Synthetical Engineering of Supramolecular Properties of Large Polycyclic Aromatic Hydrocarbons

Dissertation zur Erlangung des Grades
“Doktor der Naturwissenschaften”
am Fachbereich Chemie, Pharmazie und Geowissenschaften der
Johannes Gutenberg-Universität in Mainz

Daniel Wasserfallen

geb. in Bern, Schweiz

Mainz 2006

Dekan:

1. Berichterstatter:

2. Berichterstatter:

Tag der mündlichen Prüfung:

Die vorliegende Arbeit wurde in der Zeit vom März 2002 bis November 2005 im Max-Planck-Institut für Polymerforschung unter der Leitung von Herrn Prof. Dr. K. Müllen durchgeführt.

Ich danke Herrn Prof. Dr. K. Müllen sowohl für seine wissenschaftliche und persönliche Unterstützung als auch für seine stetige Diskussionsbereitschaft.

Dedicated to my mother

"Die Schwierigkeiten scheinen nur da zu sein, um überwunden zu werden."

Hoffmann von Fallersleben (1798-1874)

Contents

Index of Abbreviations

2D-WAXS	two-dimensional **w**ide **a**ngle **X**-ray **s**cattering
BPMPM	trans-2-[3-(4-tert-**b**utyl**p**henyl)-2-**m**ethyl-2-**p**ropenylidene] **m**alononitrile
DSC	**d**ifferential **s**canning **c**alorimetry
FET	**f**ield-**e**ffect **t**ransistor
HBC	**h**exa-*peri*-hexa**b**enzo**c**oronene
HOMO	**h**ighest **o**ccupied **m**olecular **o**rbital
HPLC	**h**igh **p**ressure **l**iquid **c**hromatography
LUMO	**l**owest **u**noccupied **m**olecular **o**rbital
MALDI-TOF MS	**m**atrix **a**ssisted **l**aser **d**esorption **i**onization-**t**ime of **f**light **m**ass **s**pectrometry
NMR	**n**ucleus **m**agnetic **r**esonance
PAH	**p**olycyclic **a**romatic **h**ydrocarbon
(O)LED	(**o**rganic) **l**ight **e**mitting **d**iode
POM	**p**olarized **o**ptical **m**icroscopy
PR-TRMC	**p**ulsed-**r**adiolysis **t**ime-**r**esolved **m**icrowave **c**onductivity
RFID	**r**adio **f**requency **i**dentification
STM	**s**canning **t**unneling **m**icroscopy
TCNQ	7,7,8,8-**t**etra**c**ya**n**o**q**uino-dimethane
TOF	**t**ime-**o**f-**f**light

1 Introduction

1.1 Benzene and Aromaticity

In 1825 discovered by Michael Faraday,[1] the structure of benzene (**1-1**) remained for a long time a centre of dispute in the scientific community. Many different options were proposed and in 1865 Kekulé suggested that benzene consists of quickly transforming isomers of cyclohexatriene and applied the term aromatic to compounds containing a benzene ring. It was later proven that the real topology of benzene is better described by Robinson's circle (Figure 1-1),[2] which pointed out the observed equal bond lengths. This phenomenon of π-bond delocalization is the reason for the high stability of benzene.

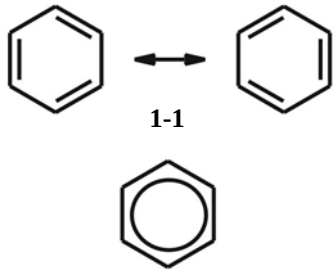

1-1

Figure 1-1: a) Kékulé and b) Robinson structures of benzene

At that time, all unsaturated systems with cyclic conjugation were considered to be aromatic, until Willstaetter[3] showed that cyclooctatetraenes have no chemical similarity to benzenes and even nowadays, aromaticity still remains in the focus of current research.[4]

Nevertheless, most chemists agreed by the 1960s that aromatic compounds are (planar) cyclic, delocalized π-electron systems and are typified by the following ground state properties.[5-7]

a) more stable than their olefinic analogues by an energy called the "resonance energy".[8,9]

b) with bond lengths intermediate between those of typical single and double bonds, and

c) with a π-electron ring current induced by an external magnetic field, leading to increased diamagnetic susceptibility and typical diatropic (low field) chemical shifts of exocyclic protons in ^{1}H NMR spectra.[10]

An additional characteristic very frequently used by organic chemists, is that:

d) aromatic compounds generally undergo substitution reactions (the so-called aromatic substitution) more easily than addition.

Because of its high stability, electronic properties and well developped substitution chemistry, benzene is found in a wide variety of compounds and is also considered as the technically most important aromatic raw material in chemistry.[11]

1.2 Polycyclic Aromatic Hydrocarbons

PAHs have not only been of academic interest since their discovery in coal tar in the 19th century. They are also important products in numerous hydrocarbon technologies as the catalytic hydrocracking of petroleum to produce gasoline, pyrolytic processes used in the formation of lower olefins and soot or the carbonization of coal in coke production.[12] The structures of benzene and PAHs can be found in many industrial products such as polymers,[13] specialized dyes and luminescence materials,[14] liquid crystals and other materials.[15] The electronic properties of aromatic compounds promoted their use in the design of organic conductors,[16] solar cells,[17] photo- and electroluminescent devices,[14,18] optically active polymers[19] and in many other fields of research. Besides the practical importance of aromatic compounds, there has always been an interest in theoretical problems like the scope, limitation and effects of electron delocalization in aromatic materials. Therefore, PAHs are of special interest as they serve as model compounds for graphite.[20]

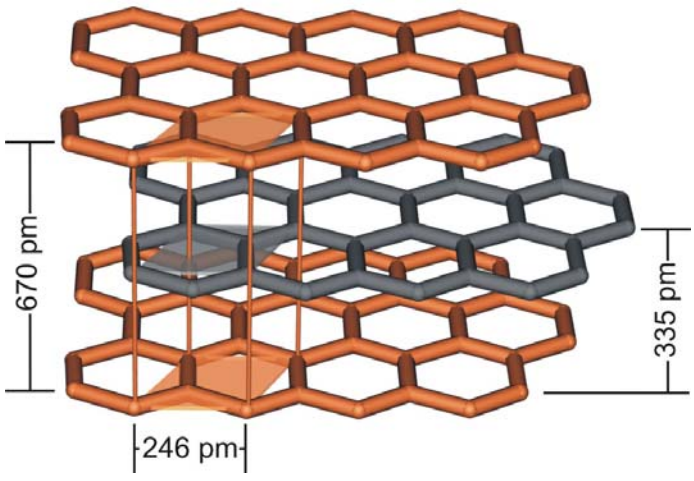

Figure 1-2: Schematic representation of a graphite lattice.

An important question is, at which size of the PAHs, their properties converge to those of graphite. Therefore, one important goal is the synthesis of defined, monodispersed PAHs with increasing size.

Graphite is the thermodynamically most stable allotrope of carbon and can be regarded as an example of an almost infinitely extended conjugated π-system. In this state, every carbon atom requires only three of its four valence electrons for the covalent binding. The fourth electron is therefore available to participate in an additional delocalized π-bond, which leads to the metallic mobility of the π-electrons parallel to the sheets. Graphite has a sheet like structure, where the atoms all lie in a plane and are only weakly bonded by van-der-Waals forces to the graphite sheets above and below (Figure 1-2). The graphite layers can be easily sheared among each other, which is the reason for its applicability as a lubricant. From this extremely different bond situation along (π-bonds) and perpendicular (van der Waals) also results a high anisotropy of the electrical and thermal properties of graphite.

1.3 The "Aromatic Sextet" and Fully Benzenoid PAHs

Not only the size, but also the topology of the PAHs play an important role concerning their reactivity or properties like absorption and fluorescence. Already 1925, many years before the wave-mechanical treatment of the aromatic bond, Robinson introduced a circle inside the hexagon to symbolize the six π-electrons of benzene.[2] This symbol stands for the mobility of the π-electrons and the stability of benzenoid compounds. By drawing aromatic structures like this, one receives a very depicted way to explain and visualize the different reactivities of PAHs. While benzene (**1-1**) exhibits a low reactivity, this argument is not true for naphthalene (**1-2**), as it can be sulfonated easily at room temperature with concentrated sulfuric acid, although it contains more π-electrons than benzene (**1-1**).

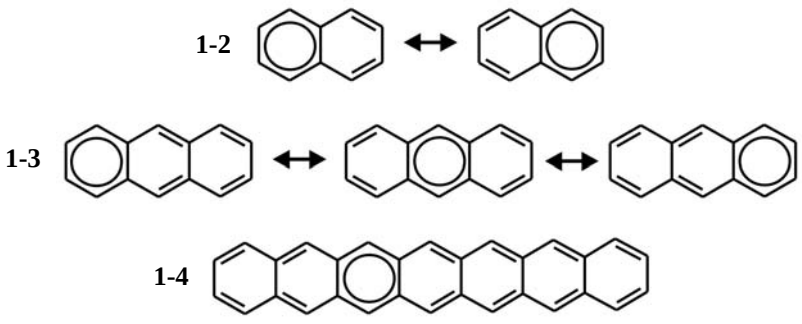

Figure 1-3: Robinson notation of acenes.

As seen in Figure 1-3, there can be only one sextet in naphthalene (**1-2**) resulting in two possible ways of drawing the molecule. The two remaining double bonds are weakening the benzenoid character, making it more "olefin-like", which is the explanation of the beforementioned higher reactivity of naphthalene. It is obvious that in the higher acenes, one sextet is shared among several rings, leading to a further gradual loss of benzenoid character. In fact the reactivity increases rapidly in the series: benzene, naphthalene, anthracene (**1-3**), tetracene (**1-7**), pentacene, hexacene and heptacene (**1-4**). While naphthalene can be, as mentioned before, sulphonated, anthracene (**1-3**) is even more reactive and can be oxidized in the middle ring to anthraquinone. Finally, the dark green heptacene is so unstable that it has never been obtained in a pure state.[21]

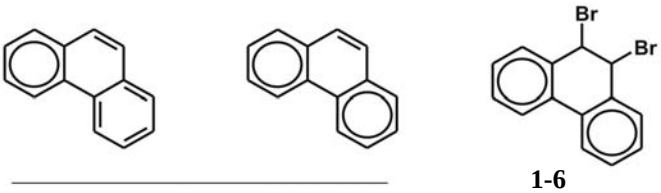

Figure 1-4: Robinson structures of phenantrene (**1-5**) and 9,10-dibromo-9,10-dihydro-phenanthrene (**1-6**).

Similar differences in reactivity can also be observed between anthracene (**1-3**) and phenanthrene (**1-5**). While for anthracene (**1-3**), one can insert only one Robinson circle, it is possible to write two for phenantrene (**1-5**). Therefore the aromatic energy of phenantrene is greater than that of anthracene.[22,23] However, this statement only applies to the whole molecule. While the rings marked with the sextet show benzene-like stability, the central ring has a "fixed" double-bond, which is indeed as reactive as any olefinic bond and adds bromine without any catalyst to form the relatively stable dibromide (**1-6**).

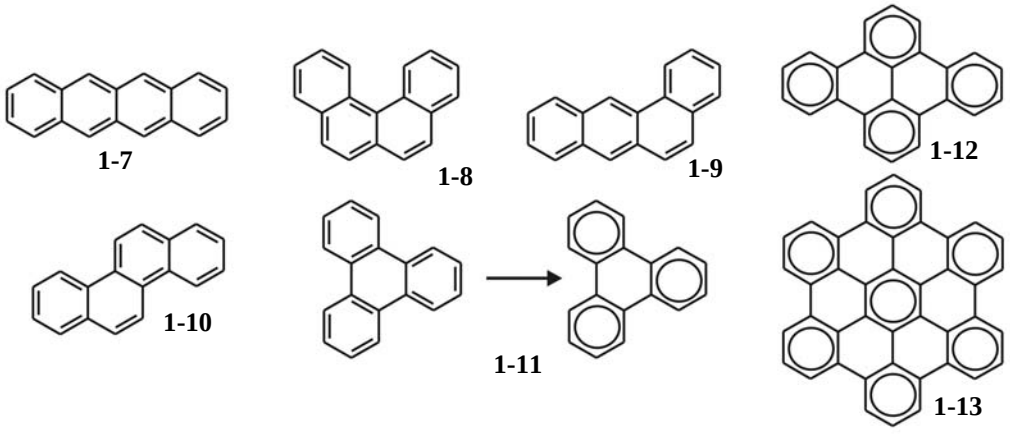

Figure 1-5: Isomers (**1-7**)-(**1-10**) of triphenylene (**1-11**). Fully benzenoid compounds dibenzopyrene (**1-12**) and hexa-*peri*-hexabenzocoronene (**1-13**) (HBC).

The simplest "fully benzenoid" PAH is triphenylene (**1-11**), whose properties differ strongly from the ones of the isomers (**1-7**)-(**1-10**) (Figure 1-5), as it is the compound with the lowest chemical reactivity, highest thermal stability, highest resonance energy and largest HOMO-LUMO gap. Triphenylene, dibenzopyrene (**1-12**), hexa-*peri*-hexabenzocoronene (HBC) (**1-13**) and all other "fully benzenoid" PAHs can be formally divided into benzene rings connected through covalent bonds or drawn with Robinsons circles with no redundant double bonds remaining, which is not possible for other PAHs (see triphenylene structure in Figure 1-5). E. Clar developped this idea into a qualitative model,[24,25,26-28] identifying the fully benzenoid PAHs as clearly less reactive and and thermodynamically more stable than the corresponding "non-fully benzenoid" isomers. The Clar structure represents hereby the energetically most stable condition and enables the differentiation between bonds, which are more olefinic or more aromatic (Figure 1-4,5). Robinsons circle[2] was used again in this context in its cassical meaning, namely as a symbol for six electrons, which illustrates the benzene likeness of the electron sextet. The "fully benzenoid" PAHs are a relatively small group of polycyclic aromatic hydrocarbons as in the case of about 20’600 possible alternating PAHs with 4-10 benzene rings only 17 are full-benzoid.[29]

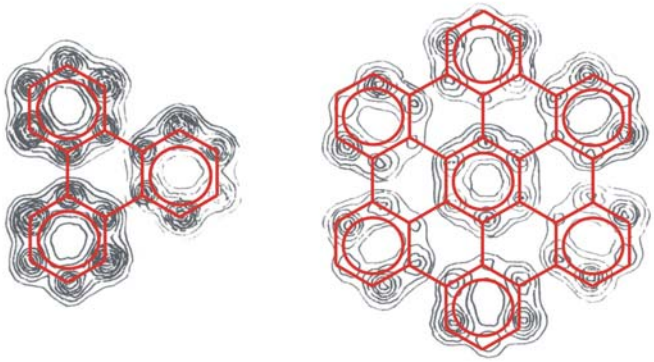

Figure 1-6: Electron contour digrams of triphenylene (**1-11**) and HBC (**1-13**) (based upon the contributions of the 3 highest occupied π-MOs).

This qualitative concept was further confirmed by a wide variety of quantum mechanical studies. One impressive result is shown in Figure 1-6, where one can clearly see the agreement between the calculated electron density distribution of the ground state and the corresponding Clar formulae.[30]

1.4 Synthesis of PAHs

Small PAHs like naphthalene, anthracene or phenantrene can be often isolated by separating mixtures, either from coal tar[31,33] or the side-products of the catalytic hydrocracking of petroleum.[32] In this case, even compounds, which are only present in small amounts in the crude material are accessible, due to the industrial scale of the process.[34] However, a far more specific assembly of PAHs is possible, as was shown by the studies of R. Scholl,[35-37] E. Clar [24,28,38-41] and M. Zander.[42-46]

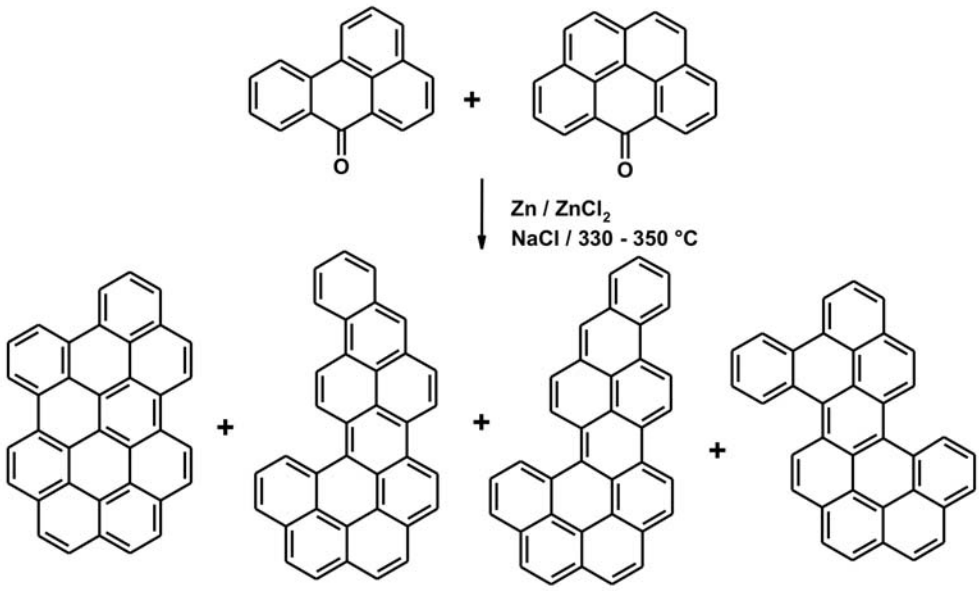

Figure 1-7: Unselective Synthesis of PAHs.[47]

Specific synthetic methods for the preparation of PAHs can be subdivided into two kinds, namely the selective and the unselective method. From the latter procedure, one gains a mixture of different compounds, which is usually formed under drastic conditions. This preparation method can be sometimes advantageous, especially if the starting material is accessible in large scale and the resulting mixture is reasonably well separable.

The selective preparation of PAHs requires a high synthetic effort, as one starts with small synthons, reaching the final product only after a multistep procedure. Two examples for such an approach can be found in Figure 1-8.

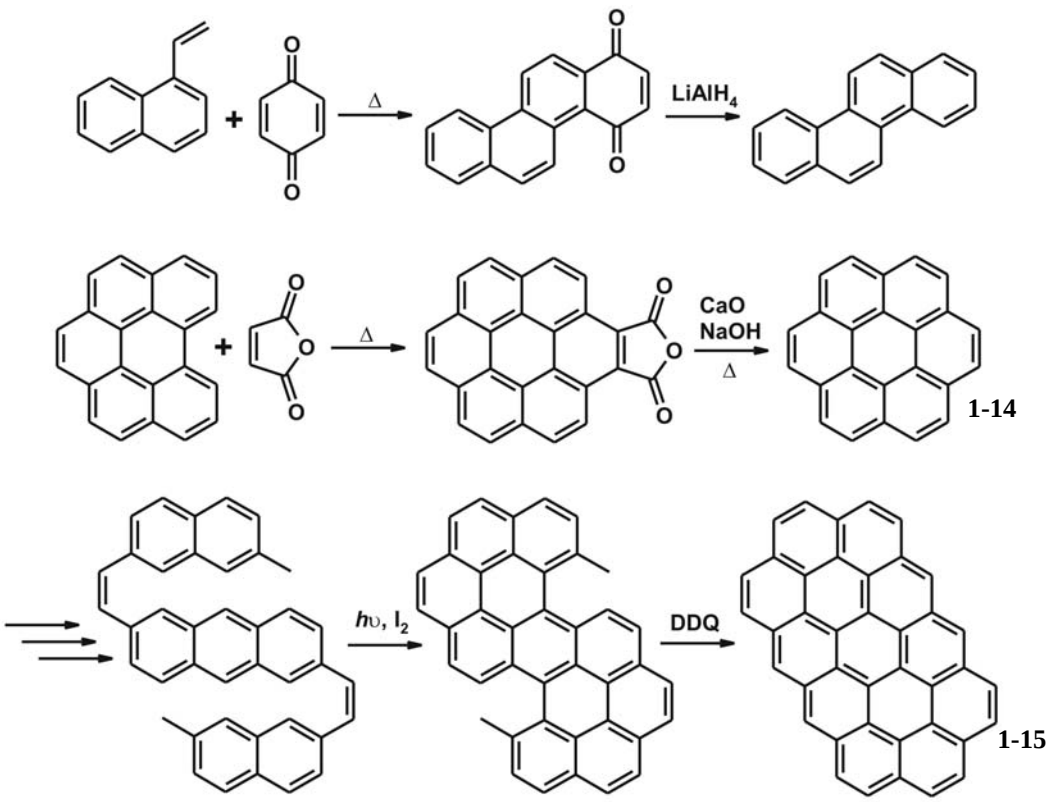

Figure 1-8: Selective synthesis of chrysene (**1-10**), coronene (**1-14**) and circumanthracene (**1-15**).

However, during the synthesis of large PAHs one often encounters the problem of a reduction of the solubility of the compounds, due to the increasing size of the rigid aromatic segment. This can lead to insoluble intermediates that are not susceptible to any further reaction step and is called "dead end" synthesis.[48] To circumvent such problems, it is necessary to find a synthetic route, in which the sparingly soluble final compound was formed during the last step, as was for example done in the synthetic approach towards kekulene.[48-51] Even though the synthesis was successful, the analytics often appear very difficult because of the pronounced insolubility of the compounds. In the case of kekulene for example the ^{1}H NMR spectrum had to be measured in 1,3,5-trichlorobenzene at 215 °C with 50'000 scans.

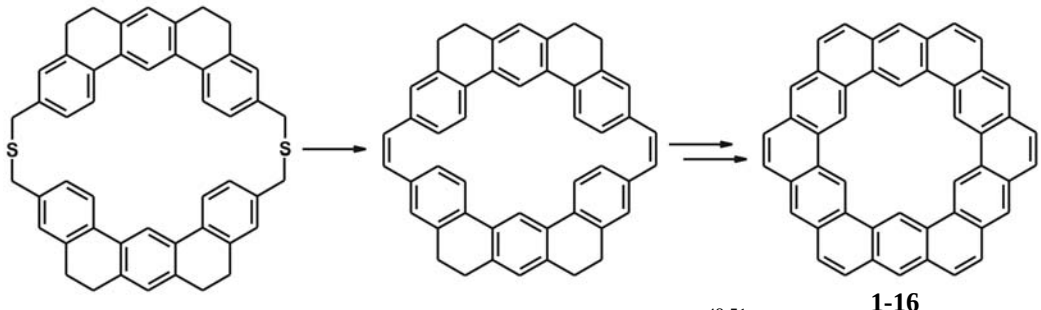

Figure 1-9: Synthesis of kekulene (**1-16**) according to Diederich and Staab.[48-51]

A commonly used concept to increase the solubility of PAHs is the attachment of flexible alkyl chains to their periphery, which happens already at an early stage of the synthetic procedure. By using this method, it is possible to synthesize alkylated, high molecular weight PAHs, which possess far better solubility in common organic solvents than their core structures.[52-54] This is not only an advantage for the analytics of spectroscopic and physical properties, but also for the processing of such compounds, whereby the alkyl substituents generally have no significant influence upon the electronic properties of the compounds.[54]

In recent years a novel synthetic approach towards monodisperse PAHs was developped in the group of Prof. Müllen. The key idea is the synthesis of soluble, structurally well-defined oligophenylene precursors and their consecutive planarization to disc-like PAHs *via* intramolecular cyclodehydrogenation.[55] For the preparation of the oligophenylene precursors three different methods are used: the cyclotrimerization of diphenylacetylene derivatives and the intra- as well as the intermolecular Diels-Alder reaction.

1.4.1 Cyclotrimerization of Diphenylacetylenes

A very efficient synthesis towards symmetrically hexafold-substituted PAHs, especially HBC, is the cobalt-catalyzed cyclotrimerization of diphenylacetylenes to hexaphenylbenzene derivatives with a subsequent planarization reaction (Figure 1-10). This opens up the possibility for introducing a wide variety of different solubilizing alkyl substituents as well as functional groups. However, it has to be kept in mind that only symmetrical diphenylacetylenes can lead to isomerically pure hexaphenylbenzenes.

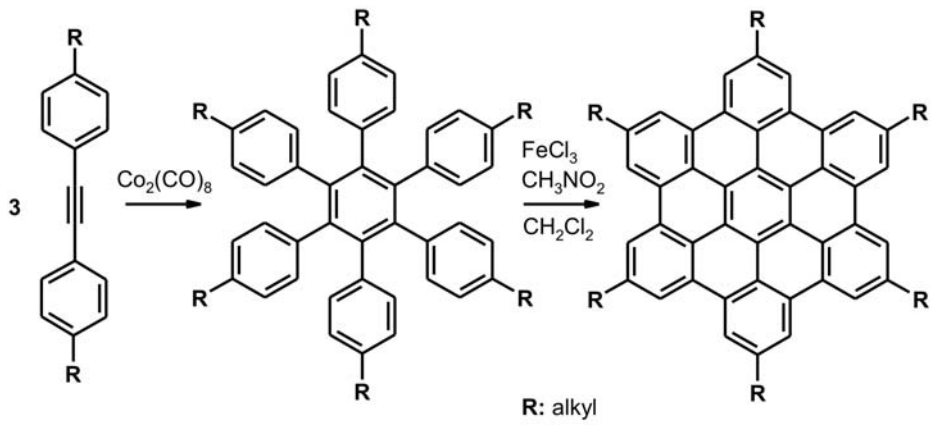

Figure 1-10: Synthesis of HBC by cyclotrimerization of a diphenylacetylene derivative and oxidative cyclodeydrogenation.[56]

Iron (III) chloride, predissolved in nitromethane,[56] proved to be one of the most effective reagents for the oxidative cyclodehydrogenation of alkyl-substituted hexaphenylbenzenes to the corresponding HBCs. Unlike the stronger Lewis-acid aluminium (III) chloride this reagent does not promote a cleavage or migration of alkyl side chains, which can occur during the course of the reaction.[57]

1.4.2 Intramolecular Diels-Alder Reaction

M. Müller[58,59] succeeded in the preparation of the phenylene-vinylene derivative **1-17**, in which the diene- and the dienophile structures are arranged in a way that they can react upon heating to 135 °C to the compound **1-18**. After a rearomatization of **1-18** using DDQ, the resulting oligophenylene **1-19** is converted to the 54 carbon atoms containing PAH **1-20** (Figure 1-11).[58, 60]

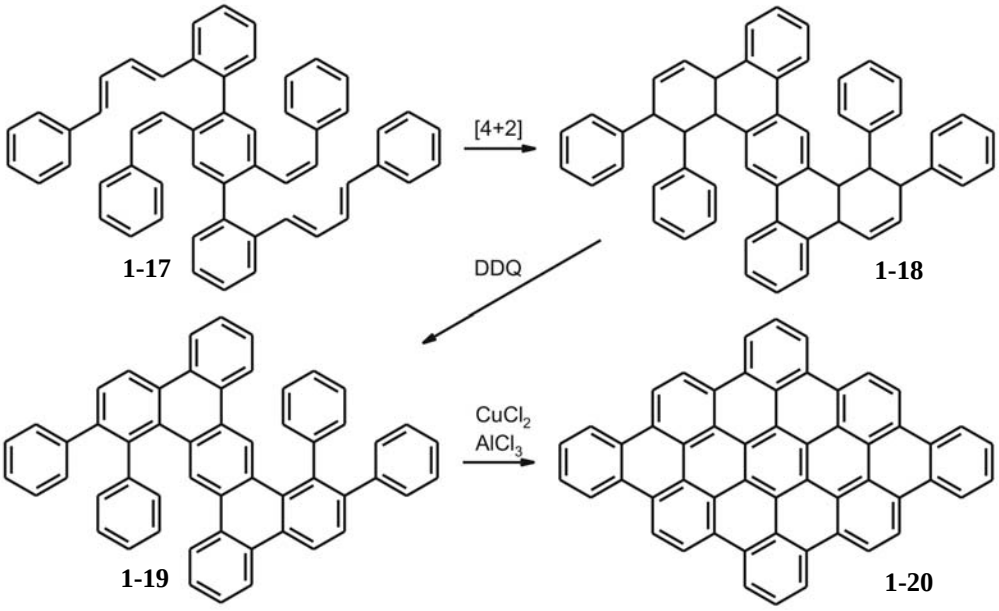

Figure 1-11: Synthesis of a rhombus shaped PAH accoording to Müller.[58]

Despite the elegance of this synthetic route, it is of rather limited use due to the complicated preparation of the precursors and is therefore not applicable as a general concept for a wide variety of PAH topologies and substitution patterns.

1.4.3 Intermolecular Diels-Alder Reaction

A versatile synthetic approach towards a concerted substitution patterns and a large variety of oligophenylenes is the intermolecular Diels-Alder reaction (Figure 1-12). In 1934, Dilthey et al. discovered that hexaphenylbenzenes were accessible *via* the reaction

of diphenylacetylenes and tetracyclones.[61,63] At a temperature of 200-250 °C the carbonyl bridged intermediate cycloaddition adduct spontaneously reacts further and expels carbon monoxide.[64]

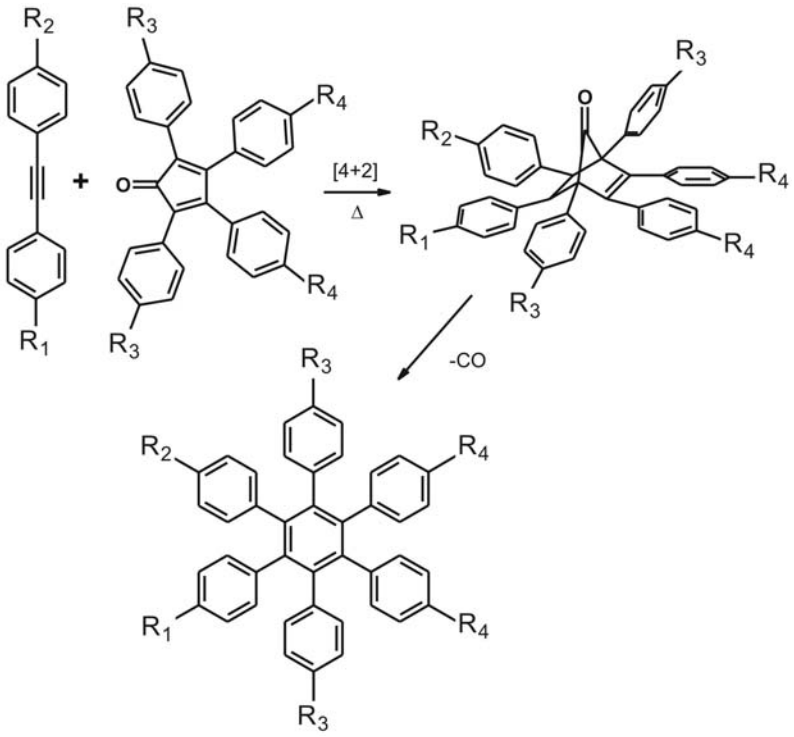

Figure 1-12: Diels-Alder-reaction for the synthesis of hexaphenylbenzene derivatives.

While phenylacetylenes with terminal acetylene functionalities already react with tetracyclone in boiling *o*-xylene as solvent, severely higher boiling solvents, like diphenylether and 1-methylnaphthalene, are necessary for a successful conversion of the diphenylacetylene derivatives.

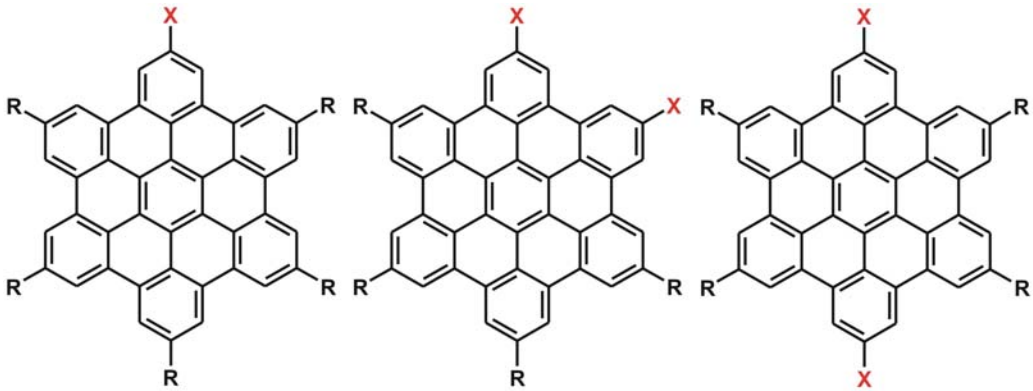

Figure 1-13: Substitution patterns of HBC-derivatives.

The versatility of this concept becomes clear, regarding the defined preparation of asymmetrically substituted hexaphenylbenzenes and their subsequently received HBC derivatives. Different substitution patterns can be accessed by modifying the alkyl substituents of the diphenylacetylene and/or the tetracyclone, including the examples shown in Figure 1-13. The declaration of "ortho" and "para" substitution follows the analoguous nomenclature of benzene, regarding HBC as a "superbenzene". The functions X also include for example halogen atoms, which enable a further functionalization on the stage of the HBC. A large diversity of HBC derivatives have already been prepared according to this route.[56,65]

1.5 Supramolecular Properties of PAHs

Molecules can be designed in a way that they meet the requirements as building blocks for nanoscale devices. They can either be covalently bonded or self-assembled *via* weak interactions like hydrogen-bonds[66-71] to form larger structures. This strategy leads to the field of supramolecular chemistry. This new branch of chemistry was introduced in the late 1970s by researchers like J. M. Lehn and has developped amazingly fast within the past decades.[72-74] Lehn defines it as:

"*the chemistry beyond the molecule, bearing on organized entities of higher complexity that result from the association of two or more chemical species held together by intermolecular forces*"[75]

These forces include all types of intermolecular interactions like hydrogen-bonding, π-interactions or van der Waals forces, which can also appear in a combined fashion.[76-84] A special feature of these structures is that their properties can be superior to the sum of the properties of the molecules they are made of. [75] A key factor for a successful formation and the amplification of the size of these nanosized structures lies within the single monomeric molecule. Therefore, monodispersed, large, nevertheless well-defined molecular building blocks are a prerequisite and are absolutely essential for the future development of this field of science.

One example of compounds, which exhibit such three-dimensional self-assemblies, are PAHs. By substituting these compounds in their periphery with the appropriate flexible alkyl chains, they can self-organize into columnar superstructures and form discotic mesophases due to their pronounced π-stacking.[56]

1.5.1 Discotic Liquid Crystals

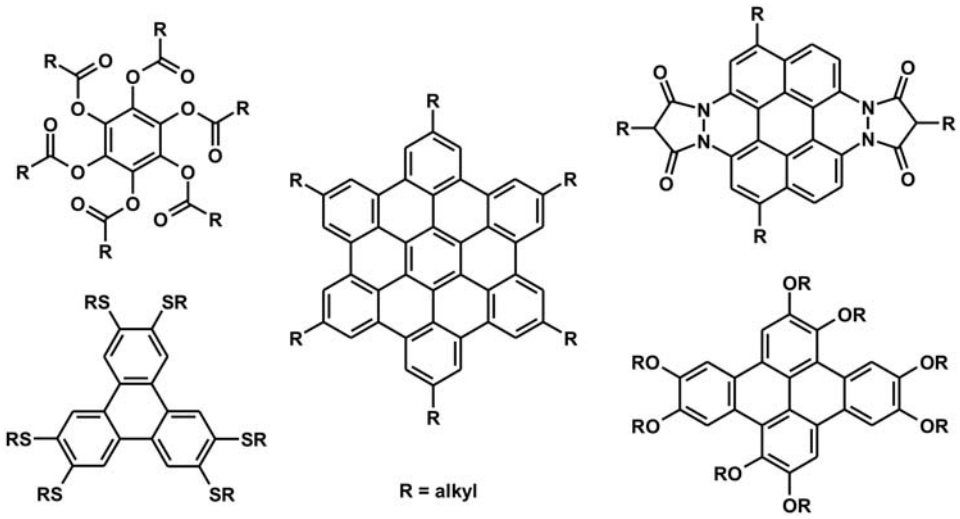

Figure 1-14: Different discotic mesogens.

The term mesophase was first given in 1977 by Chandrasekhar, the discoverer of discotic liquid crystals, and defines a state of order between crystals and liquids.[85] In this phase, the materials exhibit on one hand properties of a liquid (easily deformable) and on the other hand features typical for crystals (optical and electrical anisotropy, short to medium range order). Two different types of such phases were found. While lyotropic phases are formed by dissolving amphiphilic compounds in suitable solvents,[86] thermotropic phases can be found during the heating of a solid or the cooling of an isotropic liquid.

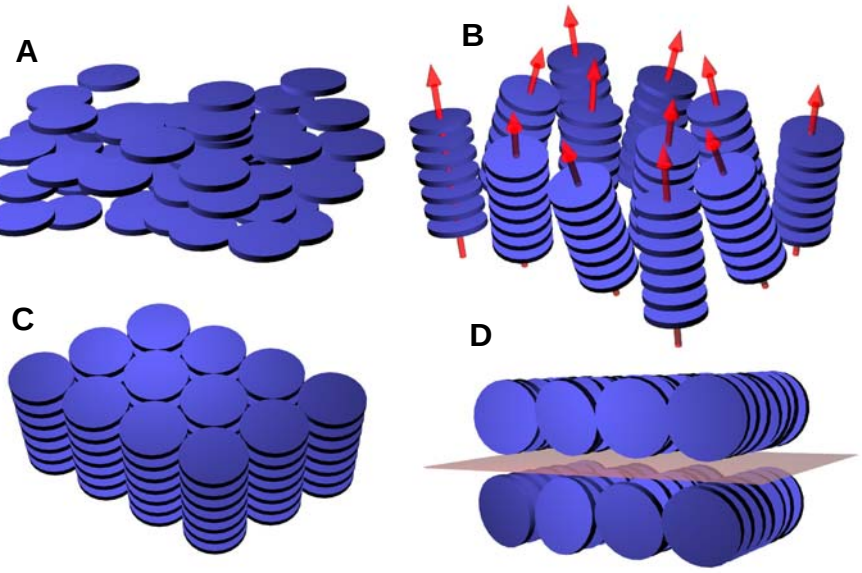

Figure 1-15: Different mesophases of discotic liquid crystals with A) discotic-nematic, B) columnar-nematic, C) columnar arrangement and D) lamellar phases.[87]

Thermotropic mesogens generally consist of a rigid core substituted with flexible peripheral moieties. Hereby, the shape of the molecule forms the basis for the further differentiation of the compounds into calamitic (rod-like core) and discotic (disc-like core) liquid crystals (Figure 1-14). Discotic liquid crystalline materials are composed of a central disc-like rigid core substituted with aliphatic alkyl chains in the periphery. These materials show different types of mesophases, which are illustrated in Figure 1-15, with a varying degree of order.

While the nematic phases reveal a preferred orientation, but no translational order, the columnar phases, which are commonly adopted by discotic molecules, show a distinct columnar self-assembly of the mesogens. These columns arrange furthermore into a two-dimensional unit cell, whereby different intercolumnar assemblies can be found (Figure 1-16A).[88,89] Finally, also the degree of order within the columns can vary between ordered, disordered and a tilted stacking behavior, as depicted in Figure 1-16B.

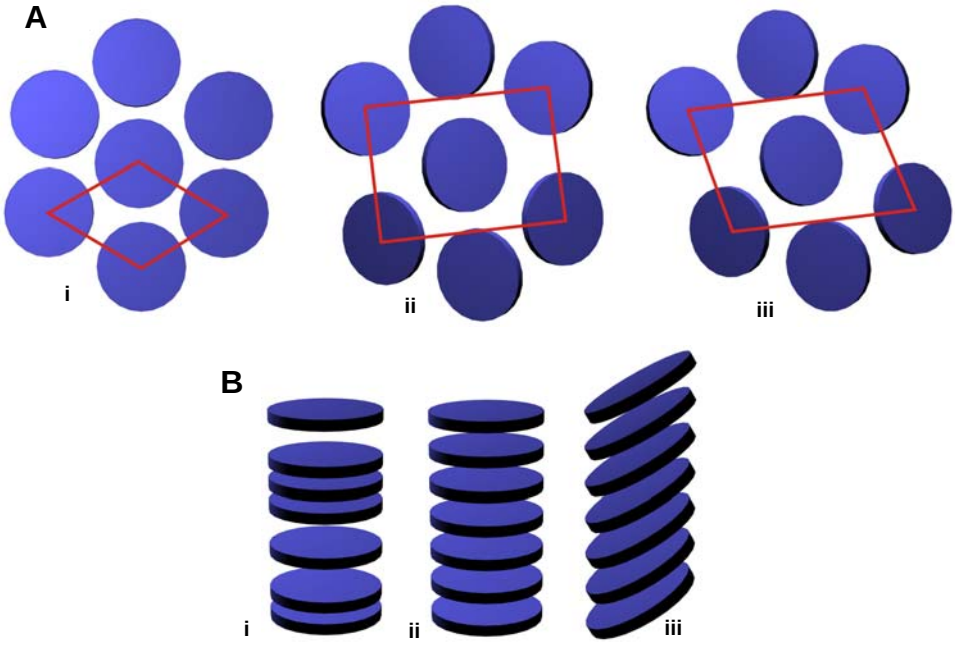

Figure 1-16: A) Two-dimensional intercolumnar arrangements with i) hexagonal (Col_h) lattice, ii) rectangular lattice (Col_r) and iii) an oblique lattice (Col_{ob}); B) common variations in intracolumnar stacking i) ordered (o) ii) disordered (d) iii) tilted (t).

In the case of alkyl substituted HBCs, three main phases are found. At low temperatures the aromatic cores are generally tilted with respect to the columnar axis as seen in Figure 1-17. This phase is usually defined as "crystalline" although this might be

incorrect according to the precise meaning, but is in agreement with the terminology already introduced for triphenylenes.

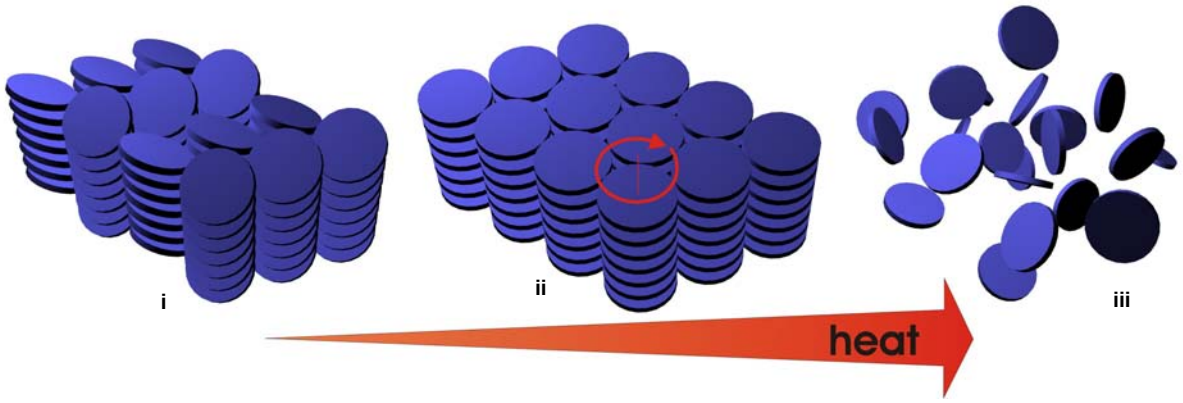

Figure 1-17: Schematic representation of thermal phase transitions: i) crystalline, ii) liquid crystalline and iii) isotropic phase

The transition to the liquid crystalline state is accompanied by a significant increase of molecular mobility. While the discs start rotating around the columnar axis, a perpendicular arrangement of the discs relative to the columnar axis is adopted, leading to a liquid-crystalline state. By heating further the isotropic state is reached, where a complete loss of any anisotropic features occurs and the material behaves like a liquid.

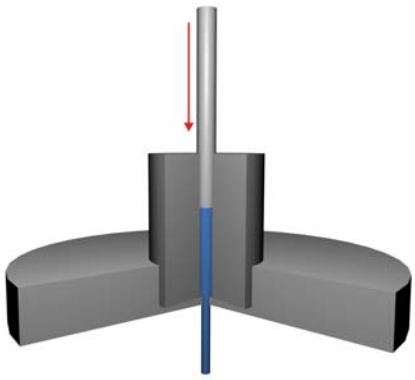

Figure 1-18: Schematic representation of an extruder.

The thermotropic phase behavior of HBCs is investigated using a wide variety of different analytical techniques. In the beginning, the phase transition temperatures and the corresponding enthalpy changes are determined with differential scanning calorimetry (DSC). By using polarized optical microscopy (POM), one can assign the type of the encountered mesophases due to the appearance of a specific birefringence of

the optical textures. For a future thermal processing, it is also important to gain information about the thermal stability of the compounds, which is achieved by thermogravimetric analysis (TGA). Another important tool for the characterization of liquid crystalline compounds is X-ray diffractometry. Small fibers of the materials are extruded, whereby the discs adopt a columnar arrangement parallel to the extrusion direction, resulting in macroscopically oriented samples, which are measured in a temperature dependent 2D X-ray diffractometer (Figure 1-19).

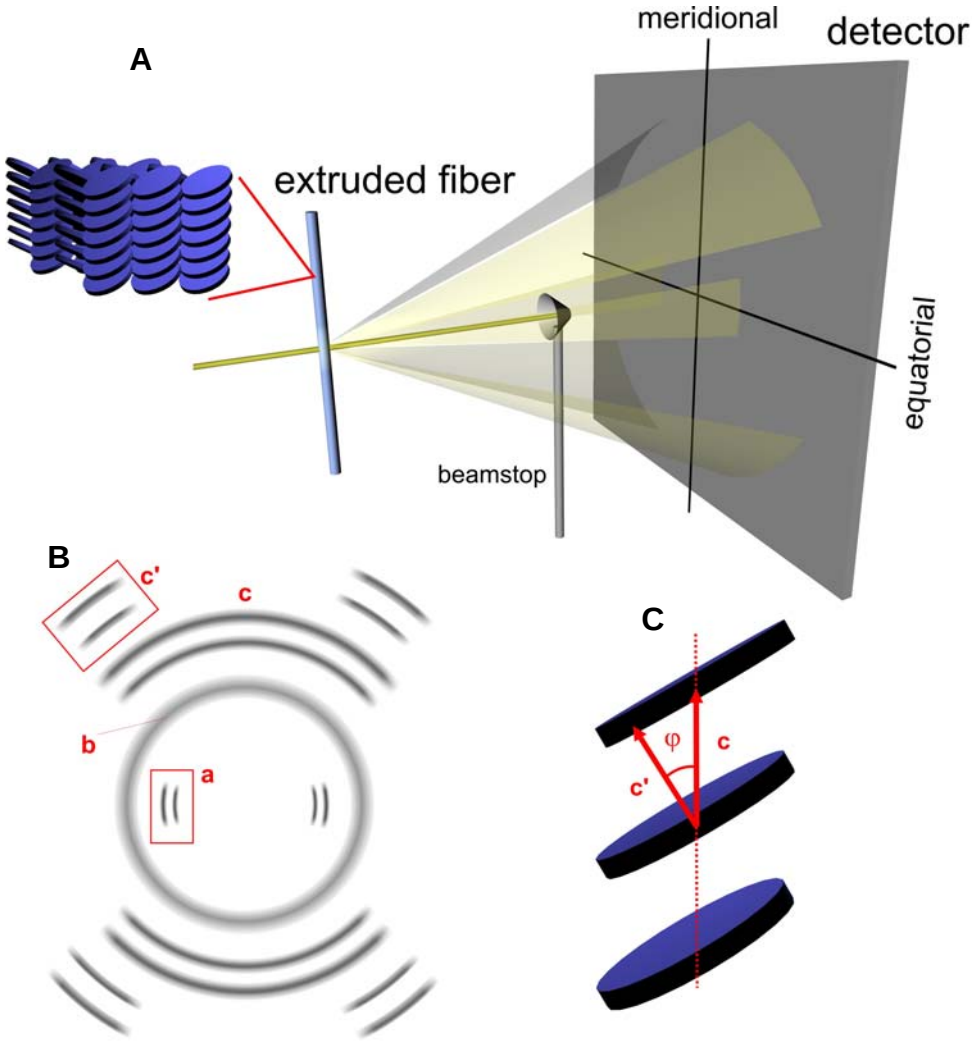

Figure 1-19: A) Experimental setup for the 2D-WAXS measurement; B) typical X-ray pattern of HBCs; C) intracolumnar arrangement.

The fibers are oriented perpendicular to the incident beam, resulting in 2D diffractograms (Figure 1-19B), where along the vertical resp. meridional axis of the spectrum the reflexes correspond to the intracolumnar stacking of the discs. In a tilted phase, one also observes reflexes on the diagonal as well as on the meridian, whereas both signals are correlated with the intracolumnar stacking (Figure 1-19B, c and c'). On

the horizontal resp. equatorial axis, the reflexes can be assigned to the intercolumnar arrangement and give an insight into the columnar packing that is aligned parallel to the extrusion direction (Figure 1-19B, a). The alkyl side-chains provide diffuse reflexes, as they cannot be oriented *via* extrusion and therefore only allow a diffuse scattering, resulting in a ring on the image (Figure 1-19B, b).

While X-ray studies are limited to a static "snapshot" of the supramolecular arrangement within the fiber, the solid-state NMR technique (Appendix A) allows a deeper insight into the dynamic bulk properties of HBCs.[90] By this method, one is able to determine not only the degree of mobility of the aromatic core components, but also the amount of mobility exerted by the alkyl substituents themselves.

1.5.2 Monolayers of PAHs

Invented in 1982, the scanning tunneling microscope (STM) was a breakthrough for nanoscience, as for the first time sub-micrometer resolution images became accessible.[91-93] For exploring organic surfaces on different length scales in various environments this technique plays an important role.[94,95] The working principle comprises of a tip that during scanning of the surface interacts locally with the surrounding vicinity (Fig 20). While atomic force microscopy (AFM) is based on interaction forces,[96-98] STM probes the tunneling probability of an electron between tip and the conducting surface.

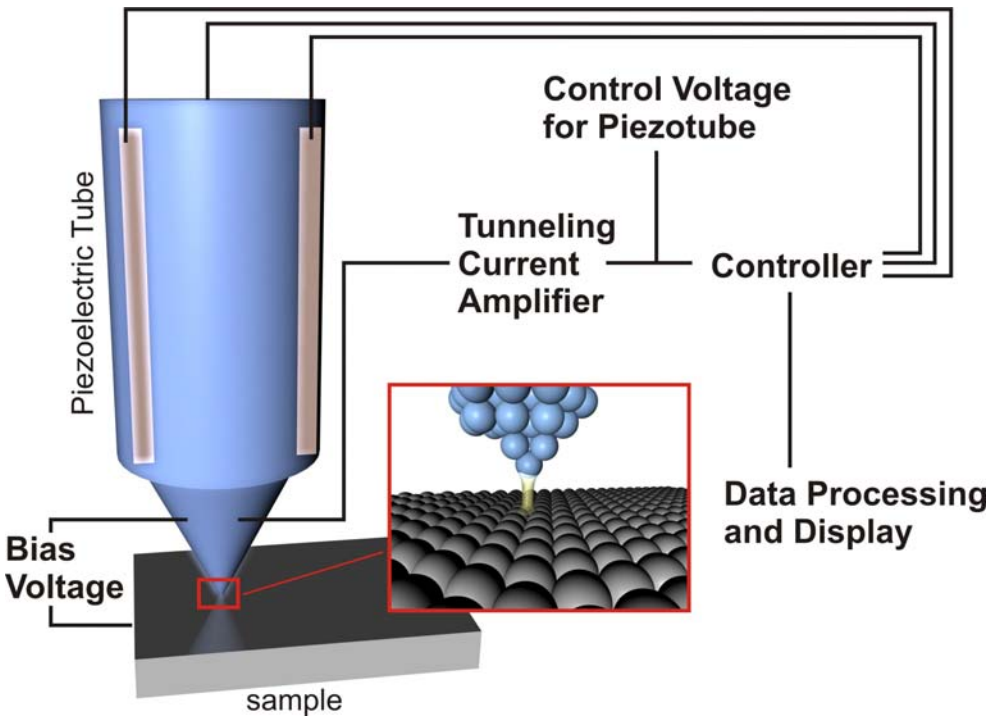

Figure 1-20: Experimental setup for STM measurements.

The quantum mechanical effect of electron tunneling occurs between two electrodes separated by a gap, which acts as a potential barrier. The tunneling current decays exponentially with the gap width, which corresponds to the distance between the conducting substrate surface and the tip. This yields a topographical image, depending on the tunneling probability through the sample. The biggest limitation for STM is the necessity for a certain conductivity of the probed materials. Insulating materials can only be visualized up to a layer thickness of 2 nm.[99]

This addresses also the necessity for localizing the molecules onto a substrate surface, preferably in monolayers. This goal can be achieved by Langmuir-Blodgett,[100] sublimation or self-assembled monolayers (SAM) at the solid-liquid interface.[99,101,102] While the Langmuir-Blodgett technique requires soluble and amphiphilic molecules, which can only be met by special functionalized PAHs,[100] only unsubstituted PAHs up to a certain size can be used for sublimation, as the high temperatures would decompose any alkyl substituents or functional groups. Monolayers can also be formed by the spontaneous self-assembly of the molecules on suitable substrate surfaces and is commonly accomplished at the solid-liquid interface.

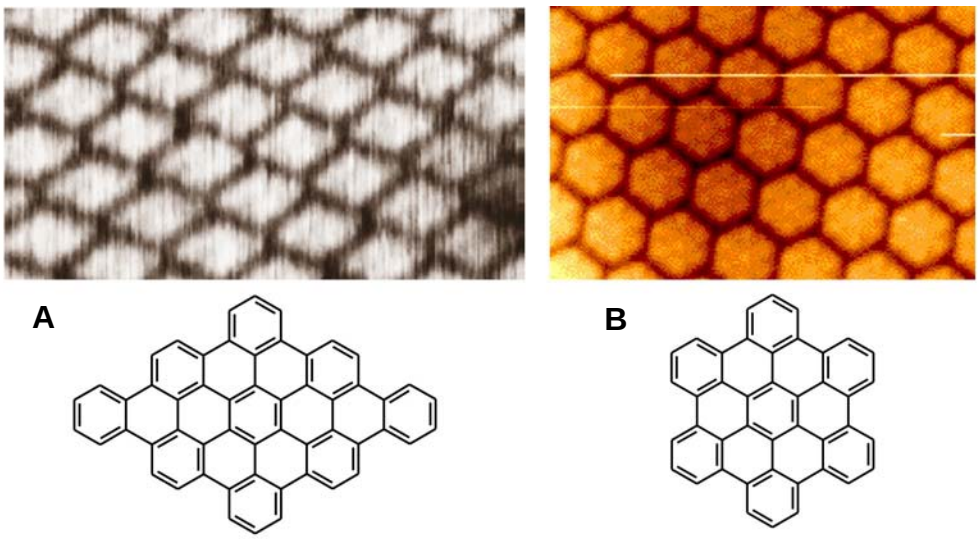

Figure 1-21: STM images of sublimed A) compound **1-20** and B) HBC **1-13**.

With the STM, it was for example possible to visualize the rhombus shaped molecule **1-20** (Figure 1-21A), which was at this time the first structure proof of this virtually insoluble molecule. The UHV-sublimation at 600 °C could only be achieved due to the high thermostability of the material. In a similar fashion, unsubstituted HBCs could also be analyzed (Figure 1-21B).[103] By using soluble, alkyl-substituted HBCs such as the

example presented in Figure 1-22 synthesized by N. Tchebotareva, monomolecular layers could be prepared *via* self-assembly from solution on a highly oriented pyrolitic graphite (HOPG) surface, which takes advantage of the tendency of certain molecules to physisorb spontaneously onto a basal plane of a flat solid surface (Figure 1-22).[56,104]

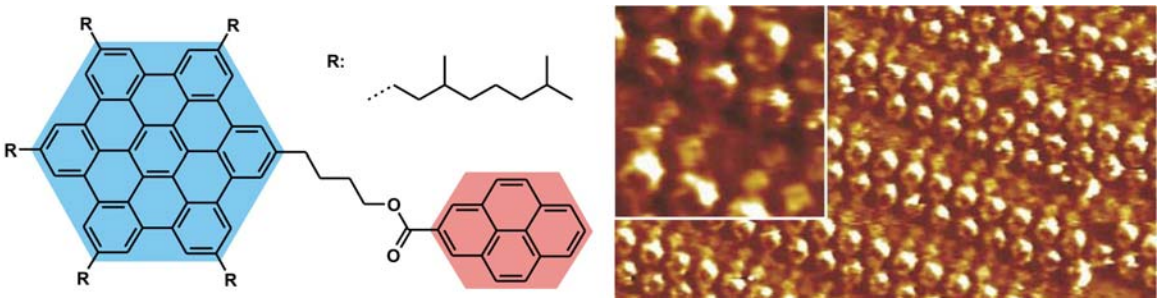

Figure 1-22: Nanoscale phase separation on HOPG.

Of course this technique is not limited to the simple visualization of molecules on surfaces, but is also used for future research towards single molecular devices (Figure 1-22).[105]

1.5.3 Intracolumnar Charge Carrier Transport

Discotic molecules, arranged in columnar stacks, exhibit one highly interesting property, what makes them very promising candidates for a future application in electronic devices. Due to their extensive molecular π-orbitals and the interaction between adjacent cores a pathway for charge-carriers can be provided (Figure 1-23).[106,107]

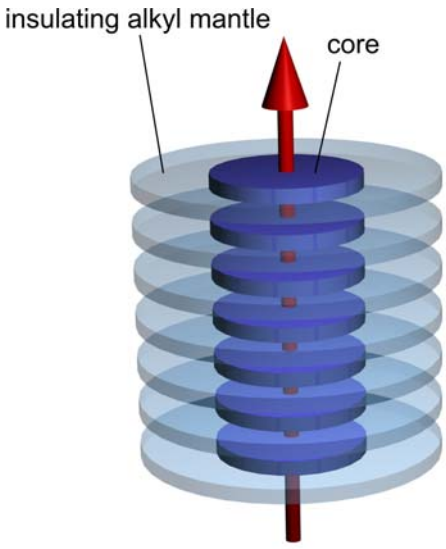

Figure 1-23: Intracolumnar pathway for charge migration.

Hereby, the peripheral substitution by alkyl chains serve as an isulating layer. In these cases one can regard the supramolecular structures as "nanowires". A detailed study of the charge transfer mechanism in discotic liquid crystalline materials was lately provided by A. van de Craats using the pulse-radiolysis time-resolved microwave conductivity (PR-TRMC) technique and by a theoretical study by Lever et al..[108,109]

By the PR-TRMC technique, one determines the charge carrier mobility on a nanometer length scale, which means that traps caused by structural defects and impurities are far less disturbing. It is important to point out that the values obtained by this technique can differ from the ones measured with time-of-flight (TOF) or field-effect transistor (FET) experiments. PR-TRMC only reveals charge carrier mobilities in relation to migration between several molecules, whereas the TOF or FET methods are usually several order of magnitudes lower due to the higher degree of disorder and possible trapping sites at grain boundaries.

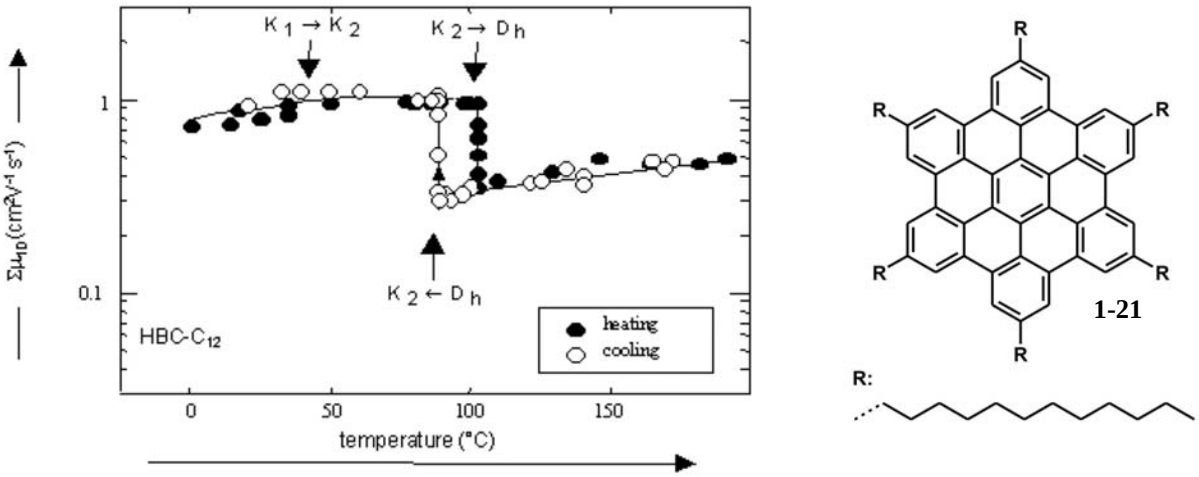

Figure 1-24: Temperature dependent charge carrier mobility values for hexa-dodecyl-HBC (**1-21**).

It was also found that the charge carrier mobility was more dependent on the size of the aromatic core component than on the cofacial distance between neighboring cores within the columnar stack.[108,110] This relation was accounted to the increased π-interactions of the larger aromatic cores leading to a more stable columnar structure and thus a better charge carrier transport. Also the phase behavior plays an important role, as was observed by A. van de Craats in the case of hexa-*n*-dodecyl HBC (Figure 1-24). The mobility substantially decreased during the phase transition between the crystalline and the liquid crystalline state, which pronounces the importance of a high order within the materials to gain high charge carrier mobility values.

1.7 Devices Based on Discotic Organic Materials

By taking advantage of the high charge carrier mobilities and the distinct self-arrangement into columnar superstructures, discotic liquid crystalline materials like triphenylene or HBC were already used as active components in electronic devices.[111] For example, the first light emitting diode (LED) based on triphenylene was introduced by Wendorff et al.[112]

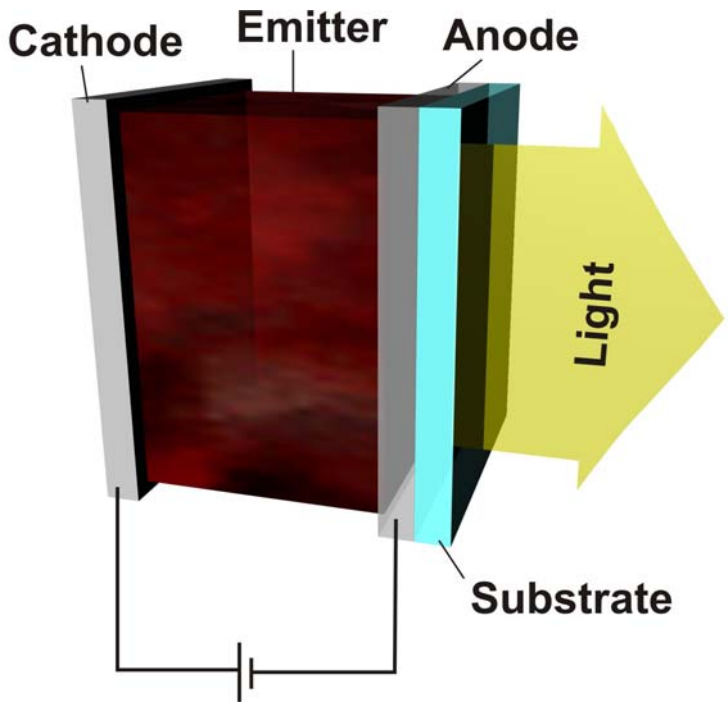

Figure 1-25: Schematic representation of an organic light emitting diode.

In Figure 1-25 the structural design of an organic light emitting diode (OLED) is depicted. This simple type consists of a thin film of an organic emitter sandwiched between a transparent anode and a metallic cathode. By applying an external voltage, electrons and holes are injected into the organic material, drift through the material under the influence of the electric field until they encounter each other and recombine to form a light-emitting exciton. For an efficient performance of the device, the discotic liquid crystals must exhibit a high fluorescence quantum efficiency combined with a high charge carrier mobility.[113] Furthermore a homeotropic alignment (Figure 1-26A) of the discotics is a prerequisite to ensure an unhindered charge transport, which occurs perpendicular to the substrate.

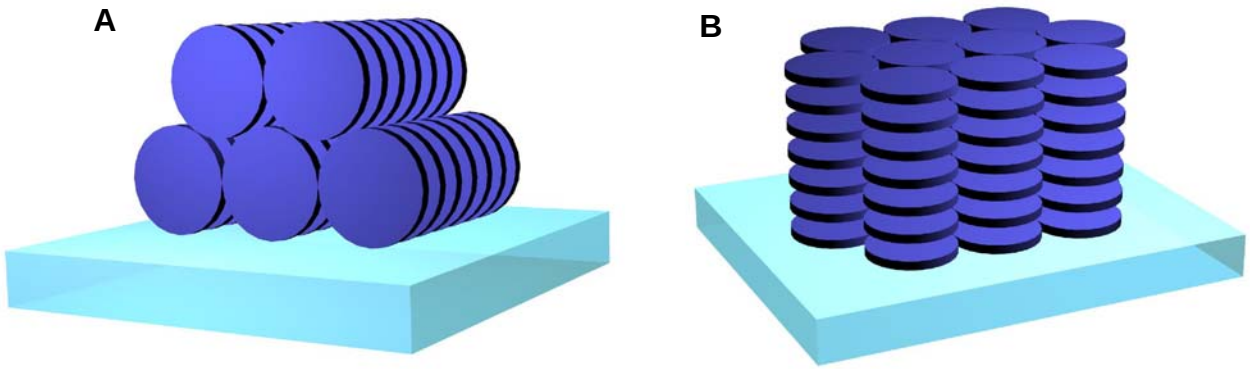

Figure 1-26: Schematic representation of the different supramolecular arrangements on surfaces with A) edge-on orientation of the molecules (columnar axis is oriented parallel to the substrate) and B) face-on arrangement (homeotropical order).

Photovoltaic cells based on organic materials encounter similar requirements as already met for OLEDs. A high efficiency can be obtained by a blending of a donor and an acceptor component (Figure 1-27). Another key issue is hereby the increase of the contact area between the two materials and an absorption profile that covers a wide area of the solar spectrum in combination with a high absorption coefficient. The latter two features are necessary to exploit the maximum number of photons.

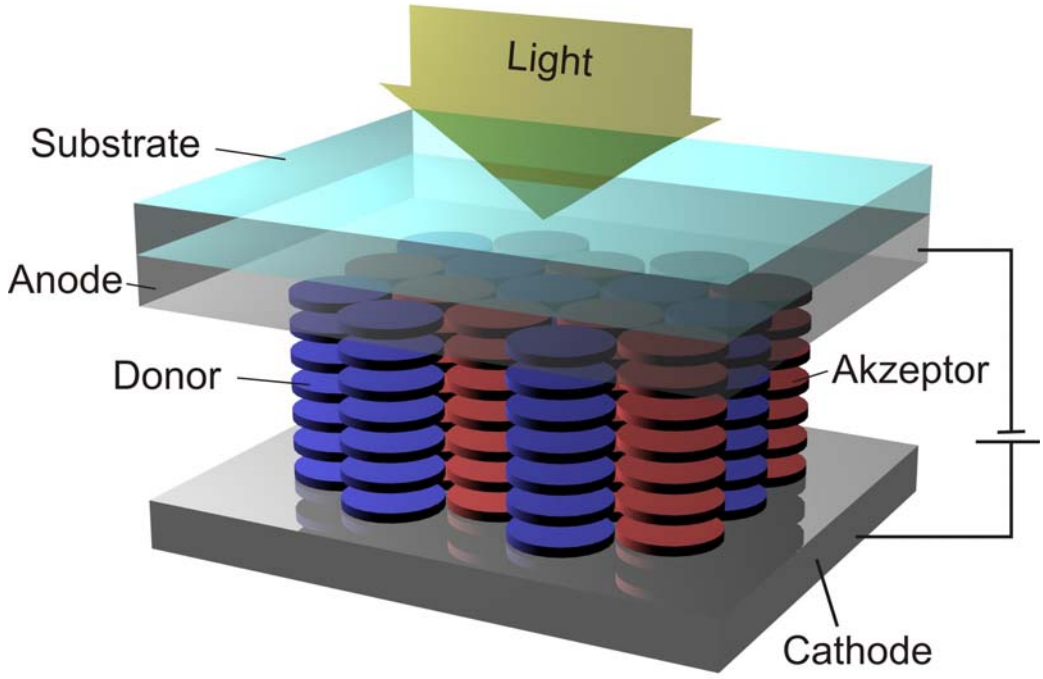

Figure 1-27: Schematic representation of an organic photovoltaic cell.

The absorbed photons generate electron-hole pairs, which after the charge separation are transported by applying an external electric field to the cathode or the electrode respectively inducing the electric current.

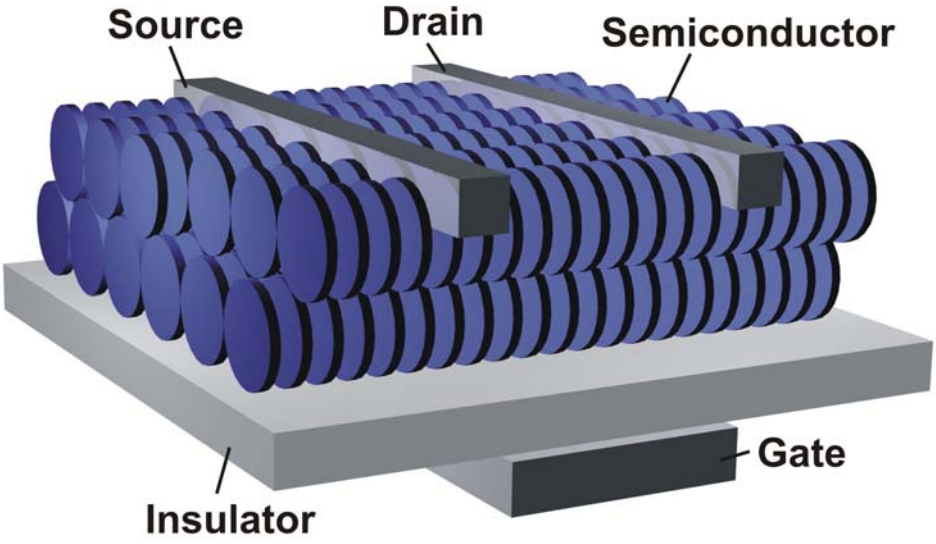

Figure 1-28: Schematic representation of an organic field-effect transistor.

In Figure 1-28, the general scheme for a field-effect transistor (FET) based on discotic mesogens is shown. In a FET, the current between the drain and the source contacts is dependent on the gate voltage. By a variation of this voltage and a constant drain voltage, it is possible to control the charge carrier density in the channel. The efficiency of such a device depends on one hand on the on/off ratio and on the other on the time that the charge carriers require to travel through the channel. Therefore, it is necessary to orient the columnar structures uniaxially in an edge-on arrangement (Figure 1-26B) along the direction of the applied electrical field between source and drain.

1.8 References

[1] M. Faraday *Phil. Trans. R. Soc. London* **1825**, 440.

[2] T. W. Armitt, R. Robinson *J. Chem. Soc. (London)*, **1925**, 1604.

[3] R. Willstaetter, E. Waser *Ber.* **1911**, *44*, 3433.

[4] T. M. Krygowski, M. K. Cyranski, Z. Czarnocki, G. Häfelinger, A. R. Katritzkyc *Tetrahedron* **2000**, *56*, 1783.

[5] F. Sondheimer *Pure Appl. Chem.* **1964**, 859.

[6] M. J. S. Dewar *Tetrahedron (Suppl.)* **1966**, *8*, 75.

[7] J. A. Elvidge, L. M. Jackman *J. Chem. Soc.* **1961**, 859.

[8] L. Pauling, G. W. Wheland *J. Chem. Phys.* **1933**, *1*, 362.

[9] G. W. Wheland *Resonance in Organic Chemistry*, Wiley: New York, **1955**.

[10] R. C. Haddon, V. R. Haddon, L. J. Jackman *Nuclear Magnetic Resonance of Annulenes. Topics in Current Chemistry*, Springer: Berlin, **1971**; Vol. 16, 2.

[11] J. Falbe, M. Regitz *Römpp-Chemielexikon* 9th ed., Georg Thieme Verlag, Stuttgart, New York, **1995**.

[12] H. G. Franck, J. W. Stadelhofer *Industrielle Aromatenchemie*, Springer, Berlin, Heidelberg, New York, **1987**.

[13] J. M. Tour *Chem. Rev.* **1996**, *96*, 537.

[14] F. O. Holtrup, G. R. J. Müller, H. Quante, S. de Feyter, F. C. de Schryver, K. Müllen *Chem. Eur. J.* **1997**, *3*, 219.

[15] S. Chandrasekhar *Liq. Cryst.* **1993**, *14*, 3.

[16] V. Gama, R. T. Henriques, G. Bonfait, M. Almeida, A. Meetsma, S. van Smaalen, J. L. de Boer *J. Am. Chem. Soc.* **1992**, *114*, 1986.

[17] M. Hiramoto, Y. Kishigami, M. Yokoyama, M.; *Chem. Lett.* **1990**, 119.

[18] J. D. Debad, J. C. Morris,P. Magnus, A. J. Bard *J. Org. Chem.* **1997**, *62*, 530.

[19] R. Fiesel, J. Huber, U. Scherf *Angew. Chem. Int. Ed. Engl.* **1996**, *35*, 2111.

[20] J. R. Dias *Thermochim. Acta* **1987**, *122*, 313.

[21] M. Bendikov, H. M. Duong, K. Starkey, K. N. Houk, E. A. Carter, F. Wudl *J. Am. Chem. Soc.* **2004**, *126*, 7416.

[22] J. W. Richardson, J. S. Parks *J. Am. Chem. Soc.* **1939**, *61*, 3543.

[23] A. Magnus, H. Hartmann, F. Becker *Z. Phys. Chem.* **1951**, *197*, 75.

[24] E. Clar *Aromatische Kohlenwasserstoffe-Polycyclische Systeme*, Springer, Berlin, Göttingen, Heidelberg, **1952**.

[25] E. Clar *The Aromatic Sextet*, 1st ed., John Wiley and Sons, London, **1972**.

[26] E. Clar, C. T. Ironside *Proc. Chem. Soc. of London* **1958**, 150.

[27] E. Clar, C. T. Ironside, M. Zander *J. Chem. Soc.* **1959**, 142.

[28] E. Clar, W. Schmidt *Tetrahedron* **1979**, *35*, 2673.

[29] I. Gutman, S. J. Cyvin *Introduction to the Theory of Benzenoid Hydrocarbons*, Springer-Verlag, Heidelberg, **1989**.

[30] H. Hosoya, *Top. Curr. Chem.* **1990**, *153*, 255.

[31] K. F. Lang, J. Kalowy, H. Buffleb *Chem. Ber. Recl.* **1962**, *95*, 1052.

[32] K. F. Lang, H. Buffleb, M. Zander *Angew. Chem. Int. Ed. Engl.* **1963**, *75*, 170.

[33] K. F. Lang, J. Kalowy, H. Buffleb *Chem. Ber. Recl.* **1964**, *97*, 494.

[34] C. Grundmann *Methoden Organischer Chemie: Arene und Arine* (Houben Weyl), Vol. 5/2b, 4. ed., Thieme Verlag, Stuttgart, New York, **1981**.

[35] R. Scholl, H. Neumann *Chem. Ber.* **1922**, 118.

[36] R. Scholl, C. Seer *Liebigs Ann. Chem.* **1912**, 111.

[37] R. Scholl, C. Seer, R. Weitzenböck *Chem. Ber.* **1910**, 2202.

[38] E. Clar *Ber. dtsch. chem. Ges.* **1936**, *69*, 607.

[39] E. Clar *Nature* **1948**, *161*, 238.

[40] E. Clar, D. G. Stewart *J. Am. Chem. Soc.* **1953**, *75*, 2667.

[41] E. Clar, C. T. Ironside, M. Zander *Tetrahedron* **1966**, *22*, 3527.

[42] M. Zander, W. Franke *Chem. Ber. Recl.* **1958**, *91*, 2794.

[43] M. Zander *Angew. Chem. Int. Edit. Engl.* **1960**, *72*, 513.

[44] H. G. Franck, M. Zander *Chem. Ber. Recl.* **1966**, *99*, 396.

[45] M. Zander *Tetrahedron Lett.* **1971**, 3245.

[46] M. Zander, W. H. Franke *Chem. Ber. Recl.* **1973**, *106*, 2752.

[47] J. C. Fetzer, W. R. Biggs *Org. Prep. Proced. Int.* **1988**, *20*, 223.

[48] H. A. Staab, F. Diederich *Chem. Ber.-Recl.* **1983**, *116*, 3487.

[49] F. Diederich, H. A. Staab *Angew. Chem. Int. Edit. Engl.* **1978**, *17*, 372.

[50] C. Krieger, F. Diederich, D. Schweitzer, H. A. Staab *Angew. Chem. Int. Edit. Engl.* **1979**, *18*, 699.

[51] H. A. Staab, F. Diederich, C. Krieger, D. Schweitzer *Chem. Ber. Recl.* **1983**, *116*, 3504.

[52] M. Rehahn, A. D. Schlüter, G. Wegner, W. J. Feast *Polymer* **1989**, *30*, 1054.

[53] M. Rehahn, A. D. Schlüter, G. Wegner *Makromolekulare Chemie-Macromolecular Chemistry and Physics* **1990**, *191*, 1991.

[54] K. H. Koch, K. Müllen *Chem. Ber.* **1991**, *124*, 2091.

[55] M. D. Watson, A. Fechtenkötter, K. Müllen *Chem. Rev.* **2001**, *101*, 1267.

[56] S. Ito, M. Wehmeier, J. D. Brand, C. Kübel, R. Epsch, J. P. Rabe, K. Müllen *Chem. Eur. J.* **2000**, *6*, 4327.

[57] M. Wehmeier *phD thesis* **1999**, Mainz.

[58] M. Müller, J. Petersen, R. Strohmaier, C. Gunther, N. Karl, K. Müllen *Angew. Chem. Int. Edit. Engl.* **1996**, *35*, 886.

[59] M. Müller *phD thesis*, Johannes-Gutenberg-Universität, Mainz, **1997**.

[60] P. Kovacic, A. Kyriakis *J. Am. Chem. Soc.* **1963**, **85**, 454.

[61] W. Dilthey, F. Quint *J. Prakt. Chem.* **1930**, *128*, 139.

[62] W. Dilthey, W. Schommer *J. Prakt. Chem.* **1933**, *136*, 293.

[63] W. Dilthey *Chem. Ber.* **1934**, *67*, 2004.

[64] L. F. Fieser *Org. Synth. V* **1973**, 604.

[65] A. Fechtenkötter, N. Tchebotareva, M. Watson, K. Müllen *Tetrahedron* **2001**, *57*, 3769.

[66] M. Suarez, J. M. Lehn, S. C. Zimmerman, A. Skoulios, B. Heinrich *J. Am. Chem. Soc.* **1998**, *120*, 9526.

[67] M. M. Conn, J. Rebek *Chem. Rev.* **1997**, *97*, 1647.

[68] L. J. Prins, J. Huskens, F. de Jong, P. Timmermann, D. N. Reinhoudt *Nature* **1999**, *398*, 498.

[69] J. H. K. Ky Hirschberg, L. Brunsveld, A. Ramzi, J. A. J. M. Vekemans, R. P. Sijbesma, E. W. Meijer *Nature* **2000**, *407*, 167.

[70] M. R. Ghadiri, J. R. Granja, L. K. Buehler *Nature* **1994**, *369*, 301.

[71] R. P. Sijbesma, F. H. Beijer, L. Brunsveld, B. J. B. Folmer, J. H. K. Ky Hirschberg, R. F. M. Lange, J. K. L. Lowe, E. W. Meijer *Science* **1997**, *278*, 1601.

[72] J. M. Lehn *Angew. Chem. Int. Ed. Engl.* **1988**, *27*, 89.

[73] G. M. Whitesides, J. P. Mathias, C. T. Seto *Science* **1991**, *254*, 1312.

[74] F. Vögtle, *Supramolecular Chemistry: An Introduction*, Wiley, Chichester, **1991**.

[75] J.-M. Lehn *Supramolecular Chemistry: Concepts and Perspectives*, VCH, Weinheim, **1995**.

[76] C. H. Lin, J. Tour *J. Org. Chem.* **2002**, *67*, 7761.

[77] D. T. Bong, T. D. Clark, J. R. Granja, M. R. Ghadiri *Angew. Chem. Int. Ed.* **2001**, *40*, 988.

[78] F. S. Schoonbeek, J. H. van Esch, B. Wegewijs, D. B. A. Rep, M. P. de Haas, T. M. Klapwijk, R. M. Kellogg, B. L. Feringa *Angew. Chem. Int. Ed. Engl.* **1999**, *38*, 1393.

[79] A. Guesquière, M. M. S. Abdel-Mottaleb, S. de Feyter, F. C. de Schryver, F. Schoonbeek, J. van Esch, R. M. Kellogg, B. L. Feringa, A. Calderone, R. Lazzaroni, J. L. Brédas *Langmuir* **2000**, *16*, 10385.

[80] R. I. Gearba, M. Lehmann, J. Levin, D. A. Ivanov, M. H. J. Koch, J. Barbera, M. G. Debije, J. Piris, Y. H. Geerts *Adv. Mater.* **2003**, *15*, 1614.

[81] M. L. Bushey, A. Hwang, P. W. Stephens, C. Nuckolls *Angew. Chem. Int. Ed. Engl.* **2002**, *41*, 2828.

[82] T. S. Balaban, A. Eichhöfer; J. M. Lehn *Eur. J. Org. Chem.* **2000**, 4047.

[83] J. J. van Gorp, J. A. J. M. Vekemans, E. W. Meijer *J. Am. Chem. Soc.* **2002**, *124*, 14759.

[84] R. E. Gillard, F. M. Raymo, J. F. Stoddart *Chem. Eur. J.* **1997**, *3*, 1933.

[85] S. Chandrasekhar, B. K. Sadashiva, K. A. Suresh *Pramana* **1977**, *9*, 471.

[86] H. Sandquist *Chem. Ber.* **1915**, *48*, 2054.

[87] S. Chandrasekhar, S. K. Prasad *Contemp. Phys.* **1999**, *40*, 237.

[88] A. M. Levelut, A. M. *J. Chem. Phys.* **1983**, *88*, 149.

[89] A. M. Levelut *J. Phys. Lett. Paris* **1979**, *40*, L-81.

[90] S. P. Brown, I. Schnell, J. D. Brand, K. Müllen, H. W. Spiess *J. Mol. Struct.* **2000**, *521*, 179.

[91] G. Binnig, H. Rohrer *Helv. Phys. Acta* **1982**, *55*, 726.

[92] G. Binnig, H. Rohrer, C. Gerber, E. Weibel *Appl. Phys. Lett.* **1982**, *40*, 178.

[93] P. Samori, J. P. Rabe *J. Phys. Condens. Matter* **2002**, *14*, 9955.

[94] A. Yazdani, C. M. Lieber *Nature* **1999**, *401*, 227.

[95] J. K. Gimzewski, C. Joachim *Science* **1999**, *283*, 1683.

[96] G. Binnig, C. F. Quate, C. Gerber *Phys. Rev. Lett.* **1986**, *56*, 930.

[97] D. Rugar, P. Hansma *Phys. Today* **1990**, *43*, 23.

[98] H. Takano, J. R. Kenseth, S. S. Wong, J. C. O'Brien, M. D. Porter *Chem. Rev.* **1999**, *99*, 2845.

[99] E. Delamarche, B. Michel, H. A. Biebuyck, C. Gerber *Adv. Mater.* **1996**, *8*, 719.

[100] N. Reitzel, T. Hassenkam, K. Balashev, T. R. Jensen, P. B. Howes, K. Kjaer, A. Fechtenkötter, N. Tchebotareva, S. Ito, K. Müllen, T. Bjornholm *Chem. Eur. J.* **2001**, *7*, 4894.

[101] E. Delamarche, B. Michel *Thin Solid Films* **1996**, *273*, 54.

[102] J. P. Rabe, S. Buchholz *Science* **1991**, *253*, 424.

[103] U. Zimmermann, N. Karl *Surf. Sci.* **1992**, *268*, 296.

[104] A. Stabel, P. Herwig, K. Müllen, J. P. Rabe *Angew. Chem. Int. Ed. Engl.* **1995**, *34*, 1609.

[105] N. Tchebotareva, X. Yin, M. D. Watson, P. Samori, J. P. Rabe, K. Müllen *J. Am. Chem. Soc.* **2003**, *125*, 9734.

[106] N. Boden, R. Bushby, J. Clements, B. Movaghar, K. Donovan, T. Kreouzis *Phys. Rev. B* **1995**, *52*, 13274.

[107] Matthias Lehmann, G. Kestemont, R. G. Aspe, C. Buess-Herman, M. H. J. Koch, M. G. Debije, J. Piris, M. P. de Haas, J. M. Warman, M. D. Watson, V. Lemaur, J. Cornil, Y. H. Geerts, R. Gearba, D. A. Ivanov *Chem. Eur. J.* **2005**, *11*, 3349.

[108] J. M. Warman, A. M. van de Craats *Mol. Cryst. Liq. Cryst.* **2003**, *396*, 41.

[109] L. J. Lever, R. W. Kelsall, R. J. Bushby Phys. Rev. B 2005, 72, 35130.

[110] A. M. van de Craats, J. M. Warman *Adv. Mater.* **2001**, *13*, 130.

[111] L. Schmidt-Mende, A. Fechtenkötter, K. Müllen, E. Moons, R. H. Friend, J. D. MacKenzie *Science*, **2001**, *293*, 1119.

[112] T. Christ, B. Glüsen, A. J. Greiner, A. Kettner, R. Sander, V. Stümpflen, V. Tsukruk, J. H. Wendorff *Adv. Mater.* **1997**, *9*, 48.

[113] I. Seguy, P. Jolinat, P. Destruel, J. Farenc, R. Mamy, H. J. Bock, T. P. Nguyen *J. Appl. Phys.* **2001**, *89*, 5442.

2 Motivations and Objectives

In the previous sections it was noted that discotic liquid crystals show a whole range of interesting features, which makes them promising candidates for applications in electronic devices. In this field, HBCs already proved their potential as could be reviewed for example in the work of A. Fechtenkötter.[1] It is also known that the columnar order of the discotics takes great influence on the charge carrier mobilities of these materials. This argument becomes obvious, as a strong decrease in the mobility could be observed when the materials change from the highly ordered crystalline phase to the less ordered liquid crystalline state.[2-8]

An approach to improve the order of the columnar stacks and reduce possible trapping sites, is the implementation of functional groups that assist the π-stacking process. One of the most important forces in nature, which drives extensively self-organization processes is hydrogen-bonding.[9] It has already been shown that a combination of π-stacking and hydrogen-bonding enables the connection of the one-dimensional π-stacking properties with the high selectivity and directionality of hydrogen-bonds.[10-18] One goal in this thesis was the implementation of functionalities that can exert hydrogen-bonds into HBCs to enforce the π-stacking and to specifically influence the self-organization behavior and the thermal properties of HBC. Although the improvement of the order between the discs is an important factor for their future use in devices, a pronounced long-range order is still inevitable. Therefore, one has to keep in mind that for such applications, solubility and thermally accessible isotropic phases are still a prerequisite to allow a further treatment of the films of the materials.[19]

In the second part, the focus was set onto the improved synthesis and characterization of a PAH, also declared as "supernaphtalene" or C72 (**2-1**), where the number indicates the amount of carbon atoms in the rigid aromatic core (Figure 2-1). While in the first part a hydrogen-bond assisted π-stacking should lead to an improved order and a higher charge carrier mobility, this challenge is already covered by the stronger π-interactions of the aromatic core of C72. In addition, the mobility and the absorption profile of the materials sensitively depend upon the area and the topology of the aromatic core component. As already mentioned, A. van de Craats et al. verified a direct correlation between the aromatic core size and the charge carrier mobility.[20] Therefore, it can be expected that an increase of the aromatic core should also lead to an improved charge carrier mobility and as a consequence to a better device performance.

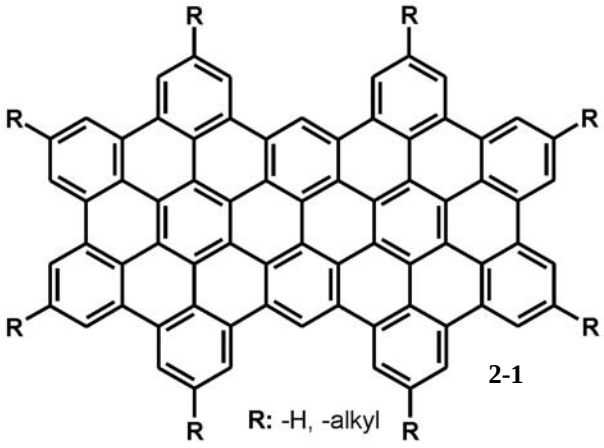

Figure 2-1: Scheme of C72 or "supernaphtalene".

In addition, these materials generally exhibit a broadened absorption profile with a strong bathochromic shift of the main absorption band compared to HBC due to the lowering of the HOMO-LUMO bandgap, which is assumed to increase the efficiency of photovoltaic applications. Additionally, it is believed that at a critical size new types of mesophases should appear as the tendency of smaller discs to tilt relative to the columnar axis is replaced by a simple lateral offset already seen for graphite.

Even though some derivatives of this material have already been prepared, several key issues, like the problem of purification, solubility and detailed analytics still remained, as for example only UV/vis and MALDI-TOF (matrix assisted laser desorption/ionization-time of flight) mass spectrometry could give some indication about the purity of the compounds. It was rather astonishing that even from highly soluble C72 derivatives no resolved ^{1}H NMR could be obtained. Therefore, it was particularly necessary to investigate the reasons for this behavior, as already small amounts of impurities can severely diminish the efficiency of a device. One possible explanation could lie within the pronounced π-stacking of this material leading to a strong aggregate formation in solution[21] and as a consequence to a reduced resolution in the NMR experiments. To gain further insight into this matter, several attempts towards an increase of the solubility and an effective suppression of the π-interactions were undertaken. Of course, attention had to be paid on not completely destroying all the supramolecular self-assembly features of these materials, as only with these forces a pronounced and distinct columnar self-organization could be achieved.

2.1 References

[1] L. Schmidt-Mende, A. Fechtenkötter, K. Müllen, E. Moons, R. H. Friend, J. D. MacKenzie *Science* **2001**, *293*, 1119.

[2] A. M. van de Craats, J. M. Warman, A. Fechtenkötter, J. D. Brand, M. A. Harbison, K. Müllen, *Adv. Mater.* **1999**, *11*, 1469.

[3] A. Fechtenkötter, K. Saalwächter, M. A. Harbison, K. Müllen, H. W. Spiess, *Angew. Chem. Int. Ed. Engl.* **1999**, *38*, 3039.

[4] A. Fechtenkötter, N. Chebotareva, M. D. Watson, K. Müllen, *Tetrahedron* **2001**, *57*, 3769.

[5] J. Wu, M. D. Watson, K. Müllen, *Angew. Chem. Int. Ed.* **2003**, *115*, 5329.

[6] S. Ito, M. Wehmeier, J. D. Brand, C. Kübel, R. Epsch, J. P. Rabe, K. Müllen, *Chem. Eur. J.* **2000**, *6*, 4327.

[7] S. Ito, P. T. Herwig, T. Böhme, J. P. Rabe, W. Rettig, K. Müllen, *J. Am. Chem. Soc.* **2000**, *122*, 7698.

[8] A. F. Thünemann, D. Ruppelt, C. Burger, K. Müllen, *J. Mat. Chem.* **2000**, *10*, 1325.

[9] J. D. Watson, F. H. C. Crick, *Nature* **1953**, 171, 737.

[10] C.-H. Lin, J. Tour, *J. Org. Chem.* **2002**, *67*, 7761.

[11] D. T. Bong, T. D. Clark, J. R. Granja, M. R. Ghadiri, *Angew. Chem. Int. Ed.* **2001**, *40*, 988.

[12] F. S. Schoonbeek, J. H. van Esch, B. Wegewijs, D. B. A. Rep, M. P. de Haas, T. M. Klapwijk, R. M. Kellogg, B. L. Feringa, *Angew. Chem. Int. Ed.* **1999**, *38*, 1393.

[13] A. Guesquière, M. M. S. Abdel-Mottaleb, S. de Feyter, F. C. de Schryver, F. Schoonbeek, J. van Esch, R. M. Kellogg, B. L. Feringa, A. Calderone, R. Lazzaroni, J. L. Brédas, *Langmuir* **2000**, *16*, 10385.

[14] R. I. Gearba, M. Lehmann, J. Levin, D. A. Ivanov, M. H. J. Koch, J. Barbera, M. G. Debije, J. Piris, Y. H. Geerts, *Adv. Mater.* **2003**, *15*, 1614.

[15] M. L. Bushey, A. Hwang, P. W. Stephens, C. Nuckolls, *Angew. Chem. Int. Ed.* **2002**, *41*, 2828.

[16] T. S. Balaban; A. Eichhöfer; J.-M. Lehn, *Eur. J. Org. Chem.* **2000**, 4047.

[17] J. J. van Gorp, J. A. J. M. Vekemans, E. W. Meijer, *J. Am. Chem. Soc.* **2002**, *124*, 14759.

[18] R. E. Gillard, F. M. Raymo, J. F. Stoddart, *Chem. Eur. J.* **1997**, *3*, 1933.

[19] W. Pisula, M. Kastler, D. Wasserfallen, T. Pakula, K. Müllen J. Am. Chem. Soc. **2004**, *126*, 8074.

[20] A. M. van de Craats, J. M. Warman *Adv. Mater.* **2001**, 13, 130.

[21] M. Kastler, W. Pisula, D. Wasserfallen, T. Pakula, K. Müllen *J. Am. Chem. Soc.* **2005**, *127*, 4286.

3 Influence of Hydrogen-Bonds on the Supramolecular Properties of Hexa-*peri*-hexabenzocoronenes

An important property for devices is the charge-carrier mobility values for the discotic organic materials.[1-5] In order to gain higher mobilities for organic materials one can follow a diversity of possible pathways such as different processing techniques.[6-14] For instance a close relation exists between the supramolecular order of the molecules and the mobilities.[15-18] In the case of the crystalline rubrene and other highly ordered materials the mobility values can even reach up to 15.0 $cm^2 V^{-1} s^{-1}$.[19,20]

For HBCs, it has been shown, that already small changes in the nature of the alkyl chains in the corona of the aromatic core component substantially influences the resulting intrinsic charge-carrier mobility.[21] Thereby, it has been observed that at the higher temperature mesophases, the values suffer from a sudden drop during the phase transition and although in the mesophase the discs still remain in a columnar ordered fashion their intracolumnar cohesion is heavily reduced, complicating an unobstructed charge transport through the columns.[22-24] It can be concluded that HBCs require a high intracolumnar order for achieving good charge-carrier mobilities. Although with a high crystallinity it is possible to achieve high charge carrier mobilities, the processability and the solubility of the materials is another key issue for those materials.[25,26] Therefore, alkylated HBCs have an indisputable advantage, as future device applications require materials, from which films can be easily gained.[27-29] As a result, HBCs incorporate both requirements, as on one hand their exceedingly large aromatic core allows mobilities up to 1.1 $cm^2 V^{-1} s^{-1}$ and on the other their alkyl side-chains induce enough disorder to impart the compounds a good solubility and thermal processability.

Indeed, it has been shown that by changing the nature of the alkyl chain one can also engineer the type of the self-assembly on surfaces. If for example a bulky alkyl chain with a branching close to the aromatic core is used, the discs will preferentially self-assemble in an edge-on manner on surfaces (see Figure 1-26).[24] This organisation is the preferred orientation for devices like FETs. However, by extending the distance between the branching and the aromatic core the discs more likely adopt a face-on self-assembly, which is the necessary organisation for solar cells.[30]

Additionally, one has to keep in mind, that the basic requirements for device manufacturers with respect to the charge-carrier mobilities are already fulfilled at the

level of 0.1 cm^2 V^{-1} s^{-1}.[31-37] Of course, with these properties, it is not possible to substitute inorganic materials like silicon with respect for high performance calculation devices or similar applications. Nevertheless, there is an undoubtable usability for such materials for cheap and flexible electronic circuits, as the manufacturing of silicon circuits require the time and cost intensive process of obtaining highly pure, crystalline silicon. For HBCs, this process can be replaced by a simple and cheap zone-casting (Appendix B) or zone-crystallization (Appendix C) technique. The devices could then be used for example as electronic tags for radio frequency identification (RFID) chips[38] and for flexible display technologies like e-paper[39-42] or even for intelligent fabrics,[43] which is not easy to obtain with silicon, as this crystalline materials requires a rigid substrate.

Within this approach an induction of a higher order *via* hydrogen-bonding is considered, which mainly points towards the improvement of the intracolumnar stacking of the materials. Hydrogen-bonds do not only concern material science for its search towards controlled self-assembled nanostructures, but are also ubiquitously found in biological systems, such as enzymes, DNA and protein structures.[44] With a combination of these interactions, it is possible to connect the one-dimensional π-stacking properties with the high selectivity and directionality of hydrogen-bonds.[45-53] These combined interactions are fundamental for future developments of devices based on organic materials, where long-range order, high charge-carrier mobilities, thermal stability and processability are prerequisites. As mentioned before, in the case of hexa-*peri*-hexabenzocoronene (HBC), it was already reported that the electronic properties sensitively depended on the temperature and phase behavior of the material, as the pseudo-crystalline phase generally exhibited higher intrinsic charge-carrier mobilities due to the improved columnar order.[21,54-59]

3.1 Hydrogen-bonds

Hydrogen-bonding is the favorite intermolecular force in self-assembling systems due to its directionality, specificity and biological relevance.[60-70] The strength depends largely on the solvent and number and sequence of the hydrogen bonds.[71] For example, a two-dimensional system of three molecules illustrates some of the features of self-complementarity involved in self-assembly (Figure 3-1). The structure designed and synthesized by Zimmerman shown in Figure 3-1 presents a pattern of hydrogen-bond donors and acceptors on one edge that is complementary to the pattern on the other functioning edge.[72] The spatial orientation of the atoms capable of hydrogen bonding at

both edges of the molecule is fixed at almost exactly 120° by the rigidity of the aromatic centerpiece of the structure. The information for the assembly is written into the hydrogen-bond patterns of the edges and their angular orientations with respect to each other. In solution a trimer is formed, and the assembly process takes place in the self-correcting (cooperative) manner, just as expected.

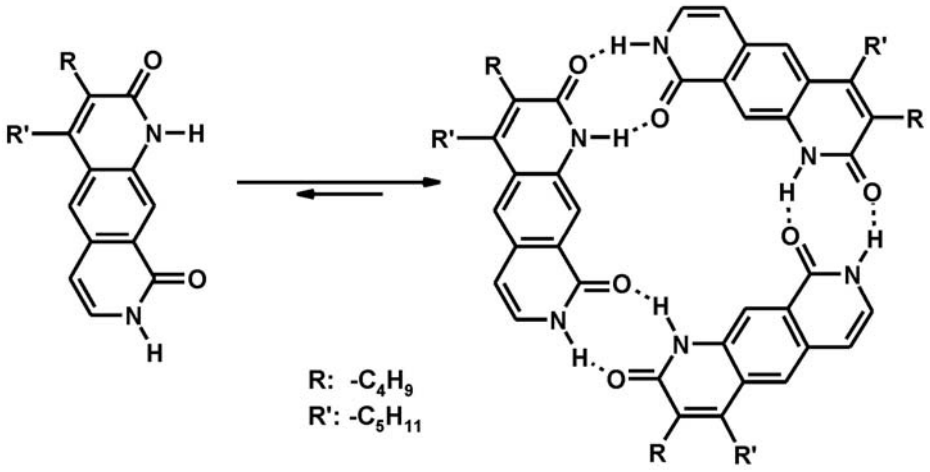

Figure 3-1: A two-dimensional assembly based upon selfcomplementary hydrogen bonding.

Although hydrogen-bonds do not belong to the strongest intermolecular forces (Table 3-1), they are definitely of prime importance as without them wooden structures would collapse, cement would crumble, oceans would vaporize, and all living things would disintegrate into random dispersions of inert matter. Moreover, the remarkable properties of H_2O, that is, its extremely high boiling point (100 °C versus 60.7 °C for H_2S), the contraction of solid H_2O on melting, and a maximum density of liquid H_2O at 3.984 °C, all rely merely on the formation of hydrogen-bonded networks.[73]

type of interaction or bonding	strength (kJ mol^{-1})
covalent bond	100-400
Coulomb	250
hydrogen bond	10-65
ion-dipole	50-200
dipole-dipole	5-50
cation-π	5-80
π-π	0-50
van der Waals forces	<5
hydrophobic effects	difficult to assess
metal-ligand	0-400

Table 3-1: Strength of several noncovalent forces.[74]

3.2 Desymmetrized HBCs

The general concept towards desymmetrized HBCs takes advantage of the synthetic approach *via* the intermolecular Diels-Alder reaction (see section 1.4.3). By this method it is possible to achieve a variety of bromo-substituted HBC derivatives[57] with substitution patterns as seen in Figure 1-13, where X=Br. Such desymmetrized HBCs have been lately used extensively to introduce functionalities into HBCs and to study the effects exerted by these groups onto different properties such as film formation and supramolecular self-assembly. It was shown for example that by attaching a carboxylic acid-terminated decyl chain in the corona of a penta-alkyl substituted HBC, an amphiphilic material resulted, which could be organized in monolayers at the air-water interface using the Langmuir-Blodgett technique.[75] This technique offered for this material a possiblity for modulating the packing mode of the aromatic cores. This strategy was successfully extended to prepare thin films of the amphiphile.[76] These films were deposited onto pretreated (poly(ethylene imine)) functionalized silicon wafers and investigated by X-ray reflectivity measurements using Synchrotron radiation. Thereby, it was shown that the columns of the aromatic cores were aligned parallel to the silicon wafer surface[76] and each of the layer is well defined in its thickness and lateral order. The same material was also used for complexing HBC with a poly(ethyleneoxide)-*block*-poly(L-lysine) polymer *via* an ionic bonding, which produced a thermotropic liquid crystalline material.[77] It was additionally found that the poly(L-lysine) blocks form an α-helical secondary structure. Every helix is thereby surrounded by six discotic columns of HBC, which results in an α-helical structure of the polymer within a discotic columnar arrangement of the HBCs. [77]

In the year 2003 more derivatives of such desymmetrized HBCs were synthesized, but this time the mono-substitution implied an attachment of a pyrene unit connected to the HBC core over an alkyl tether. The final material revealed ordered architectures both in the crystalline state and in the mesophase. During the studies, it became obvious that the two aromatic units with different sizes do not tend to stack in hybrid HBC-pyrene columns.[78] In another approach, the pyrene moiety was exchanged by an anthraquinone function. This material can self-assemble into nanophase-separated structures at surfaces and in the bulk, whereby the anthraquinone moieties play a diminished role in the packing at surfaces, compared to the HBC-pyrene dyad.[79]

3.3 Engineering the Properties of HBC via Hydrogen-Bonding

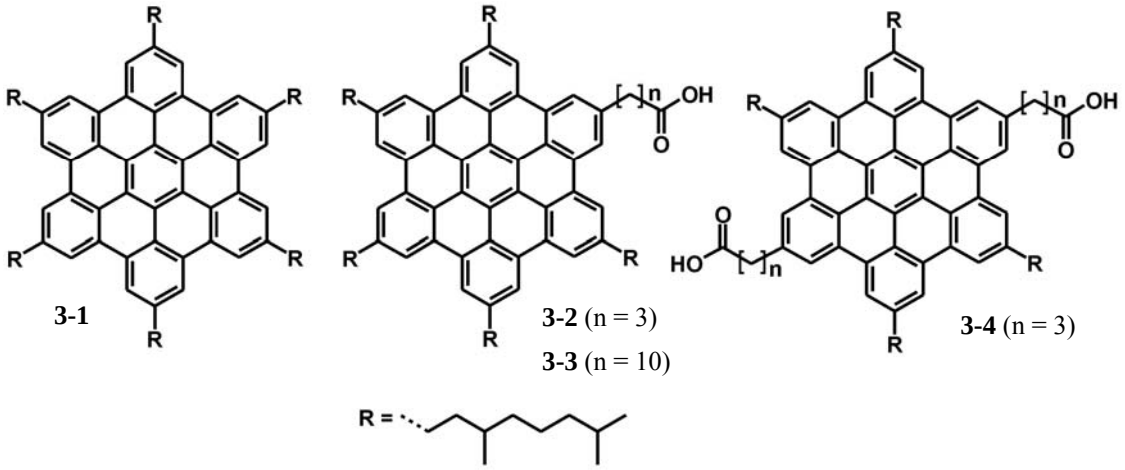

Figure 3-2: Synthesized carboxy-functionalized HBC derivatives **3-2**, **3-3**, **3-4** and parent compound **3-1**

It becomes obvious that hydrogen-bonding and desymmetrized, functionalized HBCs proved by themselves already a successful approach towards engineering of the supramolecular properties. As a logic consequence, one can regard a combination of the two concepts. Indeed, it was already reported that carboxylic acid groups tethered by relatively long alkyl chains showed little effect on the thermotropic behavior relative to unfunctionalized alkylated HBCs.[80] Likewise, a covalent linkage of two HBC discs by relatively long flexible spacers also resulted in insignificant differences compared with monomeric discs.[58]

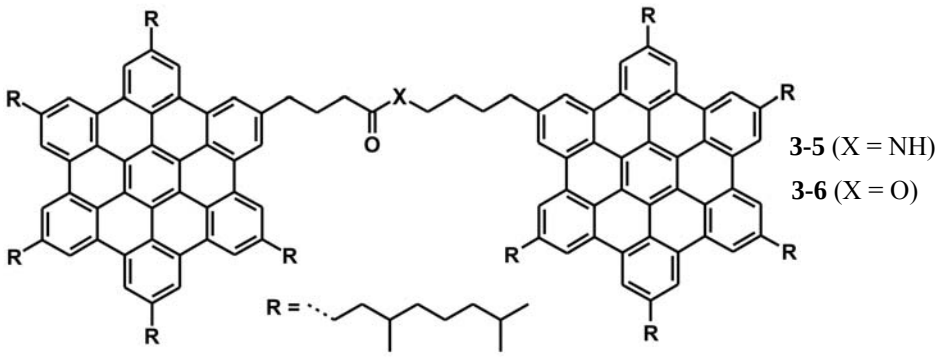

Figure 3-3: Synthesized HBC dyads **3-5** and **3-6**.

However, it was observed that in the case of HBC derivatives, which were covalently linked with either pyrene or anthraquinone entities, [78,79] not only the phase behavior, but also the order in the bulk and at the solid-liquid interface depended primarily on the length of the connecting alkyl chain. This of course made it clear, that it was necessary

to revisit the combination of HBC discs with tethered carboxylic acid groups to investigate the influence of the length of the alkyl spacers on the phase and stacking properties of the materials.

For this purpose, two different carboxy-functionalized HBCs **3-2**, **3-3** and two covalently linked HBC dyads **3-5** and **3-6** were used (Figure 3-2 and 3-3). For the investigation of the effects exerted by two carboxy-functions, compound **3-4** was synthesized according the route already established for **3-2** and **3-3**. In **3-5** and **3-6**, the connecting alkyl bridge of the two discotic units featured a similar length as the proposed intercolumnar spacer of **3-2** in the dimer state. Therefore, **3-6** was suitable to study the effects of a flexible ester linkage without any auxiliary intra- or intercolumnar interactions, whereas **3-5** provided a more rigid amide linkage and was in addition capable of establishing hydrogen-bonds *via* the amide functionality. In order to have a base point for the studies, the hexa-fold substituted HBC (**3-1**) was used as a parent compound and subjected to the same analytical methods as the other compounds.

3.3.1 Synthesis of Carboxy-functionalized HBCs

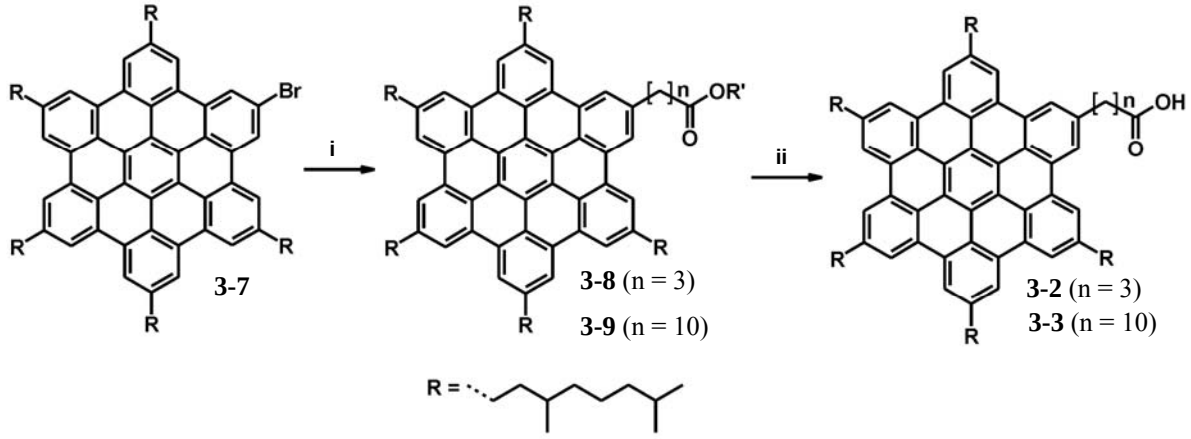

Figure 3-4: Synthesis of the mono-acid derivatives **3-2** and **3-3**. *i:* $XZn(CH_2)_nCOOR'$ (X =Br,I), $Pd[dppf]Cl_2$ x CH_2Cl_2, THF; *ii:* KOH, THF, MeOH, H_2O.

The mono-carboxylic acid functionalized HBCs **3-2** and **3-3** were synthesized according to Figure 3-4 and shall be mentioned briefly.[81]

A versatile method to introduce functional groups in the case of the mono-bromo substituted HBC (**3-7**) is the Negishi type coupling with organo zinc halides. These reagents are easily prepared from the corresponding halides. Another advantage is that many of these organo-zinc derivatives are comercially available and therefore a wide variety of different HBC derivatives can be prepared. In this case, two different spacer

lengths (n=3 and 10) were introduced. Thereby, for the long tether, 10-methoxycarbonyl-decyl zinc iodide was prepared starting from 10-methoxycarbonyl-decyl-1-bromide by substitution of bromine with iodine in boiling acetone and a subsequent treatment with activated zinc and chlorotrimethylsilane.[81]

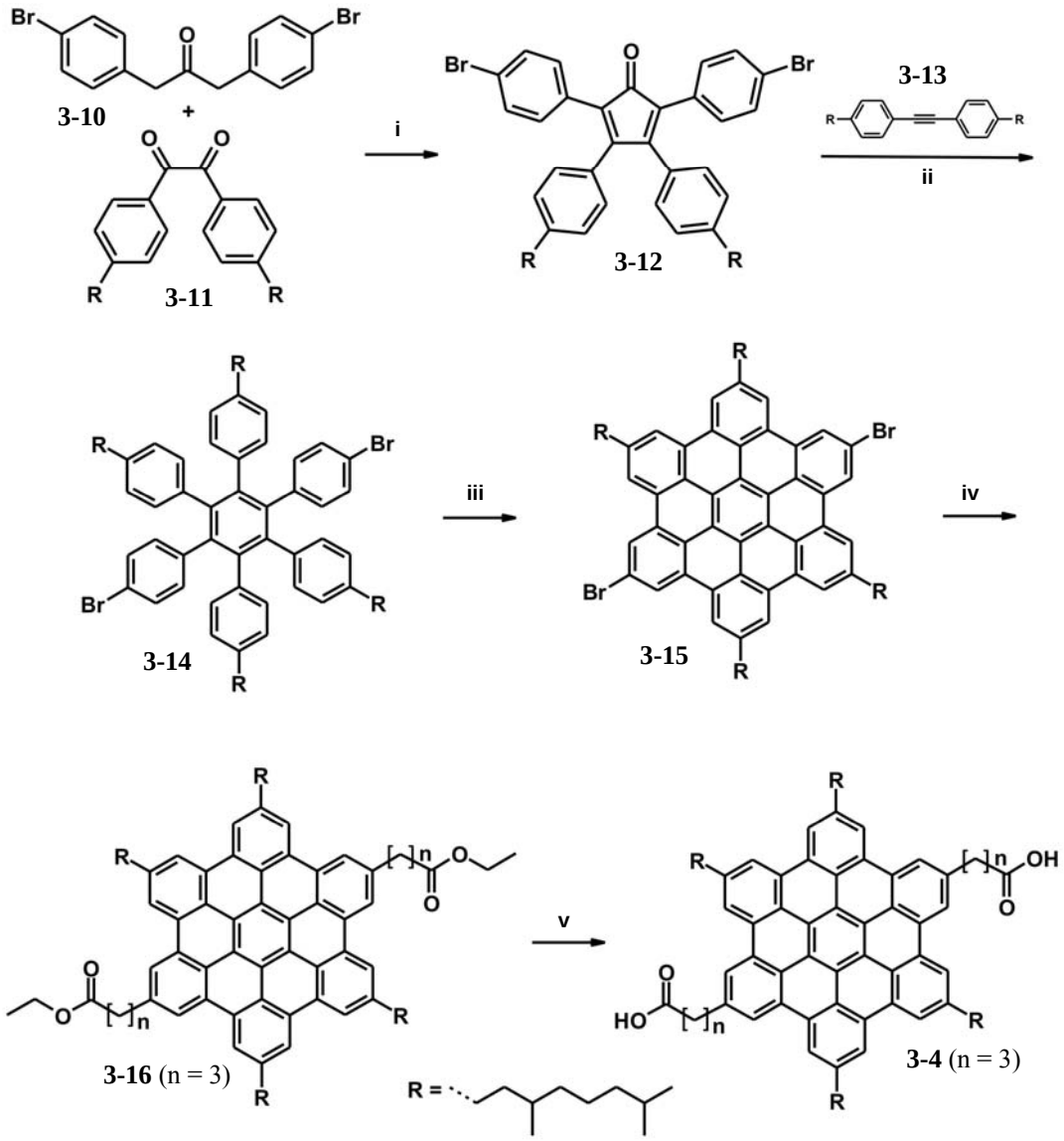

Figure 3-5: Synthesis of the diacid HBC derivative **3-4**. *i:* *n*-Bu_4NOH, *t*-BuOH; *ii:* Ph_2O; *iii:* $FeCl_3$, CH_2Cl_2, CH_3NO_2; *iv:* $BrZn(CH_2)_3COOEt$, $Pd[dppf]Cl_2$ x CH_2Cl_2, THF; *v:* NaOH, THF, MeOH, H_2O

The dibromo HBC **3-15** was prepared similar to already published procedures *via* a double Knoevennagel condensation, followed by a Diels-Alder cycloaddition and an oxidative cyclodehydrogenation with $FeCl_3$. Afterwards compound **3-15** was used in a Negishi cross-coupling reaction with commercially available organo-zinc halides. The

following saponification with potassium hydroxide solution yielded the para-diacid functionalized HBC **3-17**.

It became obvious for the dibromo derivative **3-15**, that the induced solubility of the four alkyl chains does not induce sufficient disturbance of the intracolumnar stacking for gaining an easily processable and soluble material. In the DSC, a small endothermic transition could be observed, which was attributed to some rearrangement of the alkyl chains. After the Negishi cross-coupling, compound **3-16** again showed a good solubility in standard organic solvents and also a thermal behavior due to the effects exerted by the additional ester chains. The DSC revealed a strong endothermic transition on heating (73 °C) and a similar exothermic peak during cooling (27 °C). The intensity of the signals indicated a phase transition already observed for the parent compound **3-1**. After the saponification of the ester and neutralisation with diluted hydrochloric acid, compound **3-4** precipitated as a yellow powder, which showed a limited solubility in every organic solvent. Even by adding carbondisulfide and LiCl, which proved for other cases a good way to achieve higher concentrations of such type of materials, no enhancement could be observed.

For this reason no ^{13}C NMR spectrum could be recorded, but nevertheless the received ^{1}H NMR spectrum and MALDI-TOF mass spectrometry (MALDI-TOF MS) revealed the successful preparation of compound **3-4**. It is however astonishing that although the solubility of **3-4** was rather limited such resolved spectra could be obtained. By using NMR simulation software and the found integration values, the protons were assigned to the corresponding signals. Indeed, all the signals of the protons of the side-chain with the attached carboxy-group were identified (**c**-**e**) and of course fitted the expected integration values.

These macroscopic features already indicated the strong influence of the hydrogen bonds upon the supramolecular properties of the HBC derivatives. However, it is known that these types of bonds are not restricted to the same directionality as covalently linked units but are also not that unspecific, as can be observed in a wide variety of biologically active compounds like DNA. Indeed, it has been reported that the area, where such bonds can exert their optimum bonding situation, is best described by a cone shape.[82] The geometry of this cone is thereby depending upon which atoms are involved within the actual bonding situation.

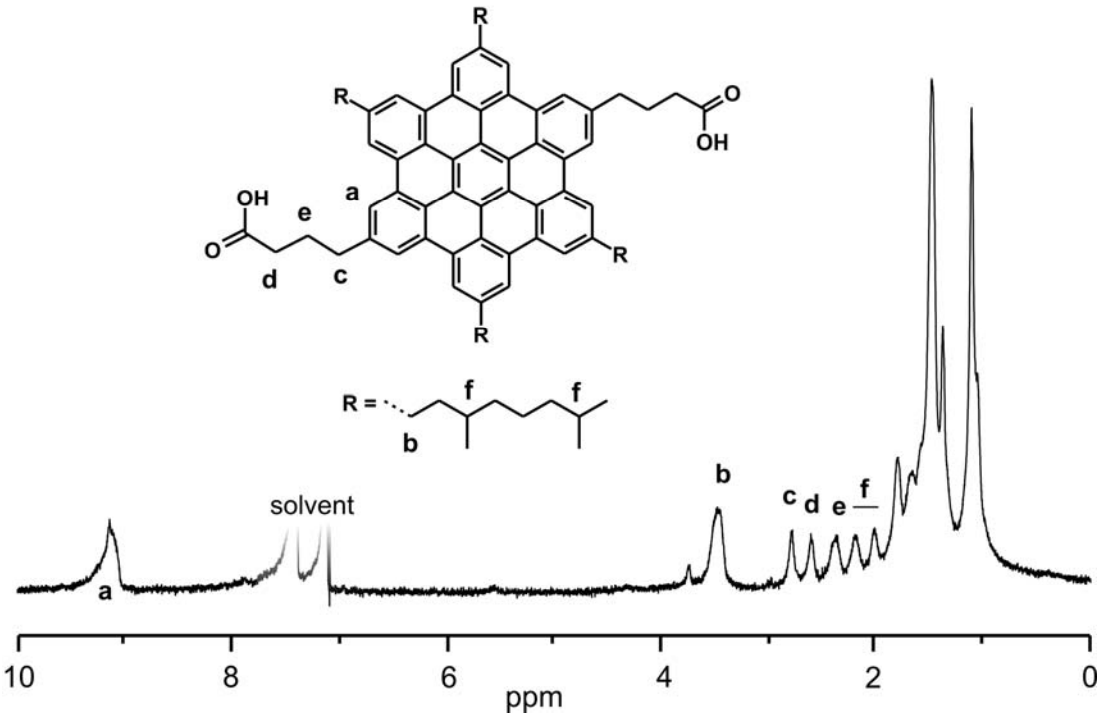

Figure 3-6: ^{1}H NMR of the diacid HBC derivative **3-4** in o-$C_6D_4Cl_2$ at 423 K.

Another important factor is, in what scope the directionality of the hydrogen bonds influences the properties in the case of the mono- (**3-2**, **3-3**) and the diacid derivatives (**3-4**). Therefore, two covalently linked HBC dyads **3-5** and **3-6** have been synthesized (Figure 3-7) as model compounds. In **3-5** and **3-6**, the connecting alkyl bridge of the two discotic units featured a similar length as the proposed intercolumnar spacer of **3-2** and **3-4** in the dimer state. An ester-linkage (**3-6**) does not exhibit additional hydrogen bonds and represents the situation of a strict intercolumnar bridging of two HBC cores. On the other hand, **3-5** provided a more rigid amide linkage, that was in addition capable of establishing hydrogen-bonds *via* the amide functionality. The example is representative for a situation, where the hydrogen bonds can still exert interactions other than intercolumnar bridging of two HBC entities. This is also more likely, when one considers that the carboxy function is connected to a small but still flexible alkyl chain.

3.3.2 Synthesis of Covalently Linked Dyads

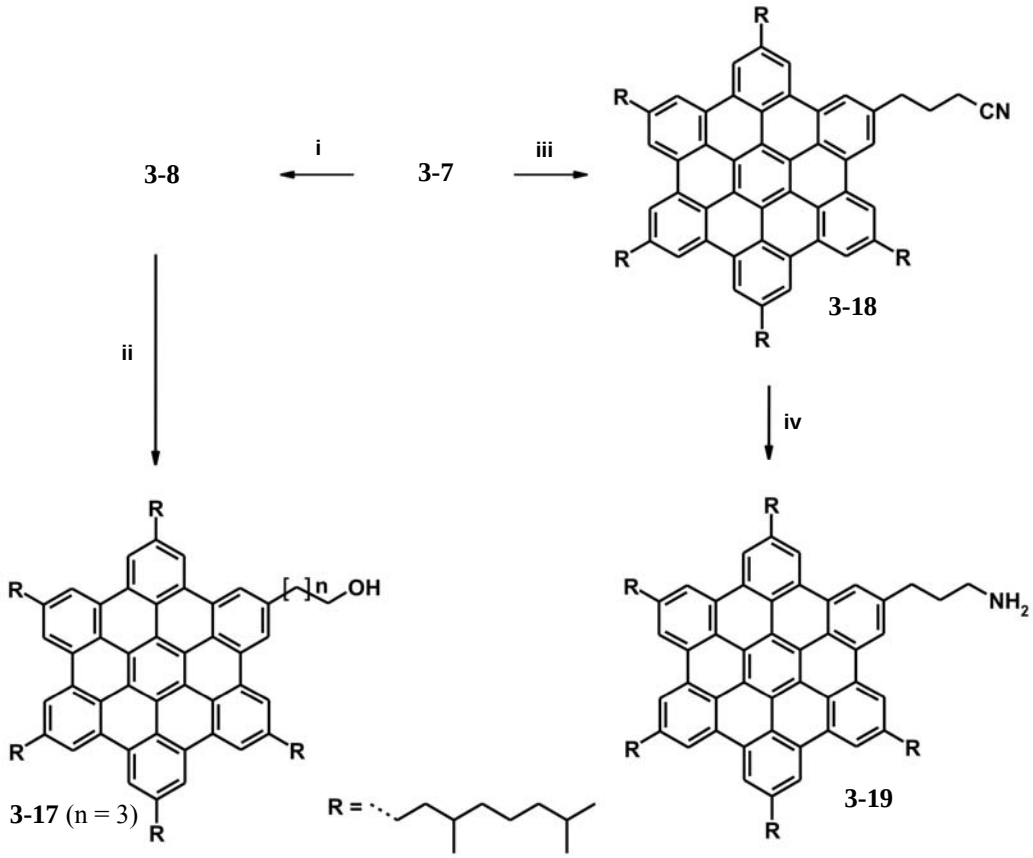

Figure 3-7: Synthesis of the amino- and hydroxy-functionalized HBC derivatives **3-17** and **3-19**. *i:* $BrZn(CH_2)_3COOEt$, $Pd[dppf]Cl_2$ x CH_2Cl_2, THF; *ii:* $LiAlH_4$, THF; *iii:* $BrZnC_3H_6CN$, $Pd[dppf]Cl_2$ × CH_2Cl_2, THF; *iv:* $LiAlH_4$, THF.

The covalently bound dimers **3-5** and **3-6** have already been synthesized and characterized and the synthetic procedure shall only be briefly mentioned. The exact procedures can be reviewed in detail in references 81 and 83. The commercially available 3-cyano-propyl-zinc-bromide was used in a Negishi cross-coupling reaction with the bromo-HBC derivative **3-7** to introduce the cyano functionality. The reduction of the ester and the cyano group with $LiAlH_4$ provided the nitrile **3-19** and the terminal alcohol derivative **3-17**. The dyads were finally prepared by a carbodiimide-promoted esterification of the mono-acid derivative **3-8** with either the amino- (**3-19**) or the hydroxyl-terminated HBC (**3-17**).

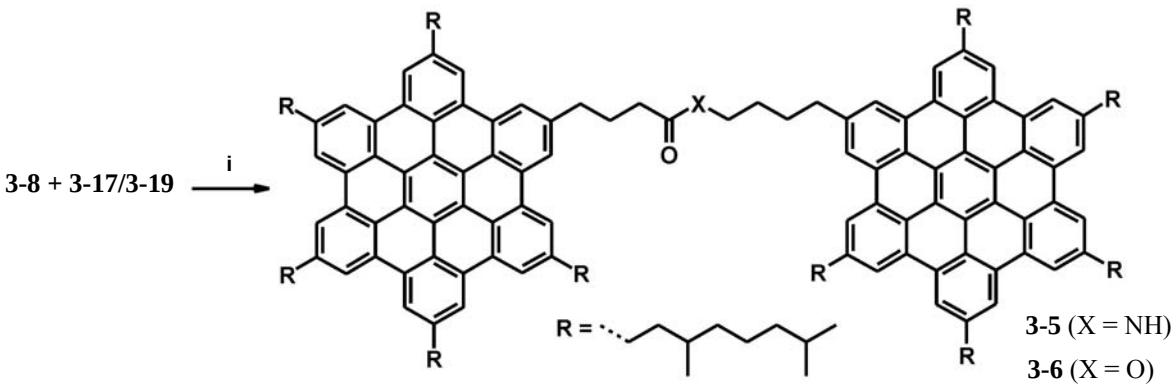

Figure 3-8: Synthesis of the HBC dyads **3-5** and **3-6**. *i:* EDC, CH_2Cl_2.

3.3.3 Bulk Properties of Carboxy-functionalized HBCs and Dyads

Bulk properties of materials are generally examined with a variety of analytical methods like DSC, X-ray and solid state NMR. The latter two methods are very valuable for the determination of the degree and type of self-organization of a compound. In the case of the HBCs **3-2**, **3-3**, **3-4** and the covalently bound dyads **3-5**, **3-6** X-ray studies were performed using powder diffraction to gain higher resolution and by 2D-WAXS (two-dimensional wide angle X-ray scattering) of an extruded fiber of the materials.

3.3.3.1 Differential Scaning Calorimetry (DSC)

Already with DSC, it became obvious that the length of the tethers exhibit a severe influence. While the long tethered species **3-3** did not show a strong difference to the parent compound, as its transition to the mesophase is almost identical to that of the hexa-alkylated HBC, the same phase was reached for **3-2** at far higher temperatures (226 °C). For the diacid- HBC (**3-4**), the DSC did not show thermal transitions anymore between -100 °C to 300 °C pointing to a very strong influence of the hydrogen bonds. Another remarkable feature is the observed transition for the short tethered derivative in the first heating at approximately 60-75 °C. This signal could stand in relation to a reoganisation of the columnar order, as during the workup, which does not include a thermal treatment, it is probable that not all of the hydrogen bonds can be oriented correctly within the material.

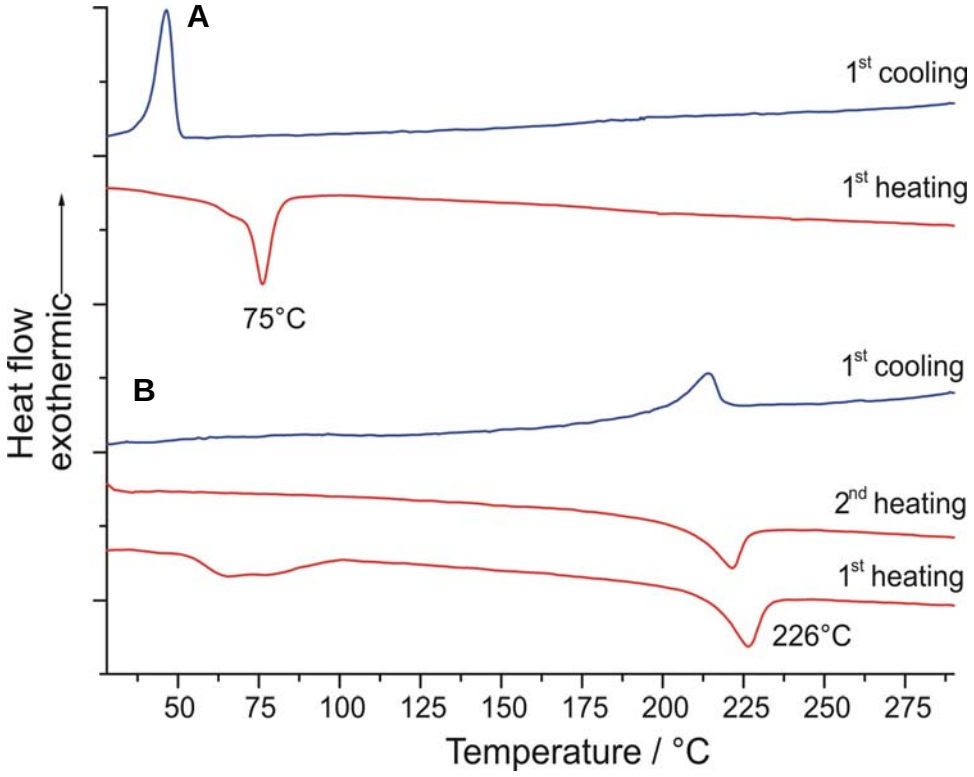

Figure 3-9: DSC traces of **A**) the long tethered (**3-3**) and **B**) the short tethered mono-acid HBC derivative (**3-2**).

Pronounced differences were also observed for the dyads **3-5** and **3-6**. The DSC diagram of the dyad **3-6** revealed a reversible, first-order transition at 14 °C to the liquid-crystalline state whereas compound **3-5** showed no thermal transition over the whole temperature range (-100 °C to 300 °C). As mentioned above this is already an indication that the hydrogen bonds do not only exert intercolumnar bridgings strictly between two HBC discs.

3.3.3.2 2D-WAXS

In the 2D-WAXS diffractogram no clear difference could be identified between the long tethered HBC derivative (**3-3**) and the parent compound, as both materials adopted in their crystalline phase a hexagonal and tilted columnar packing (Figure 3-10B) with almost the same packing parameters.

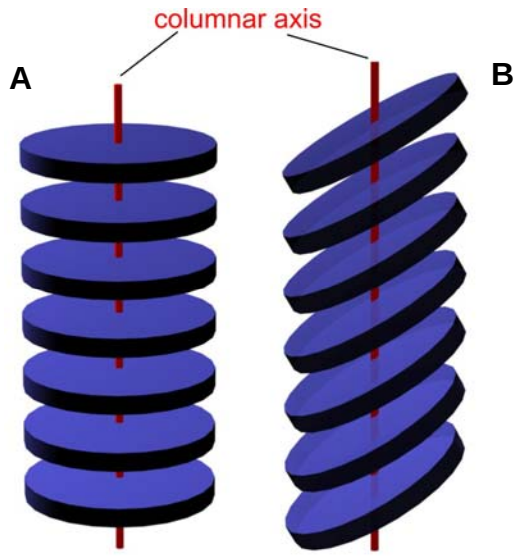

Figure 3-10: A) non-tilted and **B**) tilted columnar arrangement ("herringbone" type) with respect to the stacking axis.

The WAXS diffractogram of the short tethered derivative **3-2** in the same phase provided only broad and diffuse signals prior to thermal treatment. Already in the DSC, this material undergoes a broad irreversible endothermic transition on the first heating, which pointed towards the rearrangement of disordered structures that were induced during the workup procedure.

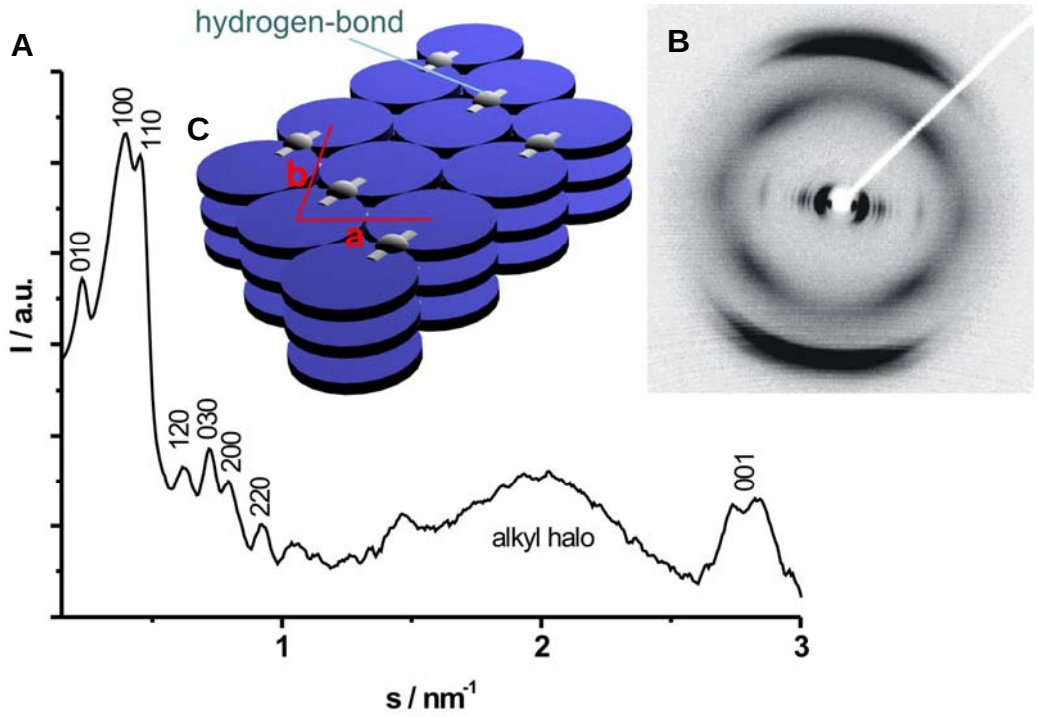

Figure 3-11: A) powder diffractogram, **B**) 2D diffractogram and **C**) schematic arrangement of the short tethered HBC derivative **3-2**.

Slow cooling to room temperature from 230 °C however resulted in a well resolved diffractogram (Figure 3-11A and B) from which an orthorhombic unit cell with a = 2.48 nm and b = 4.10 nm could be assigned (Figure 3-11C) and closely resembled a pseudo-hexagonal packing with a slight displacement of the columnar arrays. Additionally, a high intensity of the (110) signal compared to other hexagonally arranged HBCs and well resolved reflections of higher order (e.g. the (220) reflection) were observed, which is rather atypical for columnar discotic systems arranged in a 2D lateral unit cell.

Two meridional arcs were clearly identified in the range of 2.5 to 3.3 nm^{-1}. These corresponded to the intracolumnar stacking distance of 0.36 nm and indicated that the disc planes in the pseudo-crystalline phase were oriented almost perpendicular to the columnar axis (Figure 3-10A). In a tilted crystalline phase of HBC, one always receives two reflections from the stacking of the discs. One results from the arrangement between the discs parallel to the columnar axis and the other from the distance perpendicular to the disc plane. By using this information, one can calculate with a simple equation the offset angle from the columnar axis ($\varphi = \arccos c'/c$) as shown in Figure 3-12.

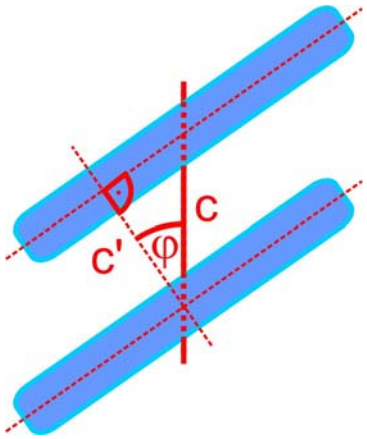

Figure 3-12: Calculation of the offset angle of the disc plane to the columnar axis.

When the axis perpendicular to the disc plane is slowly approaching the direction of the columnar axis the resulting two reflections merge into one, which is commonly seen for HBCs in the mesophase, where the discs are typically aligned perpendicular to the columnar stacking axis (Figure 3-10A).

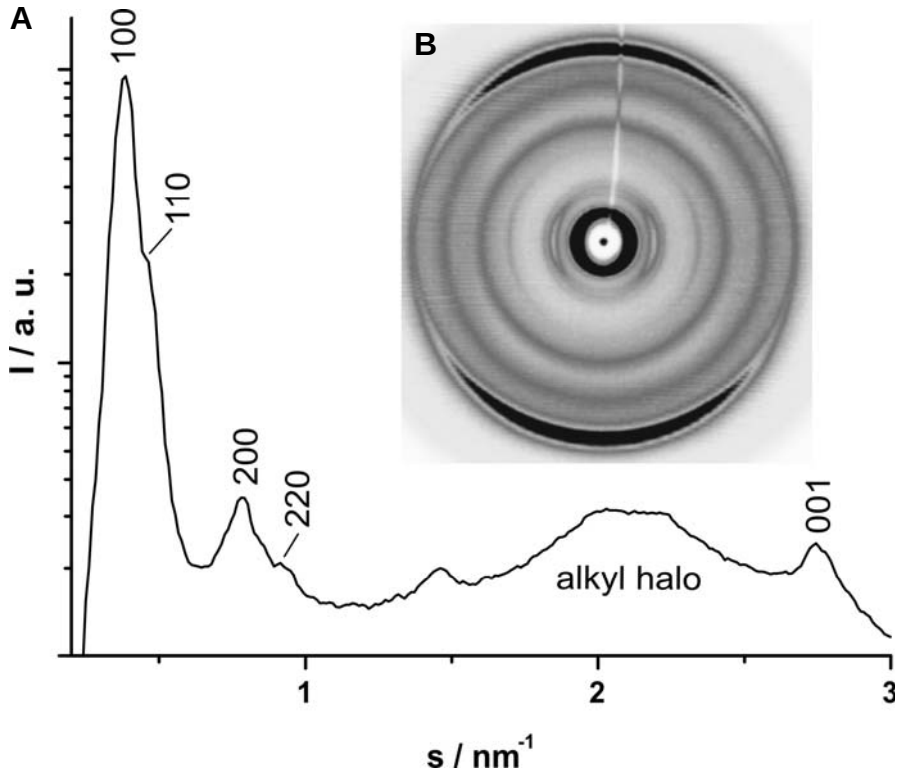

Figure 3-13: A) 360° integration plot and **B**) 2D diffractogram of the diacid HBC derivative **3-4**.

Although the diacid HBC derivative **3-4** did not undergo detectable phase transitions (DSC), it was possible to orient it *via* extrusion, due to its initial waxy state. This non-equilibrated condition caused a broadening of the reflections (Figure 3-13), but nevertheless, the equatorial distribution correlated well to an orthorhombic unit cell with the parameters a = 2.58 nm and b = 4.35 nm. The meridional reflections corresponded to a non-tilted stacking of the discs (Figure 3-10A) with a cofacial distance of d = 0.36 nm. Due to the lack of thermal annealing the reflections for the diacid derivative **3-4** were broad and unresolved. However, the main reflexes still remained visible and the tiliting of the discs showed a close similarity to the one observed for **3-2**, indicating a correlation between the arrangement observed for the diacid derivative **3-4** and the one for the short tethered mono-acid HBC **3-2**.

For **3-6**, the WAXS measurements at room temperature showed a non tilted stacking, as only one meridional reflex could be oserved (Figure 3-14). The columns self-organized in a hexagonal unit cell with a = 2.49 nm and the cofacial distance was larger than the value (0.36 nm), typical for a crystalline phase. This clearly indicated that the material was at room temperature already in the mesophase and even by cooling the material below its transition temperature only minor changes could be observed.

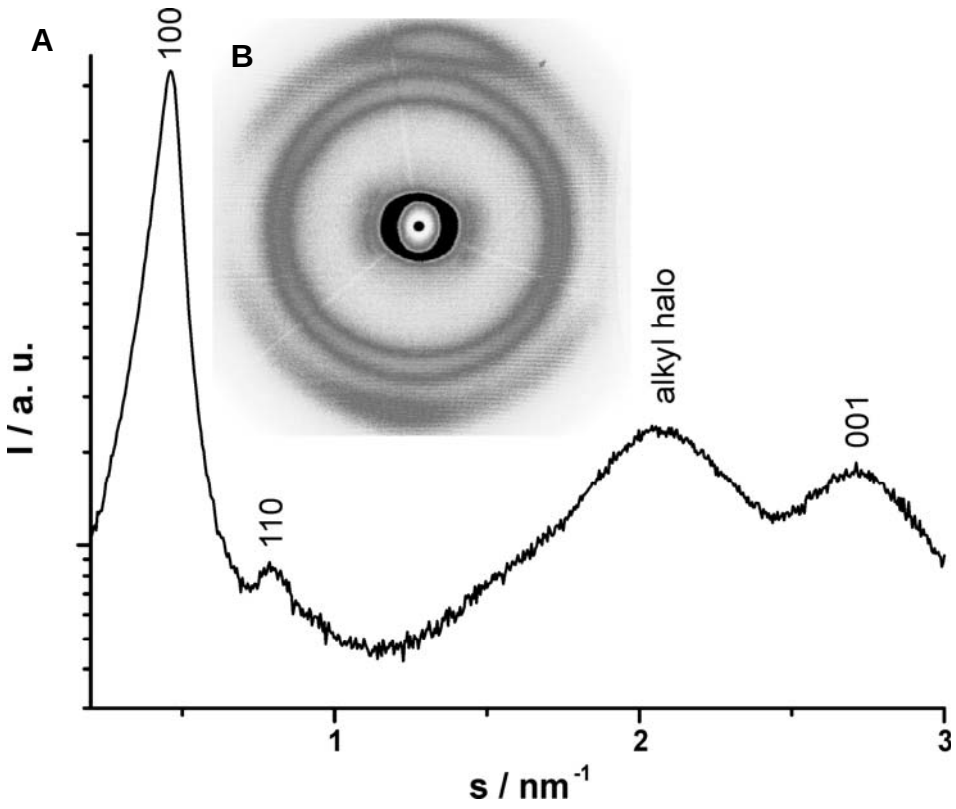

Figure 3-14: A) 360° integration plot and **B**) 2D diffractogram of the ester linke dyad derivative **3-6**.

The amide linked counterpart **3-5**, on the other hand, remained in the crystalline phase over the whole temperature range, in which the aromatic cores stacked in a tilted fashion (Figure 3-15) against the columnar axis. Interestingly, it was possible to assign two different unit cells to the equatorial reflections. By ignoring the first reflex, the reflexes corresponded to a hexagonal unit cell with a = 4.24 nm, which fitted to the dimensions of the whole extended molecule. By taking the first reflex into account, the resulting small orthorhombic cell (a = 2.10 nm, b = 3.65 nm) described a columnar packing formed by the two single aromatic cores of the dyads. In agreement with this, the diagonal of the orthorhombic cell coincided with the lattice vector of the hexagonal one (Figure 3-15C).

The signals for the intracolumnar stacking indicated a cofacial distance of 0.36 nm at 25° offset from the meridian representing the typical stacking properties of other HBC derivatives with a "herringbone" arrangement (Figure 3-10B). The remaining question was the quantization of the influence, the hydrogen bonds exerted onto the supramolecular properties of the HBCs. A classical way to address these issues is IR spectroscopy, as the frequency and broadening of the (COO-H) stretch sensitively depends on the strength and geometry of the hydrogen-bonds.[84] Unfortunately, all recorded spectra were dominated by the intense bands arising from the aliphatic and

aromatic hydrogen vibrations. An alternative method to determine hydrogen-bonding in bulk materials was provided by ^{1}H-solid-state NMR spectroscopy,[85,86] as it was used previously to detect the dynamics of the hydrogen-bonds for an hexa-carboxy-substituted HBC.[86]

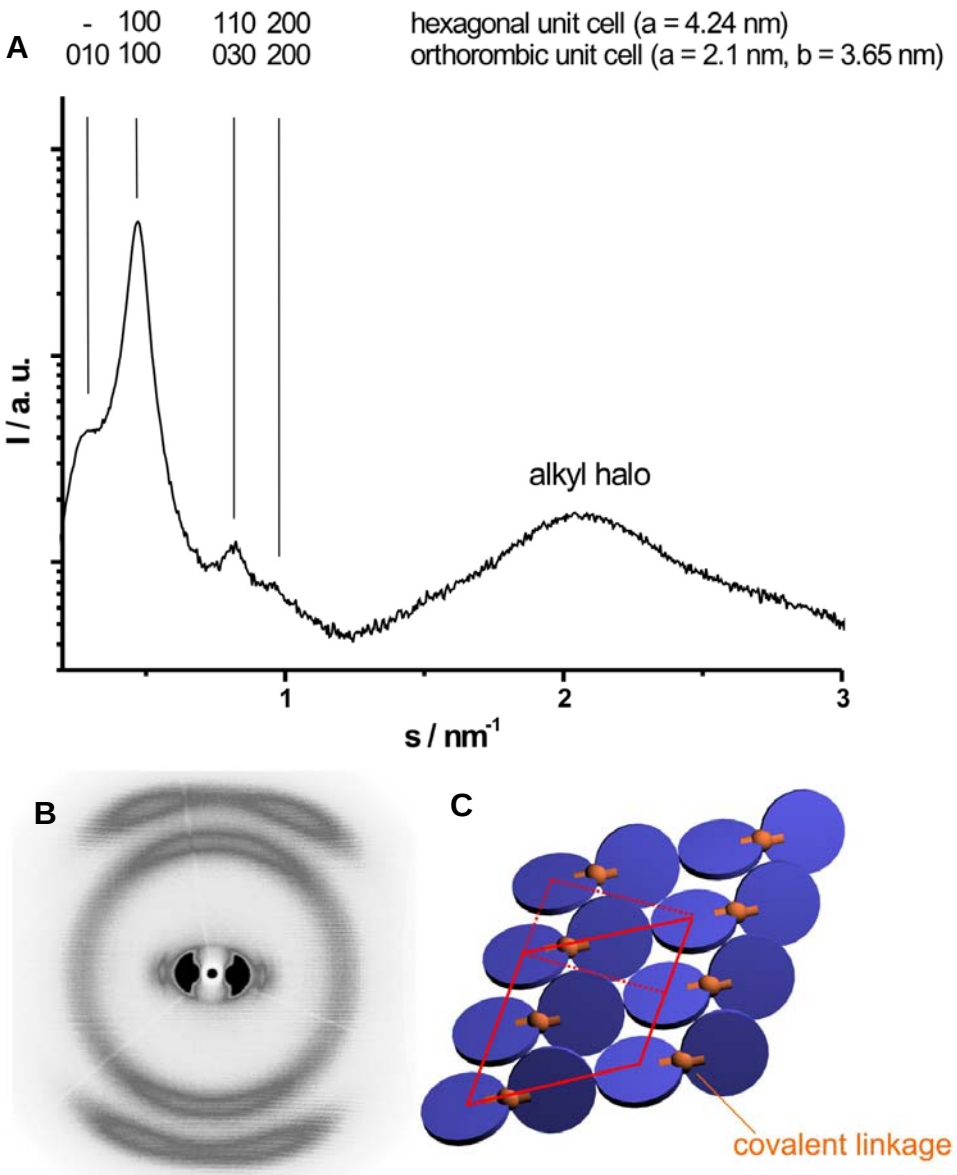

Figure 3-15: A) 360° integration plot, **B**) 2D diffractogram and **C**) schematic arrangement of the amide linked dyad **3-5**.

3.3.3.3 Solid-State NMR of Carboxy-functionalized HBCs

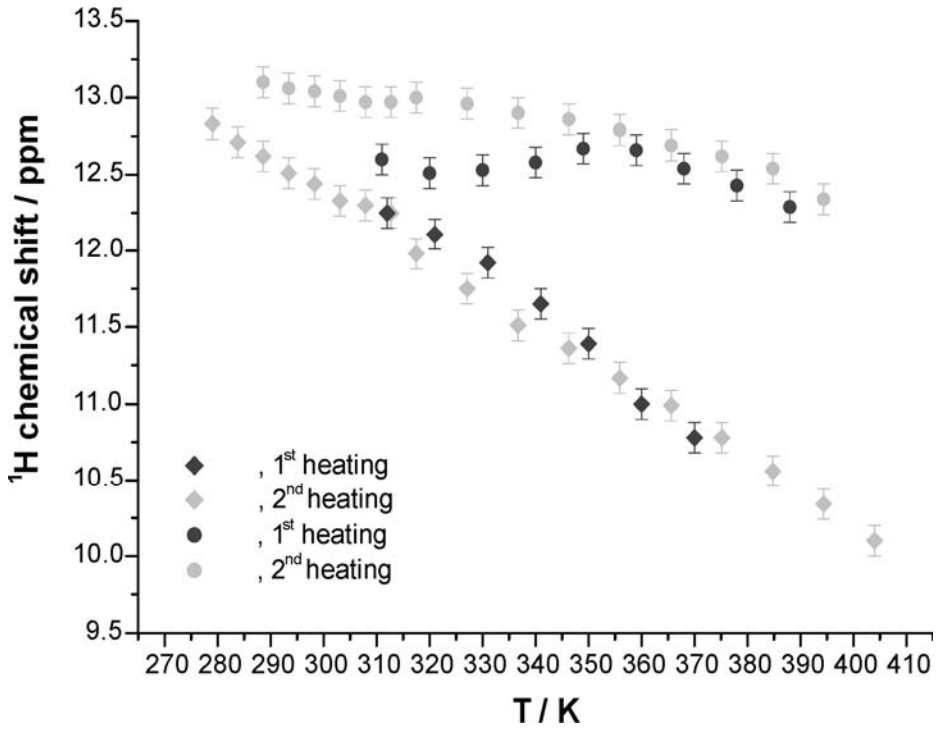

Figure 3-16: Temperature dependent ^{1}H MAS NMR of the mono-acid derivatives **3-2** and **3-3** for two heating cycles

^{1}H solid-state NMR (Appendix A) already proved to be very valuable for such systems as the chemical shift of the acid proton is very sensitive to the strength and the geometry of the hydrogen bridges. For investigating acid dimer formation, temperature dependent solid-state ^{1}H NMR spectra of the acid derivatives **3-2, 3-3** and **3-4** under fast (ν_r = 30 kHz) magic angle spinning (MAS) from 0 °C to 130 °C were recorded (Figure 3-16). The ^{1}H chemical shift could be understood assuming a chemical exchange process between the free acid and a hydrogen-bonded acid dimer resulting in a single peak located at an average position,[85,86] which directly reflected the strength and stability of the probed hydrogen-bond. The overall high chemical shift of the acid protons (>12 ppm) proved that in all samples hydrogen bonds are formed. However, at elevated temperatures significant differences for the three samples are observed. For the short tethered examples **3-2** and **3-4** the shift of the acid proton showed only a very slight change with increasing temperature, whereas the resonance of the acid proton for the long tethered HBC derivative **3-3** shifted almost linearly from approximately 12.5 ppm down to 10 ppm.

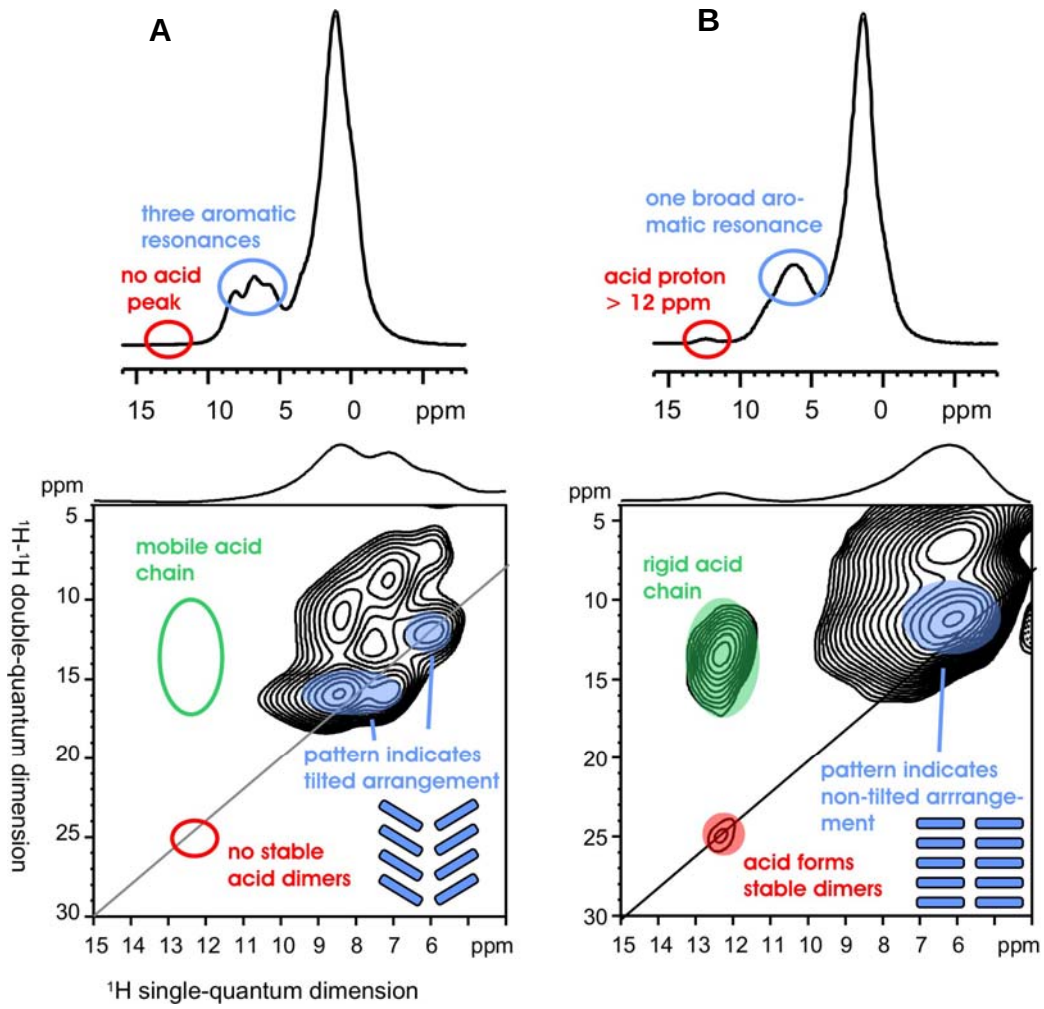

Figure 3-17: ^{1}H-^{1}H double-quantum (DQ) filtered (top) and two-dimensional ^{1}H-^{1}H DQ spectra (bottom) of the mono-acid derivatives **A**) **3-2** and **B**) **3-3** at 30 kHz MAS, T = 48 °C and one cycle of the BABA recoupling sequence for the excitation and reconversion of DQ coherences. The two-dimensional DQ spectra of 2a and 2b were recorded with WATERGATE peak suppression of the aliphatic peak at 1 ppm.

At this point, it has to be remarked that for the short tethered mono acid HBC **3-2** during the first and the second heating phase the shifts showed a strong difference. This behavior has already been observed in the DSC and the X-ray studies and was attributed to a reorganization of the system to correct the disorder in the supramolecular arrangement introduced during the workup procedure. Additionally, no significant change of the acid signal was observed for the long tethered derivative **3-3** during the transition to the mesophase suggesting that the tendency to form acid dimers did not influence the phase transition.

The formation of carboxylic acid dimers means that the hydrogen bonded acid protons are on average spatially close with a typical typical H-H separation between 0.25

and 0.3 nm. The existence of such pairs can be easily detected by ^{1}H double quantum MAS NMR as sufficiently strong dipolar coupled protons, which are not subject to a chemical exchange on the experimental timescale (100 µs) passes the double-quantum filter. For **3-3** (Figure 3-17A top) for instance the acid-proton resonance was absent indicating a fast chemical exchange of these protons on the timescale of the experiment (~100 µs). However, the clearly detectable acid resonance at 12.5 ppm for the short tethered cases **3-2** and **3-4** pointed to a far slower chemical exchange and therefore a more stable dimer than in **3-3**.

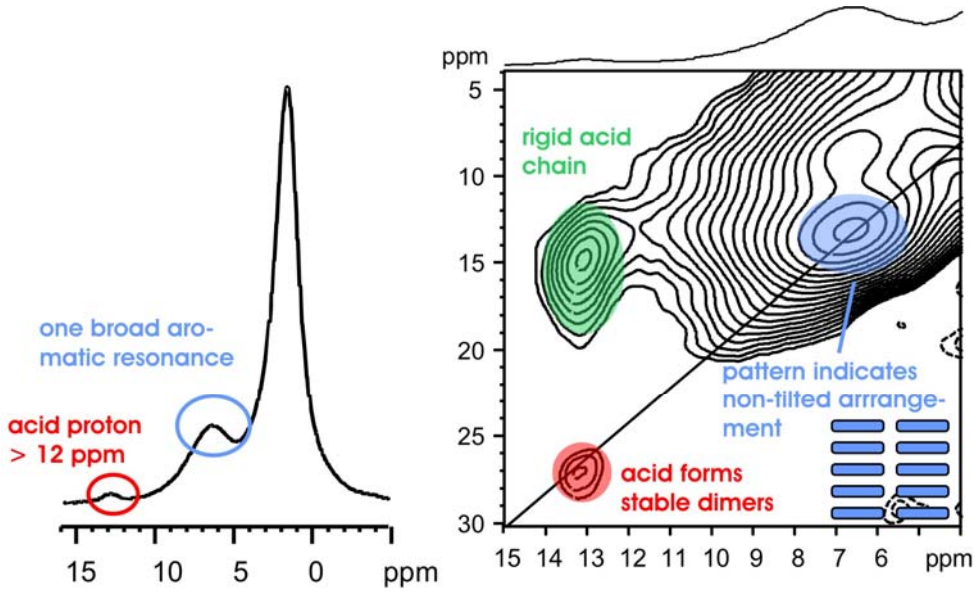

Figure 3-18: ^{1}H-^{1}H double-quantum (DQ) filtered (top) and two-dimensional ^{1}H-^{1}H DQ spectra (bottom) of the diacid derivative **3-4** at 30 kHz MAS, T = 48 °C and one cycle of the BABA recoupling sequence for the excitation and reconversion of DQ coherences. The two-dimensional DQ spectra of 2a and 2b were recorded with WATERGATE peak suppression of the aliphatic peak at 1 ppm.

While the short tethered compounds **3-2** and **3-4** showed a diagonal peak at (12.5 ppm, 25 ppm) and a cross-peak at (12.5 ppm, 13.5 ppm) in the 2D-^{1}H-^{1}H-DQ spectra (Figure 3-17B, bottom and Figure 3-18) these two signals were not observed for **3-3**. The diagonal peak appeared because the acid protons formed dipolar coupled pairs, [86] thus proving the existence of dynamically stable acid dimers for the short tethered HBCs **3-2** and **3-4** on the timescale of the experiment. Supporting evidence came from the cross-peaks due to the coupling of the acid with the neighboring aliphatic protons. Thus the long tethered compound **3-3** does not form stable dimeric structures on the same

timescale although the observed high ^{1}H chemical shift (Figure 3-16) implied that hydrogen-bonds were present most of the time.

In addition, it was further possible to confirm the columnar arrangement observed in the X-ray studies as the aromatic protons of HBCs show a specific pattern in the 2D experiments (Appendix A). As was shown by Brown et al., the tilted arrangement of the discs in the solid phase leads to different electronic environments of the aromatic protons in the stacked and therefore results in a coupling pattern as illustrated in Figure 3-17A, bottom. By this method, a tilted arrangement for the long tethered HBC **3-3** was confirmed, while for **3-2** and **3-4** no such distributions of the coherences could be found pointing towards the non-tilted arrangement.

For the determination of the molecular dynamics, ^{1}H-^{13}C-REPT-HDOR experiments[87,88] were performed, yielding coupling constants and reduction factors (Table 3-2, p. 58). These experiments generated MAS sideband patterns in the indirect dimension of a 2D experiment, which could be fitted to yield the corresponding ^{1}H-^{13}C dipole-dipole coupling constants of the aromatic ^{13}C-^{1}H peaks around 120 ppm. For rigid, directly bonded ^{1}H-^{13}C spin pairs a coupling constant of $Dis/2\pi$ = 21 kHz is typical, whereas significantly lower values were indicative of a motional process with rates above 10^4 s^{-1}. In their respective solid phases, all materials exhibited dipole-dipole coupling constants, typical for rigid, immobile C-H pairs.

All investigated materials showed no fast motions of the aromatic cores (rates higher than 10^4 s^{-1}) in the crystalline phase. While for the amide linked dyad **3-5** and the short tethered HBC acid derivatives **3-2** and **3-4** even above 100 °C no significant core motions were detected (crystalline phase), the parent compound **3-1**, the long tethered mono-acid HBC **3-3**, and the ester linked dyad **3-6** exhibited in their respective columnar mesophases strongly reduced coupling constants and therefore large core motions, pointing towards a rotation of the discs around the stacking axis.

3.3.4 Properties on Surfaces

An interesting question was, if the effects of the hydrogen bonds that were seen in the bulk, would also be visible on a surface. This is particularly important for improving the control on surface patterning with HBCs, which proves promising for molecular electronics.[89-91] Therefore, STM measurements were conducted. The epitaxially oriented two-dimensional crystals formed by the long tethered derivative **3-3** (Figure 3-19B) could be described by an hexagonal unit cell with a lateral spacing of a = (1.85 ± 0.10)

nm, which was indistinguishable from the packing arrangement of the parent compound **3-1**.[92]

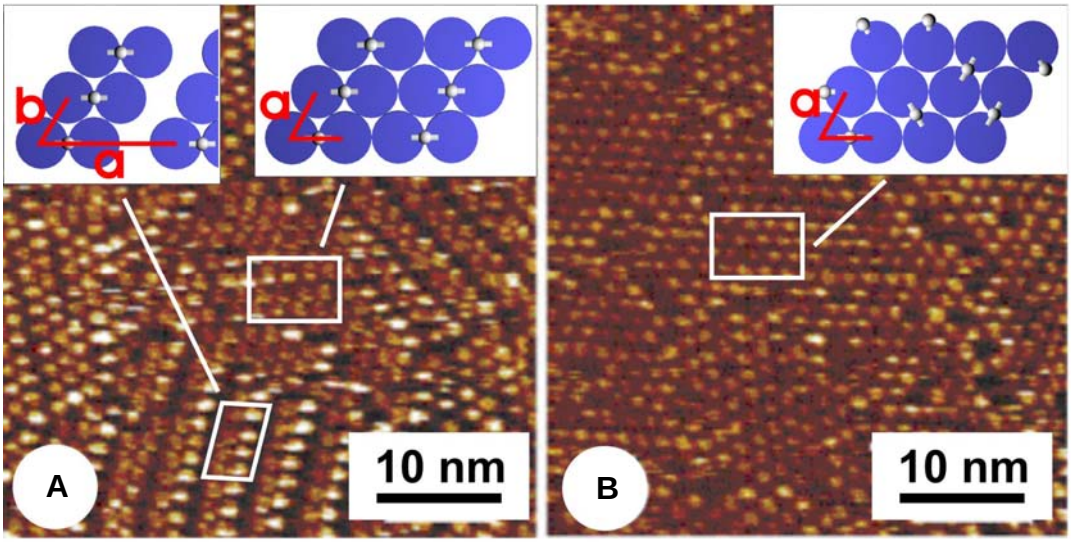

Figure 3-19: STM current image of highly ordered monolayers of **A**) the sort mono acid HBC **3-2** exhibiting dimer rows and hexagonal packing, **B**) the long tethered HBC derivative **3-3** showing hexagonal arrangement only. Tunneling conditions were sample bias U_t = -1.2 V, -0.8 V and –1.0 V and average tunneling current I_t = 100 pA, 100 pA and 150 pA, respectively.

In the case of the short tethered mono-acid HBC **3-2**, two different coexisting structures were observed (Figure 3-19A). On one hand, again a hexagonal arrangement with a lattice vector length of a = (1.92 ± 0.10) nm could be detected, whereas on the other hand a dimeric structure with a = (4.26 ± 0.18) nm and b = (1.81 ± 0.10) nm with an angle of (64 ± 2)° in between was formed. The diacid HBC **3-4** arranged in a significantly different structure than **3-2** and **3-3** (Figure 3-20A), due to its two carboxylic acid groups namely in an oblique manner with lattice parameters of a = (2.21 ± 0.10) nm, b = (1.88 ± 0.07) nm and an angle of (71.9 ± 2.3)°. The area per unit cell for the hexagonal arrangements of **3-2**, **3-3** and **3-4**, which was also observed for the parent compound **3-1** provided only enough space for the HBC core and three methylene units per side-chain to lie down flat on the substrate Figure 3-20B.

Indeed, the sterically demanding methyl branching at the γ position forced the rest of the side-chain out of plane and into an upright position.[78,92] These outer parts of the alkyl side-chains were solubilized in the supernatant solution. Therefore the parameters of the self-organized structures cannot be directly compared with the results gained in the bulk.

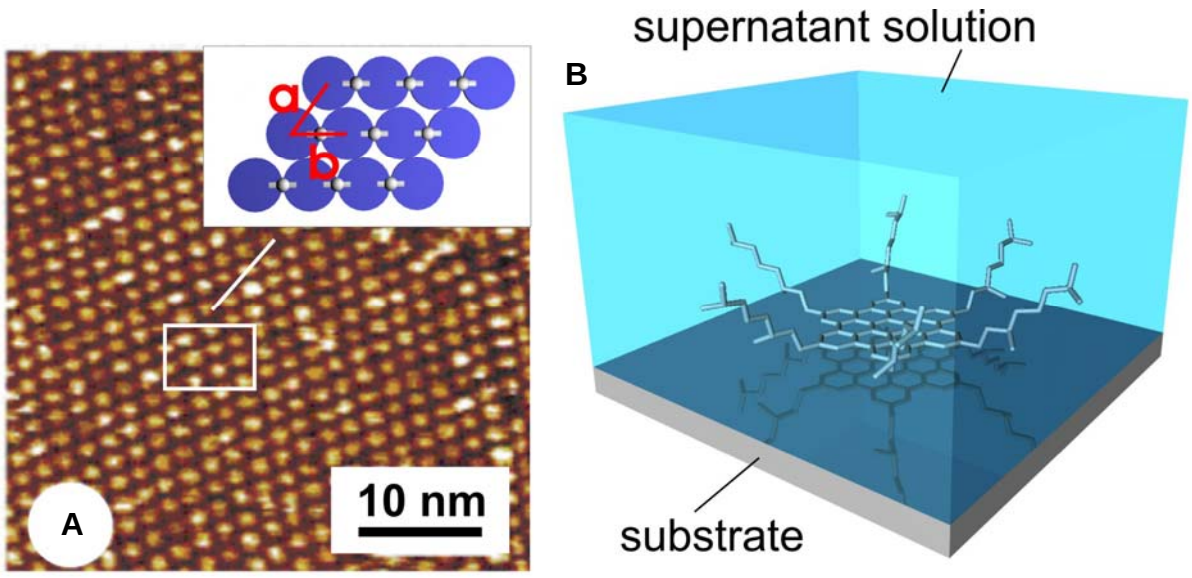

Figure 3-20: **A**) STM current image of highly ordered monolayers of the diacid HBC **3-4**, packing in an oblique structure and **B**) the schematic representation of adsorption of an HBC onto the basal plane.

3.3.5 Discussion

For **3-3**, the long tether between the aromatic disc and the carboxylic acid function showed little influence on the thermal and supramolecular behavior compared to the parent compound. Already in the DSC, the phase transition remained in the same range as for the parent compound **3-1** and the bulk properties observed by 2D-WAXS and solid-state NMR closely resembled those of **3-1**. In both cases, the discs arranged at room temperature in the pseudo-crystalline phase in a columnar, hexagonal and tilted fashion. This behavior was confirmed by STM, as the images did not reveal any influence of the hydrogen-bonds on the packing parameters.

The self-assembly of the discs of the short tethered mono-acid **3-2** in the bulk in a non-tilted, hexagonal fashion is however atypical for the packing of HBCs at room temperature and is a result of the complementary effects of the hydrogen-bonds between columns and the π-interactions of the discs (Figure 3-21A/B). This example pointed again to the importance of thermal treatment as before the treatment only broad and unresolved reflexes were observed in the 2D-WAXS. After the annealing procedure, the 2D-WAXS of the short tethered derivative **3-2** became far better resolved. With the pronounced (220) reflection in combination with a higher intensity than usually seen for hexa-substituted HBCs like **3-1**, it became apparent that this behavior had to result from an improved order. The temperature dependent ^{1}H MAS NMR additionally supported

the expected high stability of the hydrogen-bonds, as almost no decrease in chemical shift could be observed at higher temperatures (Figure 3-16).

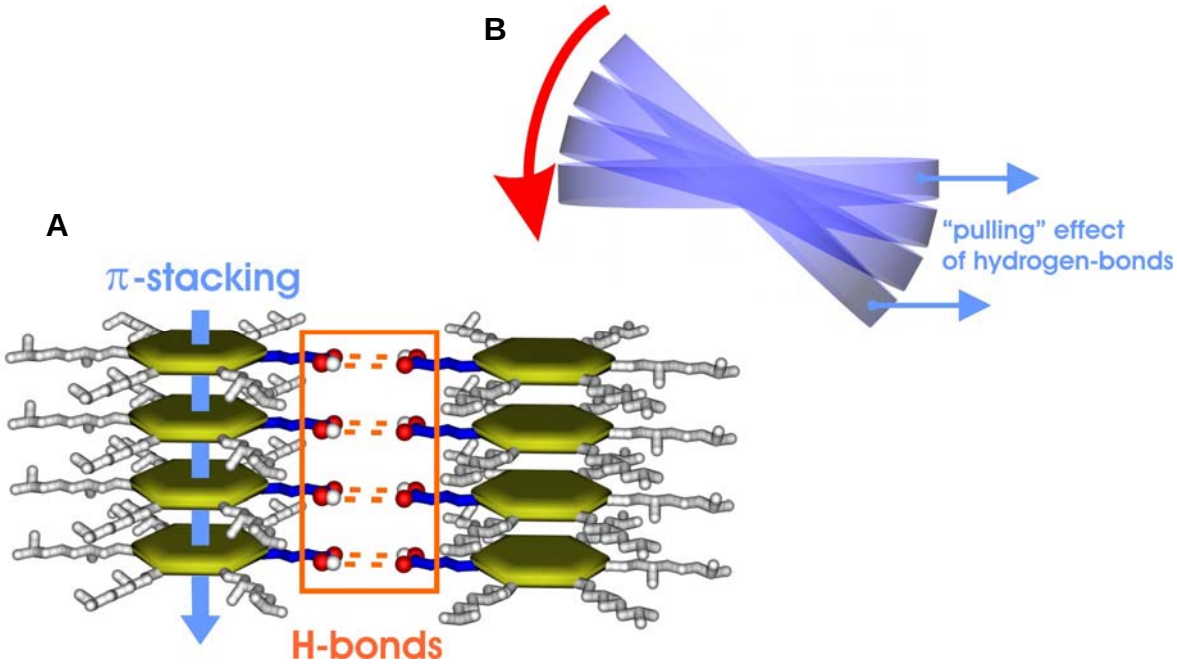

Figure 3-21: Schematic representation of the complementary effect exerted by the π-stacking with hydrogen-bonds, leading towards a non-tilted stacking behavior.

Thus different from the long tethered example **3-3**, the acid protons of **3-2** stayed on average in a hydrogen-bonded state. By assuming that the strength of the hydrogen-bonds in the short **3-2** and the long tethered case **3-3** are comparable, as both are based upon the interplay between carboxylic acid groups, this difference must originate from the flexibility of the alkylene tether. The crystalline phase of **3-2** is therefore effectively stabilized as the discs are more often encountered as hydrogen-bonded dimers than in the long tethered counterpart **3-3**. This even resulted in a distortion of the usually seen hexagonal arrangement of HBCs in the bulk. Although the differences were not severe, the discs clearly arranged in an orthorombic unit cell, which emphasized again the key role of the carboxy functions connected to the short spacer.

STM visualization of monolayers of the short tethered mono-acid HBC **3-2** at the solid-liquid interface revealed dimer formation (Figure 3-19A, left inset) due to the hydrogen-bonding of neighboring discs. Indeed, this did not hinder the self-assembly of a coexisting, more closely packed hexagonal arrangement induced by the branched side-chains (Figure 3-19A, right inset). Because of the kinetics of the self-organization

process at the solid-liquid interface, different crystalline structures are more easily observed simultaneously than in the bulk, if their difference in free energy is small. Thus, the coexistence of the two structures is attributed to the competition between hydrogen-bond formation and the effects exerted by the branching of the side-chains.

The above effects could even be amplified for the diacid HBC **3-4** by adding a second carboxylic acid group to the "para"-position of the HBC disc, while maintaining the same tether length as for the short tethered mono acid HBC **3-2**. The material showed no transition to the mesophase until degradation and stacked in a non-tilted fashion like the short tethered mono acid case **3-2**, possibly due to the same complementary effects as seen for **3-2** (Figure 3-21). The orthorhombic columnar arrangement observed in the 2D-WAXS deviated even stronger from the hexagonal case than **3-2**. The impact of the second acid group in the diacid derivative **3-4** was also found in STM, where in contrast to **3-2** exclusively an oblique arrangement was observed. Thus, a second hydrogen-bond lowers the free energy of this arrangement sufficiently to prevent the hexagonal arrangement and one is led to conclude that the diacid derivative **3-4** forms a non-covalent, hydrogen-bonded "polymer" on the substrate surface (Figure 3-20A, inset).

The specificity of the hydrogen-bonds in the bulk could be deduced from a comparison of the dyads **3-5** and **3-6**. For the ester linked example **3-6** a simple intercolumnar bridging without any auxiliary interactions was assumed. The resulting low transition temperature to the mesophase at 14 °C and the fast motions of the aromatic cores determined by solid-state NMR (Table 3-2) indicated a very unstable pseudo-crystalline phase without any long-range order below the transition temperature. This is atributed to the formation of a disordered three-dimensional network caused by the flexibility of the ester linkages, which could even allow backfolding of the HBC discs (Figure 3-22).

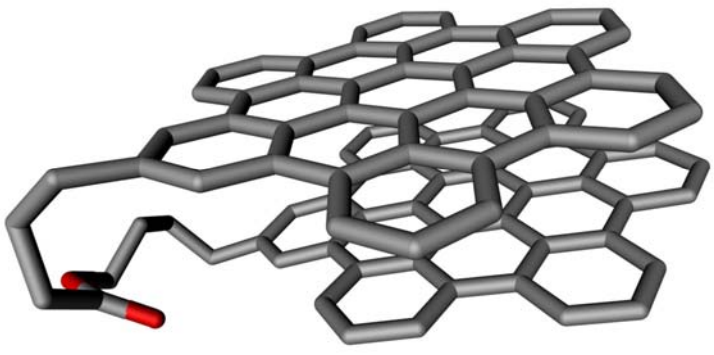

Figure 3-22: Schematic representation of backfolding of two discs of the ester linked dyad **3-6**.

At room temperature, a simple hexagonal arrangement was detected, which fitted the dimensions of single HBC discs, and a non-tilted stacking with a cofacial distance larger than 0.36 nm, typical for the mesophase. In the amide analogue **3-5**, the additional hydrogen-bond led to a drastic change of the organization behavior. The fact that the mesophase of **3-5** could not be reached before thermal decomposition in addition with the ^{1}H-^{13}C REPT-HDOR experiments (Table 3-2) revealed a low mobility of the aromatic cores, pointing towards a formation of a stable pseudo-crystalline phase.

Material	Transition	T / °C	Tilted Columnar Arrangement	D_{is} of core CH / kHz (at T)	S
1	$X_t \rightarrow Col_{ho}$ $Col_{ho} \rightarrow I$	81 420	yes	21.7 ± 0.6 (38 °C) 8.6 ± 0.3 (105 °C)	0.4
2a	$X_u \rightarrow Col_{ho}$	221	no	20.4 ± 0.5 (40 °C) 17.6 ± 0.5 (102 °C)	0.86
2b	$X_t \rightarrow Col_{ho}$	70	yes	22.0 ± 0.5 (40 °C) 8.6 ± 0.5 (93 °C)	0.39
3	* (X_u)	-	no	-	-
4a	* (X_t)	-	yes	19.1 ± 0.5 (112 °C)	> 0.9
4b	$X \rightarrow Col_{ho}$	14	not resolved	19.1 ± 1.0 (6 °C) 7.5 ± 1.5 (44 °C)	0.39

Table 3-2: Overview of the phase transition temperatures, solid-state packing and molecular dynamics of the dyads **3-5**, **3-6**, HBC dimers **3-2**, **3-3** and **3-4** and the parent compound **3-1** (X_t = pseudo-crystalline phase with tilted arrangement, X_u = pseudo-crystalline phase with untilted arrangement, Col_{ho} = ordered hexagonal columnar mesophase, I = isotropic melt, * = no transition detected in the range from -150 to 300 °C).

These findings indicate the key role of dynamic hydrogen-bonds, since a covalent linkage neither improved the order nor restricted the aromatic core motions. Thereby one carboxylic acid function of the short tethered example **3-2** stabilizes not only one neighboring disc but during breaking and reforming with other partners “distributes” its effect. A dynamic network of hydrogen-bonds is thus formed, where every column stabilizes the six adjacent columns and *vice versa*.

A short tether connecting aromatic core and carboxy functions can therefore on average stay longer in the hydrogen-bonded state due to the reduced freedom of movement. This leads to stronger intermolecular interactions and thus to an improved order in the bulk and a higher transition to the mesophase. This additional non-covalent

force distorts the preferred hexagonal and tilted columnar arrangement of the discs in the pseudo-crystalline phase towards a non-tilted, orthorhombic self-assembly. By adding a second short tethered carboxylic group to the "para"-position of the HBC (**3-4**) one can even achieve a complete distortion in the bulk, as well as on the solid-liquid interface of the usually hexagonal arranged discs towards an orthorhombic lattice.

In conclusion, a simple covalent linking of two HBCs discs without any auxiliary interactions is not responsible for the pronounced effects seen for the short tethered mono-acid case **3-2** where the dynamic behavior of the hydrogen-bonds leads to a stable network. In the case of the ester linked dyad **3-6** no improved order can be observed. By exchanging the ester to an amide function the disturbing effect of the alkylene bridge is compensated by the improved intracolumnar order based upon the hydrogen-bonds exerted via the amide functionality. The combined results of solid-state NMR, 2D-WAXS and STM thus create a complete and homogeneous picture of the effects of hydrogen-bonds on the supramolecular arrangement of HBCs in the bulk as well as on surfaces.

3.4 Inducing processability

Processability is a key issue for the use of discotic mesogens in future organic devices, but also a high order and and as a consequence of it, a high charge carrier mobility is desired.[15-18] Especially the second requirement reveals that the use of para-substituted HBC derivatives proves to be very promising for such applications, as for example HBC **3-4** already self-assembles in a kind of hydrogen bonded "polymer" on surfaces. Therefore, the recovering of the processability could lead to interesting materials that show an even higher order than the mono-substituted case **3-2**, if it is possible to retain solubility and processability. For gaining further insight into the behavior of such para-substituted materials the two derivatives with carboxy-functions **3-21** and **3-23** (Figure 3-23) were synthesized. In the first example only a phenyl entity was used as a tether. If the rigidity of the tether forces the carboxy-functions into an unfavorable geometric layout,[84] the strength of the hydrogen bonds could be severely diminished, leading to a less strong bonding situation than for derivative **3-4**, where the remaining flexibility of the propyl-tether allows a certain freedom to circumvent spatial strain. Another approach is the prolongation of the tether of **3-4**. As already observed for the mono-substituted cases, the length of the tether plays an important role for the supramolecular behavior of the compounds. As it was determined for the mono-acid

derivative **3-3** that a too long tether will show no effect, in the case of the para-substituted HBC **3-23** a shorter pentyl tether was used.

3.4.1 Synthesis

The synthesis was accomplished in a similar fashion than for the derivative **3-4**. First the corresponding ester functionalities were introduced *via* a Negishi cross-coupling and the ester entities were changed to their carboxy-analogues by using sodium hydroxide.

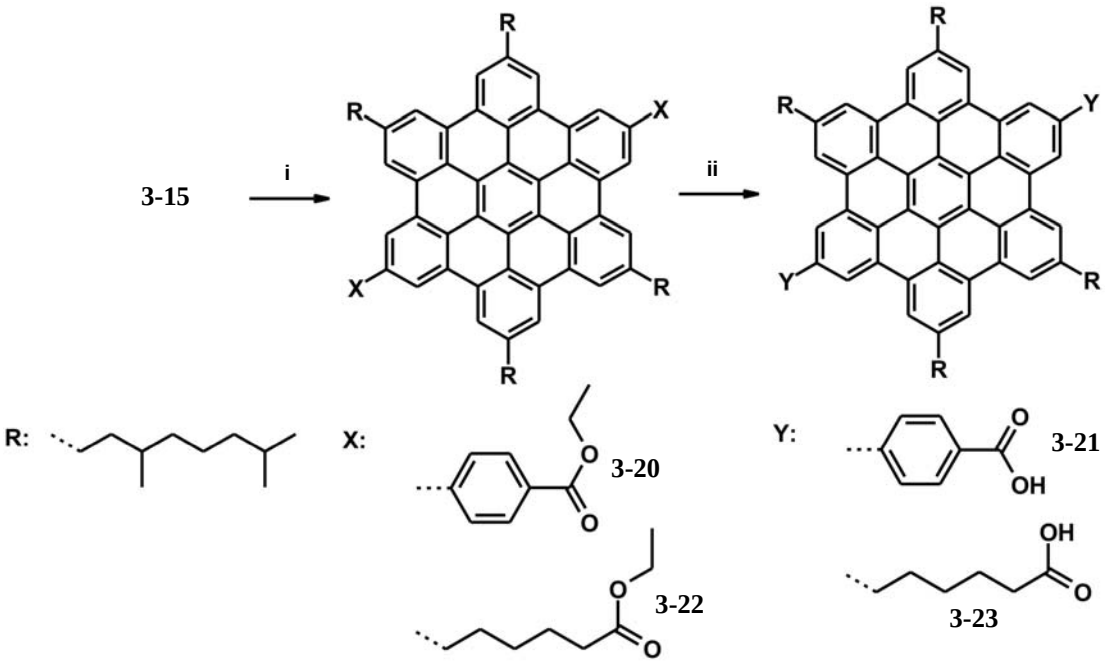

Figure 3-23: Synthesis of the diacid substituted HBC derivatives **3-21** and **3-23**. *i:* BrZnX, Pd[dppf]Cl_2 x CH_2Cl_2, THF; *ii:* NaOH, THF, MeOH, H_2O reflux.

As the before mentioned cases relied on the observations made for the mono-substituted HBC derivatives, for the para-substituted diamide case **3-24** another approach was considered. In this example, the forces exerted by the hydrogen bonding were not counteracted by a longer tether or the possible enforcing of a unfavorable geometric condition, but moreover by an attachment of a dodecyl-chain at the outer position of the hydrogen-bond exerting entity. It was assumed that the additional disturbance of such a long chain would efficiently dampen the strong effects originating from the hydrogen bonds. Therefore, it was not necessary to change the already partially successful approach with the diacid HBC derivative **3-4**. For the synthesis, the ester precursor **3-16** was used and boiled for several days in dodecylamine. Contrary to the expectations, the two acid cases revealed an even stronger insolubility in organic solvents than the previously discussed derivative **3-4**, which did as a consequence not

even allow the recording of a resolved ^{1}H NMR spectrum. Also in the thermal analysis no phase transitions could be observed.

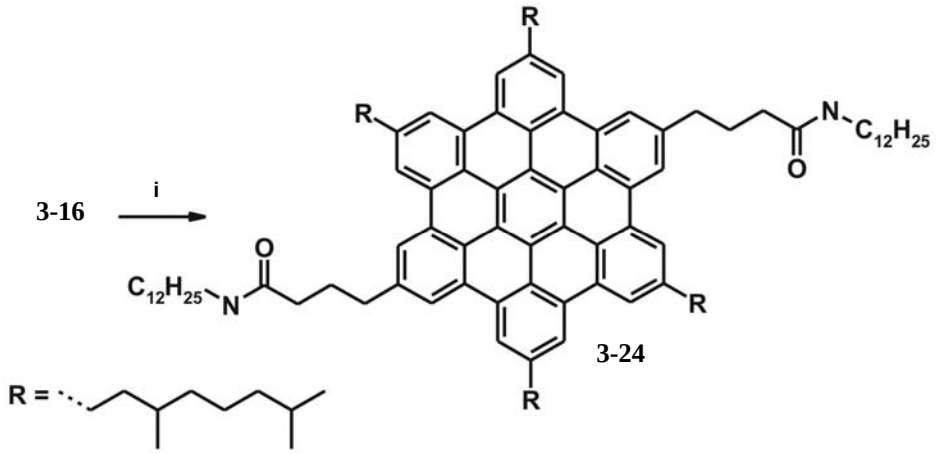

Figure 3-24: Synthesis of the para-diamide substituted HBC **3-23**. i: *n*-dodecylamine, 150 °C, 4d, 95%.

For the diamide **3-24** however a severe increase in solubility was noted and the ^{1}H NMR (Figure 3-25) confirms the solubility as also a ^{13}C NMR spectra could be recorded without the necessity to apply any severe conditions like for the diacid HBC **3-4**. It became already at this stage obvious that the approach of substituting the hydrogen-bond exerting entities with flexible alkyl chains at their outer position resulted in a more soluble material.

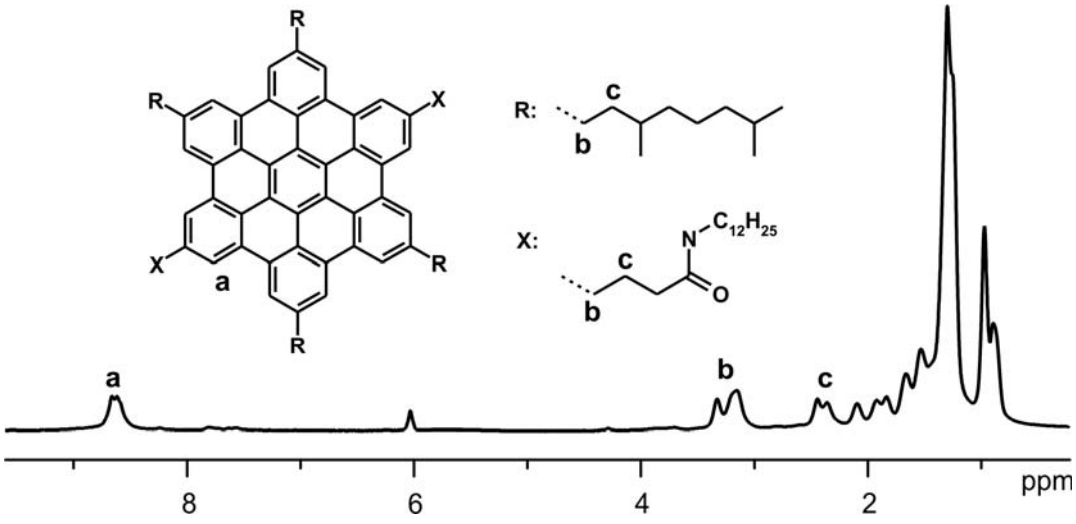

Figure 3-25: ^{1}H NMR of para-substituted diamide HBC **3-23** in $C_2D_2Cl_4$ at 403 K.

3.4.2 Bulk Properties

3.4.2.1 DSC

As already observed for the beforementioned ester compound **3-16**, also for the other derivatives **3-20** and **3-22** a thermal behavior could be observed. As ester functions do not exert any kind of pronounced secondary forces, the materials behaved generally similar to the parent case **3-1**. For compound **3-20** for example an endothermic transition at 73 °C and an exothermic transition at 48 °C appeared. A similar DSC spectrum was found for the other material **3-22**, as during the heating cycle an endothermic (20 °C) and during cooling an exothermic (-11 °C) peak was detected.

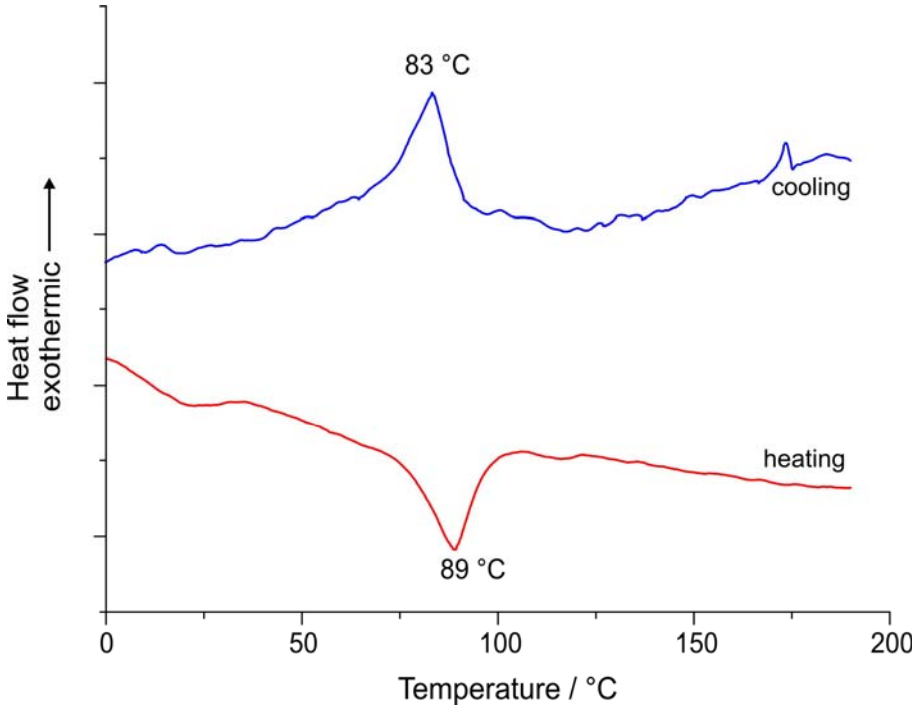

Figure 3-26: DSC plot of the diamide HBC derivative **3-24**.

For the acid derivatives **3-21** and **3-23** no thermal phase transition could be observed. For the amide analogue **3-24** however a transition was observed during heating at 89 °C and during cooling an exothermic peak at 83 °C (Figure 3-26). As these peaks were visible in repetitive cycles, they could also not be accounted to a simple reorganisation of unequilibrated structures enclosed during the workup procedure, which was for example observed for the mono acid HBC **3-2** during the first heating cycle.

3.4.2.2 2D-WAXS

The *para*-disubstituted ester HBCs **3-20** and **3-22** showed at room temperature a simple hexagonal arrangement. In both cases, one could observe thermal transitions although the temperature dependent 2D WAXS did not reveal any change of the columnar arrangements. This leads to the conclusion that the observed transition is correlated with a reversible rearrangement of the alkyl chains in the corona of the molecules. For compound **3-20** it was possible that the sterically small phenyl tether could have a minor influence upon the columnar arrangement in the bulk.

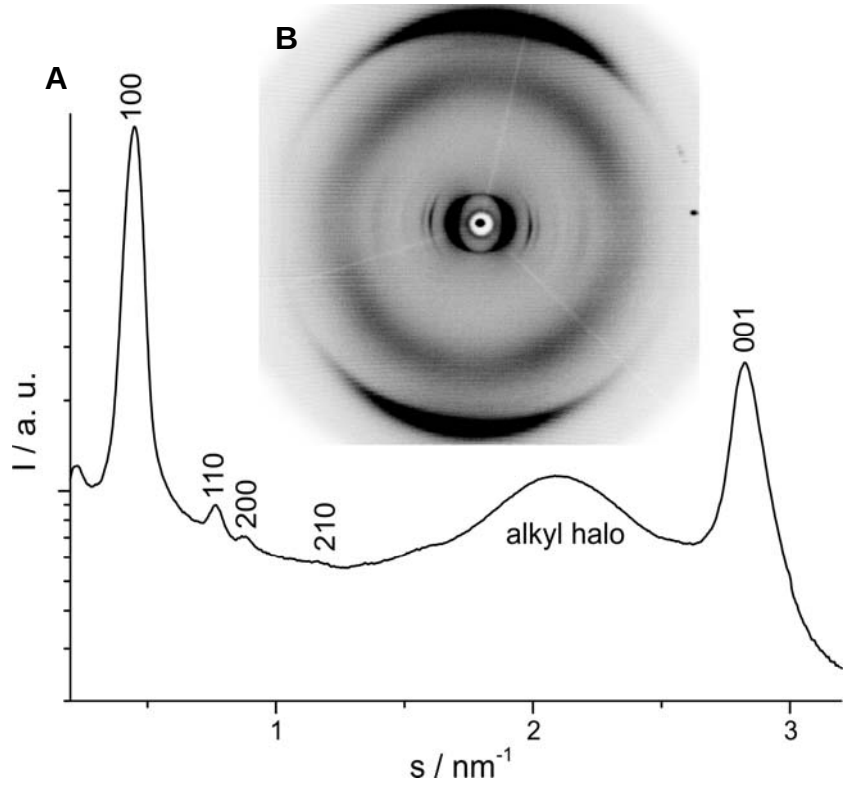

Figure 3-27: 2D WAXS of the para-substituted phenyl-ester HBC derivative **3-20 A**) 360° integration plot, **B**) 2D diffractogram.

The only difference between this case and the hexa-alkyl-substituted parent compound was the non-tilted arrangement of the discs with respect to the columnar axis (Figure 3-27). This behavior has so far only been observed for compounds in the mesophase and the beforementioned cases with hydrogen-bonding entities. Therefore, it seems likely that the material is at room temperature present in some kind of "frozen" mesophase and the peaks in the DSC indicate the transitions between different liquid-crystalline states. In fact, a similar behavior can be observed for the second ester derivative **3-22** (Figure 3-28). Also in this case the discs do not adopt a "herringbone"

arrangement (Figure 3-10B) but seem to arrange themselves in some kind of mesophase. In contrast to the two acid derivatives, the waxy state of the amide derivative **3-24** allowed the extrusion of a fiber and the recording of 2D WAXS diffractograms. In the beginning the phase transition seen in the DSC was believed to be the transition to the mesophase. However, the temperature dependent 2D WAXS measurements revealed that not a mesophase has been observed, due to the still tilted hexagonal arrangement observed for the higher temperature phase.

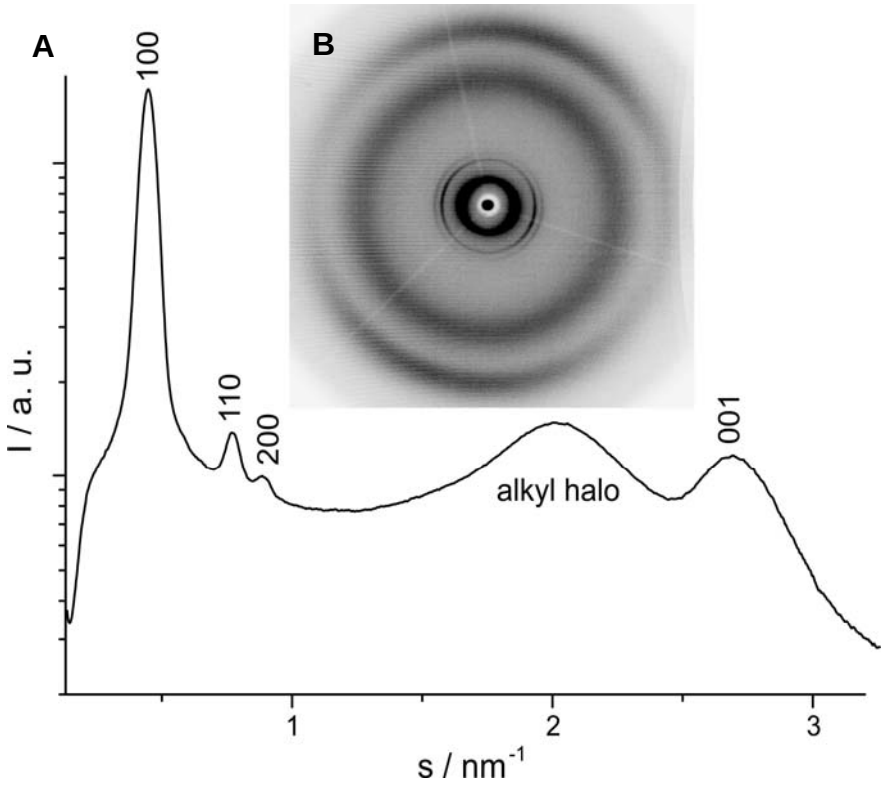

Figure 3-28: 2D WAXS of the para-substituted pentyl-ester HBC derivative **3-22 A**) 360° integration plot, **B**) 2D diffractogram.

Although the thermal transition was not due to a full phase transition, the treatment itself seemed to improve the columnar order, as can be seen from the appearance of an increased number and sharper reflexes compared to the initial state (Figure 3-29). At room temperature and at higher temperature the discs remained in a tilted configuration with respect to the columnar axis and the stacking distance was determined with 0.34 nm, which corresponds to the intermolecular stacking distance observed for other HBC derivatives.

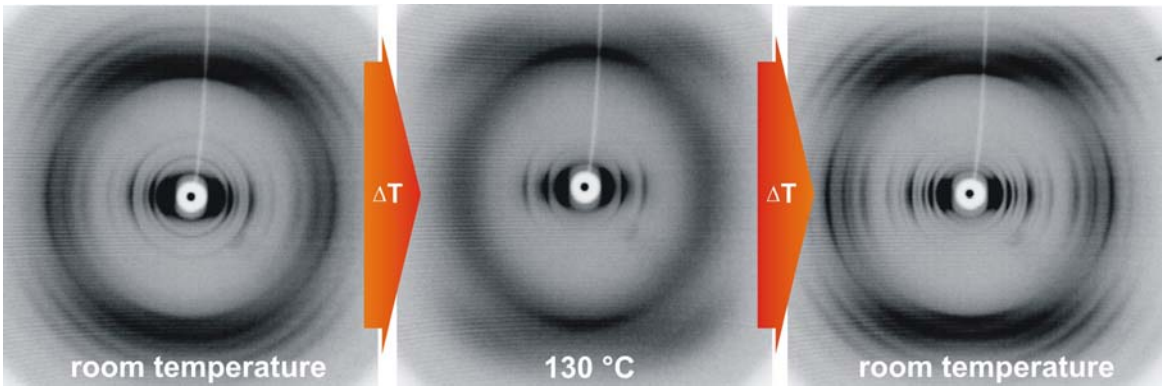

Figure 3-29: Thermal annealing of the diamide HBC derivative **3-24.**

This behavior could also be observed in the equatorial slice plot and the full integration plot of the 2D WAXS diffractograms. In the higher temperature phase the discs adopted a hexagonal packing with the cell parameter a = 2.98 nm, wich fitted approximately to the usual dimensions for a tilted columnar stacking of other hexa-alkylated cases like **3-1** in their respective "crystalline" phase (Figure 3-30B).[93]

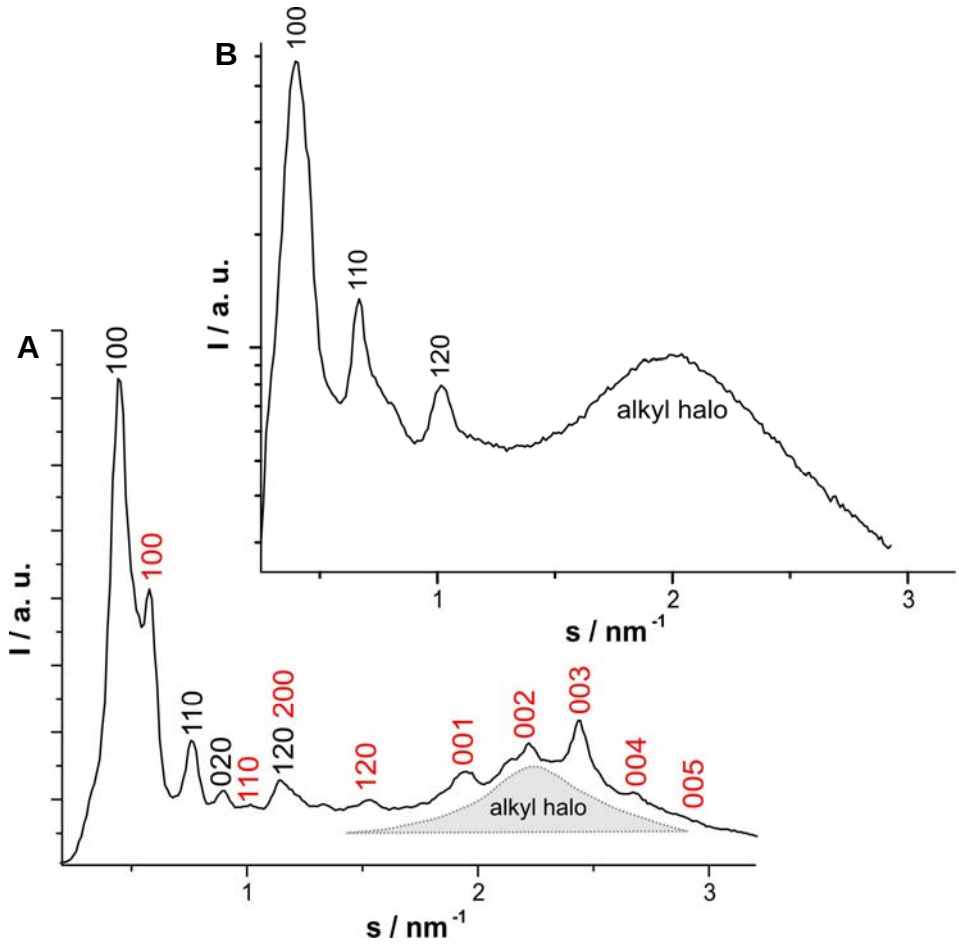

Figure 3-30: 2D WAXS of the para-substituted diamide HBC derivative **3-24 A**) 360° integration plot of annealed arrangement at room tempreature, **B**) 360° integration plot of higher temperature phase (130 °C).

During cooling to room temperature however, a diversity of new reflexes appeared next to the signals already observed at the higher temperature phase. These additional equatorial reflexes could not be correlated with the others and seemed to originate from another unit cell configuration (Figure 3-30A). Indeed, it could be proven that these two sets of signals describe two independent hexagonal unit cells. While the before mentioned cell is described with the parameter a = 2.98 nm, the second cell is significantly smaller with a = 2.23 nm. Also in the off-meridional direction several signals appeared, which originated from higher order reflexes of the intracolumnar stacking, pointing towards a stronger intracolumnar correlation of the discs and therefore a better order.

3.4.3 Discussion

Already for the mono-substituted cases a severe influence of the hydrogen bonds upon the supramolecular properties of HBCs was observed. This has been amplified by a *para*-substitution in the diacid HBC derivative **3-4** already discussed in section 3.3.5 leading to a "hydrogen-bonded" polymer formation on surfaces. The pronounced insolubility and the lack of any thermal phase behavior denied any processing of the material by zone-crystallization or zone-casting (Appendix B,C), although it showed a high order on surfaces. The distinct arrangement seen in the STM (Figure 3-20A) motivated the search for reducing the strong effects of the hydrogen-bonds in the para-substituted cases. Therefore, it was tried to force the hydrogen bond exerting entities into a geometrically unfavorable situation compared to the columnar stacking by attaching them to a rigid linker (**3-21**). Nevertheless, the resulting material showed a distinct insolubility in a way that even the recording of a ^{1}H NMR spectrum was futile, proving that the hydrogen bonds seem to be a dominating factor of the supramolecular arrangement and cannot be easily influenced by sterical demands. In addition, no thermal phase behavior could be observed.

In a second approach an extension of the alkyl tether was taken into account. As a result the expected dimer formation would not fit anymore the required intercolumnar distance and should reduce the influence of the hydrogen bonds as seen for the mono substituted case **3-3**. But also with this approach the gained material showed similar properties as **3-21**. The solubility did not allow the recording of a ^{1}H NMR spectrum and no thermal phase behavior could be determined.

Therefore, a more efficient solubilizing and perturbing approach had to be considered. By addition of a dodecyl chain at the outer rim of the hydrogen bond

exerting entity, the solubility could be recovered (**3-24**). Not only a resolved ^{1}H NMR spectrum was recorded, but moreover the concentration of the material could be raised high enough to record ^{13}C NMR spectra without the need for applying severe conditions, like extraordinarily high temperatures and/or special solvent mixtures.

The material additionally showed a signal in the DSC, which however was not due to a complete phase transition to the mesophase, as the discs remained tilted in the columnar stacking at the higher temperature phase. After cooling to room temperature, the 2D WAXS and the respective full integration plot revealed a second hexagonal unit cell with a = 2.23 nm, which is substantially smaller than the one already observed at higher temperatures (a = 2.98 nm). By consideration of the dimensions of one disc of the para-substituted diamide HBC (**3-24**), it was found that these 2.23 nm exactly fit the distance between the two amide functionalities.

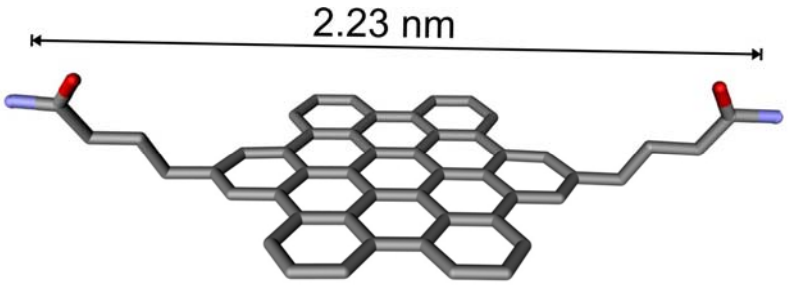

Figure 3-31: Calculated distance between the amide functionalities of the para-substituted diamide HBC **3-24**.

Therefore, the observed smaller unit cell has to originate from a closer intercolumnar packing, which was due to the hydrogen bonding of the amide entities. Such a strong interaction has already been observed for the diacid case on the solid-liquid interface in the STM, where the carboxy functions force the molecule out of its preferred hexagonal organization into a orthorombic one. Nevertheless, the larger unit cell still appears at room temperature, which points towards the fact that this packing already represents a very stable arrangement. It can be concluded that at room temperature two states of packing can coexist next to each other, resulting in a mixture of two different hexagonal unit cells (Figure 3-32).

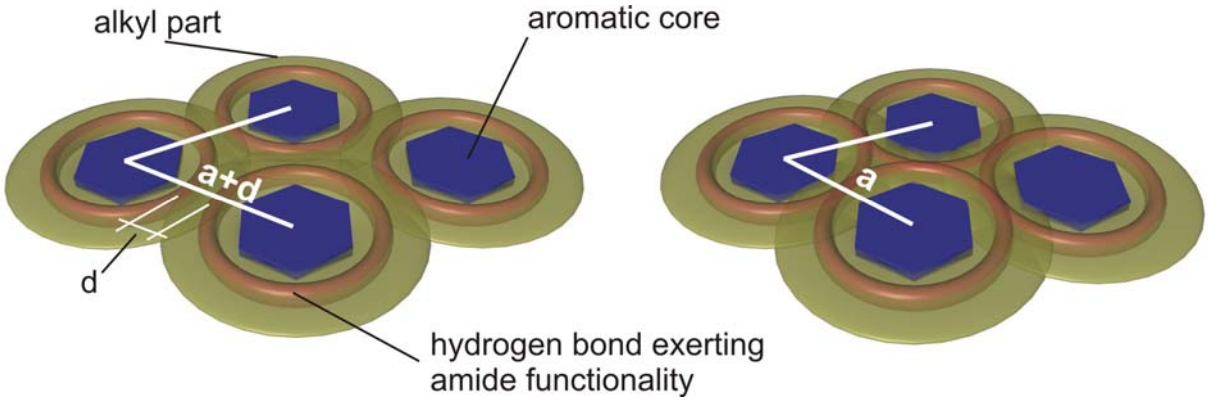

Figure 3-32: Schematic arrangement of the optimum arrangement for the para-substituted diamide HBC **3-24** for **A**) the alkyl chains and **B**) for the hydrogen-bonds.

These two states represent a competing situation between the large cell, which is based upon the spatial needs of the bulky alkyl substituents and the smaller one, which is the better organization for establishing the maximum amount of hydrogen bonds between the amide functionalities.

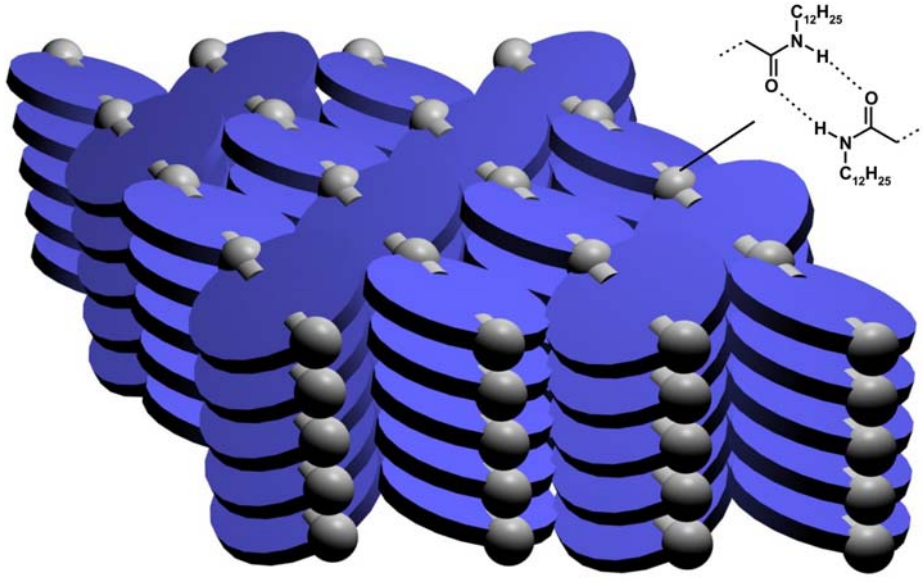

Figure 3-33: Schematic bulk arrangement for the para-substituted diamide HBC **3-24**.

Based upon the observations made for the diacid case at the solid-liquid interface, a schematic packing for the hydrogen-bonded example of **3-24** according to the smaller unit cell can be suggested. In Figure 3-33 the discs are arranged like a hydrogen bonded "polymer". With this arrangement several requirements can be fulfilled. On one hand, it allows to explain the occurrence of the small cell and only in this supercolumnar packing a maximum number of hydrogen-bonds can be established. On the other hand, the

hydrogen bonds can influence in this situation better the intracolumnar stacking, inducing a higher order, which explains the higher order reflexes for the intracolumnar stacking. Already in the dyad cases **3-5** and **3-6**, it was proven that the amide functionalities are not restricted to a intercolumnar stabilization, but exert their influence also along the columnar axis.

3.4.4 Conclusions

The para-substituted derivatives **3-4** with the carboxy- and the **3-24** with the diamide-functionalities indicated that a far higher order can be induced into the already pronounced π-stacking of the HBC discs. However, the processability of the materials should remain, as it is one of the most important features for the use of discotic mesogens in future electronic devices. Several types of alkyl tethers had to be tested. A soluble para-substituted material was only achieved due to a severe disturbance of the hydrogen-bonds by additional flexible alkyl chains attached at the outer rim of the hydrogen bond exerting entities. This compound showed also some sort of a thermal phase behavior although the peak in the DSC could not be accounted to a full transition to the mesophase. By cooling the material back to room temperature, the 2D WAXS revealed a far higher intracolumnar order due to the observed higher order reflexes in the meridional direction. Therefore, the order can be severely influenced by para-substitution of hydrogen bonding functionalities, but one has to take care that still some solubility and processability remains.

3.6 References

[1] H. Sirringhaus, N. Tessler, R. H. Friend *Science* **1998**, *280*, 1741.

[2] J. J. M. Halls, C. A. Walsh, N. C. Greenham, E. A. Marseglia, R. H. Friend, S. C. Moratti, A. B. Holmes *Nature* **1995**, *376*, 498.

[3] M. O'Neill, S. M. Kelly *Adv. Mater.* **2003**, *15*, 1135.

[4] D. Adam, P. Schuhmacher, J. Simmerer, L. Häussling, K. Siemensmeyer, K. H. Etzbach, H. Ringsdorf, D. Haarer *Nature* **1994**, *371*, 141.

[5] L. Schmidt-Mende, A. Fechtenkötter, K. Müllen, E. Moons, R. H. Friend, J. D. MacKenzie *Science*, **2001**, *293*, 1119.

[6] I. O. Shklyarevskiy, P. Jonkheijm, N. Stutzmann, D. Wasserberg, H. J. Wondergem, P. C. M. Christianen, A. P. H. J. Schenning, D. M. de Leeuw, Z. Homovic, J. Wu, K. Müllen, J. C. Maan *J. Am. Chem Soc.* **2005**, *127*, 16233.

[7] M. Mas-Torrent, D. den Boer, M. Durkut, P. Hadley, A. P. H. J. Schenning, A. P. *Nanotechnology* **2004**, *15*, S265.

[8] P. Dyreklev, M. Berggren, O. Inganas, M. R. Andersson, O. Wennerstrom, T. Hjertberg *Adv. Mater.* **1995**, *7*, 43-45

[9] V. Cimrova, M. Remmers, D. Neher, G. Wegner *Adv. Mater.* **1996**, *8*, 146.

[10] G. Xu, Z. Bao, J. T. Groves *Langumir* **2000**, *16*, 1834.

[11] M. L. Swiggers, G. Xia, J. D. Slinker, A. A. Gorodetsky, G. G. Malliaras, R. L. Headrick, B. T. Weslowski, R. N. Shashidhar, C. S. Dulcey *Appl. Phys. Lett.* **2001**, *79*, 1300.

[12] O. Karthaus, H. Ringsdorf, V. V. Tsukruk, J. H. Wendorff *Langmuir* **1992**, *8*, 2279.

[13] N. Reitzel, T. Hassenkam, K. Balashev, T. R. Jensen, P. B. Howes, K. Kjaer, A. Fechtenkötter, N. Tchebotareva, S. Ito, K. Müllen, T. Bjornholm *Chem.-Eur. J.* **2001**, *7*, 4894.

[14] O. Y. Mindyuk, P. A. Heiney *Adv. Mater.* **1999**, *11*, 341.

[15] H. Sirringhaus, P. J. Brown, P. J.; R. H. Friend, M. M. Nielsen, K. Bechgaard, B. M. W. Langeveld-Voss, A. J. H. Spiering, R. A. J. Janssen, E. W. Meijer, P. Herwig, D. M. de Leeuw *Nature* **1999**, *401*, 685.

[16] H. Sirringhaus, R. J. Wilson, R. H. Friend, M. Inbasekaran, W. Wu, E. P. Woo, M. Grell, D. D. C. Bradley *Appl. Phys. Lett.* **2000**, *77*, 406.

[17] S. Nagamatsu, N. Tanigaki, Y. Yoshida, W. Takashima, K. Yase, K. Kaneto *Synth. Met.* **2003**, *137*, 923.

[18] X. L. Chen, A. J. Lovinger, Z. Bao, J. Sapjeta *Chem. Mater.* **2001**, *13*, 1341.

[19] V. C. Sundar, J. Zaumseil, V. Podzorov, E. Menard, R. L. Willett, T. Someya, M. E. Gershenson, J. A. Rogers *Science* **2004**, *303*, 1644.

[20] N. Karl *Synth. Met.* **2003**, *133–134*, 649.

[21] A. M. van de Craats, J. M. Warman, A. Fechtenkötter, J. D. Brand, M. A. Harbison, K. Müllen *Adv. Mater.* **1999**, *11*, 1469.

[22] W. Pisula, H. Tomovic, C. Simpson, M. Kastler, T. Pakula, K. Müllen *Chem. Mater.* **2005**, *17*, 4296.

[23] W. Pisula, Z. Tomovic, M. Stepputat, U. Kolb, T. Pakula, K. Müllen *Chem. Mater.* **2005**, *17*, 2641.

[24] W. Pisula, M. Kastler, D. Wasserfallen, T. Pakula, K. Müllen *J. Am. Chem. Soc.* **2004**, *126*, 8074.

[25] W. Pisula, A. Menon, M. Stepputat, I. Lieberwirth, U. Kolb, A. Tracz, H. Sirringhaus, T. Pakula, K. Müllen *Adv. Mater.* **2005**, *17*, 684.

[26] D. W. Breiby, O. Bunk, W. Pisula, T. I. Solling, A. Tracz, T. Pakula, K. Müllen, M. M. Nielsen *J. Am. Chem. Soc.* **2005**, *127*, 11288.

[27] A. Tracz, J. K. Jeszka, M. D. Watson, W. Pisula, K. Müllen, T. Pakula *J. Am. Chem. Soc.* **2003**, *125*, 1682.

[28] M. Kastler, W. Pisula, D. Wasserfallen, T. Pakula, K. Müllen *J. Am. Chem. Soc.* **2005**, *127*, 4286.

[29] A. M. van de Craats, J. M. Warman *Adv. Mater.* **2001**, *13*, 130.

[30] W. Pisula, Z. Tomovic, B. el Hamaoui, M. D. Watson T. Pakula, K. Müllen *Adv. Funct. Mater.* **2005**, *15*, 893.

[31] T. Q. Nguyen, I. B. Martini, J. Liu, B. J. Schwartz *J. Phys. Chem. B* **2000**, *104*, 237

[32] L. S. Yu, S. A. Chen *Synth. Met.* **2002**, *132*, 81.

[33] T. Kawase, T. Shimoda, C. Newsome, H. Sirringhaus, R. H. Friend *Thin Solid Films* **2003**, *438-439*, 279.

[34] T. W. Lee, O. Kwon, M. G. Kim, S. H. Park, J. Chung, S. Y. Kim, Y. Chung, J. Y. Park, E. Han, D. H. Huh, J. J. Park, L. Pu *Appl. Phys. Lett.* **2005**, *87*, 231106.

[35] C. J. Drury, C. M. J. Mutsaers, C. M. Hart, M., Matters, D. M. deLeeuw *Appl. Phys. Lett.* **1998**, *73*, 108.

[36] H. Fuchigami, A. Ysumura, H. Koezuka *Appl. Phys. Lett.* **1993**, *63*, 1372.

[37] A. Dodabalapur, Z. Bao, A. Makhija, J. G. Laquindanum, V. R. Raju, Y. Feng, H. E. Katz, J. Rogers *Appl. Phys. Lett.* **1998**, *73*, 142.

[38] P. F. Baude, D. A. Ender, M. A. Haase, T. W. Kelley, D. V. Muyres, S. D. Theiss *Appl. Phys. Lett.* **2003**, *82*, 3964.

[39] J. M.Crowley, N. K.Sheridon, L. Romano *Journal of Electrostatics* **2002**, *55*, 247.

[40] B. Comiskey, J. D. Albert, H. Yoshizawa, J. Jacobson *Nature* **1998**, *394*, 253.

[41] J. Jacobson, B. Comiskey, C. Turner, J. Albert. P. Tsao *IBM Systems Journal* **1997**, *36*, 457.

[42] http://www.sony.jp/products/Consumer/LIBRIE/

[43] F. Clemens, M. Wegmann, T. Graule, A. Mathewson, T. Healy, J. Donnelly, A. Ullsperger, W. Hartmann, C. Papadas *Adv. Engin. Mat.* **2003**, 5, 682.

[44] J. D. Watson, F. H. C. Crick *Nature* **1953**, *171*, 737.

[45] C. H. Lin, J. Tour *J. Org. Chem.* **2002**, *67*, 7761.

[46] D. T. Bong, T. D. Clark, J. R. Granja, M. R. Ghadiri *Angew. Chem. Int. Ed.* **2001**, *40*, 988.

[47] F. S. Schoonbeek, J. H. van Esch, B. Wegewijs, D. B. A. Rep, M. P. de Haas, T. M. Klapwijk, R. M. Kellogg, B. L. Feringa *Angew. Chem. Int. Ed.* **1999**, *38*, 1393.

[48] A. Guesquière, M. M. S. Abdel-Mottaleb, S. de Feyter, F. C. de Schryver, F. Schoonbeek, J. van Esch, R. M. Kellogg, B. L. Feringa, A. Calderone, R. Lazzaroni, J. L. Brédas *Langmuir* **2000**, *16*, 10385.

[49] R. I. Gearba, M. Lehmann, J. Levin, D. A. Ivanov, M. H. J. Koch, J. Barbera, M. G. Debije, J. Piris, Y. H. Geerts *Adv. Mater.* **2003**, *15*, 1614.

[50] M. L. Bushey, A. Hwang, P. W. Stephens, C. Nuckolls *Angew. Chem. Int. Ed.* **2002**, *41*, 2828.

[51] T. S. Balaban, A. Eichhöfer, J. M. Lehn *Eur. J. Org. Chem.* **2000**, 4047.

[52] J. J. van Gorp, J. A. J. M. Vekemans, E. W. Meijer *J. Am. Chem. Soc.* **2002**, *124*, 14759.

[53] R. E. Gillard, F. M. Raymo, J. F. Stoddart *Chem. Eur. J.* **1997**, *3*, 1933.

[54] A. Fechtenkötter, K. Saalwächter, M. A. Harbison, K. Müllen, H. W. Spiess *Angew. Chem. Int. Ed.* **1999**, *38*, 3039.

[55] A. Fechtenkötter, N. Chebotareva, M. D. Watson, K. Müllen *Tetrahedron* **2001**, *57*, 3769.

[56] J. Wu, M. D. Watson, K. Müllen *Angew. Chem. Int. Ed.* **2003**, *115*, 5329.

[57] S. Ito, M. Wehmeier, J. D. Brand, C. Kübel, R. Epsch, J. P. Rabe, K. Müllen *Chem. Eur. J.* **2000**, *6*, 4327.

[58] S. Ito, P. T. Herwig, T. Böhme, J. P. Rabe, W. Rettig, K. Müllen *J. Am. Chem. Soc.* **2000**, *122*, 7698.

[59] A. F. Thünemann, D. Ruppelt, C. Burger, K. Müllen *J. Mat. Chem.* **2000**, *10*, 1325.

[60] L. J. Prins, D. N. Reinhoudt, P. Timmerman *Angew. Chem. Int. Ed.* **2001**, *40*, 2382.

[61] W. Nernst *Z. Phys. Chem.* **1892**, *8*, 110.

[62] A. Werner *Liebigs Ann. Chem.* **1902**, *322*, 261.

[63] M. L. Huggins *Angew. Chem. Int. Ed. Engl.* **1971**, *10*, 147.

[64] W. M. Latimer, W. H. Rodebush *J. Am. Chem. Soc.* **1920**, *42*, 1419.

[65] J. D. Bernal, H. D. Megaw *Proc. R. Soc. London A* **1935**, *151*, 384.

[66] M. L. Huggins *J. Org. Chem.* **1936**, *1*, 407.

[67] P. Schuster, G. Zundel, C. Sandorfy, *The Hydrogen Bond: Recent Developments in Theory and Experiments*, Vol. 1 ± 3, North-Holland, Amsterdam, **1976**.

[68] P. A. Kollman, L. A. Allen *Chem. Rev.* **1972**, *72*, 283.

[69] *Monatsh. Chem.* **1999**, *130* (special issue, No. 8).

[70] G. A. Jeffrey, W. Saenger *Hydrogen Bonding in Biological Structures*; Springer-Verlag: Berlin, **1991**.

[71] S. Shinkai *Tetrahedron* **1993**, *49*, 8933.

[72] S. C. Zimmerman, B. F. Duerr *J. Org. Chem.* **1992**, *57*, 2215.

[73] D. Hadzi, W. J. Orville-Thomas, J. Tomasi, *Theoretical Treatments of Hydrogen Bonding*, Wiley, Chichester, **1997**.

[74] F. J. M. Hoeben, P. Jonkheijm, E. W. Meijer, A. P. H. J. Schenning *Chem. Rev.* **2005**, *105*, 1491.

[75] B. W. Laursen, K. Norgaard, N. Reitzel, J. B. Simonsen, C. B. Nielsen, J. A. Nielsen, T. Bjornholm, T. I. Solling, M. M. Nielsen O. Bunk, K. Kjaer, N. Tchebotareva, M. D. Watson, K. Müllen, J. Piris *Langmuir* **2004**, *20*, 4139.

[76] S. Kubowicz, U. Pietsch, M. D. Watson, N. Tchebotareva, K. Müllen, A. F. Thünemann *Langmuir* **2003**, *19*, 5036.

[77] A. F. Thünemann, S. Kubowicz, C. Burger, M. D. Watson, N. Tchebotareva, K. Müllen *J. Am. Chem. Soc.* **2003**, *125*, 352.

[78] N. Tchebotareva, X. Yin, M. D. Watson, P. Samori, J. P. Rabe, K. Müllen *J. Am. Chem. Soc.* **2003**, *125*, 9734.

[79] P. Samori, X. Yin, N. Tchebotareva, Z. Wang, T. Pakula, F. Jäckel, M. D. Watson, A. Venturini, K. Müllen, J. P. Rabe *J. Am. Chem. Soc.* **2004**, *126*, 3567.

[80] J. D. Brand, C. Kübel, S. Ito, K. Müllen *Chem. Mater.* **2000**, *12*, 1638.

[81] N. Tchebotareva, *phD thesis* **2003**, Mainz.

[82] T. Steiner *Angew. Chem. Int. Ed.* **2002**, *41*, 48.

[83] D. Wasserfallen, I. Fischbach, N. Chebotareva, M. Kastler, W. Pisula, F. Jäckel, M. D. Watson, I. Schnell, J. P. Rabe, H. W. Spiess, K. Müllen *Adv. Funct. Mater.* **2005**, *15*, 1585.

[84] E. D. Becker, in *Hydrogen-bonding*, Wiley, Chichester, **1996** Chap. 4, 2409.

[85] B. Berglund, R. W. Vaughan, *J. Chem. Phys.*, **1980**, *73*, 2037.

[86] S. P. Brown, I. Schnell, J. D. Brand, K. Müllen, H. W. Spiess, *Phys. Chem. Chem. Phys.*, **2000**, *2*, 1735.

[87] K. Schmidt-Rohr, H. W. Spiess, in *Multidimensional solid-state NMR and polymers*, Academic Press, London, **1994**.

[88] K. Saalwächter, H. W. Spiess, *J. Chem. Phys.*, **2001**, *114*, 5707.

[89] A. Stabel, P. Herwig, K. Müllen, J. P. Rabe, *Angew. Chem. Int. Ed.* **1995**, *34*, 1609.

[90] F. Jäckel, Z. Wang, M. D. Watson, K. Müllen, J. P. Rabe, *Chem. Phys. Lett.* **2004**, *387*, 372.

[91] F. Jäckel, M. D. Watson, K. Müllen, J. P. Rabe, *Phys. Rev. Lett.* **2004**, *92*, 188303.

[92] P. Samori, A. Fechtenkötter, F. Jäckel, T. Böhme, K. Müllen, J. P. Rabe *J. Am. Chem. Soc.* **2001**, *123*, 11462.

[93] I. Fischbach, T. Pakula, P. Minkin, A. Fechtenkötter, K. Müllen, H. W. Spiess, K. Saalwächter *J. Phys. Chem. B* **2002**, *106*, 6408.

4 "Supernaphthalene"

In contrast to the before mentioned example of inducing a higher intracolumnar order by hydrogen bonding, the focus can also be set upon larger aromatic systems.[1] Such an increase in disc size has already been achieved by covalently fusing units to phtalocyanines[2-5] or by a non-covalent self-assembly of disc segments.[6,7] Additionally the charge-carrier mobility is in close relation to the size of the aromatic core and larger π-areas are expected to lead to improved mobilities.[8] For photovoltaic applications a high extinction coefficient over a broad range of the spectrum is favorable, which can also be achieved by enlarging the aromatic core component.[8-10] In addition, the stronger π-interactions between the aromatic core components should yield an improved columnar stability and order.[11] At some critical sizes, it is believed that the materials adopt novel types of mesophases, where the tendency of the smaller molecules to tilt against the columnar axis will be replaced by a simple lateral offset and would lead to a graphite-like stacking.[12] Due to their different sizes and topologies, these compounds could also provide some valuable insights for the future development of the theoretical studies and understanding of the unique properties of PAHs and graphite.[13-17] However the strengthening of the π-interactions between the aromatic core components will also lead to a reduction of the solubility and the processability due to the stronger aggregation of the molecules. This requires of course efficiently solubilizing features primarily in terms of long alkyl chains in the corona of the aromatic entity.

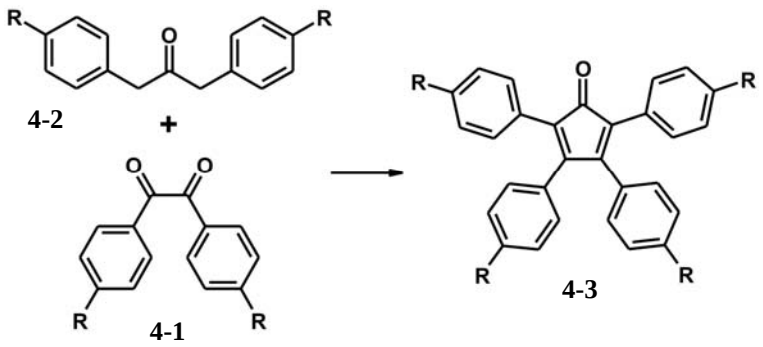

Figure 4-1: Typical Knoevenagel condensation of an alkylated benzil and a 1,3-diphenylacetone derivative to prepare an alkyl substituted tetraphenylcyclopentadienone compound.

As presented in the introduction of this thesis, several synthetic methods exist to provide a large variety of different PAHs.[18] In the group of Prof. Müllen a synthetic procedure was developed, whereby extended PAHs are mainly prepared by the initial

synthesis of large and defined oligophenylene precursor molecules, which can be achieved by a Diels-Alder cycloaddition of an ethinyl derivative with an appropriate tetraphenylcyclopentadienone (**4-3**).[19-23] The ethinyl derivatives are hereby easily accessible *via* a palladium catalyzed coupling of acetylene with bromo- or iodine substituted compounds under Hagihara-Sonogashira conditions[24] or even commercially available. The required alkylated tetraphenylcyclo-pentadienone building blocks on the other hand have to be most of the time specifically prepared by a Knoevenagel condensation.

The general conditions for the Knoevennagel reaction shown in Figure 4-1 imply the addition of a base to a mixture of a benzil (**4-1**) and a 1,3-diphenylacetone (**4-2**) derivative at elevated temperatures (50 °C). The reaction is complete within 25-40 minutes and can be usually worked up by column chromatography. In the subsequent step, the two building blocks, the tetraphenylcyclopentadienone (**4-3**) and the ethinyl derivative, are reacted in a Diels-Alder cycloaddition, yielding the before mentioned oligophenylene precursor.

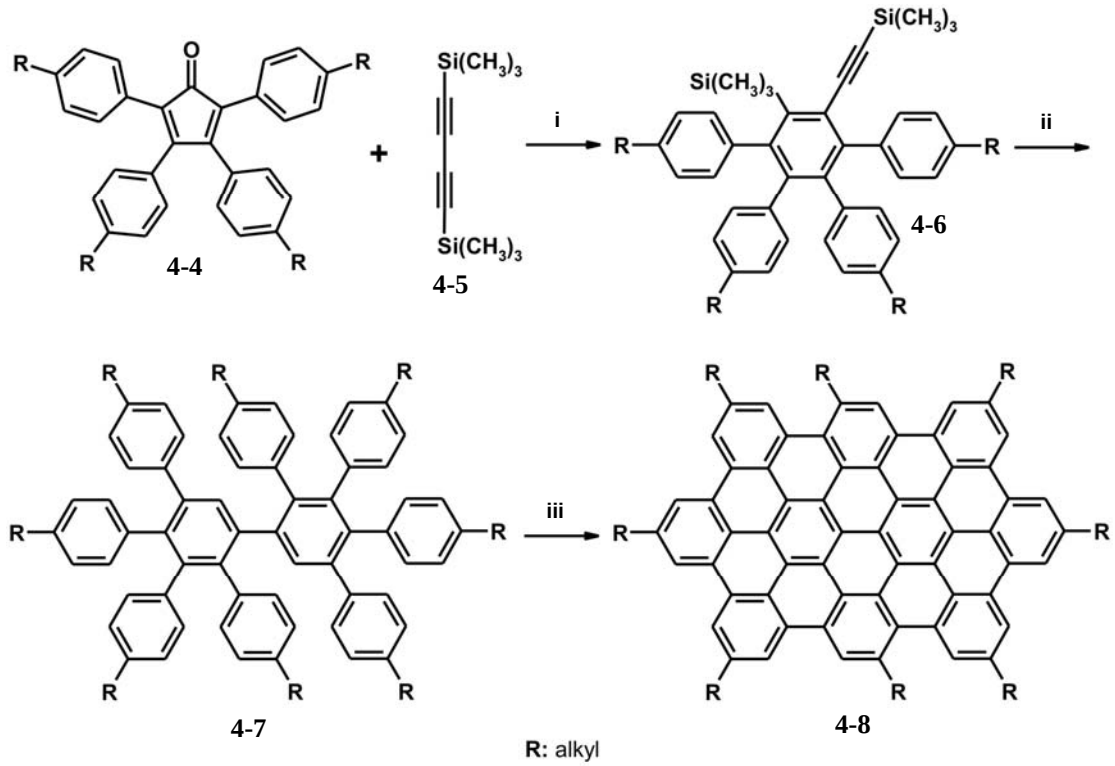

Figure 4-2: Synthesis of the alkylated PAH **4-5**: *i*: *o*-xylene 200 °C, 8 h; *ii*: n-Bu_4NF, NH4F, THF, rt, 2d; *iii*: *o*-xylene, 200 °C, 8h; *iv*: $FeCl_3$, CH_2Cl_2, rt, 3h.

Previously, oligophenylene precursors were finally planarized by an intramolecular Scholl reaction[25] with aluminum(III)chloride and copper(II) trifluoromethanesulfonate in carbon disulfide. These conditions proved to be very successful for the cyclodehydrogenation of non-alkylated oligophenylene precursors. If however alkyl substituents were present, the reaction was accompanied by a Friedel-Crafts dealkylation or a rearrangement respectively, which led as a consequence to a diversity of products.[26] Therefore milder conditions were applied by M. Wehmeier et al.[27] by exchanging the Lewis acid aluminum(III)chloride with the weaker agent iron(III)chloride, which has been initially used by P. Kovacic for the efficient synthesis of *p*-polyphenylenes.[28-31] With the resulting mild conditions for the cyclodehydrogenation, it was possible to suppress the unwanted side-reactions.

An example synthesized by C. Simpson is presented in Figure 4-2.[32] The synthesis starts by preparing compound **4-6** by a Diels-Alder cycloaddition of the 1,4-bis-trimethylsilanyl-buta-1,3-diyne (**4-5**) with an alkylated tetraphenylcyclopentadienone derivative (**4-4**) and a subsequent removal of the trimethylsily-groups under basic conditions. The Diels-Alder reaction at 250 °C in diphenylether yields the oligophenylene precursor **4-7**, which was planarized with $FeCl_3$ dissolved in dry nitromethane and dichloromethane at room temperature.

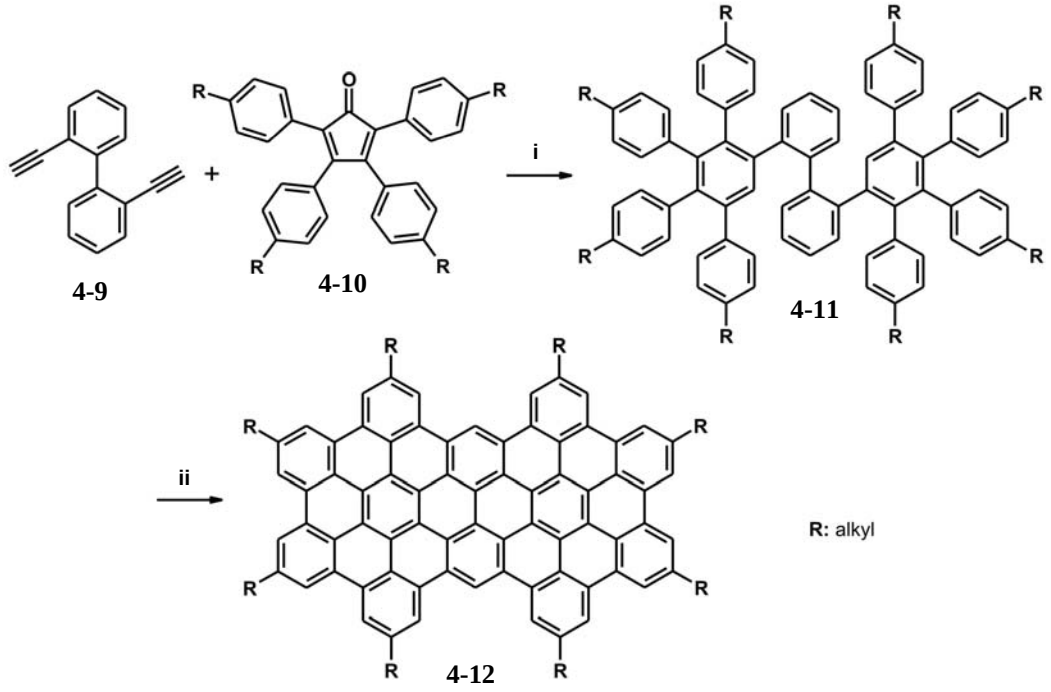

Figure 4-3: Straightforward synthesis to the extended PAH C72 (**4-12**): *i:* diphenylether, 250 °C, 8h; *ii:* : $FeCl_3$, CH_2Cl_2, rt.

An analoguous approach was used in this thesis for the synthesis towards an extended PAH, shown in Figure 4-3. In this case, it is also possible to introduce a diversity of alkyl chains at the rim of the aromatic core by using alkylated tetraphenylcyclopentadienone derivatives.

Derivatives of the compound **4-12** have already been prepared by M. Müller and M. Wehmeier.[19,33] In their work however no studies have been undertaken to determine the supramolecular properties of these materials, such as film formation or the determination of the self-organization in the bulk. This thesis tended to develop as a first step an improved synthesis for such compounds, as for the subsequent studies of the supramolecular behavior a sufficient amount of material was a prerequisite.

4.1 Synthesis

4.1.1 2,2'-Diethinylbiphenyl

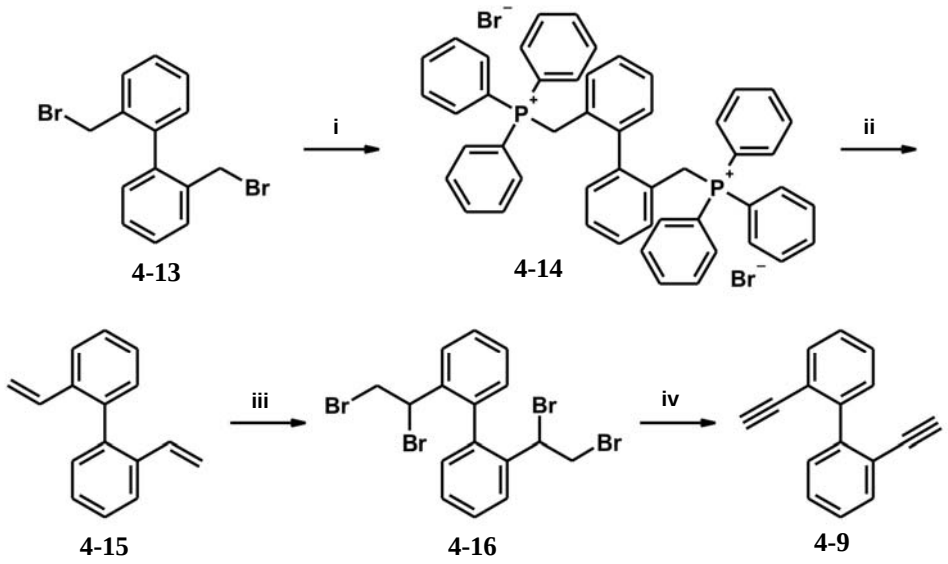

Figure 4-4: Synthesis of 2,2'-diethynylbiphenyl (**4-9**) according to M. Müller: *i:* $P(C_6H_5)_3$, DMF, 150 °C, 99%; *ii:* $(CH_2O)n$, EtONa, EtOH, 25 °C, 87%; *iii:* Br_2, $CHCl_3$, -20-0 °C, 99%; *iv:* KOtBu, THF, -20-25 °C, 91 %.

The ethynyl building block **4-9** has already been synthesized by M. Müller by the route shown in Figure 4-4 and according to a literature known procedure.[34] The commercially available 2,2'-dibromomethylbiphenyl (**4-13**) was converted under standard conditions to the 2,2'-bis[triphenylphosphonio]biphenyldibromid (**4-14**). A

double Wittig reaction of the bis(triphenyl-phosphonium)salt with formaldehyde yielded the 2,2'-divinylbiphenyl (**4-15**), which was brominated to give 2,2'-bis(dibromomethyl)biphenyl (**4-16**). In the final step the 2,2'-bis(dibromomethyl)-biphenyl (**4-16**) reacted under strong basic conditions in a fourfold elimination reaction to the product 2,2'-diethynylbiphenyl (**4-9**).

Even though the yields of the single steps are not lower than 87 %, it is obvious that the number of necessary steps should be reduced to gain the important building block (**4-9**) on a multigram scale. Therefore several synthetic routes have been examined (Figure 4-5). The palladium catalyzed Sonogashira-Hagihara reaction,[24] starting from the commercially available 2,2'-dibromobiphenyl (**4-17**) and trimethylsilylacetylene, promised a straightforward route towards a multigram preparation of 2'2'-bis[(trimethylsilyl)ethynyl)biphenyl (**4-19**). The subsequent treatment with a base to remove the trimethylsilyl groups would yield the 2,2'-diethynylbiphenyl (**4-9**). With this reaction however, the 2'2'-bis[(trimethylsilyl)-ethynyl)biphenyl (**4-19**) could not be prepared.

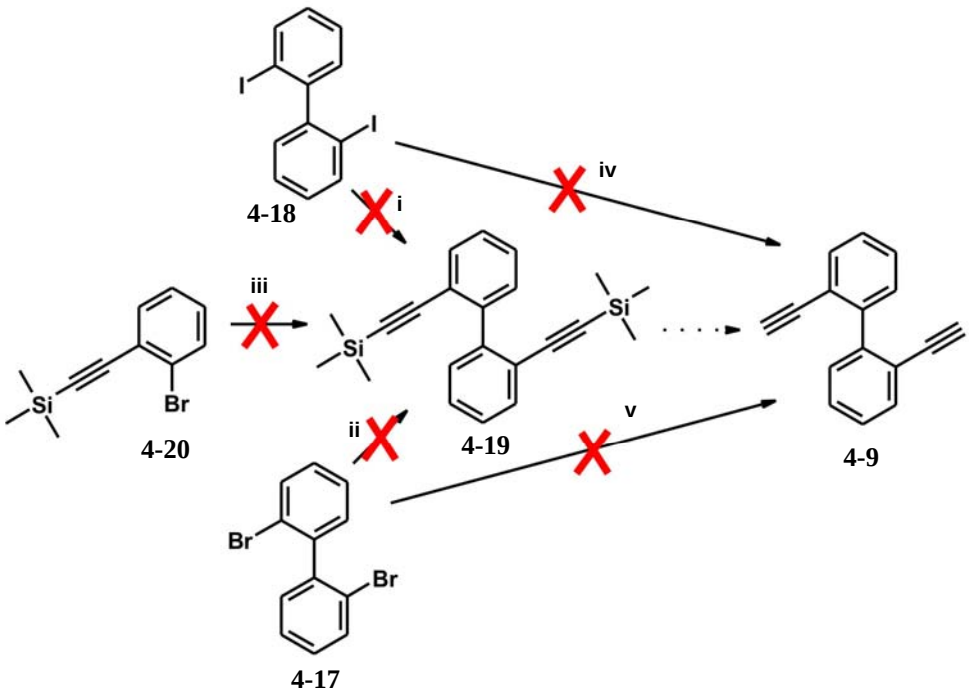

Figure 4-5: Synthetic approaches towards 2,2'-diacetylenebiphenyl (**4-9**). *i, ii:* $Pd(PPh_3)_2Cl_2$, trimethyl-silylacetylene, CuI, piperidine, 25-60 °C; iii: $Ni(COD)_2$, COD, 2,2'-bipyridine, THF, 80 °C or DMF, H_2O, isopropanol, K_2CO_3, $Pd(OAc)_2$, n-Bu_4NBr, 115 °C; *iv, v:* ethynyltri-n-butyltin, THF, $Pd(PPh_3)_4$, 25-80 °C.

Instead, the reaction stopped after the substitution of only one halogen. In the progress of the reaction the 2-bromo-2'-[(trimethylsilyl)ethynyl]-biphenyl could not be reacted further, instead the intermediate started to loose the bromine to yield the mono-substituted 2-[(trimethylsilyl)ethynyl]-biphenyl.

It is known that the iodine derivatives of aromatic compounds are more reactive in the Sonogashira-Hagihara reactions than their brominated counterparts. Therefore, 2,2'-diiodobiphenyl (**4-18**) was prepared according to a literature procedure by lithiation and addition of elementary iodine, dissolved in ether. Afterwards the compound was subjected to the same conditions as the 2,2'-dibromo-biphenyl (**4-17**). Despite the higher reactivity of the iodine no product was formed except for the already determined mono-reacted side-product 2-[(trimethylsilyl)ethynyl]-biphenyl.

As the product could not be gained on this route, an aryl-aryl coupling of the 2-[(trimethylsilyl)ethynyl]bromobenzene (**4-20**) according to Yamamoto[35,36] was tried. In this case no conversion or even debromination could be observed even at different reaction temperatures and prolonged reaction times.

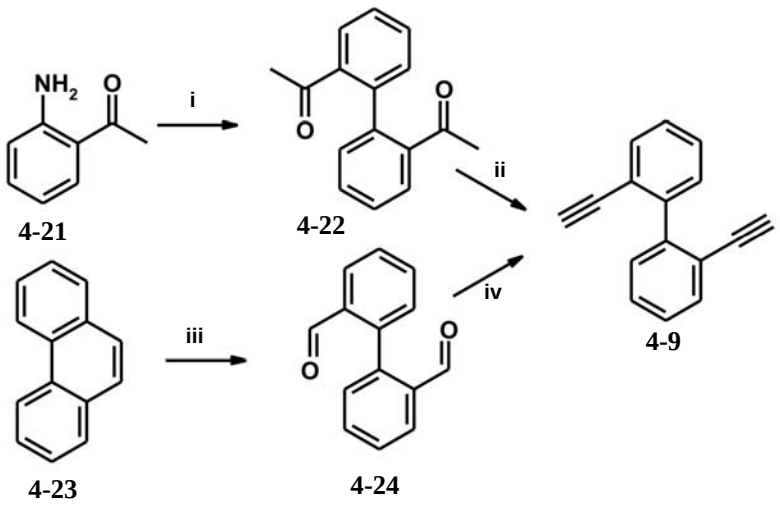

Figure 4-6: Convenient and straightforward two step synthesis of 2,2'-diethynylbiphenyl (**4-9**): *i:* HCl, H_2O, $NaNO_2$, $CuSO_4$, NH_3OHCl, NaOH, NH_3; *ii:* diisopropylamine, n-BuLi, THF, diethylchlorophosphate, -78-25 °C, 22%; *iii:* O_3, CH_2Cl_2, NaI, acetic acid; *iv:* n-BuLi, hexane, diisopropylamine, Me_3SiCHN_2, THF, -78 °C, 57%.

One reason for the breakdown of the reaction in the Sonogashira-Hagihara case could be the steric demand of the trimethylsilyl groups. Therefore a Stille-coupling[37-40] of either the 2,2'-dibromobiphenyl (**4-17**) or the 2,2'-diiodobiphenyl (**4-18**) and ethynyltri-n-butyltin was examined. In this case a smaller steric demand of the ethynyl derivative arose. Nevertheless, also in this case no conversion could be observed even at elevated

temperatures. As the problems were probably related to the palladium catalyst cycle, other alternatives were considered, which did not require a palladium-catalyzed step.

In the first example presented in Figure 4-6, 1-(2'-acetyl-biphenyl-2-yl)-ethanone (**4-22**) was prepared according to literature and afterwards treated in close relation to an already published procedure by Tour et al[42] to yield 2,2'-diethynylbiphenyl (**4-9**) with 22 % yield. Two main arguments were crucial for the search towards another route. On one hand the diazotation reaction and the workup, including a water-vapour distillation, was rather time consuming and on the other the very low yields of the second step. Therefore, the second route presented several advantages. For the first step, commercially available phenanthrene (**4-23**) could be oxidized in a straightforward manner with ozone and the conversion to the 2,2'-diethynyl-biphenyl (**4-9**)[43] could also be achieved with 57% yield. This procedure proved to be suitable for the effective preparation of 2,2'-diethynylbiphenyl (**4-9**) on a multi-gram-scale.

4.1.2 Tetraphenylcyclopentadienone Derivatives

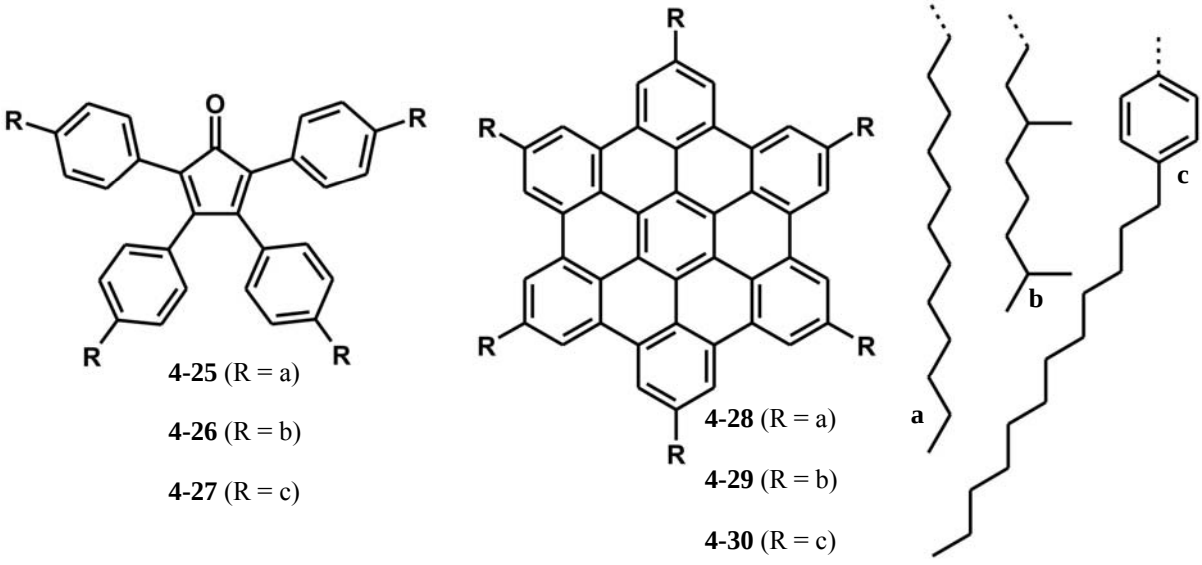

Figure 4-7: HBC and tetraphenylcyclopentadienone derivatives substituted with *n*-dodecyl- (**4-25**)(**4-28**), 3,7-dimethyloctyl- (**4-26**)(**4-29**) and dodecyl-phenyl chain (**4-27**)(**4-30**).

As presented above, the second crucial building block were the tetraphenylcyclopentadienone derivatives. With these compounds, it is possible to introduce a wide variety of different alkyl substituents into the rim of the future PAH. The used tetraphenylcyclopentadienone will show a strong influence upon the resulting material in such a sense, as the properties of the PAHs, like their liquid-crystalline

behavior, solubility and processability are strongly dependent upon the used alkyl chain.[12] For comparing the resulting compounds with HBC systems that were already studied extensively and could be used as a basis, the choice fell onto three different alkyl chains (Figure 4-7).

In the case of hexasubstituted HBCs, the dodecyl-phenyl alkyl chain (**4-30**) showed an impressive effect upon the properties of the material with respect to its charge-carrier mobility values and the use in photovoltaic devices.[41] In addition, the compound was liquid-crystalline at room temperature and exhibited a high solubility.[44] As the solubility is anyway expected to be reduced for a larger aromatic core component, this highly solubilizing effect of the dodecyl-phenyl substituents is desirable and it allows a direct comparison of the novel material with the well investigated HBC derivative (**4-30**).[12,41-54] The 3,7-dimethyl-octyl chain was already used and studied extensively for HBC chemistry (**4-29**), too.[12,46,47,49,55-62] Due to the chirality of this alkyl entity the alkyl chains did not easily crystallize and therefore a significantly improved solubility was observed also in this case, while a high supramolecular ordering was retained.[62] Moreover, it was possible to reduce the thermal transition to the liquid-crystalline mesophase to 80 °C compared to the *n*-dodecyl substituted HBC analogue (**4-28**) (107 °C). This effect is also expected to occur for PAHs with larger aromatic moieties and the resulting material should show an improved thermal processability by zone crystallization (Appendix C) to gain highly ordered films.

The *n*-dodecyl chain showed in contrast to the other two substituents a reduced solubilizing effect. In the HBC case (**4-28**) this reduced solubility turned the material into a candidate for being processed by zone-casting techniques (Appendix B), which require compounds that show a distinct preaggregation in solvents. Therefore, it is likely that the three different alkyl chains presented above would cover a wide range of possible material properties for the C72 (**4-12**) derivatives, as for the HBCs analogues these alkyl substituents led on one hand to thermal as well as to solution processable materials.

For the synthesis of the dodecyl-phenyl substituted C72 (**4-46**) derivative, the simplest approach towards the necessary tetraphenylcyclopentadienone building block (**4-27**) was a Suzuki-coupling[63] of 1,4-dodecylphenylboronic acid **4-38** with the commercially available 1,2-bis-(4-bromo-phenyl)-ethane-1,2-dione (**4-31**) and 1,3-bis-(4-bromo-phenyl)-propan-2-one (**4-33**) to receive the corresponding substances for the synthesis of the tetraphenylcyclopentadienone derivative (**4-27**).

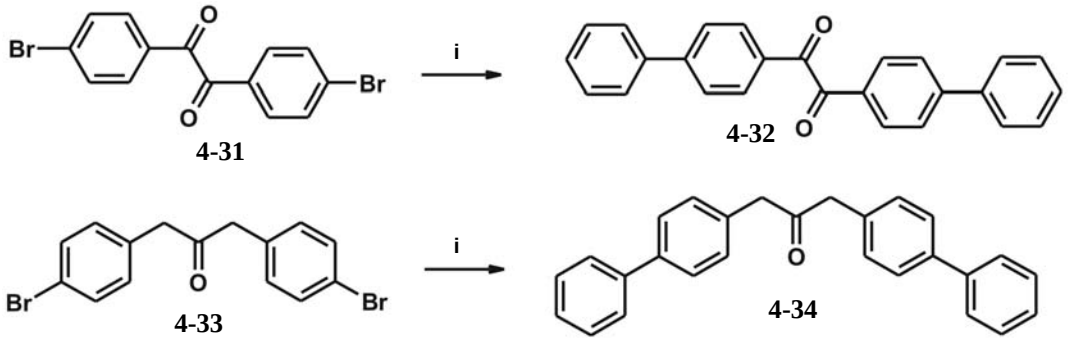

Figure 4-8: Synthesis of model compounds **4-32** and **4-34** *via* Suzuki coupling. *i:* phenylboronic acid, K_2CO_3, $Pd(PPh_3)_4$, toluene, H_2O, EtOH, 80 °C, 84-85%.

To ensure however that 1,2-bis-(4-bromo-phenyl)-ethane-1,2-dione (**4-31**) and 1,3-bis-(4-bromo-phenyl)-propan-2-one (**4-33**) can be used in this procedure, the reaction was tested in a model reaction with commercially available phenylboronic acid, whereby the compounds **4-32** and **4-34** (Figure 4-8) could be obtained in good yields. After this proof of principle, the multistep preparation of the two corresponding derivatives (**4-39**) and (**4-40**) was accomplished as described in Figure 4-9.

After the straightforward preparation of (4-bromo-phenyl)-trimethylsilane (**4-36**) according to literature known procedures by using the commercially available 1,4-dibromobenzene (**4-35**),[64] the compound was subjected to a palladium catalyzed Suzuki coupling with preliminary hydroborated 1-dodecene to prepare the 1-trimethylsilyl-4-dodecylbenzene (**4-37**). The trimethylsilyl substituent was then replaced by a boronic acid group by treating (**4-37**) with BBr_3 and by a subsequent quenching of the reaction with water, which yielded the boronic acid derivative (**4-38**).[65] This compound (**4-38**) could not only be used in the following Suzuki-type cross-coupling reaction with 1,2-bis-(4-bromo-phenyl)-ethane-1,2-dione (**4-31**) or 1,3-bis-(4-bromo-phenyl)-propan-2-one (**4-33**) but also with 4,4'-dibromodiphenylacetylene, which afforded a simplified procedure towards the diphenylacetylene derivative (**7-1**) for the synthesis of the important dodecylphenyl substituted HBC (**4-30**) (Appendix D).[12,41-54] After the preparation of the two compounds (**4-39**) and (**4-40**), the two substances were combined in a Knoevennagel condensation reaction to gain the required tetraphenyl-cyclopentadienone building block (**4-27**) in 72% yield.

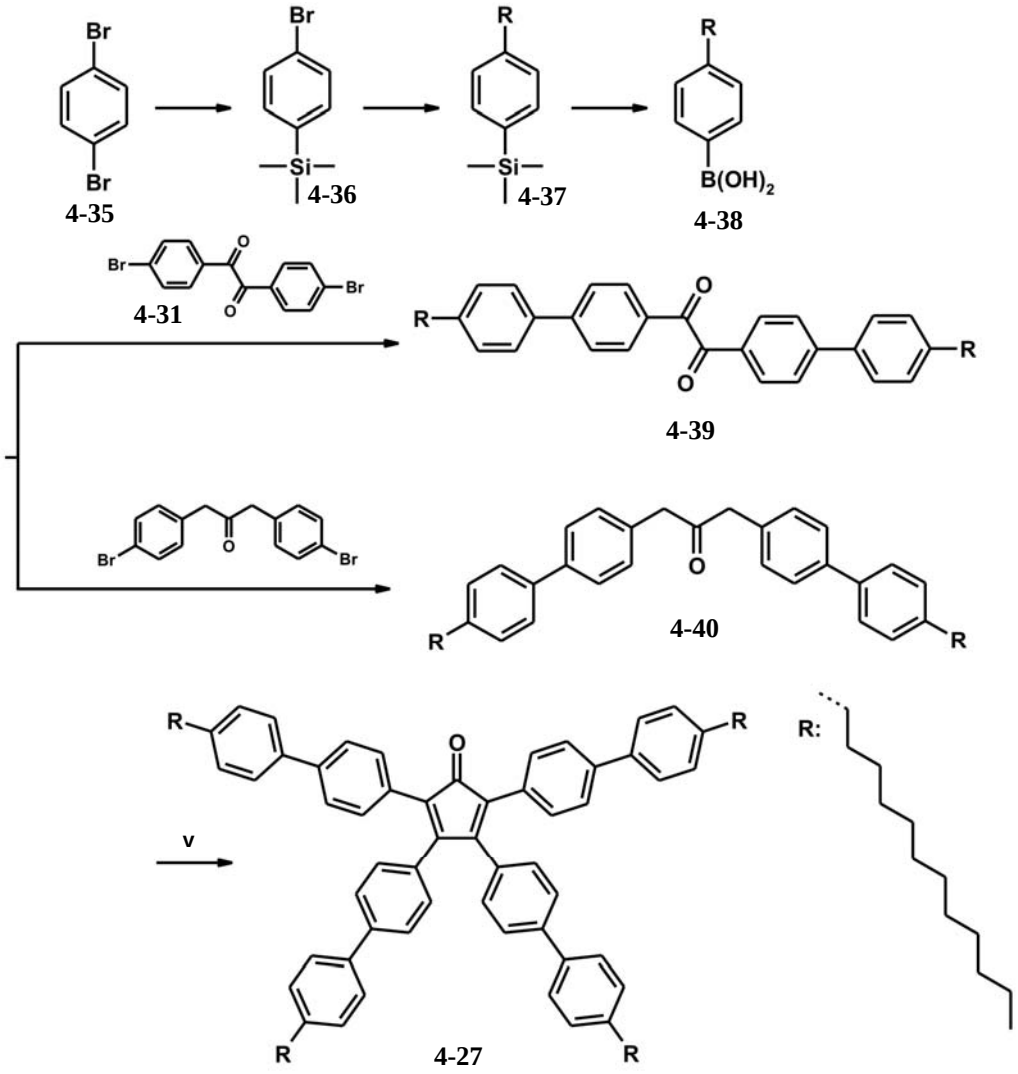

Figure 4-9: Synthesis of the tetraphenylcyclopentadienone derivative (**4-27**): i: n-BuLi, ether, TMS-Cl, -78-25 °C, 95%; ii: 1-dodecene, 9-BBN, NaOH, $Pd(dppf)Cl_2$, 25 °C,88%; iii: BBr_3, CH_2Cl_2, H_2O, 25 °C, 90%.; iv: t-BuOH, n-Bu_4NOH, 80 °C, 72%.

4.1.3 Intramolecular Cyclodehydrogenation

Remarks to the nomenclature of extended PAHs:

The official IUPAC nomenclature of the extended PAH **4-44** *is "2'',5'',8'',12'',15'',18'',21'',25''-Octa-(dodecyl)-hexabenzo-[jk,mn,pq,st: 3,4:9,10]-phen-antro[1',10',9',8':5,6,7,8]perylo-[2,11,12,11-bcdef]ovalene" (see Appendix E). It is obvious that such names are too long to be of any practical use. Therefore the extended PAHs are named according to their number of carbons in the aromatic core in combination with an abbreviation of the substituted alkyl chains and their number in the*

corona of the aromatic entity. For example the name of compound **4-44** *will become C72-(C*$_{12}$*)*$_8$.

After the preparation of the building blocks, 2,2'-diethynylbiphenyl (**4-9**) was reacted with the tetraphenylcyclopentadienone derivatives (**4-25**, **4-26** and **4-27**) in a Diels-Alder cycloaddition to yield the corresponding oligophenylenes (**4-41**), (**4-42**) and (**4-43**). In general, for the subsequent planarization the oligophenylene precursors were dissolved in dry dichloromethane, while iron(III)chloride dissolved in nitromethane was quickly added. During the whole reaction an argon flow was continuously led through the solution to expel the formed HCl and to suppress chlorination of the product, which is a possible side-reaction under these conditions. This can be easily understood as in this single final step 24 hydrogens have to be removed, forming twelve new bonds, which of course sets the demands for the efficiency of every reaction step very high. Also other conditions are possible,[25] however the beforementioned method with iron(III)chloride proved to be the most successful.

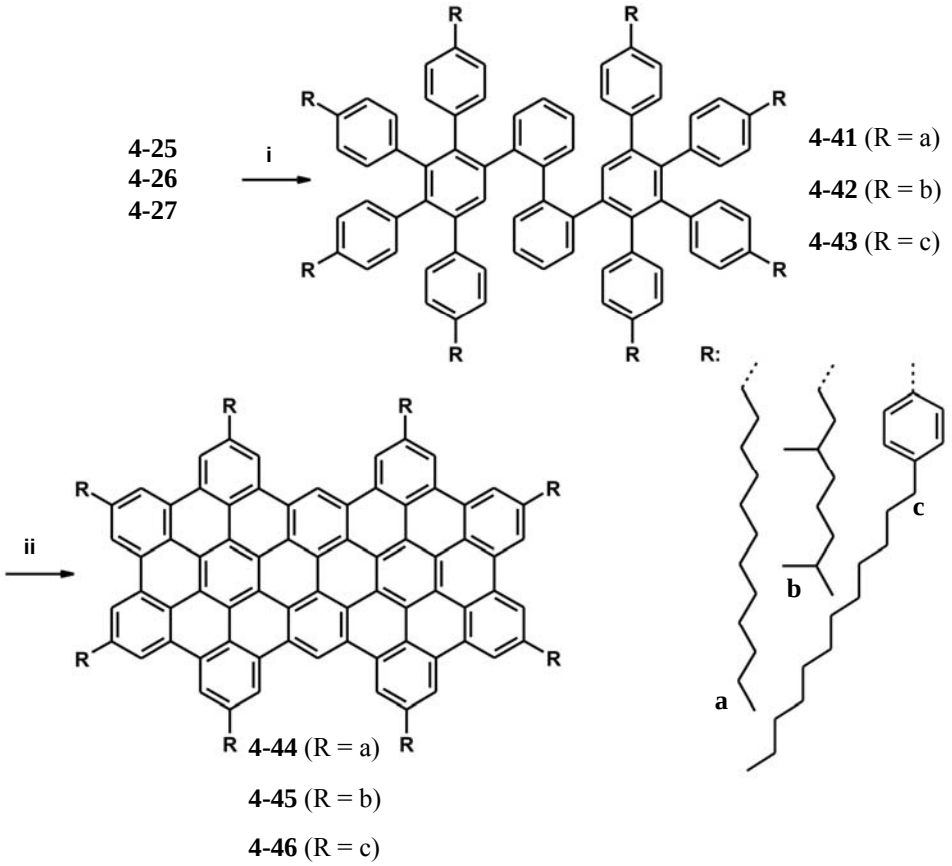

Figure 4-10: Synthesis of the three C72 derivatives C72-(C$_{12}$)$_8$ (**4-44**), C72-(C$_{8,2}$)$_8$ (**4-45**) and C72-(Ph-C$_{12}$)$_8$ (**4-46**). *i:* diphenylether, 2,2'-diethynylbiphenyl, 250 °C, 8h; *ii:* $FeCl_3$, CH_3NO_2, CH_2Cl_2.

The cyclodehydrogenation of the oligophenylene precursors is the key step towards the preparation of the PAHs. For this reaction, a complete conversion of the starting material to the product is a prerequisite. A subsequent workup, except for a repetitive precipitation of the product, is tedious and most of the times futile due to the strong π-aggregation, which leads for example to a strong tailing of the material during column chromatography. Therefore, it is necessary to determine accurately the necessary conditions for the reaction, as an excess of the oxidant can lead to the chlorination of the final PAH, while too little of the reactant results in the formation of partially fused intermediates that cannot be easily separated from the product.

4.1.3.1 C72-($C_{8,2}$)$_8$

While for the cyclodehydrogenation of smaller oligophenylene precursors like hexaphenylbenzene derivatives towards HBCs require only 3.0 equivalents of iron(III)chloride per aryl-aryl bond formation and 25-40 minutes reaction time,[33] larger PAHs require for the same step far more oxidant and substantially longer reaction times. For a PAH consisting of an aromatic core with 96 carbon atoms, which has been extensively studied by Z. Tomovic, 5.0 equivalents for every aryl-aryl bond formation and 15 hours reaction time was necessary.[1]

Therefore, a broad range of possible reaction conditions were tested for the C72 derivatives. During each test reaction, samples were taken and quenched with methanol and analyzed by matrix assisted laser desorption-ionization time-of-flight mass spectrometry (MALDI-TOF MS), which is the main analytical method used to characterize large PAHs.[66] Due to the accuracy of this method, it is even possible to record the isotopic distribution of the analyzed compounds. Every compound exhibits its own isotope pattern because of the natural isotope abundance of the elements. This can be used to compare the theoretically calculated distributions with the ones found.

In fact, the reaction conditions determined for the even larger C96 case could not be correlated to the smaller C72 cases. By using the same conditions as for C96 even after 48 hours partially fused side-products were observed in the MALDI-TOF MS. Indeed a far higher amount of oxidant (8.0 equivalents per aryl-aryl bond formation) was required, but the reaction time could be reduced to 4 hours. According to the MALDI-TOF MS spectrum however, the chlorination of the final product was not as strong as observed for C96 even by applying these large amounts of oxidant.

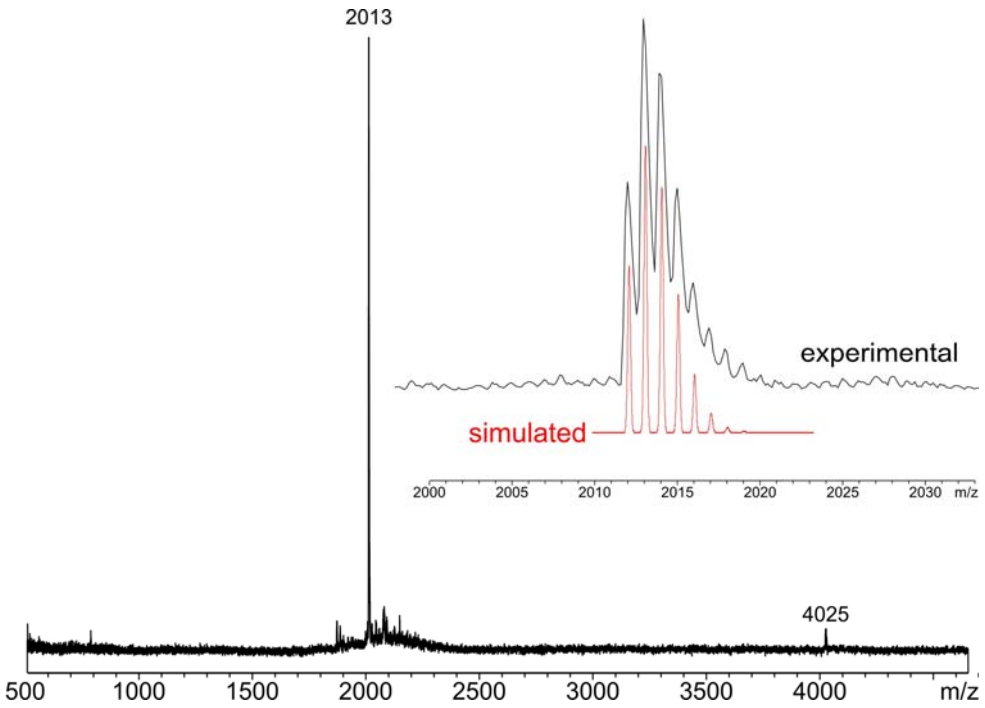

Figure 4-11: MALDI-TOF MS spectrum of C72-$(C_{8,2})_8$ (**4-45**); TCNQ matrix.

As can be seen in Figure 4-11 the simulated spectra of C72-$(C_{8,2})_8$ (**4-45**) fitted perfectly the experimental data and suggested a high degree of purity for this compound. The resulting dark red material showed a good solubility in standard organic solvents. One major disadvantage is the fact that it is very difficult to gain for PAHs, that are larger than HBCs, well resolved NMR spectra. One of the only cases which yielded well resolved NMR data was reported in the work of Simpson and Iyer[12,32,67] for a PAH, which is only slightly larger than HBC and contains eight highly solubilizing alkyl chains in its periphery (Figure 4-2). For example, the aromatic proton signals of the extended PAH C72-$(C_{8,2})_8$ (**4-45**) cannot be distinguished. Only two broad humps were observed in the aromatic region, which possibly originated from the different aromatic protons Figure 4-12. A lot of experiments were already undertaken to solve these issues, which included high temperature measurements and special solvent mixtures, like the addition of CS_2 to the deuterated solvent, which efficiently reduced π-mediated aggregation in other cases.[68] Nevertheless none of the experiments succeeded. This behavior can possibly be attributed to the aggregation in solution, which is leading to a diversity of different aggregate sizes and resulting in a broadening of the aromatic signals.

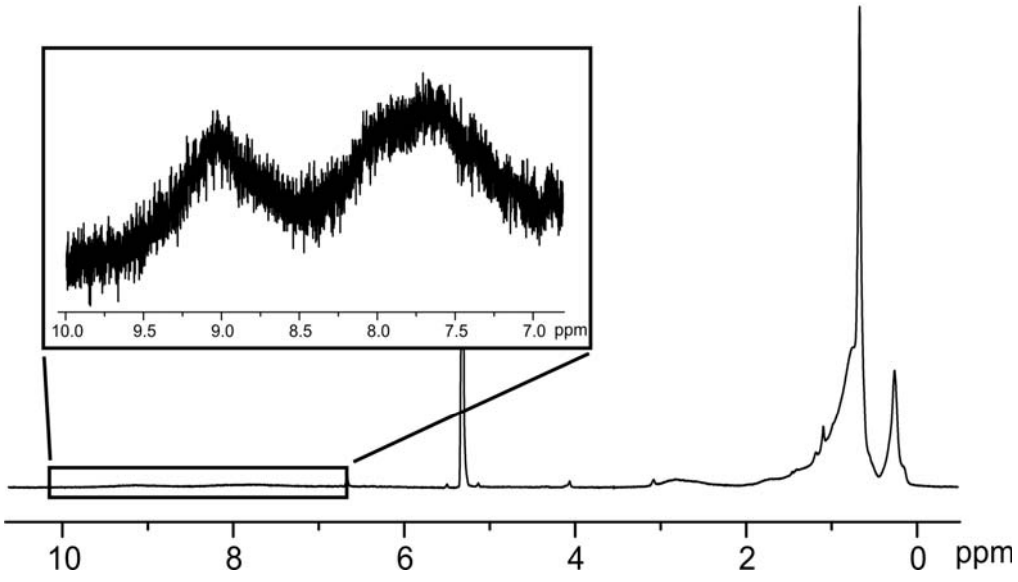

Figure 4-12: ^{1}H NMR spectrum of C72-$(C_{8,2})_8$ (**4-45**) in a CS_2/CD_2Cl_2 mixture at room temperature.

By taking into consideration the low symmetry of a molecule, as for the alkylated C72 derivatives (**4-44** to **4-46**), it is even more likely that the aromatic protons will experience different chemical environments. In addition, these aggregates might also be in a dynamic association and dissociation process and therefore broaden the spectra in the aromatic region even further. Another explanation is the presence of radicals. This did not seem plausible, as even after the addition of hydrazine the signal was not improved.

4.1.3.2 C72-$(C_{12})_8$

For the C72-$(C_{12})_8$ (**4-44**) derivative the same conditions were initially used as for the beforehand discussed C72-$(C_{8,2})_8$ (**4-45**). In this case however the 4 hours reaction time were not sufficient, as still some partially fused intermediates were found in the MALDI-TOF MS. Therefore, the reaction time was prolonged to 5 hours, which was according to the MALDI-TOF MS spectrum sufficient for the complete formation of the aryl-aryl-bonds, but resulted in a slight chlorination of the fully fused product, as can be seen in the Figure 4-13. Also in this case the material showed a reasonable solubility in standard organic solvents, but similar to the C72-$(C_{8,2})_8$ (**4-45**) (Figure 4-11) no resolved NMR spectrum could be recorded.

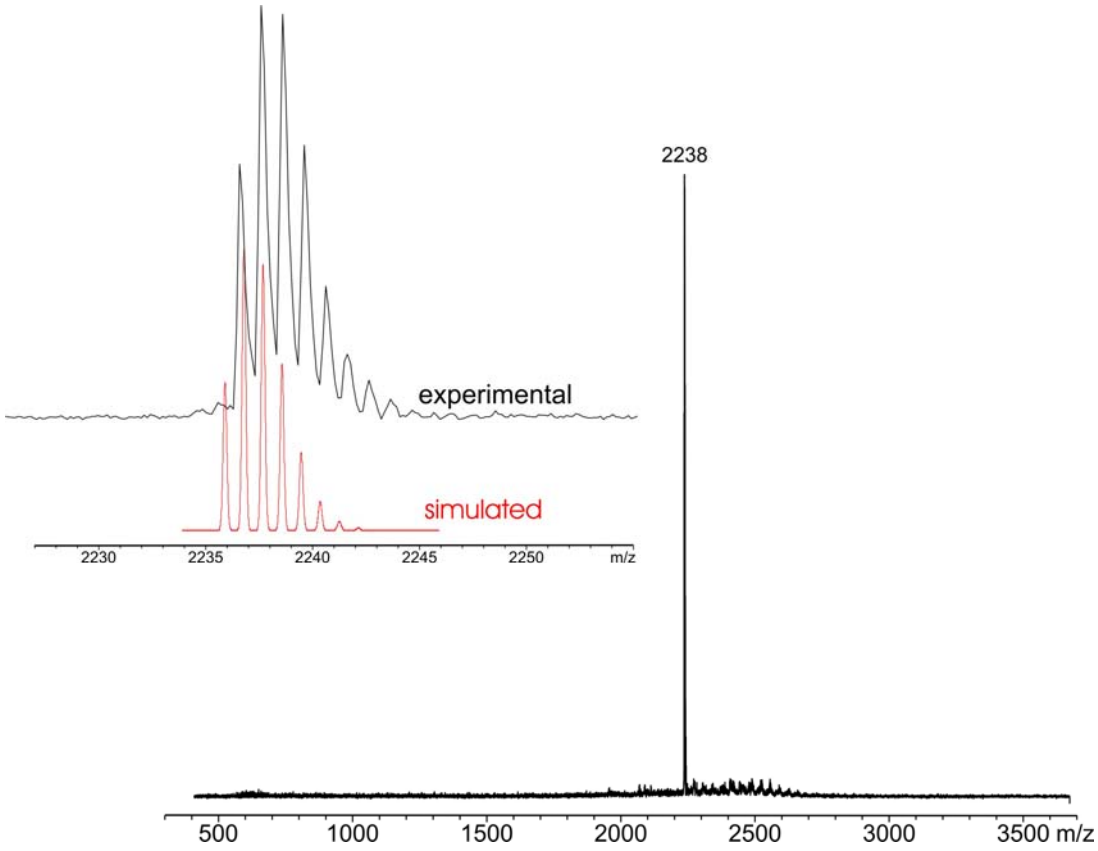

Figure 4-13: MALDI-TOF MS spectrum of C72-$(C_{12})_8$ (**4-44**); TCNQ matrix.

4.1.3.3 C72-(Ph-C_{12})$_8$

In Figure 4-14 the progressive cyclodehydrogenation towards C72-(Ph-C_{12})$_8$ (**4-46**) is shown. Even by adding excess iron chloride no product could be gained. As seen for the two former derivatives, a lowering of the reaction rate already took place between the C72-$(C_{8,2})_8$ (**4-45**) and the C72-$(C_{12})_8$ (**4-44**) case. At this point, it seemed that the alkyl substituents exerted a decisive influence onto the overall reaction rate of the cyclodehydrogenation. This proposition could however not be confirmed as only an analytical method like NMR spectroscopy could give sufficient indications about the quantification of the product and the side-products. It is nevertheless true that for the C72-$(C_{8,2})_8$ (**4-45**) derivative substantially less time was necessary to gain reasonable MALDI-TOF MS spectra.

From the HBC derivatives (**4-28**), (**4-29**) and (**4-30**) it is known that these three alkyl chains provide different degrees of solubility. For example the 3,7-dimethyloctyl alkyl chain was initially introduced in the HBC chemistry not only to achieve compounds with a higher solubility, but moreover that additionally have a lower transition temperature to the mesophase and the isotropic state. The *n*-dodecyl substituted HBC (**4-28**) on the

other hand showed a lower solubility than the derivative with six 3,7-dimethyloctyl chains (**4-29**) and also in the thermal behavior some differences were observed.[12]

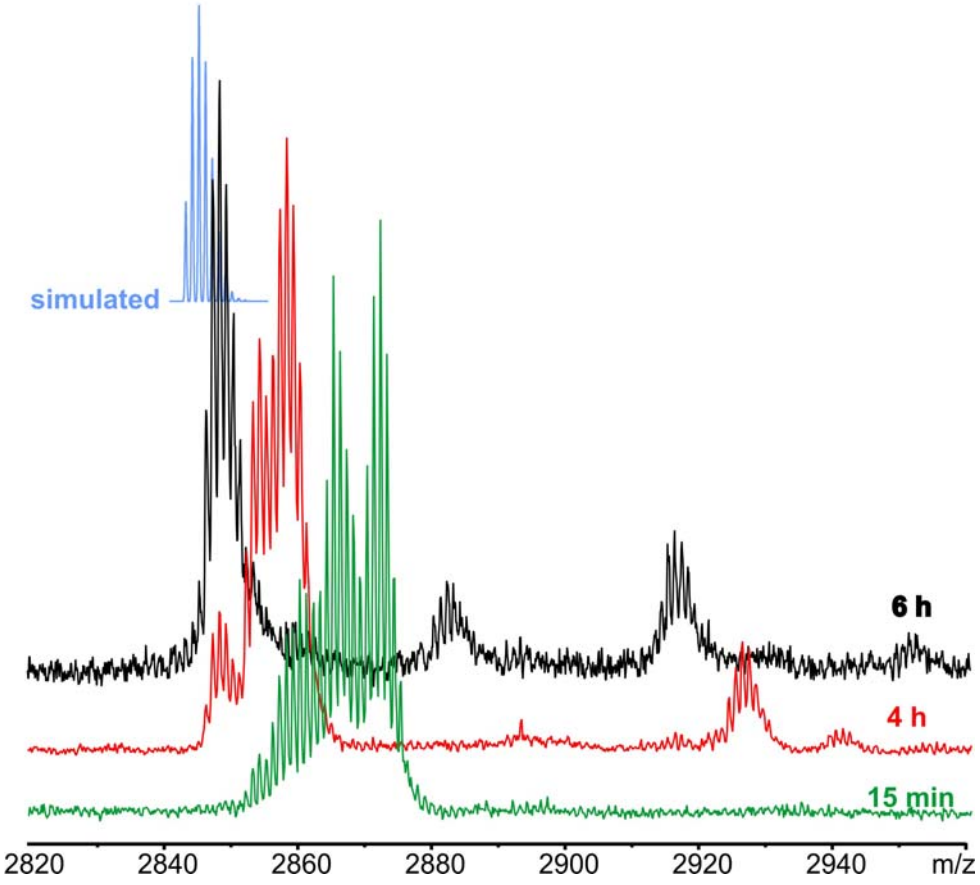

Figure 4-14: Time-dependent MALDI-TOF MS spectra of C72-(Ph-C_{12})$_8$ (**4-46**).

The reason for the different reactivities could indeed lie within the different degree of solubility. For C72-($C_{8,2}$)$_8$ (**4-45**) for example the highly solubilizing alkyl chain could lead to a better solubility of the partially closed side-products and making them accessible to further cyclodehydrogenation steps. For C72-(C_{12})$_8$ (**4-44**) on the other hand, the limited solubility exerted by the dodecyl-chains is maybe not sufficient to keep the partially closed intermediates long enough in solution to ensure a smooth conversion. This argumentation is however highly speculative and can also not be proved, as no precise analytical data is available.

An additional curious fact was, that between the batches of material obtained in the C72-($C_{8,2}$)$_8$ (**4-45**) and the C72-(C_{12})$_8$ (**4-44**) case, a limited reproduciblity occurred, for example regarding the macroscopic properties of C72-(C_{12})$_8$. Nevertheless the MALDI-TOF MS spectra indicated no differences. Not all of the C72-(C_{12})$_8$ (**4-44**) batches showed a comparable solubility and consistency. While some batches were well soluble

in common organic solvents and exhibitited a wax like appearance, others were far more crystalline and less soluble. Unfortunately, at this point no other, more detailed informations were available than those obtained by the MALDI-TOF MS spectra. As these deviations could not be satisfactorily explained on the basis of these analytical data, a closer investigation of the C72-$(C_{12})_8$ (**4-44**) batches was accomplished.

4.2 Closer Investigation on C72-$(C_{12})_8$

4.2.1 UV/vis

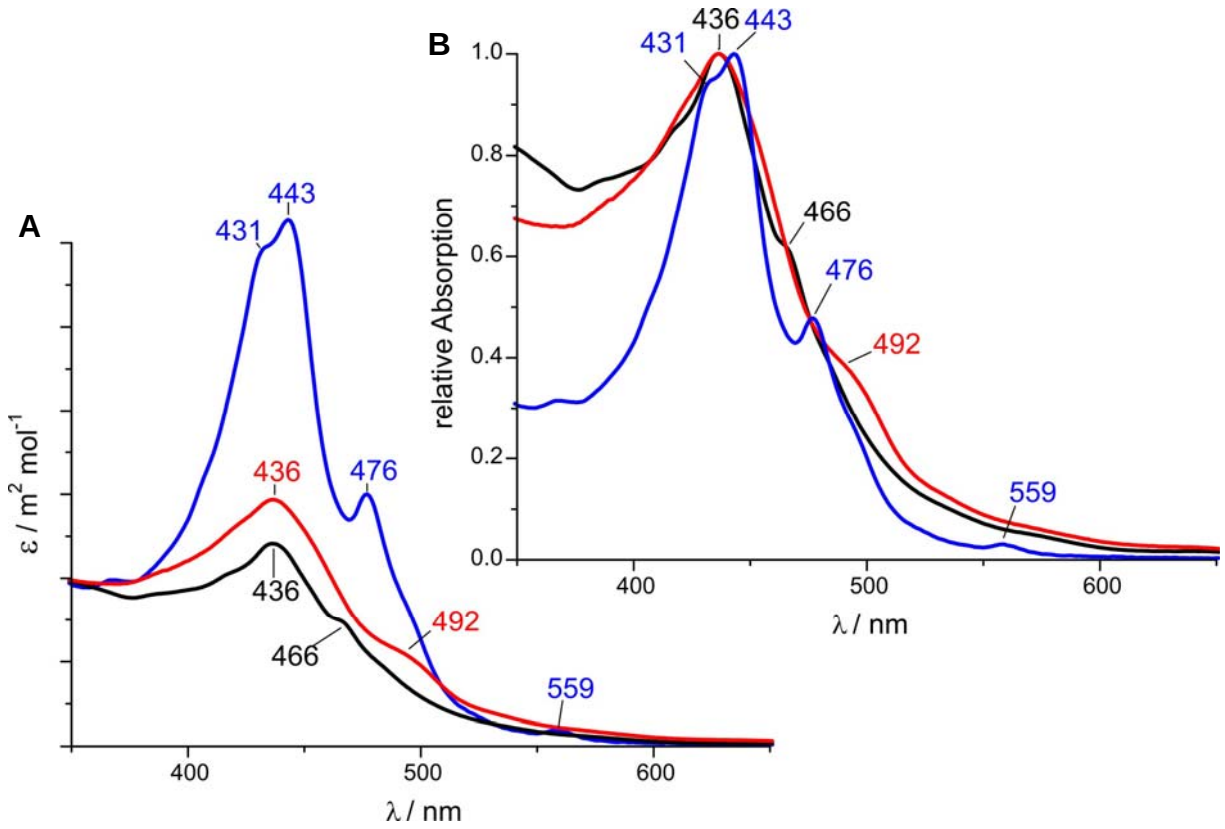

Figure 4-15: UV/vis of different batches of C72-$(C_{12})_8$ (**4-44**). **A**) according to extinction coefficients and **B**) normalized to relative maximum absorption.

An interesting feature between the batches of C72-$(C_{12})_8$ (**4-44**) were the differences in the UV/vis. In Figure 4-15A/B one can see the UV/vis absorption spectra of three different batches of C72-$(C_{12})_8$ (**4-44**). The same concentration was used in all three cases. From Figure 4-15A it becomes clear that already the molar extinction coefficients of these batches differed by a factor of three. In Figure 4-15B, the spectra were

normalized with respect to their maximum absorption value. By comparing the three curves, it becomes clear that not only the molar extinction coefficients were different, but also the position of the bands. This is already obvious for the main absorption peak, which shifted from 436 nm to 443 nm. The dilemma became even clearer by the consideration of the absorption bands at longer wavelengths next to the main absorption peaks. In one case, the band is found at 466 nm (black), in the other two cases, it is situated at 476 nm in combination with a higher resolution (blue) and at 492 nm (red) respectively.

However, the effects exerted from possible aggregation effects are difficult to determine, especially when one considers the small but existing differencies during the workup procedures. There are several possible explanations for this phenomena. On one hand, it could be due to a slightly different treatment or temperatures leading to a change in aggregation of the compound. Therefore, it could not be concluded at this stage whether these features originate from impurities or simply from the solution, aggregation properties and the history of the treatment of the investigated material.

4.2.2 HPLC

One method to determine if impurities are present is high pressure liquid chromatography (HPLC), which is a type of liquid chromatography that has been optimized to provide rapid, high resolution separations. In addition, HPLC also ranks as one of the most sensitive analytical procedures and is unique in a sense that it easily copes with multi-component mixtures.

The experiment was performed under standard conditions with a preparative column and a THF/water gradient as eluent, which already proved its versatility for other large PAHs.[69] At least three different compounds were identified, as can be seen in the amplified chromatogram in the inset of Figure 4-16A. Hereby, the small signals at shorter retention times between 20 and 22 min. are not even considered. Although the differences in the retention times are rather small, it was clear that at least three different compounds were present in the sample. This was also indicated by the fact that the UV/vis spectrum of the analyte solution differed depending on the elution times, exhibiting similar but not equal UV/vis absorption bands. For example, the main absorption band of the compound mixture with the longer retention time (red) showed a clear hypsochromic shift of 11 nm compared to the UV/vis recorded at approximately 23 min (blue) (Figure 4-16B).

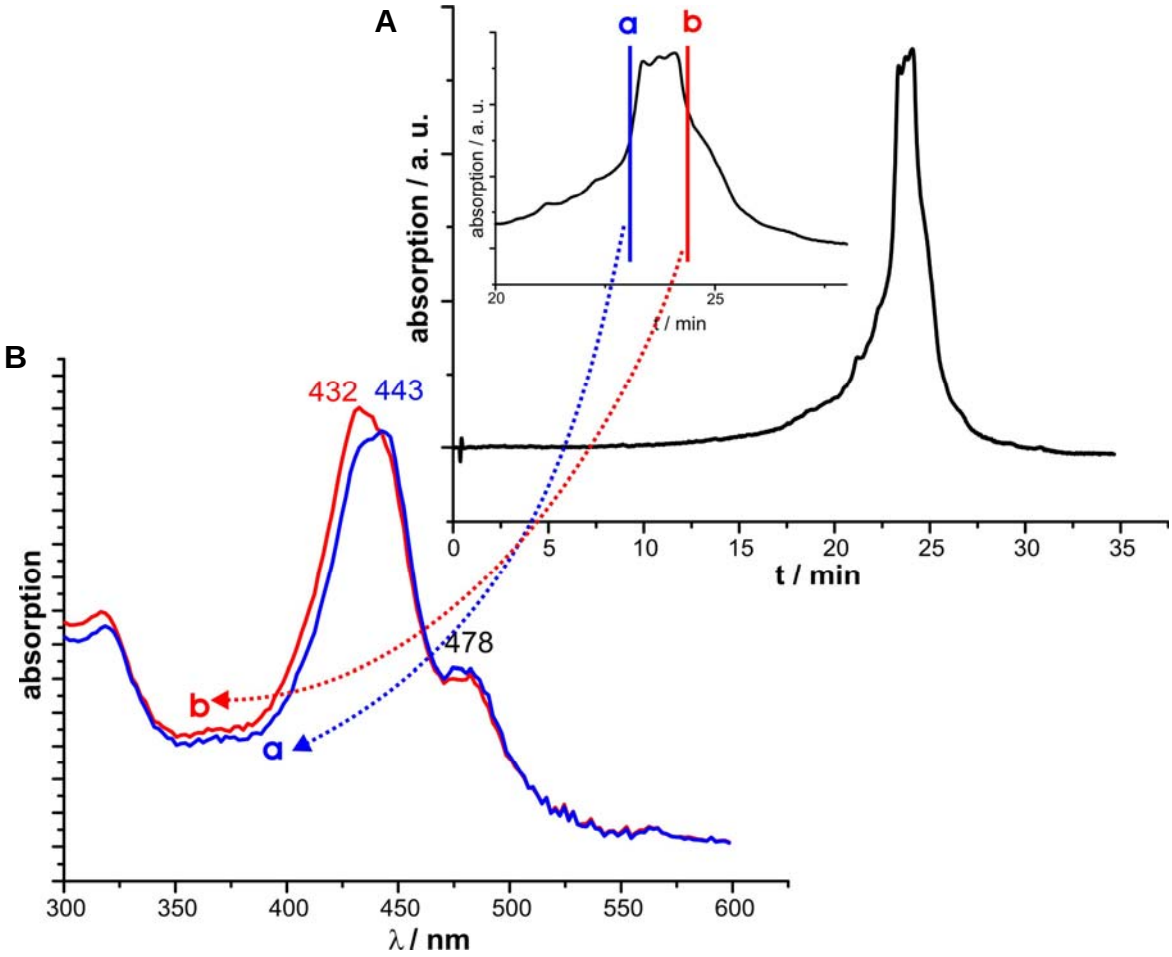

Figure 4-16: A) Time-dependent chromatogram of C72-$(C12)_8$ (**4-44**) (inset: amplification of 20 to 27 min.); **B**) UV/vis absorption spectra recorded at the elution time **a** and **b** in the inset of Figure 4-14A.

Of course, one can still argue that also this effect could be based upon an aggregation effect in solution. This would however suggest the occurrence of only three distinct main aggregates in solution, which is rather unlikely, as one has to keep in mind that the association and dissociation behavior is a dynamic process and it is not plausible for such a dynamic process to generate three distinct signals. In Figure 4-17 the three theoretically possible states are represented with aggregate formations of one, two or three discs respectively. The arrows indicate the possible association and dissociation pathways, which results already in this simple example in six different equilibrium constants. During the elution time the molecules would dynamically change in between the three different possible states. If for example one aggregate of the type **iii** would disproportionate into two species of the type **i** and **ii**, its retention time would be shortened, but this process can also occur in the reverse and the aggregate **iii** would be formed either from three times **i** or **i** and **ii** leading to an increase of the retention time.

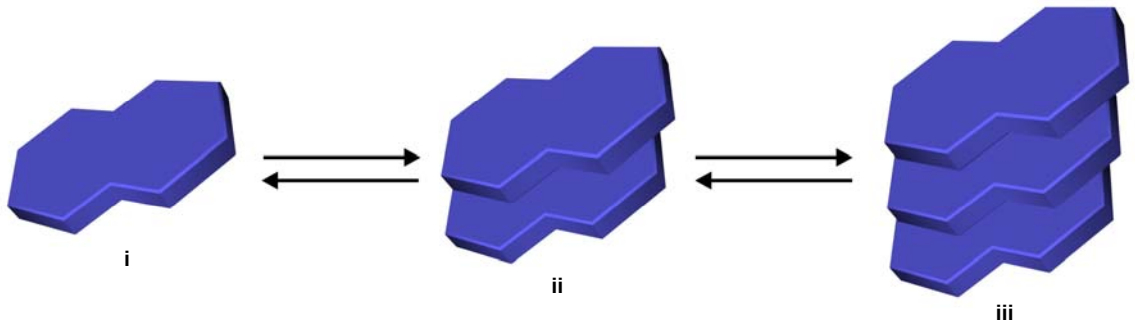

Figure 4-17: Schematic representation of three aggregate sizes in solution.

Therefore, the time a specific disc needs to pass the HPLC column is averaged in between the retention times of the different adopted states and should not lead to a separation into three signals in the chromatogram. The same assumption is also true for all the other possible aggregates and should result in the end only in a broadening of the eluent chromatogram as shown in Figure 4-18.

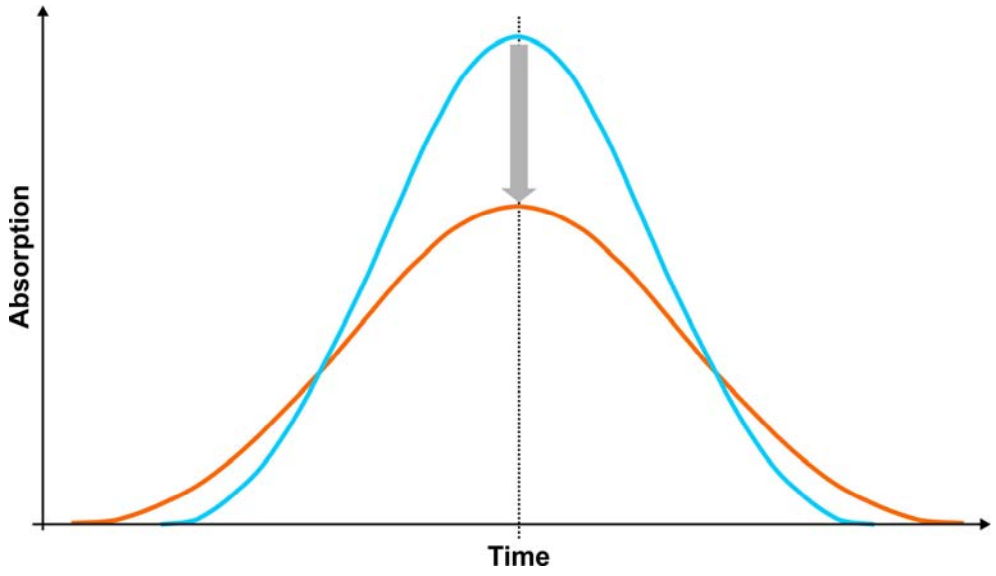

Figure 4-18: Schematic representation of the change in the HPLC chromatogram relative to time**.**

This would lead to the conclusion that the observed chromatogram can only be caused by a static distribution, if one still assumes the aggregate effects. This is however rather unlikely as HBC also shows a dynamic behavior. The UV/vis spectra seen in Figure 4-14B, confirmed that the substance consisted indeed of different compounds and not of different aggregate sizes. Unfortunately, these substances show on the HPLC column almost identical retention times, which eliminated HPLC as a possible

separation technique. Conclusively it can be said that the observed chromatogram cannot originate from aggregation effects and as a consequence, the observed peaks are due to two unidentified impurities in combination with the product.

4.2.3 Photoluminescence Experiments

Another proof for the presence of impurities was the severe difference between the photoluminescence excitation (PLE) and the UV/vis spectra of all the batches of the C72 derivatives C72-$(C_{12})_8$ (**4-44**) and even C72-$(C_{8,2})_8$ (**4-45**), as shown in Figure 4-19B.

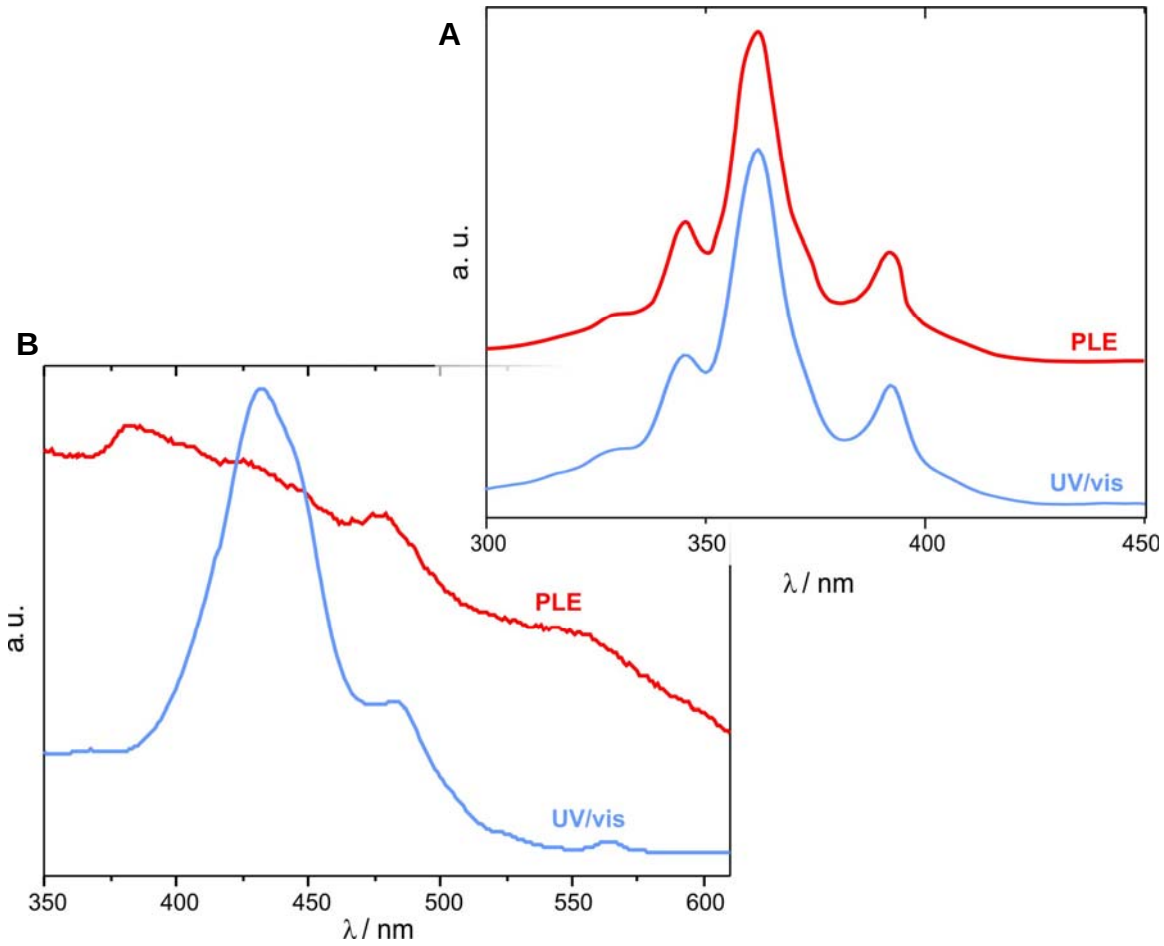

Figure 4-19: UV/vis (blue) and photoluminescence excitation spectra (red) of A) the *n*-dodecyl substituted HBC (**4-28**) and B) the C72 derivative C27-$(C_{12})_8$ (**4-44**).

Usually, the UV/vis and the PLE spectra should look similar, as despite of phosphorescence or other radiationless processes, photoluminescence is the only way for the molecule to eliminate the absorbed energy of the absorption process and to return to its ground state S_0. The PLE spectrum describes simply the amount of energy that is released by photoluminescence emission in relation to the applied excitation wavelength.

Therefore, it is obvious that a high molar extinction coefficient of a compound at a certain wavelength will also lead to a large amount of absorbed energy. Subsequently, this amount of energy has to be disposed, which will be expressed in a strong photoluminescence intensity and results in a distinct band in the PLE spectrum.

In Figure 4-19A the corresponding spectra of the *n*-dodecyl substituted HBC (**4-28**) is presented as an example for an undoubtedly pure material. The similarity is obvious, as the UV/vis shows three resolved bands at 345 nm, 360 nm and 390 nm respectively corresponding to the ones observed in the PLE. In contrast, the C72 derivatives C72-$(C_{12})_8$ (**4-44**) and C72-$(C_{8,2})_8$ (**4-45**) do not show any similarities between the UV/vis and the PLE spectra (Figure 4-19B). Of course, aggregation plays an important role for the photoluminescence measurement. This can however be reduced by lowering the concentration of the probed material. Even at the possible detection limits no resolved band structure in the PLE could be detected for the C72 species. If in contrast some impurities are present in the material, as suggested by the HPLC, no other behavior can be expected.

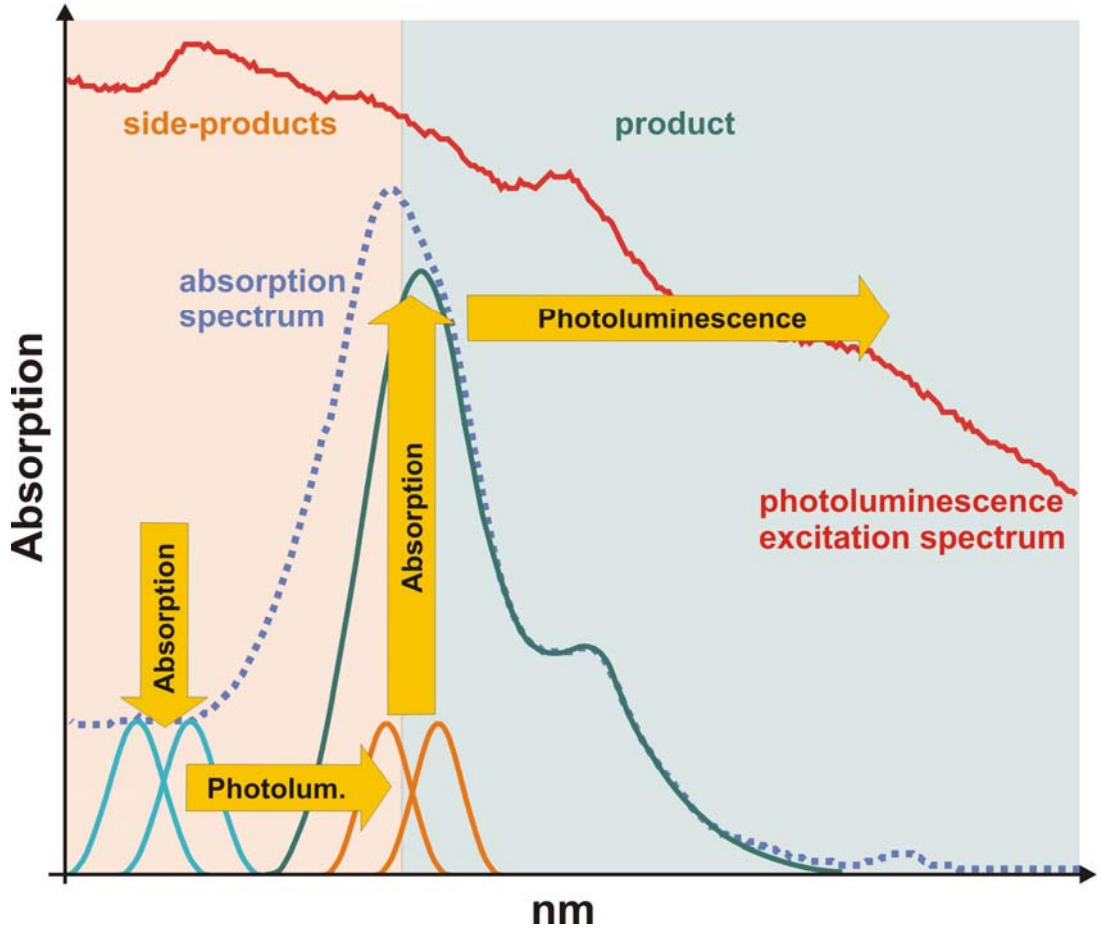

Figure 4-20: Assumed absorption profiles of the mixture of C72-$(C_{12})_8$ (**4-44**) and the side-products.

It is assumed that the side-products present in the samples are partially fused intermediates and also show an absorption towards the shorter wavelengths of the electromagnetic spectrum than the fully fused product, due to the disturbed conjugation of the aromatic entity. In Figure 4-20 the assumed simplified absorption profiles of these intermediates (orange) and the product (green) are schematically drawn. In case of the absorption spectrum the observed spectrum (dotted, blue) is a superposition of the absorptions of all the present compounds in the sample.

For the compounds with smaller aromatic moieties, the photoluminescence emission will possibly occur in a range, where the fully planarized product can absorb the emitted photons of the partially fused intermediates. The resulting photoluminescence excitation spectra will then of course show a too high response at short wavelengths, as the intermediates transfer their energy *via* photoluminescence to the C72 species and serve in some sense as a "light-collector" for the fully planarized product. This leads in the end to the observed inclination of the photoluminescence excitation spectra towards the shorter wavelengths.

Therefore, for every PAH the PLE and the UV/vis spectra need to show a similar band structure, while the intensities of the respective bands do not necessarily have to show absolutely the same ratios in both spectra due to differences in the oscillator strengths or other processes. The non-existing similarity between the PLE and the UV/vis absorption clearly indicated that not only the samples of C72-$(C_{12})_8$ (**4-44**), but also of C72-$(C_{8,2})_8$ (**4-45**) partially consisted of not completely fused, intermediate compounds.

4.2.4 Polarized Optical Microscopy

In contrast to the suggested high purity of compound C72-$(C_{12})_8$ (**4-44**) from the MALDI-TOF MS spectrum, in the polarized optical microscopy images, it was also observed that some parts of the material showed a severely different thermal behavior than others (Figure 4-21). During heating, certain parts of the material melted, indicating a transition to the isotropic state, while other parts remained crystalline and kept their birefringence until degradation of the substance. By taking into consideration the above discussed possible presence of impurities, it is likely that the areas, which contain a higher degreee of these impurities melt earlier than the areas with a higher purity, where a well ordered self-assembly can be established. These parts need far higher temperatures to overcome the stacking propensity of the discs and to melt.

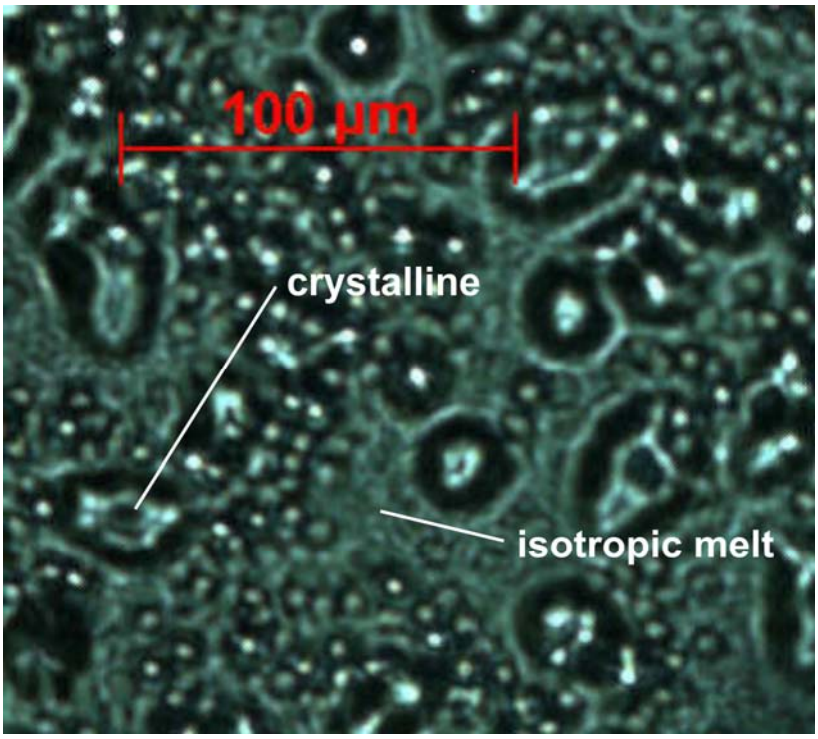

Figure 4-21: POM image of C72-$(C_{12})_8$ (**4-44**).

4.2.5 2D-WAXS

As described in the introduction of this thesis, the bulk investigations of discotic mesogens also include 2D-WAXS diffractometry on extruded fibers.[51] The material is usually heated to a temperature, at which it becomes plastically deformable and is extruded as a thin fiber. During the extrusion process, HBCs and other discotic materials self-arrange in a columnar stacking, whereby the stacking axis of the columns is along the extrusion direction. This arrangement results in a typical 2D-WAXS diffraction pattern, from which it is possible to gain information about the intra- and intercolumnar organization of the material in the bulk.

Also in this experiment, differences between the batches of C72-$(C_{12})_8$ (**4-44**) were found. In Figure 4-22 the 2D-WAXS diffractogram together with the corresponding full integration plot of two different batches of C72-$(C_{12})_8$ (**4-44**) are presented. It is obvious that in Figure 4-22A the material adopts similar to HBC as expected some sort of columnar order. The material from the other batch however only revealed a strong amorphous arrangement, as can be seen from the ring-like reflexes on the 2D-WAXS. This also supported the assumption of the possible presence of impurities, as only with

such sources of disturbance the strong π-interaction can be effectively reduced or even inibited. Although the plot in Figure 4-22A indicated some sort of columnar arrangement, it was not possible to unambiguously assign an unit cell to these reflexes.

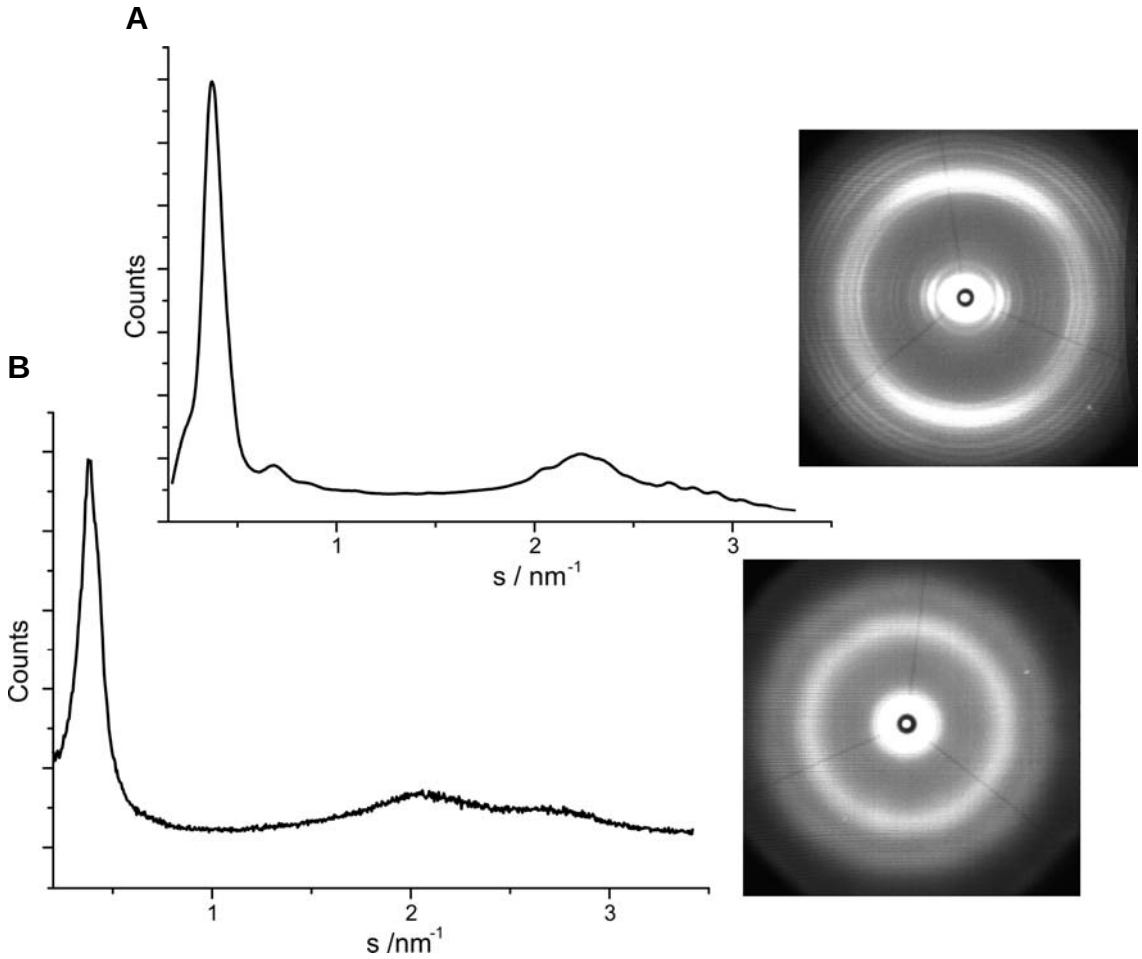

Figure 4-22: 2D-WAXS diffractogram of two batches of C72-$(C_{12})_8$ (**4-44**).

4.2.6 Conclusions

Conclusively, it was shown that the reason for the discrepancies observed in the UV/vis, PLE and HPLC spectra and the bulk behavior can be found in the presence of several impurities most probably consisting of organic compounds. However, the only methods to verify this and the nature of the impurities are NMR spectroscopy and MALDI-TOF MS. The NMR technique seems to be severely influenced by the aggregation or the possible presence of radicals, induced by the oxidative cyclodehydrogenation step, leading to a broad and unresolved aromatic region in the

spectra. This method can therefore not be used for the structural determination of the species.

MALDI-TOF MS however has so far proven to be a very versatile method in the analytics for large PAHs. One major problem is nevertheless that it did not reveal the presence of the impurities and even more important is the fact that the rate and the completeness of the cyclodehydrogenation reaction was also determined with this method. As the reliability of MALDI-TOF MS was now put into question, the cyclodehydrogenation reaction had to be of course rechecked by other methods. An easily accessible technique that allowed at least some insight into the size of the established π-system is UV/vis. It is clear that UV/vis does not yield any quantitative data on the rate or completeness of the reaction and its value is limited for detecting possible organic or inorganic impurities, however it can be consulted to at least basically verify the results gained from MALDI-TOF MS.

4.3 Verification of the MALDI-TOF MS Data

4.3.1 C72-$(C_{12})_8$

In a cyclodehydrogenation reaction towards C72-$(C_{12})_8$ (**4-44**), samples were taken after certain times and measured with MALDI-TOF MS and UV/vis. In Figure 4-23 the differences became obvious. While the MALDI-TOF MS (Figure 4-23A) spectrum confirmed a completion of the reaction already after 15 minutes and did afterwards not change anymore, in the UV/vis the bands as well as the extinction coefficients still changed after 4 hours (Figure 4-23B).

This experiment proved that MALDI-TOF MS cannot be considered alone to decide, if a cyclodehydrogenation reaction has reached its completeness. Another conclusion that can be drawn from these result is, that although organic impurities may be present, they cannot be detected by MALDI-TOF MS. However, it has to be noted that it is not probable that MALDI-TOF MS simply ignores certain molecules, but that it maybe overestimates certain substances.

Of course the question remains, why these substances could not be detected with MALDI-TOF MS. Two main criteria determine the resulting data of the experiment. The first is the sample preparation, which can take place *via* three general procedures: The matrix and the sample are both separately dissolved in a standard organic solvent. Both are then mixed together directly on the target plate leading to an efficient mixing of the

matrix with the sample. After the evaporation of the solvent, the sample can be measured.

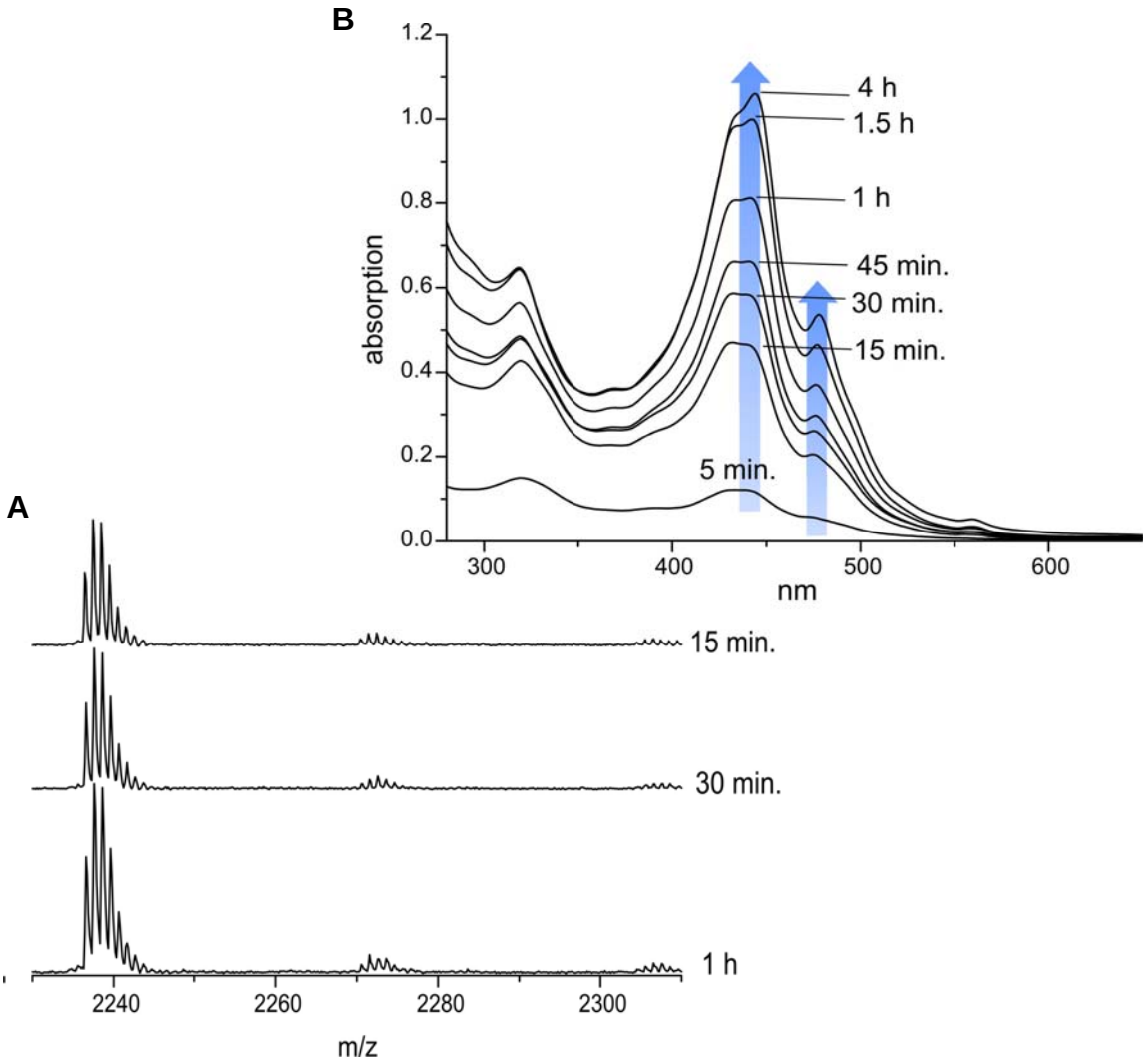

Figure 4-23: Comparison of samples taken during cyclodehydrogenation towards C72-$(C_{12})_8$ (**4-44**) with **A**) UV/vis and **B**) MALDI-TOF MS spectra.

On the other hand, it is possible to first put the dissolved matrix on the target creating after the evaporation of the solvent a thin film of the matrix substance. On top of this film a solution of the sample is carefully drop casted. After evaporation of the solvent, the sample is ready for the experiment. The last possiblity, which is generally adopted for hardly soluble compounds and large PAHs and proved already its versatility for a wide variety of compounds, is the mixing of the matrix with the sample without any solvent. In this technique, the substances are directly mixed and milled in a ball mill for 30 minutes. This yields a fine powder that can be applied with a spatula onto the target plate.

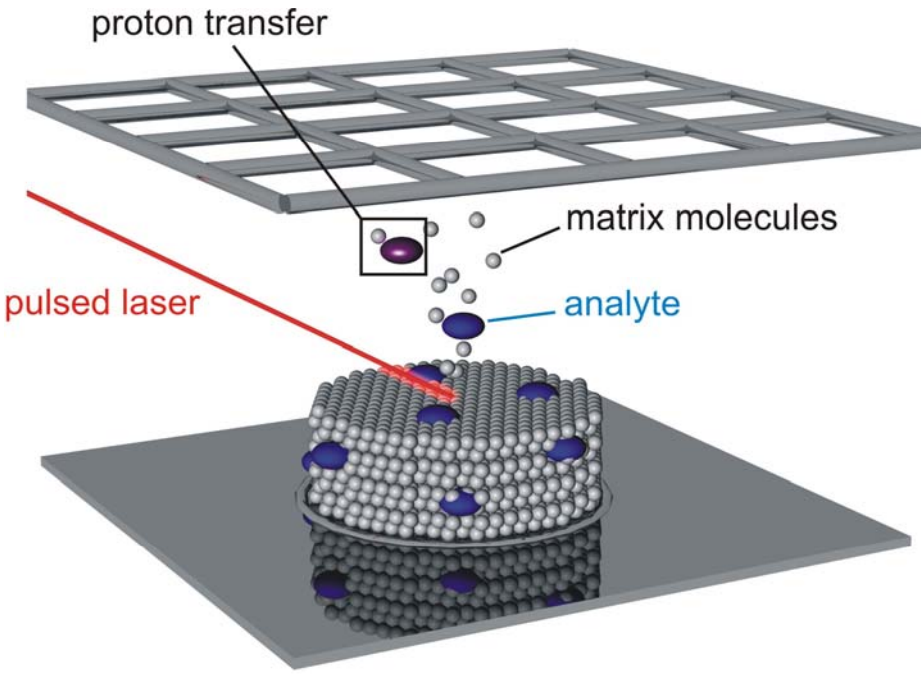

Figure 4-24: Schematic representation of ionization of analytes in the MALDI-TOF MS by laser pulse.

The second criteria is the laser power applied onto the sample, as in this method a short laser puls, which is focussed onto the target, leads to a high energy density and to a prompt heating of the analyte (Figure 4-24). This results in an explosion-like diffusion of the matrix and the analyte into the gas phase. In the small desorption cloud that forms, a diversity of complex chemical reactions take place. The analyte is ionised by a proton transfer from the matrix molecules, leading to a charged species that is accelerated in the applied electric field. Furthermore, the experiment can be carried out in the linear or in the reflex mode, whereby reflex mode provides an improved resolution of the mass distributions (see Appendix F). It is obvious that for our problem, which includes minimal mass differences, reflex mode has to be used.

Conclusively, it becomes clear that in the case of large PAHs mainly two arguments can have a sustainable influence onto the resulting spectra: the used matrix and the applied laser power. The preparation technique is not expected to exhibit a substantial impact on the measurement, as with all techniques a homogeneous sample resulted.

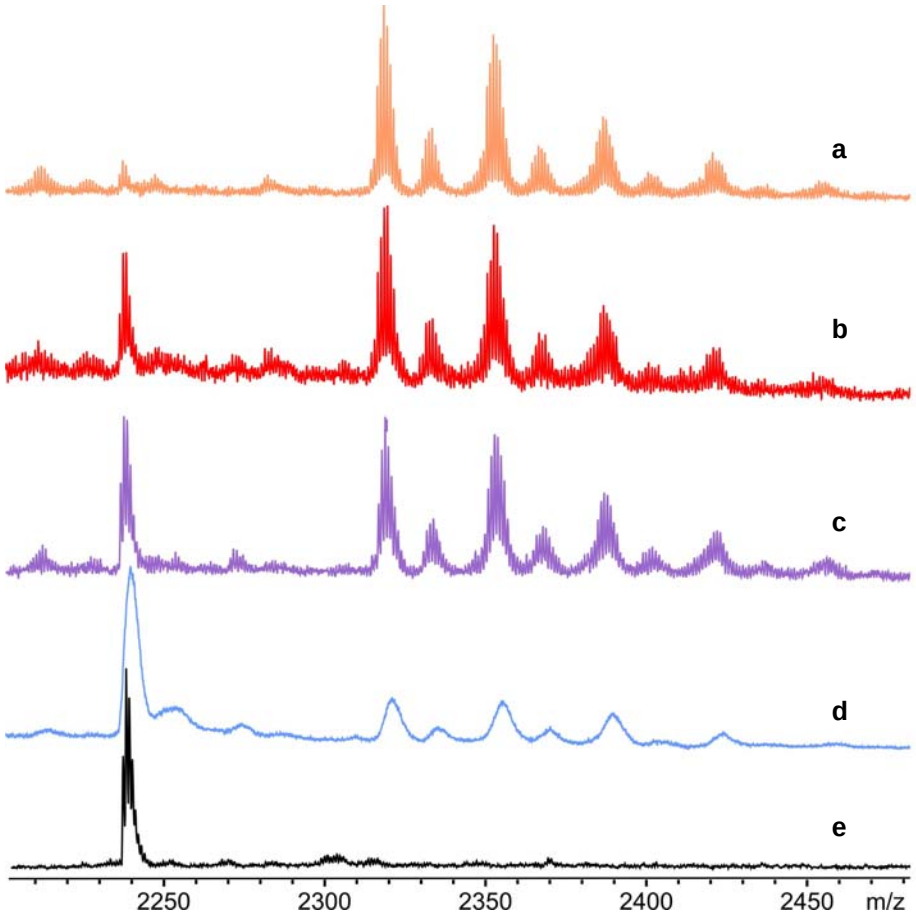

Figure 4-25: MALDI-TOF MS spectra of with different matrices of C72-$(C_{12})_8$ (**4-44**) samples during cyclodehydrogenation after 5 min. reaction time. Matrices: **a**) 9-nitroanthracene, **b**) 1,8,9-trihydroxyanthracene (dithranol), **c**) BPMPM-TCNQ mixture, **d**) trans-2-[3-(4-tert-butylphenyl)-2-methyl-2-propenylidene]malononitrile (BPMPM) **e**) 7,7,8,8-tetracyanoquino-dimethane (TCNQ).

Therefore, a range of different matrices has been tested to determine the influence of the matrix molecules on the spectra of large PAHs (Figure 4-25 and Figure 4-26). For the measurement the same samples were used, which have been collected for the comparison of the UV/vis with the MALDI-TOF MS measurements in Figure 4-23. Two samples were finally used to gather the required information. On one hand, it was necessary to get a better insight into the status, which is occupied after a short time of the reaction period (5 minutes). At this stage the chances were reasonable to receive signals from partially closed compounds or still the starting material, which will serve as a proof of principle. The second sample needs to be one close to the end of the reaction to receive detailed information about the completeness of the reaction (5 hours).

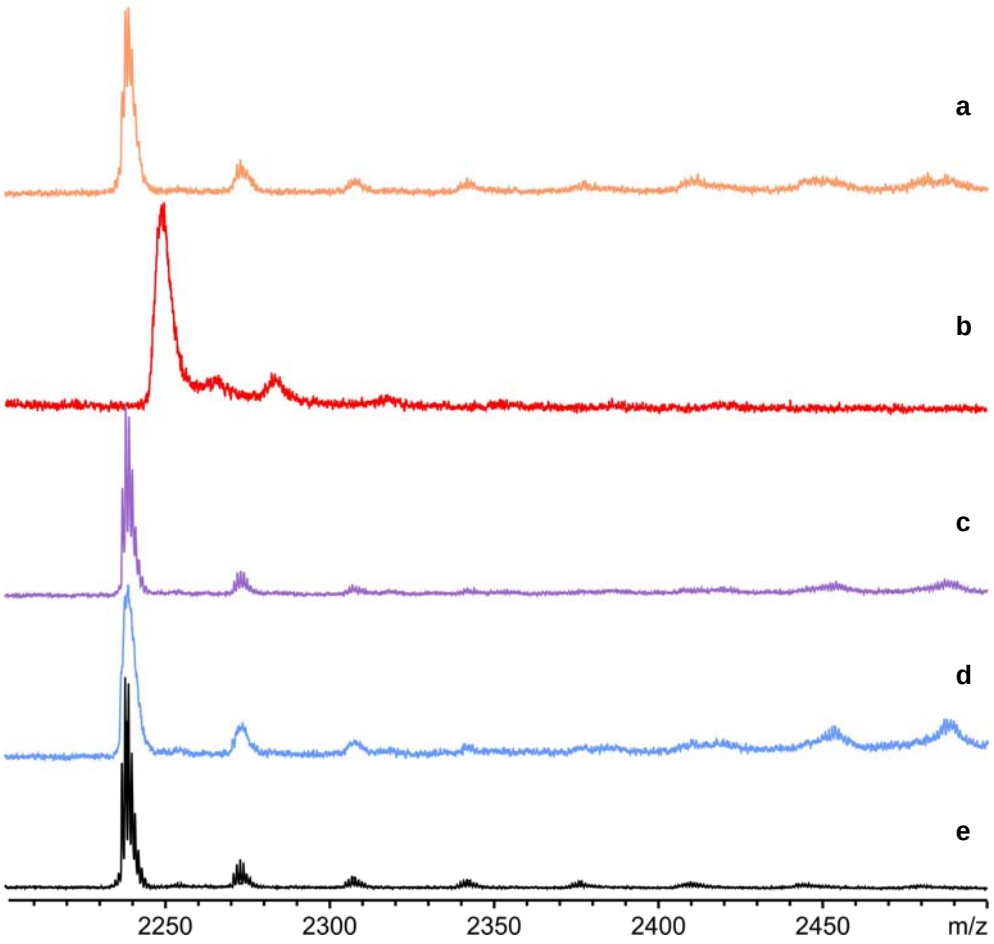

Figure 4-26: MALDI-TOF MS spectra of with different matrices of C72-$(C_{12})_8$ (**4-44**) samples during cyclodehydrogenation after 5 hours reaction time. Matrices: **a**) 9-nitroanthracene, **b**) 1,8,9-trihydroxyanthracene (dithranol), **c**) BPMPM-TCNQ mixture, **d**) trans-2-[3-(4-tert-butylphenyl)-2-methyl-2-propenylidene]malononitrile (BPMPM) **e**) 7,7,8,8-tetracyanoquino-dimethane (TCNQ).

In the first case, one clearly observes a sustainable influence of the matrix onto the resulting MALDI-TOF MS spectra (Figure 4-25). While for 7,7,8,8-tetracyanoquino-dimethane (TCNQ), which is commonly used for PAHs, only product together with a minor amount of starting material and chlorinated species could be observed, the other spectra differed quite strongly. For the samples with either BPMPM-TCNQ mixture, with 9-nitroanthracene or without any salt, a clear amplification of the chlorinated species occurred, trans-2-[3-(4-tert-butylphenyl)-2-methyl-2-propenylidene]malono-nitrile (BPMPM) as a matrix however, pronounced the partially closed compounds with a mass average of 2254 Dalton indicating seven open bonds, originating from the assumed partially closed compounds.

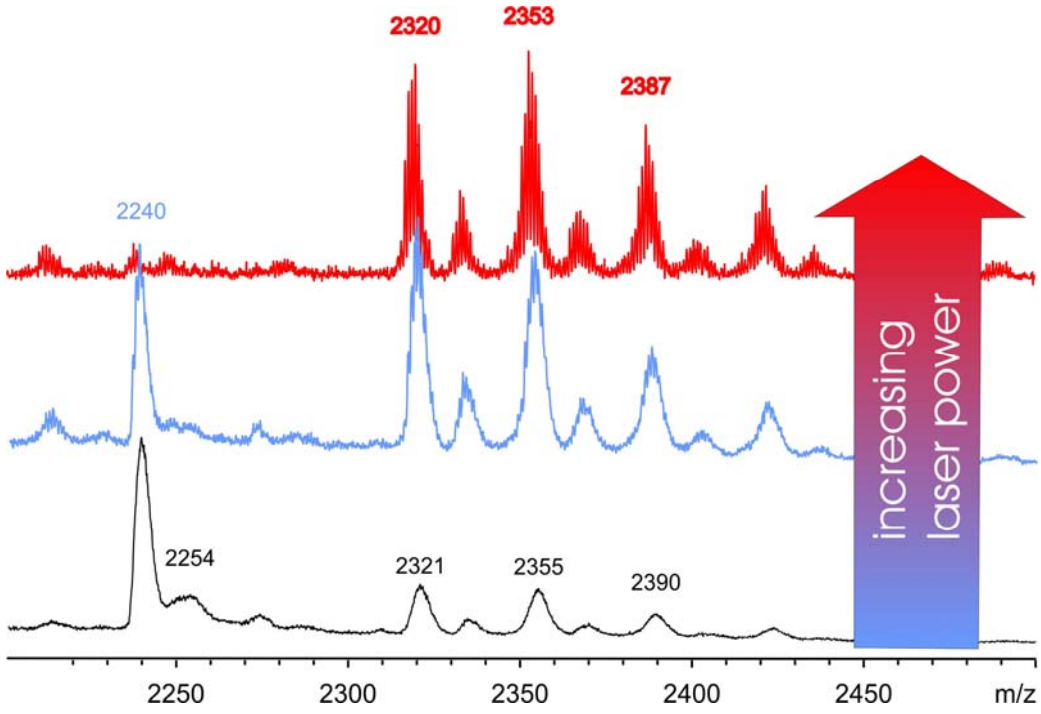

Figure 4-27: MALDI-TOF MS spectra of C72-$(C_{12})_8$ (**4-44**) recorded with different laser attenuations.

After five hours reaction time, a distinct decrease of the partially closed compounds was determined in the BPMPM case. Again the TCNQ method only revealed product in combination with some minor amount of chlorinated species. Also in the other cases no side-products could be verified except for dithranol. This matrix seemed to pronounce extraordinarily the side-products. They exhibit an average mass of 2249 Dalton and indicate a species, where five bonds are still open. Therefore, it can be concluded that even after five hours reaction time still some unclosed compounds coexist with the fully planarized product.

The remaining possibility to directly influence the result of the MALDI-TOF MS spectra is the applied laser power. From Figure 4-27 it becomes obvious that changes in laser attenuation leads to a change in the intensity of the signals. The signals react differently onto these adaptions, as can be seen from Figure 4-27. While the product and the signal originating from the partially closed species disappear with stronger laser power, the chlorinated species somehow gain in intensity. An important key point to note, is the fact that by modulating the attenuation only changes in intensities can be seen. This is the main difference between the two arguments. By applying different matrices, it is possible to completely suppress certain signals, while for changing the laser attenuation only differences in intensities are observed.

4.3.2 Investigations on Other Extended PAHs

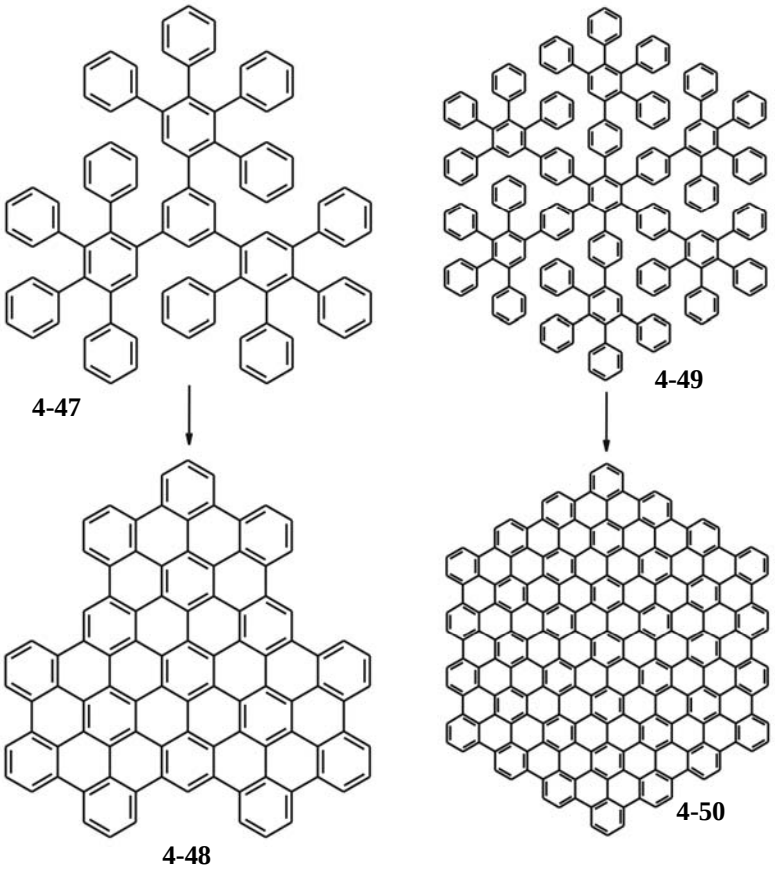

Figure 4-28: Cyclodehydrogenation step of C96 (**4-48**) and C222 (**4-50**) with $FeCl_3$, CH_3NO_2 in CH_2Cl_2.

The before mentioned issues could not only be related to the derivatives C72-$(C_{8,2})_8$ (**4-45**) and C72-$(C_{12})_8$ (**4-44**), but also other large PAHs, where no structural confirmation could be acquired by NMR methods, can possibly lack of similar partially fused side-products. In Figure 4-28 two examples (C96 (**4-48**) and C222 (**4-50**)) are presented. Indeed, after proper preparation of the MALDI-TOF MS samples, similar signals of intermediates could be observed for these cases (Figure 4-29). For example, in all three cases C72-$(C_{12})_8$ (**4-44**), C96 (**4-48**) and C222 (**4-50**) a partially fused system could be observed, where three aryl-aryl bonds were not fused, leading to a possibly distorted system. This indicated a kinetically rather stable side-product, which could even be detected in the case of C222 (**4-50**), where a large excess of the oxidant and a prolonged reaction time has been used.

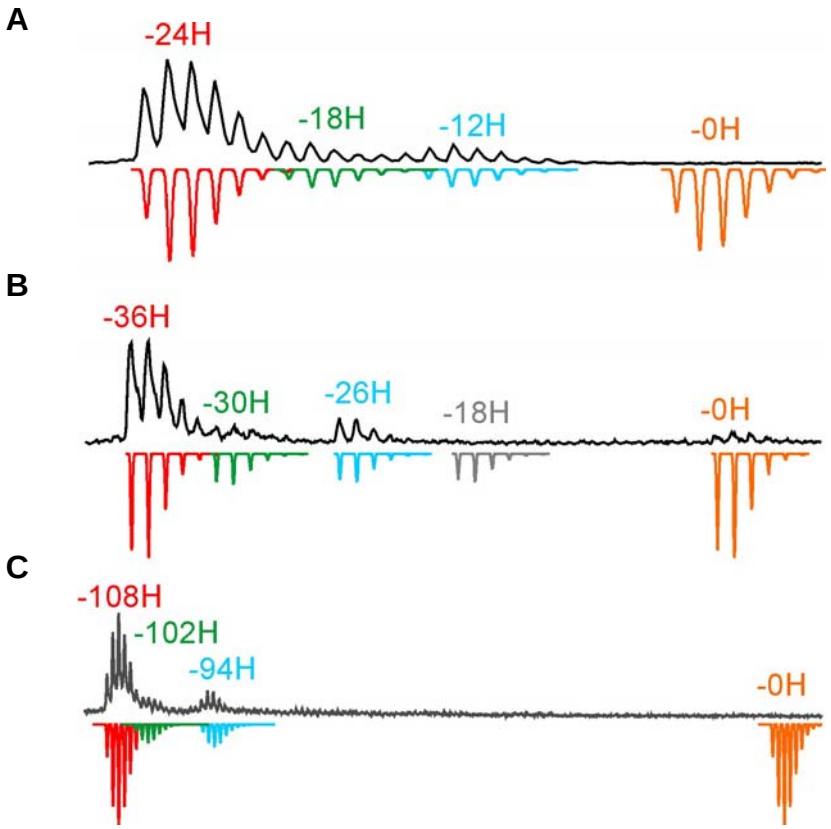

Figure 4-29: MALDI-TOF MS spectra of **A**) C72-$(C_{12})_8$ (**4-44**) (3h reaction time, TCNQ), **B**) C96 (**4-48**) (4h reaction time, TCNQ) and **C**) C222 (**4-50**) (48h reaction time, TCNQ).

For the C72 derivative C72-$(C_{12})_8$ (**4-44**) also another species could be identified, where six bonds remained open. For C96 (**4-48**) however, the other remaining species differed from the ones seen for C72-$(C_{12})_8$ (**4-44**). Indeed, two more partially fused systems were observed, where five and nine bonds were not formed, proving that this behavior was not of a general kind, but was influenced by the oligophenylene precursor molecule. In the case of the C222 (**4-50**), it was astonishing that although the size of the system is by far larger than the one of C96 (**4-48**), only two byproducts could be detected. Nevertheless, one has to mention that the applied cyclodehydrogenation reaction conditions were far harsher for C222 (**4-50**) than for C96 (**4-48**). Similar conditions could not be applied to C96 (**4-48**), as such a treatment leads to a strong chlorination of the desired product.

The occurrence of such partially fused intermediates could also explain a phenomenon, which has been encountered during the analysis of extended PAHs with the PR-TRMC measurements (Appendix G). With this method, it is possible to determine the short range intrinsic charge-carrier mobility of discotic materials. During

the studies with alkylated C96 derivatives, it was revealed that the core size of this PAH did not show the expected improved charge carrier mobility for an aromatic core component of that size and that the value was comparable or even lower to that of alkylated HBCs, although the aromatic entity is three times larger in size. With the results shown in Figure 4-29, it is likely that the charge carriers were trapped by the side-products, reducing effectively the observed charge carrier mobility values.

The presence of these partially fused intermediates would also explain the strange solubility properties of the alkylated C96 derivatives. It is known for example that the HBC derivative, which is decorated in the corona six times with dodecyl chains (**4-28**) shows a reduced solubility compared to other HBCs (Figure 4-30). This is accounted to the fact that these chains supposedly exhibit a cocrystallization effect. When one considers the fact that the aromatic core component is three times larger, it is expected that the C96 with the same number of dodecyl chains attached to the aromatic entity (**4-53**) should show a reduction in solubility, due to the stronger π-interactions. In contrast, the C96 species was very good soluble in standard organic solvents.

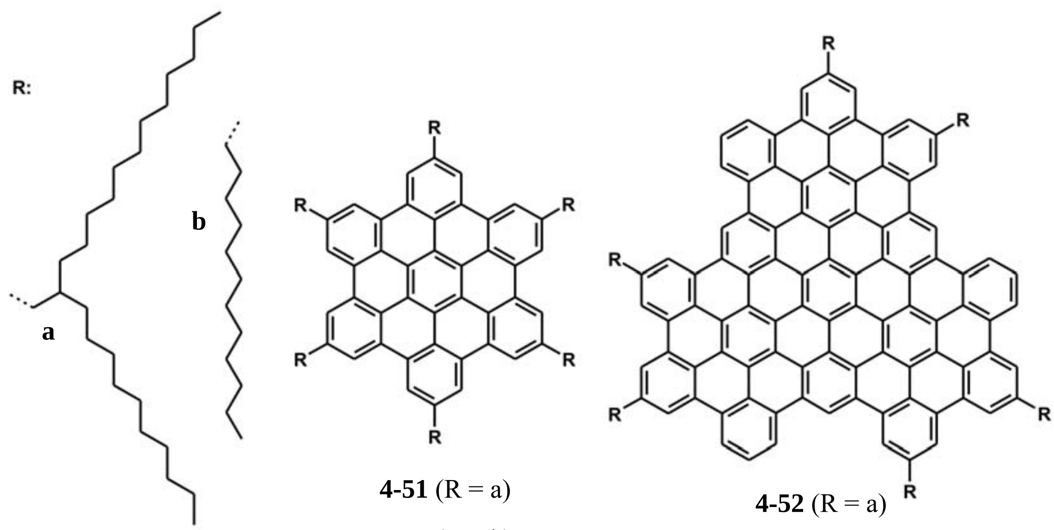

4-51 (R = a)

4-28 (R = b)

4-52 (R = a)

4-53 (R = b)

Figure 4-30: Alkylated HBC and C96 derivatives.

A similar questionable behavior was seen by considering a C96 with branched alkyl chains (**4-52**) shown in Figure 4-30. While for the HBC counterpart (**4-51**) a severe increase in solubility occurred, compared to the dodecyl substituted derivative (**4-28**), the opposite was determined for the C96 example. This is strange, as the branched alkyl chain should induce a higher solubility compared to the analogue with six dodecyl

chains due to its high steric demand close to the vicinity of the core that leads to a reduced aggregation propensity of the material.

By taking into account the presence of the disturbing side-products, this phenomena could be explained. The partially fused intermediates inhibit the proper association of the C96 discs in solution, which induces the good solubility of the dodecyl substituted derivative (**4-53**). As it has been shown above for the C72 compounds C72-C($C_{8,2}$)$_8$ (**4-45**), C72-(C_{12})$_8$ (**4-44**) and C72-(Ph-C_{12})$_8$ (**4-46**) the alkyl side-chains show some influence upon the cyclodehydrogenation reaction. This could have led to an improved cyclodehydrogenation of the C96 with the branched alkyl chains (**4-52**) and therefore to the appearance of a less disturbed association in solution. This stronger association behavior due to the improved π-interactions would induce the observed lowering of the solubility.

4.3.3 Discussion

It was proven that MALDI-TOF MS suffered from a methodological problem for the detection of partially fused side-products of solid-state prepared samples of PAHs. For a wide variety of matrices a severe overestimation of the fully closed product was observed. Nevertheless, TCNQ still ocurred to be the best matrix for getting a good overview over all the present species within a sample, when one stays aware of the strong amplification of the fully fused product.

As NMR spectroscopy could not provide any insight into the nature of these side-products, extensive MALDI-TOF MS studies were accomplished. It was shown for several cases, where oligophenylene precursors were used in the intramolecular Scholl reaction with iron(III)chloride as the oxidant, that partially fused side-products were formed during the reaction. Some similarities were found in between the examples, as all of them showed a kinetically more stable intermediate, where three bonds remained to be fused. The other species however strongly depended upon the used oligophenylene precursor. On the basis of the MALDI-TOF MS one can make several assumptions about the nature of the byproducts evolving during the intramolecular Scholl reaction.

It is important to verify the nature of the observed side-products and their origin, as only by understanding how these compounds are formed, it is possible to develop better conditions for fusing the aromatic phenyl rings and to suppress the formation of byproducts. Unfortunately, no NMR data is available, which is a prerequisite for an

accurate determination of the species. Therefore, the adjacent discussion is only based upon the results gained from MALDI-TOF MS and has to be considered as speculative.

Besides the photochemical or electrochemical means the Scholl reaction can be considered as one of the most successful chemical methods to form aryl-aryl bonds. In the earliest definitions, this reaction was confined to an intramolecular dehydrogenation of aromatic nuclei resulting in the formation of a condensed ring system. Balaban and Nenitzescu however expanded the scope of the reaction by defining it as "*the eliminination of two aryl-bound hydrogens accompanied by the formation of an aryl-aryl bond under the influence of Friedel-Crafts catalysts*".[25] The reason for emphasizing the definition was the apparent absence of differences in mechanism between the inter- and the intramolecular type of this reaction. The Scholl reaction is a dehydrogenation condensation and occurs under Friedel-Crafts conditions, but the mechanism of this condensation is far less understood than for usual Friedel-Crafts reactions. In fact the true mechanism is still unknown and a matter of current research.[70]

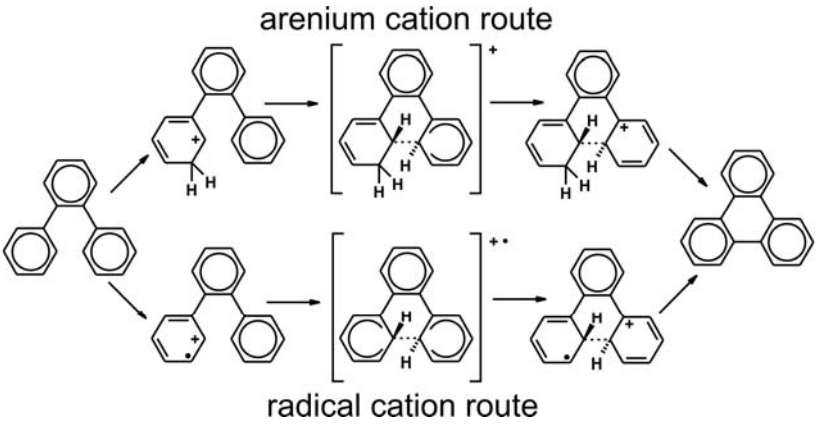

Figure 4-31: Arenium cation and radical cation reaction pathway of a *o*-terphenyl condensation.

Two different approaches evolved during all the investigations. While one explanation prefers the formation of arenium-ions as intermediate states, the other considers the induction of radical cations as the main argument. In the work of Rempala et al. an *o*-terphenyl model system was initially considered to determine, which of the proposed mechanisms,[25] arenium or radical cation based, is more likely. They concluded that the intramolecular Scholl reaction of unsubstituted hexaphenylbenzene likely proceeds by protonation, electrophilic attack, deprotonation, and a subsequent oxidation. The aryl-aryl bond formation is stepwise, contiguously and the first bond is established with the slowest rate. Therefore, the intramolecular Scholl reaction is likely to proceed

by an arenium ion promoted mechanism as presented in Figure 4-31 for the model system.[70]

One of the most important features of the intramolecular Scholl reaction for the discussion is the stepwise progression towards the fully fused products, which has also been experimentally proven by the isolation of partially fused intermediates during the reaction towards HBC.[71]

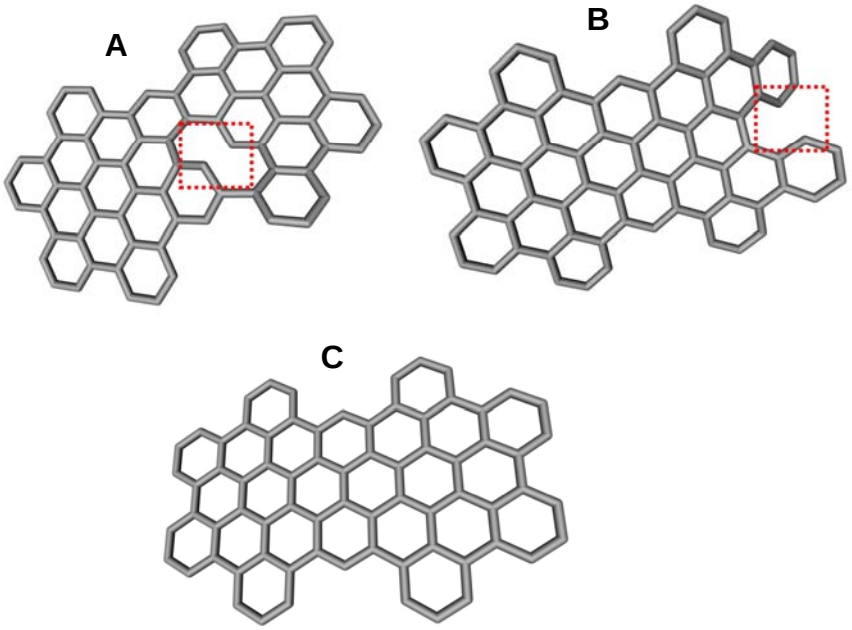

Figure 4-32: Semiemimpirical calculations (AM1) of possible defects. Heat of formation: **A**) 351.37 kcal/mol **B**) 316.89 kcal/mol and **C**) 305.71 kcal/mol.

In the beginning, one has to determine, where such open bonds are located preferentially. Therefore semiempirical AM1 calculations have been performed on two possible defect locations within the aromatic core component of the C72 species. However, it has to be emphasized that such calculations are likely to possess substantial errors and can therefore not be considered as a final proof and additionally the results correspond to thermodynamical minima and do not take kinetical arguments into account. In Figure 4-32, it is indicated that the enormous strain induced by a defect located inside the aromatic system is rather unlikely to occur due to the far less favorable heat of formation. As a consequence, the formation of such defects should preferentially occur at the rim of the aromatic core, where the induced strain can be effectively minimized. Another important factor is that the stepwise progression of the reaction will

not allow a random distribution of defects, which can therefore be excluded as the reason for the formation of possible intermediates.

As none of the phenyls provides a site with an enhanced reactivity at the beginning of the reaction, every phenyl ring in the oligophenyl precursor molecule possesses the same probability to serve as the induction site for the initial bond formation. This means that the first formation of an aryl-aryl bond can occur anywhere between two appropriate phenyl rings. If this initial bond formation occurs towards the center of the oligophenylene precursor (Figure 4-33, route A, initial state, red bonds) every succeeding step has only to overcome the steric hindrance of two hydrogens for adopting a sufficiently planarized conformation for the next aryl-aryl bond formation. The cyclodehydrogenation can then continue at the rim of the already planarized core. This pathway will be declared for future discussions as the "inside-out" pathway.

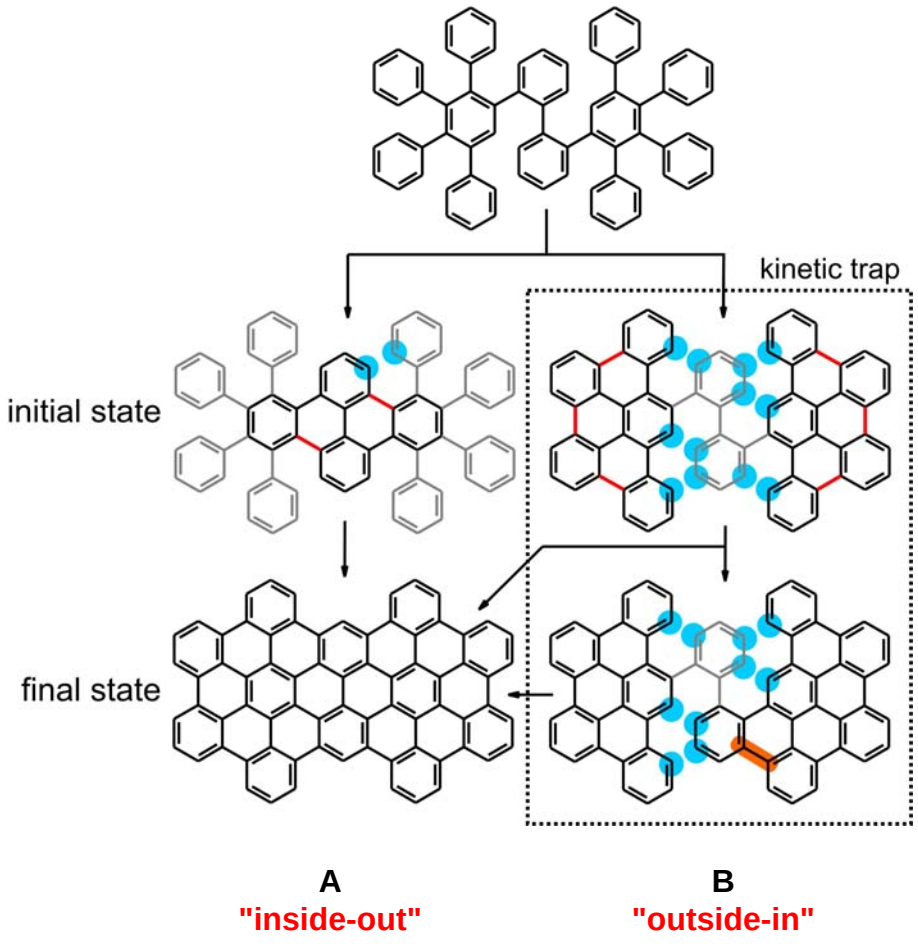

Figure 4-33: Possible cyclodehydrogenation routes **A**) initial formation of the central bonds, "inside-out" pathway **B**) initial formation of the bonds at the rim, "outside-in" pathway.

If by chance, the bonds at the rim of the precursor molecule are formed first by the so called "outside-in" pathway (Figure 4-33, initial state, route B, red bonds), one gains two panels. In this situation, the molecule would have to overcome at the same time the steric repulsion of six hydrogens. This could lead to a kinetic entrapping of the partially closed species, as the further cyclodehydrogenation steps would have to face a far higher energy barrier than for route A. Additionally, the encountered intermediate also lacks of the spatial proximity of the reaction sites for the subsequent cyclodehydrogenation step.

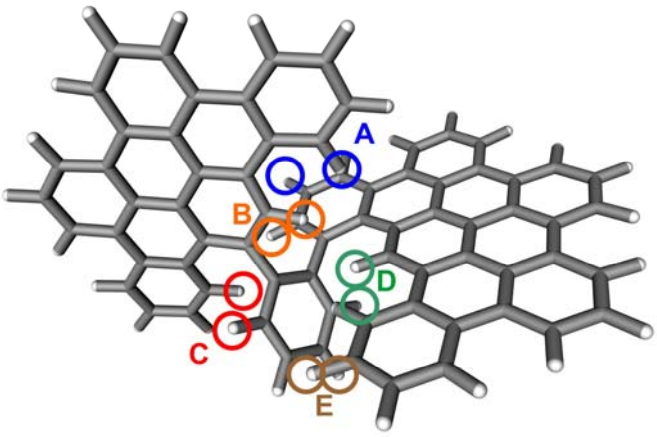

Figure 4-34: Energy minimized image of partially fused intermediate (Figure 4-33, route B, final state) and the resulting steric hindrance of the hydrogen pairs (A-E).

Of course, at this stage, as many bonds as possible are established to reach the thermodynamical minimum. By forming the next bond however (Figure 4-33, route B, final state, orange area) the molecule drives itself even further into the kinetic trap. After the formation of this bond, which fixes one central aromatic ring, also the other central phenyl ring is highly confined in conformation. Additionally, the system cannot easily adopt anymore a conformation suitable for the next cyclodehydrogenation step, without having to overcome a high activation energy due the steric hindrance of the hydrogens, as shown in Figure 4-34.

By taking into consideration the above assumed "outside-in" pathway for the cyclodehydrogenation of the C72-$(C_{12})_8$ (**4-44**) derivative, it was possible to assign from the observed mass peaks in Figure 4-29A the partially closed species presented in Figure 4-35. As it is not possible to unambiguously identify these compounds due to the lack of analytical methods, also no further insights can be gained about the partially fused systems and the stability of the proposed kinetically entrapped species. Another issue is the fact that it is not known, if the kinetically trapped intermediate species can still take

part in the intramolecular Scholl reaction and establish, although slower due to the high activation energy, additional bonds between the panels.

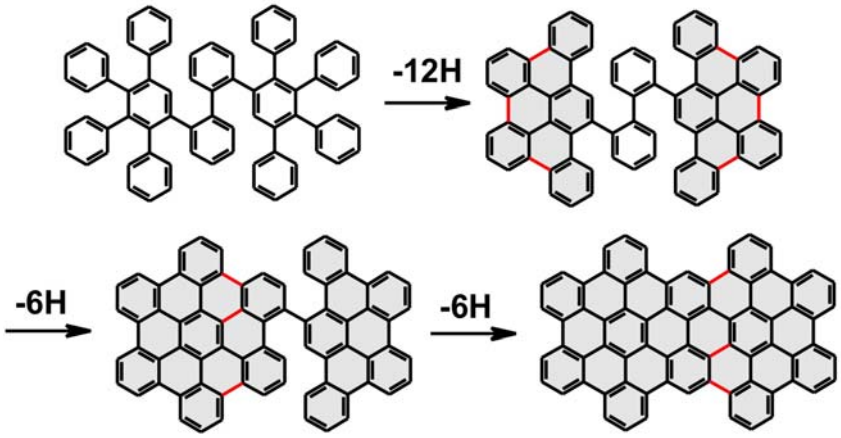

Figure 4-35: Plausible intermediates formed in the cyclodehydrogenation reaction towards C72-$(C_{12})_8$ (**4-44**) (alkyl chains are omitted for clarity)

Nevertheless, for a strained example of a HBC with 18 methoxy groups in the corona of the aromatic core component,[72] it was found that the intramolecular Scholl reaction seems not to be very sensitive towards the induced strain on the aromatic system of a large PAH. In this example, the methoxy groups forced the aromatic core component out of planarity.

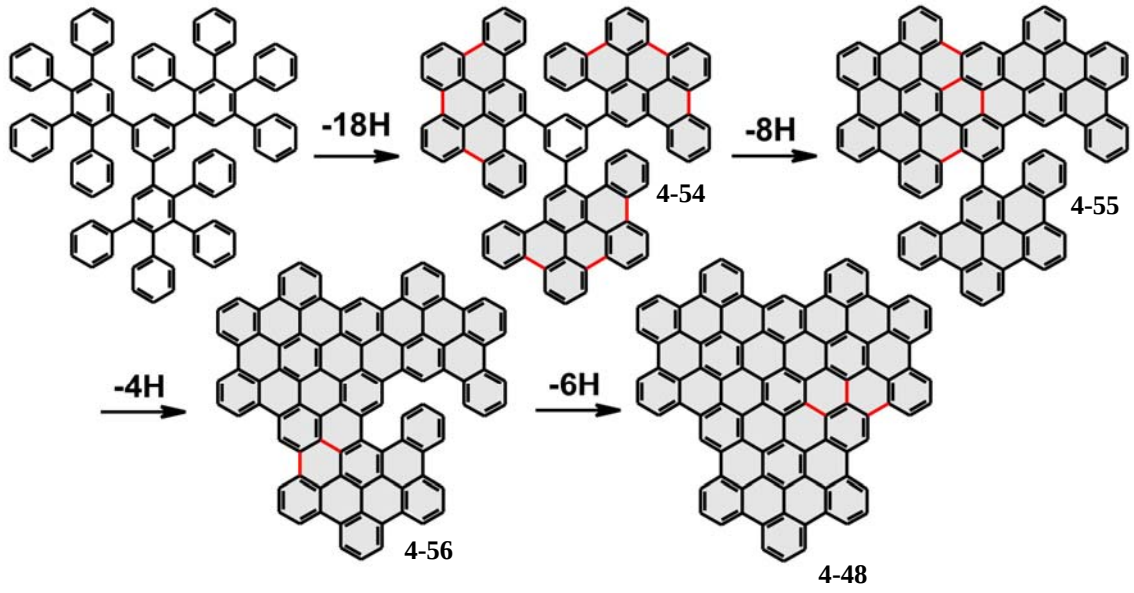

Figure 4-36: Plausible intermediates formed in the cyclodehydrogenation reaction towards C96 (**4-48**).

This steric hindrance was already built up during the cyclodehydrogenation and towards the formation of the last aryl-aryl bonds the intermediates were also encountering some steric strain. Therefore, a continued aryl-aryl bond formation of the partially fused side-products in the C72 case towards the fully planarized product seems to be probable.

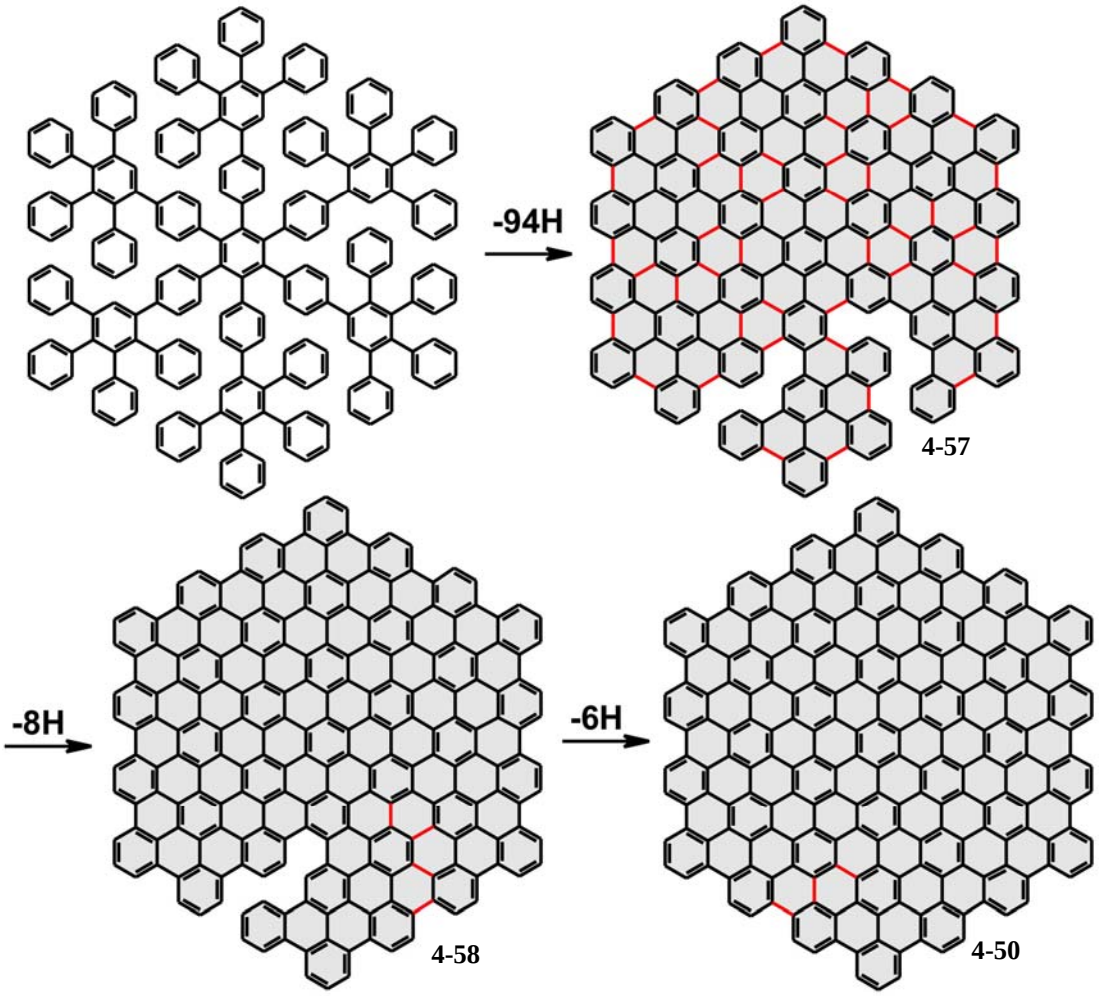

Figure 4-37: Plausible intermediates formed in the cyclodehydrogenation reaction towards C222 (**4-43**).

In a similar fashion as for the C72-C$(_{12})_8$ (**4-44**), namely by assuming the "outside-in" pathway, also for C96 (**4-48**) the mass signals of the intermediate species observed in Figure 4-29B could be correlated to the structures shown in Figure 4-36. According to the "outside-in" pathway the outer bonds were formed in the beginning of the reaction, leading to a panel formation for the C96 (**4-54**) similar to the C72 derivatives (Figure 4-35). Afterwards it seemed likely that bonds were established between the single panels, as the rest of the mass peaks in Figure 4-29B could only be explained by this proceeding of the reaction, supporting the assumption of a subsequent fusion of the panels.

Therefore, after the initial panel formation for C96 (**4-54**), which represents the first kinetic barrier, the reaction starts "stitching" together the larger aromatic systems, which further leads to the intermediates (**4-55**) and (**4-56**) shown in Figure 4-36.

For C222 (**4-50**) no such partially fused system with single panels was found, which is not surprising by considering the number of possible alternative routes in this example, by which the reaction can proceed.

As assumed by the theoretical calculations in Figure 4-32, a defect at the edge of the aromatic system is sterically and energetically far less demanding, which is the reason for the suggestion of the last partially fused compounds (**4-55** and **4-56**) for C96 and (**4-57** and **4-58**) for C222 (Figure 4-37), as for C96 for example the difference in the heat of formation between the last suggested intermediate and the final product is rather small (Figure 4-38), compared to the high degree of distortion suggested by the theoretical calculations. In the final step the last bonds are established, leading to the products C72-$(C_{12})_8$ (**4-44**), C96 (**4-48**) and C222 (**4-50**), which is undoubtedly the thermodynamically most stable state.

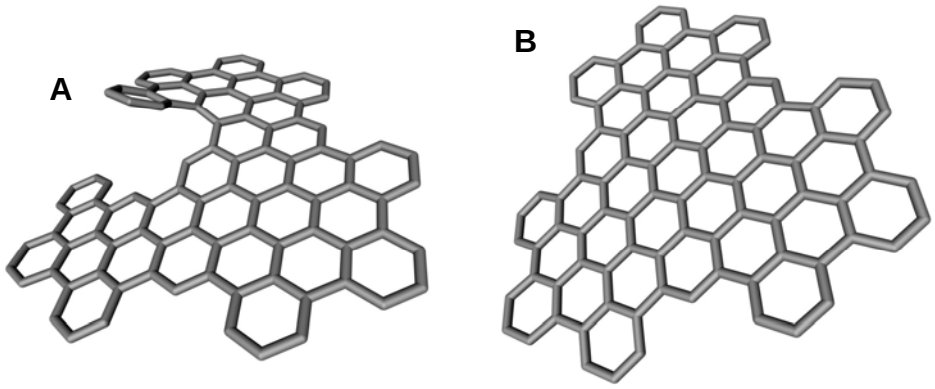

Figure 4-38: Calculated heats of formation (AM1): **A**) for intermediate **4-56**: 421.0 kcal/mol and the fully planarized product C96 (**4-48**): 403.9 kcal/mol

All of the described precursors in Figure 4-35, Figure 4-36 and Figure 4-37 had multiple "dendritic" 2,3,4,5-tetraphenylbenzene subunits in common, which allowed to establish a plausible general reaction pathway for the "outside-in" approach. In the first step, the planarization produced a singly bonded tribenzo-[b,n,pqr]perylene moiety. The next extension of the polycyclic aromatic system created a distorted system and proceeds therefore kinetically much slower.

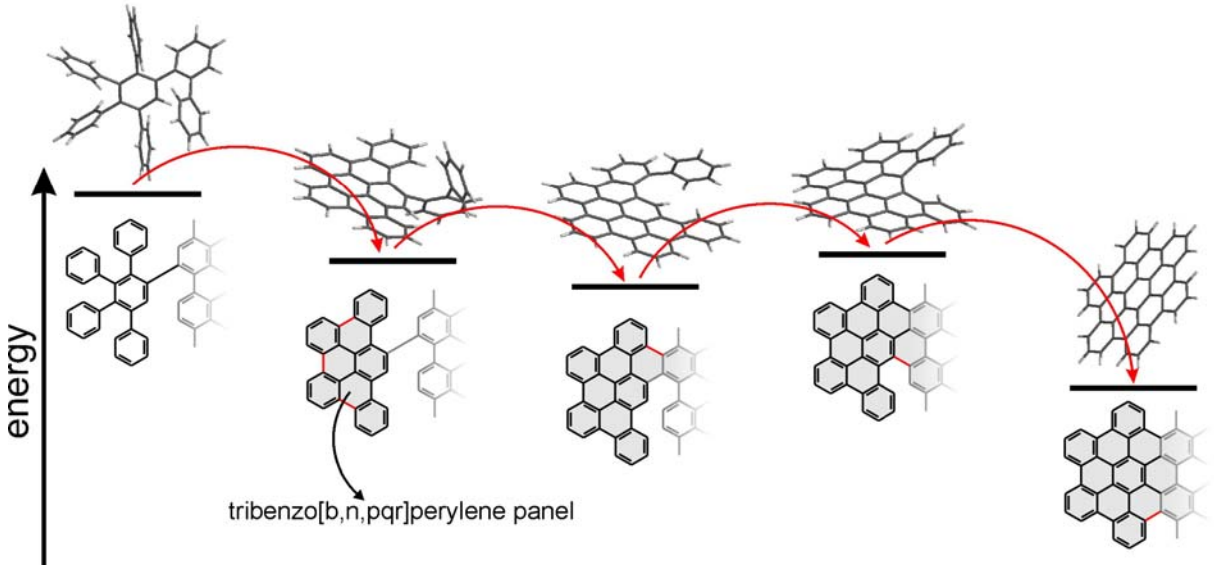

Figure 4-39: Generalized assumed pathway for cyclodehydrogenation of oligophenylene precursors according to the "outside-in" approach in combination with the calculated AM1 energies of the structures.

By the incorporation of the next phenyl unit in the “growing” PAH a highly strained intermediate was established, which presented according to the theoretical calculations an energetically higher state than the previous intermediate. Therefore, this endothermic step represents a barrier towards the full planarization and a kinetically slower step. However, a substantial amount of stabilization energy can be gained by fully planarizing the intermediate, which is possibly the driving force towards the formation of the product. This reaction pathway seemed plausible for all investigated examples (Figure 4-39).

4.3.4 Conclusions

It was found that MALDI-TOF MS amplifies strongly the fully planarized products, when treated with the corresponding matrices, which leads to a suppression of the signals of partially fused species. As MALDI-TOF MS however represents the only possible analytical technique for the determination of the side-products for large PAHs, a range of possible matrices were investigated. By applying the correct conditions, it was furthermore possible to detect several distinctive mass signals from the impurities.

It is known that the intramolecular Scholl reaction proceeds stepwise either by an arenium or a radical cation promoted pathway. As the analytical data was limited to the MALDI-TOF MS spectra, several assumptions had to be considered for reducing the number of possible products. On one hand, it was assumed by theoretical calculations that defects (unfused bonds) preferentially occur at the rim of the aromatic system.

Second, it was proposed that the formation of these partially fused species only occurred, when the initial establishment of aryl-aryl bonds happened at the rim of the oligophenylene precursor molecule. Finally, it was supposed that the observed signals in the MALDI-TOF MS spectrum originate from kinetically more stable species. This was supported by the fact that not a wide distribution but only defined signals originating from single molecules could be determined.

By using these three features, a relation was established between certain assumed intermediate structures and the observed signals from the MALDI-TOF MS spectrum. Indeed these partially fused systems could be determined for all three examples C72-$(C_{12})_8$ (**4-44**), C96 (**4-48**) and C222 (**4-50**) and additionally some similarities were found, which allowed to postulate a general hypothetical pathway for explaining the formation of the intermediate compounds.

4.4 Investigations on Workup Procedures

4.4.1 Preparative Column Chromatography

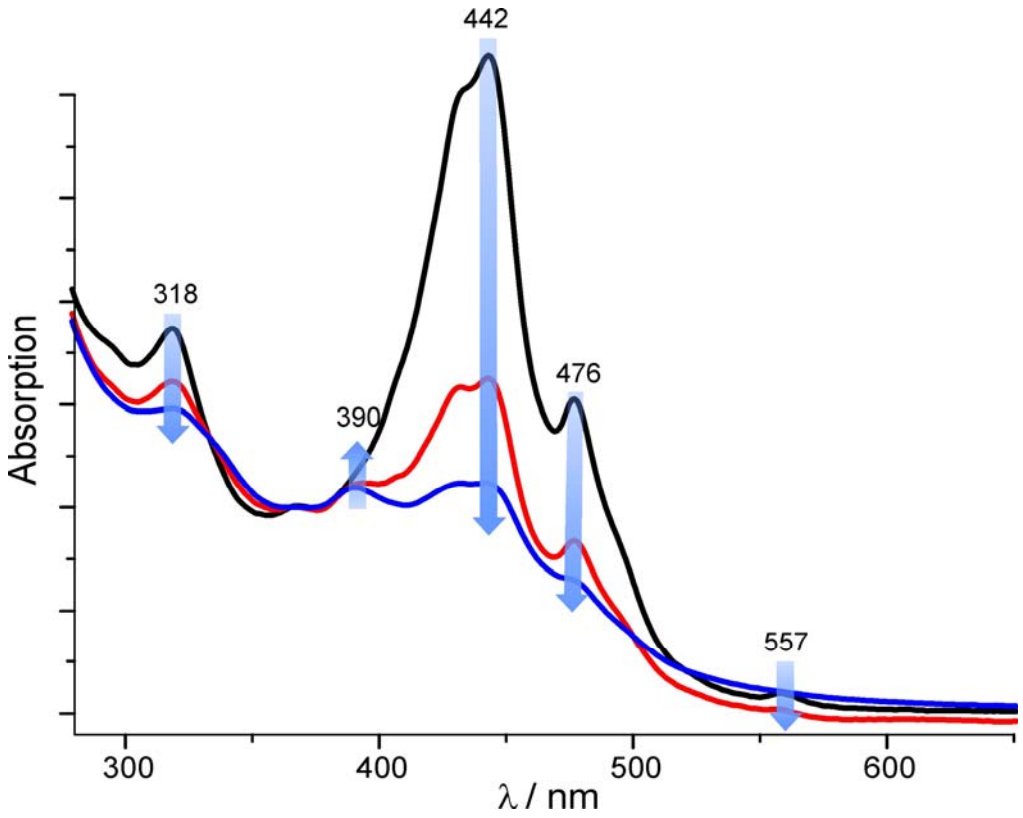

Figure 4-40: UV/vis of different fractions of C72-$(C_{12})_8$ (**4-44**) during column chromatography.

It has been shown in the HPLC that although the byproducts show only a minor difference in the retention times, that by repeated column chromatography the concentration of pure product could be gradually increased. Therefore, a simple column chromatography was conducted on a batch of C72-$(C_{12})_8$ (**4-44**). For the experiment, silica gel was used as stationary phase and toluene as eluent. During the procedure no clean separation of products was observed. However, it has to be mentioned that the alkylated C72 derivatives tend to tail strongly due to the tremendous amount of possible aggregate sizes, which are as mentioned above, possibly in a dynamic change of their size (Figure 4-17). Three different main fractions were collected, where the first one was taken immediately after the material reached the bottom line of the column (Figure 4-40, black curve). The differences between the fractions were remarkable. As already observed in Figure 4-15A, the extinction values differed significantly. Another noteworthy change was, that several bands either got weaker or even disappeared (318 nm, 442 nm, 476 nm, 557 nm), while one got stronger (390 nm). This difference in the fractions additionally indicated that the organic impurities show a small but existing deviation in their R_f values compared the fully planarized product for this type of chromatography. Unfortunately, it was observed that large amounts of the material remained on the stationary phase, which could not be removed even by a Soxhlet extraction with THF over several days. As a concequence, a repeated treatment was considered futile due to the severe permanent loss of substance.

4.4.2 Influencing the Retention Times

Even though the chromatographical separation seemed futile, several synthetical approaches were tested to induce a more pronounced difference of the retention times of the compounds. This would lead to the possibility that the substances could be separated in one chromatographical step, reducing the loss of material on the stationary phase. It was expected that the partially fused side-products would be more susceptible to substitution reactions due to their larger number of easily accessible aromatic protons, similar as observed by the differences in reactivity between HBC and hexaphenylbenzene derivatives. Dendritic oligophenylene compounds generally behave, as expected from molecules, which are built up by single benzene units, with the typical reactivities of benzene towards substitution reactions. Large PAHs like HBCs on the other hand show completely different properties, as they are not easily susceptible to such reactions. Therefore, for HBCs, one has to introduce a halogen atom already at the stage of the oligophenylene precursor, before the molecule is planarized, as an *a*

posteriori halogenation of the aromatic core component of an HBC did so far not succeed.

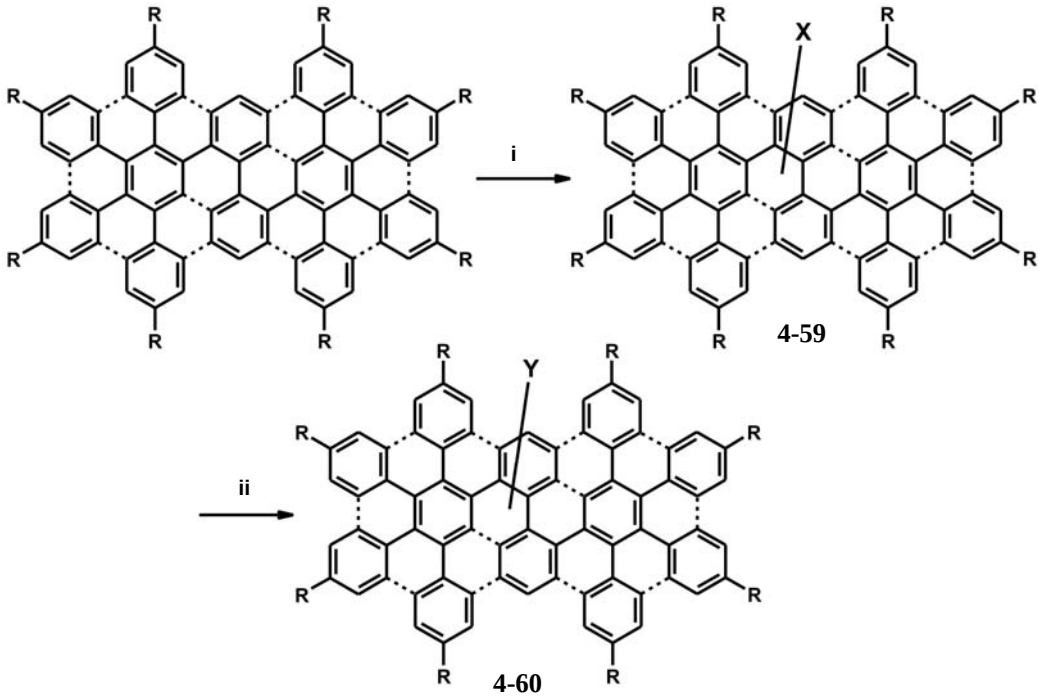

Figure 4-41: Possible reaction pathways towards attaching functional groups to partially fused side-products. *i:* bromination or treatment with *tert*-BuLi (X = Br or Li); *ii:* treatment with CO_2(s) (Y = -COOH) after lithiation.

At first, the received mixture of the cyclodehydrogenation towards C72-$(C_{12})_8$ (**4-44**) was brominated and after a succeeding functionalization with polar groups the partially fused byproducts should exhibit a higher number of polar groups and as a consequence exhibit a smaller R_f value than the fully closed product. The product, similar to HBCs, should not be as susceptible to the initial bromination. Unfortunately, the MALDI-TOF MS spectra, which has been recorded with different matrices, revealed that absolutely no bromination of either of the materials took place. It can be concluded that, with respect to bromination, no reaction differences can be observed between the fully planarized product and the partially fused intermediates. This leads to the conclusion that an additional treatment of the mixture to introduce functional groups is futile.

Another idea, was the treatment of the mixture with *tert*-buthyllithium. Again, it was expected that the lithiation will occurr preferentially at the partially closed material. A

consecutive treatment with dry ice would then directly yield the corresponding acid derivatives. However, after the treatment, no indication for a reaction was found in the MALDI-TOF MS spectra, which have been recorded in a variety of matrices. The subsequent workup by column chromatography on either silica gel or aluminum oxide as stationary phases and toluene as the eluent, showed again a strong tailing of the material. The fractions were investigated by UV/vis, but no improvement could be determined compared to Figure 4-40, which would indicate some change in the retention times of the partially fused intermediates.

As the straightforward approaches were not successful, another route was examined. In this example, it was possible to prepare the C72 derivative C72-$(C_{12})_4$-$(C_{10}$-COOH$)_4$ (**4-65**) (Figure 4-42). It was expected that after the hydrolysis of the ester functionalities of C72-$(C_{12}H_{25})_4$-$(C_{10}$-COOEt$)_4$ (**4-64**), the corresponding acid would yield a higher difference of the retention times during the column chromatography. Nevertheless, the remaining long alkyl chains on one side and the long alkyl tethers on the other were expected to induce a sufficient solubility for the workup procedure. A similar behavior has already been observed for the long tethered HBC acid derivative **3-3** in the previous chapter.

The synthesis starts with a Diels-Alder cycloaddition in *o*-xylene of 2,2´-diethinylbiphenyl (**4-9**) and an equimolar amount of the alkylated tetraphenyl-cyclopentadienone derivative **4-25**. The resulting mixture of starting materials and products was then separated chromatographically yielding the product **4-61**, which was reacted with the tetra-bromo-substituted cyclopentadienone derivative to afford the oligophenylene precursor **4-62**. This is a very convenient way to introduce a wide variety of different alkyl substituents, as the halogenated sites are susceptible to a wide range of palladium-catalyzed reactions. In the presented case, ester functionalized dodecyl chains were attached *via* a Suzuki promoted coupling to **4-62**. Therefore, the commercially available ethyl undecylate was initially hydroborated with 9-BBN to yield the boronated species of the alkyl chain. Afterwards the mixture was combined with the halogenated compound and the catalyst. This type of reaction has been chosen, as the Suzuki reactions show for these purposes usually a good yield, which is a prerequisite, as a consecutive separation of a mixture of differently reacted oligophenylene precursors would pose a difficult task.

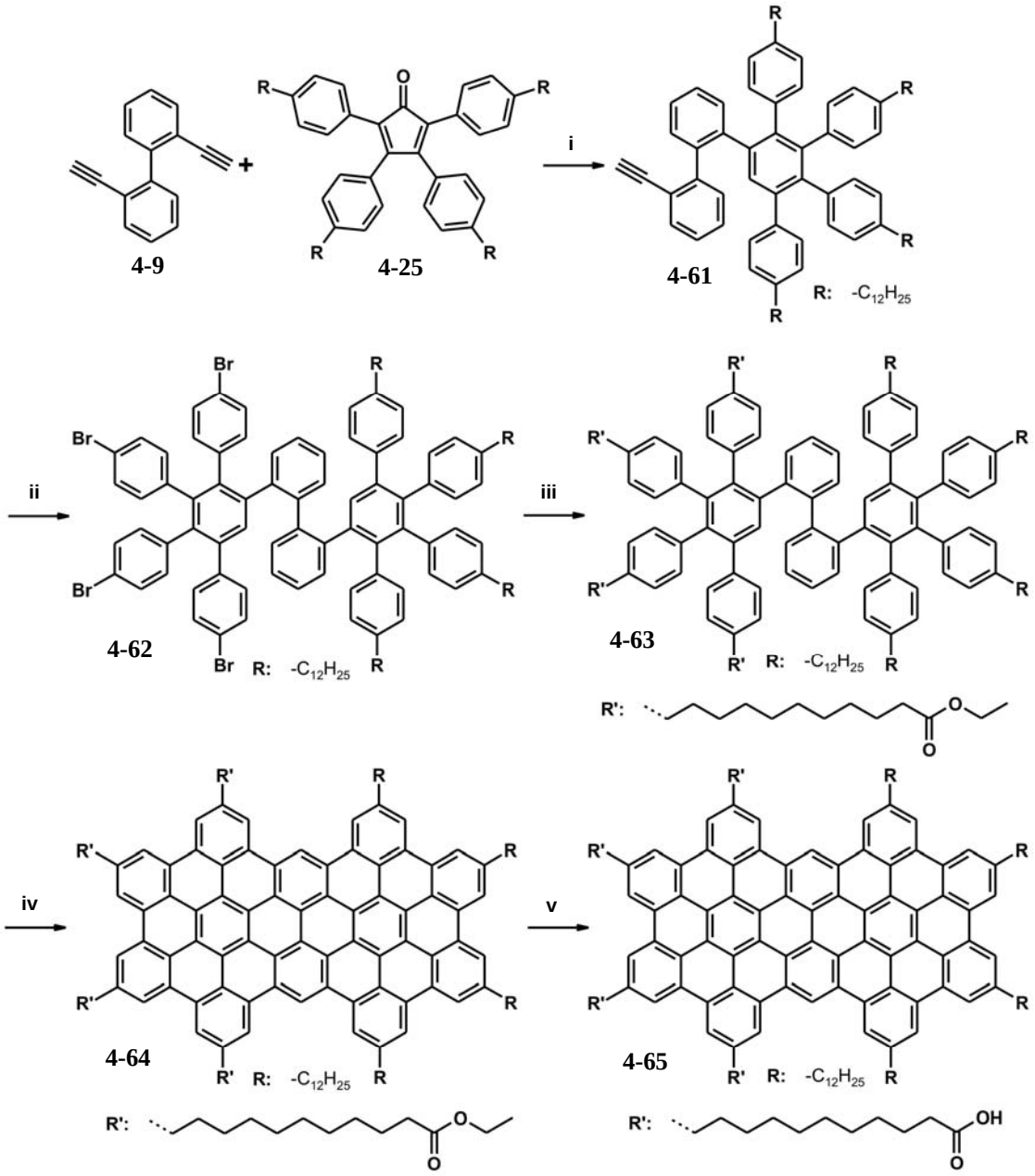

Figure 4-42: Preparation of the C72 derivative C72-$(C_{12})_4$-$(C_{10}$-COOH$)_4$ (**4-65**). *i:* o-xylene, reflux, 8h, 57%; *ii:* diphenylether, 2,3,4,5-tetrakis-(4-bromophenyl)-cyclopenta-2,4-dienone, 240 °C, 8h, 97%; *iii:* ethylundecylate, 9-BBN, THF, NaOH, H_2O, $Pd(dppf)_2Cl_2$, 64%; *iv:* $FeCl_3$, CH_3NO_2, CH_2Cl_2, 25 °C, 24h, 91%; *v:* KOH, THF, reflux, 12h, 99%.

The precursor **4-63** was then submitted to the cyclodehydrogenation step yielding C72-$(C_{12})_4$-$(C_{10}H_{20}$-COOEt$)_4$ (**4-64**). Also in this case, several test reactions had to be verified as the alkyl chains possibly show some influence upon the progression of the reaction. Indeed, due to the ester entities, the amount of oxidant had to be severely increased to 15 equivalents of $FeCl_3$ per hydrogen that needed to be removed and the

reaction time was prolongated from 14 hours to 24 hours. However, it is already known that heteroatoms often slow down or even inhibit the intramolecular Scholl reaction, as for example analoguous hexaphenylbenzene precursors incorporating nitrogen atoms can often not be planarized.[73] In this example, the oxygen atoms within the precursor possibly neutralized some of the oxidant, which led to the required increase in oxidant and reaction time.

For C72-$(C_{12})_4$-$(C_{10}$-COOEt$)_4$ (**4-64**), the MALDI-TOF MS showed only the fully planarized product together with a slight degree of chlorination. The UV/vis also looks reasonable, when compared to the previous cases C72-$(C_{8,2})_8$ (**4-45**) and C72-$(C_{12})_8$ (**4-44**). The results were reproducible and differed between the batches within the error limits. This is especially interesting, as only this slight change of the alkyl substituents seemed to influence the cyclodehydrogenation behavior substantially.

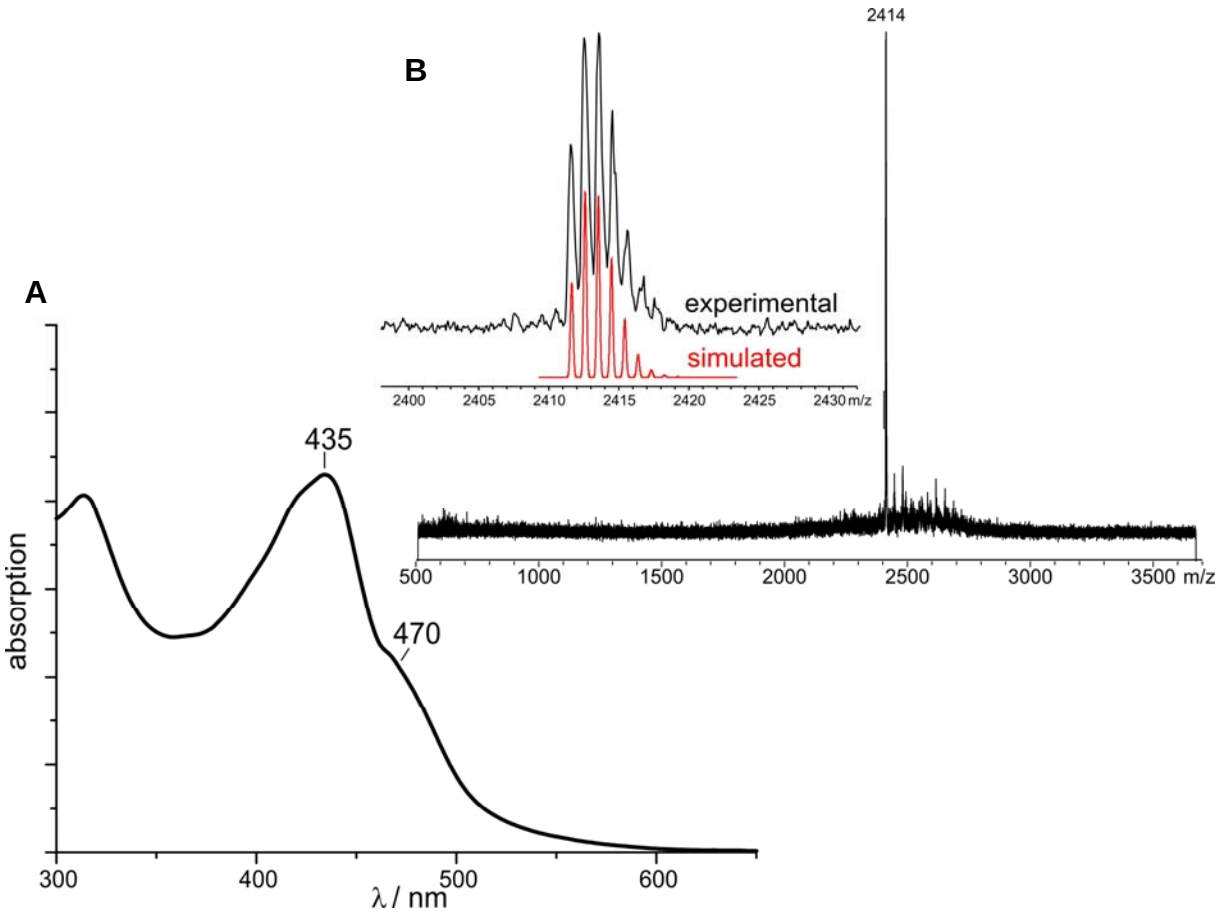

Figure 4-43: A) MALDI-TOF MS and **B**) UV/vis of C72-$(C_{12})_4$-$(C_{10}$-COOEt$)_4$ (**4-64**).

Already at the stage of the ester functionalized derivative C72-$(C_{12})_4$-$(C_{10}$-COOEt$)_4$ (**4-64**), it was expected that the product and the corresponding intermediate species should show a different retention time, due to the small but existing higher polarity, induced by the ester functionalities. Unfortunately, it was found also in this case that no improved separation compared to Figure 4-40 occurred, , indicating that the ester entities do not exhibit a sufficiently strong influence.

Therefore, the ester functionalized compound C72-$(C_{12})_4$-$(C_{10}$-COOEt$)_4$ (**4-64**) was hydrolized, using potassium hydroxide in boiling THF. By this procedure, one gained a highly crystalline, dark compound (**4-65**). This material could not be solubilized in any kind of common organic solvent, generally applied for column chromatography. This distinct low solubility, indicated the occurrence of strong hydrogen-bonds. It has already been verified in the previous chapter that the introduction of such hydrogen bonds exerted by carboxy functions can lead to a reduction in solubility. However, such a strong effect was not expected, as the carboxy functionalities were situated at the end of a long alkyl tether, similar to the mono-acid HBC derivative **3-3**.

This of course denied any of the planned chromatographical separations. Not only the insolubility prevented a further application of this compound, but also its crystallinity and lack of thermal properties denied any further processing.

4.5 Influencing the Electronic and Solubility Properties of the Oligophenylene Precursor

4.5.1 Removal of Alkyl Side-Chains

In the previous example, it became obvious that the induction of hydrogen bond exerting functional groups will lead to an insoluble material, which cannot be submitted to any kind of chromatographic separation. However, it is clear that only a strong difference in the retention times can yield a successful separation. Instead of adding functionalities, which exert the necessary influence on the solubility of the compound, it is also possible to remove some of the solubilizing alkyl chains to induce a similar effect. Thereby, it would be expected that the partially fused compounds should show a higher solubility and as a consequence shorter retention times for a chromatographic separation with standard organic solvents.

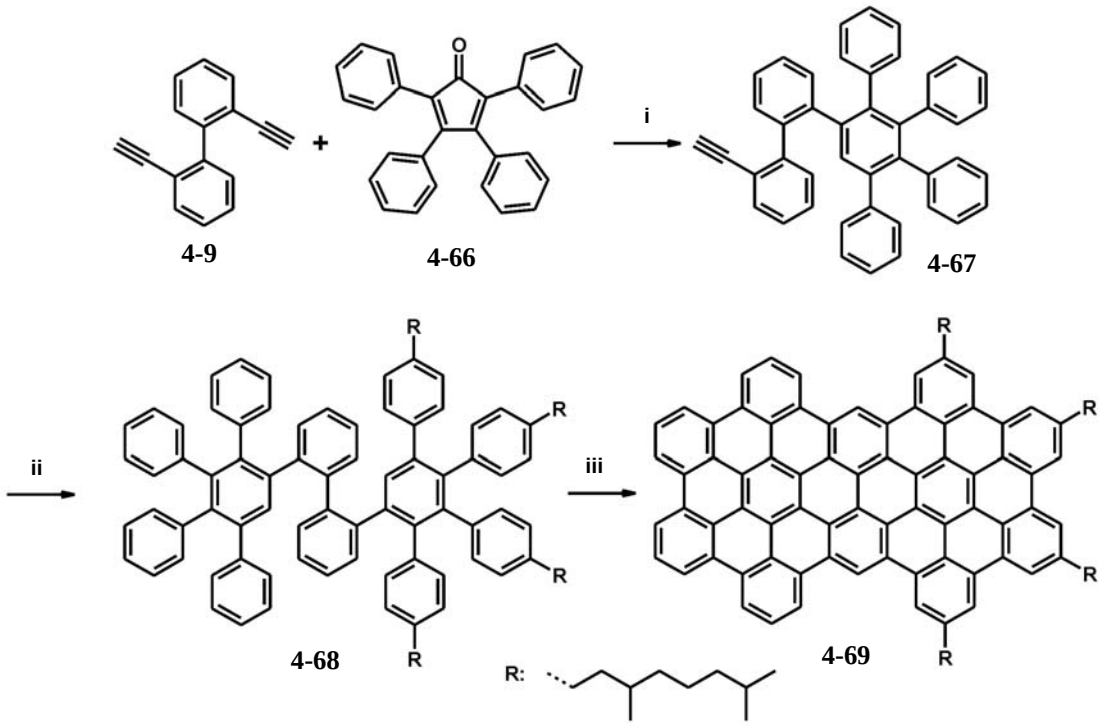

Figure 4-44: Preparation of the partially dealkylated C72-$(C_{8,2})_4$ (**4-69**). *i:* o-xylene, reflux, 8h, 71%; *ii:* diphenylether, 8h, 240 °C, 92%; *iii:* $FeCl_3$, CH_3NO_2, CH_2Cl_2, 25 °C, 24h, 92%.

In addition, it was suggested by the results presented above, that the alkyl chains show a distinct influence upon the cyclodehydrogenation progression. Whether this is due to the differences in the solubilizing effects or some electronic component could not be revealed so far. On the other hand, it was also interesting to determine, what effect a reduction of alkyl chains will show upon the scope of the intramolecular Scholl reaction. To obtain a clear difference between the octa-substituted C72 derivatives and the respective, partially dealkylated counterpart regarding the solubility, it was decided to use the 3,7-dimethyloctyl chain as the four remaining alkyl substituents. As shown in section 4.1.3, the cyclodehydrogenation of the precursor of C72-$(C_{8,2})_8$ (**4-42**) required the least amount of oxidant in combination with the shortest reaction time, until the MALDI-TOF MS revealed the completeness of the reaction. Of course, it cannot be undoubtedly determined, if this example is superior to the others on the basis of MALDI-TOF MS. However, the MALDI-TOF MS spectra for the C72 derivatives shown in section 4.1.3 were obtained under similar conditions, and therefore the results should be roughly comparable.

The synthesis corresponded to the one already described for C72-$(C_{12})_4$-$(C_{10}$-COOEt$)_4$ (**4-64**). Also in this example, the synthesis started with a Diels-Alder cycloaddition of 2,2´-diethynylbiphenyl (**4-9**) and an equimolar amount of unsubstituted tetraphenylcyclopentadienone (**4-66**) followed by a chromatographical separation of the mixture, which yielded the product **4-67**. In a second cycloaddition the oligophenylene precursor molecule **4-68** was prepared in almost quantitative yields and planarized with $FeCl_3$ dissolved in nitromethane as the oxidant.

However, even by applying up to 60 equivalents of $FeCl_3$ for every aryl-aryl bond formation and by a prolongation of the reaction time to three days, no fully planarized product (**4-69**) could be identified by MALDI-TOF MS. Instead, chlorination of the partially fused species became dominant.

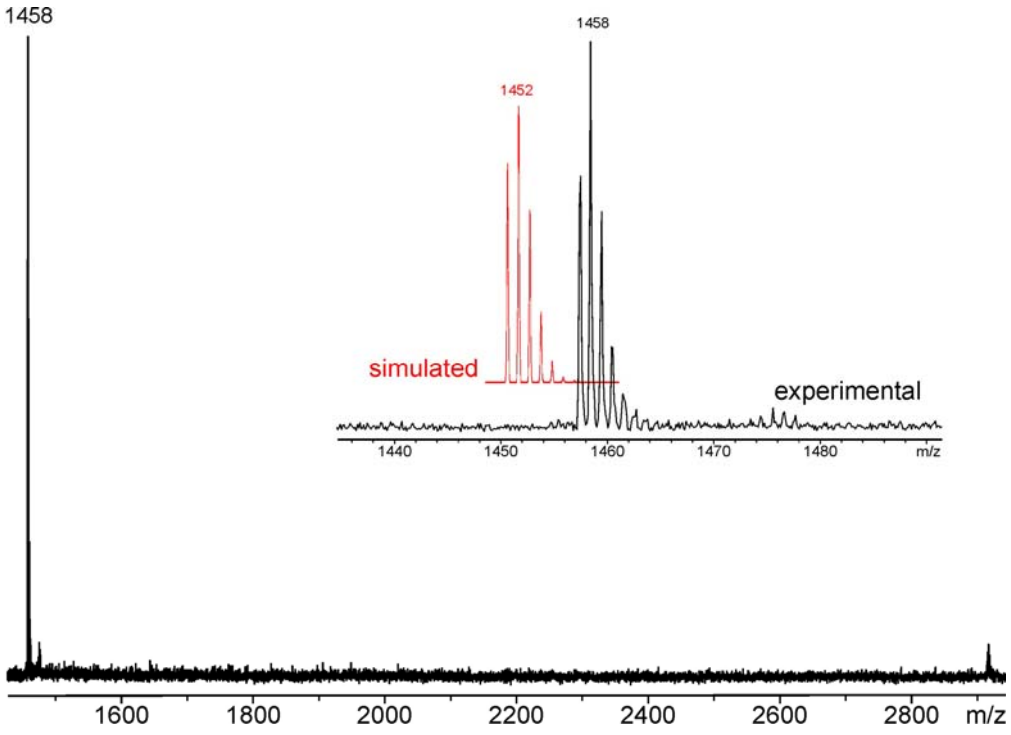

Figure 4-45: MALDI-TOF MS of the resulting product appearing during the cyclodehydrogenation of the precursor **4-68**. **A**) full spectrum, **B**) amplification of produkt signal compared to the expected value for C72-$(C_{8,2})_4$ (**4-69**).

On the other hand, in the MALDI-TOF MS a single peak was identified (Figure 4-45), which is exactly six mass units too high, indicating that exactly three bonds were not established during the cyclodehydrogenation reaction. In contrast to the other examples examined so far, where a broad distribution of different substances was found in the MALDI-TOF MS investigations with different matrices, only one distinct side-

product occurred in this case. However, it had to be noted that this compound could also be overestimated similar to the fully planarized products for the octa-substituted C72 derivatives C72-$(C_{12})_8$ (**4-44**), C72-$(C_{8,2})_8$ (**4-45**) and C72-(Ph-$C_{12})_8$ (**4-46**).

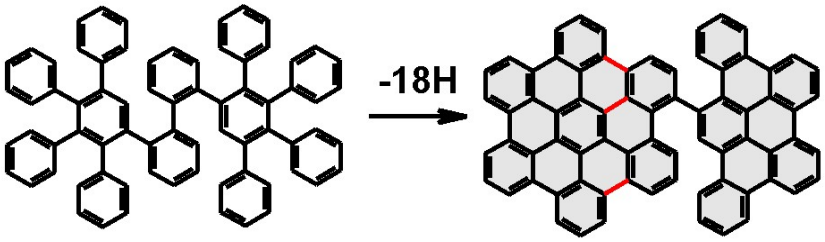

Figure 4-46: Plausible product of cyclodehydrogenation of precursor **4-68** (alkyl chains are omitted for clarity).

The mass difference to the expected value in Figure 4-45 is moreover reproducible, as in every batch only this specific material could be mass spectrometrically observed, which opens up the opportunity to determine the exact structure of this substance. Unfortunately, it was again not possible to gain a detailed NMR spectrum, as also in this case only broad and unresolved aromatic signals could be observed. As the NMR technique is next to single crystal X-ray, the only possibility for an unambiguous determination of such a compound, no clear information about the nature of the side-product could be given. Therefore, the following discussion is again purely speculative and could not be supported by additional analytical data.

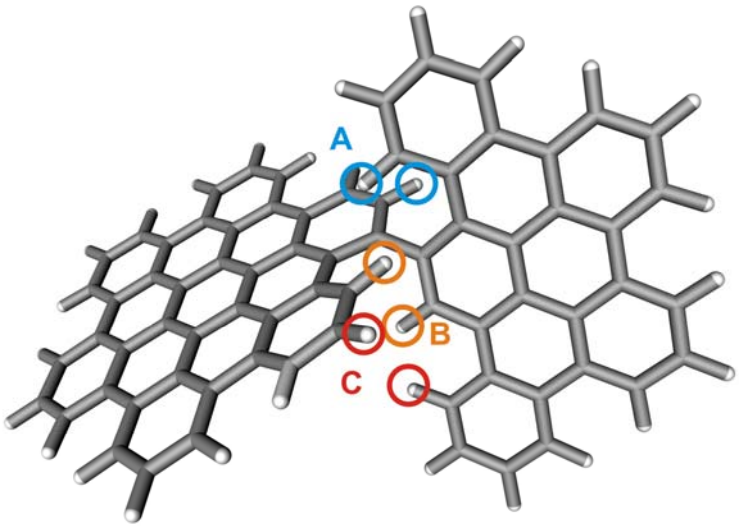

Figure 4-47: Spatial model of the assumed product formed in the cyclodehydrogenation of **4-68** (alkyl chains are omitted for clarity).

According to the assumptions made in section 4.3.3 only one possibility could be determined, which also fits the proposed structure of one byproduct of the cyclodehydrogenation of C72-$(C_{12})_8$ (**4-44**).

Nevertheless, this case can serve as an indicative example, and supports the beforehand proposed general reaction progression, pointing towards the assumed formation of tribenzo-[b,n,pqr]perylene moieties. In this proposed partially fused side-product the steric requirements of six hydrogens are expected to be too high for adopting a spatially sufficient planar status for the next aryl-aryl bond formation and to initiate the "stitching" together of the two aromatic panels. The exact reason, why in contrast to C72-$(C_{12})_8$ (**4-44**) such a monodisperse side-product was indicated by the MALDI-TOF MS is not known. However, this can also be indicative for the influence of the alkyl chains upon the scope of the reaction due to a changed electronic situation in the oligophenylene precursor molecule or due to the respective induced solubility of the side-chains. These assumptions could however not be founded, because of the lack of analytical data.

4.5.2 Changing the Oligophenylene Substitution Pattern

It has been observed by X. Feng and C. Kübel[71] that different oligophenylene precursor molecules **4-70**, **4-72**, **4-73** and **4-74** of HBC, when submitted to the same cyclodehydrogenation conditions, show distinct differences in reactivity. All the presented examples should lead to the formation of unsubstituted HBC (**4-75**). As reported by C. Kübel, the reaction pathway starting from hexaphenylbenzene (**4-70**) includes a partially fused intermediate (**4-71**), which he could isolate and prove its structure by single crystal X-ray diffractometry. Another interesting behavior is that chlorination of the product occurs rather easily during the cyclodehydrogenation reaction and requires a fine-tuning of the conditions. In addition, the reaction does not show a high degree of reproducibility, but between several batches treated with the same conditions, sometimes strong differences with respect to the chlorination can occur. The lack of reproducibility therefore limits the scope of this reaction towards unsubstituted HBC (**4-75**).

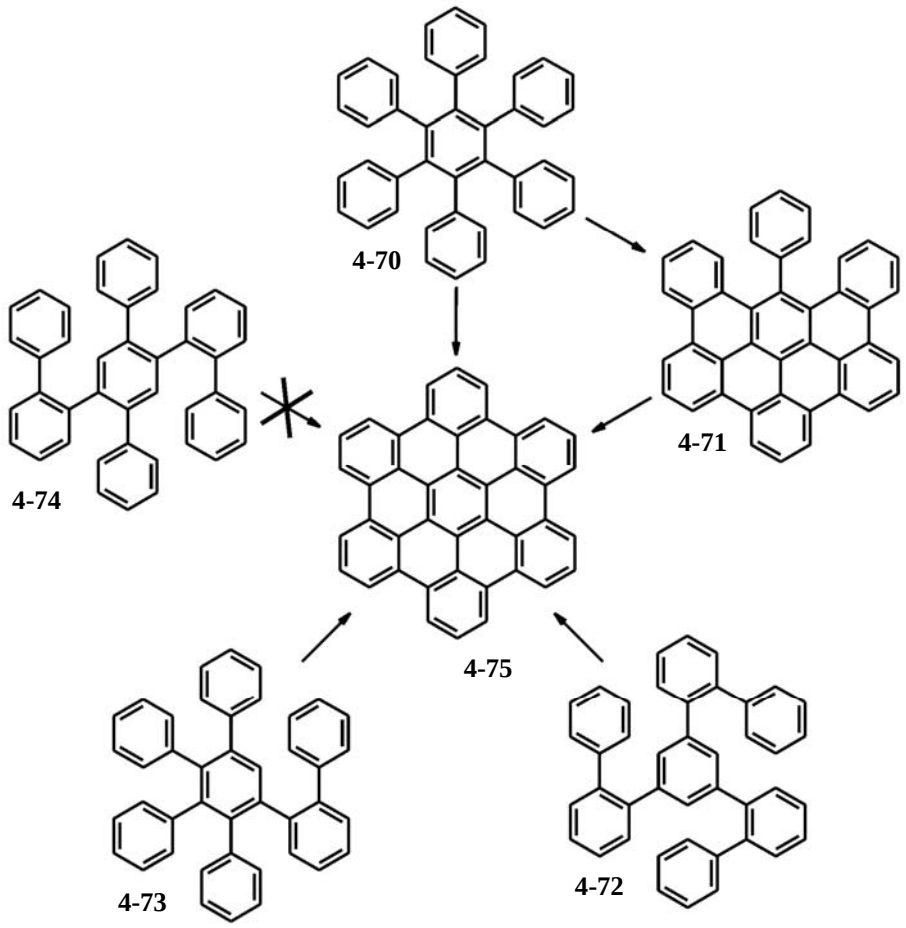

Figure 4-48: Different phenyl substitution patterns for the preparation of unsubstituted HBC (**4-75**).

X. Feng noted that by using the precursor **4-74**, where two phenyl rings are not anymore directly connected to the core benzene, but are attached in two biphenyl moieties, the reactivity of the precursor with respect to the Scholl conditions is rather low. Even by applying a huge excess of the oxidant no or only a minor reaction was observed. In the example **4-73**, which was tested by the author of this text, the reaction showed similar reactivities as for **4-70**. Again the reaction progressed smoothly, but nevertheless exhibited the same problem as seen for **4-70** concerning chlorination and reproducibility. For a novel synthetic approach by X. Feng, where three biphenyl moieties were substituted around the central benzene ring (**4-72**), a completely other reactivity was found. According to MALDI-TOF MS, the product was less susceptible to chlorination during the cyclodehydrogenation, even by applying harsher conditions like more oxidant or prolonging the reaction times and resulted in an improved purity for the gained HBC (**4-75**).

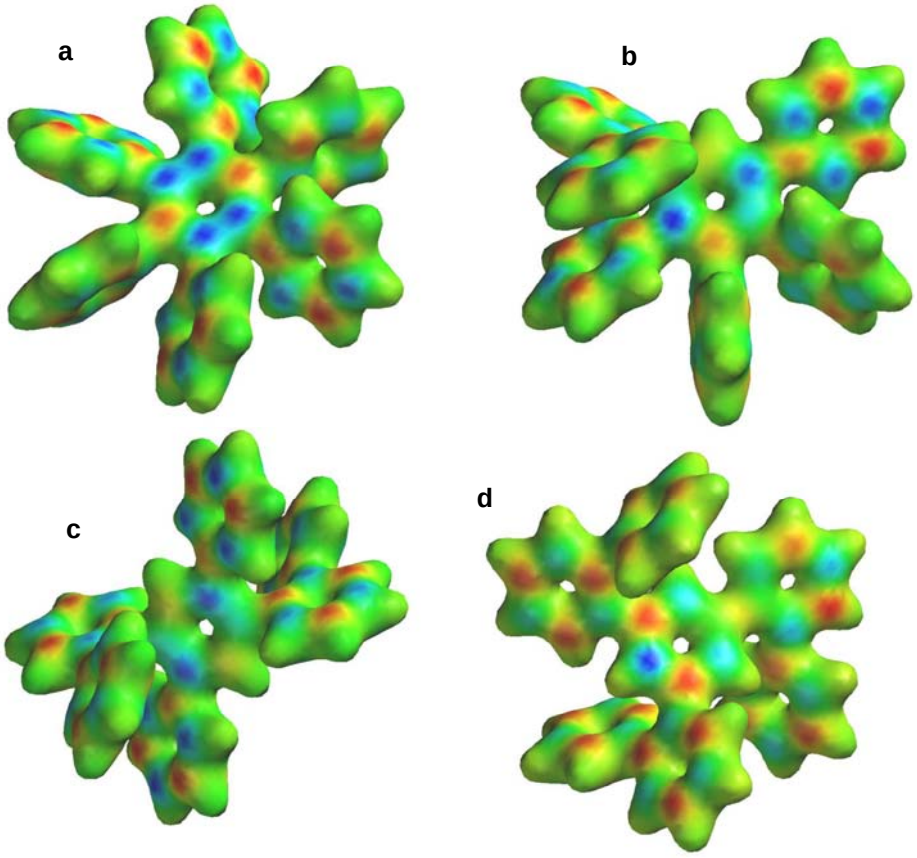

Figure 4-49: Spin density calculations of the radical cation of **a**) **4-70**, **b**) **4-73**, **c**) **4-74** and **d**) **4-72**.

As mentioned above, the true nature of the cyclodehydrogenation reaction is still unknown. It was found that the reaction proceeds either by a radical or a arenium based pathway. In both cases, a positive charge is induced on the precursor molecule. In the theoretical calculations done by using a semi-empirical method (AM1), it was indicated that the relative spin density of the respective radical cations could not be located on a specific position in the molecules (Figure 4-49). The spin density was rather uniformly distributed over the molecule. Although from a theoretical point of view, no difference is expected, the influence of the phenyl substitution pattern was impressively proven by the conducted experiments.

It has to be concluded that the progression and initiation of the intramolecular Scholl reaction remains questionable. This becomes even clearer by considering the fact that the partially fused species determined by C. Kübel does not necessarily need to be the result of a stepwise addition of benzene rings, but could have also been established by an initial formation of two triphenylene units leading to the intermediate structure **4-77** (Figure 4-50).

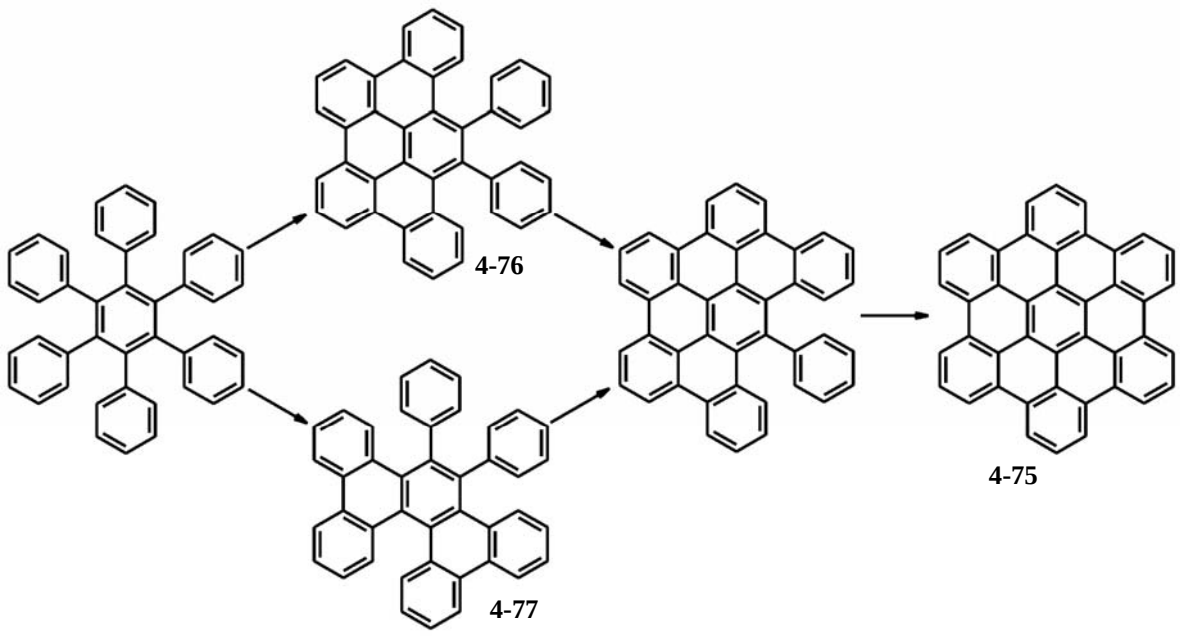

Figure 4-50: Possible intermediate states during cyclodehydrogenation towards **4-75**.

In order to adapt the topology pattern of the benzene rings within the precursor molecule for the C72 derivatives, the central biphenyl entity with the acetylene functionalities, as well as the tetraphenylcyclopentadienone derivatives have to be adapted. Indeed, the exchange of the 2,2'-diethynylbiphenyl with its 2,4'-diethynylbiphenyl derivative proved to be the most efficient way to influence the topology pattern of the C72 oligophenylene precursor (Figure 4-51).

By a Negishi cross coupling of the compound **4-78**, which was prepared according to a literature procedure from 1-iodo-2-bromobenzene and activated zinc,[79] with 1-iodo-4-bromobenzene (**4-79**), the 2,4'-dibromobiphenyl (**4-80**) could be gained in a straighforward manner. It was remarkable that for the Hagihara reaction, unlike for the 2,2'-dibromobiphenyl (**4-17**), no difficulties were encountered and the 2,4'-bis[(trimetylsilyl)ethynyl]-biphenyl (**4-81**) was obtained in good yields. This is an indication that for the 2,2'-dibromobiphenyl (**4-17**) the steric situation indeed played a major role. For the 2,4'-dibromobiphenyl (**4-80**), the substitution occurs at two sites, where after one substitution of a bromine with the corresponding trimethylsilylacetylene entity, the second substitution can occur without encountering the steric restriction of a bulky trimethylsilyl functionality, yielding compound **4-81**.

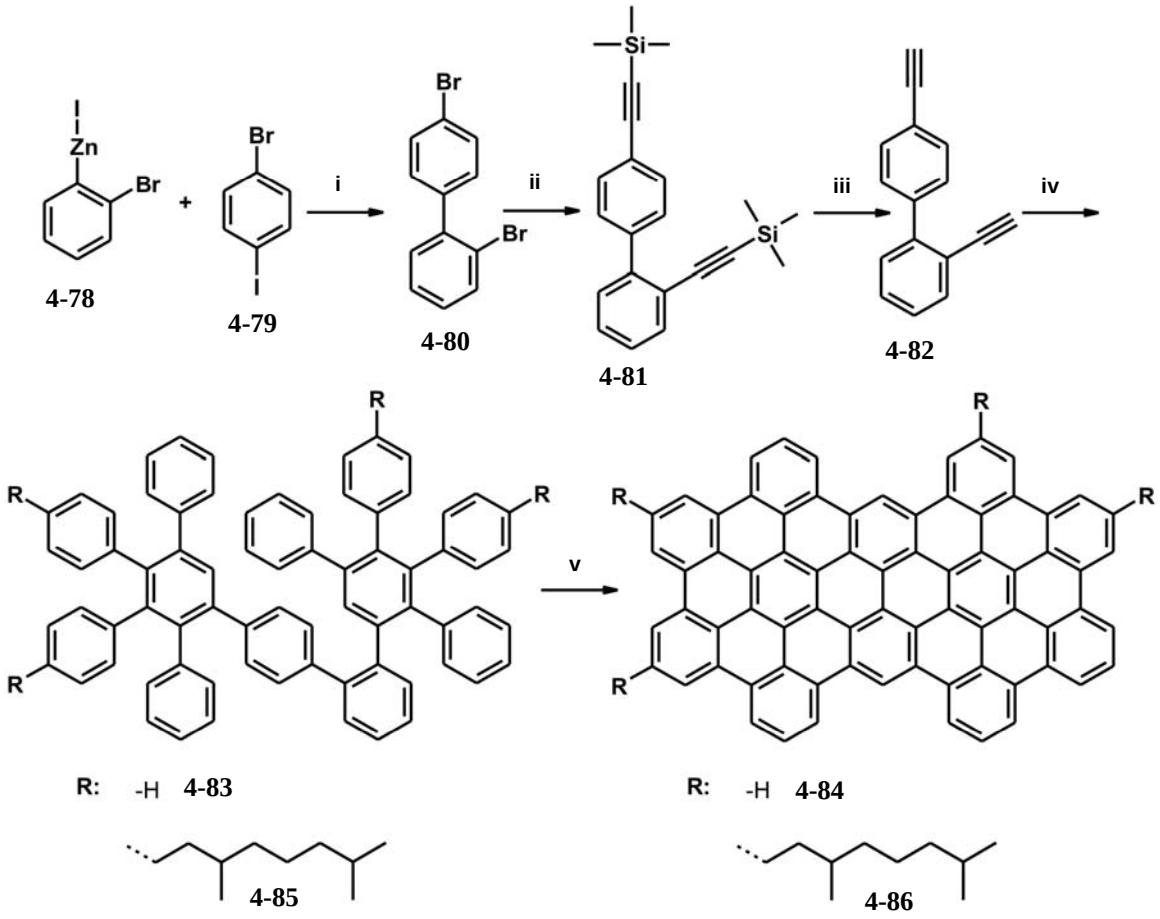

Figure 4-51: Preparation of the C72 derivatives C72 (**4-84**) and C72-$(C_{8,2})_{4(asy)}$ (**4-86**). *i:* THF, $Pd(PPh_3)_4$, 30 °C, 1h, 82%; *ii:* TMS-acetylene, $Pd(PPh_3)_2Cl_2$, CuI, piperidine, 80 °C, 12h, 92%; *iii:* NaOH aq., MeOH, 45 min., 25 °C, 98%; *iv: o*-dichlorobenzene, reflux, 8h; *v:* $FeCl_3$, CH_3NO_2, CH_2Cl_2, 25 °C.

The 2,4'-diethinylbiphenyl (**4-82**) yielded in the following Diels-Alder cycloaddition with the corresponding tetraphenylcyclopenadienone derivative the oligophenylene precursor **4-83** or **4-85** respectively. In a model reaction, the cyclodehydrogenation is examined for the precursor **4-83** to gain the unsubstituted C72 (**4-84**). For the other case, the subsequent cyclodehydrogenation of the molecule **4-85** is expected to yield the desired C72 derivative C72-$(C_{8,2})_{4(asy)}$ (**4-86**). However, only four alkyl chains can be attached in the corona of the molecule, leading possibly to a reduced solubility of the material and to a reduced reactivity under Scholl conditions, similar as observed for C72-$(C_{12})_4$ (**4-69**) Therefore, a tetraphenylcyclopentadienone with 3,7-dimethyloctyl alkyl chains was used, although the tetraphenylcyclopentadienone derivative with two dodecyl chains is easier to achieve. By using the 3,7-dimethyloctyl chain with its chiral carbon atoms one gains not only higher solubility due to the suppressed chain

crystallization, but also the larger sterical requirements close to the core reduces effectively aggregation.

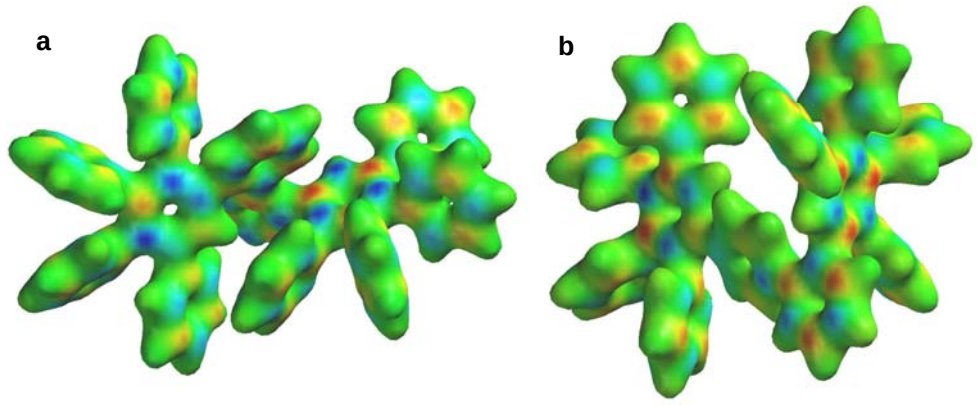

Figure 4-52: Spin density calculations of the radical cation of **a**) **4-41** to **4-43**, **b**) **4-83** and **4-85** (alkyl chains are omitted for clarity).

As expected from the results of the HBC precursor molecules above (Figure 4-48), also for the two types of the C72 precursor molecules no severe change in the spin density of the induced radical cation could be determined by theoretical calculations (Figure 4-52). In addition, the phenyl system is far larger than for the HBC, which leads to an even slightly better delocalization of the spin densities. Nevertheless, it has to be emphasized that for the HBC case, the experimental evidence clearly contradicted the theoretical results.

As a first step, it was necessary to verify, if a C72 derivative like C72-$(C_{8,2})_{4(asy)}$ (**4-86**) can indeed be synthesized *via* this route. Therefore commercially available unsubstituted tetraphenylcyclopentadienone was used in a Diels-Alder cycloaddition with 2,4'-diethynylbiphenyl to gain compound **4-83**. The precursor was in the beginning treated by using similar conditions as for the other C72 derivatives. Under these conditions however strong chlorination of the final product was observed in the MALDI-TOF MS. On the other hand, experiments with lower amounts of oxidants revealed that some intermediate species were still visible under the MALDI-TOF MS conditions. Only by a fine-tuning of the reaction time and the amount of oxidant, it was possible to achieve an optimum result, regarding the MALDI-TOF MS spectra (Figure 4-53). In the MALDI-TOF MS spectrum, it was even possible to visualize the mass signals for the dimer and the trimer of the compound (**4-84**).

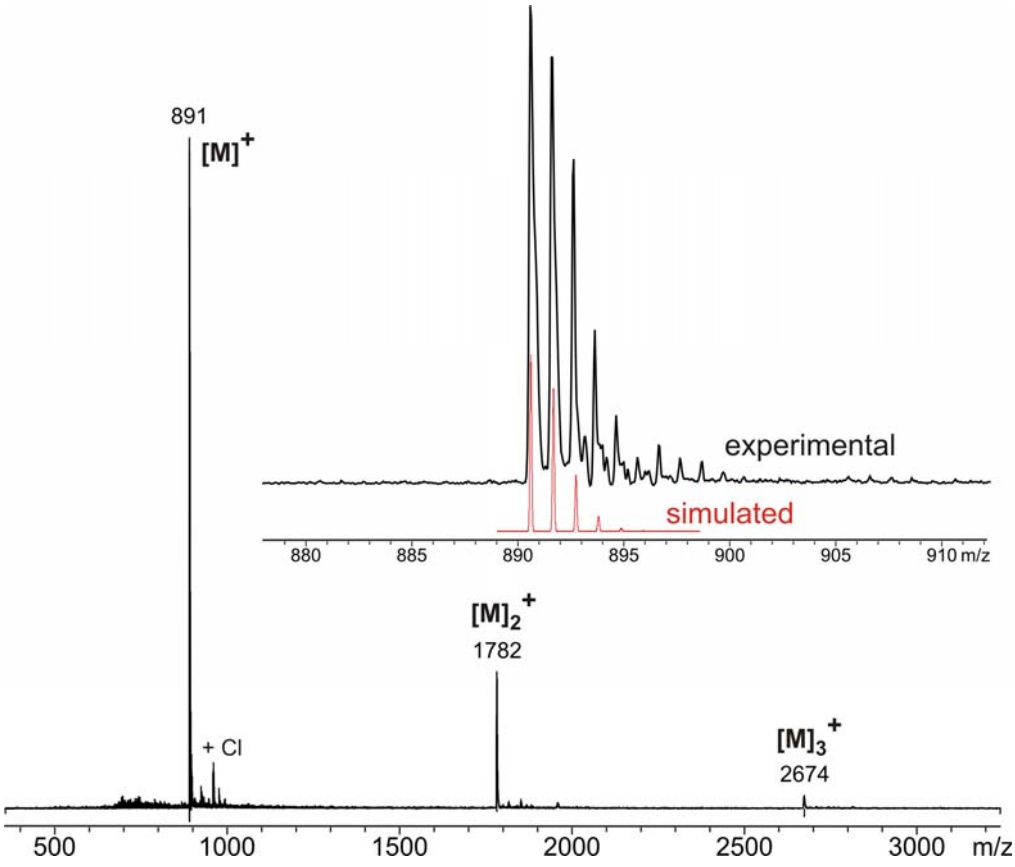

Figure 4-53: MALDI-TOF MS of **4-84** with TCNQ.

Therefore, the reaction yielded the desired product from this highly asymmetrically precursor molecule and as seen for the comparison of the simulated and the recorded spectra in the MALDI-TOF MS (Figure 4-53), also the isotopic pattern was equal to the simulated one, even though some disturbing signals in the side of the main peak could be observed. Another remarkable fact was that almost no chlorination was observed under these reaction conditions in the MALDI-TOF MS spectrum.

However, for the time-dependent MALDI-TOF MS spectra, recorded during the cyclodehydrogenation of the alkylated C72-$(C_{8,2})_{4(asy)}$ **4-86**, some small deviations from the theoretical values were observed (Figure 4-54). As shown above, the mass difference between the last partially fused intermediates and the product is rather small. Therefore, even on the basis of the MALDI-TOF MS spectrum, it becomes obvious that some of the intermediates are still present, especially by focussing on the minor, but still visible signals in the region of 1460 Dalton after 12 hours reaction time. Again, a treatment of the oligophenylene precursor with a large excess of the oxidant did not improve the results received from the MALDI-TOF MS, but moreover chlorination of the partially fused intermediates became apparent.

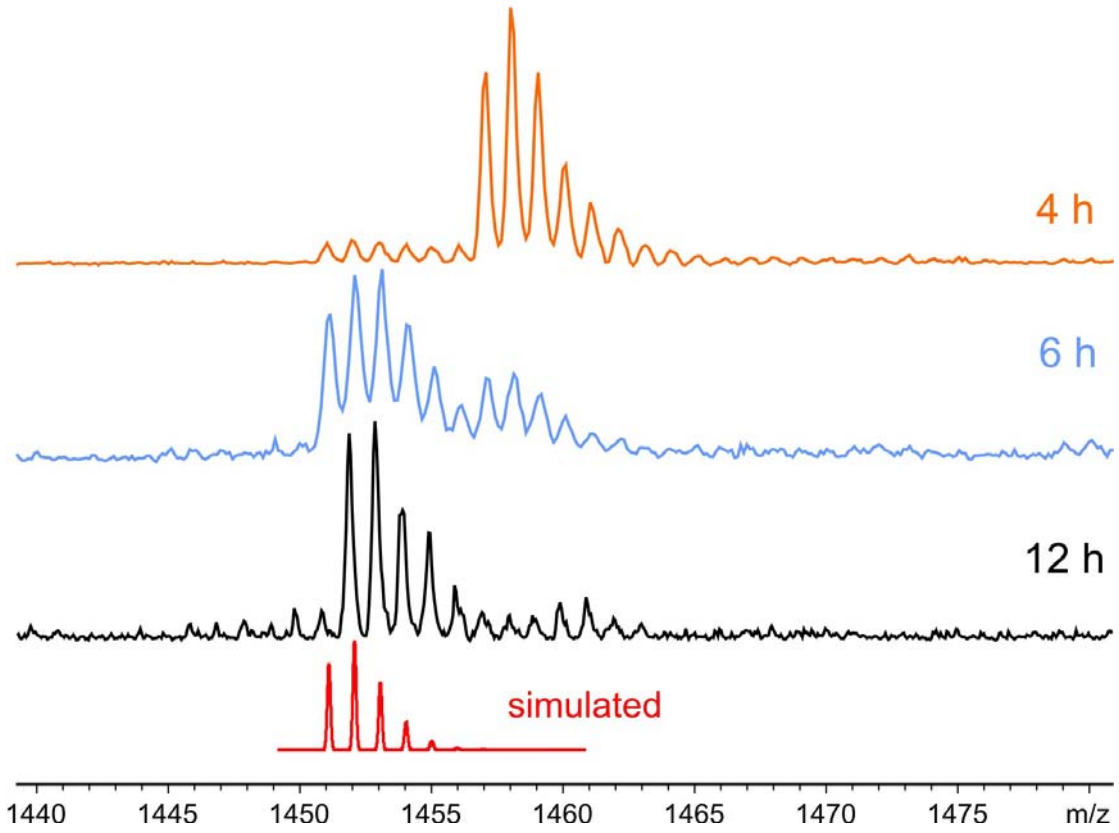

Figure 4-54: Time dependent MALDI-TOF MS measurements of the cyclodehydrogenation of **4-86.**

Therefore, the amount of oxidant was again reduced and instead an extension of the reaction time was considered. However, the same effect of the chlorination of the intermediate species was observed in this approach.

For verification of the MALDI-TOF MS results a UV/vis spectra in THF was recorded. In the UV/vis a hypsochromic shift of almost 30 nm for the maximum absorption peak was observed compared to the other derivatives C72-$(C_{12})_8$ (**4-44**) and C72-$(C_{8,2})_8$ (**4-45**) (Figure 4-55). This strong shift is not likely to be caused by an aggregation phenomena, as for other PAHs the shifts of the bands were not so strongly dependent upon concentration and therefore it has to be assumed that a larger amount of partially closed species is present in compound C72-$(C_{8,2})_{4(asy)}$ (**4-86**). Another source for the shift is the different alkyl substitution pattern and the number of attached alkyl chains, possibly exhibiting a small influence on the electronic properties of the aromatic core component. Such a strong shift however has not been observed for other PAHs like HBCs, as a change in the alkyl substitution pattern did never result in a shift of the maximum absorption peak at 360 nm of more than 1-2 nm. Therefore, the changes of the alkyl substitution pattern are presumably not the cause for the hypsochromic shift of

C72-$(C_{8,2})_{4(asy)}$ (**4-86**). Unfortunately, also in this case the NMR data did not give any indication of the status of the material or even the amount of intermediates present, as the aromatic signals were broad and unresolved. As a consequence, it was likely that the MALDI-TOF MS again severely overestimated the fully fused product.

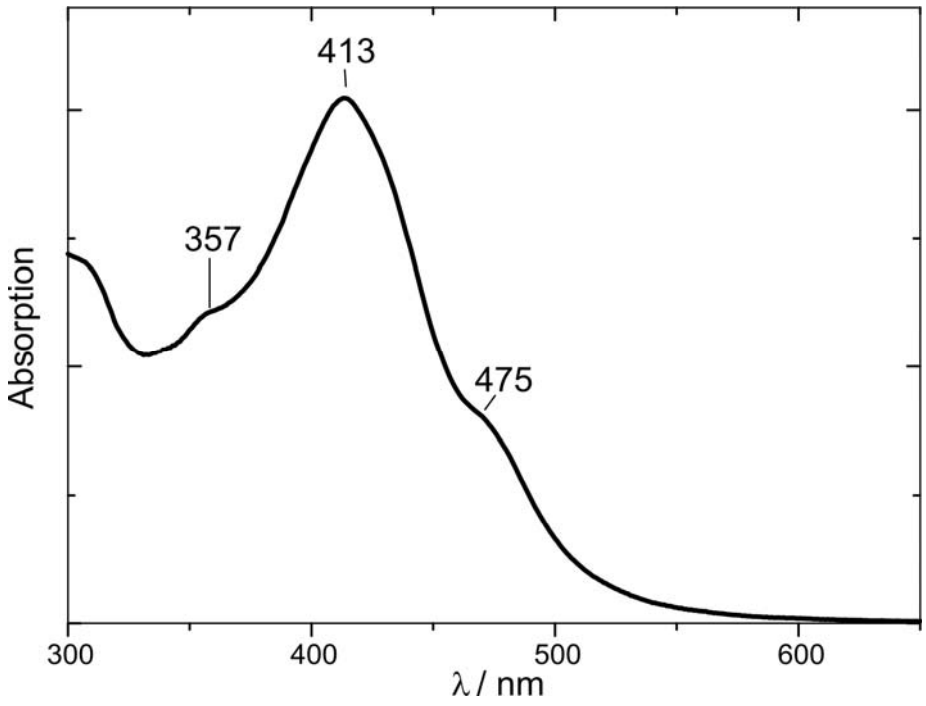

Figure 4-55: UV-vis of C72-$(C_{8,2})_{4(asy)}$ (**4-86**) in THF at room temperature.

Fortunately, it was possible to indirectly verify to some degree by a control experiment the amount of intermediates for the compound C72-$(C_{8,2})_{4(asy)}$ (**4-86**) by using for the Diels-Alder cycloaddition a tetra-alkylated derivative of the tetraphenyl-cyclopentadienone (**4-26**). This procedure also replaced in this case the time consuming search for the appropriate MALDI-TOF MS conditions. By this approach, it was possible to simply block synthetically an aryl-aryl bond formation with an alkyl chain and to prevent the full planarization of the precursor. This blocking should lead to a mixture of partially fused intermediates (**4-88**). The comparison of the mixture **4-88** with C72-$(C_{8,2})_{4(asy)}$ (**4-86**) could then give a further insight into the present amount of the intermediate species in the batches of the compound C72-$(C_{8,2})_{4(asy)}$ (**4-86**).

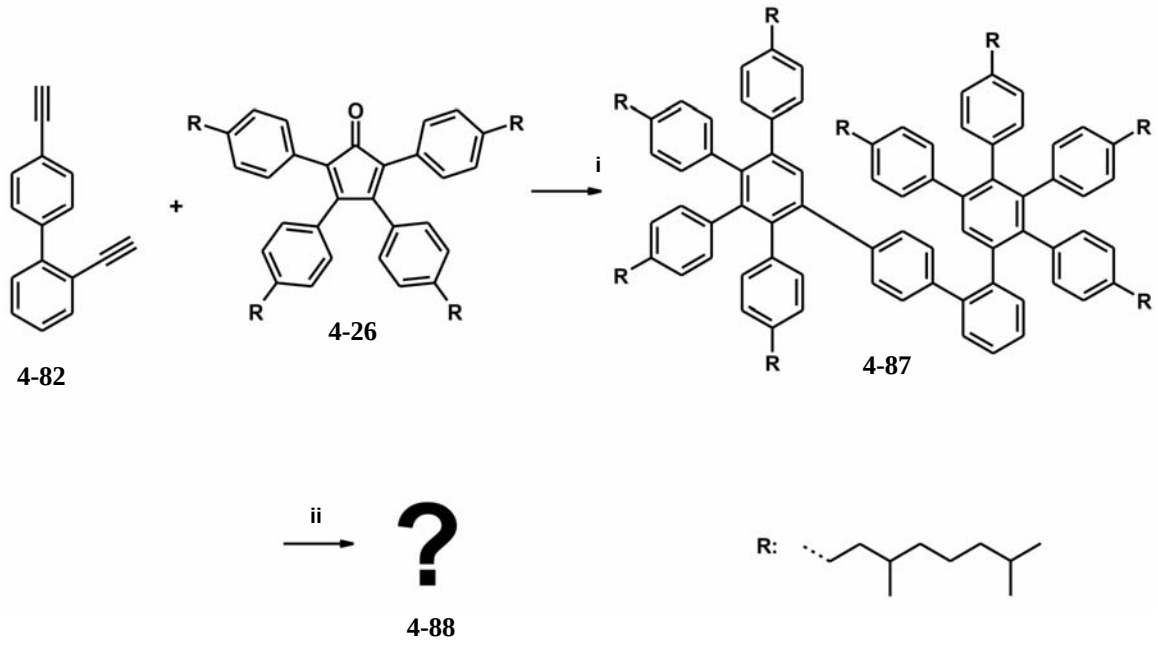

Figure 4-56: Preparation of the product mixture (**4-88**) from the cyclodehydrogenation of precursor **4-87**. *i:* o-xylene, reflux, 8h, 95%; *ii:* $FeCl_3$, CH_3NO_2, CH_2Cl_2, 25 °C, 12h, 93%;

The second information that can be gained with this experiment is the answer to the question, how much strain the Scholl reaction and the molecule tolerate towards the rim of the aromatic core, as was assumed in the discussion in section 4.3.3. Two possibilities are plausible in this scenario: either the cyclodehydrogenation immediately stops, when the steric repulsion of the blocking alkyl chain becomes iminent, which would result in the formation of only one partially fused product, or the reaction will proceed and starts "stitching" together sinlge panels as long as possible. In the second case, the progression will be dependent upon the different activation energies encountered in the variety of possible intermediates, leading to a broad distribution of partially fused products.

In Figure 4-57 the MALDI-TOF MS of the reaction product (**4-88**) and another batch of C72-$(C_{8,2})_{4(asy)}$ (**4-86**) is shown. The auxiliary batch of C72-$(C_{8,2})_{4(asy)}$ (**4-74**) has been prepared with the same amount of oxidant as for the optimum conditions, but the reaction was quenched already after one half of the necessary reaction time to gain enough intermediates for the MALDI-TOF MS analytics. A broad distribution of partially fused intermediates were revealed by the MALDI-TOF MS spectrum (Figure 4-57A), and side-products could be identified, where 5, 3 and 1 bond were not fused.

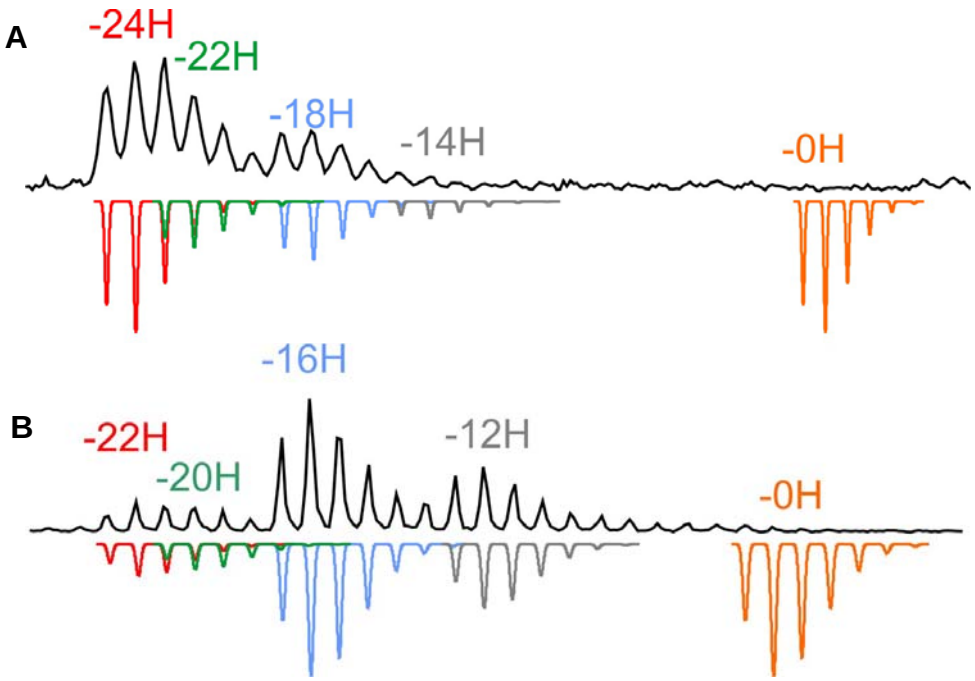

Figure 4-57: MALDI-TOF MS of **A**) C72-$(C_{8,2})_{4(asy)}$ (**4-86**) and **B**) the mixture **4-88**.

Two main signals of partially fused species were observed for the mixture **4-88**, where six and eight bonds were formed and additionally some almost fully closed products were determined, whereby ten and eleven bonds were established respectively. This indicated the formation of a strained species shown in Figure Figure 4-59 and supported the assumption of the "stitching" effect by initially formed panels during the cyclodehydrogenation (Figure 4-39). Therefore, it could be concluded that the intramolecular Scholl reaction, according to the already mentioned example of the permethoxylated HBC, did also not abort in the case of the mixture **4-88** due to encountered strain caused by sterical hindrance.

In addition, the UV/vis of the mixture **4-88** supported the assumption of the presence of a large amount of partially fused intermediates in the batches of C72-$(C_{8,2})_{4(asy)}$ (**4-86**). In Figure 4-58 the spectra of the mixture **4-88** was compared to the one from compound C72-$(C_{8,2})_{4(asy)}$ (**4-86**) and both exhibited a maximum absorption band at 413 nm. This indicated that in both cases similar amounts of partially fused species were present. This means that for the batches of the C72 derivative C72-$(C_{8,2})_{4(asy)}$, the major amount of product consisted possibly of partially fused intermediates, as for the mixture **4-88** no fully planarized product could be achieved.

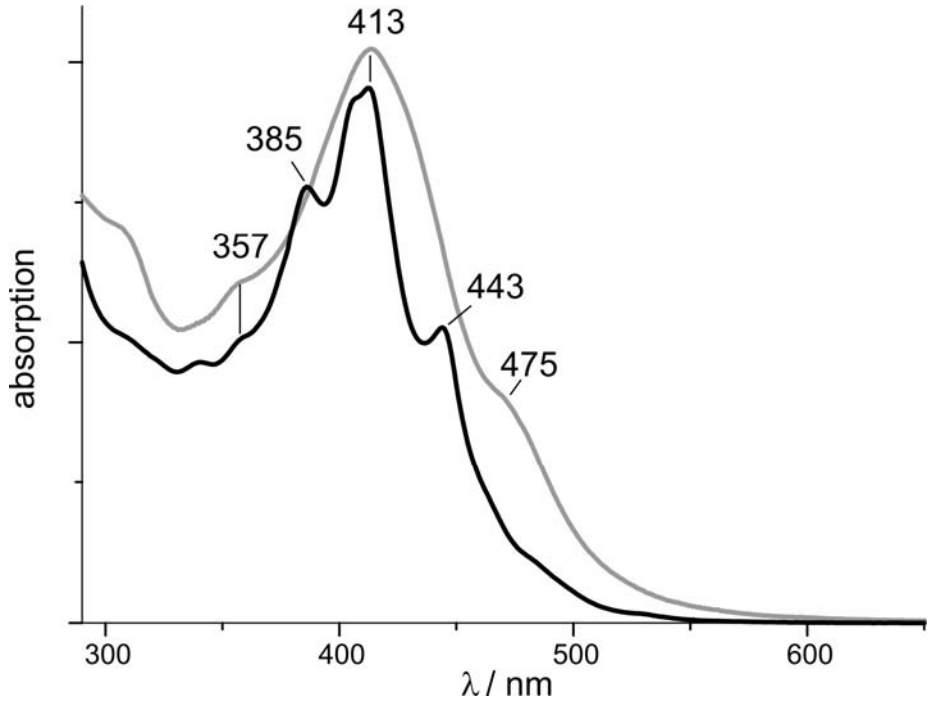

Figure 4-58: Comparison of the UV/vis of **4-88** (black) to C72-$(C_{8,2})_{4(asy)}$ (**4-86**) (grey).

Interestingly, the mixture **4-88** revealed far more resolved absorption spectra than C72-$(C_{8,2})_{4(asy)}$ (**4-86**). This effect could be due to a reduced aggregation propensity for the mixture. Hereby, it is not likely that simply a larger amount of unfused material in the mixture induced this reduction in aggregation, as for both examples similar extinction coefficients and the same location for the maximum absorption band were determined. Moreover, it was assumed that the presence of the alkyl chain, which efficiently blocked a reaction site during the cyclodehydrogenation, led to a distorted aromatic core component. This distortion could be to some extent responsible for the presumed aggregation reduction of the mixture. As detailed analytical data based on NMR spectroscopy were again not available, neither for the mixture **4-88** nor for C72-$(C_{8,2})_{4(asy)}$ (**4-86**), this argumentation remained purely speculative.

By applying the discussed assumptions in section 4.3.3, the two species **4-90** and **4-91** (Figure 4-60), corresponding to the largest signals in the MALDI-TOF MS (Figure 4-57), were probably formed during the cyclodehydrogenation of the oligophenylene precursor (**4-87**). This was contradicted by the fact that the main absorption band in the UV/vis occurred at 413 nm. The proposed intermediates should not show such a strong shift, as they consist of aromatic systems similar to 1.2,3.4,5.6,10.11-tetrabenzanthanthracene and HBC.

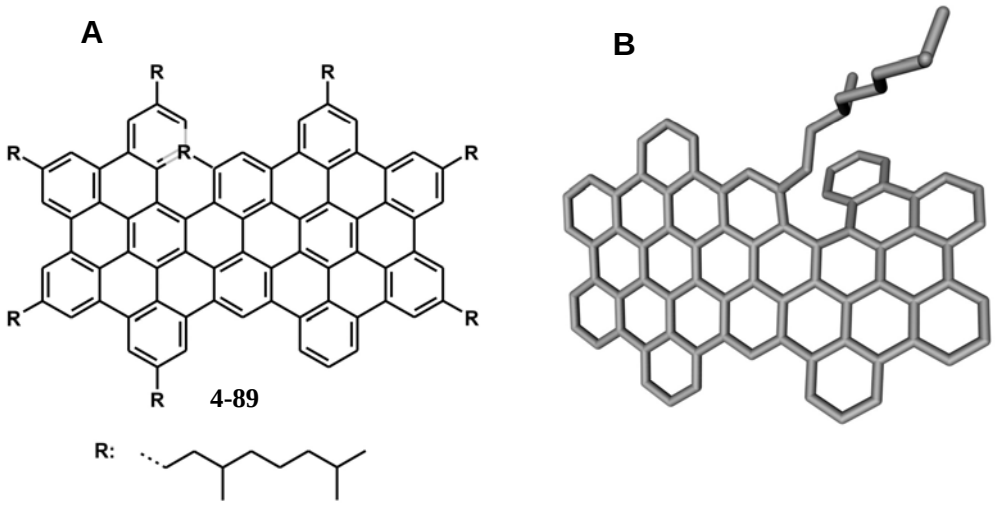

Figure 4-59: A) Schematic representation of the strained product (**4-89**) appearing during the cyclodehydrogenation of **4-87**; B) structure according to semiempirical AM1 calculations.

However, for a successful conjugation between the panels, the system would need to adopt an almost planar status, which requires to overcome the steric hindrance of at least four hydrogens (Appendix H). Therefore, a possible partial conjugation between the aromatic entities of the partially fused species could not be expected, as the steric hindrance of the hydrogens presumably forced the panels into an unfavorable conformation.

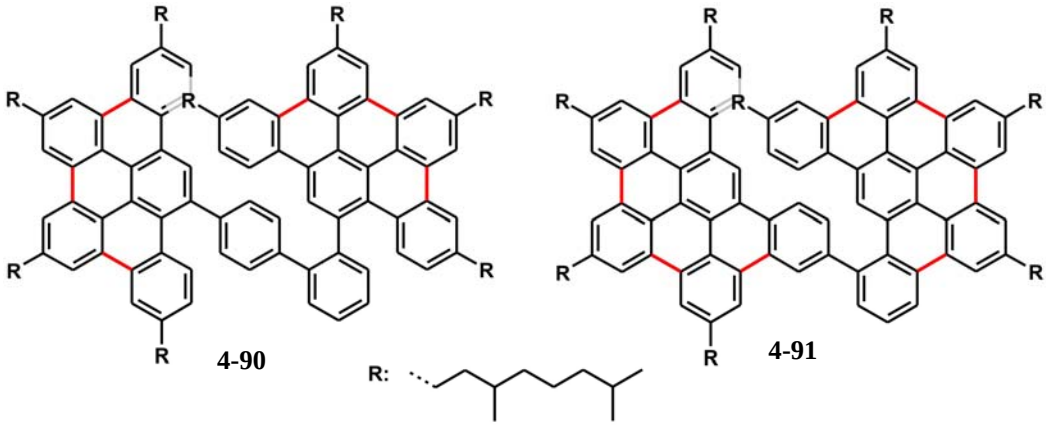

Figure 4-60: Proposed structures of the main products in the cyclodehydrogenation of precursor **4-87**.

Of course, it has to be noted that alkyl chains can migrate during the intramolecular Scholl reaction due to the present Lewis acid, leading to species, which could cause the necessary bathochromic shift observed in Figure 4-58. This behavior was already noted during the cyclodehydrogenation of alkylated hexaphenylbenzenes by using the stronger aluminum(III)chloride as the Lewis acid. This was amongst others one reason, why for

the cyclodehydrogenation step the aluminum(III)chloride was exchanged with the weaker iron(III)chloride. After exchanging the oxidant, the migration of the alkyl substitutents during the reaction seized.

Therefore, it can be concluded that the observed signals in the MALDI-TOF MS must originate from the strained side-product (**4-89**) shown schematically in Figure 4-59. These intermediates should also be responsible for the main absorption band in the UV/vis of the mixture **4-88** at 413 nm, as only these molecules could exhibit the necessary conjugation length (Appendix H).

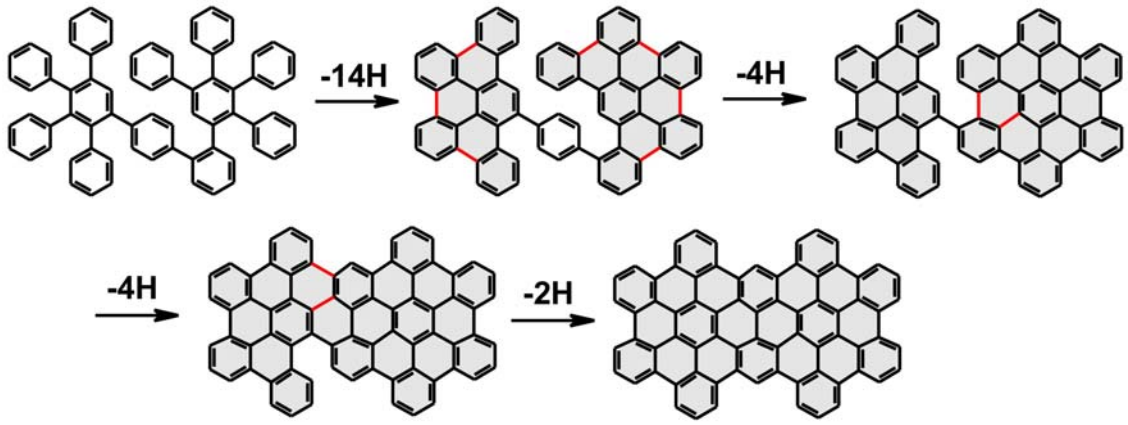

Figure 4-61: Possible intermediate structures according ot the signals observed in the MALDI-TOF MS in Figure 4-57A.

One major difference compared to the partially fused side-products of the previous example C72-$(C_{12})_8$ (**4-44**), was the occurrence of an intermediate during the cyclodehydrogenation of the oligophenylene precursor **4-85** with a molar weight of 1462 Dalton, which pointed towards five non-fused aryl-aryl bonds. This structure is special, as such an intermediate cannot appear from the precursor molecules **4-41** and **4-42**, supporting the assumptions declared in section 4.3.3 concerning the initial formation of panels. By respecting the changed symmetry of the precursor and by applying the same assumptions as for the derivatives C72-$(C_{12})_8$ (**4-44**) and C72-$(C_{8,2})_8$ (**4-45**) possible intermediate structures could be elucidated (Figure 4-61). Similar to the cyclodehydrogenation towards C72-$(C_{12})_8$ (**4-44**) and C72-$(C_{8,2})_8$ (**4-45**), a partially fused derivative appeared, where three bonds did not close. This species has already been observed for the more symmetrical example C72-$(C_{12})_8$ (**4-44**). Again it is assumed that after establishing the panels, the system seems to fall into a kinetic trap and

thereupon slowly "stitches" together the two panels. As shown in Figure 4-59 also similar strained systems appeared during the progression of this "stitching" process.

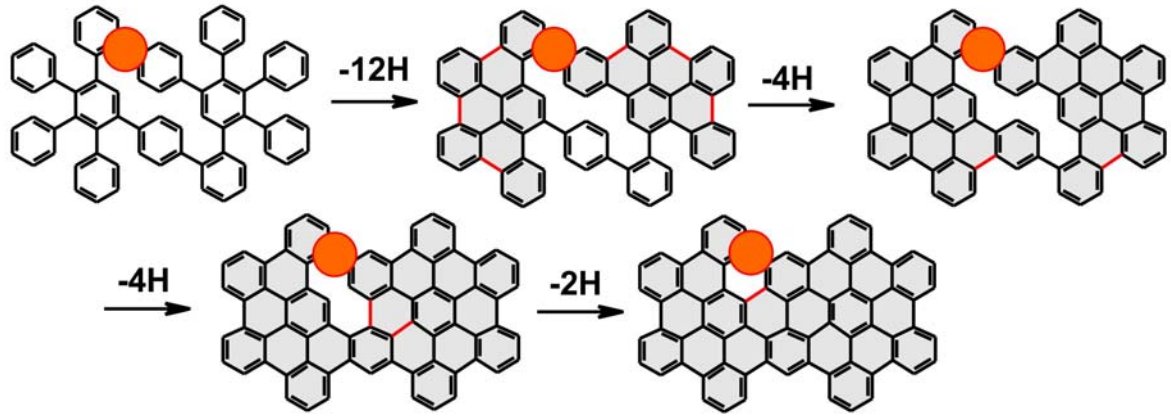

Figure 4-62: Possible intermediate structures according ot the signals observed in the MALDI-TOF MS in Figure 4-57B.

This "stitching" effect was also supported by the determined mass peaks of the cyclodehydrogenation progress of the precursor **4-87**. After the supposed initial formation of the panels the reaction proceeded again by "stitching" together the larger aromatic entities (Figure 4-62). This process could not be inhibited by the alkyl chain, which has been introduced to suppress a complete planarization of the precursor molecule. Indeed, the system even managed to establish the maximum number of aryl-aryl bonds, possibly forming the highly distorted product **4-89** (Figure 4-59) and proving the large acceptance of steric strain in the intramolecular Scholl reaction.

4.5.3 Conclusions

Already in the HPLC it was observed that the intermediate compounds of C72-$(C_{12})_8$ (**4-44**) exhibited similar retention times as the product. The differences seemed however large enough to indicate a certain possibility for a separation of the product by a consecutive chromatographical treatment. However, by this procedure a large quantity of the deployed material was left on the column and could also not be regained by a Soxhlet extraction of the stationary phase.

Another approach was the introduction of polar functional groups in the partially fused byproducts to enlargen the differences of the retention times of the compounds, which failed as neither the byproducts nor the fully planarized product were susceptible to the substitution reactions. By the adjacent synthesis of a C72 derivative C72-$(C_{12})_4$-

(C_{10}-COOH)$_4$ (**4-65**) the problem of the subsequent functionalization was circumvented by the introduction of the respective groups already at the stage of the oligophenylene precursor molecule. However, after the hydrolysis of the ester group, which by itself did not exhibit a sufficient influence on the polarity of the molecules, an insoluble material resulted, which could not be used for any subsequent workup procedure. By removing the alkyl chains from one side of the aromatic core component (C72-($C_{8,2}$)$_4$ (**4-69**)), it was again expected that a change in retention times towards preparative column chromatography would occur. Unfortunately, only one partially fused intermediate was formed in the cyclodehydrogenation step.

It has been shown in the case of unsubstituted HBCs that a change in the phenyl substitution pattern of the oligophenylene precursor also leads to a change of the reactivity of the compounds regarding the cyclodehydrogenation reaction. Therefore another C72 precursor with a different phenyl topology was prepared and submitted to the intramolecular Scholl reaction to yield C72-($C_{8,2}$)$_{4(asy)}$ (**4-86**). At a first glance from the MALDI-TOF MS it was indicated that the change of the phenyl substitution pattern did not lead to an improved purity of the resulting product. The comparison of the UV/vis with another example, where no fully closed product could be formed (**4-88**), revealed, that the major amount of the formed product in the C72-($C_{8,2}$)$_{4(asy)}$ (**4-86**) case, consisted mainly of partially fused intermediates.

4.6 Preplanarization of the Oligophenylene Precursor at the Outer Rim

4.6.1 C74, C76, C76-(*t*-Bu)

Although the change of the phenyl substitution pattern of the oligophenylene precursor did not yield an improved pathway for synthesizing C72, it is still assumed from the HBC case described in section 4.5.2, that an adaption of the aromatic system can have a severe influence upon the scope of the cyclodehydrogenation reaction. Additionally, it is still not verified, if the observed partially fused intermediates indeed originate from the assumed initial bond formation at the rim of the molecule, leading to the proposed "outside-in" pathway.

As the intramolecular Scholl reaction is initated by the formation of a radical cation or an arenium ion, it is important, how the corresponding aromatic moiety can stabilize the induced spin. It seems plausible that the capability of an aromatic system to stabilize

charges and the resulting spins increases with increasing size of the aromatic moiety.[80-87] Therefore benzopyrene units were specifically introduced into the C72 oligophenylene precursors.

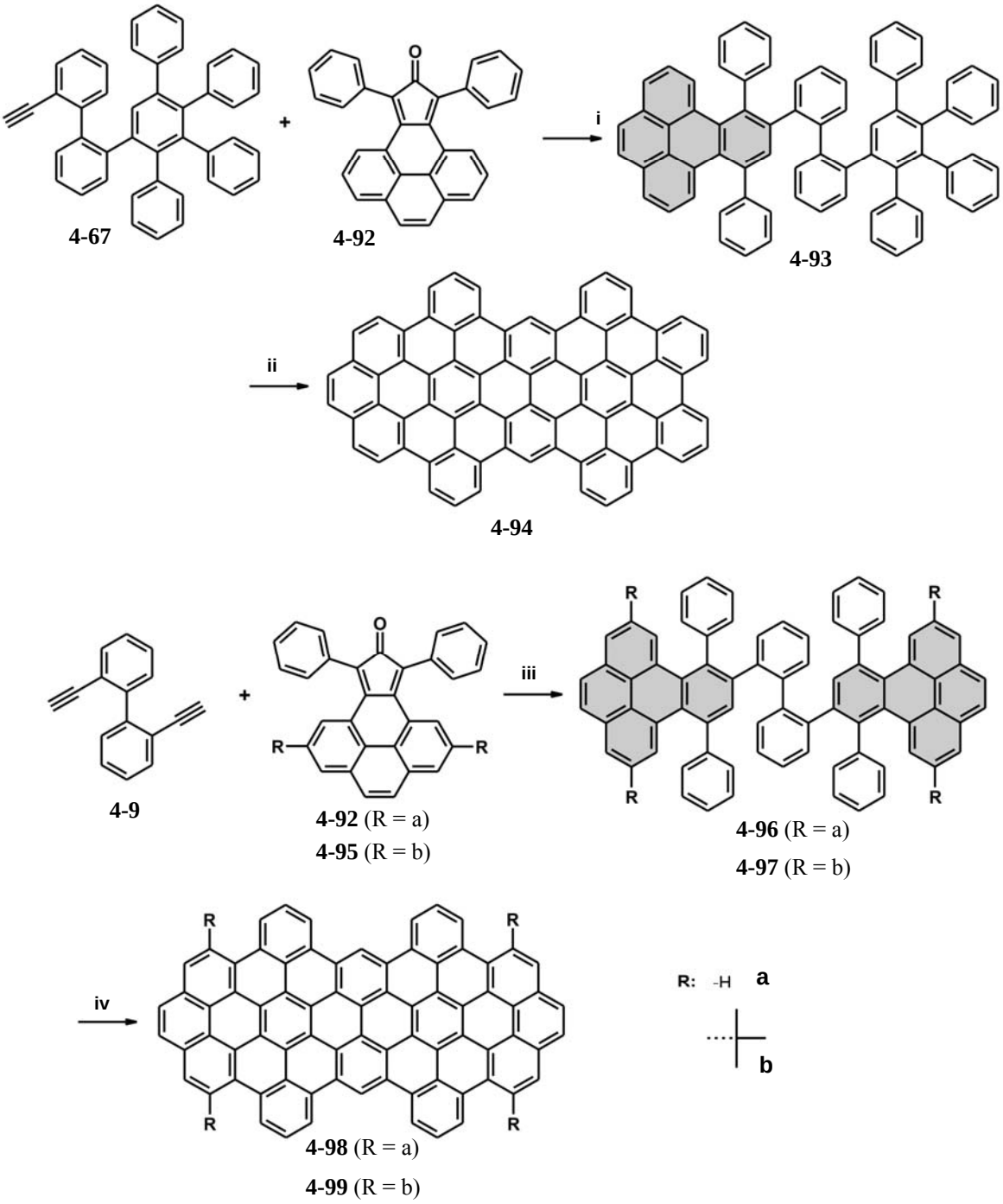

Figure 4-63: Preparation of the extended C72 compounds C74 (**4-94**), C76 (**4-98**) and C76-(t-Bu)$_4$ (**4-99**). *i:* diphenylether, reflux, 8h, 94%; *ii:* $FeCl_3$, CH_3NO_2, CH_2Cl_2, 25 °C; *iii:* diphenylether, 240 °C, 8h, 95-98%; *iv:* $FeCl_3$, CH_3NO_2, CH_2Cl_2, 25 °C, 3h, 92%.

For this purpose, another type of cyclopentadienone (**4-92** and **4-95**) was introduced (Figure 4-63), which has already been used for adapting the periphery and electronic properties of HBCs.[88] This will of course enlarge the resulting aromatic core, which will then contain 76 or 74 aromatic carbon atoms respectively, but these precursors will give the opportunity to specifically define the starting point of the cyclodehydrogenation reaction and will probably enforce the "outside-in" pathway.

Two derivatives **4-93** and **4-96** were prepared to estimate the impact exerted by such a larger aromatic subunit within the precursor, as well as another precursor **4-97**, which should show the possible influence of alkyl substituents upon the cyclodehydrogenation reaction. While for the C76 case (**4-96**) a progression from both benzopyrene moieties towards the center is expected, the C74 precursor (**4-93**) still has the possibility to adopt another panel formation and therefore to follow a different reaction pathway than the oligophenylene precursor (**4-96**) towards C76 (**4-98**).

The synthesis started for the oligophenylene precursor **4-93** with a Diels-Alder cycloaddition of the already described compound **4-67** with the literature known tetraphenylcyclopentadienone derivative **4-92**.[88] The precursor was afterwards submitted to cyclodehydrogenation conditions with iron(III)chloride in nitromethane as the oxidant. For the preparation of the unsubstituted C76 (**4-98**), 2,2'-diethynylbiphenyl (**4-9**) was subjected to a Diels-Alder cycloaddition with the tetraphenylcyclopentadienone derivative **4-92** to yield the precursor **4-96**. The cyclodehydrogenation was performed by adopting the same conditions as for C74 (**4-94**), although different reaction times and amount of oxidant were used.

In order to verify, if in these examples alkyl substituents will show a certain influence another oligophenylene precursor (**4-97**) was prepared. While **4-97** contains four *tert*-butyl groups located at the benzopyrene moiety, compounds **4-93** and **4-96** do not include any alkyl substitution. Again 2,2'-diethynylbiphenyl (**4-9**) was reacted with the also literature known tetraphenylcyclopentadienone derivative **4-95** under similar conditions as in the C76 (**4-98**) example. The cyclodehydrogenation conditions had to be adapted again to the system and did not correspond exactly to the ones for the other examples C74 (**4-94**) and C76 (**4-98**).

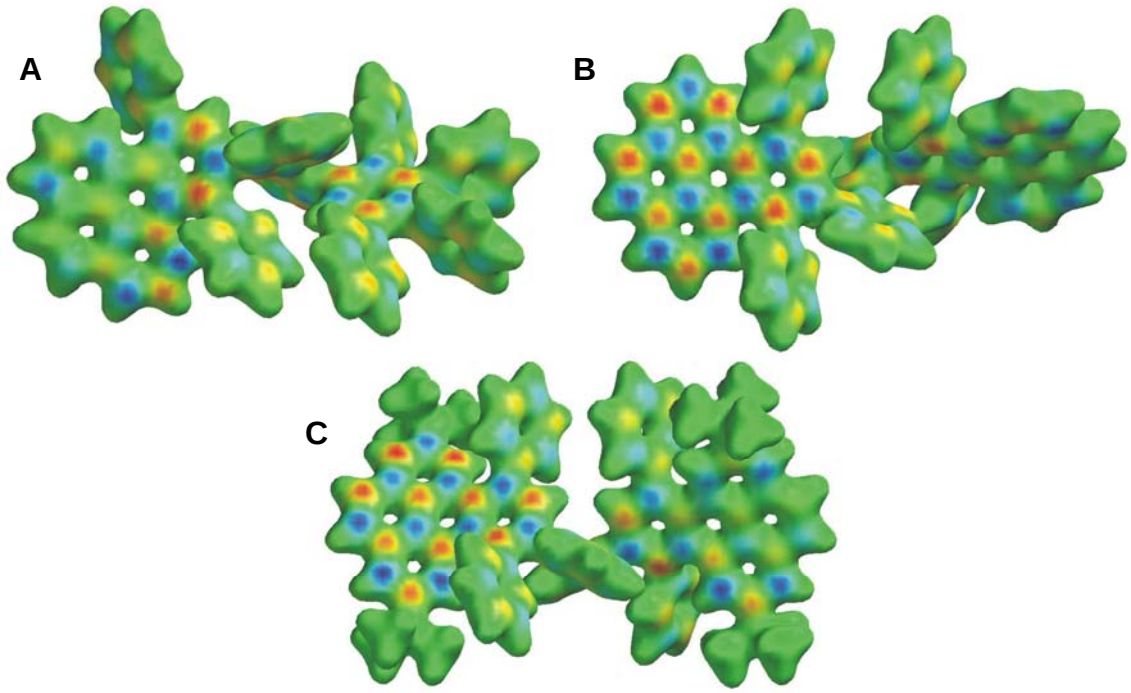

Figure 4-64: Theoretical calculations (AM1) of the spin density of the radical cation of the precursor **A**) **4-93**, **B**) **4-96** and **C**) **4-97**.

In all cases shown in Figure 4-63, it is expected that the reaction will commence at the benzopyrene parts and should progress towards the center according to the proposed "outside-in" pathway. Already for the theoretically calculated precursor molecules (semiempirical, AM1), a slightly higher spin density was predicted on the larger aromatic subunits for the radical cation. Therefore, the induction of either the radical cation or the arenium ion is expected to preferentially take place at the benzopyrene entities and the following aryl-aryl bond formations should then originate from these sites.

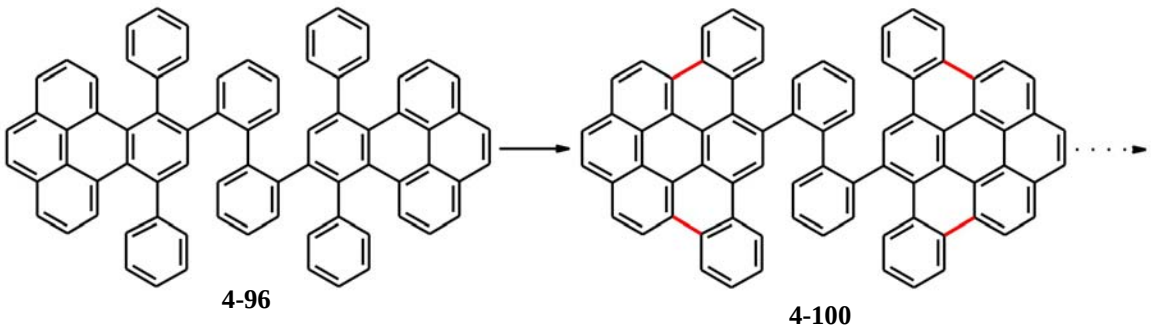

Figure 4-65: Proposed pathway for the cyclodehydrogenation of the precursor **4-96**.

If also the assumptions made in section 4.3.3 should be true, the formation of partially fused species will be preferred for the C76 precursor molecule (**4-96**), due to the induced starting point at the outer rim of the precursor leading to the intermediate **4-100** shown in Figure 4-65. Indeed, the MALDI-TOF MS spectra of the non-alkylated precursor molecules for C74 (**4-93**) and C76 (**4-96**) revealed a strong impact of the larger aromatic benzopyrene units upon the progression of the cyclodehydrogenation reaction (Figure 4-66).

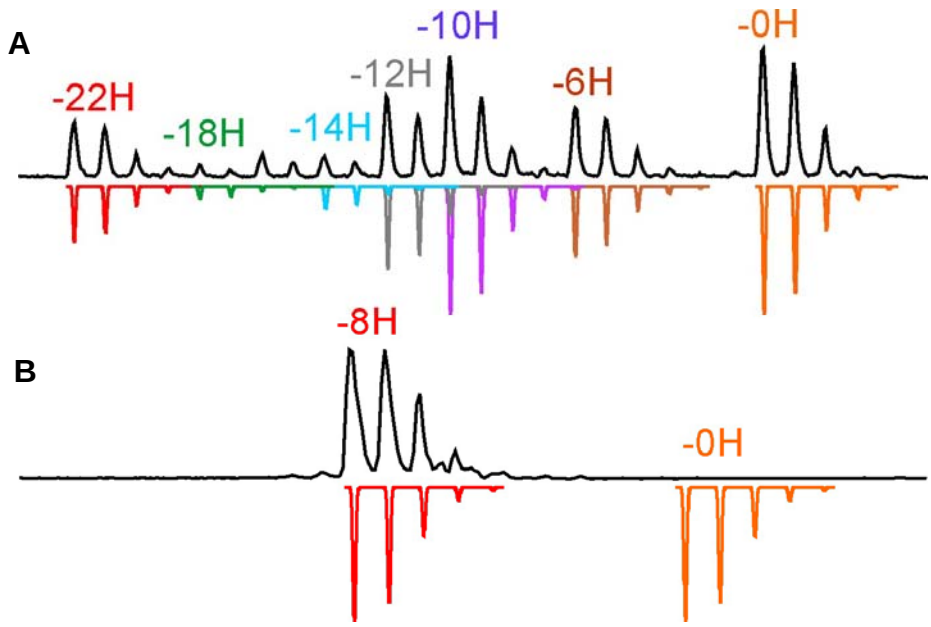

Figure 4-66: MALDI-TOF MS of the cyclodehydrogenation of the oligophenylene precursor molecules **A**) **4-93** and **B**) **4-96.**

As expected, the cyclodehydrogenation of the C74 precursor (**4-93**) exhibited in the MALDI-TOF MS spectra several partially fused intermediates, even after an extensive prolongation of the reaction time or addition of excess oxidant. Similar to the C72 derivatives C72-$(C_{12})_8$ (**4-44**) and C72-$(C_{8,2})_8$ (**4-45**) the partially fused intermediates could be assigned to the observed peaks in the MALDI-TOF MS spectrum. Also in this example, a panel formation was possibly involved during the progression of the cyclodehydrogenation reaction. After the formation of these panels, the reaction slowed down as described in section 4.3.3 and the formation of further bonds included the above mentioned "stitching" together of the already planarized panels.

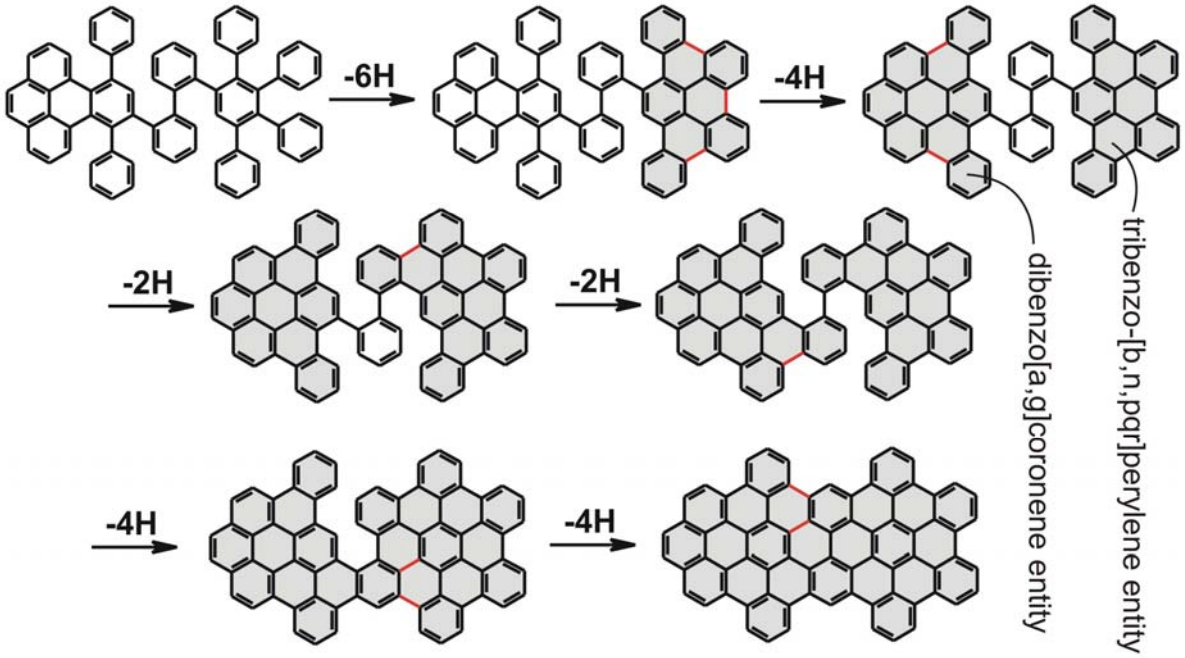

Figure 4-67: Plausible intermediates formed by the cyclodehydrogenation of the C74 precursor (**4-93**).

Independently of the used parameters for the cyclodehydrogenation reaction only one signal was observed for the cyclodehydrogenation of the unsubstituted C76 precursor (**4-96**). Even a huge excess of oxidant and reaction times up to 3 days did not yield any indication of product formation in the MALDI-TOF MS spectrum. In contrast, the chlorination of the partially fused species became dominant. For this substance, where only four aryl-aryl bonds were formed during the reaction, also no NMR data could be recorded due to the pronounced insolubility of the material in common organic solvents.

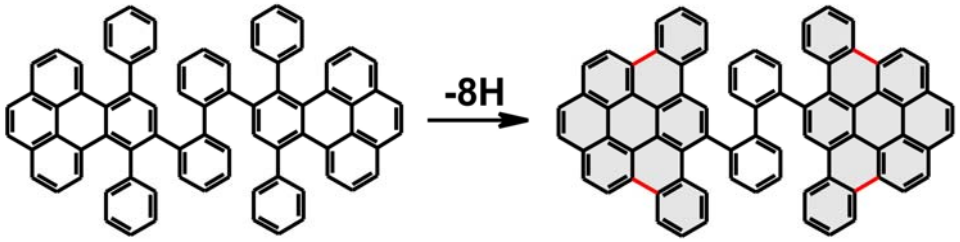

Figure 4-68: Plausible product structure of the cyclodehydrogenation of the C76 precursor (**4-96**).

Nevertheless, by using the assumptions in section 4.3.3 as a basis, a plausible structure was determined. Additionally, the strict formation of four bonds also supported the proposed reaction pathway. The initiation of the reaction occurred at the

benzopyrene moieties of the oligophenylene precursor, which consequently induced the "outside-in" pathway (Figure 4-68).

However, it was surprising that the system did not continue with the reaction similar to the C74 case with a "stitching" together of the panels, as this progression has so far been observed for all the C72, C96, C222 and C74 examples. The reason for this behavior could lie within the structure or symmetry of the formed dibenzo[a,g]coronene part (Figure 4-67). In the C74 (**4-94**) example on the other hand, the formed intermediates still had the opportunity to adopt at least one panel similar to the ones observed for C72-$(C_{12})_8$ (**4-44**). Even though the relative amount of the product cannot be verified, at least in the MALDI-TOF MS spectrum of C74 (**4-94**) some product formation was indicated (Figure 4-66A). Therefore, the "stitching" effect could be initiated from the tribenzo-[b,n,pqr]perylene panel and integrated successively the dibenzo[a,g]coronene entity into the aromatic system, leading to some extent to the fully planarized product **4-94**.

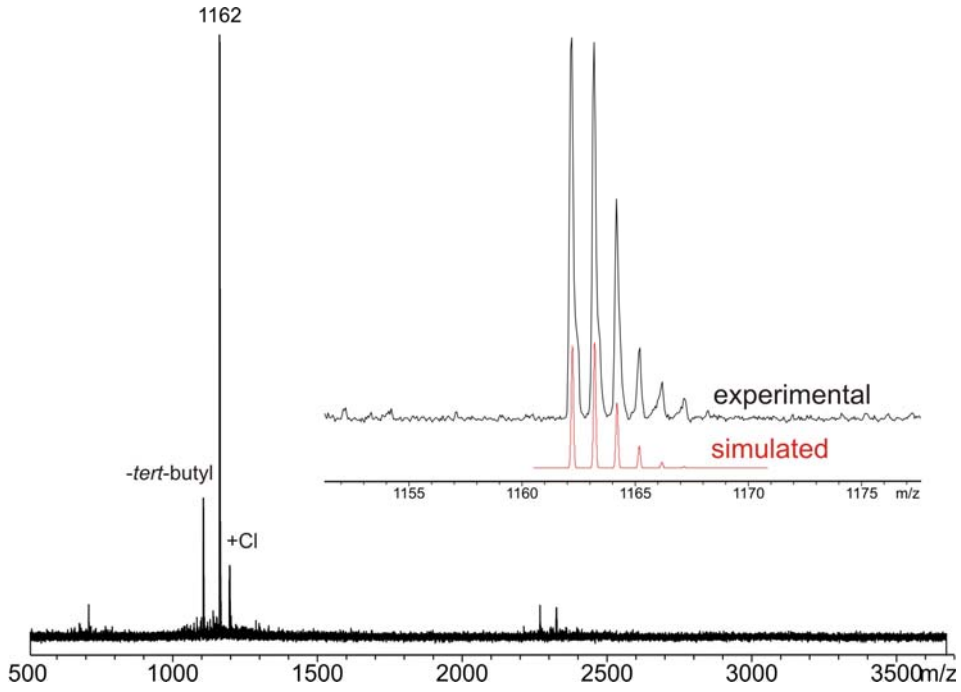

Figure 4-69: MALDI-TOF MS of C76-(t-Bu)$_4$ (**4-99**) with TCNQ.

As shown in Figure 4-69, the oligophenylene derivative with the *tert*-butyl groups (**4-97**) exhibited, according to the MALDI-TOF MS, a distinct closing towards the fully planarized product C76-(t-Bu)$_4$ (**4-99**). This indicated at least some minor influence of the *tert*-butyl groups compared to the cyclodehydrogenation towards the unsubstituted

examples C74 (**4-94**) and C76 (**4-98**). In what sense these substituents took part in the stabilization of the radical charge during the reaction or simply induced a better ionization process in the MALDI-TOF MS could not be answered on the basis of the MALDI-TOF MS spectrum. As seen from the theoretical calculations in Figure 4-64, nothing pointed towards an influence of these alkyl substitutents regarding the stabilization of induced charges. Therefore, the results from the MALDI-TOF MS were additionally verified by UV/vis, which is a quick and easy experiment for such purposes to exclude a possible overestimation of the product by MALDI-TOF MS.

Again UV/vis confirmed that MALDI-TOF MS did not reveal the true status of the compound. While for other C72 derivatives such as C72-$(C_{12}H_{25})_8$ (**4-44**) and C72-$(C_{8,2})_8$ (**4-45**) a main absorption band around 430 nm is observed, this is not the case for C76-(*t*-Bu)$_4$ (**4-99**). In contrast, the main band is located at 345 nm (Figure 4-70), which means a difference of almost 100 nm. This hypsochromic shift is so pronounced that any influence of the different topology of the aromatic core or any aggregation features can be excluded.

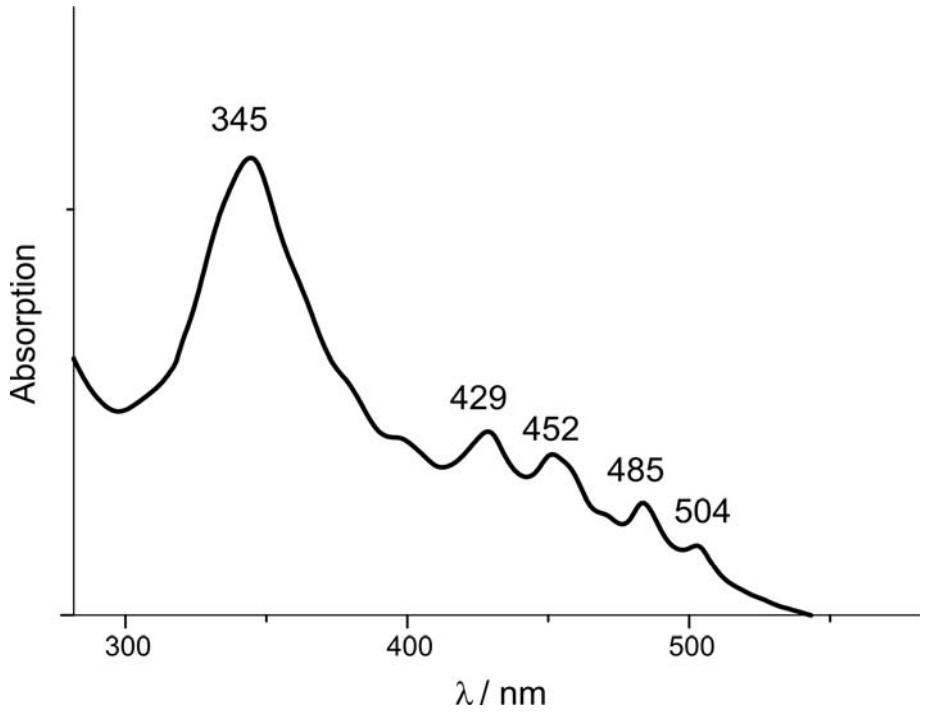

Figure 4-70: UV/vis of C76-(t-Bu)$_4$ (**4-99**) in THF at room temperature.

Already for other PAHs, it was proven that a lowering of the symmetry by adding for example double bonds in the periphery of the aromatic core, leads to additional bands due to a change in the oscillator strengths. Nevertheless, all these changes did not lead to

a similar pronounced hypsochromic shift of the main absorption bands.[88] It has been shown for HBCs that such an enlargement of the aromatic core usually resulted in a bathochromic shift of the main absorption band in the UV/vis of approximately 30 nm.

However, some additional bands were located in Figure 4-70 for C76-(*t*-Bu)$_4$ (**4-99**) at wavelengths above 420 nm. If one takes into consideration a similar mixture as already described for the C72 derivative C72-(C_{12})$_8$ (**4-44**) in Figure 4-20, it seems plausible that the bands of the partially fused intermediates would be located below 400 nm. This means that the band at 345 nm originated from an intermediate compound. The bands above 400 nm would then already be starting to exhibit the UV/vis profile of the fully planarized product C76-(*t*-Bu)$_4$ (**4-99**).

Overall, it was obvious that the MALDI-TOF MS severely overestimated the amount of the product C76-(*t*-Bu)$_4$ (**4-99**). Because of the lack of analytical data, it cannot be further determined in what relation this stood according to the presence of alkyl substitutents.

4.6.2 Specific Synthesis of Panels

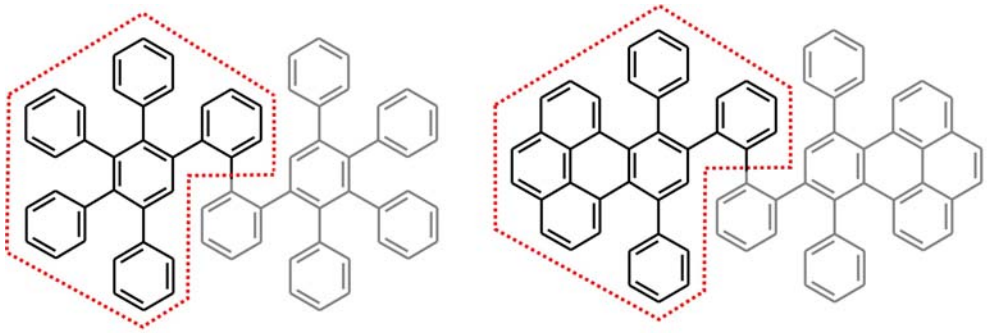

Figure 4-71: Investigated panels relative to their position within the parent structure of the precursor of C72 (**4-44** to **4-46**) and C76 (**4-96**).

For revealing, if the observed formation of the monodisperse intermediate from the unsubstituted C76 precursor (**4-96**) was related only to the supposed initiation of the cyclodehydrogenation at the rim or if symmetric and electronic effects of the dibenzo[a,g]coronene panel also played a role, compound (**4-104**) was prepared and compared to the already known example **4-101** (Figure 4-72). F. Dötz showed in his work[20] that the cyclodehydrogenation of **4-101** towards **4-102** was smooth and encountered no difficulties. In addition, it was possible to achieve a full analysis including NMR data, which unambiguously proved the structure.

These examples correspond exactly to one half of the usual C72 or C76 precursor molecules respectively, whereby in the C76 example, the non-alkylated phenyl is representing the two phenyl rings of the central biphenyl entity (Figure 4-71). It was decided to substitute the future aromatic core component **4-106** with four *tert*-butyl groups. These groups are known to inhibit aggregation effects due to their bulkiness in close proximity to the aromatic entity.[89-94] In addition, the close spatial proximity of the *tert*-butyl groups should induce a distortion of the aromatic entity, resulting in an improved solubility due to a reduced π-interaction between the distorted aromatic cores.[95-97] This should sufficiently solubilize in contrast to an unsubstituted case to achieve well resolved NMR data for the elucidation of the product and possible intermediates.

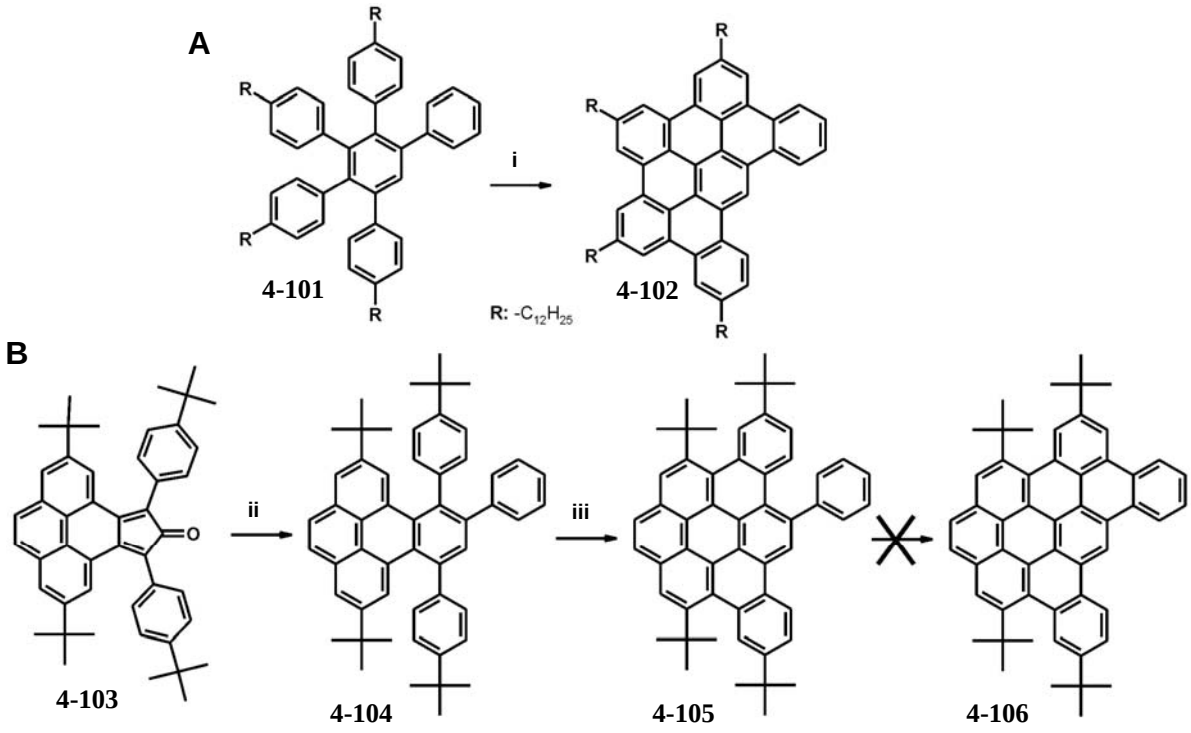

Figure 4-72: Specific synthesis of panels for **A**) the C72 case and **B**) the C76 case.

The synthesis of the precursor **4-104** started with a simple Diels-Alder cycloaddition of the literature known tetraphenylcyclopentadienone derivative **4-103** and commercially available phenylacetylene. After the workup procedure the precursor **4-104** was gained in good yields. Afterwards the precursor **4-104** was treated similar to the milder

conditions applied for the cyclodehydrogenation of hexaphenylbenzenes towards HBCs, due to the similar sizes of the structures.

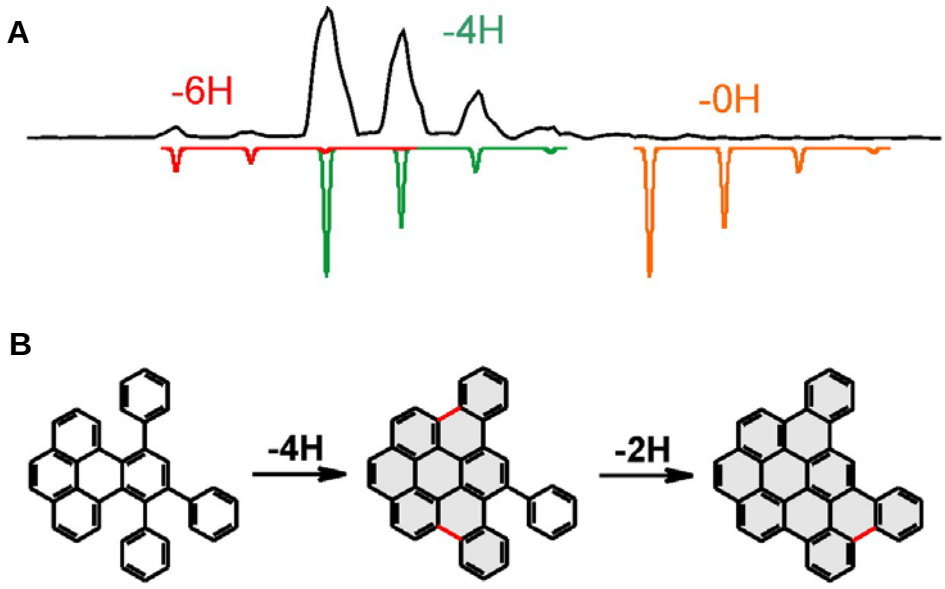

Figure 4-73: A) MALDI-TOF MS of the formed intermediate **4-105**; **B**) corresponding structures according to the MALDI-TOF MS experiment.

Already in the MALDI-TOF MS spectra it became obvious, that only two aryl bonds were formed and it was assumed that also in this case the bond formations occurred at the same positions as for the C76 precursor (**4-96**). Even by applying harsh conditions, by using for example a large excess of the oxidant, the last bond could not be easily established, instead chlorination of the intermediate (**4-105**) became significant. After the workup procedure of the product mixture by column chromatography, a light yellow compound could be isolated in 98% yield relative to the used precursor (**4-104**). Fortunately, the gained material showed sufficient solubility to record all necessary NMR spectra. In Figure 4-74 the ^{1}H NMR spectrum of the received compound (**4-105**) is shown. The spectra confirmed the results gained from the MALDI-TOF MS spectrum, as there appeared one auxiliary signal and the integration did not fit to the fully fused product.

The structure of the compound was unravelled by recording 2D NMR spectra. Due to the lack of symmetry, it would have been very difficult to exactly determine the true structure, if not two of the three phenyl rings of the precursor would have been substituted in the respective para-position with *tert*-butyl groups. These groups did not only induce the necessary solubility, but also indicated the position of the unclosed aryl bond.

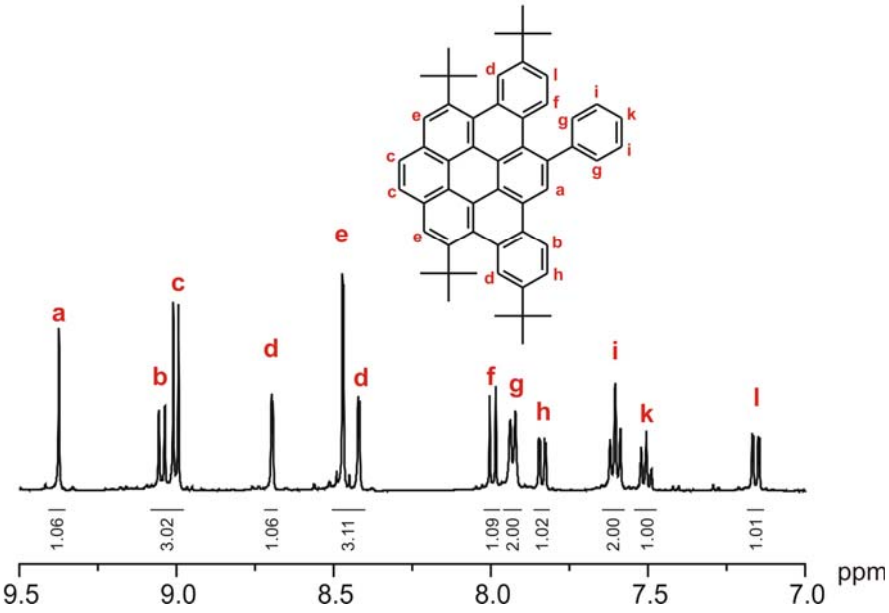

Figure 4-74: ^{1}H NMR spectrum of the compound **4-105** at room temperature in CD_2Cl_2.

The proton signal from the proton **k** can be clearly identified, as it induced next to the protons **i**, which are located at the same phenyl ring, the only triplet within the spectra, but with half of the integration value than the one of **i**. Therefore, it was obvious that the corresponding signal has to be the triplet at 7.57 ppm. By using this triplet as the starting point a coupling in the HH COSY spectrum was found to the other triplet, originating from the protons **i**. In addition, it was found that this triplet exhibited a coupling to a doublet, which was induced by the proton **g**. As the integration value from this position was indicating two protons, this proved undoubtedly that the missing aryl bond has to be located at the unsubstituted phenyl ring, else the integration value would have been one. This of course supported also the assumption that for the C76 case the corresponding bonds are missing and thus that the proposed product structure in Figure 4-68 is the one observed in the MALDI-TOF MS. Another two couplings were found for the doublet at 7.25 ppm with the doublet at 8.02 ppm and the signal at 7.87 ppm coupled with the one at 8.98 ppm. Both signals exhibited an integration value fitting to one proton respectively. The only two possible spin systems in this molecule, responsible for such a correlation are the ones of the proton **f** with **l** or the proton **b** with **h**. Although the couplings found in the NOESY confirmed the results from the HH COSY, no coupling was at first detected from the proton **g** to the proton **f**. As the NOESY indicates the spatial proximity of protons, a coupling has to be observed between **g** and **f**. As this was at first sight not the case, the only possible explanation was, that the cross peak was

covered by other signals, which can only happen in the NOESY between the signals of proton **f** and **g**. By enlarging the questionable area in the NOESY a small coupling became visible and proved that the signals at 7.25 ppm and 8.02 ppm originated from the protons **f** and **l**.

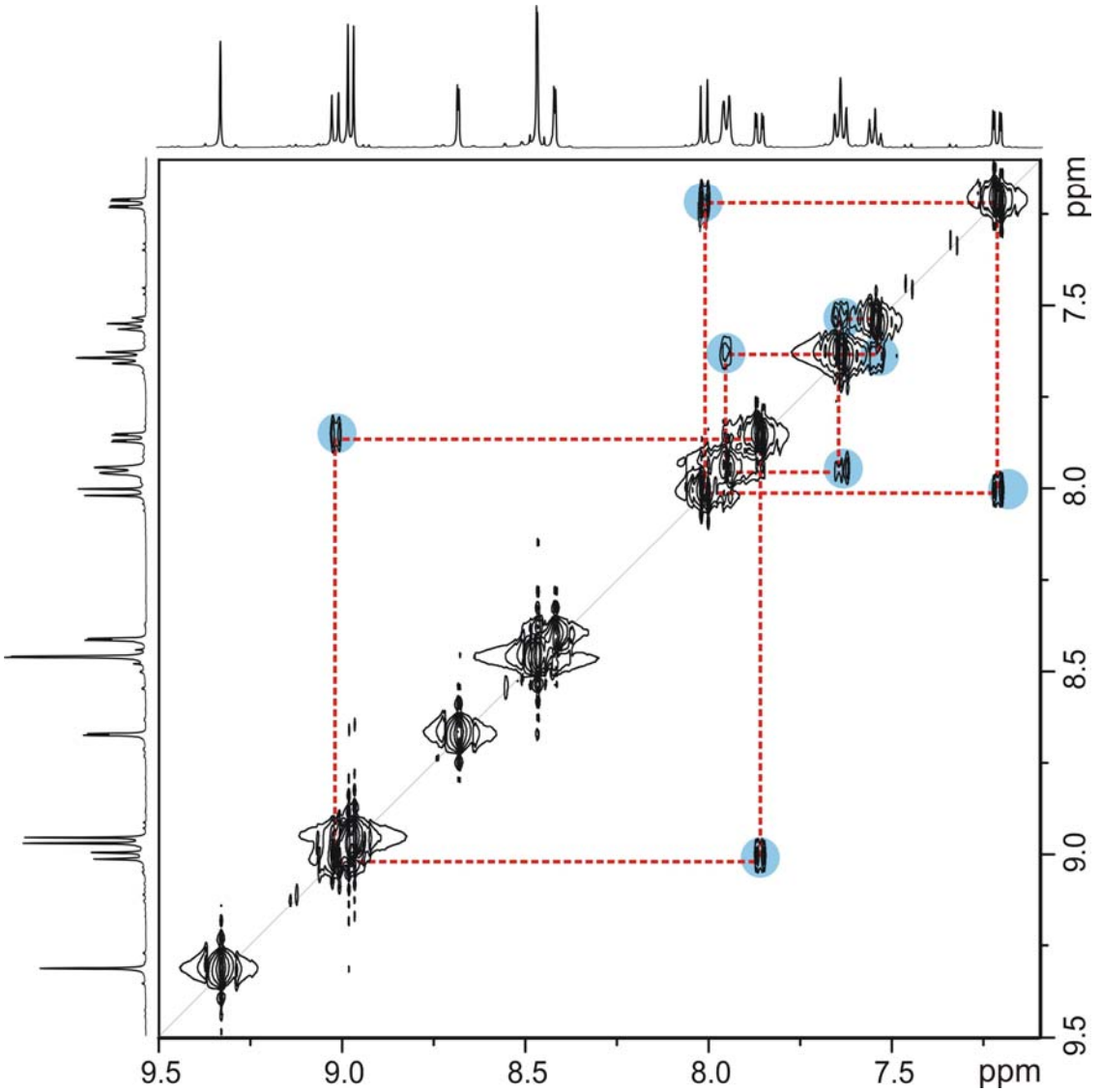

Figure 4-75: HH COSY of compound **4-105**.

The correlations found for the single phenyl ring was confirmed by the couplings found in the NOESY as the same spin system appeared. Additionally, the signals of the protons **c** and **e** could be identified based on the correlation in the NOESY and the integration values in the ^{1}H NMR spectrum. However, both protons revealed the same splitting and it was not possible to determine from the 2D spectra, which signal corresponded to which proton. For a final decision the published ^{1}H NMR spectrum of

benzopyrene was consulted, which indicated that the proton **c** in this case occurred at lower field compared to **e**. The signals were assigned for compound **4-105** accordingly. The remaining signals for **a** and **d** were determined due to the observed long range couplings, which were expressed by the small splittings of the signals in the ^{1}H NMR spectrum. While for the signals corresponding to the protons **d** such a splitting occurred, none was observed for the signal for **a**. The low field shift for **a** was also supported by a simulated spectra of the substance.

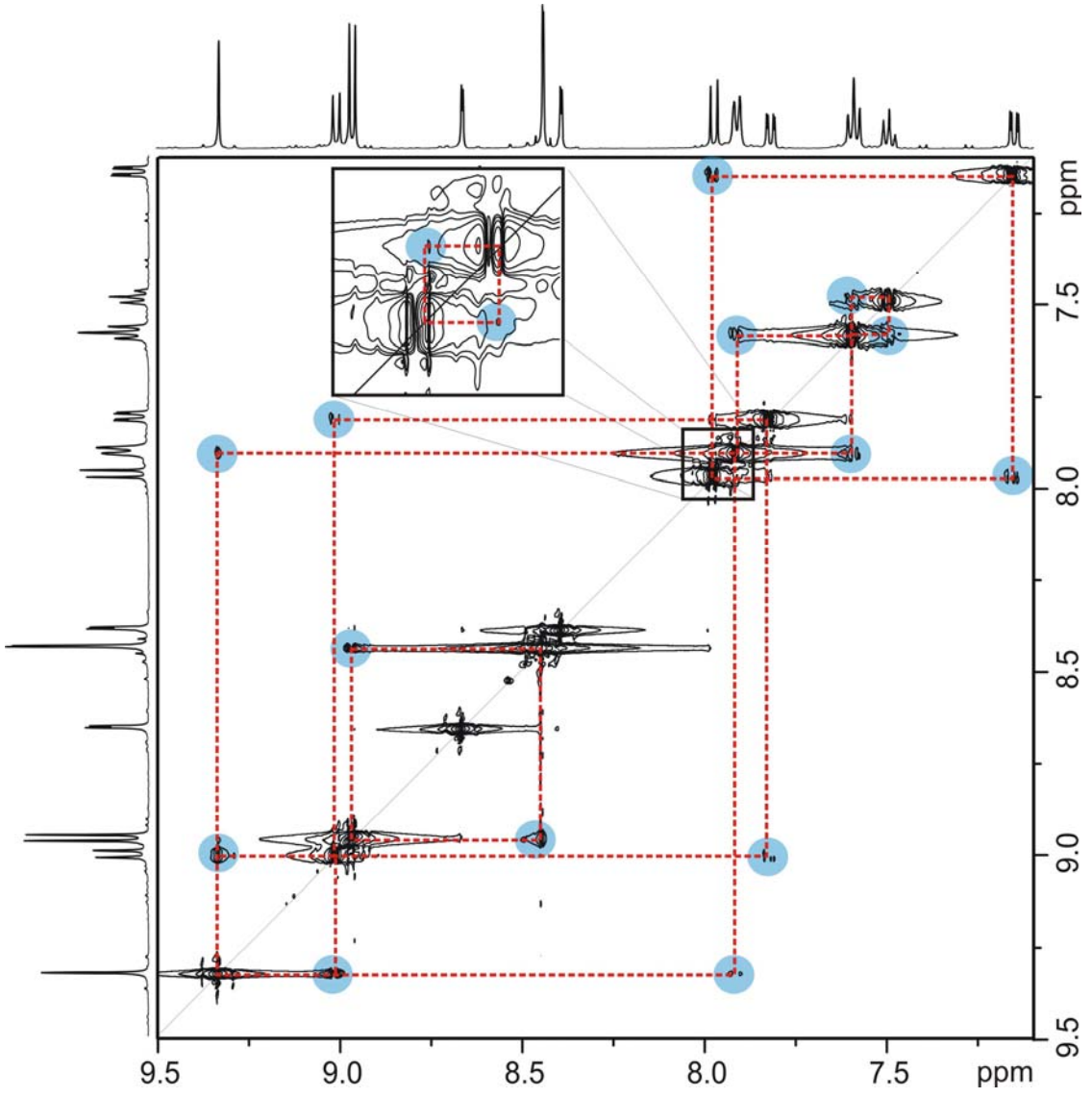

Figure 4-76: NOESY of compound **4-105.**

In the UV/vis spectra in Figure 4-77 the main absorption band was located at 347 nm. The spectra of the UV/vis and the photoluminescence-excitation (PLE) revealed very similar band structures, although with one difference. Interestingly at the same region

(347 nm), where the UV/vis exhibits a maximum, a small decrease in intensity was observed for the PLE spectrum. Additionally, in the photoluminescence emission spectra a maximum was observed at 468 nm in combination with a consecutive tailing. Usually with PAHs of such a low symmetry, only one photoluminescence band is observed. The tailing as well as the small decrease in the photoluminescence excitation spectra could originate from the substituted phenyl ring, which can adopt a diversity of different conformations with respect to the other larger aromatic entity. Therefore, one possible explanation for these features could be that two conformations with different spectral properties are present. For example, on one hand the phenyl ring can be a part of the delocalization of the aromatic entity, while on the other the delocalization is hindered due to an unfavorable angle between the phenyl ring and the aromatic entity. While the UV/vis only shows the superposition of the absorption profiles of the two conformations, similar to the case of C72-$(C_{12})_8$ (**4-44**), although with different conformations and not different substances, the photoluminescence excitation reveals mainly the response of only one conformation. This would also explain the tailing in the photoluminescence emission spectra, when one assumes that the band at 468 nm originates from one conformation, while the bathochromically shifted residual part belongs to the emission of the other conformation.

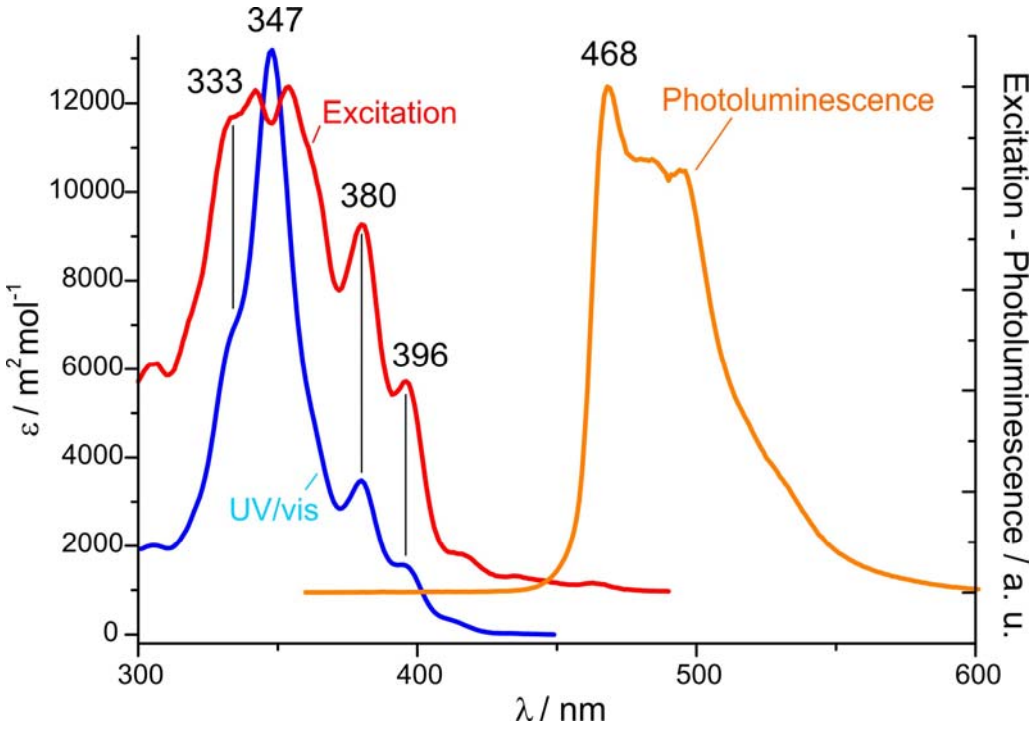

Figure 4-77: Electronic spectra of compound **4-105**.

By comparing the value of the main absorption band in the UV/vis with the one found for the alkylated case of C76-(*t*-Bu)$_4$ (**4-99**) at 345 nm (Figure 4-70), it was indicated that in contrast to the assumed large amount of product in the MALDI-TOF MS, the mixture consisted to some extent of similar partially fused intermediates as observed for the unsubstituted C76 (**4-98**).

4.7 Preplanarization in the Center of the Oligophenylene Precursor

As already described in the previous section, it is supported by several examples that the major problem of the intramolecular Scholl reaction lies within its possible "outside-in" pathway, leading to the described partially fused intermediates (section 4.3.3). These substances represent kinetically trapped states and induce the strange behavior observed for the materials such as irreproducible UV/vis spectra (section 4.2.1). It has been tried without success by improved purification or reaction conditions, changing for example the phenyl substitution pattern in the oligophenylene substitution pattern (section 4.5.2), to increase the purity of the materials. In fact, the special arrangement of oligophenylene precursors, which consist of multiple "dendritic" 2,3,4,5-tetraphenylbenzene subunits are likely to form tribenzo-[b,n,pqr]perylene moieties, when the cyclodehydrogenation proceeds *via* the "outside-in" pathway. However, it has been shown for a diversity of substituted HBCs that these compounds never showed such a distinct formation of side-products.

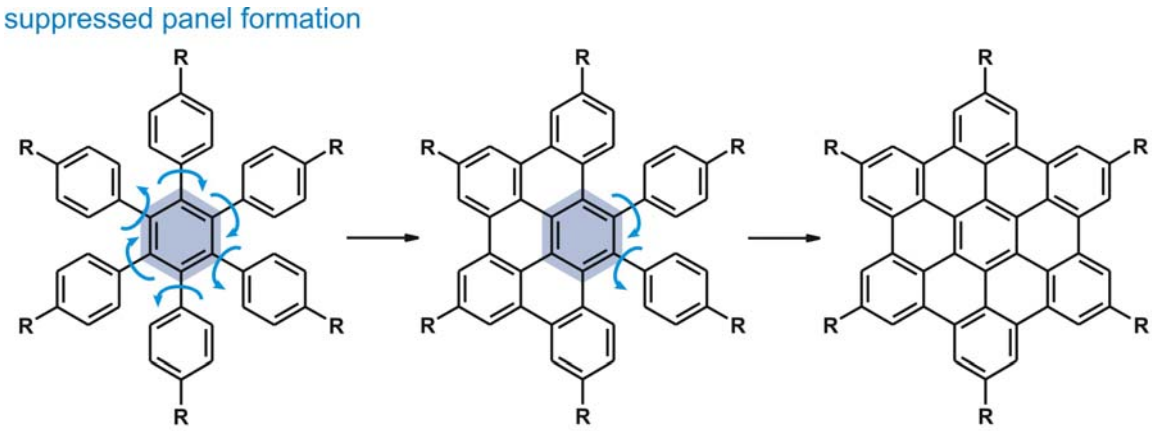

Figure 4-78: Suppressed panel formation in the HBC case.

As can be seen in Figure 4-78, the hexaphenylbenzene, representing the oligophenylene precursor molecule, does not allow a similar formation of tribenzo-

[b,n,pqr]perylene panels (Figure 4-39), as it does not consist of "dendritic" 2,3,4,5-tetraphenylbenzene subunits. This is due to the fact that the phenyl rings at the rim are only mono-substituted to the central benzene. This stands in contrast to the C72 precursors (**4-44** and **4-45**), where as shown in Figure 4-34 the formed tribenzo-[b,n,pqr]perylene panels can adopt a contorted arrangement. It seems that exactly this arrangement is one key factor leading to the kinetical entrapping of the intermediates.

In addition, the unfused entities of the hexaphenylbenzene (phenyl rings) need only to overcome the steric hindrance of one hydrogen to adopt a favorable conformation for a subsequent aryl-aryl bond formation. Only at the stage of the last intermediate shown in Figure 4-50 the last unfused phenyl ring encounters the steric demands of two hydrogens. Therefore, a similar reduction or even prevention of such bonds, where intermediately formed tribenzo-[b,n,pqr]perylene panels can rotate, should lead to an improved cyclodehydrogenation behavior and an improved material.

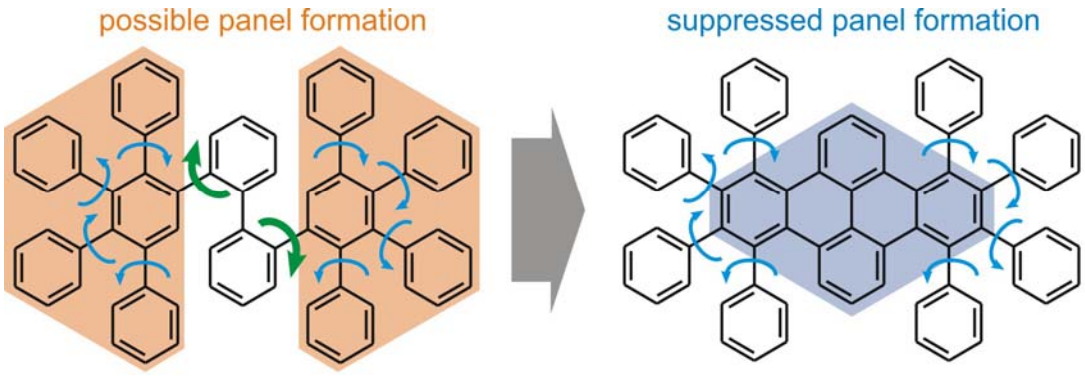

Figure 4-79: Changing the substitution pattern of the C72 precursor by fixing the central bonds.

As the HBC case is one of the most successful examples for the synthesis of large PAHs based on oligophenylene precursor molecules, this leads to the proposed analogue for the C72 precursor shown in Figure 4-79. By already fusing the two central benzene rings with the adjacent phenyls and creating a dibenzopyrene entity in the center, any possible formation of tribenzo-[b,n,pqr]perylene panels is inhibited. Of course a direct correlation between HBC and this novel system cannot be drawn, but both precursor molecules consist of singly bonded phenyl rings to a central entitity that will be fused together on the subsequent cyclodehydrogenation reaction.

As discussed in the previous section 4.2 the presence of the partially fused intermediates had a severe influence upon the supramolecular behavior of the material, as for example the solubility. It is known that HBC-$(C_{12})_6$ (**4-28**) substituted six times

with dodecyl chains is hardly soluble. As a consequence, it has to be assumed that the pure C72-$(C_{12})_8$ (**4-44**) should be rather insoluble, as the aromatic core size is doubled. This behavior has already been indicated by the fact that for the alkylated C60 (**4-8**) also no good solubility was observed and the NMR spectra had to be recorded under elevated temperatures to resolve the signals in the aromatic region (80 °C in *p*-dichloro-benzene). For C60 (**4-8**) the aromatic core unit was solubilized by eight alkyl chains, which is the same number as for the even larger C72 derivatives C72-$(C_{12})_8$ (**4-44**) and C72-$(C_{8,2})_8$ (**4-45**). That leads to the conclusion that for achieving not only a soluble, but also processable material some precaution had to be taken.

4.7.1 Inducing Solubility by Distortion of the Aromatic Core Component and Bulky Substituents

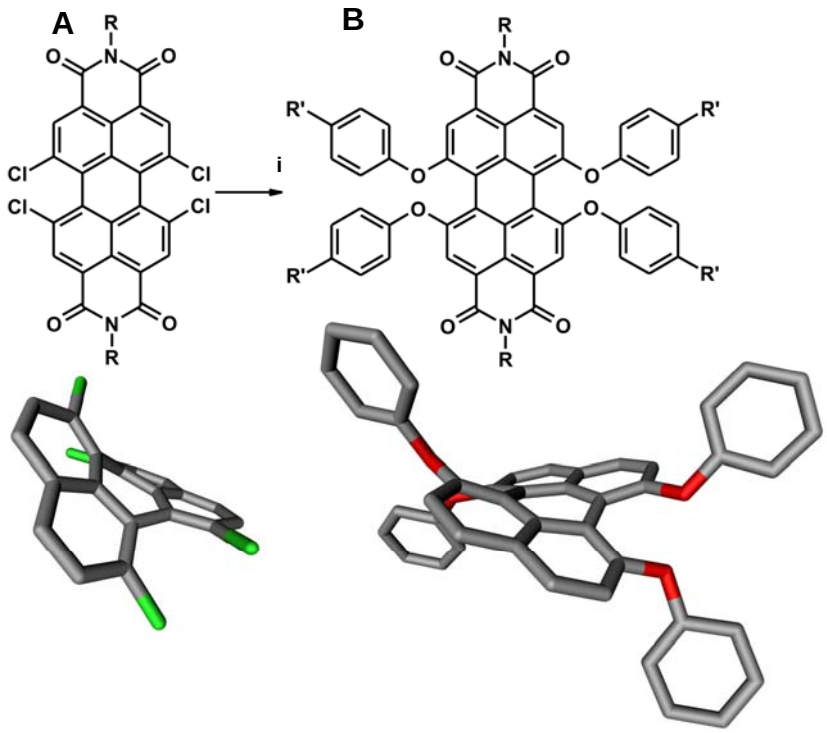

Figure 4-80: Distortion of the aromatic entity of perylene to induce solubility **A**) by halogen atoms in the bay area and **B**) after reaction with a *para*-substituted phenol. i:

Another approach towards increasing the solubility and processability of aromatic compounds is the distortion of the aromatic core unit.[95-97] As seen in Figure 4-80, dyes like perylene derivatives exhibit an improved solubility after distorting their aromatic entity. This leads similar to the introduction of bulky alkyl side chains to an efficient reduction of the π-interaction effects. After the functionalization with a phenol

derivative (Figure 4-80), the distortion of the perylene entity is additionally accompanied with a substituent that has some sterical requirements and effectively improves the solubility of the compound. The solubility can be even adapted to different solvents. For example, it was possible by the attachment of four hydrophilic substituents onto the bay region of the perylene dye to make this PAH water soluble.[98]

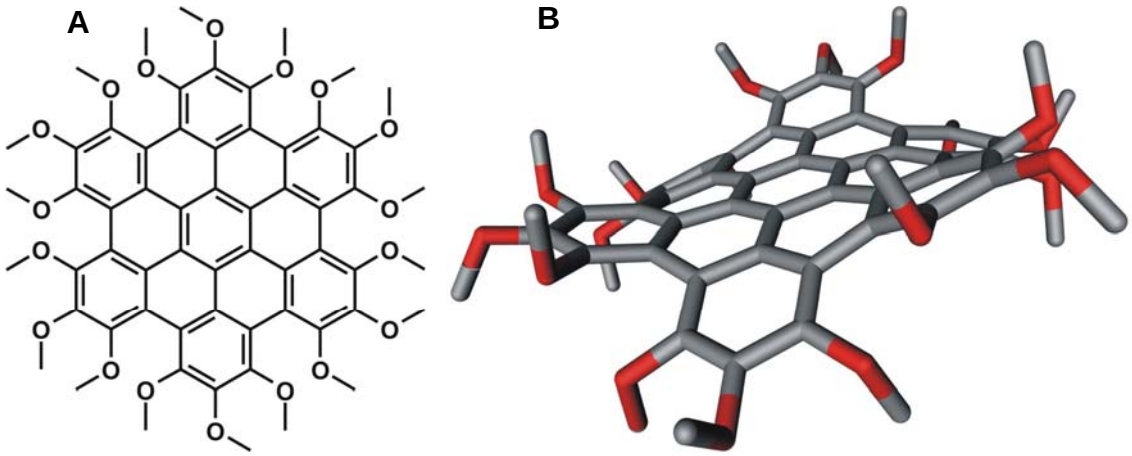

Figure 4-81: A) Permethoxy-substituted HBC and **B**) visualization of the distortion of the aromatic core component.

A similar feature based upon the distortion of an aromatic core component has also been reported for a HBC substituted eighteen times with methoxy functionalities (Figure 4-81), which represents the first persubstituted HBC derivative. The resulting distortion in combination with the small but nevertheless present steric demand of the substituents led to a reasonably well soluble material, even though the methoxy groups are rather small substituents. This distortion also allowed the use of this HBC for a host-guest system with C60-fullerene.[72] In this arrangement the fullerene is positioned exactly on the central benzene ring of the permethoxy HBC, thus yielding a perfect columnar packing arrangement.

One example, which indicates the effects of the distortion of the aromatic core component is shown in Figure 4-82. The bowl-shaped corannulene is not only well soluble, but from this compound NMR data could be recorded even at low temperatures.[74,95-97] In addition, it was revealed that the energy barrier of the bowl to bowl inversion is approximately 10 kcal mol^{-1}, which is astonishingly close to the value of the barrier of cyclohexane for the change from one chair conformation to another.

Indeed, the calculations revealed that the corannulene must invert more than 200000 times per second at room temperature, pointing towards the high tolerance of carbon-carbon bonds with respect to strain. This also indicated that under certain cirumstances the distortion of an aromatic entity can be used to induce a dynamic process, which could assist the suppression of π-mediated stacking, resulting in an improved solubility of the compounds.

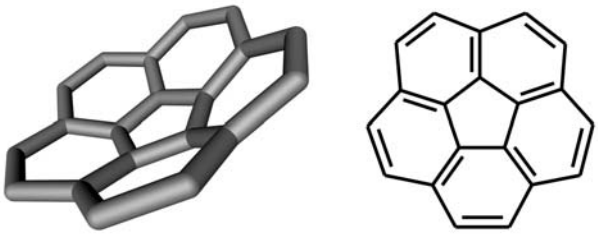

Figure 4-82: Schematic representations of corannulene.

By the introduction of *tert*-butyl groups as substituents in the corona of HBCs, the π-mediated stacking could also be efficiently supressed. For HBCs, these substituents have been introduced at the same positions as seen for the alkyl chains in Figure 4-7. A slightly larger intermolecular distance between the aromatic cores was observed in combination with a hindrance of the preferred equidistant stacking of the discs. Moreover a strong π-interaction was only found for pairs of molecules. This effect became even more distinct in solution, where only a minimum of aggregation was found based on intermolecular π-stacking, even though the compound was not well soluble due to the size of the molecule.

In the work of J. Wu an HBC was substituted six times with a first generation oligophenylene dendrimer. These compounds are known for their shape-persistency and stiffness, which led to an enormous steric demand in the vicinity of the aromatic entity. By using NMR analytics, it has been proven that in solution, this molecule only adopts a monomer or dimer state, indicating that the bulkiness of the substitutents inhibit the intermolecular aggregation. Therefore, it can be concluded that the distortion of the aromatic core component in combination with bulky substituents is an efficient initial step to improve the solubility of extended PAHs.

4.7.2 C72-$(C_{12})_8$-(t-Bu)$_2$

Hence for C72 a synthetic procedure was proposed, which combines the before mentioned features for introducing solubility and the efficient reduction of π-interactions (Figure 4-84). On one hand *n*-dodecyl chains were introduced in the corona of the molecule, as these substituents exert one of the most efficient solubilizing effects compared to other linear alkyl chains. The additional bulky *tert*-butyl groups in the corona of the C72 derivative should not only reduce the aggregation due to their steric demand,[89-94] but also distort the aromatic core component (Figure 4-83) to gain the same effect as seen for the perylene and HBC derivatives shown in Figure 4-80 and Figure 4-81. As can be seen from Figure 4-83 two possible conformations are possible for the compound C72-$(C_{12})_8$-(*t*-Bu)$_2$ **4-116**.

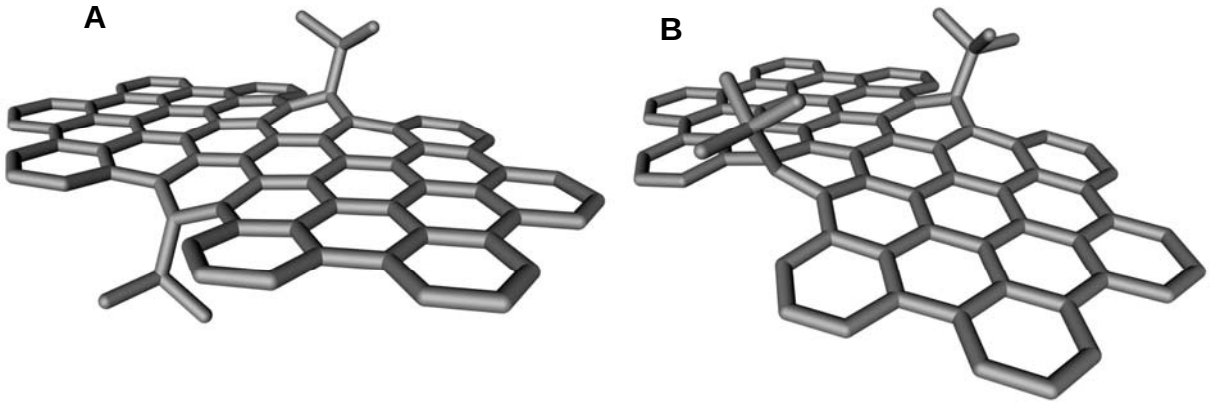

Figure 4-83: Simulated structure of the distorted C72 aromatic core component of C72 (alkyl chains are omitted for clarity); **A**) trans- and **B**) cis-conformation.

Theoretical calculations revealed that for both conformers not a large difference in the heat of formation can be expected (Figure 4-83). Therefore, it is possible that both conformations can appear simultaneously in the product, which could lead to a further disturbance of the aggregation based upon the π-interactions and therefore to an improved solubility and processability.

Nevertheless, it has to be considered that also the bulk behavior will be severely influenced. The worst case scenario would be the complete suppression of any columnar self-assembly because of the introduced disorder. A minimum of columnar self-organisation exerted by the π-interactions between adjacent aromatic cores is a prerequisite, as only by such a stacked arrangement the system will be capable of providing a channel for charge-carriers.

4.7.2.1 Synthesis

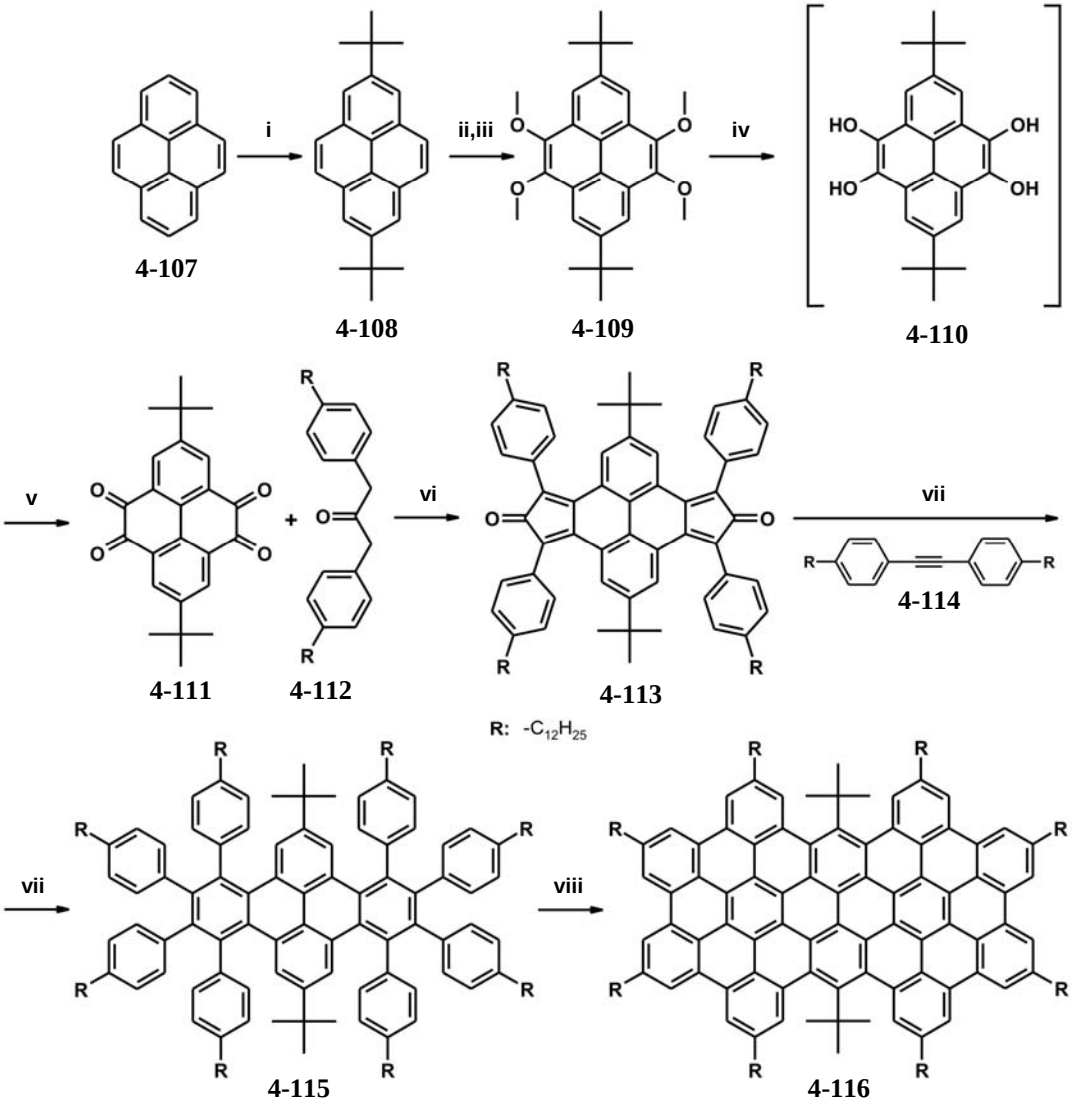

Figure 4-84: Preparation of the distorted C72 derivative C72-$(C_{12})_8$-(*t*-Bu)$_2$ **4-116**. *i:* *t*-BuCl, $AlCl_3$, CH_2Cl_2, rt, 5 h; *ii:* Br_2, $FeCl_3$, CCl_4, rt, 4h; *iii:* NaOMe. CuI, MeOH, DMF, reflux, 30h; *iv:* BBr_3, CH_2Cl_2; *v:* salcomine, O_2; *vi:* KOH, MeOH, EtOH, 48 %, rt; *vii:* Ph_2O, 21 %; *viii:* $FeCl_3$, CH_2Cl_2, CH_3NO_2, 85 %.

The synthesis of C72-$(C_{12})_8$-(*t*-Bu)$_2$ (**4-116**) started with the literature known Friedel-Crafts alkylation of commercially available pyrene[75] to yield the *tert*-butyl substituted pyrene derivative **4-108**. This compound was further subjected to literature known procedures to gain the 2,7-di-*tert*-butyl-4,5,9,10-tetramethoxypyrene (**4-109**) in 70% yield.[75,76] The subsequent synthesis towards the 2,7-di-*tert*-butyl-4,5,9,10-tetraone (**4-111**) was in the beginning performed according to the literature procedure.[76] In the first step, the unstable pyrenoquinhydrone (**4-110**) was prepared, which was subsequently

oxidized during the column chromatographical treatment. However, this procedure was not satisfying, as the oxidation during the column chromatography proved to be tedious and time-consuming due to the tailing of the substances. Therefore, a second chromatographical treatment was often necessary. By treating the resulting reaction mixture with a small amount of N,N'-bis(salicylidene)ethylene-diiminocobalt(II) and by bubbling oxygen through the solution until it turned orange, not only the yields were improved but moreover the workup procedure was reduced to a single treatment by column chromatography. With a four-fold Knoevennagel-condensation the thermally unstable bis-cyclopentadienone-derivative **4-113** could be prepared.* Only minor changes in the determined conditions resulted for this step in the formation of a wide variety of inseparable side-products. Due to the thermal instability, the material had to be directly converted in a microwave-assisted Diels-Alder cycloaddition with the alkylated diphenylacetylene (**4-114**) to afford, after a tedious chromatographical workup, the precursor **4-115**. The microwave-assisted approach was a prerequisite to prepare the oligophenylene precursor **4-115**. The reaction was initially tried under normal conditions, but no product could be identified, possibly because of the slow heating rate of the used oil baths, resulting in the decomposition of **4-113**. For tolane derivatives the reaction temperature is anyway required to be higher than for terminal alkine derivatives, where the reaction proceeds far more smoothly[77] and also allowed to reduce the reaction temperature and therefore the decomposition rate of the cyclopentadienone derivative **4-113**.

Subsequently, compound **4-115** was submitted to a well reproducible oxidative cyclodehydrogenation step using $FeCl_3$ to gain the strained C72 derivative C72-$(C_{12})_8$-(*t*-Bu)$_2$ **4-116** in 85 % yield. After quenching the reaction with methanol, usually a precipitate is immediately formed, which can then be collected *via* filtration. In this case, the gained precipitate was very fine, which did not allow a subsequent filtration of the crude product. In other examples, the precipitation was enhanced by adding some drops of a hydrazine solution, which showed in this case no effect. However, by introducing some small amounts of CS_2 a grey precipitate occurred. This substance was identified as elementary iron originating from the used $FeCl_3$. After the filtration of the iron and washing with excess THF, all traces of the compound were washed out of the precipitate. Residual traces of iron were removed by column chromatography with silica gel and toluene as eluent. The material showed a very good solubility in common

* initially synthesized by Y. Fogel.

organic solvents. In contrast to the old route, the cyclodehydrogenation step was highly reproducible and yielded no batches with differences in the solubility properties of the compounds.

4.7.2.2 MALDI-TOF MS

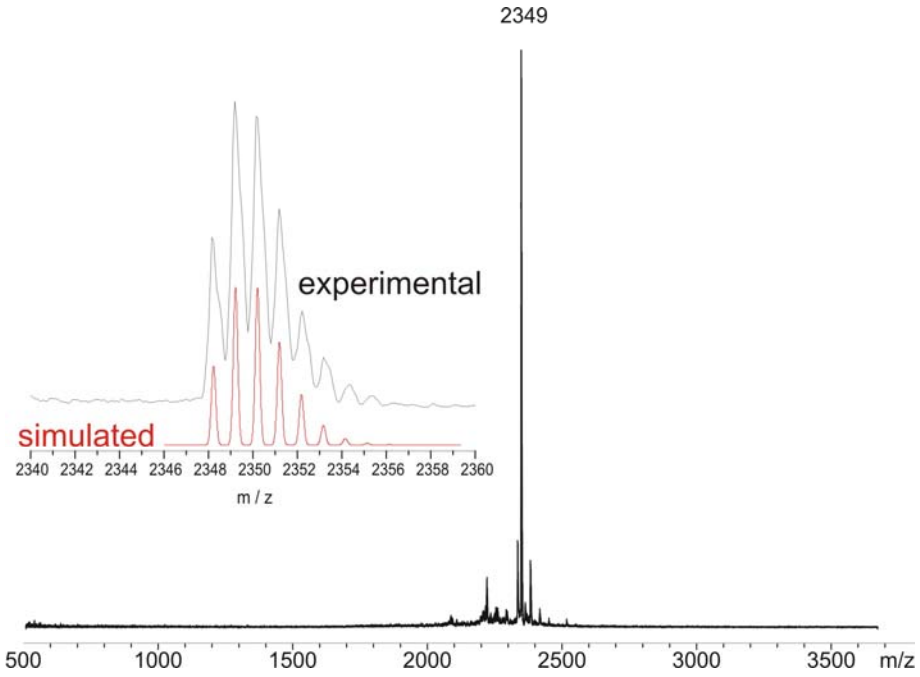

Figure 4-85: MALDI-TOF MS of C72-$(C_{12})_8$-(*t*-Bu)$_2$ (**4-116**) with BPMPM.

In the MALDI-TOF MS the product peak was clearly identified. The smaller peaks close to the main signal occurred due to the experimental conditions. One has to keep in mind that the conditions in the MALDI-TOF MS, which are required to ionize the analyte can also induce some elimination reactions. It was shown by increasing the laser attenuation, whereby the product signal was reduced and the smaller signals increased, that indeed some elimination took place during the ionization process.

By comparing the theoretical and experimental isotopic distribution pattern it was assumed that no partially fused side-products were formed. This was even supported by the choice of the matrix for the spectra presented in Figure 5-9, as trans-2-[3-(4-tert-butylphenyl)-2-methyl-2-propenylidene]malononitrile (BPMPM) normally amplifies the intermediates and not the fully fused products.

4.7.2.3 ^{1}H NMR Spectroscopy

Besides the MALDI-TOF MS, it was possible to record for the first time for a PAH of such a size a ^{1}H NMR spectrum with resolved aromatic signals in a mixture of CS_2 and deuterated dichloromethane (Figure 4-86). This mixture had to be applied, as in all other solvents even at elevated temperatures, the aromatic signals could not be resolved. CS_2 is known to inhibit efficiently the π-mediated stacking process, which is assumed to be one reason for the broad aromatic signal distribution for the other C72 derivatives.

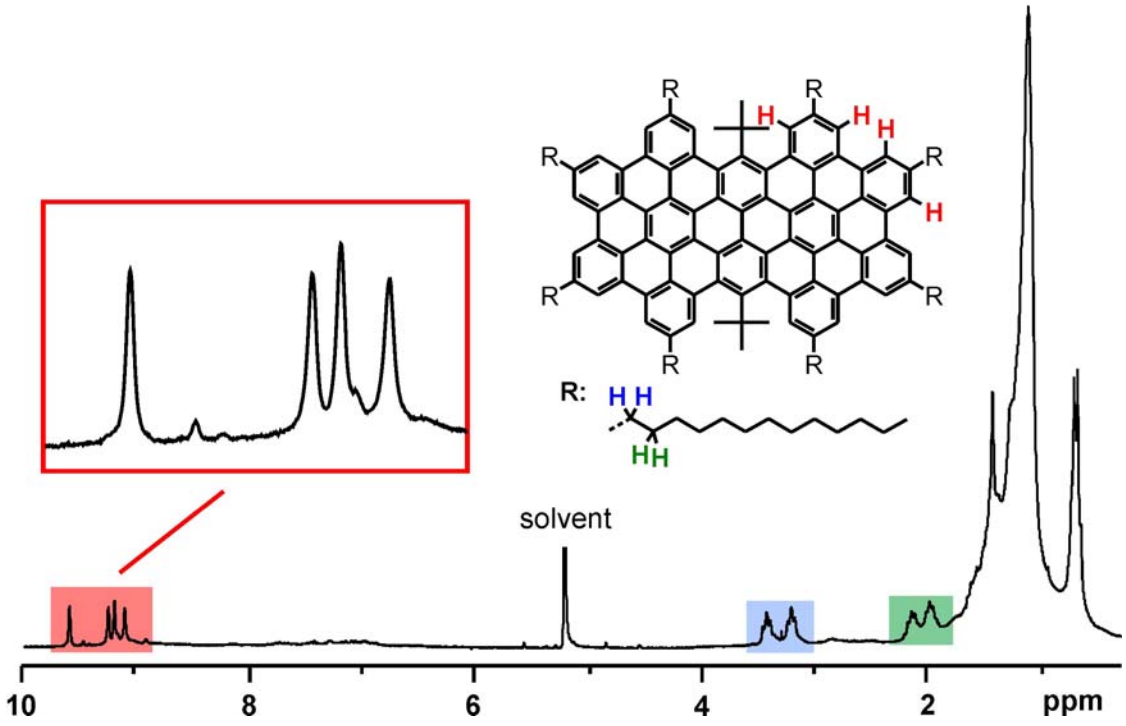

Figure 4-86: ^{1}H NMR spectrum of C72-$(C_{12})_8$-(*t*-Bu)$_2$ (**4-116**) in a CD_2Cl_2/CS_2 mixture at room temperature.

As only NMR spectroscopy can be considered as a true structural proof of a substance next to single-crystal X-ray methods, this material allowed for the first time a close analytical insight into PAHs of such sizes. On one hand, this is possibly due to the efficient reduction of the π-interaction induced by the *tert*-butyl groups, which led to a far minor disturbance of the aromatic signals by aggregation effects. In addition, this can be also an indication of a higher purity of the substance, as in this case no aromatic protons of any intermediates interfere or even suppress the signals from the fully fused product. Unfortunately, the solubility of the compound was not high enough to provide a 2D-NMR spectra with a sufficient signal to noise ratio. Therefore, the aromatic signals

could not be correlated to the corresponding protons. The α-proton signals of the alkyl side-chains were also detected in the ^{1}H NMR spectrum. All these signals have so far not been observed for the compounds prepared *via* the old pathway.

In contrast to the electronic spectra, the NMR spectrum of C72-$(C_{12})_8$-(*t*-Bu)$_2$ (**4-116**) were difficult to record and for some batches the aromatic signals were again possibly suppressed by aggregation or the presence of radicals, which could also not be solved by further diluting the samples. Therefore, a study concerning the possible shift of the aromatic resonances with respect to the concentration seemed to be questionable for C72-$(C_{12})_8$-(*t*-Bu)$_2$ (**4-116**) due to to their lack of reproducibility.

4.7.2.4 Electronic Spectroscopy

Another progress, was the increased number of absorption bands in the electronic spectra. While for the old route only one main absorption signal was identified, for C72-$(C_{12})_8$-(*t*-Bu)$_2$ (**4-116**) approximately five bands were identified, including one at 602 nm, which has not been observed for the other cases C72-$(C_{12})_8$ (**4-44**) and C72-$(C_{8,2})_8$ (**4-45**). However, a slight bathochromic shift was observed for the main absorption band in the UV/vis. This effect can be explained by the distortion of the aromatic core component by the bulky *tert*-butyl groups (Appendix H).

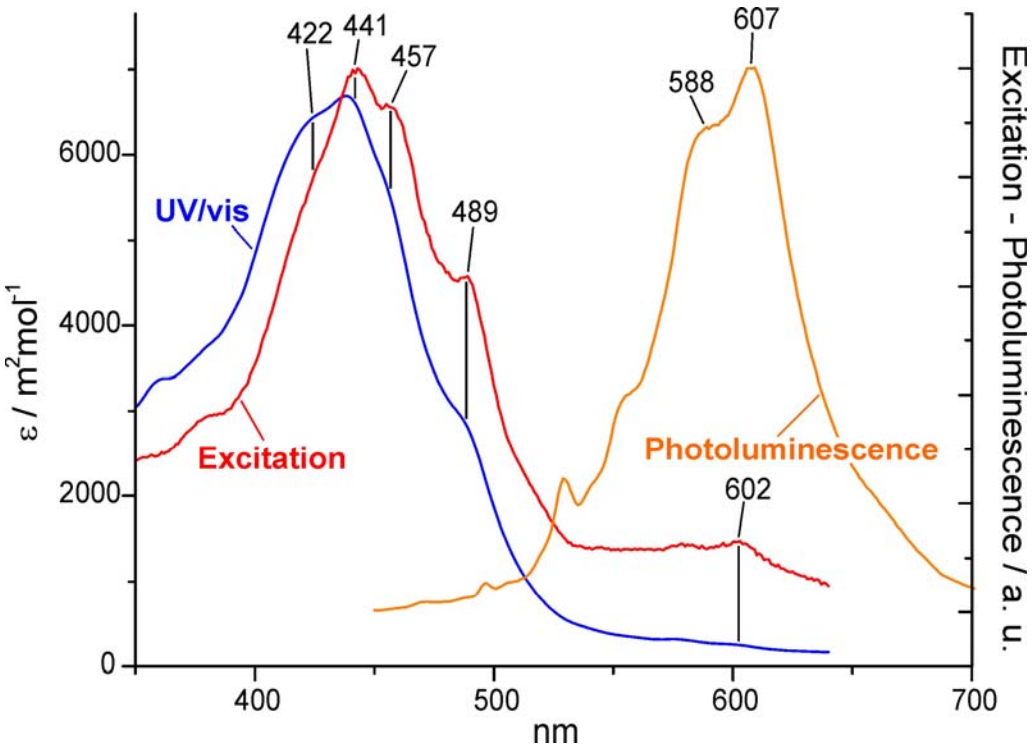

Figure 4-87: Electronic spectra of C72-$(C_{12})_8$-(*t*-Bu)$_2$ (**4-116**) in THF at room temperature.

For HBCs, which are a species with D_{6h} symmetry and therefore close to the benzene case, the α-bands correspond to a symmetry-forbidden transition and show therefore a very low oscillator strength. As C72 is reduced in its symmetry to D_{2h}, it should be expected that the α-transitions get more symmetry-allowed. Nevertheless, in Figure 4-87 one can clearly see that the spectra of C72-$(C_{12})_8$-(*t*-Bu)$_2$ (**4-116**) is still rather broad and featureless. Due to this, it was not possible to assign without any doubt the Clar nomenclature to the bands, especially when one recalls the fact that in the linear acene series the p- can completely suppress or can be found at longer wavelengths than the α-bands (Appendix H). In the literature however the β-bands were always assigned to the band with the maximum absorption and therefore the β-bands should correspond to the maximum absorption at around 441 nm.

Additionally, the fluorescence excitation spectrum of C72-$(C_{12})_8$-(*t*-Bu)$_2$ (**4-116**) showed a similar band structure as the UV/vis, which is another indication for the improved purity of the material, as no energy transfer by partially fused intermediates onto the fully fused product disturbed the recording of the photoluminescence excitation spectra. As expected, the photoluminescence emission profile appeared simplified, which can be attributed to the low symmetry of the molecule. In contrast to the materials obtained *via* the old route, where almost no intensity in the fluorescence was detected, possibly due to quenching effects based upon the π-stacking process, for this case a reasonable intensity was observed. Already by illuminating a sample in THF under a standard UV lamp, the distinct red fluorescence was impressive compared to the compounds obtained by the old route. This feature was indicating the reduction of aggregation, which has already been assumed by the successful recording of the ^{1}H NMR spectrum.

Another enhancement was the observed quantum yield, which was determined to be approximately 3 % and corresponded to the one observed for HBCs. For the other C72 examples C72-$(C_{12})_8$ (**4-44**) and C72-$(C_{8,2})_8$ (**4-45**) obtained by the old synthetic pathway, no quantum efficiency could be determined due to the severe quenching of the fluorescence. This also included other cases like C96 (**4-48**) or C222 (**4-50**). Therefore, the obtained value for C72-$(C_{12})_8$-(*t*-Bu)$_2$ (**4-116**) is another indication for the effective suppression of the aggregation.

4.7.3 Improving the Solubility Properties by Bulky Alkyl Substituents

As for C72-$(C_{12})_8$-(*t*-Bu)$_2$ (**4-116**) no 2D NMR spectrum could be recorded, possibly still due to a pronounced aggregation, further solubilizing methods had to be applied. There exist several possible approaches to induce or improve the solubility and processability of large PAHs. One key factor is hereby the nature of the alkyl substituents in the corona of the molecules, which represents one of the most important possibilities to adapt the supramolecular properties of such materials.[12] For HBCs (Figure 4-88) it has been shown that by using longer alkyl chains, the compounds exhibit a better solubility and their thermal behavior shows a reduction of the respective phase transition temperatures. The same effect can be achieved and enforced by using alkyl chains, which possess a branching site close to the aromatic core (**4-29**). The steric requirements for these chains close to the aromatic entity lead to a reduction of the π-interaction and consequently to a lower aggregation propensity in combination with an improved solubility and thermal processability (Figure 4-88).

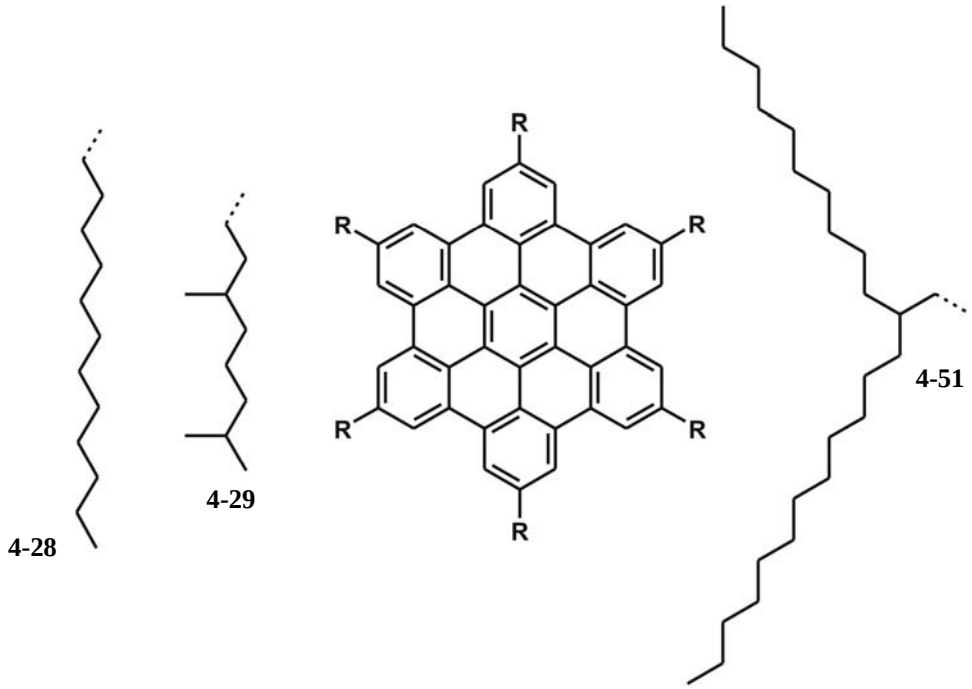

Figure 4-88: Hexa-substituted HBC derivatives.

It was recently possible to introduce the sterically highly demanding tetradecyl-decyl alkyl chain in the corona of an HBC (**4-51**), whereby the key feature of the implemented chain is the close proximity of the branching site to the aromatic core.[99] This branching at the β-position combined with the rotational freedom around the HBC-C_α bond

induced a large steric demand and decreased efficiently the strong π- interaction of the aromatic core. Moreover, this HBC derivative was the first known HBC soluble in non-polar solvents, such as pentane or hexane.[12,99]

4.7.4 C72-$(C_{12})_4$-$(C_{14,10})_4$-(*t*-Bu)$_2$

Therefore, four of the *n*-dodecyl chains of the C72-$(C_{12})_8$-(*t*-Bu)$_2$ (**4-116**) were replaced by tetradecyl-decyl chains. The combination of different types of alkyl chains also reduced the risk of a cocrystallization effect of the alkyl substituents, which would lead to a reduction of the solubility.[100]

4.7.4.1 Synthesis

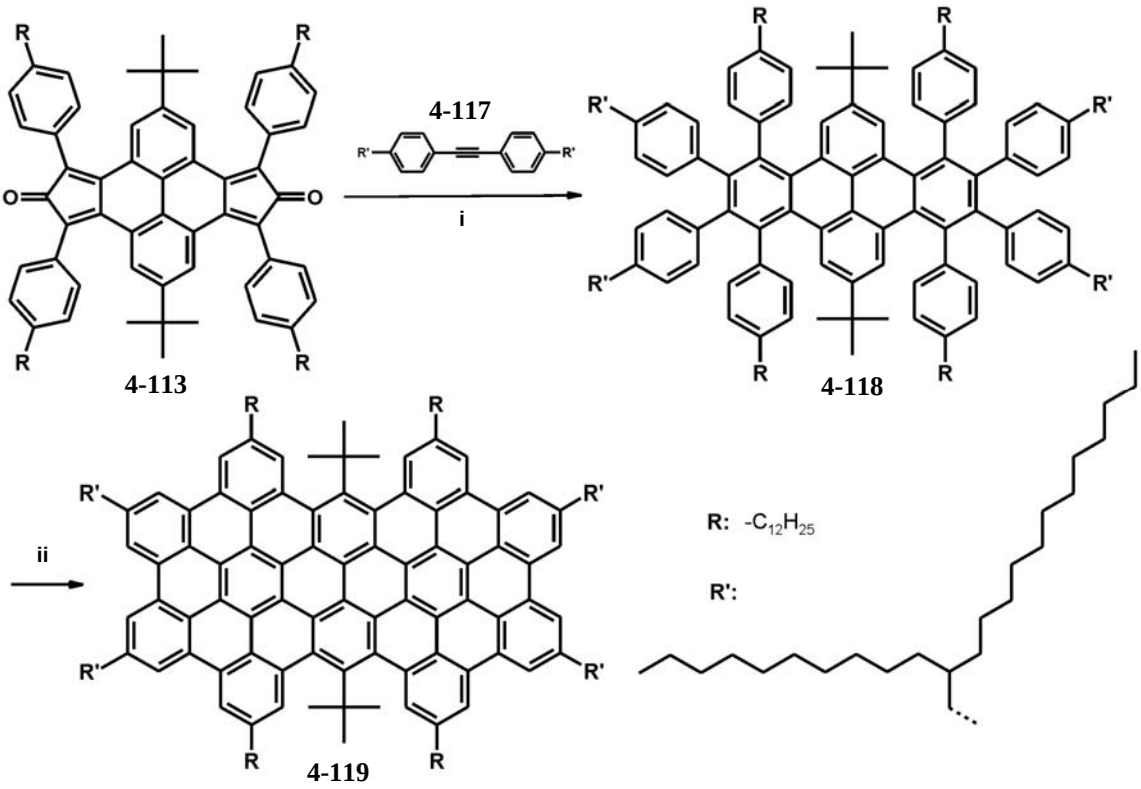

Figure 4-89: Preparation of the C72 derivative C72-$(C_{12})_4$-$(C_{14,10})_4$-(*t*-Bu)$_2$ (**4-119**). *i:* Ph_2O, 11 %; *ii:* $FeCl_3$, CH_2Cl_2, CH_3NO_2, 83%.

The synthesis had to be changed only slightly and instead of the *n*-dodecyl substituted diphenylacetylene (**4-114**), the literature known counterpart substituted with the 2-decyl-tetradecyl-chain (**4-117**) was used for the Diels-Alder reaction (Figure 4-89). With the alkyl substitutents on **4-117** the very bulky and sterically demanding 2-decyl-tetradecyl

chain was introduced into the oligophenylene precursor molecule (**4-118**). Again the cycloaddition only yielded product under the microwave conditions. The bulkiness of the diphenylacetylene derivative even led to a lower reactivity and further reduced the yield compared to the *n*-dodecyl derivative (**4-115**). Also the workup procedure proved to be as tedious as for compound **4-115**.

Subsequently, the oligophenylene precursor was subjected to the oxidative cyclodehydrogenation by using similar conditions as for C72-$(C_{12})_8$-(*t*-Bu)$_2$ (**4-116**). The precipitate formed after the quenching of the reaction was very fine, which did not allow a workup by a filtration of the product. Therefore, it was decided to perform the same workup procedure as described above for the compound C72-$(C_{12})_8$-(*t*-Bu)$_2$ (**4-116**), which yielded the product C72-$(C_{12})_4$-$(C_{14,10})_4$-(*t*-Bu)$_2$ (**4-119**). The gained material showed a very good solubility in common organic solvents and similar to C72-$(C_{12})_8$-(*t*-Bu)$_2$ (**4-116**) showed no differences in the macroscopic behavior between the batches, indicating the high reproducibility of the reaction.

4.7.4.2 MALDI-TOF MS

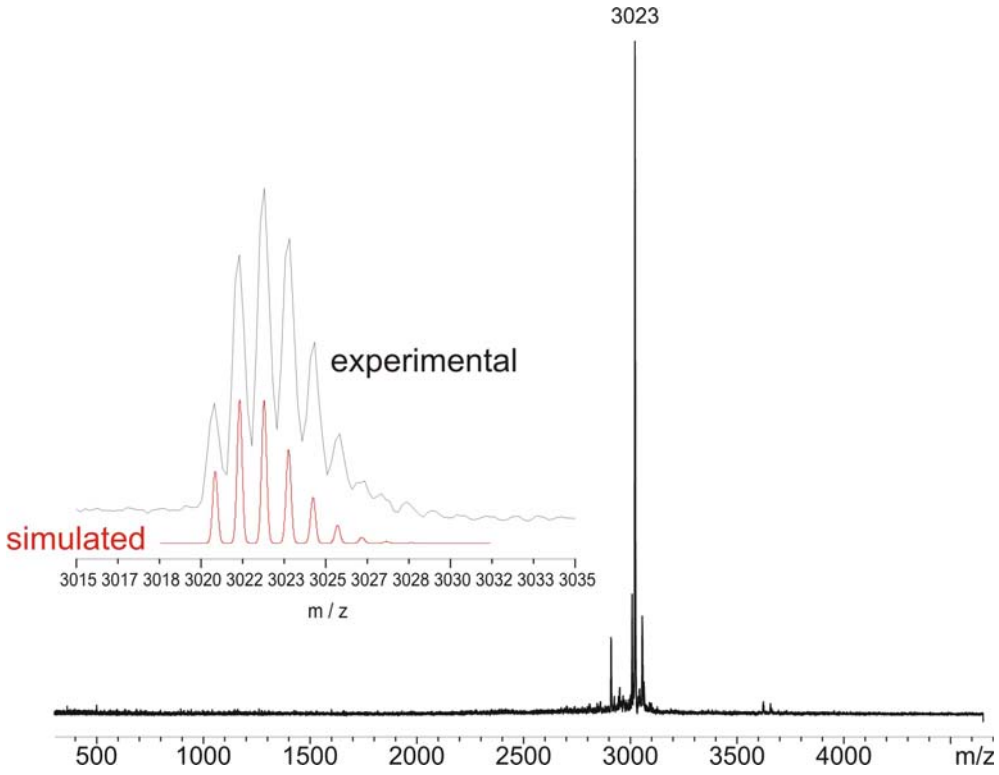

Figure 4-90: MALDI-TOF MS of C72-$(C_{12})_4$-$(C_{14,10})_4$-(*t*-Bu)$_2$ (**4-119**).

In the MALDI-TOF MS spectrum (Figure 4-90), the product was clearly identified and the comparison with the simulation indicated the successful cyclodehydrogenation. By comparing the theoretical and experimental isotopic distribution pattern, it was assumed, that no partially fused side-products were formed. This was even supported by the choice of the matrix for the spectra presented in Figure 4-90, as the used matrix (trans-2-[3-(4-tert-butylphenyl)-2-methyl-2-propenylidene] malononitrile (BPMPM)) was identical to the one used for C72-$(C_{12})_8$-(*t*-Bu)$_2$ (**4-116**), which usually amplifies the partially fused species. Therefore, it could be concluded that either no byproduct was present or that the amount of these partially fused species is sufficiently low. As already discussed for the before mentioned example C72-$(C_{12})_8$-(*t*-Bu)$_2$ (**4-116**), also a fragmentation of the molecule was observed under the MALDI-TOF MS conditions. It was shown for C72-$(C_{12})_4$-$(C_{14,10})_4$-(*t*-Bu)$_2$ (**4-119**) that by increasing the laser attenuation, the product signal was reduced, while the smaller signals simultaneously increased, which indicated some elimination process during the ionization of the analyte.

4.7.4.3 ^{1}H NMR Spectroscopy

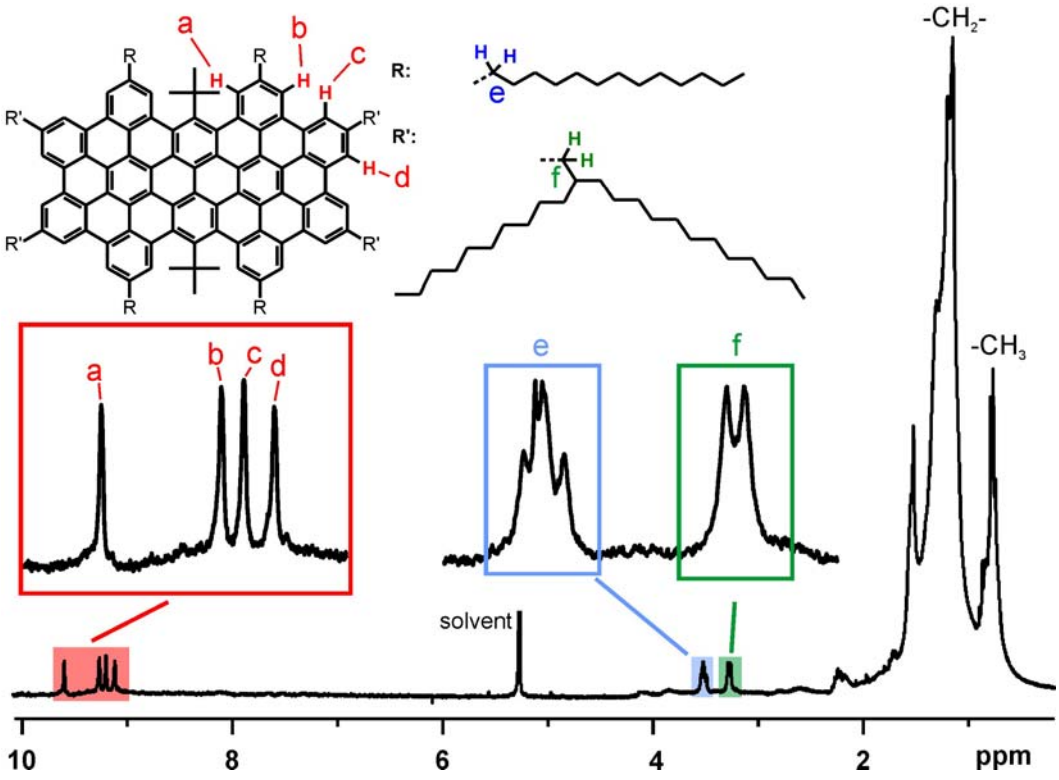

Figure 4-91: ^{1}H NMR spectrum of C72-$(C_{12})_4$-$(C_{14,10})_4$-(*t*-Bu)$_2$ (**4-119**) in a mixture of CS_2 and CD_2Cl_2 at room temperature.

For compound C72-$(C_{12})_4$-$(C_{14,10})_4$-(*t*-Bu)$_2$ (**4-119**) a ^{1}H NMR spectrum with a resolved aromatic region could be recorded (Figure 4-91), too. The α-protons of the alkyl chains were unambiguously identified as the protons from the *n*-dodecyl chain, which yielded as expected a triplet, while the ones of the branched chain exhibited a doublet. The doublet was recorded at a lower field, indicating that the positions at the aromatic core further away from the *tert*-butyl groups show a reduced effect of the aromatic core component upon the chemical shift of the α-protons. This assumed that a similar effect could occur for the aromatic protons, meaning that proton **a** should probably show the largest low-field shift. Similar to C72-$(C_{12})_8$-(*t*-Bu)$_2$ (**4-116**), compound C72-$(C_{12})_4$-$(C_{14,10})_4$-(*t*-Bu)$_2$ (**4-119**) only exhibited this degree of resolution, when the sample was dissolved in a CS_2/CD_2Cl_2 mixture. By changing the solvent to THF for example, the aromatic signals were reduced in their intensity as well as their resolution. Even by applying elevated temperatures for the other solvents, the resolution could not be achieved. This still points towards some remaining degree of aggregation in solution, which can only be inhibited by the addition of CS_2.

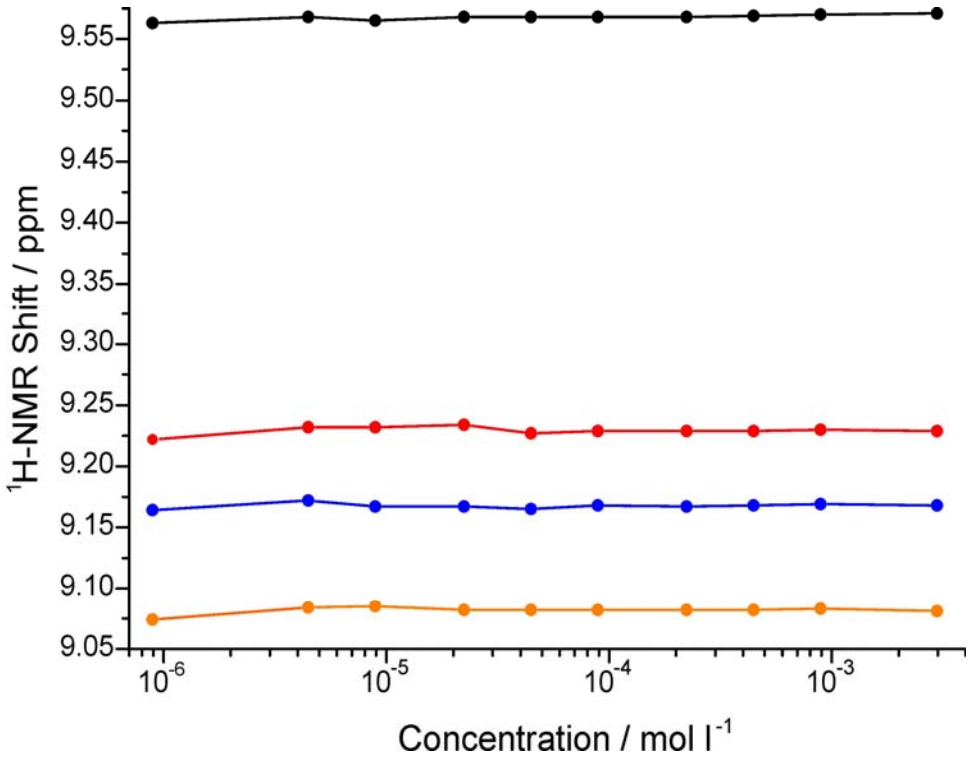

Figure 4-92: Concentration dependent chemical shifts of the aromatic protons of C72-$(C_{12})_4$-$(C_{14,10})_4$-(*t*-Bu)$_2$ (**4-119**) at room temperature in CD_2Cl_2/CS_2.

Therefore, a series of concentration dependent ^{1}H NMR spectra were recorded in the solvent mixture CD_2Cl_2 and CS_2 (Figure 4-92). It has been reported that the chemical sift of the aromatic signal of hexaalkylated HBCs is dependent upon the degree of aggregation in solution.[91] This effect is based upon the influence of the ring current from adjacent molecules, causing the shift of the aromatic protons. The influence of these neighbouring molecules decreases with decreasing concentration, as the sizes of the stacks, which are in a dynamic association and dissociation process, become smaller at lower concentrations. In this study, it was also revealed that the nature of the solvent influences the aggregation process of the PAHs in solution, too. Therefore, if a residual aggregation is present for the C72 derivative C72-$(C_{12})_4$-$(C_{14,10})_4$-(*t*-Bu)$_2$ (**4-119**) in the solvent mixture CD_2Cl_2/CS_2, a shift in the ^{1}H NMR spectra for the aromatic signals, similar to HBCs, should be observed.

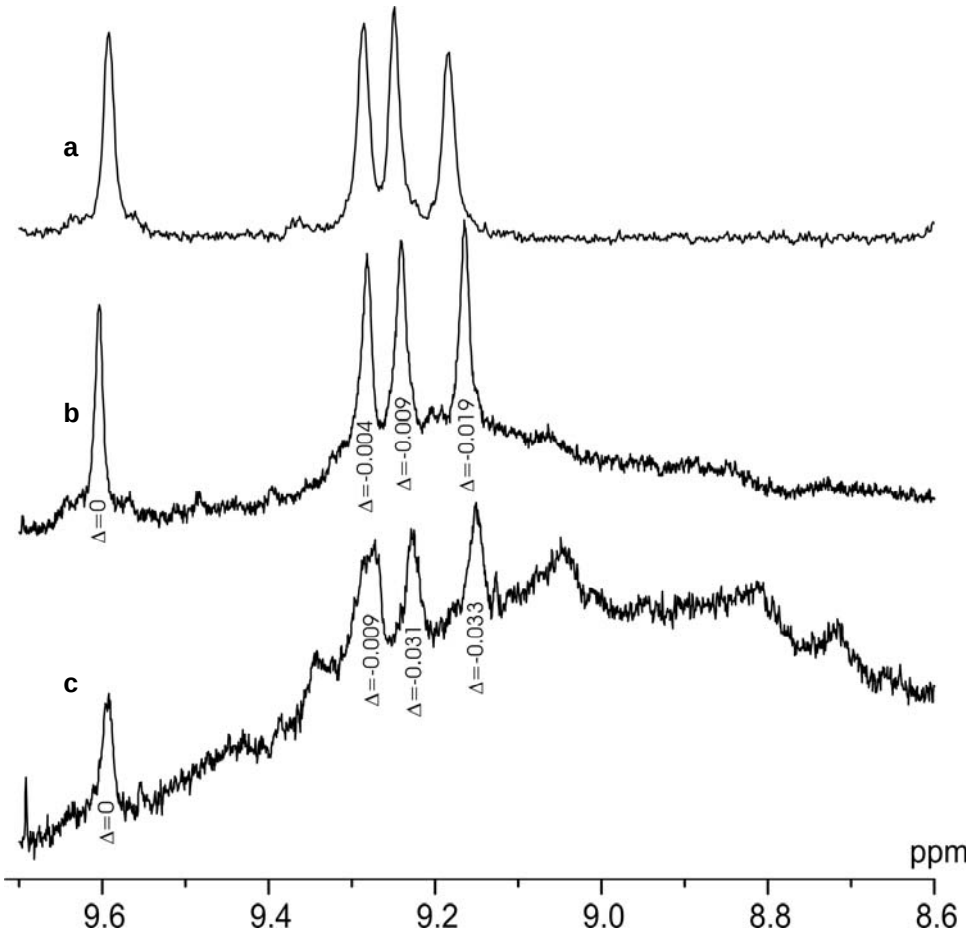

Figure 4-93: Time-dependent chemical shifts of aromatic protons for C72-$(C_{12})_4$-$(C_{14,10})_4$-(*t*-Bu)$_2$ (**4-119**). Sample after **a**) 1 h, **b**) 6 weeks and **c**) 18 weeks

However, it became obvious from the data in Figure 4-92 that no concentration dependent shift of the aromatic signals appeared. If a concentration dependence according to the HBC example could be seen, the shifts should change to higher ppm values at lower concentrations. Therefore, it has to be assumed that the aggregation effects are rather limited in this solvent, which again pointed out the strong suppression of the π-mediated aggregation by CS_2.

In Figure 4-93, it is shown that the spectra of the samples change with respect to time. While the intensity for the distinct aromatic signals is reduced after some time, a hump appeared in the aromatic region, which seemed to originate from molecules entrappped in an aggregate. Consequently, this pointed towards the argument that a minor degree of aggregation was present, as such a broad hump in the aromatic region has already appeared for the undistorted C72 derivatives as shown in Figure 4-9.

In addition, three of the four aromatic signals showed a slight decrease in their respective chemical shift, which has also been observed for HBCs situated in aggregates. Therefore a small but existing aggregation effect probably remained even in such a good solvent mixture as CD_2Cl_2/CS_2 and by applying a series of solubilizing and aggregation suppressing features as for C72-$(C_{12})_4$-$(C_{14,10})_4$-(*t*-Bu)$_2$ (**4-119**).

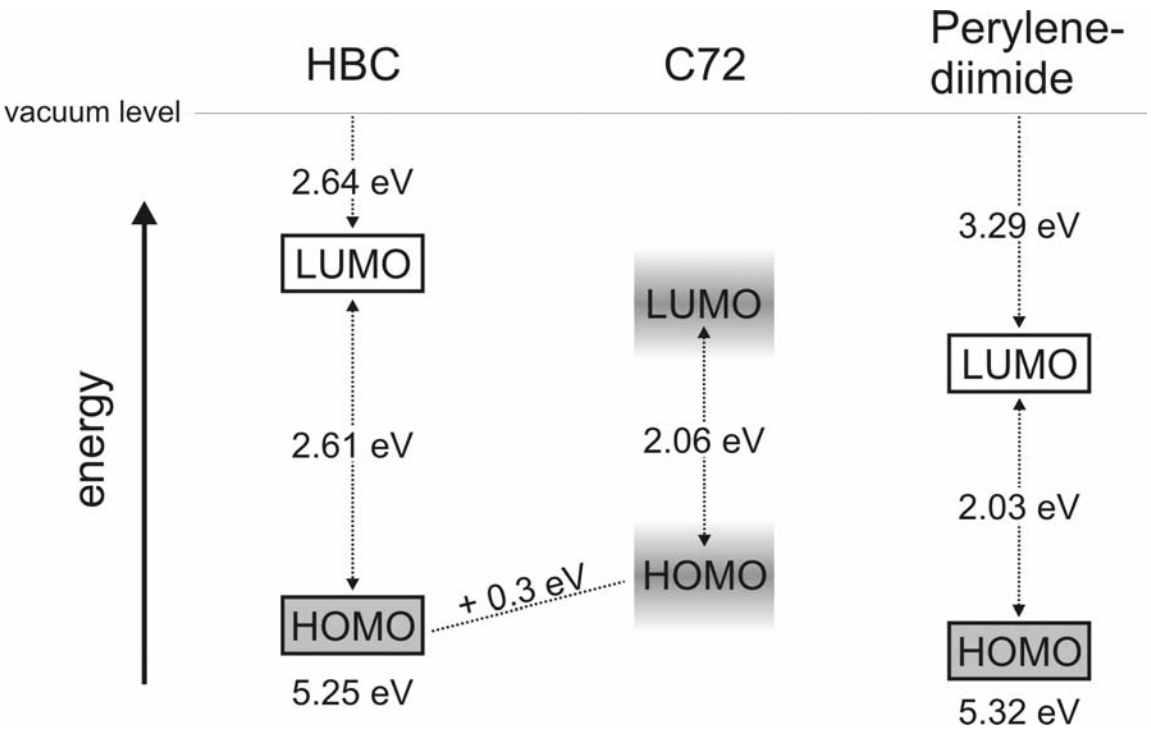

Figure 4-94: Energy level scheme for the HOMO and LUMO of HBC, C72 and perylene-diimide.

However, no precipitation was observed in the NMR solutions during this time, which contradicts the assumption of a slow aggregation in solution. Another possibility for the disappearance of the aromatic proton signals could be, that the aromatic core component is slowly oxidized by the oxygen in the overlaying atmosphere in the NMR tube. This process would generate radical species, which severely influence the ^{1}H NMR spectrum in a similar fashion, as shown in Figure 4-93. This pathway becomes even more probable, when one considers that also solutions of highly soluble HBCs are aging. Already for HBCs, the HOMO level is energetically quite high, as pointed out in Figure 4-94. From the UV/vis absorption at 603 nm for C72-$(C_{12})_4$-$(C_{14,10})_4$-(*t*-Bu)$_2$ (**4-119**) (Figure 4-103), which corresponds to the p-band, a HOMO-LUMO gap of 2.06 eV was derived (for detailed discussion refer to section 4.7.4.6). This gap is 0.55 eV smaller than the one for HBCs. As known from the literature, the reduction of the HOMO-LUMO gap for PAHs in a series like acene or rylene occurs in such a sense, that the HOMO is raised and the LUMO is lowered in energy by increasing the size of the conjugated aromatic entity (Appendix I).

Additionally, theoretical calculations (AM1) indicated an energetical difference of +0.3 eV of the C72 HOMO level with respect to the one of the HBC. Although the theoretical values cannot be considered as a final proof, it can be taken as granted that the HOMO level of the C72 should exhibit a higher energy level than the one of HBC. As a consequence, the possible oxidation could occur even easier than for HBCs.

4.7.4.4 2D NMR Spectroscopy

In contrast to the already discussed example C72-$(C_{12})_8$-(*t*-Bu)$_2$ (**4-116**), which seemed to exhibit not enough solubility, for C72-$(C_{12})_4$-$(C_{14,10})_4$-(*t*-Bu)$_2$ (**4-119**) it was possible to record 2D NMR spectra of the aromatic region. In the HH COSY (Figure 4-95), it was revealed that two spin systems exist, which can be assigned to the couplings of protons **a** with **b** and **c** with **d** (Figure 4-91). While cross-peaks were identified for the signal at 9.61 ppm with the one at 9.27 ppm, the other proved the correlation for the signal at 9.22 ppm and 9.13 ppm (Figure 4-91). Unfortunately, no cross peaks could be identified for the alkyl region. When the chemical shift differences between the coupled protons are small, the cross peaks, which are close to the diagonal, are difficult to recognize, as this is the region where the strong diagonal peaks with their broad wings interfere.

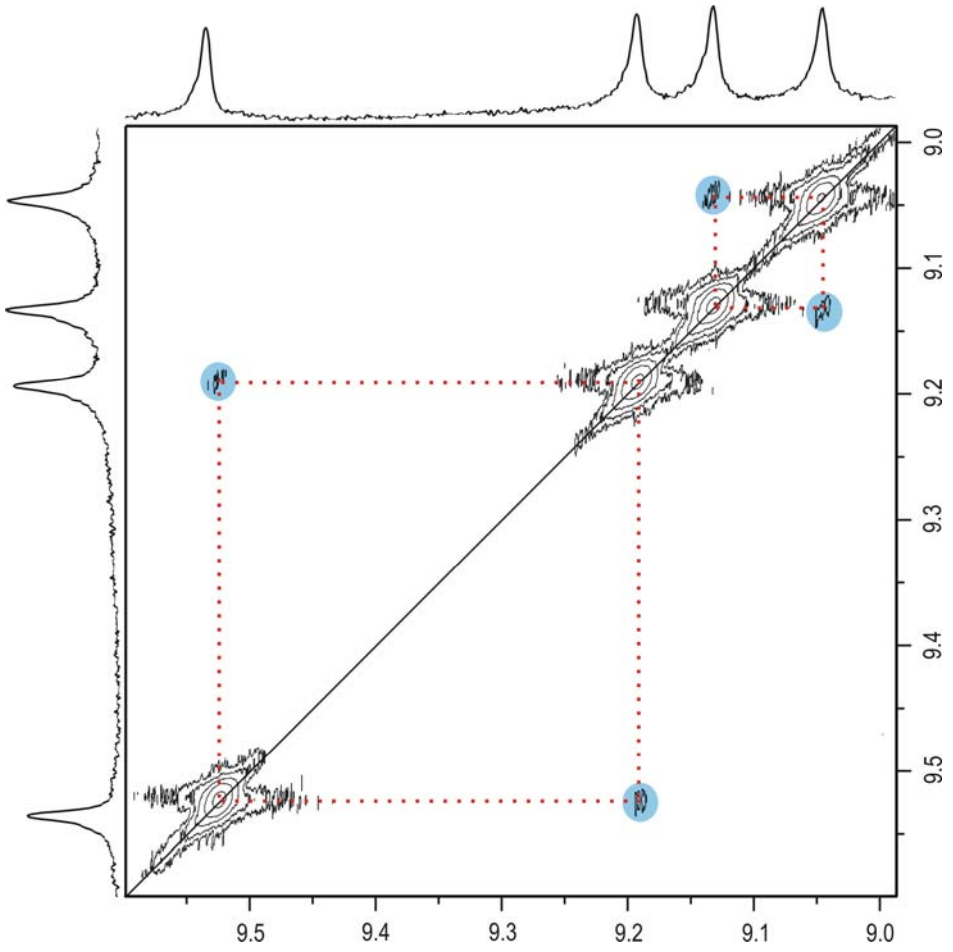

Figure 4-95: HH COSY spectrum of C72-$(C_{12})_4$-$(C_{14,10})_4$-(*t*-Bu)$_2$ (**4-119**) in CD_2Cl_2/CS_2 at room temperature.

From the NOESY spectrum (Figure 4-97), it became clear that two protons of the two spin systems observed from the HH COSY spectrum need to be located in a close spatial arrangement. This correlates to the situation expected from the protons **b** and **c**.

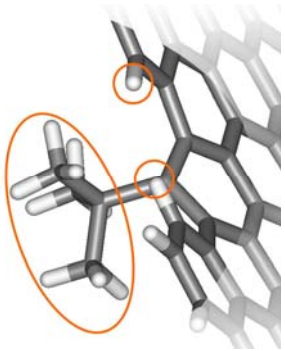

Figure 4-96: Spatial arrangement of the aromatic protons **a** with the protons of the *tert*-butyl groups.

In the NOESY spectrum, this coupling was indeed found for the signals at 9.27 and 9.22 ppm. This corresponds to the expected situation for the protons **b** and **c**. However, it was expected that in the spectrum also an indication would be found for the coupling between the protons of the *tert*-butyl groups and the aromatic proton **a**. As seen in Figure 4-96 the theoretical distance between the two protons should be sufficiently small (0.22 nm) for the occurrence of the NOE effect.

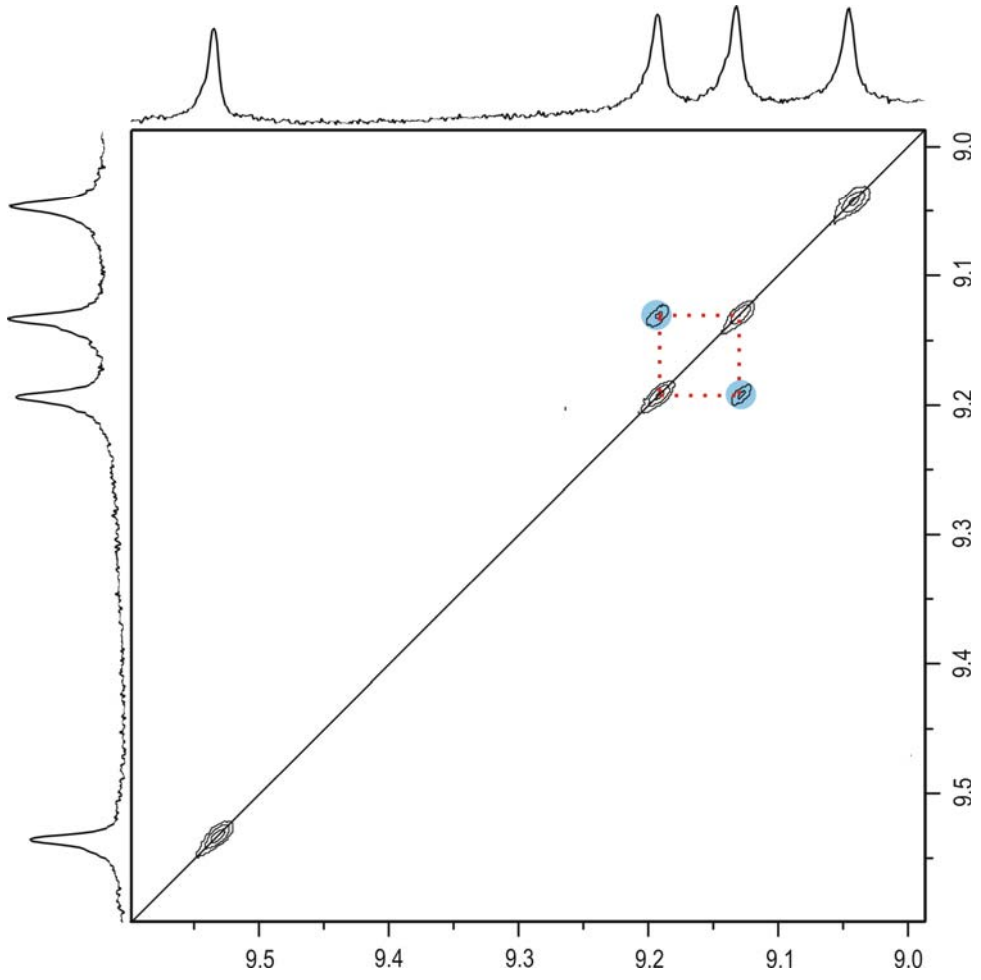

Figure 4-97: NOESY spectrum of C72-$(C_{12})_4$-$(C_{14,10})_4$-$(t\text{-Bu})_2$ (**4-119**) in CD_2Cl_2/CS_2 at room temperature.

However, the signals from the *tert*-butyl groups distributed their intensity over the whole range of the NOESY spectrum. As the intensity for the coupling of the **b** and **c** proton was already low, the noise induced by the *tert*-butyl groups and to some extent from the alkyl protons led to a suppression of the coupling by the large signal to noise ratio. This signal is necessary to unambiguously determine, which peak originates from the proton **a**. Until now, it is only sure that the signals at 9.27 and 9.22 ppm cannot

originate from the proton **a**, as for this proton no correlation between any other aromatic proton is possible.

Based upon the above discussed chemical shift of the α-protons of the alkyl side chains, it seems probable that the aromatic proton **a** should occur at lower fields than all other aromatic protons and therefore it was assumed that the signal at 9.52 ppm is the corresponding signal. Also simulations of the ^{1}H NMR spectrum could not reveal coherent indications about the relative positions of the aromatic protons, which is due to the enormous size of the molecule and the resulting, unpredictable ring current effects.

4.7.4.5 Theoretical Calculations

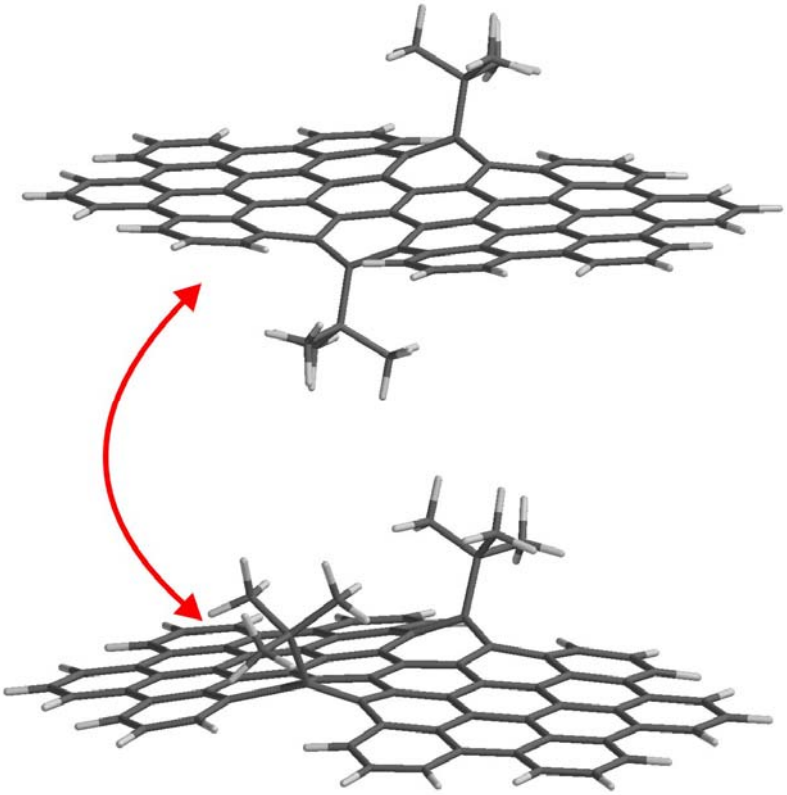

Figure 4-98: Possible flipping of the *tert*-butyl groups between cis and trans conformation.

The possibility of a flipping of the *tert*-butyl groups (Figure 4-98) had to be adressed due to the fact that the conformation of the molecule could not be undoubtedly determined by the NMR measurements. Therefore, the four aromatic signals could not only originate from a single cis or trans arrangement, but it could be also due to a flipping process of the *tert*-butyl groups. As a consequence, it had to be verified, if the efficient aggregation reduction was only due to the bulkiness of the *tert*-butyl groups and

the induced distortion of the aromatic entity, or if a flipping of these groups from one side of the aromatic core to the other disturbed the aggregation process further. Based on theoretical calculations, it was shown that the “cis” and the “trans” conformation exhibit almost the same heat of formation and therefore both conformers can be formed during the cyclodehydrogenation (Figure 4-83).

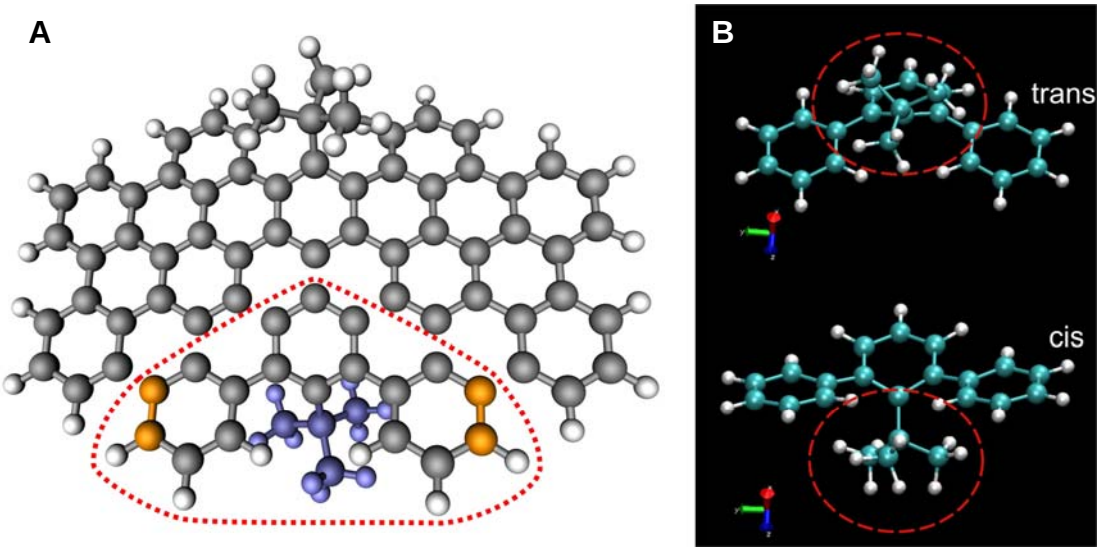

Figure 4-99: A) Structure of “trans”-conformation, selected section (red dotted line) for the density functional simulation and carbon atoms fixed in the simulations (orange), the *tert*-butyl group was colored blue for a better visualization; **B**) ground state conformation of “cis” and “trans” functional groups.

The calculations regarding the possibility for the conformational change from "cis" to "trans" were performed by Dr. W. Hofer at the University of Liverpool, which included density functional calculations of a section of the molecule (Figure 4-99A/B).[101,102] Within this section, the space coordinates of four carbon atoms were fixed in the simulations (Figure 4-99A, orange), whereby all other atoms were fully relaxed. As the rigid entities were placed at the very end of the substructure, this fragment showed a similar flexibility with respect to the elasticity of the carbon-carbon bonds of the whole molecule. It also has to be considered that this part is usually connected to the rest of the molecule by seven covalent bonds, exerting further resistance to a conformational change. The energy barrier for transitions was calculated with the so-called nudged elastic band method[103] and was found to exceed 1 eV/atom. This indicates that every bond of the segment would have to stabilize at least a strain energy of 450 kJ/mol, hence the molecule is more likely to fragment than changing its conformation. As a

consequence, the efficient aggregation suppression observed in the ^{1}H NMR spectra was due to the bulky side-chains and the fixed *tert*-butyl groups and was not partially enhanced by any disturbing effect of a dynamic conformational change, as for example exhibited by corannulene (Figure 4-82).

Therefore, the molecule had to be present in a single conformation. Unfortunately, it was not possible to elucidate, which of the two possibilities was preferred. In Figure 4-100 the two arrangements are presented schematically. It becomes obvious that the conformations cannot be determined by standard techniques, as a clear indication of a cross-peak in the NOESY method can only be revealed, when on one hand the two protons are rather close. This is due to the fact that the NOE effect falls off with distance in inverse proportion to r^{6}. In addition, a cross peak can only be observed, when a deviation in chemical shift of the two questionable protons appears.

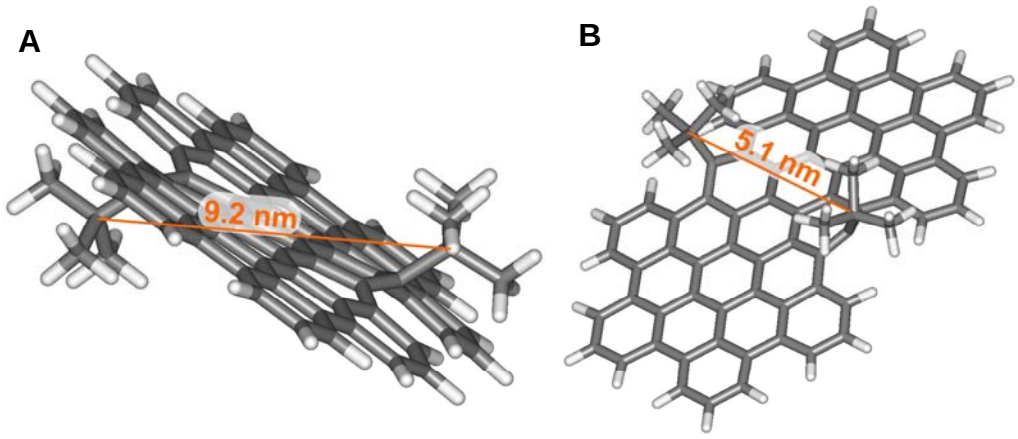

Figure 4-100: Distance between the two *tert*-butyl groups with respect to the conformation **A**) trans and **B**) cis.

It is obvious that even for the cis arrangement, where the distance between the protons is around 5.1 nm, the possible resulting effect is minimal. Additionally, the chemical shifts of the two groups will not be different as for both cases the chemical environment is similar. In Figure 4-101 it is shown that the "trans" arrangement exhibits a reduced symmetry compared to the "cis" case. This however only concerns the removal of one mirror plane and cannot be exploited for some kind of polarimetric analysis due to the remaining plane and the addition of the symmetric center. Neither of the two conformations will show an optical activity with respect to polarized light, as the

molecules would need to be chiral and therefore feature the lack of symmetry planes or symmetry centers.

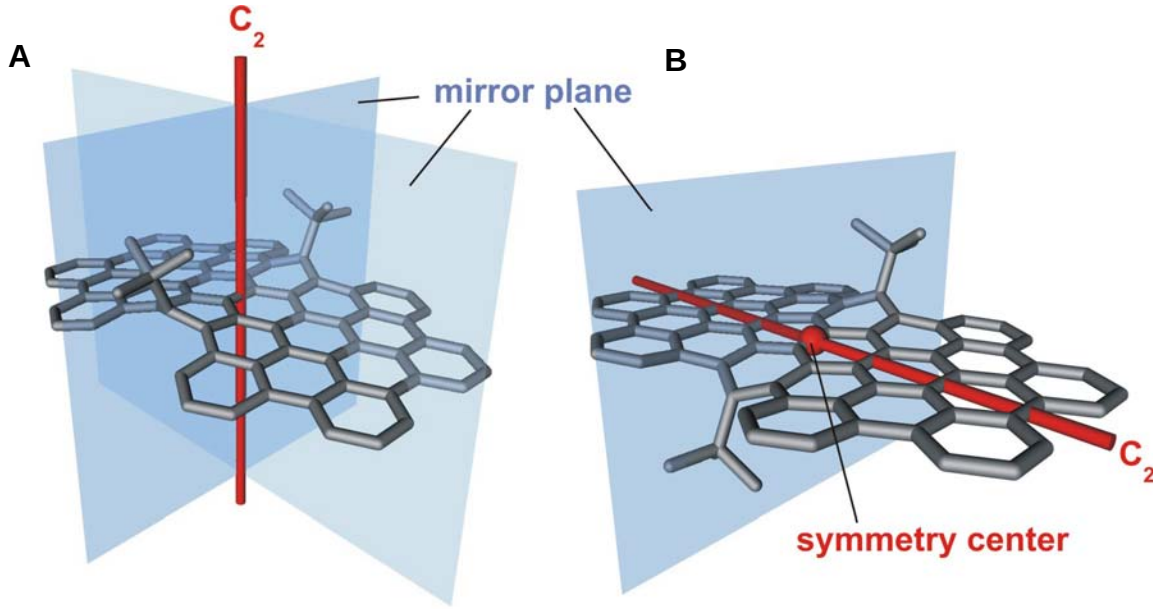

Figure 4-101: Symmetry of the respective conformations. **A**) cis and **B**) trans.

4.7.4.6 Electronic Spectroscopy

Figure 4-102: Picture taken from a sample of C72-$(C_{12})_4$-$(C_{14,10})_4$-(*t*-Bu)$_2$ (**4-119**) dissolved in THF at room temperature and illuminated by an UV-lamp.

Already in Figure 4-102 the strong fluorescence became apparent. This effect has not yet been observed in this intensity for the materials obtained *via* the old synthetic route,

where the fluorescence from the fully fused products was possibly efficiently quenched by the aggregation effect.

In Figure 4-103 the electronic spectra of C72-$(C_{12})_4$-$(C_{14,10})_4$-(*t*-Bu)$_2$ (**4-119**) are presented, which revealed a more than three times higher molar extinction coefficient than observed from HBCs. From the UV/vis it becomes obvious that the additional aggregation suppression resulted in a far more resolved spectrum and confirmed, as expected, that a strong aggregation leads to a broadening of the spectra. Compared to the previous example C72-$(C_{12})_8$-(*t*-Bu)$_2$ (**4-116**), it was therefore proven that the incorporated bulky side-chain enhanced efficiently the aggregation suppression. Indeed, it was shown that at 603 nm the first absorption band can be found, which is observed at even longer wavelengths than the first band for C96 derivatives. The determined quantum yields of C72-$(C_{12})_4$-$(C_{14,10})_4$-(*t*-Bu)$_2$ (**4-119**) are comparable to the ones observed for the C72-$(C_{12})_8$-(*t*-Bu)$_2$ (**4-116**), indicating no severe influence of the proposed improved soubility upon this property.

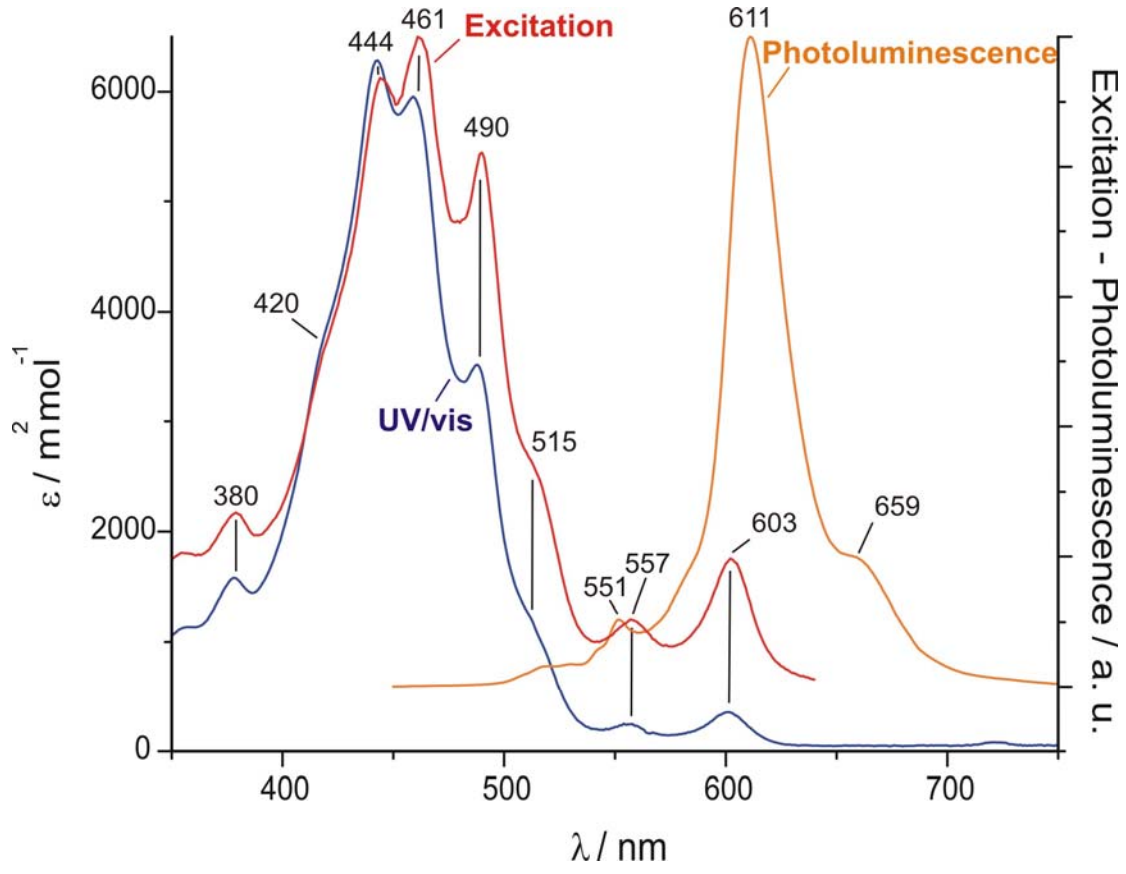

Figure 4-103: Electronic spectra of C72-$(C_{12})_4$-$(C_{14,10})_4$-(*t*-Bu)$_2$ (**4-119**); blue: absorption; red: photoluminescence excitation; orange: photoluminescence emission.

The similarity between the UV/vis and the fluorescence excitation spectrum is striking, supporting additionally the high purity of the material. As expected the photoluminescence spectra only exhibits one main peak at 611 nm corresponding to the one observed for C72-$(C_{12})_8$-(*t*-Bu)$_2$ (**4-116**) at 607 nm, which is due to the reduced symmetry of the molecule. Another small signal was found at 659 nm, which has not been observed for C72-$(C_{12})_8$-(*t*-Bu)$_2$ (**4-116**) and was possibly suppressed by aggregation effects.

As the enhanced resolution of the UV/vis spectra of C72-$(C_{12})_4$-$(C_{14,10})_4$-(*t*-Bu)$_2$ (**4-119**) allowed a better identification of the maxima, the argument of the respective bands, corresponding to the nomenclature introduced by Clar (Appendix H), was easier to accomplish. One has to be careful however, as similar to the acene series, the p-bands can suppress or even be found at longer wavelengths than the α-bands (Figure 4-104, Appendix H).[18]

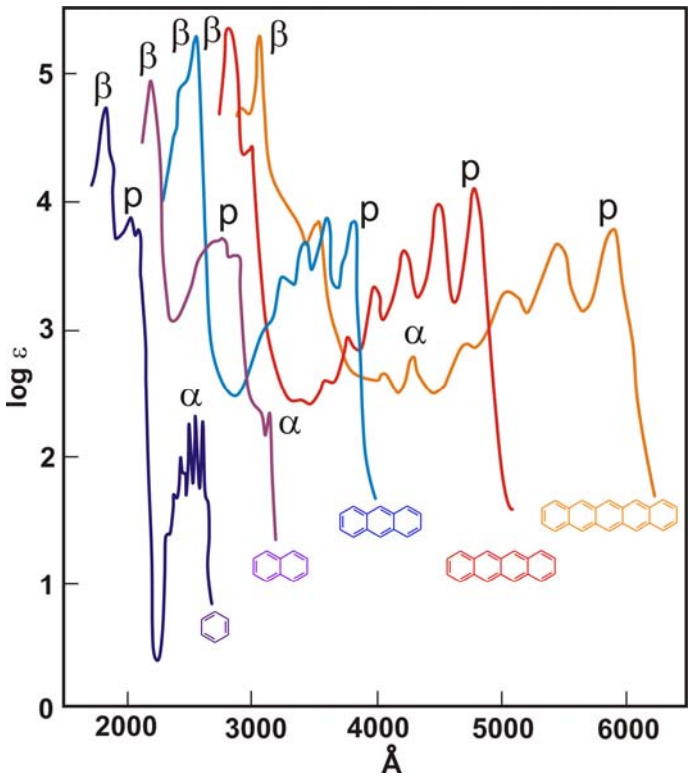

Figure 4-104: UV/vis spectra of the acene series.

By considering the symmetry, HBC corresponds to the benzene case shown in Figure 4-104. Indeed, the α-bands are located for HBC and benzene at the longest wavelengths in the spectrum.[18] If one continues in the series to naphthalene, which would be the corresponding example to C72-$(C_{12})_4$-$(C_{14,10})_4$-(*t*-Bu)$_2$ (**4-119**), it becomes obvious, that

the extension of the conjugation by one benzene unit, leads to a substantial convergence of the α- and the p-bands. By adding another one or two benzene entities to accomplish the anthracene and the tetracene, the p- already covers the α-band. Interestingly, for the pentacene, the α- and the p-bands are exchanged and exhibit a substantial difference in wavelength.

Therefore, theoretical semi-empirical calculations (AM1) for C72-$(C_{12})_4$-$(C_{14,10})_4$-(*t*-Bu)$_2$ (**4-119**) were performed to label the bands. The calculations indicated that the observed band at 603 nm does not comply to the α-transition, as the HOMO-LUMO transition, which corresponds to the p-band, was calculated to be the gap with the lowest energy. It has to be noted that semi-empirical methods with AM1 can only be considered as an approximation. However, due to the number of the atoms in the aromatic core component, other theoretical methods require significantly longer computational time. In conclusion, it was indicated that the band at 603 nm originates from the p-transition and the α-bands should be found at shorter wavelengths and can be possibly correlated to the small absorption at 557 nm. The β-bands in contrast can be clearly dedicated to the strongest absorptions in the UV/vis spectrum from 444-490 nm. Similar to other known PAHs,[18] the Stokes shift of 8 nm of C72-$(C_{12})_4$-$(C_{14,10})_4$-(*t*-Bu)$_2$ (**4-119**) is relatively small, indicating the low changes in polarity of such systems.[18]

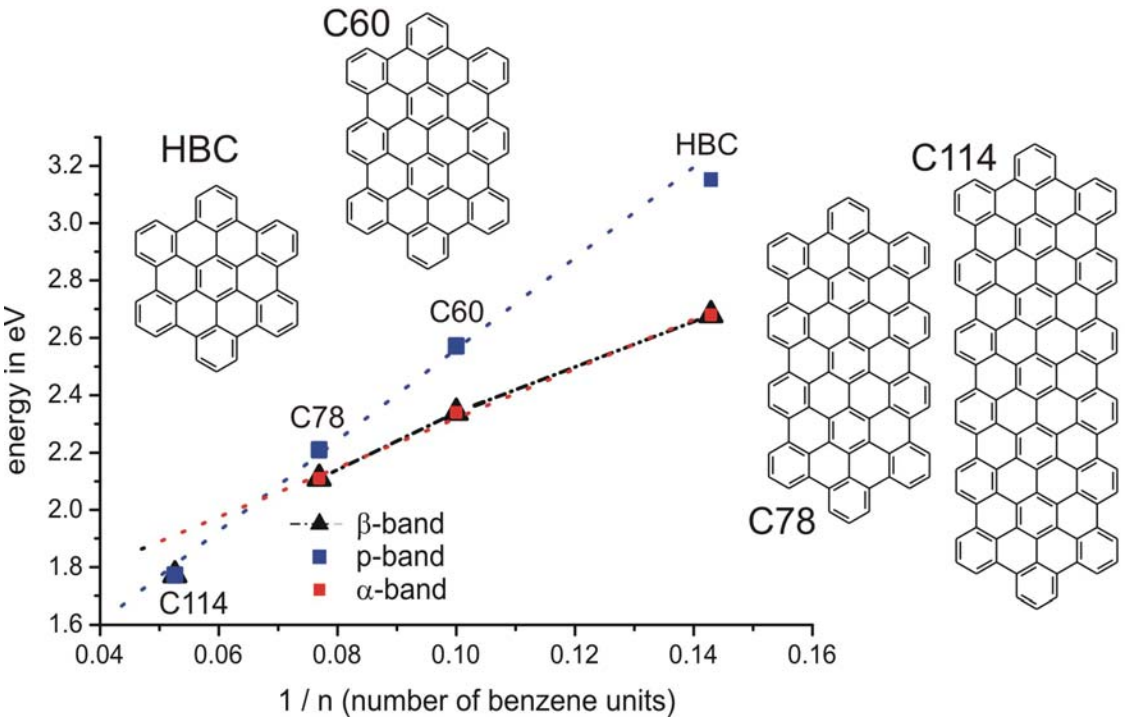

Figure 4-105: PPP- Self concistent field calculations (PM3) of HBC, C60 C78 and C114 by M. Baumgarten.

Another indication for the above assumed labelling of the bands was provided by the calculations for the PAH series shown in Figure 4-105, which has been carried out by M. Baumgarten. In this series, the continuous enlargement of the HBC to the C114 aromatic core and the additional symmetry reduction led to a switching of the α- and the p-band, indicating the same behavior for large PAHs as for the acene series. For the smaller three examples, namely from the HBC to the C78, the α-bands remained energetically lower than the p-bands but at the size of the C114 the α- and the p-bands were exchanged. When one compares the C72-$(C_{12})_4$-$(C_{14,10})_4$-(*t*-Bu)$_2$ (**4-119**) with the presented PAH series, two facts become apparent. On one hand, the C72-$(C_{12})_4$-$(C_{14,10})_4$-(*t*-Bu)$_2$ (**4-119**) exhibits the same symmetry as the C60, C78 and C114 and second possesses only six aromatic carbon atoms less than C78. Although, it has to be noted that according to the plots in Figure 4-105, the exchange of the α- and the p-bands occurs in the series approximately at a core size of 90 aromatic carbon atoms, the theoretically determined values cannot be considered as irrevocable. Indeed, by comparing the UV/vis spectra of C72-$(C_{12})_4$-$(C_{14,10})_4$-(*t*-Bu)$_2$ (**4-119**) and the C60 molecules synthesized by C. Simpson, a substantial bathochromic shift for the C72 example is found, indicating the different electronic situation.

4.8 Solution Properties of C72-$(C_{12})_8$-(t-Bu)$_2$ and C72-$(C_{12})_4$-$(C_{14,10})_4$-(t-Bu)$_2$

For device fabrication, it is a prerequisite to align the active component between the electrodes in such a way that the charge carriers can migrate effectively. This requires to establish distinct columnar pathways over large domains, which is directly correlated to the future device performance. For zone casting (Appendix B) for example, it is necessary to deposit preaggregated species onto the substrate. On the other hand, materials with an improved solubility also exhibit lower isotropization temperatures and can therefore be easier processed thermally *via* zone crystallization (Appendix C) from the melt. Therefore, the solution behavior of a discotic compound is a good indication for the further treatment of the material and yields some indications about the general aggregation propensity of the materials.[104]

4.8.1 C72-$(C_{12})_8$-(*t*-Bu)$_2$

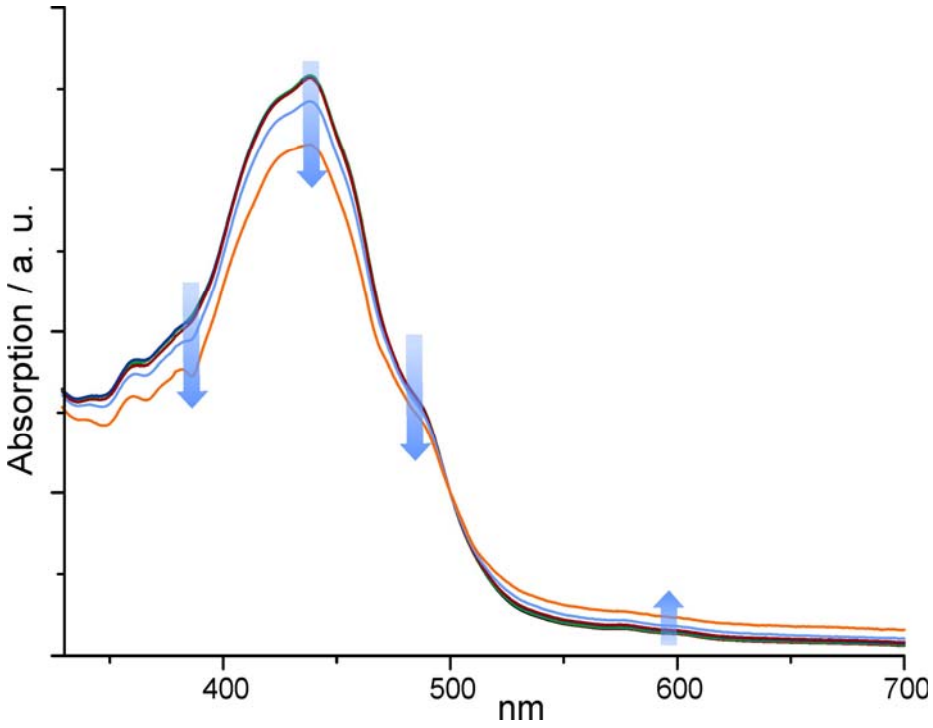

Figure 4-106: Concentration dependent UV/vis spectra of C72-$(C_{12})_8$-(*t*-Bu)$_2$ (**4-116**) in THF at room temperature (normalized to the value at 500nm).

To gain a first insight into the self-association behavior of C72-$(C_{12}H_{25})_8$-(*t*-Bu)$_2$ (**4-116**) concentration dependent UV/vis was recorded (Figure 4-106). Only small differences were observed between the concentrations of 2.6×10^{-5} and 1.0×10^{-6} mol l^{-1}. After a normalization at the absorption value at 500 nm some differences became better visible, as the suggested β-bands showed a reduction of their extinction values, while the bands at the longer wavelengths exhibited a small increase with decreasing concentration. These minor changes have already been observed for HBCs and already in those examples, it seemed that the absorption spectra were not very sensitive towards the aggregation of the discs in solution.

However, it is also known from HBC derivatives that in the same concentration range the photoluminescence emission and the photoluminescence excitation spectra revealed a far more pronounced effect. Compared to the absorption, the photoluminescence is far more susceptible to changes in the concentration, as the emission of a PAH can be strongly quenched by aggregation effects.

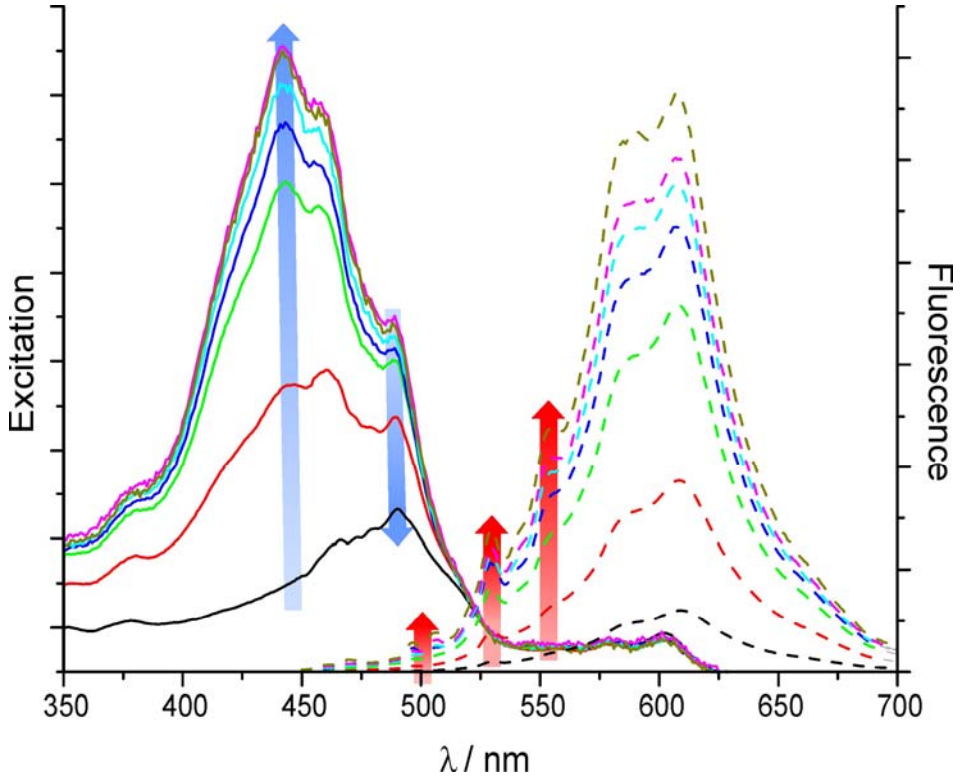

Figure 4-107: Concentration dependent photoluminescence excitation and photoluminescence spectra of C72-$(C_{12})_8$-(*t*-Bu)$_2$ (**4-116**) in THF at room temperature (normalized to the respective concentration).

In Figure 4-107 the spectra were all corrected regarding their respective concentration. It becomes obvious that not only the intensity of the spectra changed, but also several bands were highly dependent upon the concentration changes. For the photoluminescence excitation for example, the band at 441 nm was almost not visible at larger concentrations, but slowly evolved by diluting the solution. The band at 489 nm on the other hand did not change that severely, but at higher concentrations even became the band with the highest intensity. The photoluminescence emission spectra did not exhibit similar dependencies for individual bands. Moreover, the spectra were more or less changing *en bloc* and the intensity became stronger at lower concentrations. However, small deviations became obvious, as for example the bands in the range of 500-560 nm appeared.

Therefore, the photoluminescence was normalized to the main peak to gain a further insight on the evolution of single bands (Figure 4-108). Indeed, it could be shown that not only the before mentioned range changed more strongly according to the concentration but also the band at 588 nm was evolving above average.

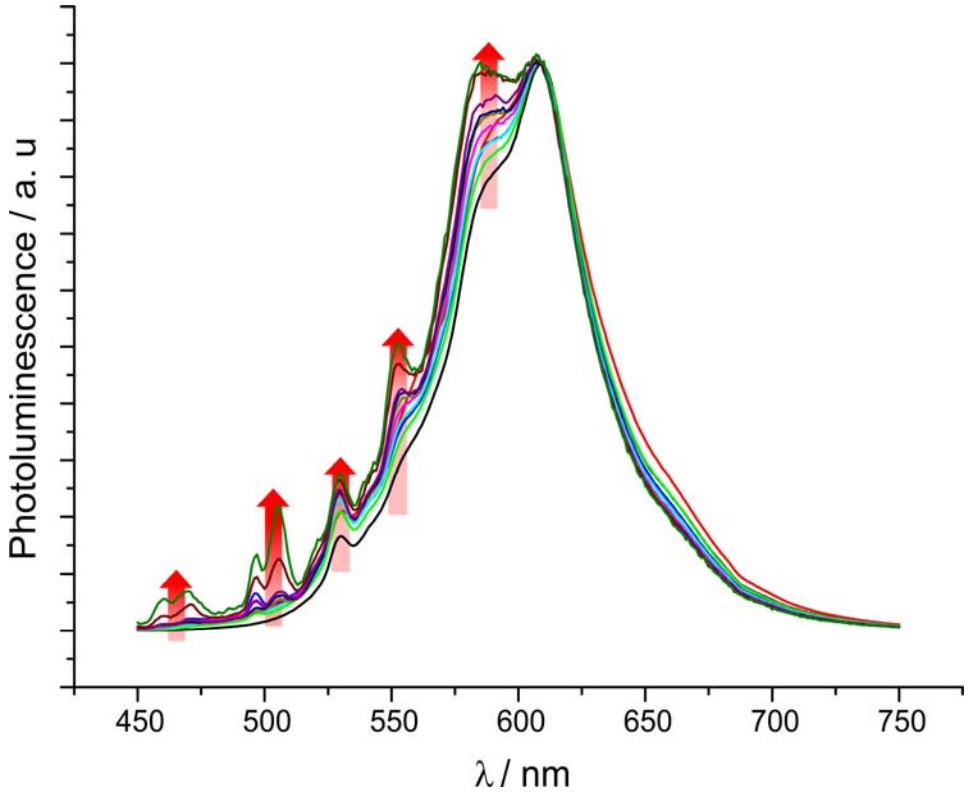

Figure 4-108: Concentration dependent photoluminescence spectra of C72-$(C_{12})_8$-(*t*-Bu)$_2$ (**4-116**) (normalized to the main band).

For an even better visualization of the respective changes in intensities of the single bands, their respective values have been depicted in Figure 4-109 for the photoluminescence excitation and in Figure 4-110 for the emission spectra with respect to the concentration. In the cases of soluble HBC derivatives, it has been observed that the relative intensities plotted according to Figure 4-109 or Figure 4-110 approach a plateau,[91] which exhibited the presence of the monomeric species. At these concentrations it was found that mainly monomers were present in the solution and the intensities did not further change by lowering the concentration. In addition, the respective concentrations, where the plateau was reached, was a direct indication of the solubility character of the examined species. Before reaching this plateau however, a linear increase in intensity occurred. For the well soluble HBC cases, which of course did not exhibit such strong π-interactions as C72, due to the smaller aromatic core component, the plateau was reached usually at around 10^{-4}-10^{-5} mol l^{-1}.

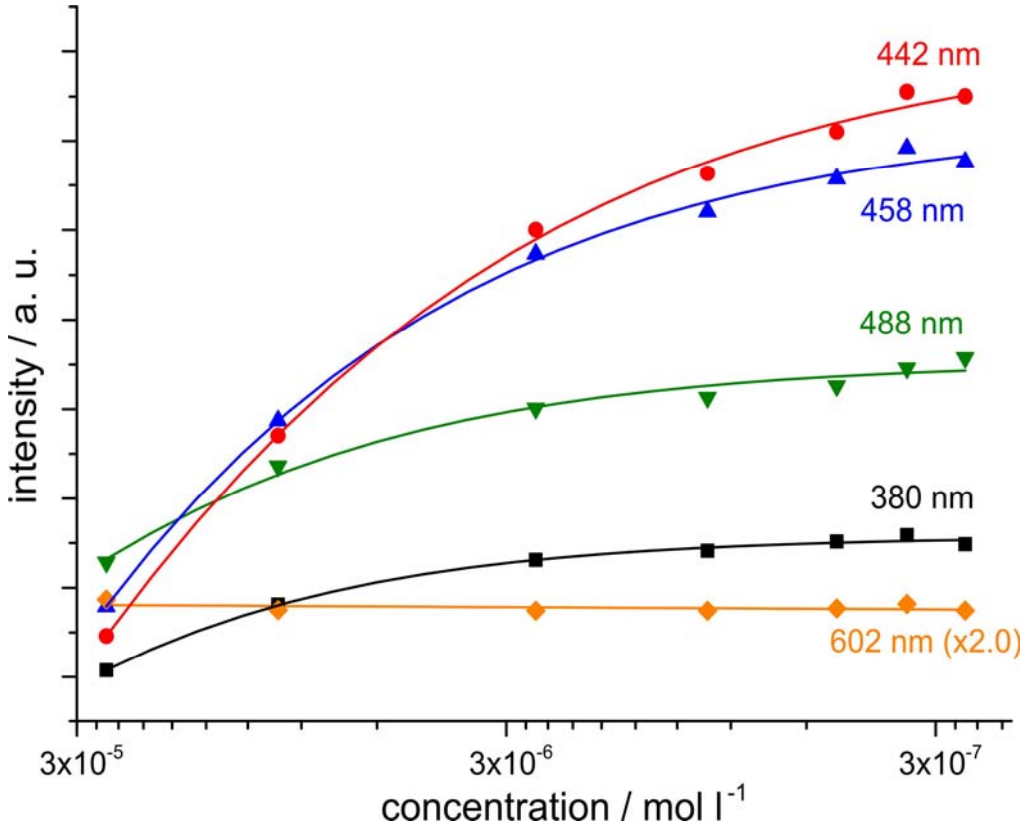

Figure 4-109: Band intensities of the photoluminescence excitation spectra of C72-$(C_{12})_8$-(*t*-Bu)$_2$ (**4-116**) in THF at room temperature.

One remarkable difference between the published HBC examples and the C72-$(C_{12})_8$-(*t*-Bu)$_2$ (**4-116**) is that the values of the intensities could not reach a plateau even at a concentration of 10^{-7} mol l^{-1}. Already the less soluble HBC derivative substituted with *n*-dodecyl chains (**4-28**) reached the plateau at a concentration of 5 x 10^{-5} mol l^{-1}. This indicated that the residual aggregation of C72-$(C_{12})_8$-(*t*-Bu)$_2$ (**4-116**) exceeds the one of the before mentioned HBC derivative at least by a factor of 100. This means that the aggregation propensity for C72-$(C_{12})_8$-(*t*-Bu)$_2$ (**4-116**) does not seem to be linearly correlated with the area of the aromatic core component. If this would be the case only a two times stronger aggregation effect, due to the two times larger aromatic core size, can be expected and the plateau should already be reached at a concentration of 10^{-6} mol l^{-1}. This result pointed out that the aggregation propensity of extended PAHs have possibly been underestimated and cannot be extrapolated from the values received by smaller PAHs. In contrast, the intensity of the band at 602 nm was not concentration dependent. This band is therefore directly related with the electronic properties of the molecule and is not influenced by differing aggregate sizes.

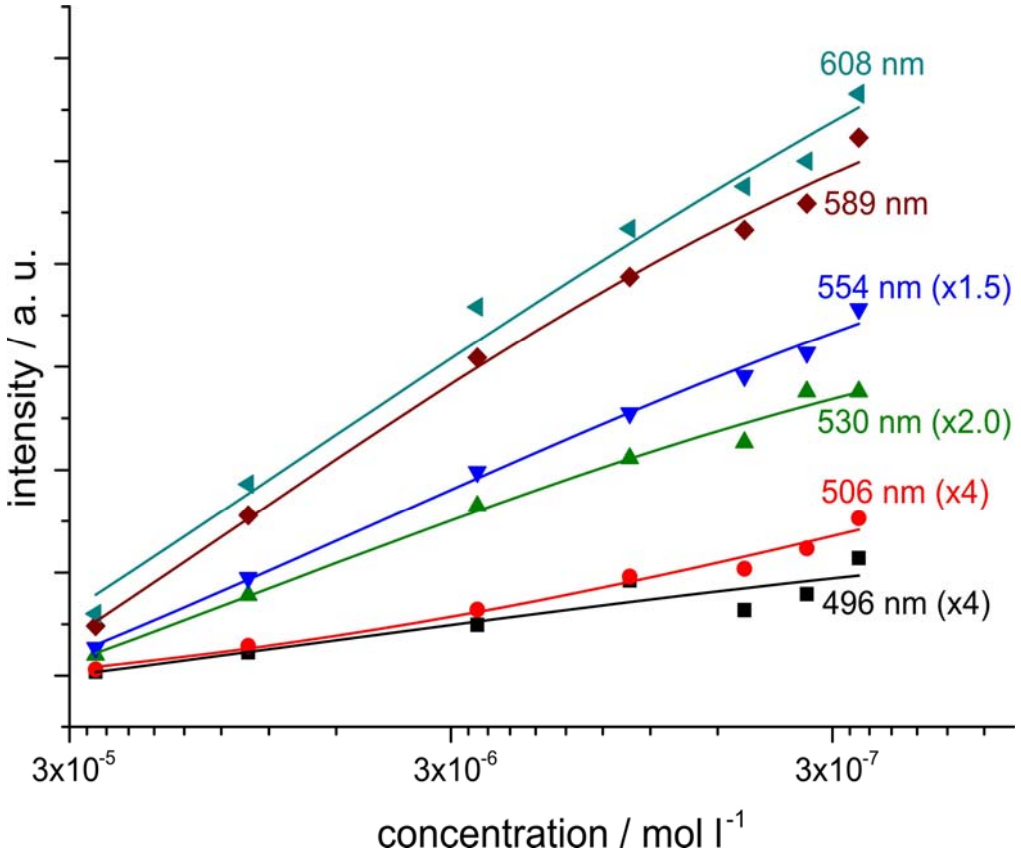

Figure 4-110: Band intensities of the photoluminescence emission spectra of C72-$(C_{12})_8$-(*t*-Bu)$_2$ (**4-116**) in THF at room temperature.

In Figure 4-110 the same graphs were plotted for the bands in the photoluminescence emission spectrum with respect to the concentration. All bands with small intensities over the observed range were multiplied with appropriate values, so that their concentration dependence could be plotted in a similar fashion as the others. For the emission intensities not even a deviation towards a plateau was observed. All bands showed in the investigated concentration range a linear increase of the intensity with decreasing concentration. In the HBC examples such linear dependencies were only found at higher concentrations, where the stacking sizes were still rather large. It can be concluded that the values extracted from the concentration dependent emission spectra depict an even stronger aggregation propensity of C72-$(C_{12})_8$-(*t*-Bu)$_2$ (**4-116**) than the plots of the excitation values. Therefore, it is not surprising that for a successful ^{1}H NMR measurement, which probably requires a sufficient amount of monomers in solution, CS_2 had to be added to sufficiently suppress the aggregation and to reveal the aromatic proton signals.

4.8.2 C72-$(C_{12})_4$-$(C_{14,10})_4$-(*t*-Bu)$_2$

In contrast to compound C72-$(C_{12})_8$-(*t*-Bu)$_2$ (**4-116**), where a change in the extinction coefficients of the particular bands was observed depending upon the respective concentration, no such clear deviations were found for C72-$(C_{12})_4$-$(C_{14,10})_4$-(*t*-Bu)$_2$ (**4-119**). This pointed towards a reduced influence of the aggregation upon the absorption values of the material. Nevertheless, photoluminescenc excitation and emission analytics were again far more susceptible to the aggregation effects.

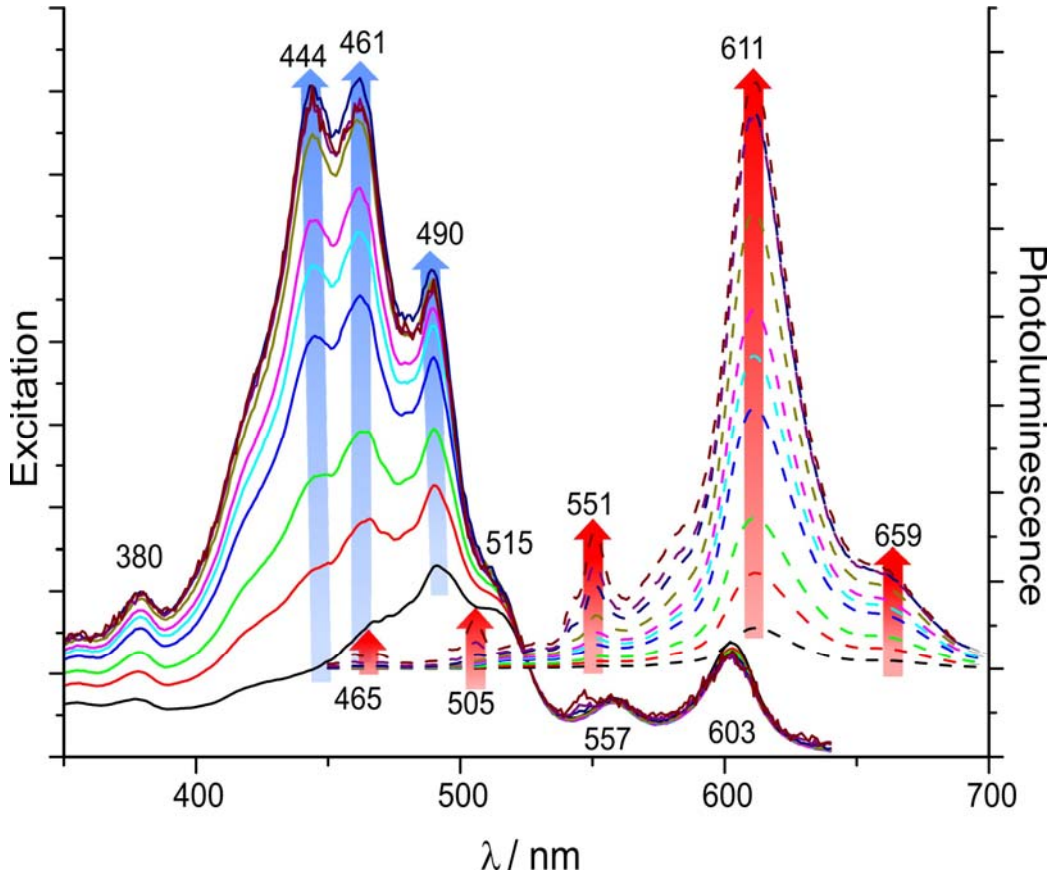

Figure 4-111: Concentration dependent photoluminescence excitation and photoluminescence spectra of C72-$(C_{12})_4$-$(C_{14,10})_4$-(*t*-Bu)$_2$ (**4-119**) in THF at room temperature (normalized to the respective concentration).

In the excitation spectra, a similar arrangement of the bands was found as for C72-$(C_{12})_8$-(*t*-Bu)$_2$ (**4-116**). In this case however, the possible reduction of the aggregation propensity due to the additional sterically demanding 2-decyl-tetradecyl side-chains led to a far better resolved spectrum. In the concentration dependent series, it was determined that for the excitation spectra the bands at 557 and 603 nm are not susceptible to any aggregation effect. The rest of the bands at smaller wavelengths

exhibited not only a simple change of the intensities, but also several signals were strongly dependent on the concentration, corresponding to the observations for C72-$(C_{12})_8$-(*t*-Bu)$_2$ (**4-116**). For example the bands at 444 nm and 461 nm even disappeared at higher concentrations, similar to the band at 441 nm in the spectra shown in Figure 4-107 for C72-$(C_{12})_8$-(*t*-Bu)$_2$ (**4-116**). The residual band at 490 nm did not change as severely as the ones at 444 and 461 nm.

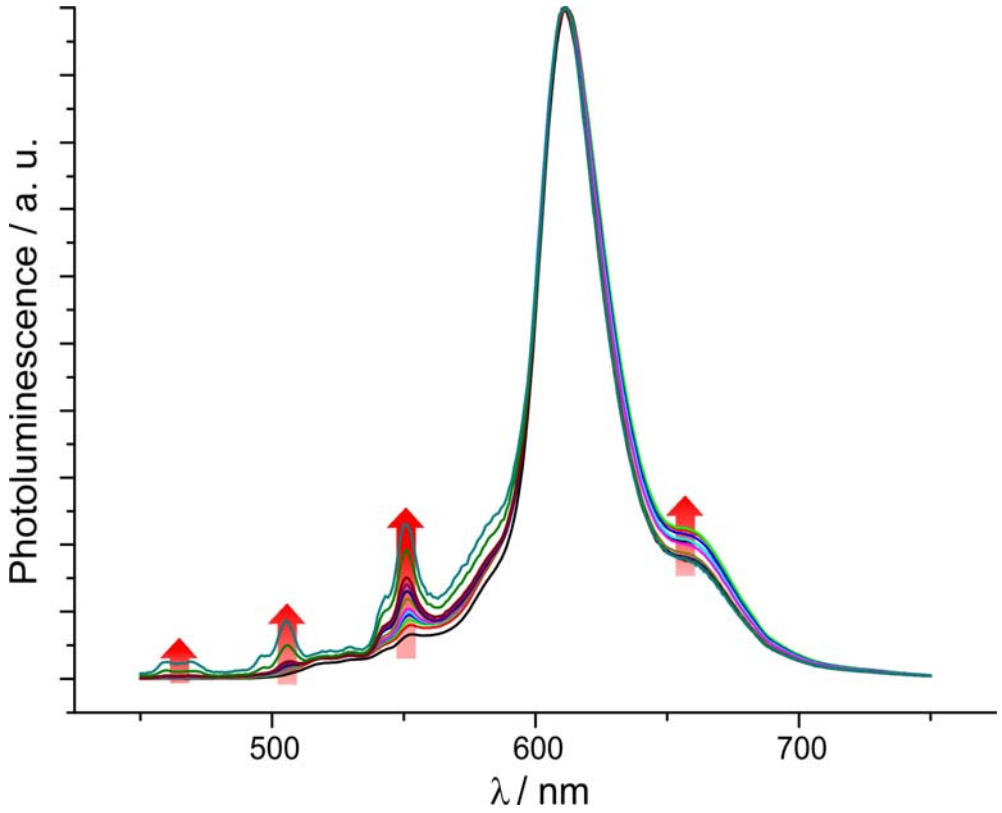

Figure 4-112: Concentration dependent photoluminescence spectra C72-$(C_{12})_4$-$(C_{14,10})_4$-(*t*-Bu)$_2$ (**4-119**) (normalized to the main band).

For the emission spectra, the main band at 611 nm is expected to be the S1→ S0 transition and all bands changed sensitively with respect to the concentration, whereby at lower concentrations additional bands evolved (Figure 4-112). These bands, which are situated at shorter wavelengths than the main band for the S1→S0 transition at 611 nm, are presumably thermal bands and originate directly from the electronic properties of the single molecules. This also indicates that the thermal bands are suppressed, while the molecules are members of a stacked arrangement.

The differences in concentration dependence between the bands became even clearer by applying the same plots for the main intensities in the photoluminescence excitation and emission as previously for C72-$(C_{12})_8$-(*t*-Bu)$_2$ (**4-116**).

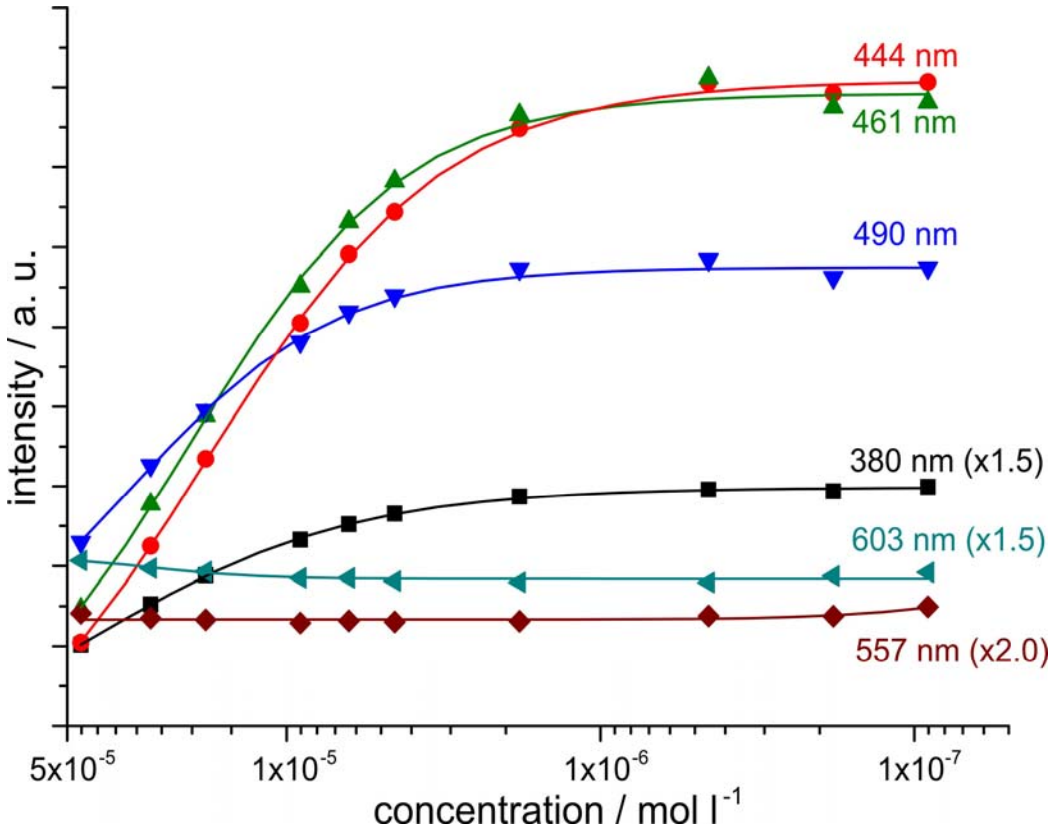

Figure 4-113: Band intensities of the photoluminescence excitation spectra of C72-$(C_{12})_8$-$(C_{14,10})_4$-(*t*-Bu)$_2$ (**4-119**) in THF at room temperature.

In Figure 4-113 the respective maximum intensities of the bands of C72-$(C_{12})_4$-$(C_{14,10})_4$-(*t*-Bu)$_2$ (**4-119**) in the photoluminescence excitation spectra are plotted. In contrast to C72-$(C_{12})_8$-(*t*-Bu)$_2$ (**4-116**), a clear plateau became visible. This means that at a concentration of approximately 10^{-6} mol l^{-1} mainly monomers are present in the solution. As the before mentioned HBC derivative (**4-28**), which exhibits a limited solubility in standard organic solvents, reaches its plateau at 5 x 10-5 mol l-1, it can be assumed that the aggregation propensity of C72-$(C_{12})_4$-$(C_{14,10})_4$-(*t*-Bu)$_2$ (**4-119**) is still stronger by approximately a factor of 10. This clearly indicates that even after applying a whole series of solubilizing features, like the distortion of the aromatic core, the presence of two bulky substituents and the substitution with four bulky, branched alkyl chains, the tendency for aggregation seems to be still stronger than for the hexaalkylated HBC derivative (**4-28**).

Similar to the band at 602 nm for the C72-$(C_{12})_8$-(*t*-Bu)$_2$ (**4-116**), also for C72-$(C_{12})_4$-$(C_{14,10})_4$-(*t*-Bu)$_2$ (**4-119**) two bands occurred at 557 nm and 603 nm, which did not change their relative intensities, meaning that these are also originating from the molecule properties themselves and were not susceptible to a stacking phenomenon.

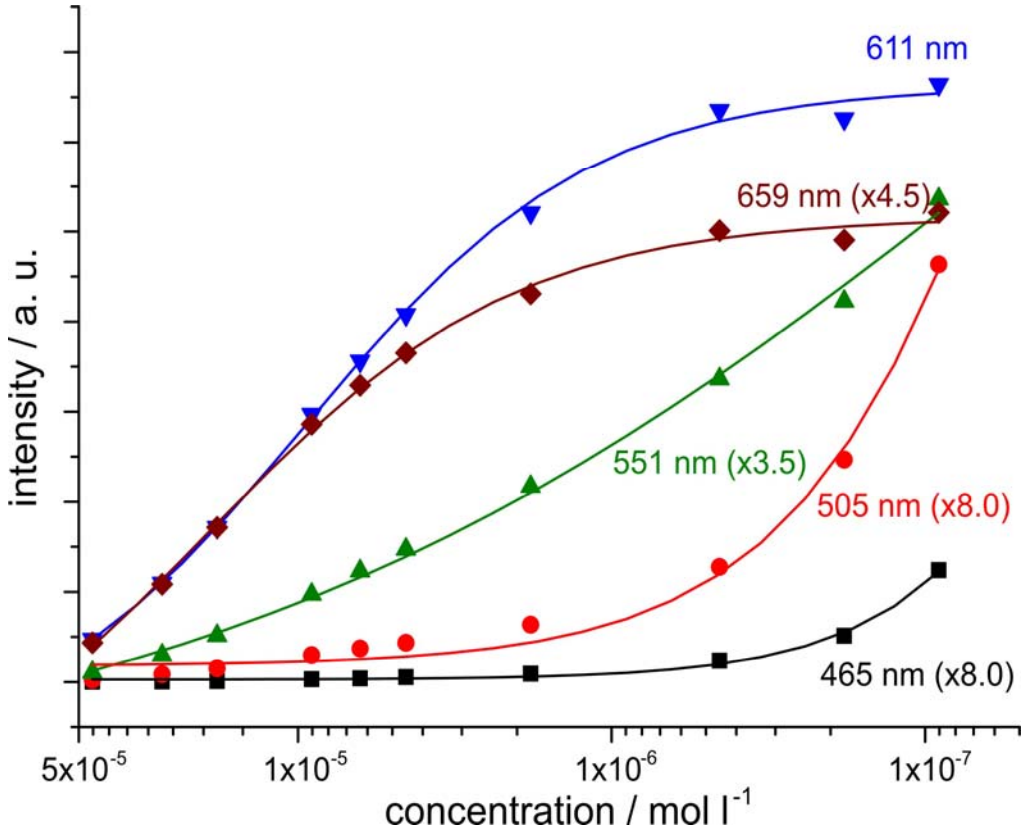

Figure 4-114: Band intensities of the photoluminescence emission spectra of C72-$(C_{12})_8$-$(C_{14,10})_4$-(*t*-Bu)$_2$ (**4-119**) in THF at room temperature.

In Figure 4-114 the same plotting was performed as in Figure 4-113, but this time for the intensities of the emission bands, whereby two features became apparent. While the bands originating from transitions with lower energy, which includes the S1→ S0 transition (611 nm) and the band at 659 nm, are consistent with the concentration dependent plots in the excitation (Figure 4-113), the bands previously identified as thermal bands show a mirror like behavior. Instead of slowly approaching a plateau, they show an exponential increase towards lower concentrations, which supports the assumption that they originate from the single molecule. Indeed, the exponential increase starts exactly at the same concentration, where the other two bands at longer wavelengths are slowly evolving towards the plateau.

Conclusively, it can be said that the substitution of four *n*-dodecyl chains with the sterically demanding tetradecyl-decyl chains, which have already shown their solubilizing effects in combination with their efficient suppression of aggregation, resulted in a material with extraordinary solubility properties. While for the C72-$(C_{12})_8$-(*t*-Bu)$_2$ (**4-116**) not even a plateau could be reached until the detection limits of the spectrometer, C72-$(C_{12})_4$-$(C_{14,10})_4$-(*t*-Bu)$_2$ (**4-119**) showed an astonishingly improved solubility.

According to the concentration dependent NMR spectra shown in Figure 4-92 it was assumed that an exchange of the solvent from THF to CS_2 should yield a concentration independent photoluminescence response.

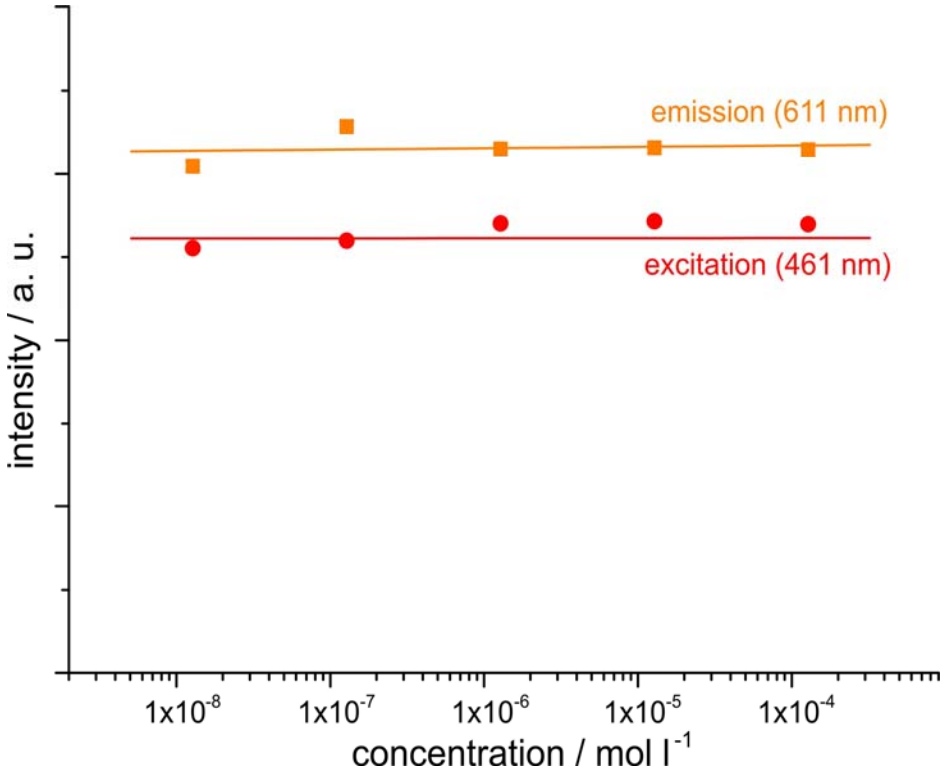

Figure 4-115: Band intensities of the photoluminescence excitation and emission spectra of C72-$(C_{12})_8$-$(C_{14,10})_4$-(*t*-Bu)$_2$ (**4-119**) in CS_2 at room temperature.

The results obtained by the concentration dependent ^{1}H NMR spectra were confirmed by the electronic spectra. In all concentrations, the relative observed intensities did not change with concentration, indicating the additional strong aggregation suppression initiated by the CS_2. These differences in the concentration dependent photoluminescence spectra, according to different solvents, also indicated, why no resolved aromatic signals were seen in the ^{1}H NMR spectra for deuterated THF. The required monomer concentration of C72-$(C_{12})_4$-$(C_{14,10})_4$-(*t*-Bu)$_2$ (**4-119**) for THF is

below 10^{-6} mol l^{-1}, which is a very low concentration to record NMR data. Therefore, CS_2 in combination with CD_2Cl_2 had to be chosen to reach the monomer concentration at values, which are still appropriate for the NMR technique. Therefore, it can be assumed that a resolved NMR spectrum of a C72 derivative can only be recorded, when at least a sufficient amount of the molecules is present in the monomeric state.

4.9 Bulk Properties

C72-$(C_{12})_8$-(*t*-Bu)$_2$ (**4-116**) did not show a thermal phase transition in the DSC until degradation of the material, which was already indicated from the observed distinct aggregation in solution. It was furthermore not possible to gain a well aligned sample by extrusion due to the crystallinity of the compound. In the 2D WAXS only broad and diffuse reflexes were found. This is not necessarily the result of a severe suppression of the π-mediated self-assembly in the bulk, but can also originate from the still too strong π-interactions during the extrusion processs, inhibiting the proper alignment of the sample. In contrast, C72-$(C_{12})_4$-$(C_{14,10})_4$-(*t*-Bu)$_2$ (**4-119**) revealed interesting properties in the bulk, which are presented in the following.

4.9.1 DSC

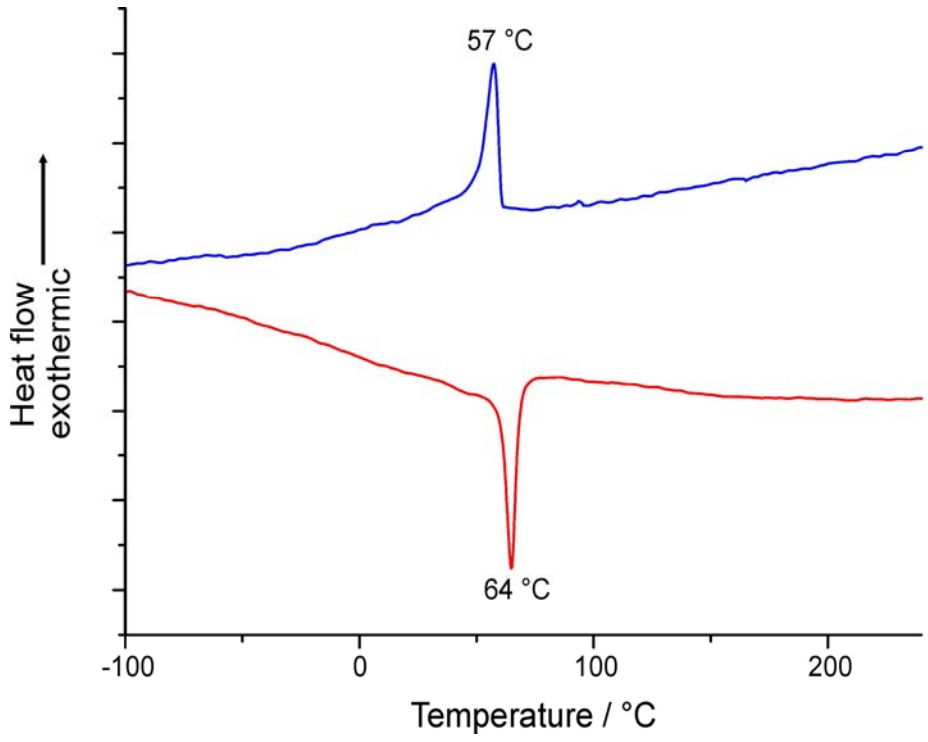

Figure 4-116: DSC traces of C72-$(C_{12})_4$-$(C_{14,10})_4$-(*t*-Bu)$_2$ (**4-119**). **red**) heating, **blue**) cooling.

This started with a distinct endothermic signal during heating and a corresponding exothermic signal during cooling in the DSC at around 60 °C (Figure 4-116) for C72-$(C_{12})_4$-$(C_{14,10})_4$-(*t*-Bu)$_2$ (**4-119**). This feature however could not be accounted to a phase transition correlated with the aromatic core component as neither in the subsequent POM a change in the optical birefringence nor different diffractograms in the 2D-WAXS were determined. This leads to the conclusion that the appearance of this thermal property was presumably correlated with some rearrangement of the alkyl substituents.

4.9.2 2D-WAXS

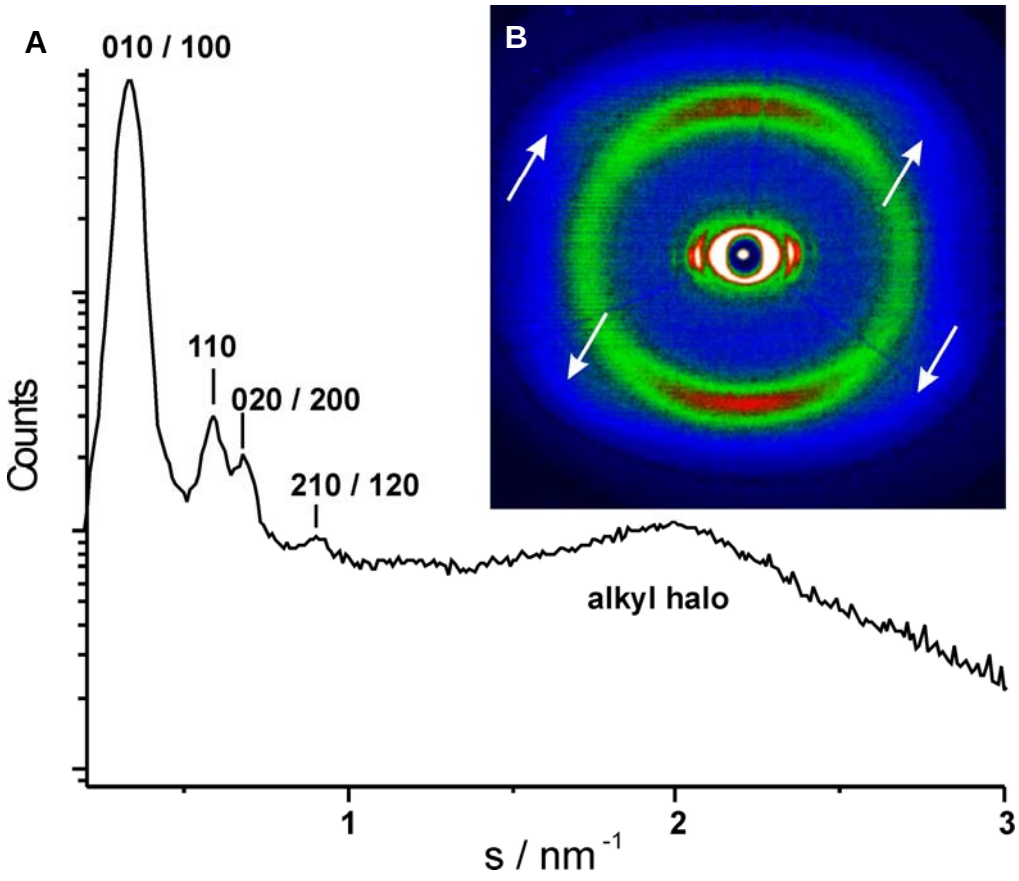

Figure 4-117: 2D-WAXS of C72-$(C_{12})_4$-$(C_{14,10})_4$-(*t*-Bu)$_2$ (**4-119**). **A**) 2D-WAXS and **B**) equatorial slice plot.

In a fiber of C72-$(C_{12})_4$-$(C_{14,10})_4$-(*t*-Bu)$_2$ (**4-119**), which has been extruded according to the same principle as shown in the introduction, the discs self-organized in columnar structures along the extrusion direction (Figure 4-117). From the equatorial reflections in Figure 4-117B an intercolumnar hexagonal unit cell could be assigned with a = 3.3 nm as the packing parameter, which fits the calculated dimensions by taking into account an interdigitation of the alkyl chains (Figure 4-119B). The meridional reflections combined

with the weak offset signals (Figure 4-117B, arrows) implied that the discs adopted a tilted arrangement with respect to the columnar axis. Although the effective suppression of the π-stacking was expected to lead to a strong reduction of the supramolecular organization of the material in the bulk, C72-$(C_{12})_4$-$(C_{14,10})_4$-(*t*-Bu)$_2$ (**4-119**) featured a high degree of order in the 2D-WAXS experiment. This indicated that the remaining π-interaction was sufficient for the self-assembly into the already known columnar superstructures.

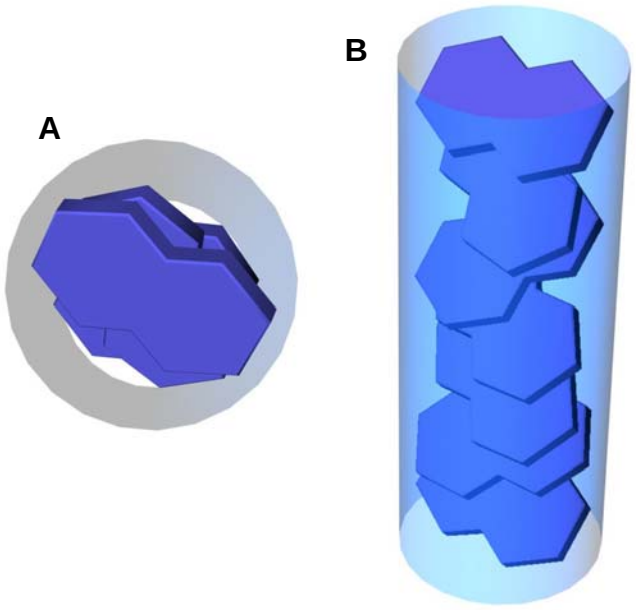

Figure 4-118: Schematic representation of the columnar self-assembly of C72-$(C_{12})_4$-$(C_{14,10})_4$-(*t*-Bu)$_2$ (**4-119**) and the resulting round structure of a column. **A**) top and **B**) side view.

The found hexagonal arrangement is nevertheless contradictory to the symmetry of the molecule. As shown in Figure 4-101 the molecular symmetry of the molecule is C_{2h} for the trans and C_{2v} for the cis case. Generally, the symmetry of the molecule is inherited by the crystal packing or the supramolecular self-assembly. This behavior is explained by the intermolecular arrangement induced by the bulky *tert*-butyl groups. Thereby, the molecules self-assembled with an offset angle between the discs to gain a larger π-contact area, which resulted in a round columnar structure (Figure 4-118A/B). After this intracolumnar arrangement was adopted, there was no further hindrance for the columnar self-organisation into the observed hexagonal arrangement as presented in Figure 4-119A.

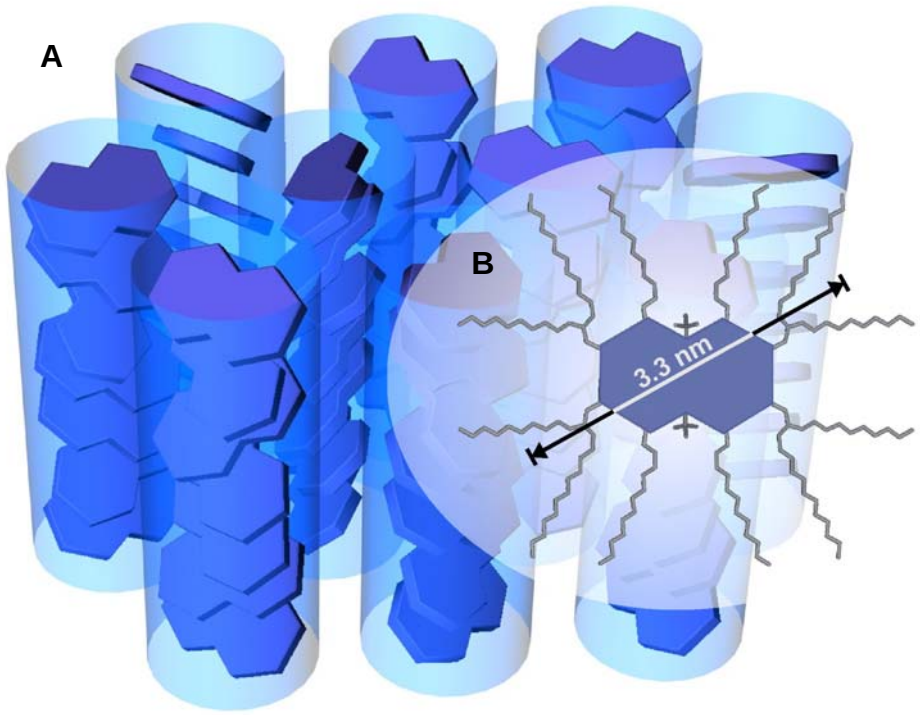

Figure 4-119: A) Hexagonal columnar arrangement of C72-$(C_{12})_4$-$(C_{14,10})_4$-(*t*-Bu)$_2$ (**4-119**) in the bulk (alkyl chains are ommitted for clarity); **B**) calculated dimensions of C72-$(C_{12})_4$-$(C_{14,10})_4$-(*t*-Bu)$_2$ (**4-119**) with respect to hexagonal packing parameter (a = 3.3 nm).

The high transition temperature to the isotropic melt determined in the POM confirms the significant degree of intracolumnar π-stacking, which is favorable for the columnar order in the bulk.

4.9.3 Polarized Optical Microscopy

Polarized optical microscopy (POM) allowed to apply high heating rates to suppress thermal decomposition of the material, which was not that accurately possible with DSC, and was used to investigate the crystallization behavior from the isotropic phase. Compound C72-$(C_{12})_4$-$(C_{14,10})_4$-(*t*-Bu)$_2$ (**4-119**) was sandwiched between two glass slides and heated under nitrogen flow at maximum heating rate. After reaching the isotropic phase at roughly 430 °C, the sample was immediately cooled down. At approximately 370 °C a dendritic texture appeared, which did not reveal birefringence in polarized light, except for some defects. This indicated a homeotropic order (Figure 4-120A/B), which is the favored orientation on substrates for photovoltaic applications.

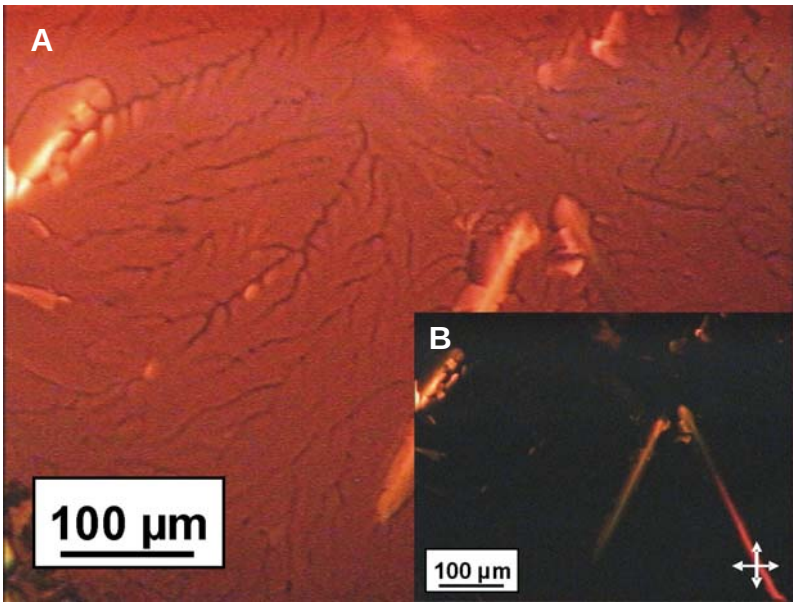

Figure 4-120: A) Optical microsopy image of C72-$(C_{12})_4$-$(C_{14,10})_4$-(*t*-Bu)$_2$ (**4-119**) at 370 °C **B**) image with applied cross-polarizers at 370°C.

In contrast to the other C72 derivatives, C72-$(C_{12})_4$-$(C_{14,10})_4$-(*t*-Bu)$_2$ (**4-119**) is the first derivative, which exhibited a thermal phase behavior similar to HBCs. It has to be pointed out that the observed transition temperatures between the phases occurrred at fairly high temperatures, indicating that the π-mediated aggregation propensity in the solid state was still rather distinct. These observations were supported by the aggregation studies in solution presented before. It has been shown that for example the HBC derivative decorated with six linear dodecyl alkyl chains (**4-28**) exhibited a less pronounced aggregation behavior and even for this material the transition to the mesophase was determined at 107 °C and the isotropic phase was reached above 430 °C. Therefore, it is not surprising that due to the far stronger aggregation propensity for C72-$(C_{12})_4$-$(C_{14,10})_4$-(*t*-Bu)$_2$ (**4-119**), the changes in thermal phases started to appear at 370 °C and above.

4.10 Removing the tert-Butyl Groups

Although the *tert*-butyl groups seemed to be an efficient way to inhibit the aggregation process of the materials, inducing a high degree of solubility and processability, their presence could reduce the charge-carrier mobilities of the compounds. On the other hand, this was an option to reveal the nature of truly planar PAHs larger than HBCs, as with this approach no disturbing intermediates are expected to be formed due to the suppressed formation of side-products.

If the final compound still shows a minimum of solubility and processability, the previous approach *via* the dendritic oligophenylene precursors has to be reconsidered. Although the novel pathway incorporated several advantages, its main problem is the preparation of large amounts of material, required for materials science. This is mainly caused by the thermally unstable compound **4-113**, which results in low yields for the Diels-Alder step. In addition, the subsequent separation by column chromatography of the oligophenylene precursor molecule **4-115** or **4-118** respectively, is tedious.

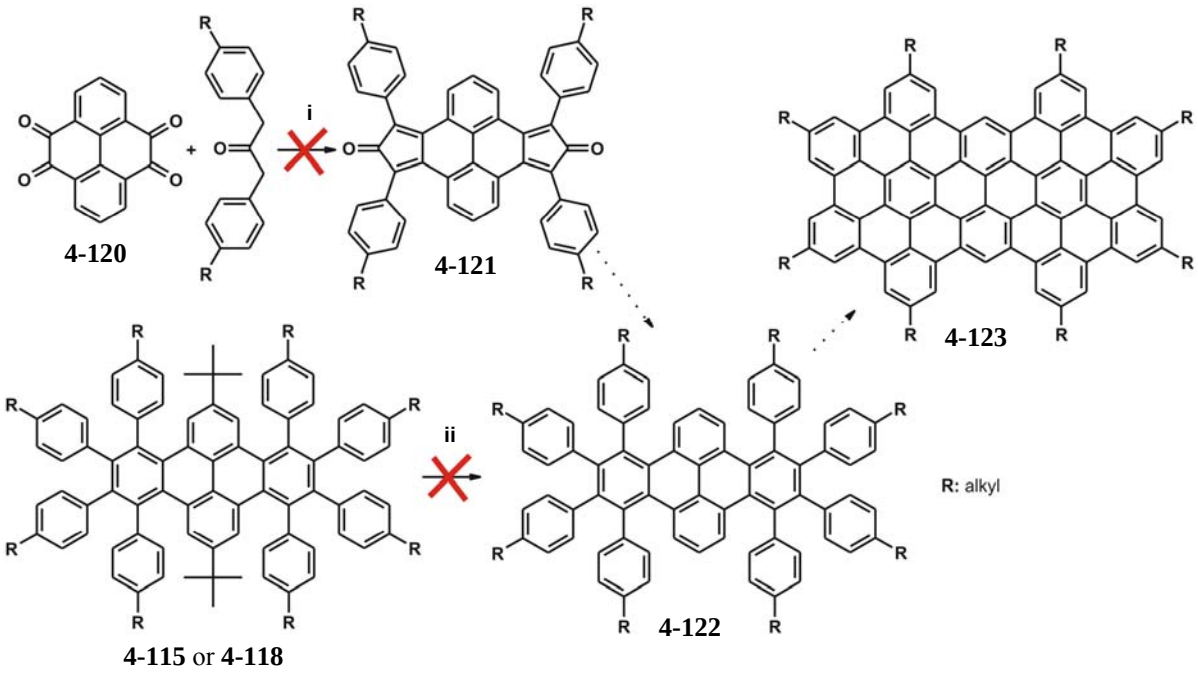

Figure 4-121: Examined synthetic routes towards the fully planarized C72 derivatives.

Therefore, several approaches were tested towards the non-distorted derivative, according to the novel concept of the preplanarization of the oligophenylene precursor. In Figure 4-121 two possibilities are shown. In the first example, it was tried to simply exchange the 2,7-di-*tert*-butyl-pyrene-4,5,9,10-tetraone (**4-111**) by its derivative without the *tert*-butyl entities **4-120**. Several conditions for the Knoevennagel condensation were examined, including different temperatures and base. However, it was not possible to achieve the compound **4-121** under any of the applied conditions and the reaction stopped after the presumed formation of intermediates. It seemed that for compound 2,7-di-*tert*-butyl-pyrene-4,5,9,10-tetraone (**4-111**) the *tert*-butyl groups had a severe influence upon the stabilisation and formation of the derivative **4-113** during the Knoevennagel condensation.

A similar observation was made for the cyclopentadienone derivatives presented in Figure 4-122.

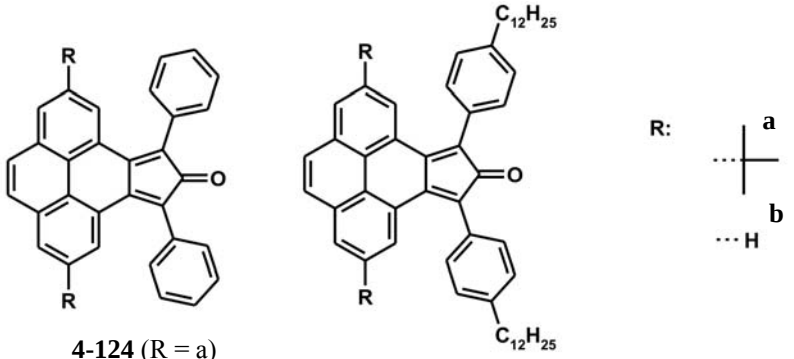

4-124 (R = a)

4-125 (R = b)

4-126 (R = a)

4-127 (R = b)

Figure 4-122: Cyclopentacienone derivatives.

In these examples, the presence of the *tert*-butyl groups proved to stabilize the cyclopentadienone product. The compounds **4-124** and **4-125** were prepared by a Knoevennagel condensation with the unsubstituted 1,3-diphenyl-propan-2-one. The derivative without the *tert*-butyl groups (**4-125**) could be synthesized, but was not stable at room temperature. The compound slowly decomposed after the synthesis and denied for example a time-consuming treatment by column chromatography, as during this workup process a large amount of the substance degraded on the column. The derivative with the *tert*-butyl groups (**4-124**) however could be synthesized and treated similar to other tetraphenylcyclopentadienone compounds such as **4-25** to **4-27**.

For the derivatives, which were prepared with the alkylated version of the 1,3-diphenyl-propan-2-one, the stabilizing property of the *tert*-butyl groups, which is also one of the most versatile protection groups,[105] became even clearer. While the protected compound **4-126** could be prepared under common conditions for the Knoevennagel condensation and did not show a propensity for degradation, not even an indication of product formation could be found for its unprotected counterpart (**4-127**). This pointed out the distinct stabilization and protection behavior of the *tert*-butyl groups and furthermore supported the observations made for the cyclopentadienone derivative (**4-121**) shown in Figure 4-121, as in this unprotected example not even traces of product could be found, too.

Therefore in the second example, the procedure included the removal of the *tert*-butyl group at the stage of the oligophenylene precursor (**4-115** or **4-118**) under Friedel-Crafts

conditions, circumventing the difficulties encountered in the previous approach for the Knoevennagel condensation. The reaction conditions consisted of benzene as solvent and some drops of oleum (65%). The reaction mixture was then heated in a sealed microwave tube to suppress a change in the concentration of the acid. Even after a prolonged reaction time of three days at 150 °C no reaction was observed and it was astonishing to note that neither the *tert*-butyl nor the alkyl groups showed any reactivity under these conditions.

4.10.1 Synthesis

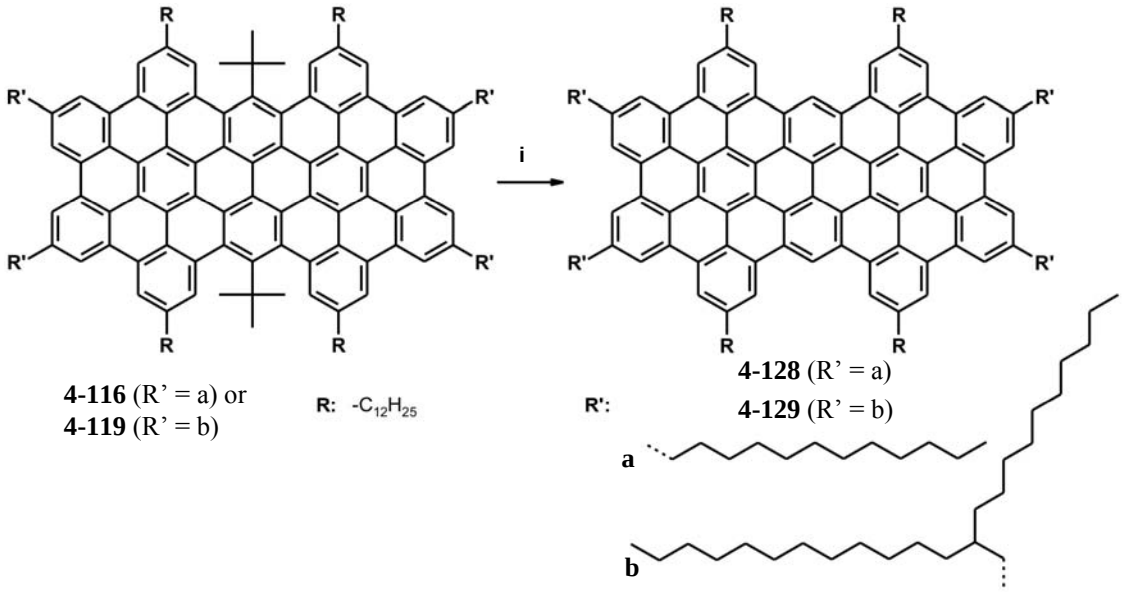

Figure 4-123: Preparation of the fully planarized C72 derivatives C72-$(C_{12})_{8p}$ (**4-128**) and C72-$(C_{12})_4$-$(C_{14,10})_{4p}$ (**4-129**).

As the before mentioned reaction conditions were possibly rather mild towards the removal of alkyl substituents the same procedure was repeated for the already planarized compounds C72-$(C_{12})_8$-(*t*-Bu)$_2$ (**4-116**) and C72-$(C_{12})_4$-$(C_{14,10})_4$-(*t*-Bu)$_2$ (**4-119**). After twelve hours the MALDI-TOF MS revealed that all *tert*-butyl groups had been removed and interestingly the alkyl side-chains showed again no reactivity under these conditions. For the cyclodehydrogenated compounds C72-$(C_{12})_8$-(*t*-Bu)$_2$ (**4-116**) and C72-$(C_{12})_4$-$(C_{14,10})_4$-(*t*-Bu)$_2$ (**4-119**) the relaxation of the twisted aromatic core into the planar product C72-$(C_{12})_{8p}$ (**4-128**) and C72-$(C_{12})_4$-$(C_{14,10})_{4p}$ (**4-129**) was a key driving force for the cleavage of the substituents. As shown in Figure 4-124 the theoretical calculations

(AM1) suggested a large gain in energy by the planarization of approximately 25 kcal/mol.

After the workup procedure, the received compounds C72-$(C_{12})_{8p}$ (**4-128**) and C72-$(C_{12})_4$-$(C_{14,10})_{4p}$ (**4-129**) were almost insoluble in common organic solvents. While C72-$(C_{12})_4$-$(C_{14,10})_{4p}$ (**4-129**) still exhibited sufficient solubility in hot THF for measuring for example reliable UV/vis spectra, no such spectra could be recorded for the compound C72-$(C_{12}H_{25})_{8p}$ (**4-128**). As the solubility of this compound was even too low for recording an UV/vis spectrum, other methods like photoluminescence were not applied. This clearly contradicts the observations made for the well soluble compounds C72-$(C_{12})_8$ (**4-44**) and C72-$(C_{8,2})_8$ (**4-45**), which were prepared *via* the old synthetic route.

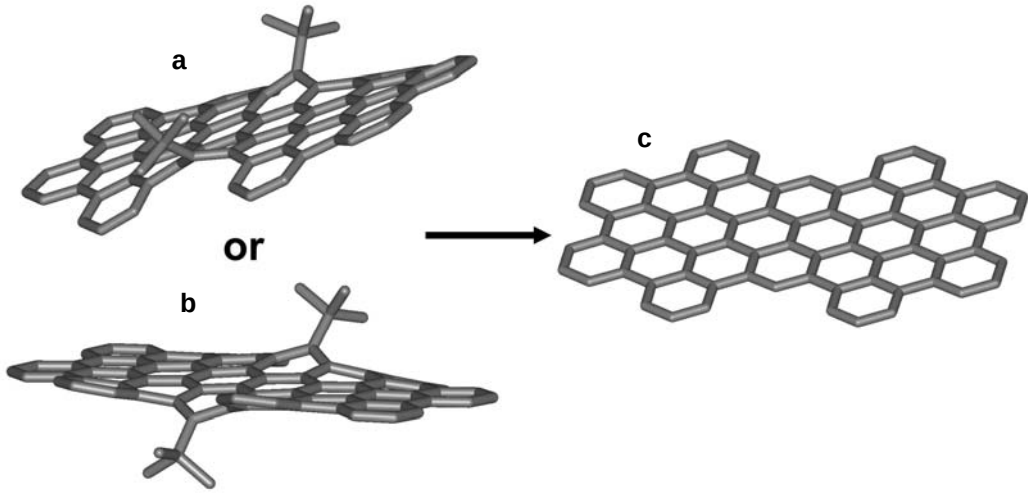

Figure 4-124: Semiempirical calculations of the energy gain by removal of the *tert*-butyl groups: **a**) cis: 330.17 kcal/mol; **b**) trans: 330.10 kcal/mol; **c**) planar: 305.71 kcal/mol.

This means that the pronounced difference in solubility, observed for the two identical compounds, originated from the partially fused intermediates, which strongly interfere with the π-mediated stacking process and induce the exhibited solubility. Therefore eight *n*-dodecyl chains for C72-$(C_{12})_8$ (**4-44**) are definitely insufficient for inducing solubility or processability for a PAH with such a large aromatic core unit. In addition, it can be assumed that this is also valid for even larger systems as C96 (**4-48**), where only six *n*-dodecyl chains are expected to solubilize an aromatic entity, which exhibits a three times larger size than HBC. This indicates that all the prepared C96 derivatives should show similar solubility properties as C72-$(C_{12})_{8p}$ (**4-128**) and leads to

the conclusion that the aggregation propensity for large aromatic cores have been severely underestimated until now.

4.10.2 MALDI-TOF MS

In the MALDI-TOF MS the isotope patterns of the measurement show a close similarity to the theoretical ones, which further indicated a higher purity. There were no indications of the presence of partially fused species.

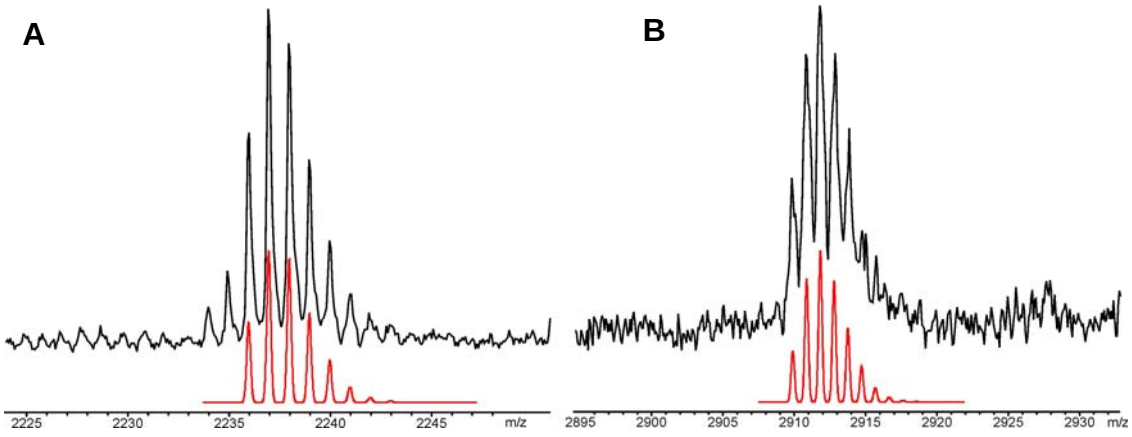

Figure 4-125: MALDI-TOF MS spectra of **A**) C72-$(C_{12})_{8p}$ (**4-128**) and **B**) C72-$(C_{12})_4$-$(C_{14,10})_{4p}$ (**4-129**) with TCNQ; red: simulated spectra.

An interesting fact was that even by using TCNQ as the matrix, which usually pronounces the presence of the fully planarized species, the signal to noise ratio remained rather high, meaning that the intensity of the signal was rather low. This could point towards the possibility that even the strong signals observed for the C72 derivatives, prepared according to the dendritic pathway, could simply have borrowed some intensity of the partially fused intermediates. Another explanation could be the less tight columnar stacking due to the interference with the partially fused intermediates, which resulted for example in the good solubility of C72-$(C_{12})_8$ (**4-44**). Due to this reduced stacking, the molecules could be more easily "evaporated" during the interaction with the laser light, inducing the observed high intensity of the peak of the fully planarized product.

In the ^{1}H NMR measurements of C72-$(C_{12})_4$-$(C_{14,10})_{4p}$ **(4-129)**, a similar spectrum was recorded as for the compounds achieved *via* the old route, which was due to the pronounced insolubility and the strong aggregation. Even though the branched alkyl

chains induce a high steric demand and effectively reduce the π-mediated stacking behavior, no NMR spectrum could be gained from this species.

4.10.3 Electronic Spectroscopy

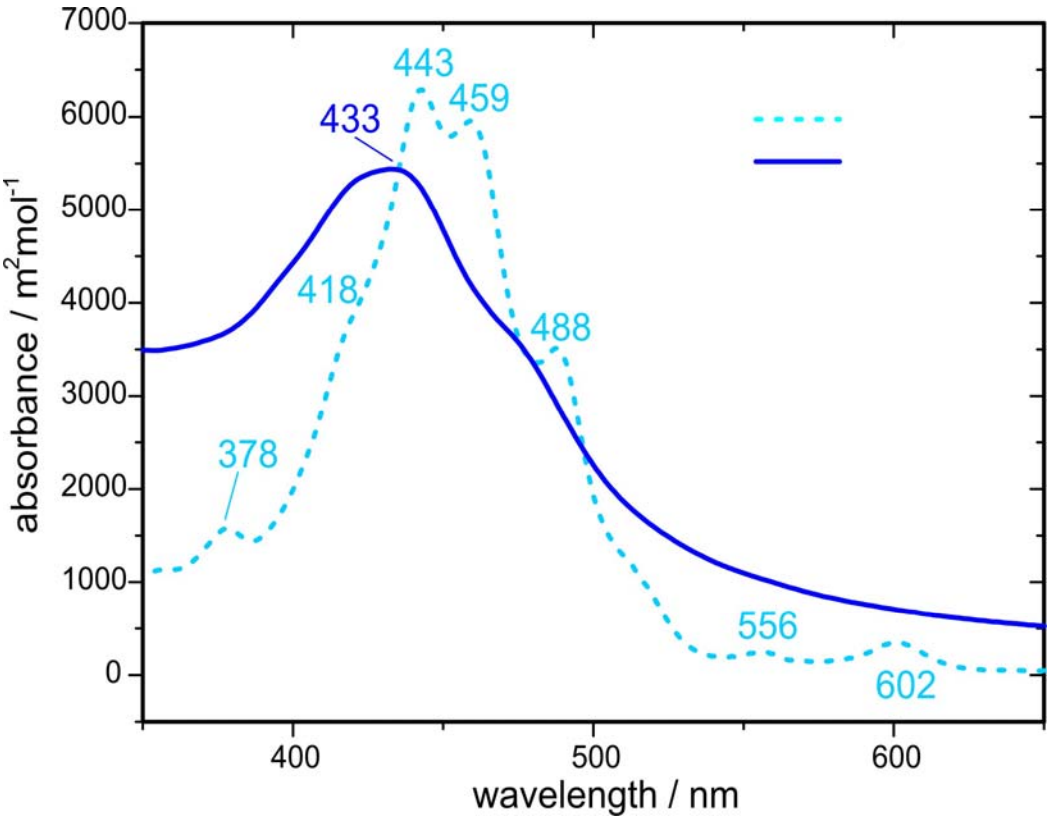

Figure 4-126: UV/vis absorption spectra of C72-$(C_{12})_4$-$(C_{14,10})_{4p}$ (**4-129**) (blue) and C72-$(C_{12})_4$-$(C_{14,10})_4$-(*t*-Bu)$_2$ (**4-119**) (cyan).

In Figure 4-126 the absorption spectra of C72-$(C_{12})_4$-$(C_{14,10})_{4p}$ (**4-129**), which corresponds to the spectra observed for the compounds C72-$(C_{12})_8$ (**4-44**) and C72-$(C_{8,2})_8$ (**4-45**), and the spectra of the distorted precursor molecule C72-$(C_{12})_4$-$(C_{14,10})_4$-(*t*-Bu)$_2$ (**4-119**) are compared. It becomes obvious that the main absorption band shifted hypsochromically by 10 nm, which is indeed due to the distortion of the precursor (Appendix H). The removal of the *tert*-butyl groups and as a consequence thereof, the induced higher aggregation led to a severe reduction of the resolution of C72-$(C_{12})_4$-$(C_{14,10})_{4p}$ (**4-129**). Therefore, the resolution of the absorption spectra of a large PAH is correlated with the specific aggregation of the investigated material. Some indications

for this behavior have already been determined for HBCs, but appeared not as strong as in this example.

4.10.4 Solution Properties

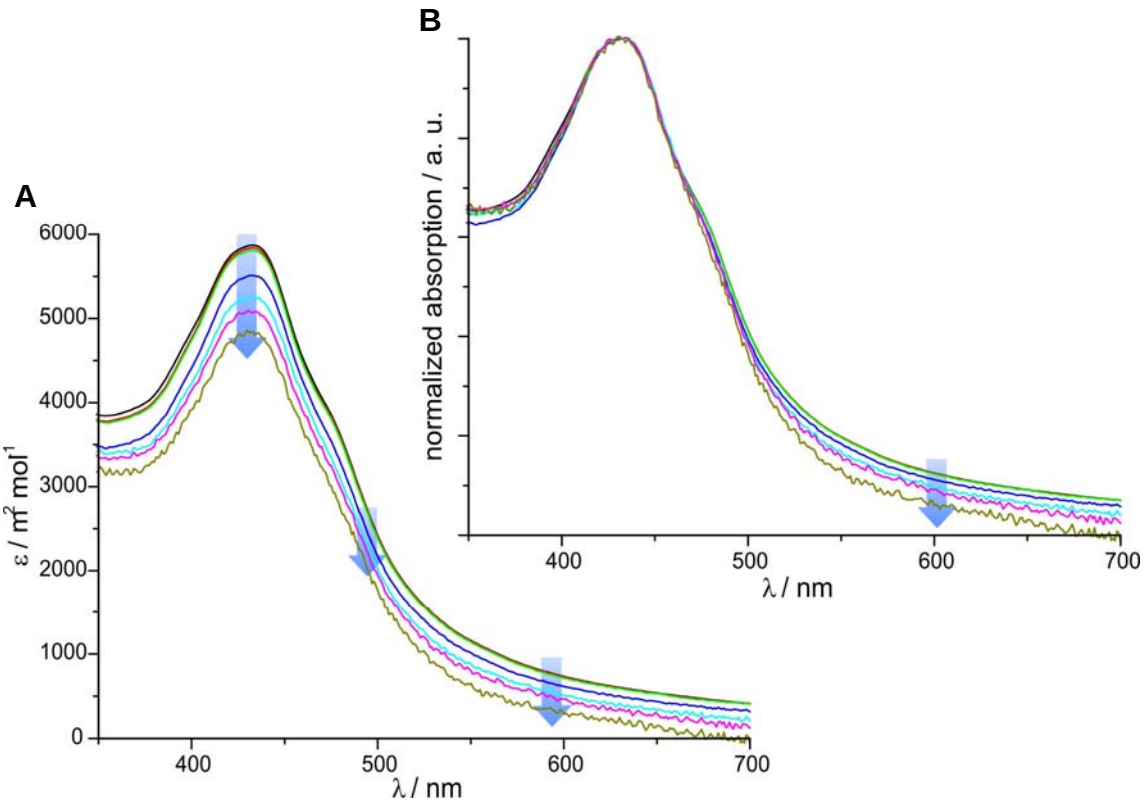

Figure 4-127: Concentration dependent absorption spectra of C72-$(C_{12})_4$-$(C_{14,10})_{4p}$ (**4-129**) **A**) with respect to concentration and **B**) normalized to the main absorption band.

By changing the concentration as shown in Figure 4-127 the extinction coefficient differed far stronger than for C72-$(C_{12})_4$-$(C_{14,10})_4$-(*t*-Bu)$_2$ (**4-119**). Interestingly over the whole range the absorption was reduced by a lowering of the concentration (Figure 4-127A). Due to the lack of an isosbestic point, the spectra were normalized to the value of the maximum absorption peak (Figure 4-127B). It became clear that the strongest deviation of the values occurred at wavelengths of 500 nm and above. Consistent with the measurements for C72-$(C_{12})_4$-$(C_{14,10})_4$-(*t*-Bu)$_2$ (**4-119**), also for C72-$(C_{12})_4$-$(C_{14,10})_{4p}$ (**4-129**) the photoluminescence spectra showed a far stronger effect on the change of the concentrations (Figure 4-128).

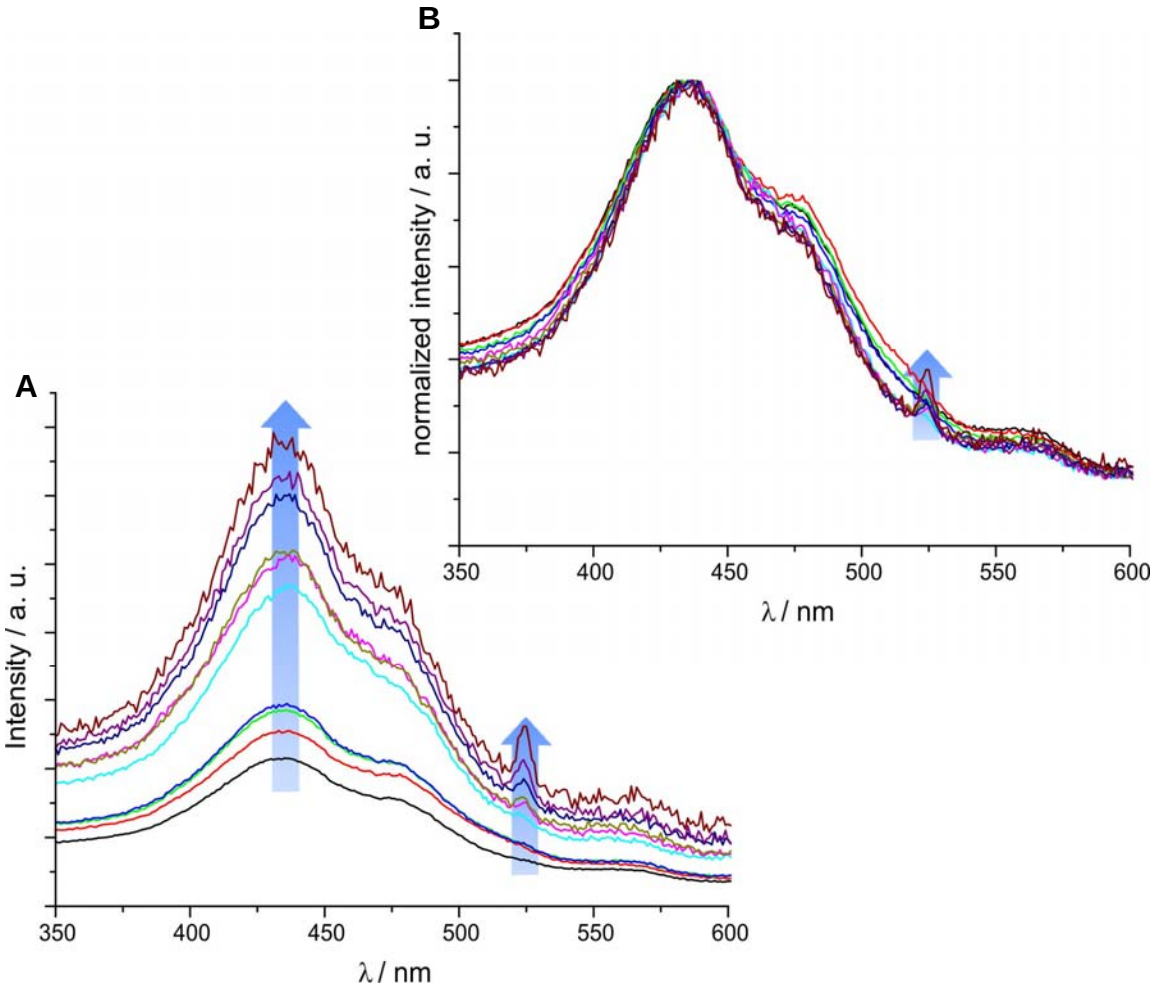

Figure 4-128: Concentration dependent photoluminescence excitation spectra of C72-$(C_{12})_4$-$(C_{14,10})_{4p}$ (**4-129**) **A**) with respect to concentration and **B**) normalized to the main absorption band.

From Figure 4-128 it becomes obvious that lower concentrations for C72-$(C_{12})_4$-$(C_{14,10})_{4p}$ (**4-129**) lead to a higher intensity in the photoluminescence excitation spectra, which fully complies with the properties for other PAHs and again indicates the influence of the aggregation upon the quenching of the fluorescence.

In contrast with the results of the UV/vis, the strongest changes in intensity were observed not above 500 nm, but between 450 and 600 nm. In addition, a small band occurred at approximately 525 nm at lower concentrations, which presumably indicated a stronger presence of monomeric species in the solution. Similar to the values observed for C72-$(C_{12})_8$-(*t*-Bu)$_2$ (**4-116**) also for C72-$(C_{12})_4$-$(C_{14,10})_{4p}$ (**4-129**) a linear dependence of the photoluminescence excitation intensities upon the concentration in THF was found. Even though the averaged plot assumes a slow progression towards a plateau,

typical for the presence of only monomeric species, the errors of the data points do not allow any assumption about the possible occurrence or even an interpolation of the necessary concentration for reaching the monomeric state. Moreover, it has to be pointed out that a linear increase until the detection limits of the spectrometer is more probable.

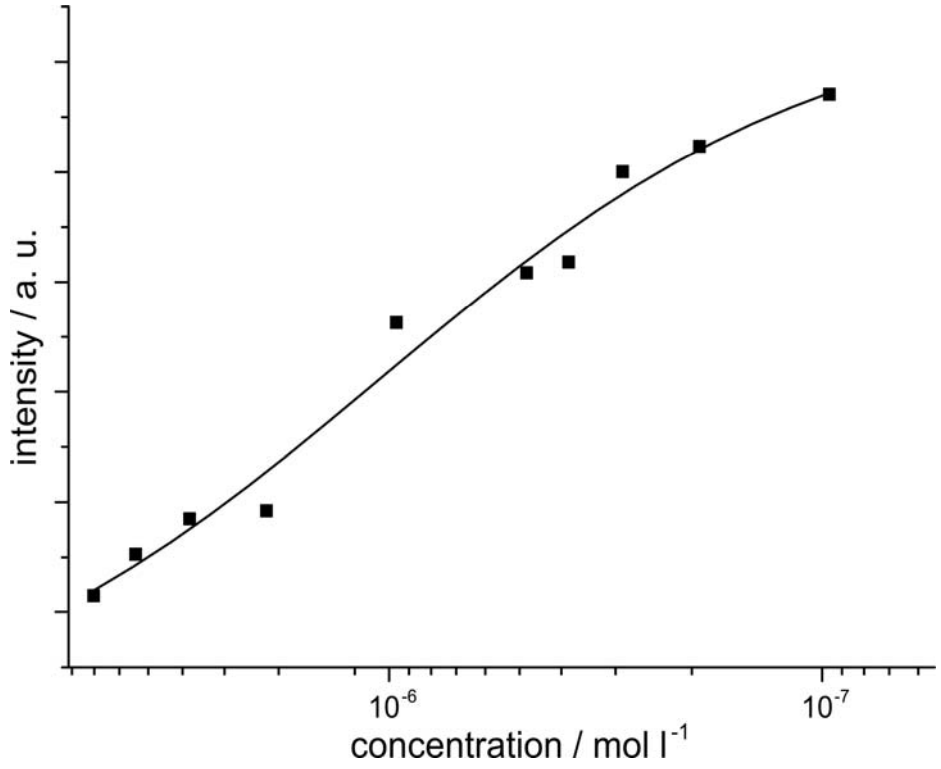

Figure 4-129: Intensity values of the photoluminescence excitation band at 435 nm with respect to the concentration of C72-$(C_{12})_4$-$(C_{14,10})_{4p}$ (**4-129**), recorded in THF.

Such a linear increase is characteristic for a strong propensity of aggregation. As mentioned earlier, the HBC derivative decorated with six linear *n*-dodecyl chains (**4-28**), which is a material that does not exhibit a very pronounced solubility in common organic solvents, reaches its plateau or rather the concentration value, where the molecules enter the monomeric status, at 5 x 10^{-5} mol l^{-1}. Even the distorted C72-$(C_{12})_8$-(*t*-Bu)$_2$ (**4-116**), which exhibited presumably a 100 times stronger aggregation propensity than the before mentioned HBC derivative showed a clear progression towards a plateau in Figure 4-109. Therefore it can be assumed that the aggregation observed for C72-$(C_{12})_4$-$(C_{14,10})_{4p}$ (**4-129**) need to be very high, supporting the macroscopic observation of the limited solubility of the compound.

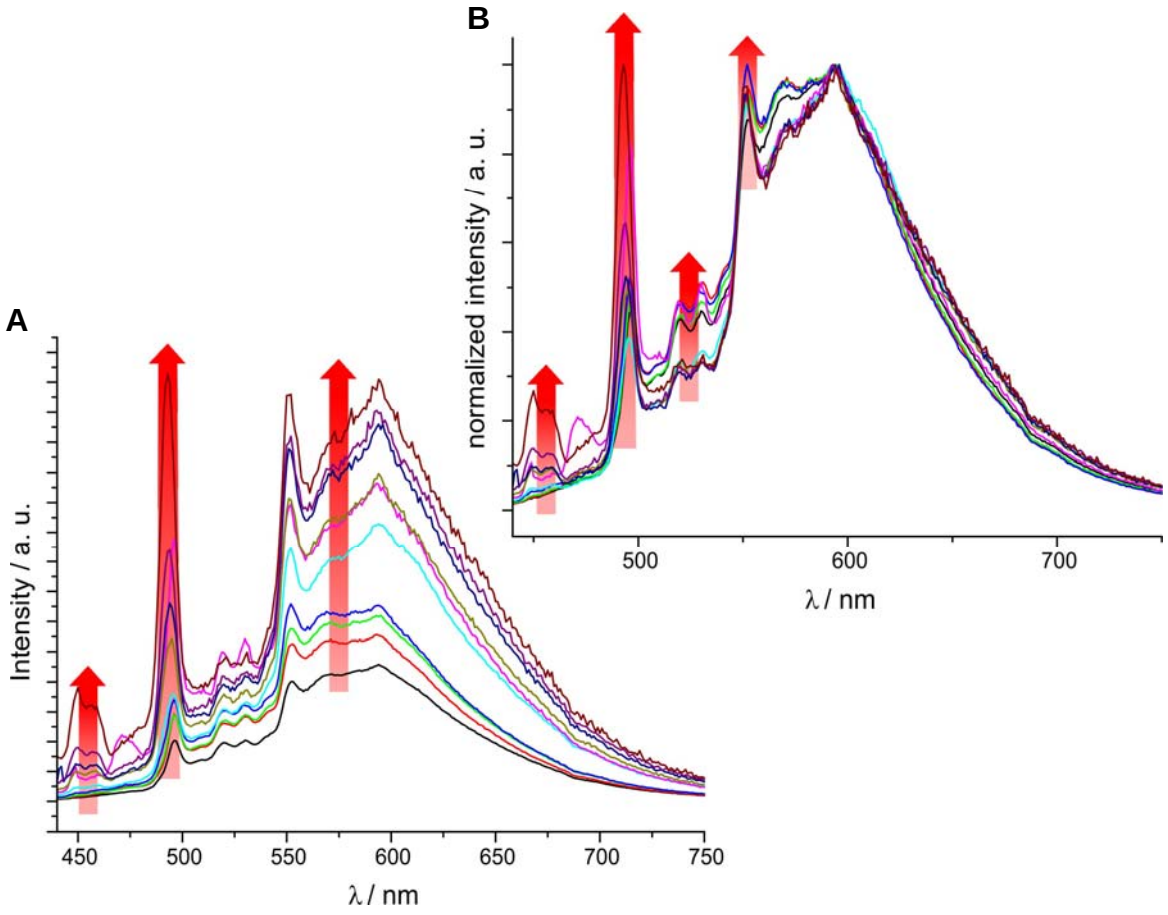

Figure 4-130: Concentration dependent photoluminescence spectra of C72-$(C_{12})_4$-$(C_{14,10})_{4p}$ (**4-129**) **A**) with respect to concentration and **B**) normalized to the main band at 600 nm.

The same effect appeared for the photoluminescence emission spectra, where at lower concentrations an increase of intensity was observed, too. The resulting band structure however revealed a slightly higher number of bands compared to the precursor molecule C72-$(C_{12})_4$-$(C_{14,10})_4$-(*t*-Bu)$_2$ (**4-119**), and is presumably due to the removal of the *tert*-butyl groups and the resulting planarization of the aromatic core unit. For most cases however, the wavelengths of the bands correlated to the ones observed for C72-$(C_{12})_4$-$(C_{14,10})_4$-(*t*-Bu)$_2$ (**4-119**) at low concentrations. Especially the three bands at the shorter wavelengths seemed to originate from the same transitions, although with slight deviations in their respective shift. While the bands for C72-$(C_{12})_4$-$(C_{14,10})_{4p}$ (**4-129**) at 453 and 495 nm exhibited the same hypsochromic shift of 10 nm as the main absorption band of the UV/vis, the bands at 550 nm did not show any change according to their position.

In Figure 4-130B the intensities were normalized to the value of the band with the highest intensity at 600 nm. In contrast to Figure 4-108, where the same normalization was performed, the band at 495 nm showed this time the strongest dependence upon the concentration, indicating that this band is apparently not originating from an aggregate but from the monomeric species.

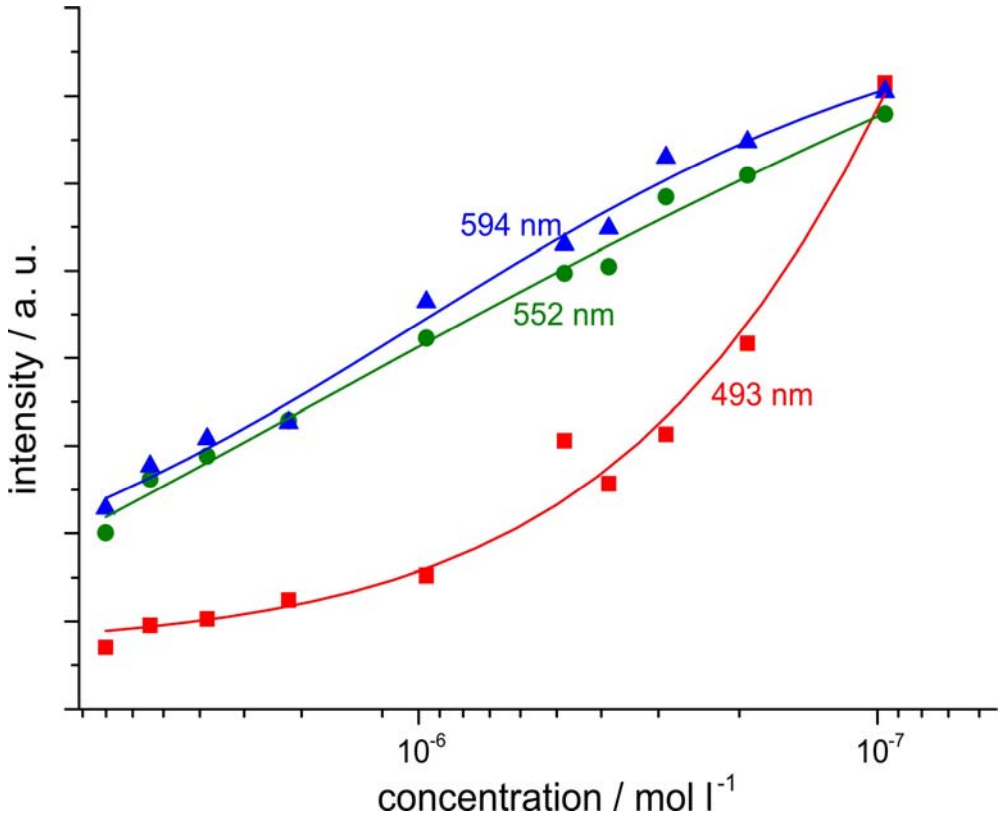

Figure 4-131: Intensity values of the photoluminescence emission bands at 493 nm, 552 nm and 594 nm with respect to the concentration of C72-$(C_{12})_4$-$(C_{14,10})_{4p}$ (**4-129**), recorded in THF.

The plots of the intensities of the photoluminescence emission bands at 594 nm and 552 nm supported the observations made for the concentration dependent excitation values in Figure 4-129, namely that the concentration value for the occurrence of mainly monomers will be below the detection limits of the spectrometer. However, in this case an interesting thermal band was observed, which started evolving at around 10^{-6} mol l^{-1} and increased exponentially by lowering the concentration. Similar bands have been observed for the photoluminescence emission of C72-$(C_{12})_4$-$(C_{14,10})_4$-(*t*-Bu)$_2$ (**4-119**) and were assumed to originate only from the monomeric species. In this example however, it was shown that the exponential increase of the intensity of the thermal band did not occur at the same concentration values as the progression towards a plateau of other

bands like for C72-$(C_{12})_4$-$(C_{14,10})_4$-(*t*-Bu)$_2$ (**4-119**). This means that the thermal bands are not necessarily completely suppressed by the aggregation, as indicated from the results shown in Figure 4-131. Therefore, it is questionable, if for C72-$(C_{12})_4$-$(C_{14,10})_4$-(*t*-Bu)$_2$ (**4-119**) the simultaneous appearance of the progression towards a plateau of the band at 611 nm and the emergence of the exponential increase of the thermal bands at shorter wavelengths, is not simply a coincidence and that thermal bands are not necessarily directly correlated with the monomeric status of the compound.

4.10.5 Polarized Optical Microscopy

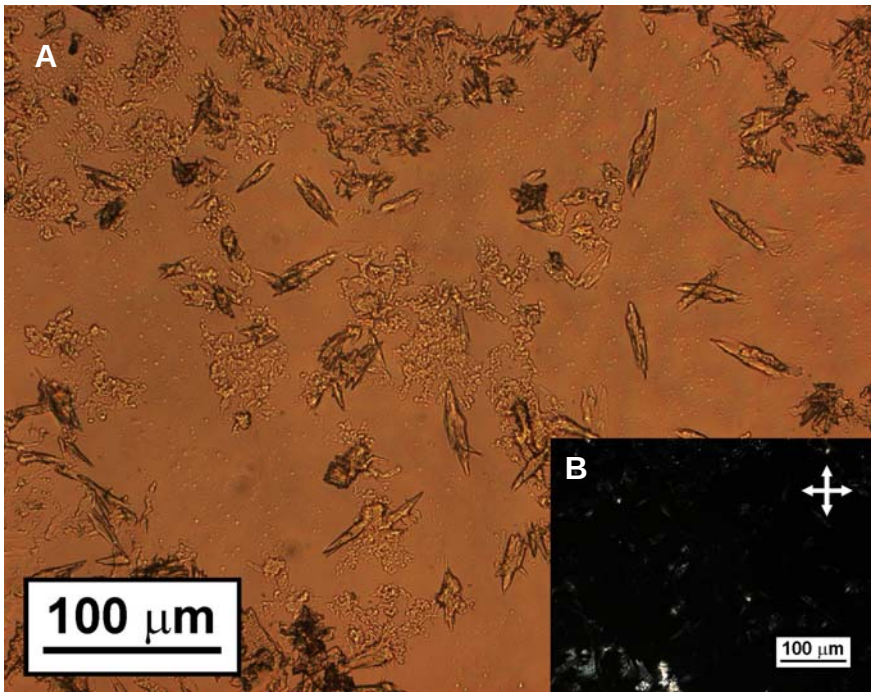

Figure 4-132: A) Optical microsopy image of a drop-casted film of C72-$(C_{12})_4$-$(C_{14,10})_{4p}$ (**4-129**) at room temperature **B**) image with applied cross-polarizers.

As for C72-$(C_{12})_4$-$(C_{14,10})_{4p}$ (**4-129**) no thermal transitions were observed, any further thermal processing of this material is futile. Nevertheless, it was possible to gain drop-casted films from THF (Figure 4-132A/B), where small crystalline-like objects formed, which has already been predicted by the aggregation propensity of the material in solution. As mentioned above, only compounds with already high association constants of the discs in solution provided films with a high degree of crystallinity. Therefore, it was supported by the appearance of C72-$(C_{12})_4$-$(C_{14,10})_{4p}$ (**4-129**) in the solid state that this material exhibits a high association constant in solution, pointing towards a

pronounced degree of aggregation. As a consequence, the future treatment of such materials will imply rather solution based than thermal film forming techniques.[91]

4.10.6 Powder X-ray Diffraction

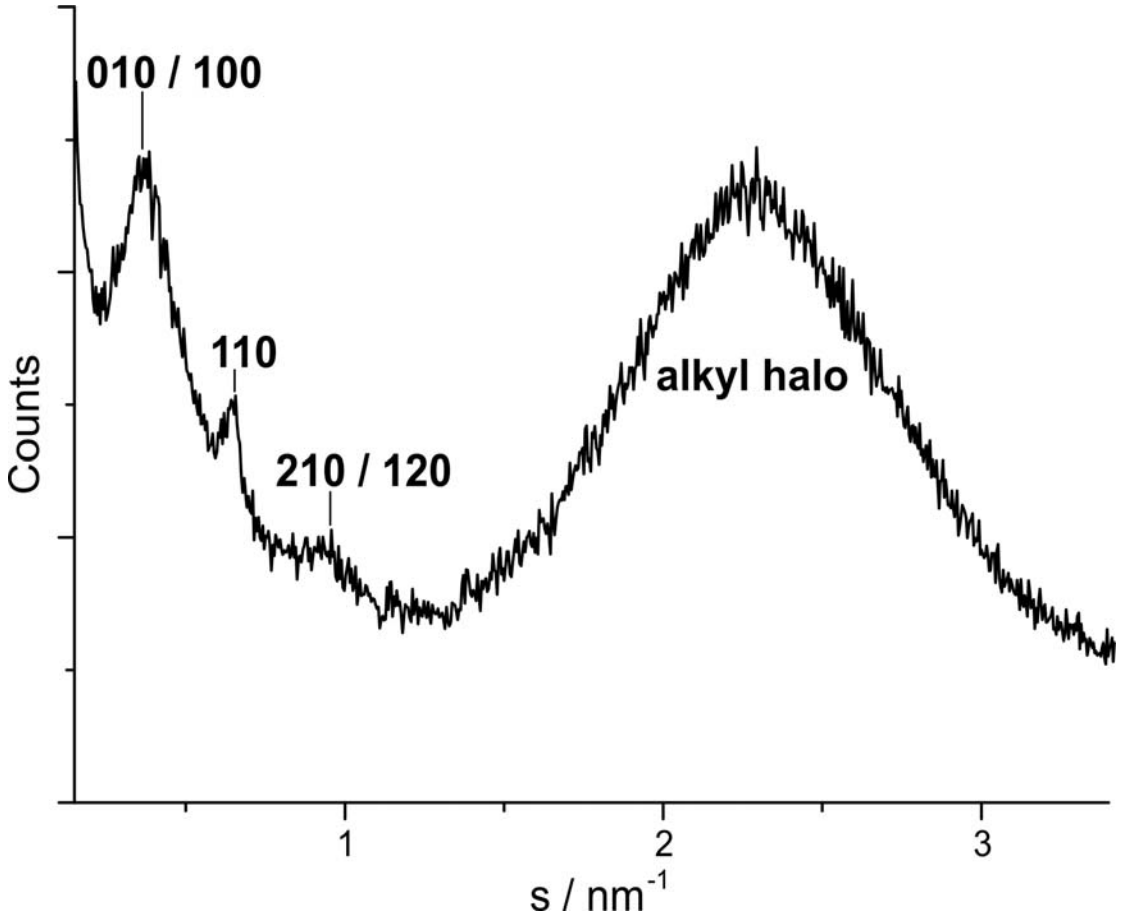

Figure 4-133: Powder X-ray diffractogram of C72-$(C_{12})_4$-$(C_{14,10})_{4p}$ (**4-129**).

Due to the high crystallinity of the material, it was not possible to extrude a fiber and consecutively record a 2D-WAXS diffractogram. Therefore, the compound was further investigated by using powder X-ray methods. The diffractogram revealed a hexagonal arrangement of the molecules with a packing parameter of a = 3.07 nm. This unit cell is slightly smaller than the one for the distorted precursor compound C72-$(C_{12})_4$-$(C_{14,10})_4$-(*t*-Bu)$_2$ (**4-119**), which possibly indicates the reduced steric demand for the alkyl substituents within the columnar organization, due to the absence of the *tert*-butyl groups. The π-stacking reflex (001) was so far not readily observed, but is presumably located within the broad alkyl halo region, as the reflex is usually found at 2.9-3.0 nm^{-1}.

4.11 Discussion

Although the classical synthetic route *via* dendritic oligophenylene precursor molecules is a simple way to gain a wide diversity of different PAHs, due to the flexible preparation of the precursors, the planarization step consisting of an intramolecular Scholl reaction suffered from severe problems. The reaction showed not only chlorination of the fully fused products, but also the presence of partially fused intermediates. These byproducts could neither be separated nor suppressed by adapting the oligophenylene precursors.

Although the change of the phenyl substitution pattern in the oligophenylene precursor did not reveal a strong influence upon the scope of the cyclodehydrogenation reaction, it was still assumed that an adaption of the aromatic system of the oligophenylene precursor can have a severe influence upon the scope of the intramolecular Scholl reaction. For gaining further insight into the propagation of the Scholl reaction oligophenylene precursor (C74 (**4-94**), C76 (**4-98**) and C76-(*t*-Bu)$_4$ (**4-99**)) with benzopyrene entities were prepared to enforce an initiation of the reaction at the rim of the precursor. Indeed, the resulting MALDI-TOF MS analytics revealed that for the C74 precursor (**4-93**) a wide diversity of intermediates were determined similar to the assumed structures for the C72 example C72-(C$_{12}$)$_8$ (**4-44**). For the C76 (**4-98**) case only one signal of a partially fused intermediate was found. Additionally an influence of alkyl substituents appeared, as for the alkylated C76-(t-Bu)$_4$ (**4-99**) precursor only the fully fused product was observed in the MALDI-TOF MS. However, the UV/vis clearly contradicted this result, as the main absorption band was located at a too short wavelength for such an aromatic system. This proved again that MALDI-TOF MS overestimated the product, but how much of this effect was due to the presence of the alkyl chains could not be verified.

Finally, it had to be considered, if the formation of the observed monodisperse intermediate C76 (**4-98**) was related only to the supposed initiation of the cyclodehydrogenation at the rim or if symmetric and electronic effects of the dibenzo[a,g]coronene panel also played a role. Therefore, a small version of the precursor was prepared, which was related to one half of the C76 precursor **4-96**. During the reaction only the above described intermediate was formed, in which one alkyl bond was not established. This clearly indicated that an electronic influence played the major role in the formation of the partially fused intermediate during the cyclodehydrogenation of **4-96**.

At this stage, it was necessary to develop a completely novel synthetic pathway towards the C72 derivatives. According to the experiences made that far, two arguments became relevant for a successful synthesis of such a compound. The possible formation of panels had to be suppressed by an initial preplanarization of the oligophenylene precursor molecule, providing a similar starting configuration for the unfused phenyl rings as in hexaphenylbenzene. Second, only by applying a whole series of solubilizing features it was possible to induce sufficient solubility and processability for a C72 derivative. The sterical demand and the resulting distortion of the aromatic core unit by the bulky *tert*-butyl groups showed in this context an especially strong influence. But it has to be mentioned that only the combination of the methods proved to be successful as two features alone did not introduce sufficient effects. For example, the results gained from the derivative C72-$(C_{12})_8$-(*t*-Bu)$_2$ (**4-116**), where only one type of alkyl chain and the *tert*-butyl groups induced the solubility, difficulties were encountered with respect to the reproducibility of the ^{1}H NMR spectra. In addition, no 2D NMR measurements could be performed as the aggregation in solution still remained high. This distinct aggregation behavior became obvious during the concentration dependent photoluminescence studies, which revealed the assumed strong aggregation in solution. Also in the bulk, the lack of solubility became manifest in the poor processability, as for example the material showed no thermal phase behavior and could not be aligned *via* extrusion.

After the substitution of four *n*-dodecyl alkyl chains with their 2-decyl-tetradecyl counterparts, the properties were dramatically improved. Due to the steric requirements close to the vicinity of the aromatic core component this alkyl side-chain further suppressed the aggregation behavior. This led to the successful recording of 2D NMR spectra in addition to the analytical methods, already achieved with the other derivative. Nevertheless, a certain aggregation remained in solution, which was detected by concentration dependent photoluminescence measurements. Another improvement was the evolution of the UV/vis spectra, as for C72-$(C_{12})_4$-$(C_{14,10})_4$-(*t*-Bu)$_2$ (**4-119**) a large number of bands were detected, whereby the first absorption band was found above 600 nm. It was additionally proven that even for such extended PAHs, the UV/vis as well as the photoluminescence excitation spectra need to exhibit the same bands. Due to the easily reproducible ^{1}H NMR spectra, concentration dependent NMR studies were performed. It was revealed that in a CD_2Cl_2/CS_2 mixture no aggregation could be determined as the NMR shifts, in contrast to other PAHs, did not exhibit any changes at

different concentrations. However, it is known that CS_2 sufficiently suppresses the π-aggregation, which resulted in this case in the presence of only the monomeric species.

Moreover C72-$(C_{12})_4$-$(C_{14,10})_4$-(*t*-Bu)$_2$ (**4-119**) showed a thermal phase behavior and even a homeotropic arrangement on a glass substrate at higher temperatures. In addition, it was possible to align the discs *via* extrusion and record a 2D WAXS diffractogram. Similar to HBC, a columnar hexagonal arrangement was observed, which was presumably adopted due to the steric repulsion induced by the bulky *tert*-butyl groups, leading to an intermolecular offset within the same column. This offset resulted in a round intracolumnar arrangement, which yielded the observed hexagonal arrangement.

This arrangement was also adopted by the fully planar derivative C72-$(C_{12})_4$-$(C_{14,10})_{4p}$ (**4-129**). It is difficult to define, whether or not this was induced by the already established arrangement of the precursor compound C72-$(C_{12})_4$-$(C_{14,10})_4$-(*t*-Bu)$_2$ (**4-119**) in some kind of template effect. Logically, the molecules should prefer a self-organization similar to the one in the graphite lattice. In the case of HBCs for example this becomes apparent by the tilting of the discs relative to their stacking axis. In addition the self-arrangement should also include the maximum possible aromatic overlap, which is not given for the proposed twisted arrangement of the fully planar compound C72-$(C_{12})_4$-$(C_{14,10})_{4p}$ (**4-129**). This indicates that the reaction occurs maybe not only at the monomeric species, but can directly attack the *tert*-butyl groups of molecules, which are members of a stacked arrangement. The resulting lower solubility and higher aggregation then "freezes" the position of the molecule relative to its neighbors, preserving the offset induced by the *tert*-butyl groups. During the workup procedure the aggregated entities simply move closer together due to the additional space provided by the removal of the *tert*-butyl groups. This then resulted in the observed hexagonal arrangement in the bulk.

For the derivative C72-$(C_{12})_4$-$(C_{14,10})_{4p}$ (**4-129**), where the branched alkyl side-chain induced a residual solubility, a strong effect of the aggregation upon the recorded concentration dependent electronic spectra was found and several bands exhibited a surprisingly high amplification upon a lowering of the concentration. In addition, it was proven that the aggregation is indeed responsible for the disappearance of the resolution in the UV/vis spectra.

In combination with the experiences made with the fully planarized derivatives C72-$(C_{12})_{8p}$ (**4-128**) and C72-$(C_{12})_4$-$(C_{14,10})_{4p}$ (**4-129**) it became obvious that the strength of the π-mediated aggregation for these extended PAHs is rather distinct. Even with such a

small aromatic system as C72, compared to C96 (**4-48**) or even C222 (**4-50**), a highly insoluble material has been gained, which showed also no thermal phase transitions anymore. One has to keep in mind that in this case the symmetry of the molecule is rather low and should therefore assist the aggregation suppression induced by the alkyl side-chains. On the other hand, this indicates that all the alkylated substances (C72, C96 and C222) received by the old route should probably be less soluble and highly crystalline.

4.12 Conclusions

The intramolecular Scholl reaction was influenced by the presence of a larger aromatic moiety within the oligophenylene precursor molecule. In addition, it was shown that the type of the initially formed aromatic entity, establishing either a tribenzo-[b,n,pqr]perylene or a dibenzo[a,g]coronene panel, can be decisive for the consecutive "stitching" process. For example, if dibenzo[a,g]coronene moieties are present, the further cyclodehydrogenation ("stitching") is substantially slowed down.

In accordance, the novel synthetic approach by a preplanarization of the center of the precursor proved to be highly reproducible and no discrepancies between the batches like for C72-$(C_{12})_8$ (**4-44**) could be observed for C72-$(C_{12})_8$-(*t*-Bu)$_2$ (**4-116**) and C72-$(C_{12})_4$-$(C_{14,10})_4$-(*t*-Bu)$_2$ (**4-119**). It was verified that one can record well-resolved NMR and UV/vis spectra from large PAHs, as compounds C72-$(C_{12})_8$-(*t*-Bu)$_2$ (**4-116**) and C72-$(C_{12})_4$-$(C_{14,10})_4$-(*t*-Bu)$_2$ (**4-119**) are the largest reported PAHs with a resolved ^{1}H NMR spectrum. To achieve this goal, several solubilizing features had to be introduced, whereby the induced distortion and the steric requirements of the bulky tert-butyl groups proved to be the main argument for the solubility and the effective aggregation suppression of C72-$(C_{12})_8$-(*t*-Bu)$_2$ (**4-116**) and C72-$(C_{12})_4$-$(C_{14,10})_4$-(*t*-Bu)$_2$ (**4-119**). Although C72-$(C_{12})_8$-(*t*-Bu)$_2$ (**4-116**) could not be oriented via extrusion due to the still pronounced aggregation, C72-$(C_{12})_4$-$(C_{14,10})_4$-(*t*-Bu)$_2$ (**4-119**) showed the necessary columnar self-assembly in the bulk, which is a prerequisite for a successful charge-carrier migration along the columnar axis. Also from drop-casting C72-$(C_{12})_4$-$(C_{14,10})_4$-(*t*-Bu)$_2$ (**4-119**) already formed homogeneous films with low crystallinity, indicating good film forming properties. With the more than three times higher molar extinction coefficient of C72-$(C_{12})_4$-$(C_{14,10})_4$-(*t*-Bu)$_2$ (**4-119**) and the bathochromically shifted absorption profile relative to HBCs the material becomes an interesting candidate for future photovoltaic applications.

4.13 References

[1] Z. Tomovic, M. D. Watson, K. Müllen *Angew. Chem. Int. Ed.* **2004**, *43*, 755.

[2] B. Mohr, G. Wegner, K. Ohta *J. Chem. Soc. Chem. Commun.* **1995**, 995.

[3] J. M. Fox, T. J. Katz, S. V. Elshocht, T. Verbiest, M. Kauranen, A. Persoons, T. Thongpanchang, T. Krauss, L. Brus, *J. Am. Chem. Soc.* **1999**, *121*, 3453.

[4] A. N. Cammidge, H. Gopee *Chem. Commun.* **2002**, 966.

[5] C. F. van Nostrum, S. J. Picken, A. J. Schouten, R. J. M. Nolte *J. Am. Chem. Soc.* **1995**, *117*, 9957.

[6] R. P. Sijbesma, E.W. Meijer *Chem. Commun.* **2003**, 5.

[7] V. Percec, M. Glodde, T. K. Bera, Y. Miura, I. Shiyanovskaya, K. D. Singer, V. S. K. Balagurusamy, P. A. Heiney, I. Schnell, A. Rapp, H.W. Spiess, S. D. Hudsonk, H. Duank *Nature* **2002**, *419*, 384.

[8] A. M. van de Craats, J. M. Warman *Adv. Mater.* **2001**, *13*, 130.

[9] V. Lemaur, D. A. da Silva Filho, V. Coropceanu, M. Lehmann, Y. Geerts, J. Piris, M. G. Debije, A. M. van de Craats, L. Senthilkumar, L. D. A. Siebbeles, J. M. Warman, J. L. Brédas, J. Cornil *J. Am. Chem. Soc.* **2004**, *126*, 3271.

[10] M. G. Debije, J. Piris, M. P. de Haas, J. M. Warman, H. Tomovic, C. D. Simpson, M. D. Watson, K. Müllen *J. Am. Chem. Soc.* **2004**, *126*, 4641.

[11] H. Sirringhaus, P. J. Brown, R. H. Friend, M. M. Nielsen, K. Bechgaard, B. W. M. Langeveld-Voss, A. J. H. Spiering, R. A. J. Janssen, E. W. Meijer, P. Herwig, D. M. de Leeuw *Nature* **1999**, *401*, 685.

[12] W. Pisula, H. Tomovic, C. Simpson, M. Kastler, T. Pakula, K. Müllen *Chem. Mater.* **2005**, *17*, 4296.

[13] I. Gutman, S. J. Cyvin *Introduction to the Theory of Benzenoid Hydrocarbons*, Springer, Berlin, **1989**.

[14] D. Moran, F. Stahl, H. F. Bettinger, H. F. Schäfer, P. Schleyer *J. Am. Chem. Soc.* **2003**, *125*, 6746.

[15] M. Randic, X. F. Guo *New J. Chem.* **1999**, *23*, 251.

[16] I. Gutman, V. Ivanov-Petrovic, J. R. Dias *Polycyclic Aromat. Compd.* **2000**, *18*, 221.

[17] F. Negri, C. Castiglioni, M. Tommasini, G. Zerbi *J. Phys. Chem. A* **2002**, *106*, 3306.

[18] E. Clar *Polycyclic Hydrocarbons*, Academic Press and Springer Verlag, Berlin, **1964**.

[19] M. Müller, C. Kübel, F. Morgenroth V. S. Iyer, K. Müllen *Carbon* **1998**, 36, 827.

[20] F. Dötz, J. D. Brand, S. Ito, L. Ghergel, K. Müllen *J. Am. Chem. Soc.* **2000**, 122, 7707.

[21] M. D. Watson, A. Fechtenkötter, K. Müllen *Chem. Rev.* **2001**, *101*, 1267.

[22] M. Lee, J.-W. Kim, S. Peleshenko, K. Larsen, Y.-S. Yoo, D. Vaknin, S. Markutsya, V. V. Tsukruk *J. Am. Chem. Soc.* **2002**, *124*, 9121.

[23] R. Rathore, C. L. Burns *J. Org. Chem.* **2003**, *68*, 4071.

[24] S. Takahashi, Y. Kuroyama, K. Sonogashira, N. Hagihara *Synthesis-Stuttgart* **1980** 627.

[25] Balaban, A. T.; Nenitzescu, C. D. In Friedel-Crafts and Related Reactions; Olah, G. A., Ed.; Wiley & Sons: New York **1964**; Vol. 2, part 2, 979.

[26] G. A. Olah, P. Schilling, I. M. Gross *J. Am. Chem. Soc.* **1974**, *96*, 876.

[27] M. Wehmeier *phD thesis* **1999**, Mainz.

[28] P. Kovacic, C. Wu *J. Org. Chem.* 1961, 26, 759.

[29] P. Kovacic, F. W . Koch *J. Org. Chem.* 1963, 28, 1864.

[30] P. Kovacic, F. W . Koch *J. Org. Chem.* 1965, 30, 3176.

[31] P. Kovacic, M. B. Jones *Chem. Rev.* 1987, 87, 357.

[32] C. Simpson *phD thesis* **2003**, Mainz.

[33] V. S. Iyer, M. Wehmeier, J. D. Brand, M. A. Keegstra, K. Müllen *Angew. Chem.* **1997**, *109*, 1676.

[34] W. Ried, V. B. Saxena *Angew. Chem.* **1968**, *80*, 366.

[35] T. Yamamoto, A. Morita, Y. Miyazaki, T. Maruyama, H. Wakayama, Z. Zhou, Y. Nakamura, T. Kanbara *Macromol.* **1992**, *25*, 1214.

[36] I. Colon, D. R. Kelsey *J. Org. Chem.* **1986**, *51*, 2627.

[37] V. Farina, V. Krishnamurthy, W. J. Scott, *Org. React.* **1997**, 1-652.

[38] V. Farina, V. Krishnamurthy, W. J. Scott *The Stille Reaction.* - John Wiley & Sons, New York **1998**.

[39] T. N. Mitchell *Synthesis* **1992**, 803.

[40] J. K. Stille *Angew. Chem.* **1986**, 504.

[41] L. Schmidt-Mende, A. Fechtenkötter, K. Müllen, E. Moons, R. H. Friend, J. D. MacKenzie *Science*, **2001**, *293*, 1119.

[42] E. B. Stephens, J. M. Tour *Macromolecules* **1993**, *26*, 2420.

[43] A. Fürstner, V. Mamane *J. Org. Chem.* **2002**, *67*, 6264.

[44] A. M. van de Craats, J. M. Warman, A. Fechtenkötter, J. D. Brand, M. A. Harbison, K. Müllen *Adv. Mater.* **1999**, *11*, 1469.

[45] T. Hassheider, S. A. Benning, M. W. Lauhof, H. S. Kitzerow, H. Bock, M. D. Watson, K. Müllen *Mol. Cryst. Liq. Cryst.* **2004**, *413*, 2597.

[46] J. Piris, M. G. Debije, N. Stutzmann, A. M. van de Craats, M. D. Watson, K. Müllen, J. M. Warman Adv. Mater. **2003**, *15*, 1736.

[47] L. Schmidt-Mende, M. D. Watson, K. Müllen, R. H. Friend Mol. Cryst. Liq. Cryst. **2003**, *396*, 73.

[48] C. Im, W. Tian, H. Bässler, A. Fechtenkötter, M. D. Watson, K. Müllen *J. Chem. Phys.* **2003**, *119*, 3952.

[49] A. J. Fleming, J. N. Coleman, A. B. Dalton, A. Fechtenkötter, M. D. Watson, K. Müllen, H. J. Byrne, W. J. Blau *J. Phys. Chem. B* **2003**, *107*, 37.

[50] L. Schmidt-Mende, A. Fechtenkötter, K. Müllen, R. H. Friend, J. D. MacKenzie *Physica E* **2002**, *14*, 263.

[51] I. Fischbach, T. Pakula, P. Minkin, A. Fechtenkötter, K. Müllen, H. W. Spiess, K. Saalwächter *J. Phys. Chem. B* **2002**, *106*, 6408.

[52] P. Samori, A. Fechtenkötter, F. Jäckel, T. Böhme, K. Müllen, J. P. Rabe *J. Am. Chem. Soc.* **2001**, *123*, 11462.

[53] A. M. van de Craats, J. M. Warman Synth. Met. **2001**, *121*, 1287.

[54] A. Fechtenkötter, K. Saalwächter, M. A. Harbison, K. Müllen, H. W. Spiess *Angew. Chem. Int. Ed.* **1999**, *38*, 3039.

[55] J. M. Warman, J. Piris, W. Pisula, M. Kastler, D. Wasserfallen, K. Müllen *J. Am. Chem. Soc.* **2005**, *127*, 14257.

[56] R. Friedlein, X. Crispin, W. Osikowicz, S. Braun, M.P. de Jong, C. D. Simpson, M. D. Watson, F. von Kieseritzky, P. Samori, S. K. M. Jonsson, M. Fahlman, F. Jäckel, J. P. Rabe, J. Hellberg, K. Müllen, W. R. Salaneck *Synthetic Metals* **2004**, *147*, 79.

[57] P. Samori, X. Yin, N. Tchebotareva, Z. Wang, T. Pakula, F. Jäckel, M. D. Watson, A. Venturini, K. Muellen, J. P. Rabe *J. Am. Chem. Soc.* **2004**, *126*, 3567.

[58] M. D. Watson, M. G. Debije, J. M. Warman, K. Muellen *J. Am. Chem. Soc.* **2004**, *126*, 766.

[59] N. Tchebotareva, X. Yin, M. D. Watson, P. Samori, J. P. Rabe, K. Müllen *J. Am. Chem. Soc.* **2003**, *125*, 9734.

[60] P. Miskiewicz, A. Rybak, J. Jung, I. Glowacki, J. Ulanski, Y. Geerts, M. D. Watson, K. Müllen *Synth. Met.* **2003**, *137*, 905.

[61] O. Bunk, M.M. Nielsen, T. I. Solling, A. M. van de Craats, N. Stutzmann *J. Am. Chem. Soc.* **2003**, *125*, 2252.

[62] A. Fechtenkötter, N. Tchebotareva, M. D. Watson, K. Müllen *Tetrahedron* **2001**, *57*, 3769.

[63] N. Miyaura, A. Suzuki *Chem. Rev.* **1995**, 2457.

[64] B. H. Ye, Y. Naruta *Tetrahedron* **2003**, *59*, 3593.

[65] V. Hensel, A. D. Schlüter *Liebigs Ann. - Rec.* **1997**, 303.

[66] L. Przybilla, J. D. Brand, K. Yoshimura, H. J. Räder, K. Müllen *Anal. Chem.* **2000**, *72*, 4591.

[67] V. S. Iyer, Viveka, K. Yoshimura, V. Enkelmann, R. Epsch, J. P. Rabe, K. Müllen *Angew. Chem. Int. Ed.* **1998**, *37*, 2696.

[68] D. Wasserfallen, I. Fischbach, N. Tchebotareva, M. Kastler, W. Pisula, F. Jäckel, M. D. Watson, I. Schnell, J. P. Rabe, H. W. Spiess, K. Müllen *Adv. Funct. Mater.* **2005**, *15*, 1585.

[69] Z. Tomovic *phD thesis* **2004**, Mainz.

[70] P. Rempala, J. Kroulik, B. T. King *J. Am. Chem. Soc.* **2004**, *126*, 15002.

[71] C. Kübel, K. Eckhardt, V. Enkelmann, G. Wegner, K. Müllen *J. Mater. Chem.* **2000**, *10*, 879.

[72] Z. Wang, F. Dötz, V. Enkelmann, K. Müllen *Angew. Chem. Int. Ed.* **2005**, *44*, 1247.

[73] J. Wu - unpublished results

[74] L. T. Scott, M. M. Hashemi, M. S. Bratcher *J. Am. Chem. Soc.* **1992**, *114*, 1920.

[75] Y. Mima, E. Yamano, A. Miyazawa, M. Tashiro *J. Chem. Soc. Perkin Trans. 2* **1995**, 359.

[76] T. Yamato, M. Fujimoto, A. Miyazawa. K. Matsuo *J. Chem. Soc. Perkin Trans. 1* **1997**, 1201.

[77] Y. Fogel, unpublished results, **2005**.

[78] A. Tracz, J. K. Jeszka, M. D. Watson, W. Pisula, K. Müllen, T. Pakula *J. Am. Chem. Soc.* **2003**, *125*, 1682.

[79] R. Ikegami, A. Koresawa, T. Shibata, K. Takagi J. Org. Chem. **2003**, *68*, 2195.

[80] N. Boden, R. Borner, D. R. Brown, R. J. Bushby, J. Clements *Liq. Cryst.* **1992**, *11*, 325.

[81] L. Gherghel, J. D. Brand, M. Baumgarten, K. Müllen *J. Am. Chem. Soc.* **1999**, *121*, 8104.

[82] H. van Willigen, J. A. M. van Broekhaven, E. de Boer *Mol. Phys.* **1967**, *12*, 533.

[83] R. E. Jesse, P. Biloen, R. Prins, J. D. W. van Voorst, G. J. Hoijtink *J. Chem. Phys.* **1963**, *6*, 633.

[84] K. Bechgaard, V. D. Parker *J. Am. Chem. Soc.* **1972**, *94*, 4749.

[85] T. J. LePage, R. J. Breslow *J. Am. Chem. Soc.* **1987**, *109*, 6412.

[86] J. Thomaides, P. Maslak, R. Breslow *J. Am. Chem. Soc.* **1988**, *110*, 3870.

[87] D. A. Dixon, J. C. Calabrese, R. L. Harlow, J. S. Miller *Angew. Chem.* **1989**, *101*, 81.

[88] Z. Wang, Z. Tomovic, M. Kastler, R. Pretsch, F. Negri, V. Enkelmann, K. Müllen *J. Am. Chem. Soc.* **2004**, *126*, 7794.

[89] C. Y. Liu, A. J. Bard *Chem. Mater.* **2000**, 12, 2353.

[90] D. Perahia, D. Traiphol, U. H. F. Bunz *Macromolecules* **2001**, *34*, 151.

[91] M. Kastler, W. Pisula, D. Wasserfallen, T. Pakula, K. Müllen *J. Am. Chem. Soc.* **2005**, *127*, 4286.

[92] J. Piris, M. G. Debije, N. Stutzmann, B. W. Laursen, W. Pisula, M. D. Watson, T. Bjornholm, K. Müllen, J. M. Warman *Adv. Funct. Mater.* **2004**, *14*, 1053.

[93] W. Pisula, Z. Tomovic, M. Stepputat, U. Kolb, T. Pakula, K. Müllen *Chem. Mater.* **2005**, *17*, 2641.

[94] D. W. Breiby, O. Bunk, W. Pisula, T. I. Solling, A. Tracz, T. Pakula, K. Müllen, M. M. Nielsen *J. Am. Chem. Soc.* **2005**, *127*, 11288.

[95] G. Seybold, G. Wagenblast *Dyes Pigm.* **1989**, *11*, 303.

[96] L. T. Scott, P. C. Cheng, M. M. Hashemi, M. S. Bratcher, D. T. Meyer, H. B. Warren *J. Am. Chem. Soc.* **1997**, *119*, 10963.

[97] S. Hagen, M. S. Bratcher, M. S. Erickson, G. Zimmermann, L. T. Scott *Angew. Chem. Int. Ed. Engl.* **1997**, *36*, 406.

[98] C. Kohl, T. Weil, J. Qu, K. Müllen *Chem. Eur. J.* **2004**, *10*, 5297.

[99] W. Pisula, M. Kastler, D. Wasserfallen, T. Pakula, K. Müllen *J. Am. Chem. Soc.* **2004**, *126*, 8074.

[100] G. Wegner, G. *Macromol. Chem. Phys.* **2003**, *204*, 347.

[101] G. Kresse, J. Hafer *Phys. Rev. B* **1993**, *47*, 558.

[102] G. Kresse, J. Furthmüller *Phys. Rev. B* **1996**, *54*, 11169.

[103] Mills, G.; Jonsson, H.; Schenter, G. K. *Surf. Sci*. **1995**, *324*, 305.

[104] R. B. Prince, J. G. Saven, P. G. Wolynes, J. S. Moore *J. Am. Chem. Soc.* **1999**, *121*, 3114.

[105] *Protective Groups in Organic Synthesis*, 3rd ed., T. W. Greene, P. G. M. Wuts, John Wiley and Sons, **1999**.

5 Summary and Outlook

5.1 HBCs

By the addition of hydrogen-bond exerting moieties, covalently linked to the aromatic core by different types of linkers, the supramolecular properties of HBCs were substantially influenced. This did not only affect the thermal behavior of these materials, but also their intra- as well as intercolumnar order in the bulk as well as on surfaces. For example, by the addition of only one single carboxy-functionality into the system the length of the alkyl tether can be used to tune the thermal behavior of the materials. Thermally more stable pseudo-crystalline phases thereby appear as prerequisites due to their enhanced columnar order.

The introduction of a higher number of hydrogen-bonding functionalities led initially to the loss of the solubility, as well as the processability of the HBC derivatives. Nevertheless, it is important to retain the processability of these compounds, as this property is an important factor for the film formation capabilities of these materials. Only by a minimum of either a thermal phase behavior or solubility, it is possible to achieve the films required for future device applications.

As a consequence, a variety of approaches were considered to suppress the effects of the hydrogen-bonds onto the supramolecular properties of the HBCs and to keep the improved columnar order. This goal was partially achieved, as the addition of a flexible alkyl chain at the terminal site of the hydrogen-bond exerting entity led not only to a better soluble material, which exerted again a thermal phase behavior, but retained also the columnar order. The higher order reflexes, which appeared in the meridional direction of the 2D-WAXS, even suggested an improved intracolumnar order. In conclusion, it can be said that it is possible to introduce a better order into the columnar order of HBC by adding hydrogen-bonding functionalities, but one has to be aware not to introduce too many of these, as not to loose the processability of the materials.

Although the 3,7-dimethyloctyl chains in the corona of the HBC have in a variety of cases proven their usefulness in combination with such strong secondary forces like hydrogen-bonds, it is worthwile to regard other opportunities. It is obvious that the addition of multiple hydrogen-bonding functionalities will also require a corresponding counterpart to achieve on one hand the improved columnar order, as well as to keep the

solubility and the processability of the compounds. One possible substitution for the 3,7-dimethyloctyl alkyl chain is the recently introduced tetradecyldecyl chain (Figure 5-1).

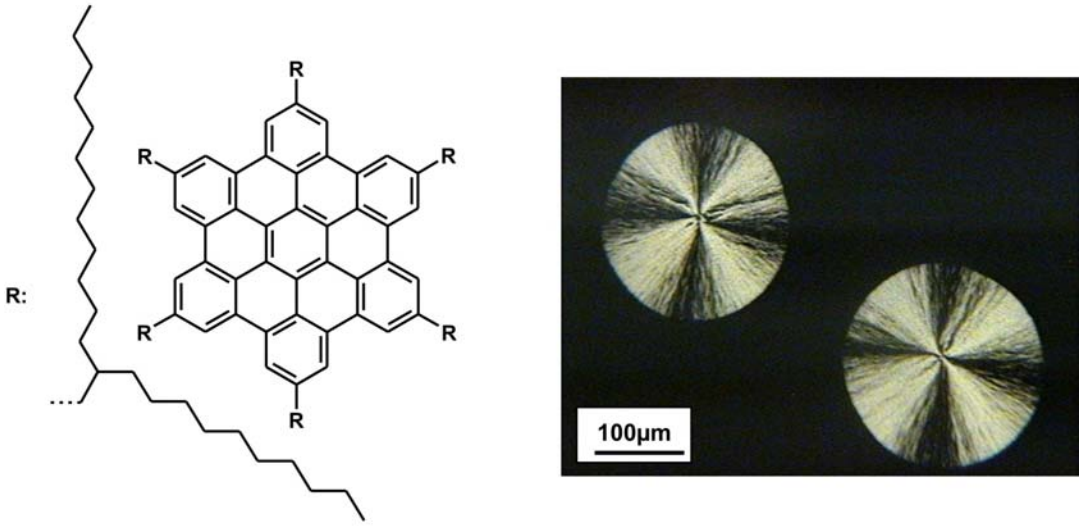

Figure 5-1: A) HBC substituted with six tetradecyldecyl chains (**5-1**); B) drop-cast film of the HBC (**5-1**)

Not only did their extremely solubilizing character allow the workup of compound **5-1** by column chromatography with hexane as eluent, but also did the reduction of the transition temperature to the isotropic state result in their good processability by zone-crystallization (Appendix C). In addition, the material showed already a strong self-aggregation tendency into long-range well-ordered films by simple drop-casting. As a consequence, the combination of hydrogen-bonding entities with such alkyl chains in the corona of HBC derivatives should allow to gain materials with high local order due to the assistance of the hydrogen-bonding entities in combination with the required processability induced by the bulky alkyl chains. With this approach, it is possible to engineer para-substituted HBC derivatives that can be specifically adapted to the actual requirements.

If for example a processing at lower temperatures is necessary, one reduces the effect of the hydrogen-bonds by either adding another alkyl chain at the outer rim of the hydrogen-bonding group, using a reduced number of the functionalities, by introducing a longer alkyl tether between the aromatic core component and the functional group or by attaching better solubilizing alkyl chains in the corona of the aromatic core.

5.2 Extended PAHs

The extension of the aromatic core component is an important factor to increase the charge-carrier mobility values of discotic materials.[1] In addition, the covering of a wider part of the electromagnetic spectrum by absorption and the lowering of the HOMO-LUMO bandgap will also lead to other interesting electronic properties regarding the use of these materials in future device applications.

The generally used pathway for the preparation of such compounds required the initial synthesis of a dendritic oligophenylene precursor molecule, which was subsequently planarized by an intramolecular Scholl reaction. It was revealed in this thesis that with such an approach, several side-products occurred in the last synthetic step, mainly consisting of partially fused intermediates. All purification attempts for separating the fully planarized product failed. This required a novel synthetic concept by a prepalanarization of the center of the oligophenylene precursor to suppress the formation of the before mentioned side-products.

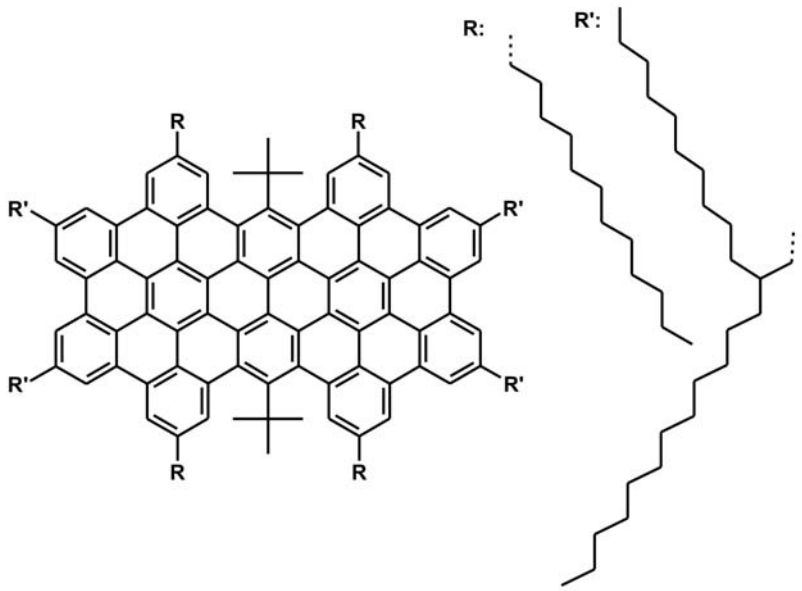

Figure 5-2: C72 derivative.

By this method, it was possible to synthesize an extended PAH (Figure 5-2), which contains 72 aromatic carbon atoms in its core. By the application of a variety of solubilizing features, including the distortion of the aromatic core and the introduction of bulky alkyl substituents in the corona of the aromatic moiety, one could achieve a material, which showed for the first time a well-resolved ^{1}H NMR spectrum of the aromatic hydrogens. The solubilization of the molecule was mainly focussing on the

reduction of the π-interactions of the aromatic core components, which is responsible for the aggregation phenomena in these compounds.

For the first time, a distinct thermal phase behavior could be demonstrated, including a high temperature phase, where the discs arranged homeotropically on the substrate surface. This arrangement is the favored orientation of the discs for an application in photovoltaic devices. Nevertheless, the π-interactions between the aromatic moieties were still strong enough to establish a well-ordered hexagonal columnar arrangement. This columnar self-assembly is one prerequisite for the intrinsic charge-carrier mobility of discotic compounds.

By concentration dependent measurements of the UV/vis and the photoluminsecence excitation as well as the emission spectra, it could be shown that the aggregation is not completely suppressed in solution. The removal of the *tert*-butyl groups resulted in a full planarization of the molecule, which led to a crystalline material with low solubility in common organic solvents.

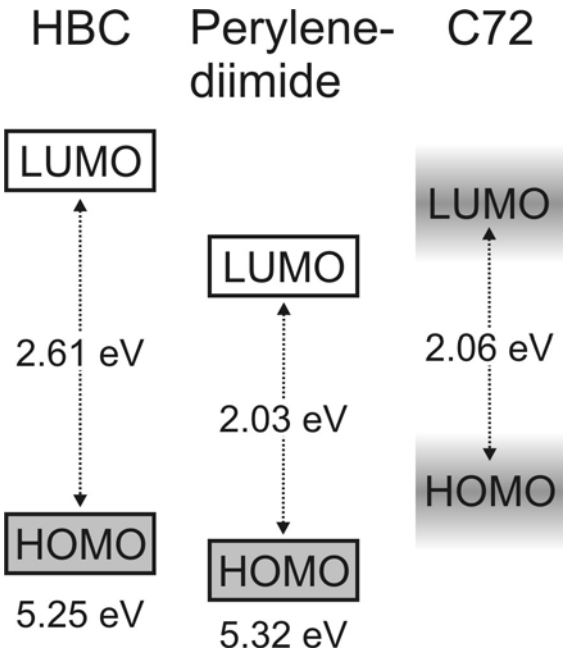

Figure 5-3: HOMO-LUMO bandgaps of HBC, perylene-diimide and the C72 derivative shown in Figure 5-2.

The electronic spectra of the C72 derivative shown in Figure 5-2, revealed that the p-band of the compound was located at 603 nm, which is identical to a HOMO-LUMO bandgap of 2.06 eV[2,3] and is similar to the one of perylene. It has to be pointed out that perylene is an electron acceptor materials, whereby C72 should act, similar to HBC, as

an electron donating system. So far, this is the first example known of a discotic donor material with such a low bandgap value of 2.06 eV. The difference between the two bandgaps consists only of 0.03 eV. If the assumed elevation of the HOMO of the C72 derivative compared to HBC, which has also been shown for other systems in the literature (Appendix I), is true, the C72 derivative would be another candidate for the donor component in a photovoltaic cell together with perylene as the acceptor component. In accordance to the low bandgap, the material showed a more than three times higher extinction coefficient than HBC and covers a far wider area of the electromagnetic spectrum, which makes it an even better candidate for such device applications.

5.3 References

[1] A. M. van de Craats, J. M. Warman *Adv. Mater.* **2001**, *13*, 130.

[2] E. Clar *Angew. Chem. Int. Ed.* **1956**, *68*, 528.

[3] E. Clar, O. Kuhn *Annalen der Chemie-Justus Liebig* **1956**, *601*, 181.

6 Experimental

6.1 General Methods

Chemicals and solvents:

The chemicals and solvents were obtained from the companies Fluka, Lancaster, Merck, Riedel-de Haen, Sigma-Aldrich, ABCR and Strem and used as obtained.

Chromatography:

Preparative column chromatography was performed on silica gel from Merck with a grain size of 0.04-0.063 mm (Geduran Si 60). For analytical thin layer chromatography (TLC) silica gel coated substrates 60 F254 from Merck were used. Compounds were detected by fluorescence quenching at 254 nm, self-fluorescence at 366 nm.

NMR spectroscopy:

^{1}H NMR and ^{13}C NMR spectra were recorded in CD_2Cl_2, $C_2D_2Cl_4$, d_8-THF, d_4-DMSO or d_4-o-dichlorobenzene on a Bruker DPX 250, Bruker AMX 300, Bruker DRX 500 or Bruker DPX 700 by using the solvent proton- or carbon-signal as internal standard.

Mass spectrometry:

FD mass spectra were obtained on a VG Instruments ZAB 2-SE-FPD. MALDI-TOF mass spectra were measured on a Bruker Reflex II-TOF spectrometer using a 337 nm nitrogen laser and 7,7,8,8-tetracyanoquinodimethane (TCNQ), 9-nitroanthracene, 1,8,9-trihydroxy anthracene (dithranol), trans-2-[3-(4-tert-butylphenyl)-2-methyl-2-propenylidene]malono- nitrile (BPMPM) as matrix.

UV/Vis spectroscopy:

UV/Vis spectra were recorded at room temperature on Perkin-Elmer Lambda 9 or Perkin-Elmer Lambda 5 spectrometers with chloroform or THF as solvent.

Quantum yields:

The quantum yields were determined by comparison of the investigated compounds dissolved in THF with a known standard (9,10-diphenylanthracene) at three different concentrations and according to Appendix H.

IR spectroscopy:

Infrared spectra were recorded on a Nicolet FT-IR 320 spectrophotometer as KBr pellets.

Elemental analysis:

Elemental analyses were carried out on a Foss Heraeus Vario EL at the Institute for Organic Chemistry at the Johannes-Gutenberg-University of Mainz. (Because of the high carbon content in large PAHs, combustion may be incomplete (soot formation), resulting sometimes in values lower than expected for the carbon content.)

Differential scanning calorimetry (DSC) and thermogravimetric analysis (TGA):

DSC was measured on a Mettler DSC 30 with heating and cooling rates of 10 K/min. First order transition temperatures were reported as the minima of their endothermic peaks during heating. For TGA a Mettler 500 thermogravimetric analyzer was used.

Polarization microscopy:

A Zeiss Axiophot with a nitrogen flushed Linkam THM 600 hot stage was used to perform polarization microscopy.

X-ray:

X-ray diffraction experiments were performed using a Siemens D 500 Kristalloflex with a graphite-monochromatized CuKα X-Ray beam, emitted from a rotating Rigaku RU-300 anode. 2D-WAXS measurements of oriented filaments were conducted using a rotating anode (Rigaku 18 kW) X-ray beam (CuKα, pinhole collimation, double graphite monochromator) and CCD camera. The patterns were recorded with vertical orientation of the filament axis and with the beam perpendicular to the filament.

Analytical HPLC:

The High Performance Liquid Chromatography was performed on a Hewlett-Packard HP 1100 system, equipped with a HP 1050 photo diode array detector. The column was

filled with Purospher Star RP18e reverse phase silica gel (particle size: 3 µm). As solvents HPLC-grade THF and millipore water were used.

6.2 Synthesis

6.2.1 Hexa-*peri*-hexabenzocoronene Derivatives

6.2.1.1 2,5-Bis-(4-bromo-phenyl)-3,4-bis-[4-(3,7-dimethyl-octyl)-phenyl]-cyclo penta-2,4-dienone (3-12)

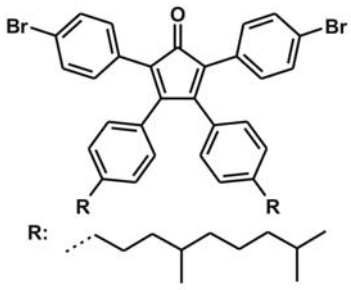

In a 100 ml 2-neck flask equipped with condenser and magnetic stirrer 4,4'-(3,7-dimethyloctyl)benzil (1.0 g, 1.43 mmol),[1] 1,3-bis-(4-bromophenyl)-propan-2-one (0.75 g, 1.43 mmol)[2] and 2.5 ml *tert*-butanol were combined and degassed. The solution was heated to 85 °C and tetrabutyl-ammoniumhydroxide (0.8 M in methanol, 1.42 ml) was quickly added. The reaction mixture was stirred at 85 °C for 20 min. under argon. The reaction was quenched with 10 ml of water and the aqueous phase extracted with dichloromethane. The combined organic phases were washed with water, dried over magnesium sulfate and the solvent was removed under reduced pressure. The crude product was purified by column chromatography (silica gel; eluent: petroleum ether: dichloromethane = 8: 2) to yield (**3-12**) as a violet oil (78%): ^{1}H-NMR (250 MHz, CD_2Cl_2, 293 K): δ = 7.35 (d, 4H, ^{3}J(H,H) = 8.63Hz, Ar-*H*), 7.08 (d, 4H, ^{3}J(H,H) = 8.65Hz, Ar-*H*), 6.99 (d, 4H, ^{3}J(H,H) = 8.20Hz, Ar-*H*), 6.78 (d, 4H, ^{3}J(H,H) = 8.20Hz, Ar-*H*), 2.70-2.40 (m, 4H, α-CH_2), 1.70-1.00 (m, 20H, -CH_2, -C*H*), 0.91-0.81 (m, 18H, -CH_3); ^{13}C-NMR (62 MHz, CD_2Cl_2, 293 K): δ = 200.31 (*C*O), 156.31, 145.21, 132.50, 131.92, 130.93, 130.66, 129.97, 128.83, 124.84, 122.32, 40.11, 39.34, 37.92, 34.08, 33.29, 28.79, 25.54, 23.27, 23.20, 20.17; MS (FD, 8 kV): m/z (%) = 822.8 (100%, M^+) (calc. for $C_{49}H_{58}Br_2O$ = 822.82 g mol^{-1}).

6.2.1.2 1,4-Bis-(4-bromo-phenyl)-2,3,5,6-tetrakis(3,7-dimethyloctylphen-1-yl)benzene (3-14)

In a dry 25 ml Schlenk tube equipped with condenser and magnetic stirrer a solution of 2,5-bis-(4-bromo-phenyl)-3,4-bis-[4-(3,7-dimethyl-octyl)-phenyl]-cyclopenta-2,4-dienone (**3-12**) (4.0 g, 4.86 mmol), 4,4'-bis-(3,7-dimethyloctyl)-diphenylacetylene (2.44 g, 5.32 mmol)[1] in 6 ml of diphenylether was degassed for 10 min. The solution was then

heated to reflux and stirred overnight. The diphenylether was removed *in vacuo* and the crude product was purified by column chromatography on silica gel (eluent: petroleum ether: dichloromethane = 20:1) to yield (**3-14**) as a colorless oil (90%): ^{1}H-NMR (250 MHz, CD_2Cl_2, 293 K): δ = 7.01 (d, 4H, ^{3}J(H,H) = 8.44Hz, Ar-*H*), 6.80-6.70 (m, 20H , Ar-*H*), 2.60-2.30 (m, 8H, α-C*H*$_2$), 1.70-1.00 (m, 40H, -C*H*$_2$, -C*H*), 1.00-0.80 (m, 36H, -C*H*$_3$); ^{13}C-NMR (62 MHz, CD_2Cl_2, 293 K): δ = 141.22, 141.01, 140.32, 138.46, 134.00, 132.03, 130.43, 127.61, 119.99, 40.27, 39.45, 37.98, 33.69, 32.89, 28.87, 25.59, 23.44, 23.37, 20.32; MS (FD, 8 kV): m/z (%) = 1256.2 (100%, M^+) (calc. for $C_{82}H_{108}Br_2$ = 1253.58 g mol^{-1}).

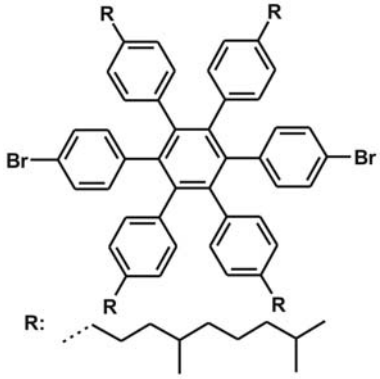

6.2.1.3 2,11-Dibromo-5,8,14,17-tetra-(3,7-dimethyloctyl)-hexa-*peri*-hexa-benzocoronene (3-15)

A 2 L three neck flask was charged with 1,4-bis-(4-bromo-phenyl)-2,3,5,6-tetrakis(3,7-dimethyloctylphen-1-yl)benzene (**3-14**) (1.25 g, 1.0 mmol) and 800 ml of dry dichloromethane. While bubbling argon through the solution, $FeCl_3$ (3.89 g, 23.9 mmol) dissolved in CH_3NO_2 (19 ml) was added and the mixture was stirred at room temperature for 40 min. The reaction was quenched by adding methanol and the precipitate was filtered and washed with methanol. The resulting brownish solid was dissolved in toluene and filtered through a short pad of silica gel and dried under vacuum to yield (**3-15**) as a brown, waxy solid (92 %): ^{1}H-NMR (500 MHz, CD_2Cl_2, 293 K): δ = 7.43 (s, 4H, Ar-*H*); 7.22 (s, 4H, Ar-*H*); 7.09 (s, 4H, Ar-*H*); 2.66 (s, 8H, α-C*H*$_2$), 2.10-0.70 (m, 76H, -C*H*$_2$, -C*H*$_3$, -C*H*); ^{13}C-NMR (125 MHz, CD_2Cl_2, 293 K): δ = 137.01, 128.04, 125.90, 124.87, 119.02, 115.01, 38.19, 37.63, 36.036, 32.73, 32.07, 26.52, 23.44, 21.12, 21.05, 18.34; MS (MALDI-TOF (TCNQ-matrix)): 1239.54 (11.4 %), 1240.54 (10.2 %), 1241.57 (21.9 %), 1242.55 (18.8 %), 1243.54 (18.5 %), 1244.52 (11.5 %), 1245.52 (5.4 %), 1246.48 (2.3 %) (calc. for $C_{82}H_{96}Br_2$ = 1241.49 g mol^{-1}, isotope distr.: 1238.59 (10.2 %), 1239.59 (9.4 %), 1240.59 (24.2 %), 1241.59 (19.7 %), 1242.59 (18.4 %), 1243.59 (11.6 %), 1244.59 (4.6 %), 1245.59 (1.3 %)); DSC: on heating: 100 °C endothermic, on cooling:

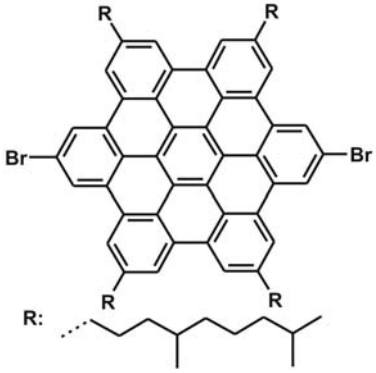

87 °C exothermic; UV/vis (THF, 293K): λ (nm) = 360 (1226 m^2 mol^{-1}); EA: C = 79.36 %, H = 7.83 % (calc.: C = 79.33 %, H = 7.79 %, Br = 12.87 %).

6.2.1.4 2,11-Di-(3-ethoxycarbonyl-propyl)-5,8,14,17-tetra-(3,7-dimethyl-octyl)-hexa-*peri*-hexabenzocoronene (3-16)

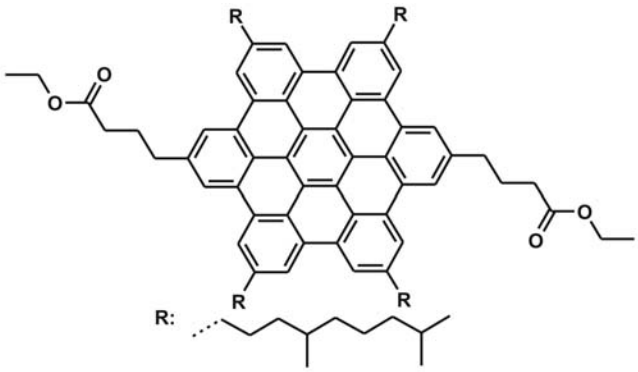

In a degassed and well dried 100 mL Schlenk tube, equipped with septum and magnetic stirrer, 2,11-dibromo-5,8,14,17-tetra-(3,7-dimethyloctyl)-hexa-*peri*-hexabenzocoronene (**3-15**) (0.5 g, 0.40 mmol) and 5 mol% $Cl_2Pd[dppf] \times CH_2Cl_2$ were evacuated for 30 min. After purging the flask with argon, a 0.5 M solution of 4-ethoxy-4-oxobutylzinc bromide in anhydrous THF (50 mL) was added. The reaction mixture was stirred under argon for 48 h at 50 °C and quenched with methanol. The resulting yellow precipitate was filtered off from solution and purified by flash chromatography on silica gel (eluent: petrol ether:CH_2Cl_2:ethyl acetate = 6:3:1) to yield (**3-16**) as a yellow solid (95%): ^{1}H-NMR (300 MHz, CD_2Cl_2, 293 K): δ = 8.50 (s, 12 H, Ar-*H*), 4.12 (q, 4H, ^{3}J(H,H) = 7.12Hz, -C*H*$_2$OCO), 3.30-2.80 (m, 12H, α-C*H*$_2$), 2.49 (t, 4H, ^{3}J(H,H) = 7.44Hz, -C*H*$_2$COO), 2.30-2.10 (m, 4H, -C*H*$_2$CH$_2$COO), 2.08-1.00 (m, 58H, -C*H*$_2$, -C*H*$_3$), 0.87 (d, 24H, ^{3}J(H,H) = 6.8 Hz, -CH(C*H*$_3$)$_2$); ^{13}C-NMR (75 MHz, CD_2Cl_2, 293 K): δ = 174.02 (*C*O), 140.18, 138.53, 129.71, 129.61, 129.52, 123.01, 121.09, 119.27, 61.00 (O*C*H$_2$), 41.04, 40.39, 38.37, 37.00, 35.52, 34.97, 34.29, 28.95, 25.88, 23.46; MS (MALDI-TOF (TCNQ-matrix)): 1310.25 (31.66 %),1311.25 (30.66 %), 1312.24 (20.83 %), 1313.24 (8.99 %), 1314.26 (4.57 %), 1315.24 (3.29 %) (calc. for $C_{94}H_{118}O_4$ = 1311.99 g mol^{-1}, isotope distr.: 1310.90 (34.40 %), 1311.91 (36.63 %), 1312.91 (19.57 %), 1313.91 (7.00 %), 1314.92 (1.88 %), 1315.92 (0.41 %)); DSC: on heating: 73 °C endothermic, on cooling: 27 °C exothermic; UV/vis (THF, 293K): λ (nm) = 362 (1052 m^2 mol^{-1}); EA: C = 86.22 %, H = 8.90 % (calc.: C = 86.06%, H = 9.07 %, O = 4.88 %).

6.2.1.5 2,11-Di-(4-carboxypropyl)-5,8,14,17-tetra-(3,7-dimethyloctyl)-hexa-*peri*-hexabenzocoronene (3-4)

In a 25 mL Schlenk tube equipped with a reflux-condenser, 4 ml of an aqueous 1N sodium hydroxide solution and 0.05 g/0.04 mmol of 2,11-di-(3-ethoxycarbonyl-propyl)-

5,8,14,17-tetra-(3,7-di-methyloctyl)-hexa-peri-hexabenzocoronene (**3-16**) in 4 mL of THF were degassed for 5 min. The reaction mixture was refluxed under argon for 96 h. After the mixture has cooled down to room temperature, a 1N aqueous hydrochloric acid solution was added until the pH of the mixture became neutral. The product was then extracted three times with dichloromethane and the combined organic phases were washed two times with water. The organic phase was dried with magnesium sulfate and finally the solvent was removed under reduced pressure to yield (**3-4**) as a dark yellow solid (99%). ^{1}H-NMR (500 MHz, o-$C_6D_4Cl_2$, 423 K): δ = 9.14 (s, 12H, Ar-*H*), 3.48 (s, 12H, α-C*H*$_2$), 2.78 (s, 4H, -C*H*$_2$-(CH$_2$)$_2$-COOH), 2.60 (s, 4H, -C*H*$_2$-COOH), 2.38 (s, 4H, -C*H*$_2$-CH$_2$-COOH), 2.19 (s, 4H, -C*H*-), 2.01 (s, 4H, -C*H*-), 1.90-1.25 (m, 32H, alkyl-C*H*$_2$), 1.11 (m, 36H, -C*H*$_3$); ^{13}C-NMR (solubility of compound too low for appropriate signal-to-noise ratio); MS (MALDI-TOF (TCNQ-matrix)): 1254.60 (34.8 %), 1255.58 (33.3 %), 1256.57 (19.4 %), 1257.54 (7.9 %), 1258.49 (4.7 %) (calc. for $C_{90}H_{110}O_4$ = 1255.88 g mol^{-1}, isotope distr.: 1254.84 (36.0 %), 1255.84 (36.7 %), 1256.85 (18.8 %), 1257.85 (6.4 %), 1258.85 (1.7 %)); UV/vis (THF, 293K): λ (nm) = 360 (1230 m^2 mol^{-1}); IR (KBr, 293 K): 2953.8, 2923.9, 2853.3, 1709.7 (-COOH), 1611.9, 1457.6, 1375.2, 852.9; EA: C = 86.15 %, H = 8.93 % (calc.: C = 86.08%, H = 8.83 %, O = 5.10 %).

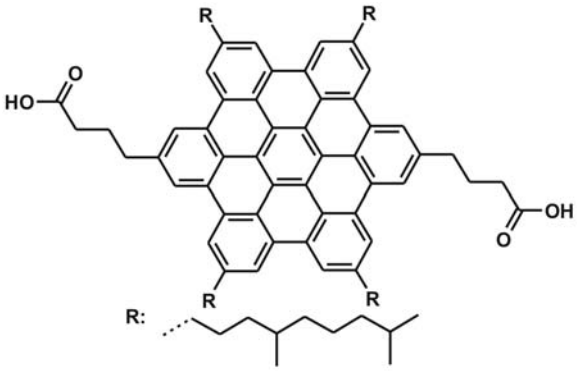

6.2.1.6 2,11-Di-(4-N-dodecyl-butyramide)-5,8,14,17-tetra-(3,7-dimethyl-octyl)-hexa-*peri*-hexabenzocoronene (3-24)

In a well-dried 25 ml Schlenk tube equipped with a reflux condenser a solution of 2,11-dibromo-5,8,14,17-tetra-(3,7-dimethyloctyl)-hexa-*peri*-hexabenzo-coronene (**3-15**) (0.1 g, 0.08 mmol) in dodecylamin (5 ml) was degassed for 5 min. The mixture was heated to 150 °C and stirred for 4 days under argon. The reaction was

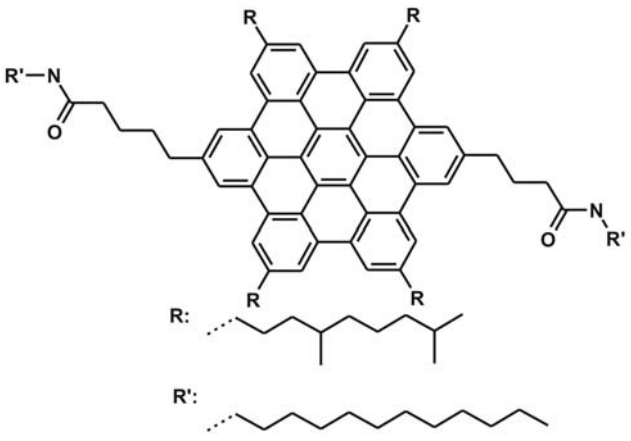

quenched with methanol. The precipitate was filtered, washed with methanol and dried in vacuo to yield (**3-24**) as a dark yellow solid (95 %): ^{1}H-NMR (500 MHz, $C_2D_2Cl_4$, 403 K): δ = 8.69 (s, 12H, Ar-*H*), 5.36 (s, 2H, -N*H*-), 3.25 (s, 16H, α-CH_2, NH-CH_2), 2.41 (s, 8H), 2.10 (s, 4H), 1.93 (s, 4H), 1.82 (s, 4H), 1.63 (s, 8H), 1.55-1.10 (m, 60H alkyl-CH_2), 1.05-0.75 (m, 42H, -CH_3); ^{13}C-NMR (125 MHz, $C_2D_2Cl_4$, 403 K): δ = 172.44 (*C*O), 141.24, 139.71, 130.61, 130.46, 130.37, 124.08, 123.87, 122.03, 121.95, 121.87, 121.76, 121.66, 120.19, 120.10, 39.81, 39.62, 37.75, 34.94, 33.44, 31.92, 30.12, 29.73, 29.62, 29.40, 29.28, 28.17, 27.19, 25.03, 22.76, 22.70, 22.63, 22.59, 20.07, 13.86, 40.14, 36.77, 31.97, 27.59; MS (MALDI-TOF (Dithranol)): 1590.20 (30.4 %), 1591.20 (32.1 %), 1592.20 (23.1 %), 1593.19 (9.9 %), 1594.19 (4.5 %) (calc. for $C_{114}H_{160}N_2O_2$ = 1590.56 g mol^{-1}, isotope distr.: 1589.25 (27,3 %), 1590.25 (35.5 %), 1591.25 (23.0 %), 1592.26 (9.9 %), 1593.26 (3.2 %)); DSC: on heating: 85 °C endothermic, on cooling: 80 °C exothermic; UV/vis (THF, 293K): λ (nm) = 367 (1816 m^2 mol^{-1}); EA: C = 84.50 %, H = 10.41 % (calc.: C = 86.09 %, H = 10.14 %, N = 1.76 %, O = 2.01 %).

6.2.1.7 2,11-Di-(4-ethoxycarbonylphenyl)-5,8,14,17-tetra-(3,7-dimethyloctyl)-hexa-*peri*-hexabenzocoronene (3-20)

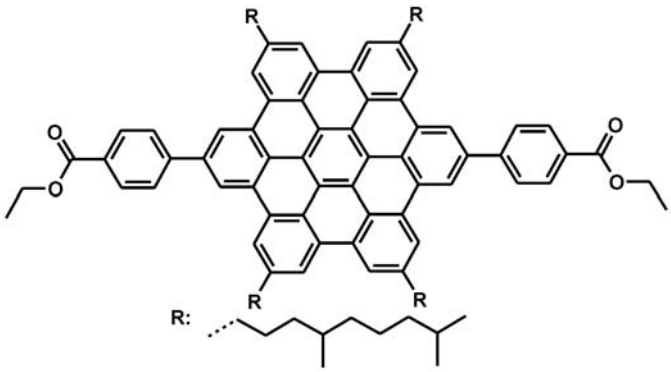

In a degassed and well dried 100 mL Schlenk tube, equipped with reflux condenser and magnetic stirrer, 2,11-dibromo-5,8,14,17-tetra-(3,7-dimethyl-octyl)-hexa-*peri*-hexabenzocoronene (**3-15**) (0.062 g, 0.050 mmol) and 5 mol% Cl_2Pd[dppf] x CH_2Cl_2 were evacuated for 30 min. After purging the flask with argon, a 0.5 M solution of 4-(ethoxycarbonyl)phenylzinc in anhydrous THF (20 mL) was added. The reaction mixture was refluxed for 5 d and quenched with methanol. The resulting yellow precipitate was filtered off, washed with methanol and purified by column chromatography on silica gel (eluent: petrol ether:CH_2Cl_2:ethyl acetate = 6:3:1) to yield (**3-20**) as a yellow solid (97%): ^{1}H-NMR (250 MHz, CD_2Cl_2, 293 K): δ = 8.50-6.90 (m, 20H, Ar-*H*), 4.54 (m, 4H, -COO-CH_2-CH$_3$), 2.36 (s, 8H, α-CH$_2$), 1.90-0.70 (m, 82H, alkyl-CH_2, C*H*, CH_3); ^{13}C-NMR (125 MHz, CD_2Cl_2, 293 K): δ = 166.47 (*C*O), 146.10, 144.53, 138.99, 131.80, 130.57, 130.38, 129.35, 128.88, 128.54, 128.38, 128.21, 128.13,

127.55, 127.44, 127.21, 121.52, 120.42, 120.34, 120.06, 118.70, 118.40, 118.31, 118.13, 117.93, 61.44 (-COO*C*H_2CH_3), 40.35, 39.88, 37.79, 34.82, 33.85, 30.07, 28.51, 25.47, 23.02, 22.89, 19.97, 14.73, 14.50; MS (MALDI-TOF (TCNQ-matrix)): 1379.75 (32.3 %), 1380.75 (32.9 %), 1381.75 (20.5 %), 1382.76 (8.9 %), 1383.78 (3.4 %), 1384.78 (1.8 %) (calc. for $C_{100}H_{114}O_4$ = 1380.02 g mol^{-1}, isotope distr.: 1378.87 (32.2 %), 1379.88 (36.4 %), 1380.88 (20.7 %), 1381.88 (7.8 %), 1382.89 (2.2 %), 1383.89 (0.5 %)); UV/vis (THF, 293K): λ (nm) = 368 (1618 m^2 mol^{-1}); EA: C = 86.93 %, H = 8.24 % (calc.: C = 87.04 %, H = 8.33 %, O = 4.64%).

6.2.1.8 2,11-Di-(4-benzoic acid)-5,8,14,17-tetra-(3,7-dimethyloctyl)-hexa-*peri*-hexabenzocoronene (3-21)

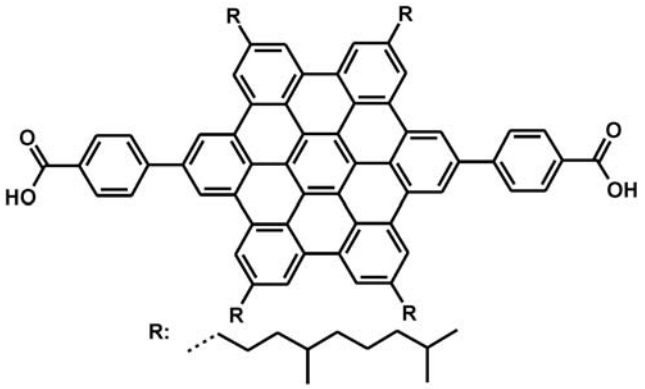

In a 25 mL Schlenk tube equipped with a reflux-condenser, 1 ml of an aqueous 5N sodium hydroxide solution and 0.05 g/0.04 mmol 2,11-di-(3-ethoxycarbonyl-propyl)-5,8,14,17-tetra-(3,7-di-methyl-octyl)-hexa-peri-hexabenzocoronene (**3-20**) in 12 mL of THF and 1 mL of methanol were degassed for 5 min. The reaction mixture was refluxed under argon for 96 h. After the mixture had cooled down to room temperature, a 1N aqueous hydrochloric acid solution was added until the pH of the mixture became neutral. The product was filtered off and washed with methanol. The solvent was removed under reduced pressure to yield (**3-21**) as a light yellow solid (95%): ^{1}H-NMR (solubility too low); ^{13}C-NMR (solubility too low); MS (MALDI-TOF (TCNQ-matrix)): 1323.17 (31.2 %), 1324.17 (35.6 %), 1325.22 (18.0 %), 1326.10 (10.1 %), 1327.22 (5.1 %) (calc. for $C_{96}H_{106}O_4$ = 1323.91 g mol^{-1}, isotope distr.: 1322.81 (33.7 %), 1323.81 (36.5 %), 1324.82 (19.9 %), 1325.82 (7.3 %), 1326.82 (2.0 %)); EA: C = 87.08 %, H = 8.12 % (calc.: C = 87.10 %, H = 8.07 %, O = 4.83 %).

6.2.1.9 2,11-Di-(3-ethoxycarbonyl-pentyl)-5,8,14,17-tetra-(3,7-dimethyloctyl)-hexa-*peri*-hexabenzocoronene (3-22)

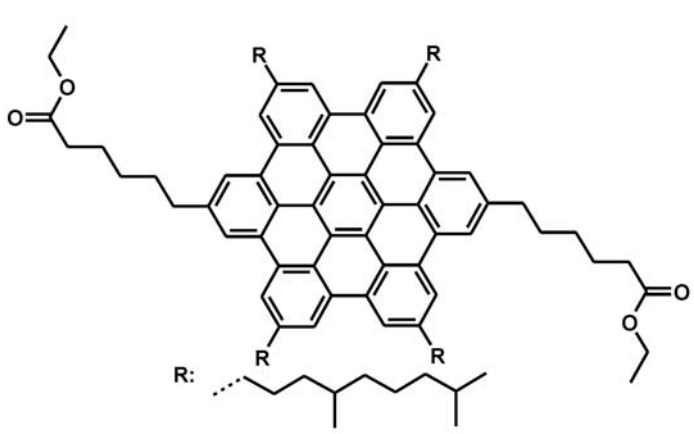

In a degassed and well dried 100 mL Schlenk tube, equipped with septum and magnetic stirrer, 2,11-dibromo-5,8,14,17-tetra-(3,7-di-methyloctyl)-hexa-*peri*-hexabenzo-coronene (**3-15**) (0.5 g, 0.40 mmol) and 5 mol% $Cl_2Pd[dppf]$ x CH_2Cl_2 were evacuated for 30 min. After purging the flask with argon, a 0.5 M solution of 4-ethoxy-4-oxobutylzinc bromide in anhydrous THF (50 mL) was added. The reaction mixture was stirred under argon for 48 h at 50 °C and quenched with methanol. The resulting yellow precipitate was filtered off from solution and purified by flash chromatography on silica gel (eluent: petrol ether:CH_2Cl_2:ethyl acetate = 6:3:1) to yield (**3-22**) as a yellow solid (92%): ^{1}H-NMR (250 MHz, CD_2Cl_2, 293 K): δ = 8.00 (s, 12H, Ar-*H*), 4.16 (q, 4H, ^{3}J(H,H) = 7.12Hz, -COOC*H*$_2$CH$_3$), 2.85 (s, 12H, α-C*H*$_2$), 2.43 (t, 4H, ^{3}J(H,H) = 7.40Hz, -C*H*$_2$COOEt), 2.10-1.10 (m, alkyl-CH2), 0.99 (d, 24H, ^{3}J(H,H) = 6.58Hz, -C*H*$_3$); ^{13}C-NMR (125 MHz, CD_2Cl_2, 293 K): 173.79 (*C*O), 140.03, 139.43, 129.41, 129.37, 122.83, 122.76, 120.92, 119.01, 60.48 (-COO*C*H$_2$CH$_3$), 40.54, 39.96, 37.92, 35.14, 34.78, 33.81, 30.08, 28.52, 25.58, 25.44, 23.02, 22.92, 20.12, 14.54; MS (MALDI-TOF (TCNQ-matrix)): 1367.91 (27.5 %), 1368.90 (29.7 %), 1369.88 (22.2 %), 1370.87 (12.0 %), 1372.87 (5.5 %), 1372.87 (3.1 %) (calc. for $C_{98}H_{126}O_4$ = 1368.09 g mol^{-1}, isotope distr.: 1366.97 (32.9 %), 1367.97 (36.5 %), 1368.97 (20.3 %), 1369.98 (7.6 %), 1370.98 (2.1 %), 1371.98 (0.5 %)); DSC: on heating: 73 °C endothermic, on cooling: 48 °C exothermic; UV/vis (THF, 293K): λ (nm) = 362 (1010 m^2 mol^{-1}); EA: C = 84.64 %, H = 9.49 % (calc.: C = 86.04 %, H = 9.28 %, O = 4.68 %).

6.2.1.10 2,11-Di-(4-carboxypentyl)-5,8,14,17-tetra-(3,7-dimethyloctyl)-hexa-*peri*-hexabenzocoronene (3-23)

In a 25 mL Schlenk tube equipped with a reflux-condenser, 1 ml of an aqueous 5N sodium hydroxide solution and 0.05 g/0.04 mmol 2,11-di-(3-ethoxycarbonyl-pentyl)-5,8,14,17-tetra-(3,7-di-methyloctyl)-hexa-peri-hexabenzocoronene (**3-22**) in 12 mL of THF and 1 mL of methanol were degassed for 5 min. The reaction mixture was refluxed

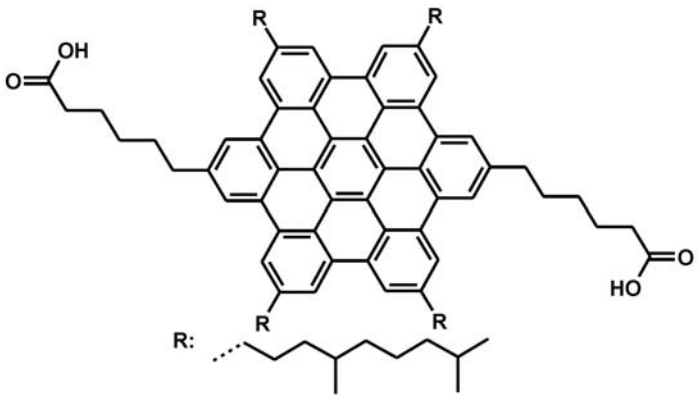

under argon for 96 h. After the mixture had cooled down to room temperature, a 1N aqueous hydrochloric acid solution was added until the pH of the mixture became neutral. The product was filtered off and washed with methanol. The solvent was removed under reduced pressure to yield (**3-23**) as a yellow solid (97%): ^{1}H-NMR (solubility too low); ^{13}C-NMR (solubility too low); MS (MALDI-TOF (TCNQ-matrix)): 1311.85 (33.5 %), 1312.85 (35.9 %), 1313.86 (19.2 %), 1314.86 (7.5 %), 1315.90 (3.9 %) (calc. for $C_{94}H_{118}O_4$ = 1311.99 g mol^{-1}, isotope distr.: 1310.90 (34.4 %), 1311.91 (36.6 %), 1312.91 (19.6 %), 1313.91 (7.0 %), 1314.92 (1.9 %)); EA: C = 86.06 %, H = 9.02 % (C = 86.06 %, H = 9.07 %, O = 4.88 %).

6.2.1.11 2'',3'',5''-Triphenyl-[1,2';1',1'';4'',1''']quaterphenyl (4-73)

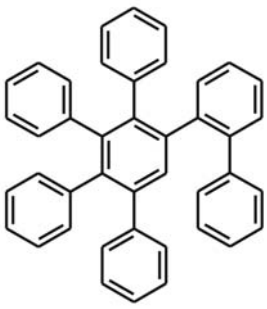

In a dry 25 ml Schlenk tube equipped with condenser and magnetic stirrer a solution of 2,3,4,5-tetraphenyl-cyclopenta-2,4-dienone (0.43 g, 1.12 mmol), 2-ethinylbiphenyl (0.20 g, 1.12 mmol)[3] in 6 ml of o-xylene was degassed for 10 min. The solution was then heated to reflux and stirred overnight. The o-xylene was removed *in vacuo* and the crude product was purified by column chromatography on silica gel (eluent: petroleum ether: toluene = 4:10) to yield (**4-73**) as a colorless solid (91%): ^{1}H-NMR (250 MHz, CD_2Cl_2, 293 K): δ = 7.50-6.50 (m, 29H, Ar-*H*), 5.89 (s, 1H, Ar-*H*); ^{13}C-NMR (62 MHz, CD_2Cl_2, 293 K): δ = 142.18, 141.95, 141.57, 141.20, 140.87, 140.62, 140.53, 140.42, 140.06, 139.84, 133.00, 132.20, 131.98, 131.93, 131.86, 131.64, 131.60, 131.54, 130.29, 130.12, 127.92, 127.80, 127.61, 127.10, 126.87, 126.78, 126.74, 126.51, 125.86, 125.56, 125.50, 119.18; MS (FD, 8 kV): m/z (%) = 534.2 (100%, M^+) (calc. for $C_{42}H_{30}$ = 534.71 g mol^{-1}).

6.2.1.12 Hexa-*peri*-hexabenzocoronene (4-75)

In a 100 mL Schlenk tube 2",3",5"-triphenyl-[1,2';1',1";4",1'"]quaterphenyl (0.192 g, 0.24 mmol) (**4-73**) was dissolved in 30 mL of dry dichloromethane. $FeCl_3$ (0.778 g, 4.8 mmol) in 3 ml of CH_3NO_2 was quickly added and the reaction was kept stirring for 40

min. while a constant flow of argon was led through the solution. The reaction was stopped by adding methanol. The resulting precipitate was filtered, washed with methanol and dried *in vacuo* to yield (**4-75**) as a dark yellow solid (68 %): MS (MALDI-TOF (TCNQ-matrix)): 522.45 (46.6 %), 523.45 (25.5 %), 524.47 (17.4 %), 525.45 (10.5 %) (calc. for $C_{42}H_{18}$ = 522.61 g mol^{-1}, isotope distr.: 522.14 (62.7 %), 523.14 (29.4 %), 524.15 (6.8 %), 525.15 (1 %)).

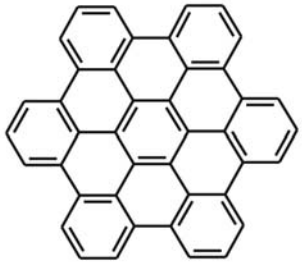

6.2.2 Hexabenzo-[jk,mn,pq,st:3,4:9,10]-phenantro-[1', 10',9',8':5,6, 7,8]-perylo-[2,11,12,11-bcdef]ovalen Derivatives (C72)

6.2.2.1 2,2'-Diethinyl-biphenyl (4-9)

Procedure A:

1) To a cooled solution (-78 °C) of diisopropylamine (1.5 ml) in dry THF (10.0 ml) 6.5 ml of a 1.6M solution of n-buthyllithium was slowly added under argon. The mixture was stirred for 3 min. and was allowed to warm up to 0 °C for 5 min. The solution was again cooled to -78 °C and 2,2'-diacetylbiphenyl (1.2 g, 5 mmol)[4,5] dissolved in 10 ml THF was added. The mixture was stirred for 1 h at -78 °C. Then diethylchlorophosphate (1.5 ml, 10.4 mmol) was added and the solution was allowed to warm up to room temperature and stirred for 30 min.

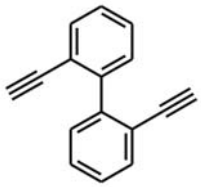

2) In a 250 ml Schlenk flask 14.1 ml of a 1.6 M solution of *n*-buthyl-lithium was slowly added to a cooled solution (-78 °C) of diisopropylamine (3.22 ml, 23.0 mmol) in 25 ml THF. The mixture was stirred for 3 min. and was then allowed to warm up to 0 °C for 5 min.

The solutions 1) and 2) were cooled to -78 °C and 1) was then added to solution 2) *via* a canula. The combined solutions were stirred for 5 min. at -78 °C and was then warmed up to room temperature and stirred for 1 h. Finally the mixture was poured onto 30 ml of water. The product was extracted three times with dichloromethane and the combined organic phases were washed two times with water. The organic phase was dried with magnesiumsulfate and the solvent was removed under reduced pressure. The crude product was purified by column chromatography on silica gel with a dichloromethane/hexane (2/8) mixture to yield (**4-9**) as a colorless solid (22 %).

Procedure B:

At 0 °C, 18.6 mL (30.0 mmol) of a 1.6 M *n*-BuLi solution in hexane was added to diisopropylamine (4.52 mL, 32.2 mmol). After stirring for 10 min, the resulting solution of LDA was cooled to −78°C and Me_3SiCHN_2 (2.0 M in hexane, 15.0 mL, 30.0 mmol) was added dropwise and kept stirring at this temperature for another 30 min. A solution of biphenyl-2,2'-dicarboxaldehyde (2.60 g, 12.4 mmol)[6] in 30 mL of dry THF was slowly added and the mixture was allowed to warm to room temperature at which it was kept for 3 h. The reaction was finished by adding water, and the crude product was extracted with *tert*-butyl-methyl ether. The product was purified chromatographically using silica gel and a hexane:dichloromethane (8:2) mixture to yield (**4-9**) as a colorless solid (57 %): ^{1}H-NMR (250 MHz, CD_2Cl_2, 293 K): δ = 7.50 (dd, 2H, ^{3}J(H,H) = 7.1 Hz, ^{3}J(H,H) = 1.1 Hz, Ar-*H*), 7.32-7.19 (m, 6H, Ar-*H*), 2.90 (s, 2H, -C≡C*H*); ^{13}C-NMR (63 MHz, CD_2Cl_2, 293 K): δ = 143.63, 133.42, 130.53, 128.80, 127.99, 121.84, 82.94, 80.83; MS (EI, 70 eV): m/z (%) = 203.4 (7.3 %, $[M^{+1}]^+$); 202.3 (44.1 %, $[M]^+$); 201.3 (19.0 % $[M^{-1}]^+$); 200.3 (21.5 % $[M^{-2}]^+$); 176.3 (4.0 % $[M-(HC\equiv C-)]^+$); 150.3 (4.0 % $[M-(HC\equiv C-)_2]^+$) (calc. for $C_{16}H_{10}$ = 202.26 g mol^{-1}).

6.2.2.2 1,2-Bis-biphenyl-4-yl-ethane-1,2-dione (4-32)

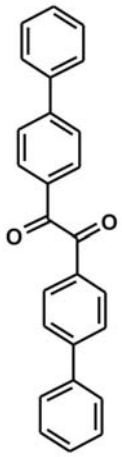

In a 500 ml 2-neck flask equipped with condenser a solution of 4,4'-dibromobenzil (2.2 g, 6.0 mmol), phenylboronic acid (3.8 g, 31.2 mmol), potassiumcarbonate (14.7 g, 106.4 mmol), 53 mL water, 106 mL toluene and 8.3 mL of ethanol was degassed for 10 min. $Pd(PPh_3)_4$ (0.66 g, 0.6 mmol) was quickly added and the reaction mixture was vigorously stirred overnight under argon at 80 °C. After the mixture had cooled to room temperature the product was extracted with toluene. The combined organic phases were dried with magnesuimsulfate and the solvent removed under reduced pressure. The crude product was purified by column chromatography (silica, petrolether/dichloromethane 1/1) to yield (**4-32**) as a yellow solid (85 %): ^{1}H-NMR (300 MHz, CD_2Cl_2, 293 K): δ = 8.11 (d, 4H, ^{3}J(H,H) = 8.5 Hz, Ar-*H*), 7.82 (d, 4H, ^{3}J(H,H) = 8.6 Hz, Ar-*H*), 7.71 (d, 4H, ^{3}J(H,H) = 6.8 Hz, Ar-*H*), 7.60-7.42 (m, 6H, Ar-*H*); ^{13}C-NMR (75 MHz, CD_2Cl_2, 293 K): δ = 194.57 (*C*O), 147.86, 139.77, 132.12, 130.79, 129.39, 129.02, 127.98, 127.69; MS (FD, 8 kV): m/z (%) = 362.7 (100%, M^+) (calc. for $C_{26}H_{18}O_2$ = 362.43 g mol^{-1}); EA: C = 87.48 %, H = 5.19 % (calc.: C = 86.17 %, H = 5.01 %, O = 8.83%).

6.2.2.3 1,3-Bis-biphenyl-4-yl-propan-2-one (4-34)

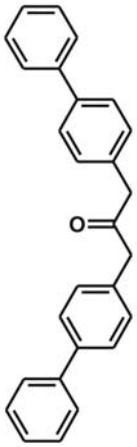

In a 500 ml 2-neck flask equipped with condenser a solution of 1,3-bis-(4-bromophenyl)-propan-2-one (2.2 g, 6.0 mmol),[2] phenylboronic acid (3.8 g, 31.2 mmol), potassiumcarbonate (14.7 g, 106.4 mmol), 53 mL water, 106 mL toluene and 8.3 mL of ethanol was degassed for 10 min. $Pd(PPh_3)_4$ (0.66 g, 0.6 mmol) was quickly added and the reaction mixture was vigorously stirred overnight under argon at 80 °C. After the mixture cooled to room temperature the product was extracted with toluene. The combined organic phases were dried with magnesuimsulfate and the solvent removed under reduced pressure. The crude product was purified by column chromatography (silica, petrolether/dichloromethane 1/1) to yield (**4-34**) as a colorless solid (84 %): ^{1}H-NMR (300 MHz, CD_2Cl_2, 293 K): δ = 7.66-7-55 (m, 8H, Ar-*H*), 7.50-7.41 (m, 4H, Ar-*H*), 7.40-7.32 (m, 2H, Ar-*H*), 7.27 (d, 4H, ^{3}J(H,H) = 8.2 Hz, Ar-*H*); ^{13}C-NMR (75 MHz, CD_2Cl_2, 293 K): δ = 205.662 (*C*O), 141.05, 140.20, 133.78, 130.46, 129.18, 127.71, 127.62, 127.35, 49.19 (Ar-*C*H_2-CO-); MS (FD, 8 kV): m/z (%) = 362.8 (100%, M^+) (calc. for $C_{27}H_{22}O$ = 362.48 g mol^{-1}); EA: C = 91.15 %, H = 5.99 % (calc.: C = 89.47 %, H = 6.12 %, O = 4.41 %).

6.2.2.4 (4-Dodecyl-phenyl)-trimethyl-silane (4-37)

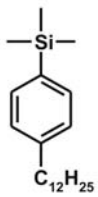

In a dry 1000 ml Schlenk flask equipped with septum 1-dodecene (53.4 ml, 238 mmol) and a 0.5 M solution of 9-BBN in THF (500 ml, 250 mmol) was stirred overnight under argon at room temperature. 118 ml of an aqueous NaOH solution (3 N) was added and the resulting mixture was vigorously stirred for 20 min. 1-Bromo-4-(trimethylsilyl)benzene (34.1 g, 149 mmol)[7] and $Pd(dppf)Cl_2$ (2.4 g, 3.3 mmol) were added and the reaction was stirred overnight at room temperature. The solvent was removed and the crude product purified by column chromatography (silica, petrolether) to yield (**4-37**) as a transparent oil (88 %): ^{1}H-NMR (250 MHz, CD_2Cl_2, 293 K): δ = 7.42 (d, 2H, ^{3}J(H,H) = 7.9 Hz, Ar-*H*), 7.15 (d, 2H, ^{3}J(H,H) = 7.9 Hz, Ar-*H*), 2.57 (t, 2H, ^{3}J (H,H) = 7.7 Hz, α-CH_2), 1.70-1.16 (m, 20H, -CH_2-), 0.88 (t, 3H, ^{3}J(H,H) = 6.5 Hz, alkyl-CH_3), 0.24 (s, 9H, -Si-(CH_3)$_3$); ^{13}C-NMR (63 MHz, CD_2Cl_2, 293 K): δ = 144.18, 137.43, 133.74, 128.31, 36.40, 32.44, 32.05, 30.19, 30.12, 30.03, 29.91, 29.88, 23.20, 14.39, 0.00; MS (FD, 8 kV): m/z (%) = 318.5 (100%, M^+) (calc. for $C_{21}H_{38}Si$ = 318.62 g mol^{-1}).

6.2.2.5 (4-Dodecyl-phenyl)-boronic acid (4-38)

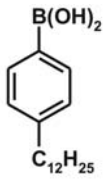

In a dry 500 ml Schlenk flask equipped with septum 4-dodecyl-phenyl)-trimethyl-silane (10.0 g, 31.4 mmol) (**4-37**) was dissolved in 350 ml of dry dichloromethane. The resulting solution was degassed for 5 min. Over a period of 15 min. borontribromide (47.0 ml, 47.0 mmol, 1 M in CH_2Cl_2) was added and the mixture was stirred under argon for 3 h at room temperature. The reaction was quenched by adding 125 ml of water. The water phase was extracted two times with dichloromethane, the combined organic phases were extracted two times with water and dried with magnesiumsulfate. The solvent was removed under reduced pressure to yield (**4-38**) as a light brown solid. The crude product was used without further purification: MS (FD, 8 kV): 1632.7 (25 %, $[(M_{trimer})_2]^+$), 817.1 (100 %, $[M_{trimer}]^+$), 741.0 (72 %), 648 (26 %).

6.2.2.6 1,2-Bis-(4'-dodecyl-biphenyl-4-yl)-ethane-1,2-dione (4-39)

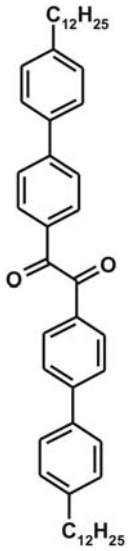

In a 500 ml 2-neck flask equipped with condenser a solution of 4,4'-dibromobenzil (2.2 g, 6.0 mmol), (4-dodecyl-phenyl)-boronic acid (7.0 g, 24.0 mmol) (**4-38**), potassiumcarbonate (14.7 g, 106.4 mmol), 53 mL water, 106 mL toluene and 8.3 mL of ethanol was degassed for 10 min. $Pd(PPh_3)_4$ (0.66 g, 0.6 mmol) was quickly added and the reaction mixture was vigorously stirred overnight under argon at 80 °C. After the mixture had cooled to room temperature the product was extracted with toluene. The combined organic phases were dried with magnesuimsulfate and the solvent removed under reduced pressure. The crude product was purified by column chromatography (silica, petroleum ether:dichloromethane 1:1; R_f = 0.67) to yield (**4-39**) as a yellow solid (54 %) with NMR suggesting a minor amount of impurities. The material was used without further purification: ^{1}H-NMR (250 MHz, CD_2Cl_2, 293 K): δ = 8.20-8.00 (m, 4H, Ar-*H*), 7.90-7.75 (m, 4H, Ar-*H*), 7.70-7.24 (m, 8H, Ar-*H*), 2.84-2.60 (m, 4H, α-C*H*$_2$), 1.82-1.60 (m, 4H, β-C*H*$_2$), 1.50-1.20 (m, 36H, alkyl-C*H*$_2$), 1.00-0.87 (m, 6H, -CH$_2$C*H*$_3$); ^{13}C-NMR (75 MHz, CD_2Cl_2, 293 K): δ = 194.66 (*C*O), 148.20, 147.89, 144.42, 139.78, 137.05, 132.14, 131.96, 130.83, 130.79, 129.55, 129.32, 129.23, 128.02, 127.85, 127.72, 127.55, 125.05, 36.38, 36.02, 32.36, 31.98, 31.84, 30.09, 30.03, 29.93, 29.79, 23.12, 14.30; MS (FD, 8 kV): m/z (%) = 699.1 (90%, $[M]^+$), 349.6 (10 %, $[M]^{2+}$) (calc. for $C_{50}H_{66}O_2$= 699.08 g mol^{-1}).

6.2.2.7 1,3-Bis-(4'-dodecyl-biphenyl-4-yl)-propan-2-one (4-40)

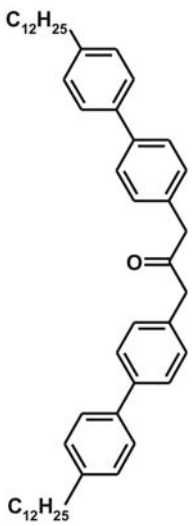

In a 500 ml 2-neck flask equipped with condenser a solution of 1,3-bis-(4-bromophenyl)-propan-2-one (2.2 g, 6.0 mmol),[2] (4-dodecyl-phenyl)-boronic acid (7.0 g, 24.0 mmol) (**4-38**), potassiumcarbonate (14.7 g, 106.4 mmol) in 53 ml of water, toluene (106 ml) and 8.3 ml of ethanol was degassed for 10 min. $Pd(PPh_3)_4$ (0.66 g, 0.6 mmol) was quickly added and the reaction mixture was vigorously stirred overnight under argon at 80 °C. After the mixture cooled to room temperature, the product was extracted with toluene. The combined organic phases were dried with magnesiumsulfate and the solvent removed under reduced pressure. The crude product was purified by column chromatography (silica, petrolether:dichloromethane 3:2; R_f = 0.46) to yield (**4-40**) as a colorless solid (45 %) with NMR suggesting a minor amount of impurities. The material was used without further purification: ^{1}H-NMR (250 MHz, CD_2Cl_2, 293 K): δ = 7.60-7.00 (m, 16H, Ar-*H*), 3.73 (s, 4H, -C*H*$_2$COC*H*$_2$-), 2.70-2.45 (m, 4H, α-C*H*$_2$), 1.65-1.45 (m, 4H, β-C*H*$_2$), 1.40-1.05 (m, 36H, alkyl-C*H*$_2$), 0.90-0.70 (m, 6H, -C*H*$_3$); ^{13}C-NMR (63 MHz, CD_2Cl_2, 293 K): δ = 205.72 (*C*O), 144.05, 142.77, 140.95, 140.45, 140.16, 138.27, 133.63, 133.42, 130.37, 129.24, 129.01, 127.83, 127.62, 127.50, 127.40, 127.10, 124.61, 49.17 (Ph-*C*H$_2$-CO), 36.39, 35.92, 32.32, 32.01, 31.93, 30.06, 29.10, 29.91, 29.75, 23.08, 14.26; MS (FD, 8 kV): m/z (%) = 699.1 (86%, $[M]^+$), 349.6 (14 %, $[M]^{2+}$) (calc. for $C_{51}H_{70}O$ = 699.13 g mol^{-1}).

6.2.2.8 4,4'-Bis(4-*n*-dodecylphen-1-yl)diphenylacetylene (7-1)

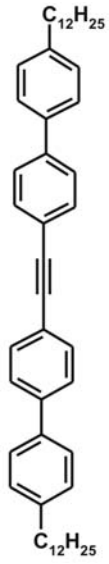

In a 2000 ml 3-neck flask equipped with dropping funnel and condenser, a solution of (4-dodecyl-phenyl)-boronic acid (45.0 g, 155 mmol) (**4-38**), potassiumcarbonate (94.8 g, 686 mmol) in 342 ml water, 480 ml toluene and 54.0 ml ethanol was degassed for 10 min. $Pd(PPh_3)_4$ (4.26 g, 3.7 mmol) was quickly added and the solution was heated to 80 °C. 4,4'-dibromodiphenylacetylene (13.0 g, 38.7 mmol)[8] was dissolved in 200 ml of toluene and added dropwise to the reaction solution *via* the dropping funnel. The complete solution was vigorously stirred overnight under argon at 80 °C. The hot water phase was removed and the toluene phase washed with 500 ml water. The organic phase was dried over magnesiumsulfate and the hot solution filtered over a short silica pad. On cooling a colorless solid precipitated, which

was filtered off and washed with cold toluene and petroleum ether to yield (**7-1**) as a colorless solid (49 %): ^{1}H-NMR (500 MHz, $C_2D_2Cl_4$, 413K): δ = 7.80-7.40 (m, 12H, Ar-*H*), 7.30-7.20 (s, 4H, Ar-*H*), 2.75-2.60 (s, 4H, α-C*H*$_2$), 1.78-1.62 (s, 4H, β-C*H*$_2$), 1.50-1.20 (m, 36H, alkyl-C*H*$_2$), 0.91 (s, 6H, -C*H*$_3$); ^{13}C-NMR (125 MHz, $C_2D_2Cl_4$, 413K): δ = 143.13, 141.45, 138.02, 132.57, 129.32, 127.31, 127.23, 122.69, 90.76, 36.08, 32.36, 31.51, 30.09, 29.97, 29.83, 29.70, 29.63, 23.05, 14.43; MS (FD, 8 kV): m/z (%) = 666.7 (100 %, $[M]^+$), 333.4 (25 %, $[M]^{2+}$) (calc. for $C_{50}H_6$ = 667.08 g mol^{-1}).

6.2.2.9 2,3,4,5-Tetrakis-(4'-dodecyl-biphenyl-4-yl)-cyclopenta-2,4-dienone (4-27)

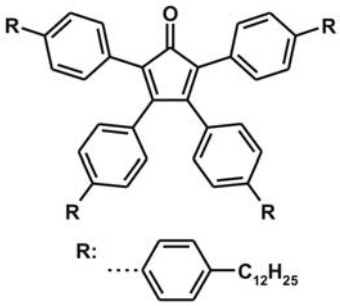

In a 50 ml 2-neck flask equipped with condenser a solution of 1,2-bis-(4'-dodecyl-biphenyl-4-yl)-ethane-1,2-dione (1 g, 1.43 mmol), 1,3-bis-(4'-dodecyl-biphenyl-4-yl)-propan-2-one (1 g, 1.43 mmol) in 7 ml *tert*-butanol was degassed for 15 min. The solution was heated to 80 °C and a solution of tetrabutylammoniumhydroxide (0.8 M in methanol, 1.0 ml) was quickly added. The reaction mixture was stirred for 20 min. at 80 °C under argon. The reaction was quenched with 10 ml of water and the solution extracted with dichloromethane. The organic phase was washed with water, dried with magnesiumsulfate and the solvent was removed under reduced pressure. The crude product was purified by column chromatography on silica with a petroleum ether/dichloromethane solvent mixture (3/2; R_f = 0.76) to yield (**4-27**) as a dark violet solid (72 %): ^{1}H-NMR (250 MHz, CD_2Cl_2, 293 K): δ = 7.48-6.94 (m, 32H, Ar-*H*), 2.60-2.46 (m, 8H, α-C*H*$_2$), 1.62-1.40 (s, w, 8H, β-C*H*$_2$), 1.35-1.05 (m, 72H, alkyl-C*H*$_2$), 0.78 (t, 12H, ^{3}J(H,H) = 6.3 Hz, -C*H*$_3$); ^{13}C-NMR (63 MHz, CD_2Cl_2, 293 K): 200.68 (*C*O), 154.69, 144.14, 144.06, 143.22, 142.91, 141.71, 141.41, 140.79, 140.64, 140.34, 138.11, 137.65, 132.51, 132.31, 130.99, 130.41, 130.23, 129.32, 129.28, 129.09, 129.05, 127.44, 127.35, 127.05, 126.10, 126.89, 126.78, 126.63, 125.56, 125.64, 124.56, 36.42, 35.96, 32.06, 31.93, 31.88, 32.35, 30.09, 29.78, 29.94, 23.11, 14.31; MS (FD, 8 kV): m/z (%) = 1360.8 (100%, $[M]^+$) (calc. for $C_{101}H_{132}O$ = 1362.18 g mol^{-1}).

6.2.2.10 2,3,4,5,2''',3''',4''',5'''-Octa-(4-dodecyl-biphenyl)-[1,1';2',1'';2'',1''']quaterphenyl (4-43)

In a dry 25 ml Schlenk tube equipped with condenser a solution of 2,3,4,5-tetrakis-(4'-dodecyl-biphenyl-4-yl)-cyclopenta-2,4-dienone (0.68 g, 0.5 mmol) (**4-27**), 2,2'-

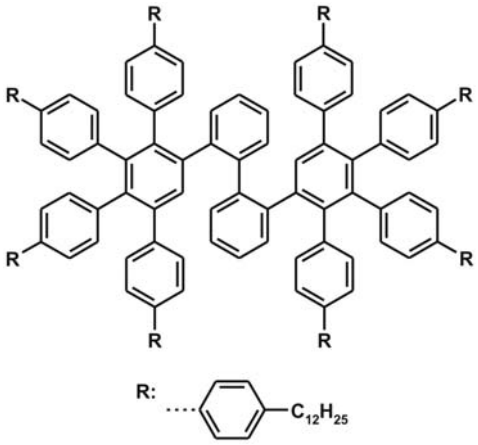

diethynyl-biphenyl (0.05 g, 0.25 mmol) (**4-9**) in 4 ml of diphenylether was degassed for 10 min. The solution was then heated to reflux and stirred overnight. The diphenylether was removed *in vacuo* and the crude product was purified by column chromatography (petroleumether:dichloro-methane 3:1 on silica gel) to yield (**4-43**) as a colorless viscous oil (95 %): ^{1}H-NMR (250 MHz, CD_2Cl_2, 293 K): δ = 7.65-6.55 (m, 74H, Ar-*H*), 2.60-2.32 (m, 16H, α-CH_2), 1.65-1.00 (m, 160H, alkyl-CH_2), 0.78 (t, 24H, ^{3}J(H,H) = 6.13 Hz, alkyl-CH_3); ^{13}C-NMR (63 MHz, CD_2Cl_2, 293 K): δ = 145.00-123.00 (Ar-*C*), 35.85, 32.34, 31.90, 30.07, 29.91, 29.77, 23.10, 14.30; MS (FD, 8 kV): m/z (%) = 1435.0 (31%, $[M]^{2+}$), 2869.6 (100%, $[M]^{+}$) (calc. for $C_{216}H_{274}$ = 2870.59 g mol^{-1}).

6.2.2.11 1,2-Bis-(4-dodecyl-phenyl)-ethane-1,2-dione

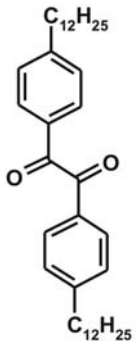

In a dry 500 ml Schlenk flask equipped with septum 1-dodecene (20.0 ml, 90.1 mmol) and a 0.5 M solution of 9-BBN in THF (190 ml, 95.0 mmol) was stirred overnight under argon at room temperature. 45.0 ml of an aqueous NaOH solution (3 N) was added and the resulting mixture was vigorously stirred for 20 min. 4,4'-dibromobenzil (10.0 g, 27.17 mmol) and Pd(dppf)Cl_2 (0.92 g, 1.27 mmol) were added and the reaction was stirred for 5 h at room temperature. The solvent was removed *in vacuo* and the resulting slurry was extracted with water and dichloromethane. The combined organic phases were dried with magnesiumsulfate and after removing the solvent, the crude product was purified by column chromatography (silica, petrolether:dichloromethane 3:1) to yield 1,2-bis-(4-dodecyl-phenyl)-ethane-1,2-dione as a yellow solid (64 %): ^{1}H-NMR (300 MHz, CD_2Cl_2, 293 K): δ = 7.85 (d, 4H, ^{3}J(H,H) = 8.35 Hz, Ar-*H*), 7.33 (d, 4H, ^{3}J(H,H) = 8.38 Hz, Ar-*H*), 2.67 (t, 4H, ^{3}J(H,H) = 7.7 Hz, α-CH_2), 1.75-1.10 (m, 40H, alkyl-CH_2), 0.88 (t, 6H, ^{3}J(H,H) = 6.7 Hz, -CH_3); ^{13}C-NMR (75 MHz, CD_2Cl_2, 293 K): δ = 195.00 (*C*O), 151.63, 131.20, 130.25, 129.47, 36.54, 32.31, 31.42, 30.02, 29.93, 29.81, 29.74, 29.63, 23.08, 14.27; MS (FD, 8 kV): m/z (%) = 273.4 (61 %, $[M]^{2+}$), 546.7 (100%, $[M]^{+}$) (calc. for $C_{38}H_{58}O_2$ = 546.88 g mol^{-1}).

6.2.2.12 1,3-Bis(4-dodecylphen-1-yl)propan-2-one

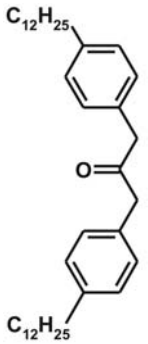

In a dry 500 ml Schlenk flask equipped with septum 1-dodecene (16.0 ml, 72.1 mmol) and a 0.5 M solution of 9-BBN in THF (150 ml, 75.0 mmol) was stirred overnight under argon at room temperature. 36.0 ml of an aqueous NaOH solution (3 N) was added and the resulting mixture was vigorously stirred for 20 min. Then bis(4-bromophen-1-yl)propan-2-on (9.4 g, 25.50 mmol) and Pd(dppf)Cl_2 (0.73 g, 1.00 mmol) were added and the reaction was stirred for 5 h at room temperature. The solvent was removed *in vacuo* and the resulting slurry was extracted with water and dichloromethane. The combined organic phases were dried with magnesiumsulfate and after removing the solvent, the crude product was purified by column chromatography (silica, petrolether:dichloromethane 3:1) to yield 1,3-bis(4-dodecylphen-1-yl)propan-2-one as a colorless solid (56 %): ^{1}H-NMR (250 MHz, $CDCl_3$, 293 K): δ = 7.15 (d, 4H, ^{3}J(H,H)=8.0 Hz, Ar-C*H*), 7.07 (d, 4H, ^{3}J(H,H) = 8.0 Hz, Ar-C*H*), 3.69 (s, 4H, OC-CH_2), 2.60 (t, 4H, ^{3}*J*=7.4 Hz, α-CH_2), 1.10-1.70 (m, 40H, alkyl-CH_2), 0.91 (t, 6H, ^{3}J(H,H) = 6.9 Hz, -CH_3); ^{13}C-NMR (75 MHz, CD_2Cl_2, 293 K): δ = 206.28 (*C*O), 142.11, 131.81, 129.76, 128.95, 49.03 (Ph-*C*H_2-CO, 35.90, 32.33, 31.96, 30.08, 29.92, 29.76, 23.10, 14.30; MS (FD, 8 kV): m/z (%) = 546.9 (100%, $[M]^+$) (calc. for $C_{39}H_{62}O$ = 546.93 g mol^{-1}).

6.2.2.13 2,3,4,5,2''',3''',4''',5'''-Octa-(4-dodecyl-phenyl)-[1,1';2',1'';2'',1'''] quaterphenyl (4-41)

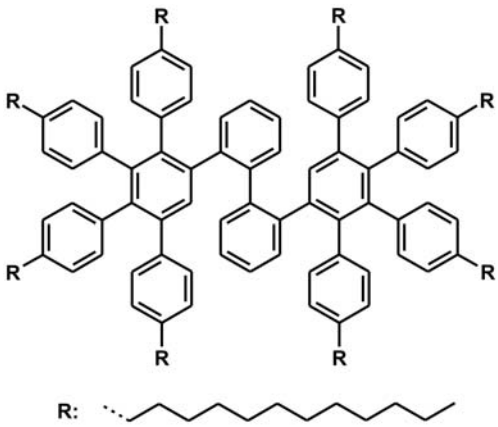

In a dry 25 ml Schlenk tube equipped with condenser a solution of 2,3,4,5-tetrakis-(4-dodecyl-phenyl)-cyclopenta-2,4-dienone (0.5 g, 0.53 mmol),[9] 2,2'-diethynyl-biphenyl (0.053 g, 0.26 mmol) (**4-9**) in 2 ml of diphenylether was degassed for 10 min. The solution was then heated to reflux and stirred overnight. The diphenylether was removed *in vacuo* and the crude product was purified by column chromatography (petroleumether:toluene 10:1 on silica gel) to yield (**4-41**) as a transparent oil (89 %): ^{1}H-NMR (300 MHz, CD_2Cl_2, 293 K): δ = 7.50-6.10 (m, 42H, Ar-C*H*), 2.60-2.20 (m, 16H, α-CH_2), 1.70-1.00 (m, 160H, alkyl-CH_2), 0.90 (t, 24H, ^{3}J(H,H) = 6.6 Hz, -CH_3); ^{13}C-NMR (75 MHz, CD_2Cl_2, 293 K):

145.00-125.00 (Ar-*C*), 35.85, 32.34, 31.90, 29.91, 30.07, 29.77, 23.10, 14.30; MS (FD, 8 kV): m/z (%) = 1131.3 (11%, $[M]^{2+}$)2261.8 (100%, $[M]^{+}$) (calc. for $C_{168}H_{242}$ = 2261.80 g mol^{-1}).

6.2.2.14 2,3,4,5,2''',3''',4''',5'''-Octa-[4-(3,7dimethyloctyl)-phenyl]-[1,1';2',1'';2'', 1'''] quaterphenyl (4-42)

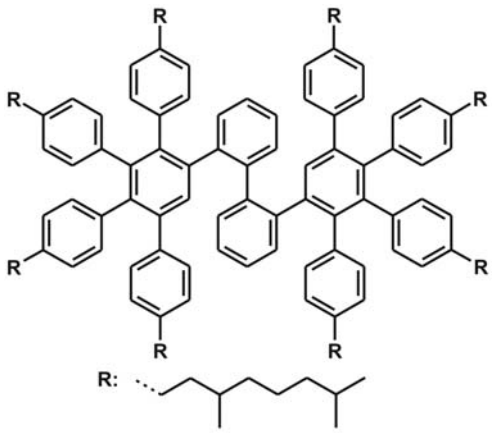

In a dry 25 ml Schlenk tube equipped with condenser a solution of 2,3,4,5-tetrakis-(4-(3,7-dimethyloctanyl)phen-1-yl)-cyclopenta-2,4-dienone (0.5 g, 0.53 mmol),[1] 2,2'-diacetylenbiphenyl (0.053 g, 0.26 mmol) (**4-9**) in 2 ml of diphenylether was degassed for 10 min. The solution was then heated to reflux and stirred overnight. The diphenylether was removed in vacuo and the crude product was purified by column chromatography (petroleumether:toluene 10:1 on silica gel) to yield (**4-42**) as a transparent viscous oil (95 %): ^{1}H-NMR (250 MHz, $CDCl_3$, 293 K): δ = 7.80-6.40 (m, 40H, Ar-*H*), 6.02 (s, 2H, Ar-*H*), 2.60 (s, w, 16H, α-CH_2), 2.00-0.90 (m, 152H, alkyl-CH_2, -CH_3); ^{13}C-NMR (75 MHz, CD_2Cl_2, 293 K): 142-137 (m), 134-129 (m), 128-125 (m), 39.93, 37.74, 37.69, 28.53, 25.30, 25.27, 23.13, 23.05, 19.99; MS (FD, 8 kV): m/z (%) = 2039.3 (100%, $[M]^{+}$) (calc. for $C_{152}H_{210}$ = 2037.37 g mol^{-1}).

6.2.2.15 2,2'-Bis(9,12-diphenyl-benzo[e]pyrene-10-yl)-biphenyl (4-96)

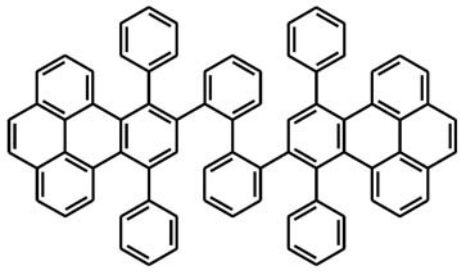

In a dry 25 ml Schlenk tube equipped with a condenser a solution of 1,3-diphenyl-cyclopenta[e]pyren-2-one (0.100 g, 0.24 mmol),[10] 2,2'-diacetylenbiphenyl (0.025 g, 0.12 mmol) (**4-9**) in 3 ml of diphenylether was degassed for 10 min. The solution was then heated to reflux and stirred overnight. The reaction was quenched with methanol and the resulting colorless precipitate was filtered off and washed with methanol. The product was purified by column chromatography (silica, petroleum ether:dichloromethane 7:3) dried *in vacuo* (85 %): ^{1}H-NMR (500 MHz, $C_2D_2Cl_4$, 413 K): δ = 7.91 (m, 8H, Ar-*H*), 7.82 (d, 2H, ^{3}J=7.9 Hz, Ar-*H*), 7.55 (s, 2H, Ar-*H*), 7.39 (t, 2H, ^{3}J=7.9 Hz, Ar-*H*), 7.25-6.50 (m, 32H,

Ar-*H*); ^{13}C-NMR: solubility too low; MS (FD, 8 kV): m/z (%) = 959.1 (100%, $[M]^+$) (calc. for $C_{76}H_{46}$ = 959.21 g mol^{-1}).

6.2.2.16 2-(9,12-Diphenyl-benzo[e]pyrene-10-yl)-2'-(2,3,4,5-tetraphenylbenzene)-biphenyl (4-93)

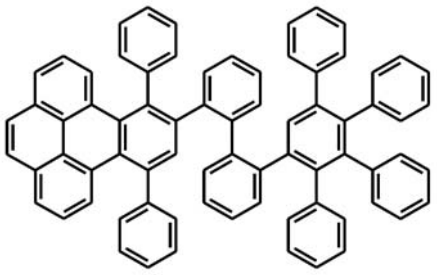

In a dry 25 ml Schlenk tube equipped with condenser a solution of 1,3-diphenylcyclopenta[e]-pyren-2-one (0.10 g, 0.24 mmol),[10] 2''-ethynyl-2,3,4,5-tetraphenyl-[1,1';2',1''] terphenyl (0.13 g, 0.34 mmol) (**4-9**) in 3 ml of diphenylether was degassed for 10 min. The solution was then heated to reflux and stirred overnight. The reaction was quenched with methanol and the resulting colorless precipitate was filtered off and washed with methanol. The product was purified by column chromatography (silica, petroleum ether:dichloromethane 7:3) dried in vacuo (92 %): ^{1}H-NMR (500 MHz, $CDCl_3$, 413 K): δ = 7.91 (d, 1H, ^3J=7.7 Hz, Ar-*H*), 7.87 (m, 3H, Ar-*H*), 7.81 (d, 1H, ^3J=7.2 Hz, Ar-*H*), 7.67 (s, 1H, Ar-*H*), 7.37 (t, 1H, ^3J=7.8 Hz, Ar-*H*), 7.30-7.13 (m, 6H, Ar-*H*), 7.10-6.35 (m, 35H, Ar-*H*); ^{13}C-NMR: solubility too low; MS (FD, 8 kV): m/z (%) = 936.7 (100%, $[M]^+$) (calc. for $C_{74}H_{48}$ = 937.2 g mol^{-1}).

6.2.2.17 2,2'-Bis(2,7-di-tert-butyl-9,12-diphenyl-benzo[e]pyrene-10-yl)-biphenyl (4-97)

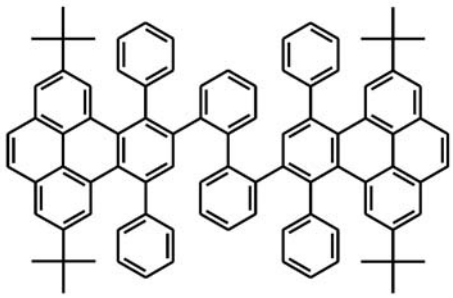

In a dry 25 ml Schlenk tube equipped with condenser a solution of 2,7-di-tert-butyl-9,11-diphenyl-cyclo-penta[e]pyren-10-one (0.35 g, 0.68 mmol),[11] 2,2'-diacetylenbiphenyl (0.068 g, 0.34 mmol) (**4-9**) in 3 ml of diphenylether was degassed for 10 min. The solution was then heated to reflux and stirred overnight. The reaction was quenched with methanol, the resulting colorless precipitate was filtered off and washed with methanol. The product was purified by column chromatography (silica, petroleum ether:dichloromethane 8:2) dried in vacuo (83 %): ^{1}H-NMR (500 MHz, CD_2Cl_2, 300 K): δ = 8.32 (s, 2H, Ar-*H*), 8.17 (s, 2H, Ar-*H*), 8.10-7.85 (m, 8H, Ar-*H*), 7.80-7.10 (m, 24H, Ar-*H*), 7.05-6.60 (m, 6H, Ar-*H*), 1.19 (s. 36H, -C*H*$_3$); ^{13}C-NMR (125 MHz, CD_2Cl_2, 300 K): 147.73, 147.59, 146.05, 143.92, 140.36, 140.05, 139.29, 138.91, 133.89, 133.73, 133.53, 131.85, 131.62, 131.02, 130.98,

129.90, 129.73, 129.28, 128.93, 127.81, 127.68, 127.57, 127.48, 127.29, 126.60, 126.38, 125.95, 123.95, 123.59, 122.59, 31.81, 31.66; MS (FD, 8 kV): m/z (%) = 1185.1 (100%, $[M]^+$) (calc. for $C_{92}H_{78}$ = 1183.65 g mol^{-1}).

6.2.2.18 2''-Ethynyl-2,3,4,5-tetraphenyl-[1,1';2',1'']terphenyl (4-67)

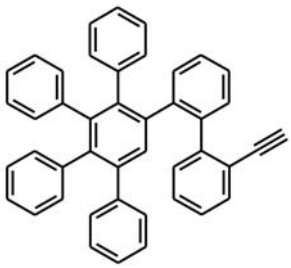

2,3,4,5-Tetraphenyl-cyclopenta-2,4-dienone (0.93 g, 2.4 mmol), 2,2'-diethinyl-biphenyl (0.5 g, 2.5 mmol) (**4-9**) and 25 mL of o-xylene were combined in an inert 50 mL Schlenk tube equipped with a reflux condenser. The mixture was heated to reflux temperature and left stirring overnight under argon. The solvent was removed *in vacuo* and the crude product was purified using column chromatography (silica, toluene:petroleum ether, 1:2), which yielded (**4-67**) as a colorless solid (71 %): ^{1}H-NMR (300 MHz, CD_2Cl_2, 293 K): δ = 7.70-6.50 (m, 29H, Ar-*H*), 2.95 (s, 1H, -C≡C*H*); ^{13}C-NMR (75 MHz, CD_2Cl_2, 293 K): δ = 142.54, 142.32, 141.35, 141.16, 140.94, 140.59, 140.42, 140.27, 139.90, 138.56, 133.76, 132.69, 132.22, 131.56, 131.40, 130.64, 130.54, 129.78, 128.99, 128.56, 128.25, 127.60, 127.47, 127.28, 127.16, 126.93, 126.53, 126.33, 126.09, 126.01, 123.99, 123.12, 119.61, 84.09, 81.46; MS (FD, 8 kV): m/z (%) = 559.0 (100%, $[M]^+$) (calc. for $C_{44}H_{30}$ = 558.73 g mol^{-1}).

6.2.2.19 2''-Ethynyl-2,3,4,5-tetrakis-(4-dodecylphenyl)-[1,1';2',1'']terphenyl (4-61)

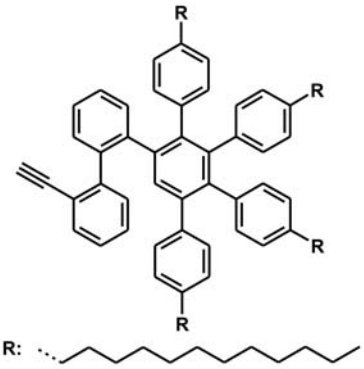

2,3,4,5-Tetrakis-(4-dodecyl-phenyl)-cyclopenta-2,4-dienone (0.78 g, 0.74 mmol),[9] 2,2'-diethinyl-biphenyl (0.15 g, 0.74 mmol) (**4-9**) and 5 mL of o-xylene were combined in an inert 50 mL Schlenk tube equipped with a reflux condenser. The mixture was heated to reflux temperature and left stirring overnight under argon. The solvent was removed *in vacuo* and the crude product was purified using column chromatography (silica, dichloromethane:petroleum ether, 1:4), which yielded (**4-61**) as a viscous, transparent oil (57 %): ^{1}H-NMR (300 MHz, CD_2Cl_2, 293 K): δ = 7.50-6.20 (m, 24H, Ar-*H*), 2.81 (s, 1H, -C≡C*H*), 2.50-2.10 (m, 8H, α-CH_2), 1.60-0.90 (m, 80H, alkyl-CH_2), 0.79 (t, 12H, ^{3}J(H,H) = 6.5 Hz, -CH_3); ^{13}C-NMR (75 MHz, CD_2Cl_2, 293 K): δ = 142.21, 141.34, 141.08, 140.39, 140.30, 140.02, 139.87, 139.66, 138.50, 138.17, 137.50, 133.43, 133.16, 132.45, 131.80, 131.14, 130.18, 128.16,

127.80, 127.19, 126.98, 126.81, 126.53, 122.64, 83.86, 80.57, 35.78, 32.45, 31.84, 31.76, 31.70, 30.21, 30.04, 29.90, 29.81, 29.58, 29.36, 23.20, 14.40; MS (FD, 8 kV): m/z (%) = 1231.3 (100%, $[M]^+$) (calc. for $C_{92}H_{126}$ = 1232.03 g mol^{-1}).

6.2.2.20 2,3,4,5-Tetra-phenyl-2''',3''',4''',5'''-tetra-[4-(3,7dimethyloctyl)-phenyl]-[1,1';2',1'';2'',1'''] quaterphenyl (4-68)

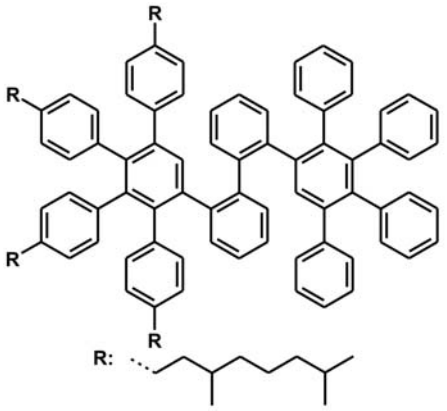

2,3,4,5-Tetrakis-(3,7-dimethyloctyl)-cyclopenta-2,4-dienone (0.21 g, 0.22 mmol),[1] 2"-ethynyl-2,3,4,5-tetraphenyl-[1,1';2',1"]terphenyl (0.14 g, 0.24 mmol) (**4-67**) and 2.5 mL of diphenylether were combined in an inert 50 mL Schlenk tube equipped with a reflux condenser. The mixture was heated to reflux temperature (240 °C) and left stirring overnight under argon. The solvent was removed *in vacuo* and the crude product was purified using column chromatography (silica, dichloromethane:petroleum ether 1:4), which yielded (**4-68**) as a viscous, transparent oil (92 %): ^{1}H-NMR (250 MHz, CD_2Cl_2, 293 K): δ = 7.50-6.10 (m, 46H, Ar-*H*), 2.60-2.00 (m, 8H, α-CH_2), 1.60-0.85 (m, 40H, alkyl-CH_2), 0.85-0.60 (m, 36H, -CH_3); ^{13}C-NMR (63 MHz, CD_2Cl_2, 293 K): δ = 144.00-137.00 (Ar-*C*), 134.00-129.00 (Ar-*C*), 128.00-125.00 (Ar-*C*), 39.77, 39.26, 39.08, 39.03, 37.54, 33.38, 33.23, 32.96, 32.55, 28.39, 25.12, 22.91, 22.83, 19.79; MS (FD, 8 kV): m/z (%) = 1476.7 (100%, $[M]^+$) (calc. for $C_{112}H_{130}$ = 1476.28 g mol^{-1}).

6.2.2.21 2,3,4,5-Tetra-bromo-2''',3''',4''',5'''-tetra-[4-(3,7dimethyloctyl)-phenyl]-[1,1';2',1'';2'',1'''] quaterphenyl (4-62)

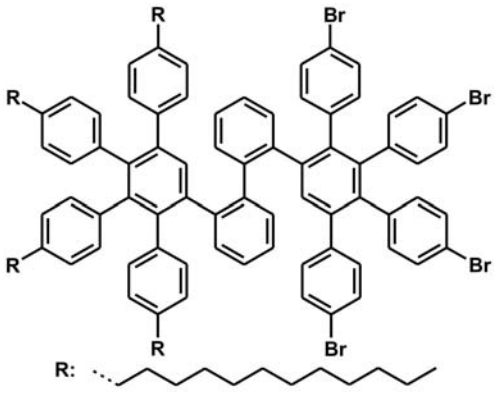

2,3,4,5-Tetrakis-(4-bromo-phenyl)-cyclopenta-2,4-dienone (0.07 g, 0.1 mmol),[12] 2"-ethynyl-2,3,4,5-tetrakis-(4-dodecylphenyl)-[1,1';2',1"]terphenyl (0.12 g, 0.1 mmol) (**4-61**) and 3.0 mL of diphenylether were combined in an inert 50 mL Schlenk tube equipped with a reflux condenser. The mixture was heated to reflux temperature (240 °C) and left stirring overnight under argon. The solvent was removed *in vacuo* and the crude product was purified using column chromatography (silica, dichloromethane:petroleum ether 1:4),

which yielded (**4-62**) as a viscous, transparent oil (97 %): ^{1}H-NMR (250 MHz, CD_2Cl_2, 293 K): δ = 7.60-6.20 (m, 42H, Ar-*H*), 2.62-2.22 (m, 8H, α-C*H*$_2$), 1.62-1.05 (m, 80H, alkyl-C*H*$_2$), 0.98-0.80 (m, 12H, -C*H*$_3$); ^{13}C-NMR (63 MHz, CD_2Cl_2, 293 K): δ = 144.00-136.00 (Ar-*C*), 135.00-129.00 (Ar-*C*), 128.00-124.00 (Ar-*C*), 35.71, 32.38, 31.66, 30.14, 29.98, 29.83, 29.75, 29.59, 29.32, 23.14, 14.34; MS (FD, 8 kV): m/z (%) = 1905.5 (100%, $[M]^+$) (calc. for $C_{112}H_{142}Br_4$ = 1904.09 g mol^{-1}).

6.2.2.22 2,3,4,5-Tetra-4-(phenyl-undecanoic acid ethyl ester)-2''',3''',4''',5'''-tetra-[4-(3,7dimethyloctyl)-phenyl]-[1,1';2',1'';2'',1'''] quaterphenyl (4-63)

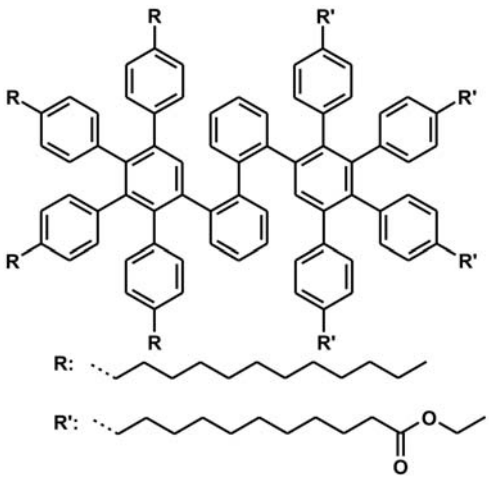

In a dry 500 ml Schlenk flask equipped with septum ethyl undecylate (25.3 g, 28.7 mL, 119.0 mmol) and a 0.5 M solution of 9-BBN in THF (250 ml, 125.0 mmol) was stirred overnight under argon at room temperature. 59.0 ml of an aqueous NaOH solution (3 N) was added and the resulting mixture was vigorously stirred for 20 min. 10 ml of the so prepared solution were transferred to another 50 mL Schlenk flask. Afterwards 2,3,4,5-tetra-bromo-2''',3''',4''',5'''-tetra-[4-(3,7dimethyloctyl)-phenyl]-[1,1';2',1'';2'',1''']quarterphenyl (0.18 g, 0.095 mmol) (**4-62**) and Pd(dppf)Cl_2 (0.01 g) were added and the resulting mixture was stirred at room temperature for 5 h. The solvent was removed *in vacuo* and the resulting slurry was extracted with water and dichloromethane. The combined organic phases were dried with magnesiumsulfate and after removing the solvent, the crude product was purified by column chromatography (silica, petroleum ether:ethylacetate 9:1) to yield (**4-63**) as a transparent viscous oil (64 %): ^{1}H-NMR (300 MHz, $CDCl_3$, 293 K): δ = 7.50-6.30 (m, 40H, Ar-*H*), 5.81 (s, 1H, Ar-*H*) , 5.79 (s, 1H, Ar-*H*), 4.08 (q, 8H, ^{3}J(H,H) = 7.1 Hz, -O-C*H*$_2$-CH$_3$), 2.60-2.15 (m, 24H, α-C*H*$_2$, -C*H*$_2$-COOEt), 1.80-1.00 (m, 156H, alkyl-C*H*$_2$), 0.88 (t, 12H, ^{3}J(H,H) = 6.6 Hz, -C*H*$_3$); ^{13}C-NMR (125 MHz, CD_2Cl_2, 293 K): 173.90 (*C*O), 142.91, 142.68, 141.71, 141.01, 140.85, 140.48, 140.23, 140.11, 139.99, 139.93, 139.71, 139.64, 139.36, 138.81, 138.24, 137.91, 137.72, 134.88, 134.25, 133.35, 133.11, 132.32, 132.11, 131.99, 131.83, 131.76, 130.35, 127.74, 127.60, 127.31, 127.06, 126.66, 126.55, 126.05, 125.09, 60.38, 35.90, 35.72, 34.70, 32.37, 31.71, 31.67, 30.13, 29.98, 29.81, 29.76, 29.60, 29.34, 25.43,

23.13, 14.49, 14.31; MS (FD, 8 kV): m/z (%) = 2436.3 (100%, $[M]^+$) (calc. for $C_{172}H_{242}O_8$ = 2437.84 g mol^{-1}).

6.2.2.23 2'',5'',8'',12'',15'',18'',21'',25''-Octa-(dodecyl)-hexabenzo-[jk,mn,pq,st: 3,4:9,10]-phenantro[1',10',9',8':5,6,7,8]perylo-[2,11,12,11-bcdef]ovalen (4-44)

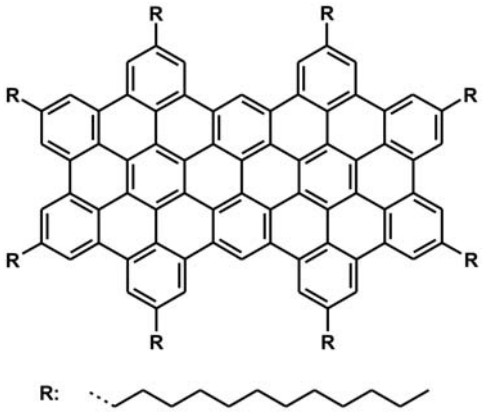

In a 250 ml 2-neck flask a solution of 2,3,4,5,2''',3''',4''',5'''-octa-(dodecyl)-[1,1';2', 1";2",1'''] quaterphenyl (0.1 g, 0.05 mmol) (**4-41**) in 140 mL of dry dichloromethane was degassed for 15 min., afterwards $FeCl_3$ (0.686 g, 4.80 mmol) in 6.9 ml nitromethane was quickly added. The reaction mixture was vigurously stirred at room temperature, while continuously bubbling argon. After 5 h the reaction was quenched with 100 ml of methanol and the precipitate was filtered and washed with methanol. The crude product was dissolved in hot toluene and filtered over a short silica column to yield (**4-44**) as a dark red solid (98 %): MS (MALDI-TOF (TCNQ-matrix)): 2237.42 (15.8 %), 2238.43 (25.6 %), 2239.43 (25.6 %), 2240.43 (16.8 %), 2241.45 (8.6 %), 2242.44 (4.5 %), 2243.43 (3.1 %) (calc. for $C_{168}H_{218}$ = 2237.61 g mol^{-1}, isotope distr.: 2235.71 (15.1 %), 2236.71 (28.7 %), 2237.71 (27.1 %), 2238.72 (17.0 %), 2239.72 (7.9 %), 2240.72 (2.9 %), 2241.73 (0.9 %)); UV/vis (THF, 293 K): λ (nm) = 434, 443, 477, 558.

6.2.2.24 2'',5'',8'',12'',15'',18'',21'',25''-Octa-(3,7dimethyloctyl)-hexabenzo-[jk,mn,pq,st:3,4:9,10]-phenantro[1',10',9',8':5,6,7,8]perylo-[2,11,12,11-bcdef]ovalen (4-45)

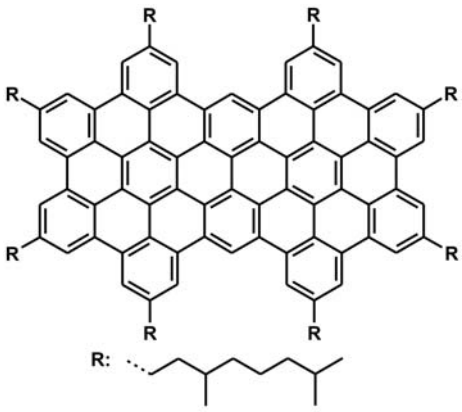

In a 250 ml 2-neck flask a solution of 2,3,4,5,2''',3''',4''',5'''-octa-(3,7dimethyloctyl)-[1,1';2',1"; 2",1''']quaterphenyl (0.1 g, 0.05 mmol) in 140 mL of dry dichloromethane was degassed for 15 min., afterwards $FeCl_3$ (0.764 g, 4.71 mmol) dissolved in 7.6 mL nitromethane was quickly added. The reaction mixture was vigurously stirred at room temperature, while continuously bubbling argon. After 4 h the reaction was quenched with 100 mL of methanol and the precipitate

was filtered and washed with methanol. The crude product was dissolved in hot toluene and filtered over a short silica column to yield (**4-45**) as a dark red solid (95 %): MS (MALDI-TOF (TCNQ-matrix)): 2011.16 (18.2 %), 2012.17 (31.4 %), 2013.16 (24.5 %), 2014.24 (17.5 %), 2015.19 (8.3 %) (calc. for $C_{152}H_{186}$ = 2013.18 g mol^{-1}, isotope distr.: 2011.46 (18.1 %), 2012.46 (31.1 %), 2013.46 (26.6 %), 2014.47 (15.0 %), 2015.47 (6.3 %); UV/vis (THF, 293 K): λ (nm) = 421, 434, 478.

6.2.2.25 2'',5'',8'',12'',15'',18'',21'',25''-Octa-(4-dodecylphenyl)-hexabenzo-[jk,mn,pq,st:3,4:9,10]-phenantro[1',10',9',8':5,6,7,8]perylo-[2,11,12,11-bcdef]ovalen (4-46)

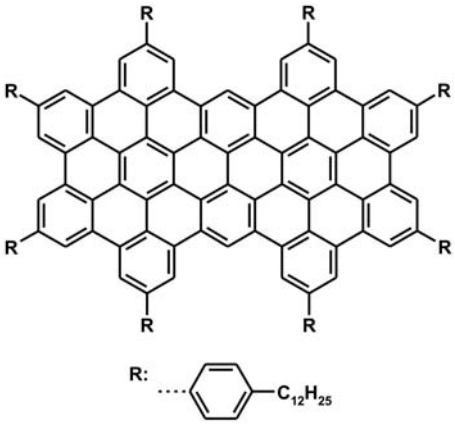

In a 250 ml 2-neck flask a solution of 2,3,4,5,2''',3''',4''',5'''-Octa-(4-dodecyl-biphenyl)-[1,1';2', 1";2",1'''] quaterphenyl (0.05 g, 0.02 mmol) (**4-43**) in 70 mL of dry dichloromethane was degassed for 15 min., afterwards $FeCl_3$ (0.271 g, 1.7 mmol) dissolved in 2.7 mL nitromethane was quickly added. The reaction mixture was vigorously stirred at room temperature, while continuously bubbling argon. After 24 h the reaction was quenched with 50 mL of methanol and the precipitate was filtered and washed with methanol. The crude product was dissolved in hot toluene and filtered over a short silica column to yield (**4-46**) as a dark red solid (95 %): MS (MALDI-TOF (TCNQ-matrix)): 2846.35 (11.5 %), 2847.34 (19.9 %), 2848.34 (23.5 %), 2849.34 (19.7 %), 2850.35 (15.0 %), 2851.33 (10.4 %) (calc. for $C_{216}H_{250}$ = 2846.40 g mol^{-1}, isotope distr.: 2843.96 (8.8 %) 2844.96 (21.6 %), 2845.96 (26.2 %), 2846.97(21.1%), 2847.97 (12.7 %), 2848.97 (6.1 %)).

6.2.2.26 1,6,14,19-Tetra-(1,1-dimethylethyl)-hexabenzo-[7,8:13,14:bc,ef,hi,uv]-ovaleno-[10,11-d]-ovalen (4-99)

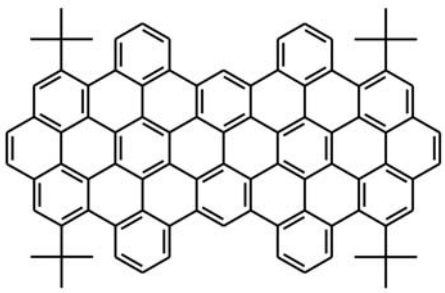

In a 250 ml 2-neck flask a solution of 2,2'-bis(2,7-di-tert-butyl-9,12-diphenyl-benzo[e]pyrene-10-yl)-bi-phenyl (0.05 g, 0.05 mmol) (**4-97**) in 100 ml of dry dichloromethane was degassed for 15 min., afterwards $FeCl_3$ (0.25 g, 4.80 mmol, 4 eq. per H) in 3.0 ml nitromethane was quickly added. The reaction mixture was stirred at room temperature and an argon flow was

continuously bubbling through, removing HCl formed during reaction. After 3 h the reaction was quenched with 50 mL of methanol and the precipitate was filtered and washed with methanol. The product was dried *in vacuo*. MS (MALDI-TOF (TCNQ-matrix)): 1162.19 (33.3 %), 1163.20 (32.9 %), 1164.20 (19.7 %), 1165.18 (7.1 %), 1166.14 (4.3 %), 1167.20 (2.8 %) (calc. for $C_{92}H_{58}$ = 1163.49 g mol^{-1}, isotope distr.: 1162.45 (35.8 %), 1163.46 (37.0 %), 1164.46 (18.9 %), 1165.46 (6.4 %), 1166.47 (1.6 %), 1167.47 (0.3 %).

6.2.2.27 2'',5'',8'',25''-Tetra-(dodecyl)- 12'',15'',18'',21''-tetra-(undecanoic acid ethyl ester)-hexabenzo-[jk,mn,pq,st:3,4:9,10]-phenantro [1',10',9',8': 5,6,7,8]perylo-[2,11,12,11-bcdef]ovalen (4-64)

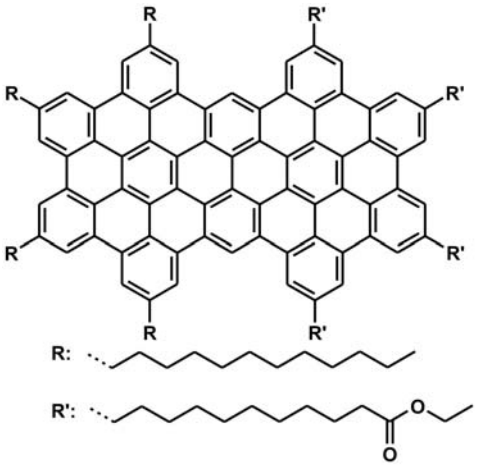

In a 100 ml Schlenk tube a solution of 2,3,4,5-tetra-4-(phenyl-undecanoic acid ethyl ester)-2''',3''',4''',5'''-tetra-[4-(3,7dimethyloctyl)-phenyl]-[1,1';2',1'';2'',1'''] quaterphenyl (0.01 g, 0.004 mmol) (**4-63**) in 30 mL of dry dichloromethane was degassed for 15 min., afterwards $FeCl_3$ (0.25 g, 1.5 mmol) dissolved in 2.5 mL nitromethane was quickly added. The reaction mixture was vigorously stirred at room temperature, while continuously bubbling argon. After 24 h the reaction was quenched with 50 mL of methanol and the precipitate was filtered and washed with methanol. The crude product was dissolved in hot toluene and filtered over a short silica column to yield (**4-64**) as a dark red solid (91 %): MS (MALDI-TOF (TCNQ-matrix)): 2411.60 (17.2 %), 2412.58 (26.1 %), 2413.57 (26.5 %), 2414.59 (20.1 %), 2415.59 (10.1 %) (calc. for $C_{172}H_{218}O_8$ = 2413.65 g mol^{-1}, isotope distr.: 2411.67 (14.2 %), 2412.67 (27.6 %), 2413.67 (27.0 %), 2414.68 (17.6 %), 2415.68 (8.7 %)); UV/vis (THF, 293 K): λ (nm) = 435, 468.

6.2.2.28 2,7-Di-(1,1-dimethylethyl)-9,12-bis-(4-(1,1-dimethylethyl)-phenyl)-10-phenyl-benzo[e]pyrene (4-104)

2,7-Di-*tert*-butyl-9,11-di-(4-*tert*-butyl-phenyl)-cyclo-penta[e] pyren-10-one (0.18 g, 0.3 mmol),[13] phenylacetylene (0.03 g, 0.3 mmol) and 3.0 mL of o-xylene were placed in a microwave tube, which was purged with argon and sealed. The reaction was carried out in a CEM Discover microwave at 300 W and activated cooling, keeping the temperature between 150 °C and 160 °C for 3 h. The solvent was removed *in vacuo* and

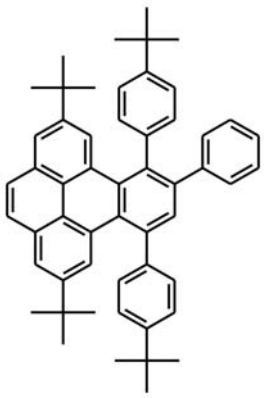

the crude product was chromatographically purified (silica, hexane:dichloromethane 9:1) to yield (**4-104**) as a transparent oil (95 %): ^{1}H-NMR (300 MHz, $CDCl_3$, 293 K): δ = 8.22 (dd, 2H, ^{3}J(H,H) = 1.7 Hz, Ar-*H*), 8.01-7.89 (m, 4H, Ar-*H*), 7.70 (s, 1H, Ar-*H*), 7.51-7.41 (m, 4H, Ar-*H*), 7.30-7.13 (m, 5H, Ar-*H*), 7.12-7.02 (m, 4H, Ar-*H*), 1.37 (s, 9H, -C*H*$_3$), 1.29 (s, 9H, -C*H*$_3$), 1.13 (s, 9H, -C*H*$_3$), 1.09 (s, 9H, -C*H*$_3$); ^{13}C-NMR (75 MHz, CD_2Cl_2, 293 K): δ = 150.35, 149.85, 147.44, 147.32, 142.81, 142.46, 140.97, 140.29, 139.35, 137.71, 132.94, 132.69, 131.84, 131.07, 130.80, 130.74, 130.29, 129.65, 129.61, 128.92, 127.81, 127.44, 127.21, 126.69, 126.60, 126.31, 125.97, 123.80, 123.41, 122.179, 35.12, 35.06, 34.86, 34.70, 31.65, 31.54, 31.51, 31.46; MS (FD, 8 kV): m/z (%) = 704.7 (100%, $[M]^+$) (calc. for $C_{54}H_{56}$ = 705.05 g mol^{-1}).

6.2.2.29 4,6,11,13-Tetra-(1,1-dimethylethyl)-dibenzo[a,m]-coronene (4-105)

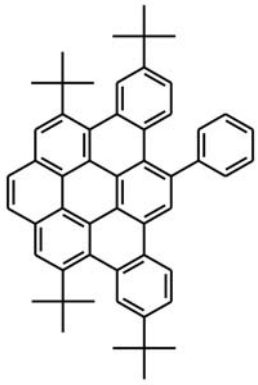

In a 100 ml Schlenk tube a solution of 2,7-di-(1,1-dimethylethyl)-9,12-bis-(4-(1,1-dimethylethyl)-phenyl)-10-phenyl-benzo[e]pyrene (0.02 g, 0.03 mmol) (**4-104**) in 30 mL of dry dichloromethane was degassed for 15 min., afterwards $FeCl_3$ (0.043 g, 0.27 mmol) dissolved in 0.33 mL nitromethane was quickly added. The reaction mixture was vigorously stirred at room temperature, while continuously bubbling argon. After 20 min. the reaction was quenched with 50 mL of a methanol/water mixture. All solvent except for the water was removed and the precipitate was filtered and washed excessively with water and 2 N HCl. The crude product was purified chromatographically (silica, petroleum ether:CH_2Cl_2 9:1) to yield (**4-105**) as a light yellow solid (98 %): ^{1}H-NMR (300 MHz, CD_2Cl_2, 293 K): δ = 9.29 (s, 1H, Ar-*H*), 8.98 (d, 1H, ^{3}J(H,H)=8.8 Hz, Ar-*H*), 8.94 (d, 2H, ^{3}J(H,H)=7.5 Hz, Ar-*H*), 8.66 (d, 1H, ^{4}J(H,H)=2.0 Hz, Ar-*H*), 8.45 (d, 2H, ^{4}J(H,H)=1.4 Hz, Ar-*H*), 8.41 (d, 1H, ^{4}J(H,H)=2.0 Hz, Ar-*H*), 8.02 (d, 1H, ^{3}J(H,H)=8.8 Hz, Ar-*H*), 7.96 (d, 2H, ^{3}J(H,H)=7.1 Hz, Ar-*H*), 7.87 (dd, 1H, ^{3}J(H,H)=6.7 Hz, Ar-*H*), 7.66 (t, 2H, ^{3}J(H,H)=7.6 Hz, Ar-*H*), 7.57 (t, 1H, ^{3}J(H,H)=7.4 Hz, Ar-*H*), 7.25 (dd, 1H, ^{3}J(H,H)=6.7 Hz, Ar-*H*), 1.83 (s, 9H, -CH_3), 1.78 (s, 9H, -CH_3), 1.56 (s, 9H, -CH_3), 1.43 (s, 9H, -CH_3); ^{13}C-NMR (75 MHz, CD_2Cl_2, 293 K): δ = 146.91, 146.40, 146.09, 145.86, 145.11, 138.07, 132.31, 131.20, 130.93, 130.40, 130.12, 129.99, 129.35, 129.13, 129.03, 128.95, 128.42, 128.38, 128.01, 127.78, 127.53,

127.36, 127.18, 126.99, 126.09, 125.43, 125.21, 125.08, 124.71, 124.02, 123.42, 123.24, 121.58, 121.50, 39.61, 39.38, 35.96, 35.70, 35.44, 35.32, 32.13, 31.99; MS (MALDI-TOF (TCNQ-matrix)): 700.16 (43.7 %), 701.15 (36.2 %), 702.16 (16.0 %), 703.10 (4.1 %) (calc. for $C_{54}H_{52}$ = 701.02 g mol^{-1}, isotope distr.: 700.39 (54.6 %), 701.39 (33.2 %), 702.40 (9.9 %), 703.40 (1.9 %)); UV/vis (THF, 293 K): λ (nm) = 334 (6841 m^2 mol^{-1}), 348 (13104 m^2 mol^{-1}), 380 (3425 m^2 mol^{-1}), 396 (1505 m^2 mol^{-1}).

6.2.2.30 2,4'-Dibromo-biphenyl (4-80)

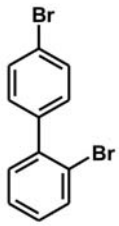

1-Bromo-4-iodobenzene (8.63 g, 30.5 mmol) and a solution of (2-bromophenyl)zinc-iodine (30.5 mmol) in THF, which was prepared according to published procedures,[14,15] were combined in a 100 mL Schlenk tube. After the addition of $Pd(PPh_3)_4$ (0.7 g) the mixture was stirred at 30 °C for 1 h. The reaction was quenched with methanol, the solvent was removed *in vacuo* and the crude product was purified with column chromatography (silica, hexane) to yield (**4-80**) as a transparent viscous oil (73 %): ^{1}H-NMR (250 MHz, CD_2Cl_2, 293 K): δ = 7.62 (d, 1H, ^{3}J(H,H) = 7.9 Hz, Ar-*H*), 7.51 (d, 2H, ^{3}J(H,H) = 8.3 Hz, Ar-*H*), 7.42-7.10 (m, 5H, Ar-*H*); ^{13}C-NMR (63 MHz, CD_2Cl_2, 293 K): δ = 142.13, 140.84, 134.03, 132.84, 131.99, 130.01, 129.37, 128.46, 123.15, 122.67; MS (EI, 70 eV): m/z (%) = 314.5 (29.6 %, $[M^{+1}]^+$), 312.6 (56.5 %, $[M]^+$), 310.6 (30.2 %, $[M^{-1}]^+$), 234.8 (1.7 %, $[M-(Br)]^+$), 152.4 (100.0 %, $[M-(Br)_2]^+$), 76.9 (33.1 %, $[(M-Br_2)/2]^+$) (calc. for $C_{12}H_8Br_2$ = 312.01 g mol^{-1}).

6.2.2.31 2,4'-Bis-trimethylsilanylethinyl-biphenyl (4-81)

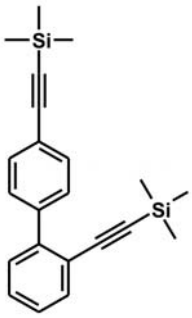

2,4'-Dibromo-biphenyl (3.5 g, 11.2 mmol), $Pd(PPh_3)_2Cl_2$ (0.28 g, 0.42 mmol), copper iodine (0.02 g, 0.21 mmol) and piperidine (50 mL were combined in a 100 mL Schlenk tube and degassed. Afterwards trimethylsilylacetylene (2.8 g, 3.9 mL, 28.1 mmol) was added via the septum and the mixture was vigorously stirred at 80 °C under argon. After 8 h a second portion of trimethylsilylacetylene (2.8 g, 3.9 mL, 28.1 mmol) was added and the reaction was continued for another 4 h. The solvent was evaporated and the crude product purified chromatographically (silica, hexane) to yield (**4-81**) as a transparent oil (92 %): ^{1}H-NMR (250 MHz, CD_2Cl_2, 293 K): δ = 7.70-7.20 (m, 8H, Ar-*H*), 0.35 (s, 9H, -C*H*$_3$), 0.23 (s, 9H, -C*H*$_3$); ^{13}C-NMR (63 MHz, CD_2Cl_2, 293 K): δ = 143.50, 140.86, 133.89, 131.99, 131.93, 131.76, 129.73,

129.36, 127.84, 127.78, 105.43, 104.82, 80.97, 78.08, 0.18, 0.01; MS (FD, 8 kV): m/z (%) = 346.3 (100%, $[M]^+$) (calc. for $C_{22}H_{26}Si_2$ = 346.62 g mol^{-1}).

6.2.2.32 2,4'-Diethinyl-biphenyl (4-82)

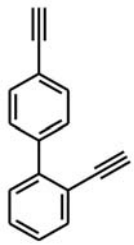

A degassed solution of 2,4'-bis-trimethylsilanylethinyl-biphenyl (3 g, 8.7 mmol) (**4-81**) in 50 mL of methanol was treated with 10.4 mL of aqueous NaOH (5 N). The resulting mixture was stirred under argon for 45 min. at room temperature and afterwards acidified with HCl (1 N). The product was extracted three times with dichloromethane and the combined organic phases dried with $MgSO_4$. After evaporation of the solvent, the crude product was purified by column chromatography (petroleum ether: dichloromethane 9:1) to yield (**4-82**) as a transparent oil (98 %): ^{1}H-NMR (250 MHz, CD_2Cl_2, 293 K): δ = 7.78-7.58 (m, 5H, Ar-*H*), 7.57-7.36 (m, 3H, Ar-*H*), 3.29 (s, 1H, -C≡C*H*), 3.21 (s, 1H, -C≡C*H*); ^{13}C-NMR (63 MHz, CD_2Cl_2, 293 K): δ = 143.75, 141.12, 134.32, 133.01, 132.16, 129.82, 129.69, 129.55, 127.86, 127.30, 121.68, 120.67, 83.85, 83.15, 81.09, 78.35; MS (EI, 70 eV): m/z (%) = 202.1 (44.1 %, [M]) (calc. for $C_{16}H_{10}$ = 202.26 g mol^{-1}).

6.2.2.33 2,3,4,5,2''',3''',4''',5'''-Octaphenyl-[1,1';4',1'';2'',1''']quaterphenyl (4-83)

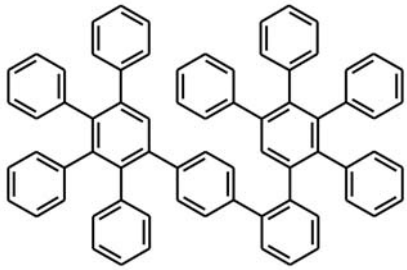

In a dry 25 ml Schlenk tube equipped with condenser a solution of 2,3,4,5-tetraphenyl-cyclopenta-2,4-dienone (1.16 g, 3.0 mmol), 2,4'-diethinyl-biphenyl (0.24 g, 1.2 mmol) (**4-82**) in 10 ml of o-dichlorobenzene was degassed for 10 min. The solution was then heated to reflux and stirred overnight. The solvent was removed *in vacuo* and the crude product was purified by column chromatography (silica, petroleumether:toluene 1:1) to yield (**4-83**) as a colorless solid (80 %): ^{1}H-NMR (250 MHz, CD_2Cl_2, 293 K): δ = 7.60-6.60 (m, 48H, Ar-*H*), 6.39 (s, 1H, Ar-*H*), 5.74 (s, 1H, Ar-*H*); ^{13}C-NMR (63 MHz, CD_2Cl_2, 293 K): δ = 142.42, 142.24, 141.88, 141.25, 140.92, 140.88, 140.78, 140.67, 140.61, 140.57, 140.38, 140.25, 139.70, 139.67, 139.57, 139.53, 132.80, 132.09, 131.99, 131.92, 131.77, 131.55, 130.34, 130.29, 130.00, 129.76, 129.53, 127.99, 127.90, 127.77, 127.65, 127.34, 127.24, 127.16, 126.94, 126.89, 126.79, 126.68, 126.58, 126.13, 126.00, 125.92, 125.68, 125.64, 125.48; MS (FD, 8 kV): m/z (%) = 915.9 (100%, $[M]^+$) (calc. for $C_{72}H_{50}$ = 915.20 g mol^{-1}).

6.2.2.34 Hexabenzo-[jk,mn,pq,st:3,4:9,10]-phenantro[1',10',9',8':5,6,7,8] perylo-[2,11,12,11-bcdef]ovalen (4-84)

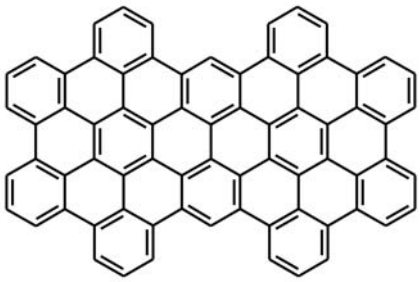

In a 100 ml Schlenk tube a solution of 2,3,4,5,2''',3''',4''',5'''-octaphenyl-[1,1';4',1'';2'',1''']-quarter-phenyl (0.05 g, 0.05 mmol) (**4-83**) in 50 mL of dry dichloromethane was degassed for 15 min., afterwards $FeCl_3$ (0.532 g, 3.3 mmol) dissolved in 5.3 mL nitromethane was quickly added. The reaction mixture was vigorously stirred at room temperature, while continuously bubbling argon. After 8 h the reaction was quenched with 50 mL of methanol and the precipitate was filtered and washed extensively with methanol to yield (**4-84**) as a dark solid (90 %): MS (MALDI-TOF (TCNQ-matrix)): 889.85 (39.5 %), 890.86 (32.4 %), 891.89 (18.9 %), 892.97 (6.7 %), 894.00 (2.5 %) (calc. for $C_{72}H_{26}$ = 891.01 g mol^{-1}, isotope distr.: 890.20 (44.9 %), 891.21 (36.1 %), 892.21 (14.3 %), 893.21 (3.7 %), 894.22 (0.7 %)).

6.2.2.35 2,3,2''',3'''-Tetra-[4-(3,7-dimethyloctyl)-phenyl)]-4,5,4''',5'''-tetraphenyl-[1,1';4',1'';2'',1''']quaterphenyl (4-85)

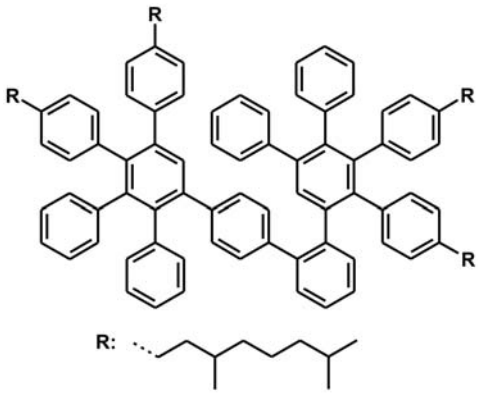

In a dry 25 ml Schlenk tube equipped with condenser a solution of 3,4-bis-[4-(3,7-dimethyl-octyl)-phenyl]-2,5-diphenyl-cyclopenta-2,4-dienone (0.3 g, 0.45 mmol),[16] 2,4'-diethinyl-biphenyl (0.044 g, 0.22 mmol) (**4-82**) in 8 ml of o-dichlorobenzene was degassed for 10 min. The solution was then heated to reflux and stirred overnight. The solvent was removed *in vacuo* and the crude product was purified by column chromatography (silica, petroleumether:toluene 2:1) to yield (**4-85**) as a transparent oil (87 %): ^{1}H-NMR (300 MHz, CD_2Cl_2, 293 K): δ = 7.70-6.50 (m, 44H, Ar-*H*), 6.40 (s, 1H, Ar-*H*), 5.76 (s, 1H, Ar-*H*), 2.45 (m, 8H, α-CH_2), 1.70-1.05 (m, 40H, alkyl-CH_2), 1.00-0.80 (m, 36H, -CH_3); ^{13}C-NMR (75 MHz, CD_2Cl_2, 293 K): δ = 142.65, 142.51, 142.47, 142.12, 141.24, 140.87, 140.82, 140.76, 140.72, 140.69, 140.63, 140.58, 140.52, 140.43, 140.34, 140.26, 140.22, 139.92, 139.89, 139.75, 139.59, 139.53, 138.13, 138.10, 137.89, 137.79, 132.65, 132.13, 131.98, 131.86, 131.80, 131.52, 131.41, 130.80, 130.40, 130.34, 130.06, 129.99, 129.75, 129.51, 127.95, 127.87, 127.78, 127.66, 127.59, 127.26, 127.19, 126.96, 126.84,

126.55, 126.46, 126.24, 126.00, 125.36, 39.80, 39.07, 37.55, 33.28, 32.58, 28.42, 25.15, 22.93, 22.85, 19.80; MS (FD, 8 kV): m/z (%) = 1475.4 (100%, $[M]^+$) (calc. for $C_{112}H_{130}$ = 1476.28 g mol^{-1}).

6.2.2.36 2'',5'',12'',15''-Tetra-(3,7-dimethyloctyl)-hexabenzo-[jk,mn,pq,st: 3,4: 9,10]-phenantro[1',10',9',8':5,6,7,8]perylo-[2,11,12,11-bcdef] ovalen (4-86)

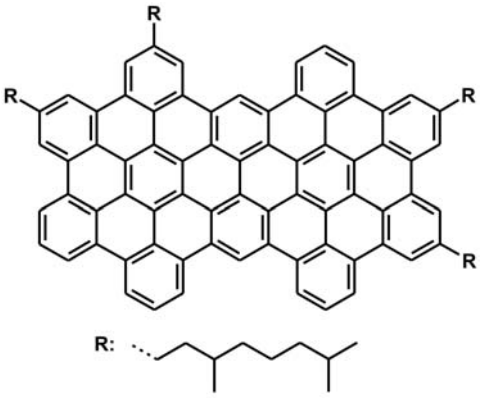

In a 100 ml Schlenk tube a solution of 2,3,2''',3'''-tetra-[4-(3,7-dimethyloctyl)-phenyl)]-4,5,4''',5'''-tetraphenyl-[1,1';4',1";2",1''']quaterphenyl (0.050 g, 0.034 mmol) (**4-85**) in 40 mL of dry dichloromethane was degassed for 15 min., afterwards $FeCl_3$ (0.33 g, 2.1 mmol) dissolved in 3.0 mL nitromethane was quickly added. The reaction mixture was vigorously stirred at room temperature, while continuously bubbling argon. After 12 h the reaction was quenched with 50 mL of methanol and the precipitate was filtered and washed extensively with methanol to yield (**4-86**) as a red solid (91 %): MS (MALDI-TOF (TCNQ-matrix)): 1451.89 (28.5 %), 1452.88 (30.1 %), 1453.89 (18.2 %), 1454.93 (15.1 %), 1455.96 (8.1 %) (calc. for $C_{112}H_{106}$ = 1452.09 g mol^{-1}, isotope distr.: 1451.83 (25.8 %), 1452.83 (36.0 %), 1453.84 (22.5 %), 1454.84 (9.3 %), 2415.84 (2.5 %)); UV/vis (THF, 293 K): λ (nm) = 413.

6.2.2.37 2,3,4,5,2''',3''',4''',5'''-Octa-[4-(3,7-dimethylocty]-phenyl)-[1,1';4',1''; 2'',1''']quaterphenyl (4-87)

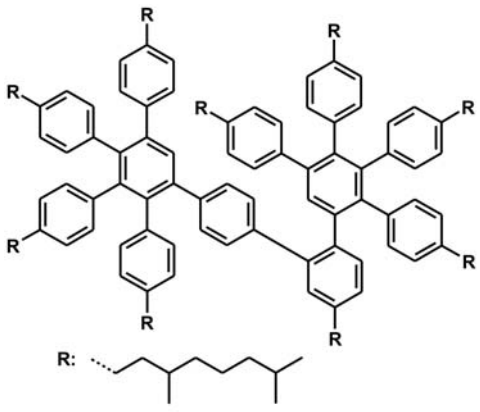

In a dry 25 ml Schlenk tube equipped with condenser a solution of 2,3,4,5-tetrakis-(4-(3,7-dimethyloctanyl) phen-1-yl)-cyclopenta-2,4-dienone (0.1 g, 0.1 mmol),[1] 2,4'-diacetylenbiphenyl (0.01 g, 0.05 mmol) (**4-82**) in 3 mL of o-xylene was degassed for 10 min. The solution was then heated to reflux and stirred overnight. The diphenylether was removed in vacuo and the crude product was purified by column chromatography (silica, petroleumether:dichloromethane 17:3) to yield (**4-87**) as a transparent viscuous oil (89 %): ^{1}H-NMR (250 MHz, CD_2Cl_2, 293 K): δ = 7.50-6.40 (m, 40H, Ar-*H*), 6.05 (s, 1H,

Ar-*H*), 5.59 (s, 1H, Ar-*H*), 2.70-2.10 (m, 16H, α-C*H*$_2$), 1.70-1.00 (m, 80H, alkyl-C*H*$_2$, -C*H*), 0.95-0.70 (m, 72H, -C*H*$_3$); ^{13}C-NMR (63 MHz, CD_2Cl_2, 293 K): δ = 145.00-135.00 (Ar-*C*), 133.00-125.00 (Ar-*C*), 35.76, 32.40, 31.88, 31.73, 30.21, 30.16, 30.01, 29.85, 29.58, 29.37, 29.31, 23.15, 14.34; MS (FD, 8 kV): m/z (%) = 1475.4 (100%, $[M]^+$) (calc. for $C_{112}H_{130}$ = 1476.28 g mol^{-1}).

6.2.2.38 Product mixture resulting from 2,3,4,5,2''',3''',4''',5'''-Octa-[4-(3,7-dimethylocty]-phenyl)-[1,1';4',1'';2'',1''']quaterphenyl (4-87) by cyclodehydrogenation (4-88)

In a 100 ml Schlenk tube a solution of 2,3,4,5,2''',3''',4''',5'''-octa-[4-(3,7-dimethylocty]-phenyl)-[1,1';4',1'';2'',1''']quaterphenyl (0.023 g, 0.01 mmol) (**4-87**) in 50 mL of dry dichloromethane was degassed for 15 min., afterwards $FeCl_3$ (0.078 g, 0.5 mmol) dissolved in 0.8 mL nitromethane was quickly added. The reaction mixture was vigorously stirred at room temperature, while continuously bubbling argon. After 2 h the reaction was quenched with 50 mL of methanol and the precipitate was filtered and washed extensively with methanol to yield the product mixture as a red solid (93 %).

6.2.2.39 2,7-Di-(1,1-dimethylethyl)-pyrene-4,5,9,10-tetraone (4-111)

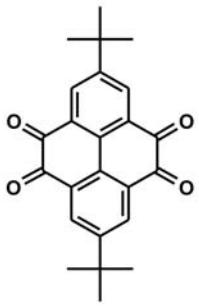

BBr_3 in CH_2Cl_2 (400 mL, 1 M) was added to a solution of 2,7-di-*tert*-butyl-4,5,9,10-tetramethoxy-pyrene (20.2 g, 46.0 mmol)[17] in CH_2Cl_2 (2 L) at 0 °C. The reaction mixture was allowed to warm up to room temperature and stirred for 6h. Afterwards, it was poured into ice-water and extracted with CH_2Cl_2. The organic phases were washed with water, dried with $MgSO_4$ and concentrated to afford the pyrenoquinhydrone as a dark violet solid. The material was dissolved in methanol and 0.02 g of N,N'-bis(salicylidene)ethylene-diiminocobalt(II) (Salcomine) were added. While bubbling oxygen, the solution was stirred at room temperature until it turned orange. Finally, the product was chromatographically purified using silica gel and CH_2Cl_2 as eluent and recrystallized from ethanol to yield (**4-111**) as orange needles (65 %): ^{1}H-NMR (250 MHz, CD_2Cl_2, 293 K): δ = 8.46 (s, 4H, Ar-*H*); 1.42 (s, 18H, -C(C*H*$_3$)$_3$); ^{13}C-NMR (63 MHz, CD_2Cl_2, 293 K): δ = 178.63(*C*O), 155.04, 133.90, 132.56, 131.01, 35.64, 30.75; MS (FD, 8kV): m/z (%) = 374.5 (100%, M^+) (calc. for $C_{24}H_{24}O_4$ = 376.46 g mol^{-1}).

6.2.2.40 1,8-Bis(1,1-dimethylethyl)-3,4,5,6,10,11,12,13-octa(4-dodecyl-tetraphenyl)-benzenepyrene (4-115)

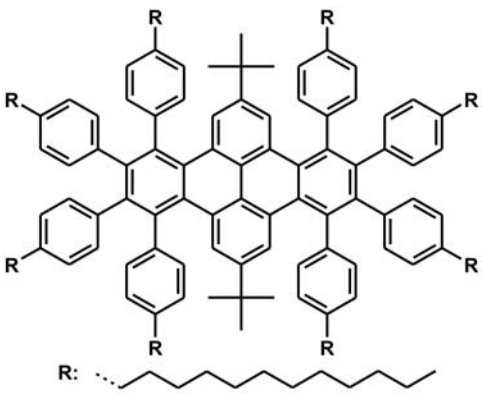

4,9-Di-tert-butyl-1,2:6,7-bis-[2,5-di-p-dodecyl-cy-clopenta-2,4-dienone]-pyrene (0.05 g, 0.036 mmol),[18] 4,4'-di-n-dodecyltolane (0.111 g, 0.215 mmol)[16] and 0.3 ml of diphenylether were placed in a microwave tube, which was purged with argon and sealed. The reaction was carried out in a CEM Discover microwave at 300 W and activated cooling, keeping the temperature between 230 °C and 250 °C for 8 h. The solvent was removed *in vacuo* at 80 °C and the residue was treated *via* column chromatography using silica. In the beginning pure petroleum ether was used to remove the excess 4,4'-di-n-dodecyltolane (5), afterwards the polarity of the solvent was slowly increased to petroleum ether:dichloromethane (19:1), yielding the product as a light yellow oil (21 %): ^{1}H-NMR (250 MHz, CD_2Cl_2, 293 K): δ = 7.89 (s, 4H, Ar-*H*); 6.97 (d, 8H, ^{3}J(H,H) = 7.92 Hz, Ar-*H*); 6.88 (d, 8H, ^{3}J(H,H) = 7.31 Hz, Ar-*H*); 6.70 (d, 8H, ^{3}J(H,H) = 7.9 Hz, Ar-*H*); 6.61 (d, 8H, ^{3}J(H,H) = 7.8 Hz, Ar-*H*); 2.55-2.35 (m, 16H, α-CH_2); 1.58-1.43 (m, 16H, β-CH_2); 1.36-1.20 (m, 144H, alkyl-CH_2); 0.95-0.87 (m, 24H, alkyl-CH_3); 0.67-0.62 (s, 18H, -C(CH_3)$_3$); ^{13}C-NMR (125 MHz, CD_2Cl_2, 293 K): δ = 141.31, 140.88, 139.83, 138.69, 137.70, 132.26, 131.96, 131.87, 146.00, 129.000, 128.50, 126.93, 125.85, 124.24, 32.43, 32.41, 32.01, 31.95, 31.30, 30.30, 30.24, 30.20, 30.13, 30.04, 29.88, 29.85, 29.27, 23.17, 14.36, 36.00, 35.81, 34.97; MS (FD, 8kV): m/z (%) = 2370.0 (100%, M^+) (calc. for $C_{176}H_{254}$ = 2369.99 g mol^{-1}); R_f: 0.12 (PE:DCM 19:1).

6.2.2.41 1,8-Bis(1,1-dimethylethyl)-3,6,10,13-tetra(4-dodecyl-tetraphenyl)-4,5,11,12-tetrakis(2-decyl-tetradecyl)-benzenepyrene (4-118)

4,9-Di-tert-butyl-1,2:6,7-bis-[2,5-di-p-dodecyl-cyclopenta-2,4-dienone]-pyrene (0.35 g, 0.036 mmol),[18] 4,4'-bis(2-decyl-tetradecyl)diphenylacetylene (1.0 g, 0.215 mmol)[19] and 2.0 ml of diphenylether were placed in a microwave tube, which was purged with argon and sealed. The reaction was carried out in a CEM Discover microwave at 300 W and activated cooling, keeping the temperature between 230 °C and 250 °C for 8 h. The solvent was removed under reduced pressure at 80 °C and the residue was treated via column chromatography using silica. In the beginning pure petroleum ether was used to

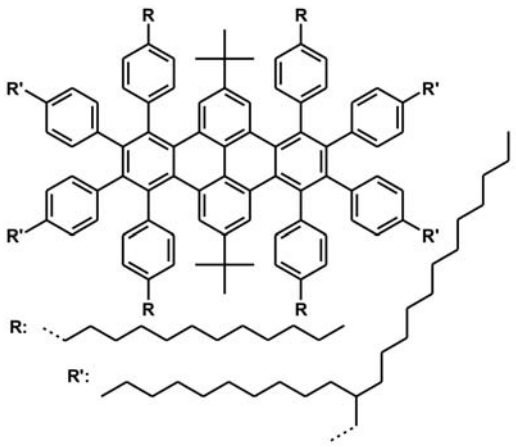

remove the excess 4,4'-bis(2-decyl-tetradecyl)di phen-yl acetylene, afterwards the polarity of the solvent was slowly increased to petroleum ether:dichloromethane (19:1), yielding the product as a light yellow oil (11 %): ^{1}H-NMR (250 MHz, CD_2Cl_2, 293 K): δ = 7.88 (s, 4H, Ar-*H*); 6.98 (d, 8H, ^{3}J(H,H) = 8.0 Hz, Ar-*H*); 6.87 (d, 8H, ^{3}J(H,H) = 8.0 Hz, Ar-*H*); 6.67 (d, 8H, ^{3}J(H,H) = 8.02 Hz, Ar-*H*); 6.60 (d, 8H, ^{3}J(H,H) = 7.94 Hz, Ar-*H*); 2.45 (t, 8H, ^{3}J(H,H) = 7.46 Hz, α-CH_2); 2.37 (d, 8H, ^{3}J(H,H) = 6.24 Hz, α-CH2); 1.65-1.05 (m, 244H, alkyl-CH_2); 0.95-0.83 (m, 36H, alkyl-CH_3); 0.67-0.62 (s, 18H, -C(CH_3)$_3$); ^{13}C-NMR (125 MHz, CD_2Cl_2, 293 K): δ = 146.02, 141.27, 141.22, 140.91, 138.67, 138.60, 137.61, 132.31, 132.00, 131.73, 129.02, 128.50, 127.70, 125.79, 124.14, 40.01, 36.06, 34.95, 33.22, 32.40, 32.05, 31.31, 30.61, 30.24, 30.18, 30.12, 30.03, 29.85, 26.91, 23.15, 14.34; MS (FD, 8kV): m/z (%) = 3043.9 (100%, M^+) (calc. for $C_{224}H_{330}$ = 3043.29 g mol^{-1}).

6.2.2.42 13, 26-Bis(1,1-dimethylethyl) 2,5,8,11,15,18,21,24-octakis(n-dodecyl)-tetrabenzo[jk,mn,pq,st]dibenzo[3,4:9,10]phenanthro[1',10',9',8':5,6,7,8]pe-rylo[2,1,12,11-bcdef]ovalene (4-116)

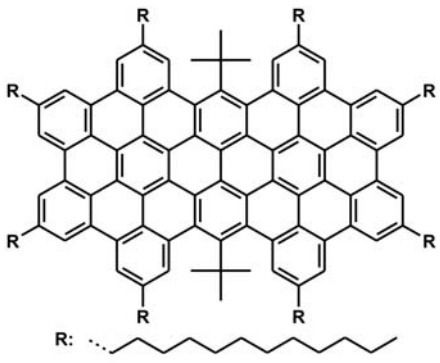

A 100 mL Schlenk tube was charged with 1,8-bis(1,1-dimethylethyl)-3,4,5,6,10,11,12,13-octa(4-dodecyl-tetraphenyl)-benzenepyrene (0.03 g, 0.013 mmol) (**4-115**) and 45 mL of dry dichloromethane. A flow of argon was led through the solution, which had been preliminary enriched with CH_2Cl_2 vapor. $FeCl_3$ (0.162 g, 1.0 mmol) dissolved in CH_3NO_2 (1.62 mL) was added and the mixture was stirred at room temperature for 18 h. The reaction was quenched by adding methanol. After addition of 2 mL of hydrazine and 1 mL of CS_2, a grey substance precipitated. After filtration, the product was washed out of the precipitate using excess THF. The solvent was evaporated and the resulting dark, red solid was again dissolved in a small amount of THF and reprecipitated in 200 mL of methanol. The precipitate was filtered off, dried and dissolved in toluene and filtrated over a short silica column to remove residual iron. After removal of the solvent, the

product was again dissolved in a small amount of THF and precipitated in 200 mL of methanol, yielding (**4-116**) as a dark, red solid (85 %): ^{1}H-NMR (250 MHz, CD_2Cl_2, 293 K): δ = 9.61 (s, 4H, Ar-*H*); 9.27 (s, 4H, Ar-*H*); 9.22 (s, 4H, Ar-*H*); 9.13 (s, 4H, Ar-*H*); 3.57 (t, 16H, ^{3}J(H,H) = 7.54 Hz, α-C*H*$_2$); 3.36 (t, 16H, ^{3}J(H,H) = 7.45 Hz, α-C*H*$_2$); 2.40-2.05 (m, 32H, β-C*H*$_2$); 2.00-1.00 (m, 144H, alkyl-C*H*$_2$); 0.98-0.80 (m, 24H, -C*H*$_3$); MS (MALDI-TOF, trans-2-[3-(4-*tert*-butylphenyl)-2-methyl-2-propenylidene]-malononitrile): m/z (%) = 2348.54 (14%), 2349.52 (24%), 2350.51 (24%), 2351.50 (17%), 2352.51 (10%), 2353.53 (5%), 2354.55 (3%) (calc. for $C_{176}H_{234}$ = 2349.83 g mol^{-1}, isotope distr.: 2347.83 (14%), 2348.83 (27%), 2349.84 (27%), 2350.84 (18%), 2351.84 (9%), 2352.85 (3%), 2353.85 (1%)); EA: C = 87.28 %, H = 9.82 % (calcd.: C = 89.96 %, H = 10.04 %).

6.2.2.43 13,26-Bis(1,1-dimethylethyl)-2,11,15,24-tetrakis(n-dodecyl)-5,8,18,21-tetrakis-(2-decyl-tetradecyl)-tetrabenzo[jk,mn,pq,st]dibenzo[3,4:9,10]phenanthro[1',10',9',8':5,6,7,8]perylo[2,1,12,11-bcdef]ovalene (4-119)

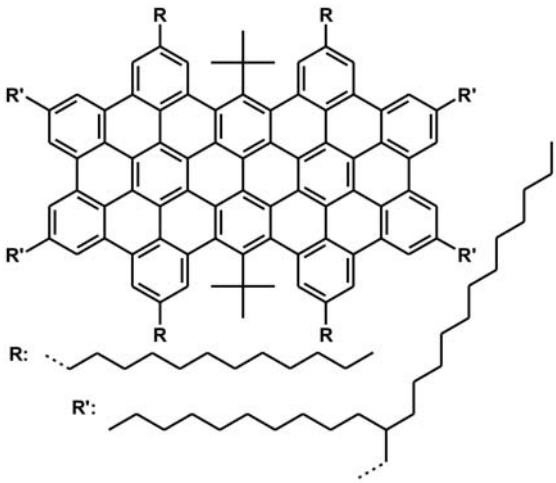

A 100 mL Schlenk tube was charged with 1,8-bis(1,1-dimethylethyl)-3,6,10,13-tetra(4-dodecyl-tetraphenyl)-4,5,11,12-tetrakis(2-decyl-tetradecyl)-benzenepyrene (0.05 g, 0.016 mmol) (**4-118**) and 60 ml of dry dichloromethane. A flow of argon was led through the solution, which had before been enriched with CH_2Cl_2 vapor. $FeCl_3$ (0.213 g, 1.3 mmol) dissolved in CH_3NO_2 (2.13 mL) was added and the mixture was stirred at room temperature for 18 h. The reaction was quenched by adding methanol. After 2 mL of hydrazine and 1 mL of CS_2 were added, a grey precipitate formed. After filtration the product was washed out of the precipitate using excess THF. The solvent was evaporated and the resulting dark, red solid was again dissolved in a small amount of THF and reprecipitated in 200 mL of methanol. The precipitate was filtered off, dried and dissolved in toluene and filtrated over a short silica column to remove residual iron. After removal of the solvent, the product was again dissolved in a small amount of THF and precipitated in 200 mL of methanol, yielding (**4-119**) as a dark, red solid (83 %): ^{1}H-NMR (250 MHz, CD_2Cl_2, 293 K): δ = 9.61 (s, 4H, Ar-*H*); 9.27 (s, 4H, Ar-*H*); 9.22 (s,

4H, Ar-*H*); 9.13 (s, 4H, Ar-*H*); 3.59 (t, 8H, ^{3}J(H,H) = 7.62 Hz, α-C*H*$_2$); 3.35 (d, 8H, ^{3}J(H,H) = 6.55 Hz, α-C*H*$_2$); 2.50-0.50 (m, 280H, alkyl-C*H*$_2$, -C*H*$_3$); MS (MALDI-TOF, trans-2-[3-(4-*tert*-butylphenyl)-2-methyl-2-propenylidene]-malononitrile): m/z (%) = 3021.51 (10%), 3022.48 (21%), 3023.50 (26%), 3024.48 (20%), 3025.50 (14%), 3026.45 (8%); (calc. for $C_{224}H_{330}$ = 3023.13 g mol^{-1}, isotope distr.: 3020.58 (8%), 3021.59 (20%), 3022.59 (26%), 3023.59 (22%), 3024.60 (14%), 3025.60 (7%)) EA: C = 90.07 %, H = 10.03 (calcd.: C = 89.00 %, H = 11.00 %).

6.2.2.44 2,5,8,11,15,18,21,24-octa-(n-dodecyl)-tetrabenzo[jk,mn,pq,st] dibenzo[3,4:9,10]phenanthro[1',10',9',8':5,6,7,8]perylo[2,1,12,11-bcdef]ovalene (4-128)

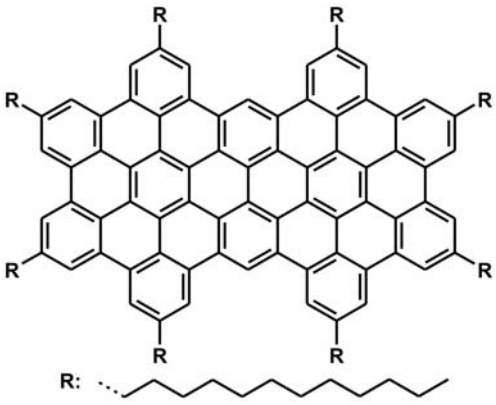

In a microwave tube (**4-116**) (0.03 g, 0.012 mmol), 6 mL of dry benzene and two drops of fuming H_2SO_4 were combined. The reaction mixture was purged with argon, the tube was sealed and the reaction mixture was stirred overnight at 150 °C. After cooling to room temperature, the reaction mixture was added drop-wise to 200 mL of methanol. The precipitate was filtered off and washed with water and excess methanol. The resulting dark solid was finally dried under vacuum (95 %): MS (MALDI-TOF, trans-2-[3-(4-*tert*-butylphenyl)-2-methyl-2-propenylidene]-malono-nitrile): m/z (%) = 2236.00 (16%), 2236.98 (24%), 2238.00 (22%), 2238.99 (15%), 2239.98 (9%), 2240.99 (6%) (calc. for $C_{168}H_{218}$ = 2237.61 g mol^{-1}, isotope distr.: 2235.71 (15%), 2236.71 (29%), 2237.71 (27%), 2238.72 (17%), 2239.72 (8%), 2240.72 (3%))

6.2.2.45 2,11,15,24-tetra-(n-dodecyl)-5,8,18,21-tetrakis(2-decyl-tetradecyl)-tetrabenzo[jk,mn,pq,st]dibenzo[3,4:9,10]phenanthro[1',10',9',8':5,6,7,8]perylo [2,1,12,11-bcdef]ovalene (4-129)

In a microwave tube (**4-119**) (0.03 g, 0.012 mmol), 6 mL of dry benzene and two drops of fuming H_2SO_4 were combined. The reaction mixture was purged with argon, the tube was sealed and the reaction mixture was stirred overnight at 150 °C. After cooling to room temperature, the reaction mixture was added droppwise to 200 mL of methanol. The precipitate was filtered off and washed with water and excess methanol. The resulting dark solid was finally dried under vacuum (95 %): MS (MALDI-TOF,

trans-2-[3-(4-*tert*-butylphenyl)-2-methyl-2-propenylidene]-malononitrile): m/z (%) = 2909.90 (11%), 2910.91 (19%), 2911.88 (22%), 2912.88 (18%), 2913.86 (14%), 2914.84 (8%), 2915.80 (7%) (calc. for $C_{224}H_{330}$ = 3023.13 g mol^{-1}, isotope distr.: 2908.46 (8%), 2909.46 (21%), 2910.46 (26%), 2911.47 (21%), 2912.47 (13%), 2913.47 (6%), 2914.48 (2%)).

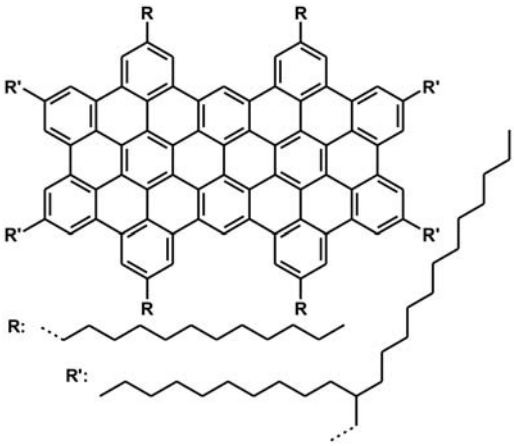

6.3 References

[1] A. Fechtenkötter, N. Chebotareva, M. D. Watson, K. Müllen *Tetrahedron* **2001**, *57*, 3769.

[2] H. Sauriat-Dorizon, T. Maris, J. D. Wuest *J. Org. Chem.* **2003**, *68*, 240.

[3] E. B. Stephens, J. M. Tour *Macromolecules* **1993**, *26*, 2420.

[4] P. A. Lottaz, T. R. G. Edwards, Y. G. Mentha, U. Burger *Tetrahedron Letters* **1993**, *34*, 639.

[5] L. F. Tietze, T. H. Eicher *Reaktionen und Synthesen*, Thieme Verlag Stuttgart, **1981**, 197.

[6] I. Agranat, M. Rabinovitz, W. C. Shaw *J. Org. Chem.* **1979**, *44*, 1936.

[7] B. H. Ye, Y. Naruta *Tetrahedron* **2003**, *59*, 3593.

[8] M. J. Mio, L. C. Kopel, J. B. Braun, T. L. Gadzikwa, K. L. Hull, R. G. Brisbois, C. J. Markworth, P. A. Grieco *Organic Letters* **2002**, *4*, 3199.

[9] M. Wehmeier, M. Wagner, K. Müllen *Chem. Eur. J.* **2001**, *7*, 2197.

[10] R. A. Pascal, W. D. McMillan, D. van Engen, R. G. Eason *J. Am. Chem. Soc.* **1987**, *109*, 4660.

[11] Wang, K. *unpublished results*, same synthetic procedure as published in ref. [13].

[12] Coan, S. B.; Trucker, D. E.; Becker, E. I. *J. Am. Chem. Soc.* **1955**, *77*, 60.

[13] Wang, Z.; Tomovic, Z.; Kastler, M.; Pretsch, R.; Negri, F.; Enkelmann, V.; Müllen, K. *J. Am. Chem. Soc.* **2004**, *126*, 7794.

[14] Okano, M.; Amano, M.; Takagi, K. *Tetrahedron Letters* **1998**, *39*, 3001.

[15] Ikegami, R.; Koresawa, A.; Shibata, T.; Takagi, K. *J. Org. Chem.* **2003**, *68*, 2195.

[16] Ito, S; Wehmeier, M.; Brand, J. D.; Kübel, C.; Epsch, R.; Rabe, J. P.; Müllen, K. *Chem. Eur. J.* **2000**, 6, 4327.

[17] T. Yamato, M. Fujimoto, A. Miyazawa, K. Matsuo *J. Chem. Soc., Perkin Trans. 1* **1997**, 1201.

[18] D. Wasserfallen, M. Kastler, W. Pisula, W. A. Hofer, Y. Fogel, Z. Wang, K. Müllen *J. Am. Chem. Soc.* **2005** - accepted.

[19] W. Pisula, M. Kastler, D. Wasserfallen, T. Pakula, K. Müllen, *J. Am. Chem. Soc.* **2004**, *126*, 8074.

7 Appendix

A Solid-State NMR

In solution NMR, the spectra consist of a series of sharp transitions, which is based upon the averaging of anisotropic NMR interactions by a rapid, random tumbling of the molecules in the solvent. In contrast, solid state NMR spectra are very broad, as the before mentioned anisotropic effects or orientation-dependent interactions are observed in the spectrum. For achieving similar information than from corresponding solution NMR spectra, two key techniques are applied: magic-angle spinning (MAS) and dipolar recoupling. With these methods, it is possible to obtain combined chemical shift and dipolar coupling informations.

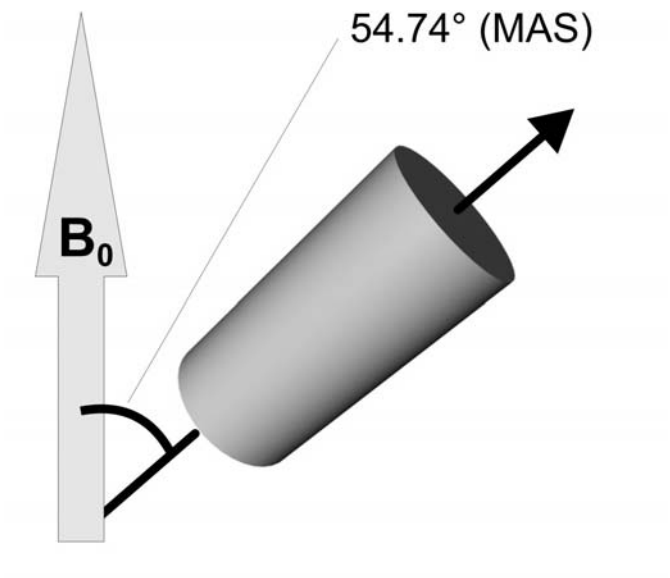

Figure 7-1: Schematic representation of the rotation of a sample with MAS.

MAS has become an indispensable tool to narrow resonance lines in the presence on anisotropic "line-broadening" interactios, such as dipole-dipole couplings or chemical shift anisotropies. By rotating the sample at frequencies of 10-30 kHz around an axis, which is oriented at the magic angle (54.7°) relative to the external magnetic field (Figure 7-1), the line broadening can be efficiently reduced. In the context of HBCs, this effect was of partiular importance for the ^{1}H chemical shifts, since they exhibit a pronounced sensitivity on nearby π-electrons. In this way, neighboring aromatic cores led to caracteristic shifts of the ^{1}H resonances either to low or high field. The shifts correspond to the extent, by which the ^{1}H nuclei experience the ring current effect either

above, below or beside an aromatic unit. Hence, ^{1}H resonances are ideal probes for the columnar packing of the aromatic HBC cores.

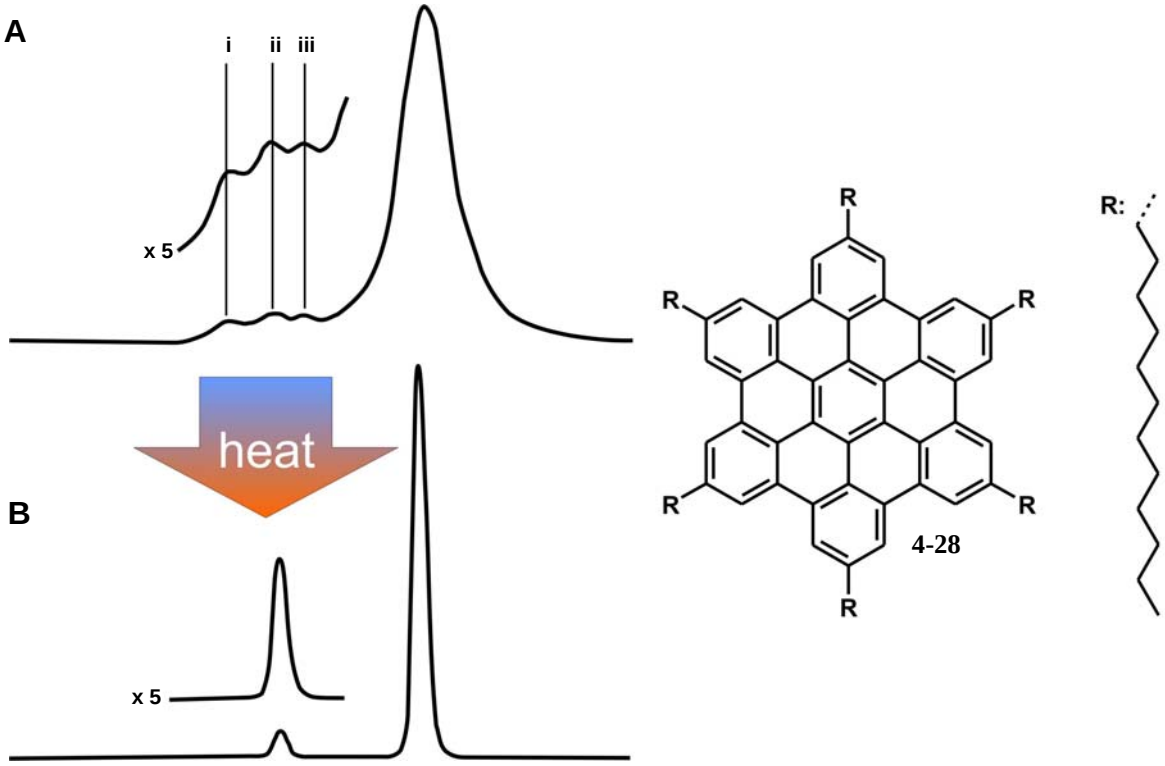

Figure 7-2: ^{1}H spectra of the HBC derivative **4-28** at **A**) "crystalline" phase and **B**) liquid-crystalline phase.

Although the MAS is a prerequisite for obtaining the chemical shift information in solid state NMR, this is achieved by the substantial reduction of dipolar interactions. This situation is commonly encountered in liquid samples, where the molecules can tumble isotropically and dipole-dipole effects are almost completely averaged to zero. However, to exploit the valuable structural and and dynamic information inherent to dipolar couplings in solids, the effect of the MAS needs to be compensated in certain periods of the experiments. The applied dipolar recoupling, which is accomplished by the application of radio-frequency pulse sequences, initiates a “counterrotation” of the spin part of the nuclear wave function. The time intervals, during which the dipolar interactions are reintroduced, can be precisely defined, and the experiments can be designed to allow a very precise measurement of dipolar coupling strengths in combination with chemical shift resolution. Translated to internuclear distances, the experimental sensitivity allows an accuracy of usually 0.01 Angstrom, with internuclear distances ranging from 1 to about 5 Angstrom. Additionally, with respect to the

molecular dynamics, kinetic or thermodynamic parameters of the processes can be determined.

Surprisingly, three distinct aromatic ^{1}H resonances were found for HBC-C_{12} (**4-28**) in the crystalline phase at room temperature (Figure 7-2A),[1,2] although the molecule exhibits a six-fold symmetry and the investigated protons are all chemically equivalent. Upon heating the sample into its liquid-crystalline state the three signals merged into one (Figure 7-2B). Therefore, in the crystalline phase, the splitting of the aromatic resonances reflected three different degrees, to which the protons experience aromatic ring current effects from the adjacent aromatic layers.

For verification, if the three resonances are resulting from different packing arrangements or from the protons of a single molecule, double-quatum (DQ) spectra were recorded. With this method, detailed information about internuclear proximities can be obtained from the signals.

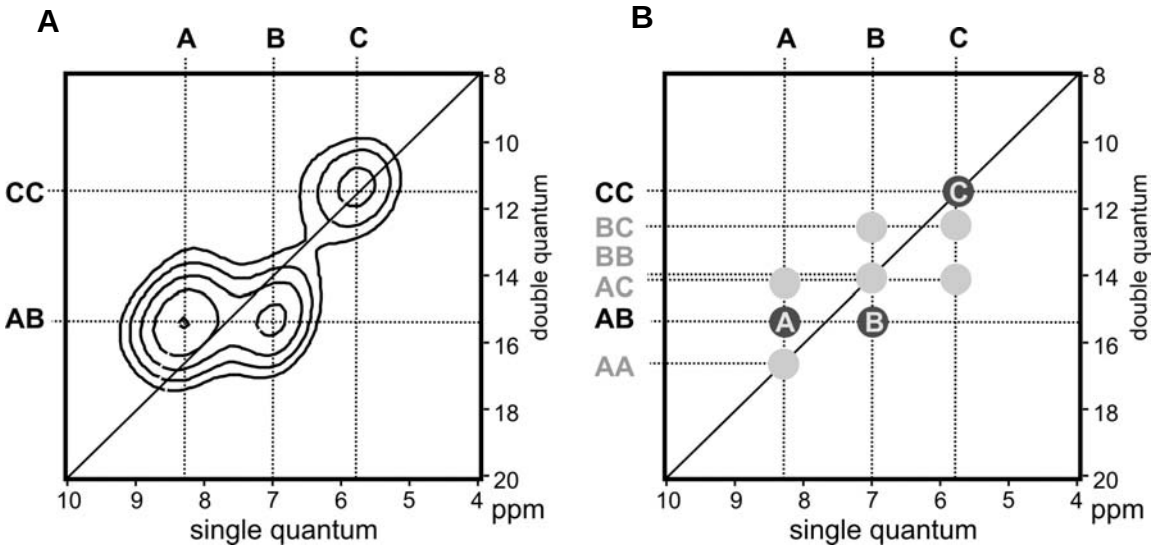

Figure 7-3: Structural implications from the signal pattern observed in the ^{1}H ^{1}H double quantum spectrum of the HBC derivative **4-28**; **A**) experimental and **B**) all signals that could be theoretically observed.

For the aromatic protons of HBC-C_{12} (**4-28**), the signal pattern observed in the two-dimensional ^{1}H ^{1}H DQ spectrum, is presented in Figure 7-3A. The presence of two off-diagonal peaks indicated a close proximity of two aromatic protons with different chemical shifts (AB), while the diagonal peak is due to a CC pair. From the relative signal intensities, it is clear that the two types of pairs, AB and CC, are present in a ratio

of 2:1. In Figure 7-3B all theoretically possible signals are depicted, and in addition the observed signals are highlighted.

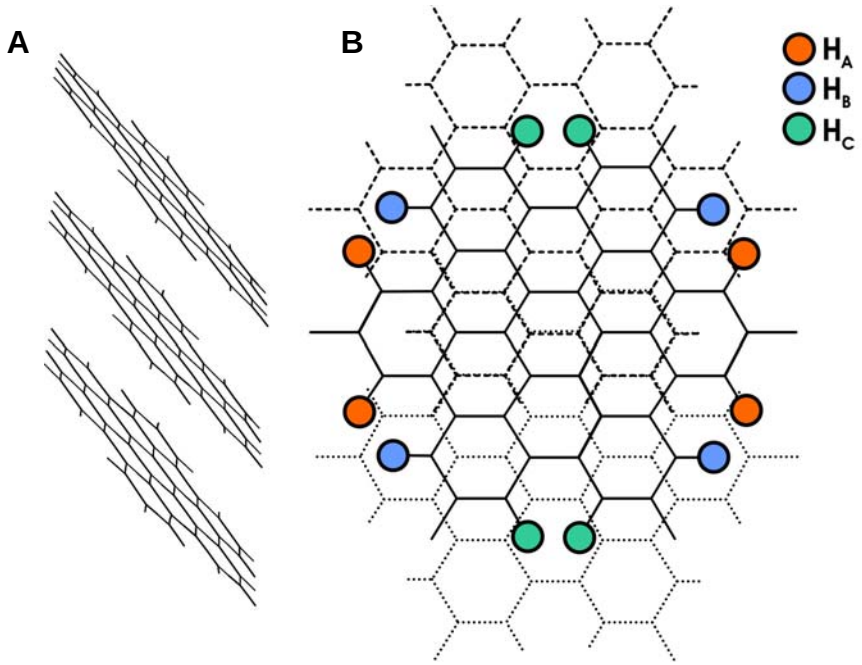

Figure 7-4: Relative arrangement of the discs in crystalline HBC; **A**) side-view and **B**) top view.

It became obvious from the crystal structure of unsubstituted HBC, that the relative arrangement of the aromatic discs is such, that the aromatic protons are exposed to three different ring curents (Figure 7-4). The types of pairs and the signal intensities observed in the ^{1}H DQ spectrum of HBC-C_{12} (**4-28**) corresponded quantitatively to the three distinguishable proton positions in crystalline HBC (Figure 7-4). Therefore, the ^{1}H NMR spectra showed that in the crystalline phase of HBC-C_{12} (**4-28**) the aromatic discs are packed in the same fashion as in crystalline HBC.[3,4]

References

[1] S. P. Brown, I. Schnell, J. D. Brand, K. Müllen, H. W. Spiess *J. Am Chem. Soc.* **1999**, *121*, 6712.

[2] S. P. Brown, I. Schnell, J. D. Brand, K. Müllen, H. W. Spiess *J. Mol. Struct.* **2000**, *521*, 171.

[3] C. Ochsenfeld, S. P. Brown, I. Schnell, J. Gauss, H. W. Spiess *J. Am Chem. Soc.* **2001**, *123*, 2597.

[4] A. Fechtenkötter, K. Saalwächter, M. Harbison, K. Müllen, H. W. Spiess *Angew. Chem. Int. Ed.* **1999**, *38*, 3039.

B Zone-Casting

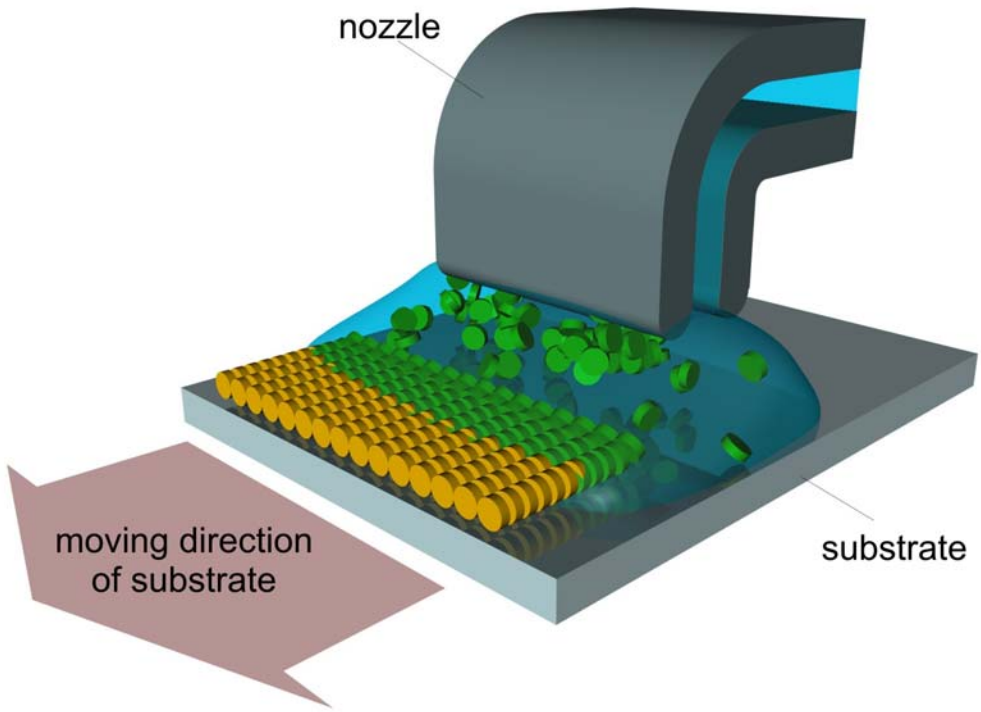

Figure 7-5: Schematic representation of an experimental setup for zone-casting

A schematic representation of the experimental setup is depicted in Figure 7-5. A solution of the investigated material is spread out by a nozzle onto a moving substrate platter. During the process, a meniscus is formed between the nozzle and the support. While the solvent evaporates, a concentration gradient occurs inside the meniscus. At the critical concentration the material starts to precipitate or nucleates from the solution and crystallizes directionally onto the moving support, establihing an aligned thin layer. The morphologies of the obtained films can be controlled by a variety of parameters, namely type of solvent, evaporation temperature, concentration and the solvent flow.

C Zone-Crystallization

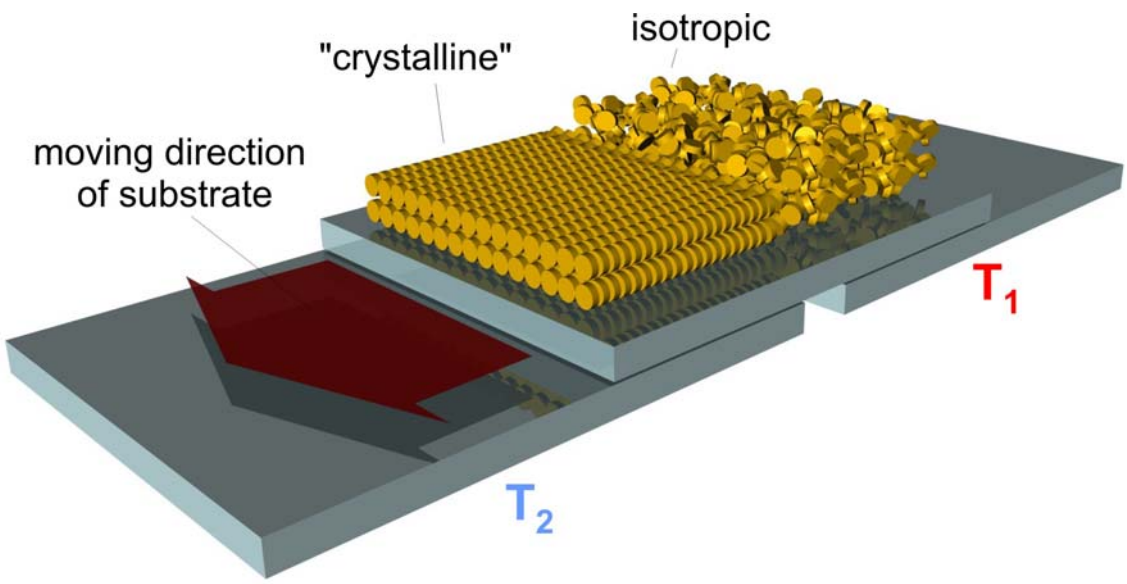

Figure 7-6: Schematic representation of an experimental setup for zone-crystallization.

In Figure 7-6 a schematic representation of the experimental setup is depicted. A prerequisite, regarding the material properties used for this treatment is that the compound exhibits an isotropic phase at reasonable temperatures. During the alignment process a substrate plate is moved at controlled velocity from a heating block with temperature T_1, where the material is in the isotropic phase, to a block with a temperature T_2, which is lower than the crystallization temperature of the material. By application of the optimum conditions only one nucleation point will appear, which is the origin of the subsequent growth in direction of the temperature gradient.

D Improved Synthesis Towards the HBC Derivative (4-30)

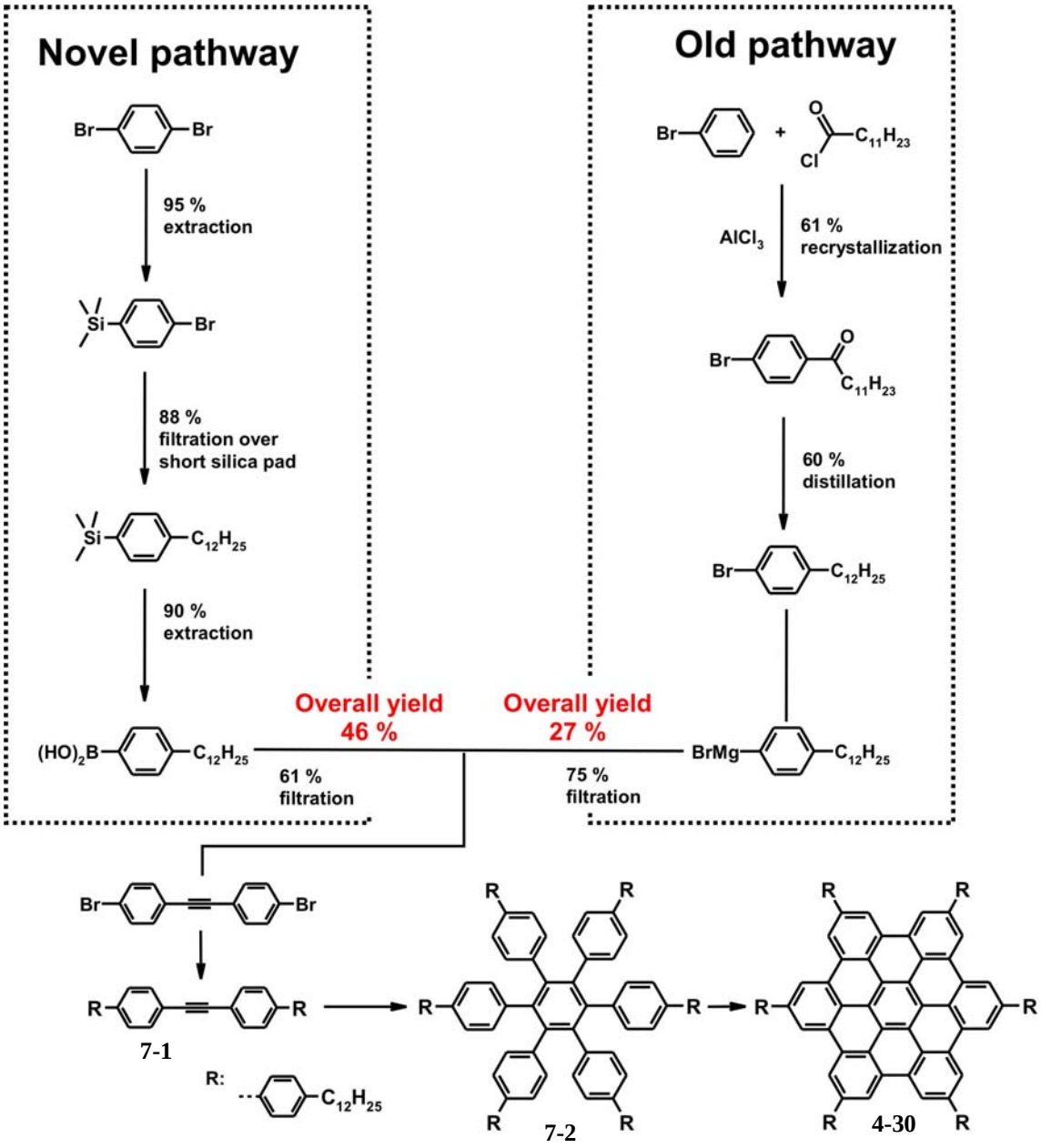

Figure 7-7: A) Synthesis towards the HBC derivative **4-30** and comparison of the old and the novel route towards the diphenylacetylene derivative **7-1**.

As the diphenylecatylene derivative **7-1** is used for the preparation of the dodecyl-phenyl substituted HBC (**4-30**), which showed the highest charge-carrier mobilites seen so far for a mesogen, the presented Suzuki-coupling in section 4.1.2 of (4-dodecyl-phenyl)-boronic acid with appropriate halogenated compounds proved to be even more valuable. On one hand, by using this approach the overall yield towards the diphenylacetylene derivative was significantly improved (47 %) compared to the

published route (27 %), on the other hand the time-consuming purification steps were replaced by a smooth, straightforward synthesis and most of the time the products could be used without further purification or required only minor workup procedures (Figure 7-7). With this method, it is now possible to synthesize the beforementioned HBC (**4-30**) in a shorter time in gram scale quantities.

E Nomenclature

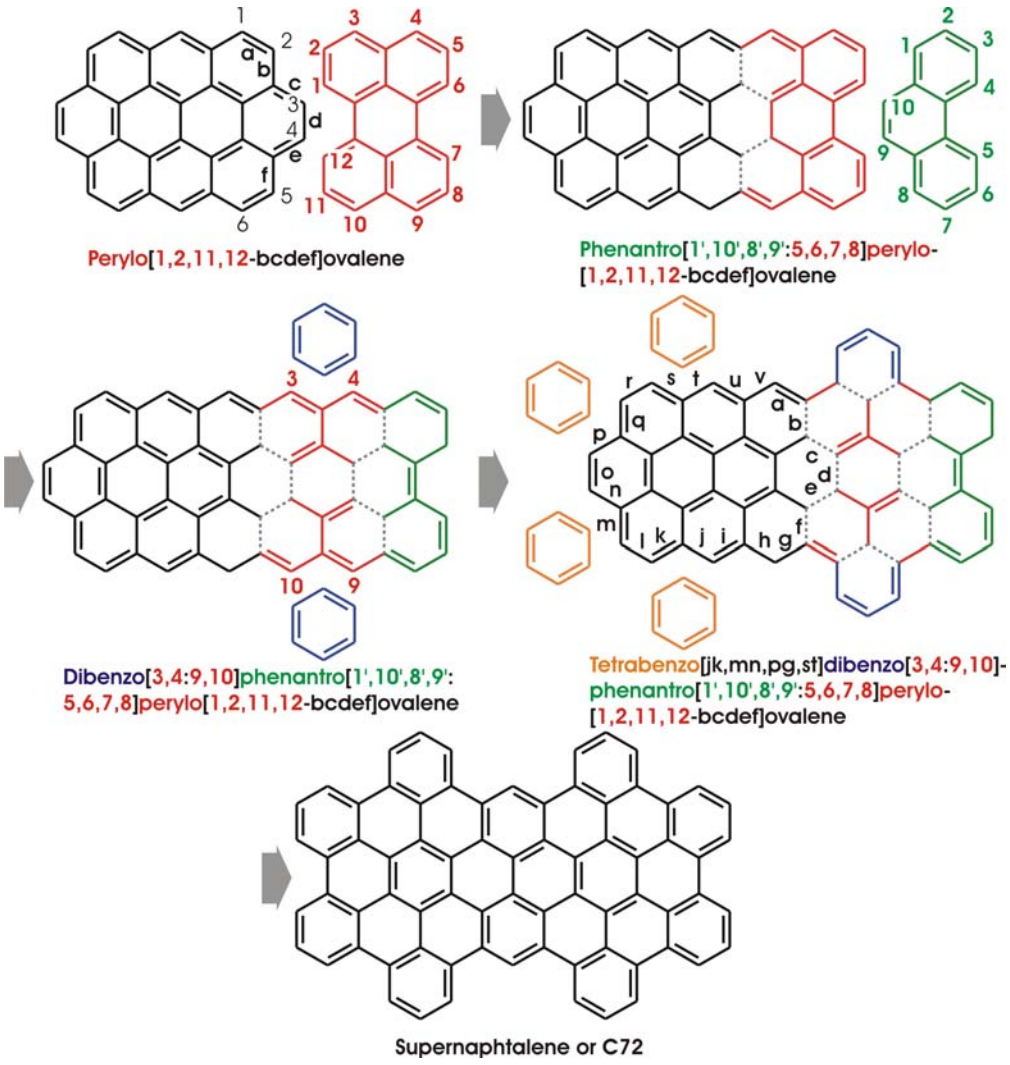

Figure 7-8: IUPAC nomenclature of C72.

According to the nomenclature introduced by the International Union of Pure and Applied Chemistry (IUPAC) the system presented in Figure 7-8 is called "Tetrabenzo[jk,mn,pg,st]dibenzo[3,4:9,10]phenantro[1',10',8',9':5,6,7,8]perylo[1,2,11,12-bcdef]ovalene". This name was derived from the existing rules of nomenclature for polycyclic aromatic hydrocarbons. In the beginning, it was necessary to locate the

largest possible PAH that could be set as the basis for the naming, which is in this example ovalene. The system was fused with perylene, whereby the numbering of the parent compound enters as characters, which define the bonds used for the fusion. For the perylene, the numbers of the virtually removed hydrogens define the sites for the addition. Therefore, after the first step the resulting PAH can be declared as perylo[1,2,11,12-bcdef]ovalene. In the second step, a phenantrene block was added. It becomes clear that a distinction between the numbers of the perylene and the phenantrene part is necessary. As the phenantrene is the "second level" PAH, a dash is added to its numbers, which results in the name phenantro[1',10',8',9':5,6,7,8]-perylo[1,2,11,12-bcdef]ovalene. This procedure was reapplied for the subsequent addition of the remaining PAH-parts. Detailed informations related to the naming and numbering of PAHs can be found in reference 1.

References

[1] http://www.chem.qmul.ac.uk/iupac/

F MALDI-TOF MS modes

After the ionization process of the analyte, one receives after the laser pulse a velocity distribution of the analyte ions. This leads to a broadening of the spectra but can be corrected by applying the reflex mode (Figure 7-9). Ions with a higher starting velocity after the ionization will also show up earlier at the end of the drifting distance. As they do have a higher kinetic energy they penetrate deeper into the electric field of the reflector and have to travel a longer distance than ions of the same species with lower kinetic energy. During this time the slower ions overtake the faster species. At the detector, the faster ions however can catch up with the slower species and reach the target at the same time, leading to a higher resolution of the spectra.

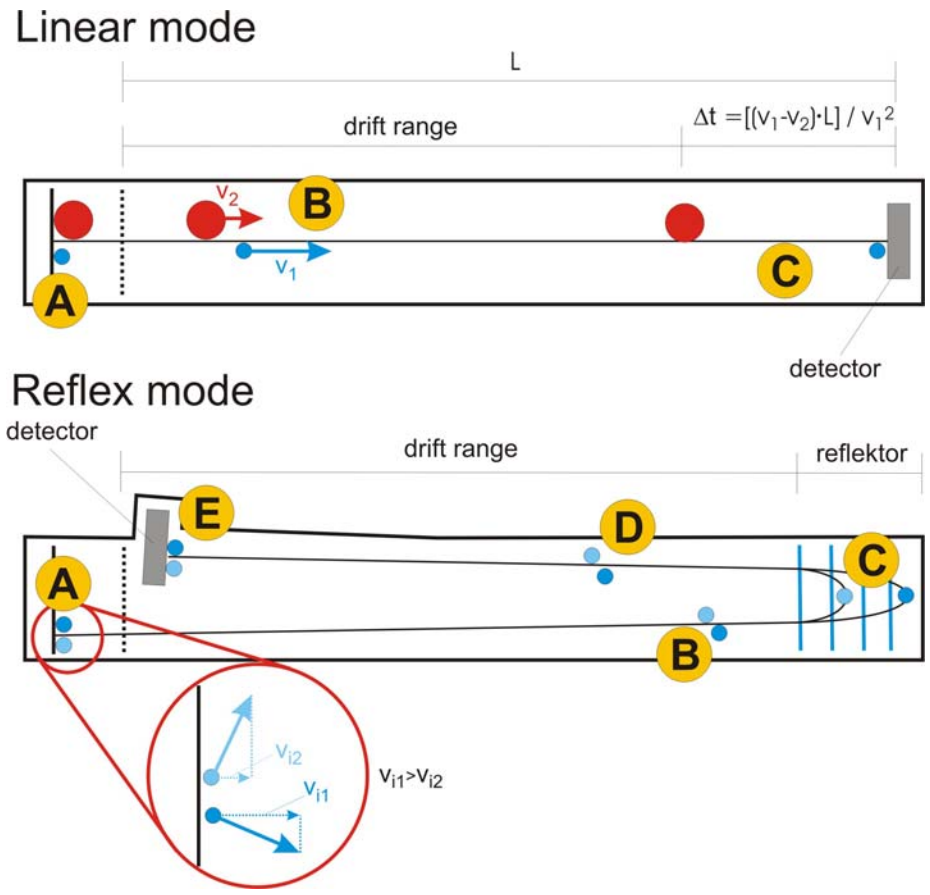

Figure 7-9: Linear mode of MALDI-TOF MS: A) ionization of the molecules with different mass weight; B) After acceleration the heavier mass will exhibit a smaller travel velocity, leading to a separation of the masses. C) Lower weight molecule is detected, while heavier molecule is still in the drift range. Reflex mode: A) ionization and vaporisation leads to differences in the initial velocity of the same molecules; B) molecules with a higher initial velocity (v_{i1}) overtake slower molecules leading to a broadening of the spectrum; C) in the reflector the faster molecules will have to travel a longer distance which allows the slower molecules to overtake; D) faster molecules are catching up; E) molecules are detected at the same time despite their differences in initial velocity.

G PR-TRMC technique

The pulse radiolysis time- resolved microwave conductivity (PR-TRMC) technique is used for the non-destructive study of charge transport in organic materials. The method can be roughly divided into two parts. On one hand, charge-carriers are created by a pulse-radiolysis using a 3 MeV electron accelerator, on the other the detection of the created mobile charges are detected by monitoring the respective absorbed microwave power.

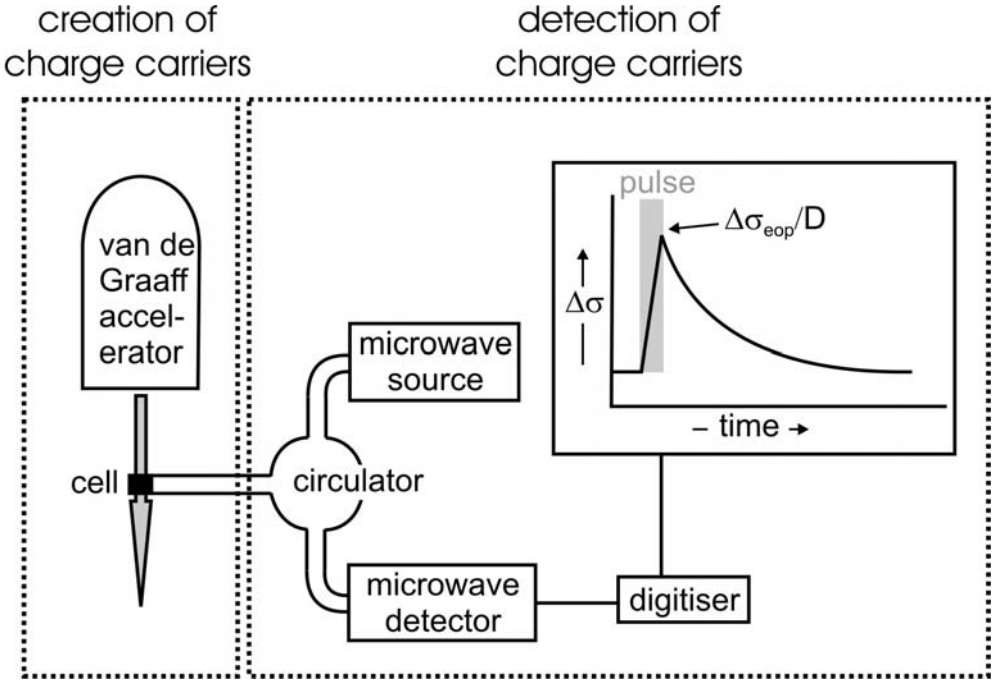

Figure 7-10: Schematic representation of the PR-TRMC setup

In the method depicted in Figure 7-10, the bulk material is irradiated with high energy electrons resulting in a low concentration of electron-hole pairs. These charge carriers will induce a change in the microwave conductivity, indicated by the change in the microwave power reflected by the cell. Microwaves are high frequency electromagnetic waves in the GHz range. These waves are attenuated, if they conduct through a medium, where charge carriers are present. The microwaves popagate through the sample and are reflected at the end of the cell by a metal plate. The reflected wave is finally directed to a detector. One important thing to note is, that with the TRMC method only the sum of the mobilities of the negative and positive charge carriers can be determined and not the charge carrier sign with the corresponding mobility value.

It has to be pointed out that the following discussion is only a short description of the necessary mathematical relations. For detailed informations, please refer to the references 1 to 3. The determined conductivity is related to the sum of the mobilities of the positive and negative charge carriers ($\Sigma\mu_{TRMC} = \mu_{+}+\mu_{-}$ [$m^2V^{-1}s^{-1}$]) and their concentration (N_p [m^{-3}]) by

$$\Delta\sigma = e\, N_p \sum \mu_{TRMC} \qquad \text{Eq. 7-1}$$

with e as the elementary charge (1.6 x 10^{-19} C). Therefore, when the concentration of charge carriers is known, it is possible to derive an estimation of the charge carrier mobility by the experimentally determined conductivity change.

For an infinitely short pulse, a dose D of (J m^{-3}) will result in an initial concentration of electron-hole pairs ($N_p(0)$) of

$$N_p(0) = \frac{D}{e\,E_p} \qquad \text{Eq. 7-2}$$

with E_p the required average energy for the formation of one electron-hole pair. For pulses of finite duration a fraction of the initially formed chage carriers may undergo a fast recombination within the pulse. This results in an end-of-pulse survival probability, W_{eop}. The actual concentration of charge carriers present at the end of the pulse will therefore be

$$N_p(eop) = \frac{W_{eop}\,D}{e\,E_p} \qquad \text{Eq. 7-3}$$

By a substitution of eq. 7-3 in 7-1, one gains for the end-of-pulse conductivity

$$\Delta\sigma_{eop} = \frac{W_{eop}\,D\,\Sigma\mu_{TRMC}}{E_p} \qquad \text{Eq. 7-4}$$

The mobility can then be estimated by the experimentally determined $\Delta\sigma/D$, when W_{eop} and E_p are known, by using the relationship

$$\Sigma\mu_{TRMC} = \frac{E_p}{W_{eop}} \cdot \frac{\Delta\sigma_{eop}}{D} \qquad \text{Eq. 7-5}$$

The mobility value determined by eq. 7-5 is an isotropic value corresponding to a random orientation of the columnar axis within the microdomains. For each domain, the charge transport is expected to be highly anisotropic and occurs preferentially along the columnar axis.[4-7] Therefore, the mean value of the mobility averaged over all

orientations is related to the one-dimensional intracolumnar mobility by a factor of 3, resulting in the equation

$$\Sigma\mu_{1D} = 3 \cdot \frac{E_p}{W_{eop}} \cdot \frac{\Delta\sigma_{eop}}{D} \qquad \text{Eq. 7-6}$$

References

[1] Warman, J.M. The Microwave Absorption Technique for Studying Ions and Ionic Processes. In *The study of fast processes and transient species by electron pulse radiolysis*; Baxendale, J. H., Busi, F., Ed.; Reidel: Dordrecht, 1982; pp 129-161.

[2] J. M. Warman, M. P. de Haas Time-Resolved Conductivity Techniques, DC to Microwave. In *Pulse Radiolysis*; Tabata, Y., Ed.; CRC Press: Boca Raton, Florida, **1991**, 101-133.

[3] P. G. Schouten *phD thesis* Delft University of Technology, **1994**.

[4] E. O. Arikainen, N. Boden, R. J. Bushby, J. Clements, B. Movaghar, A. Wood *J. Mater. Chem.* **1995**, *5*, 2161.

[5] N. Boden, R. J. Bushby, J. Clements, M. V. Jesudason, P. F. Knowles, G. Williams *Chem. Phys. Lett.* **1988**, *152*, 94.

[6] N. Boden, R. J. Bushby, J. Clements *J. Chem. Phys.* **1993**, *98*, 5920.

[7] N. Boden, R. J. Bushby, A. N. Cammidge, J. Clements, R. Luo, K. J. Donovan *Mol. Cryst. Liq. Cryst.* **1995**, *261*, 251.

H Electronic spectroscopy of PAHs

Historical

For PAHs a classification of the bands into α- p- and β-bands has been introduced by Clar.[1,2] These three bands, which can be generally found in PAHs are distinguished by their relative intensities where the α-band shows the weakest and the β-band the strongest absorption behavior. In the series from benzene to heptaphene (Figure 7-11A), these bands remain in a specific sequence, where β is found at the smaller, α at the larger wavelengths and the p-band in between. By increasing size of the systems a strong shift towards the red is observed, which is called the annellation effect.

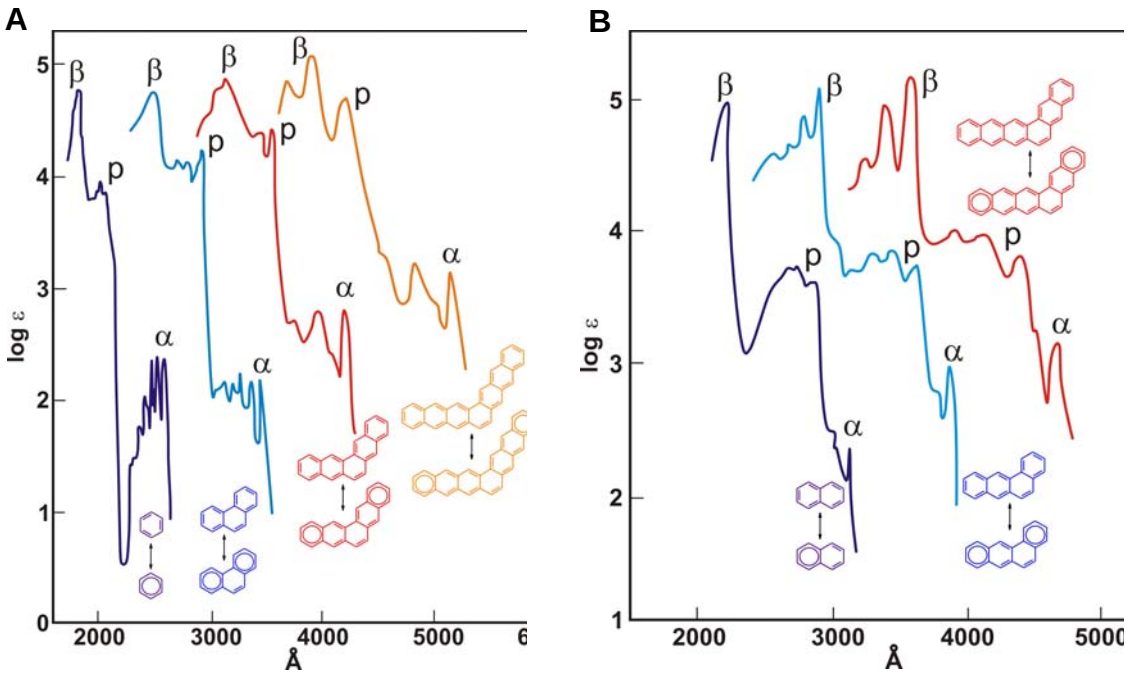

Figure 7-11: UV/vis absorption profiles in the phene series (**A**) and the asymmetric phene series (**B**).

It demonstrates that the two branches are in aromatic conjugation, each ring producing a constant shift to the red, which is valid as long as the systems contain only two sextets. If the annellation of the two rings does not take place in a symmetric way (Figure 7-11B), it causes a stronger bathochromic shift for the p- than for the α- and the β-bands, leading to a partial superimposition of the α-bands. The migration of the p-bands is essentially dependent on the longest branch, while the other two bands respond equally to the linear annellation of the rings to any of the two branches. The ratio of the wavelengths of the α- and β-bands remain however at 1:1.35. The extreme case can be found in the linear acene series (Figure 7-12), where the p bands move far more to the red with the annellation than the α- and β-bands. Thus for anthracene and tetracene the α-bands get completely hidden by the p-bands. They reappear faintly in the minimum of the spectrum of pentacene. However the p-bands still show a constant shift relative to the annellation. Conclusively, it can be said that the b bands prove to be the most reliable bands for comparing annellation effects, as they are not only the most intense bands in the spectra but also shift towards the red with linear annellation of the two branches. In addition the β-bands are never superimposed by other bands and can always be observed, independent of the symmetry of the molecule. However, it is also known that the stability of the isomers increases with the number of sextets, which is combined with big shifts of the absorption bands towards the violet.

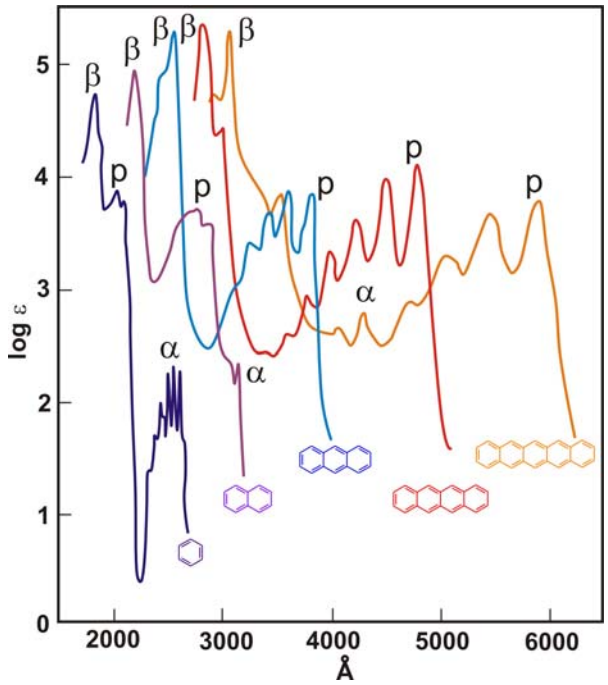

Figure 7-12: UV/vis absorption profiles in the acene series.

Theory

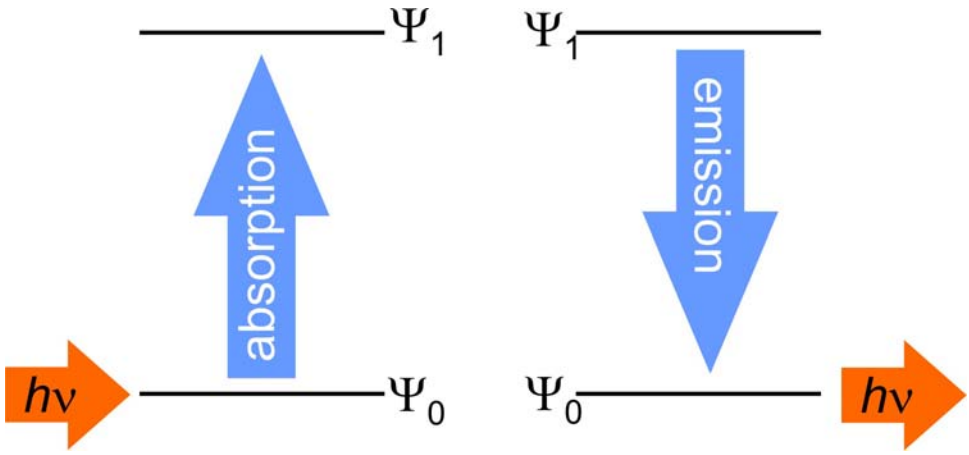

Figure 7-13: Electron transition and emission process.

When light with an appropriate wavelength (ν) interacts with a molecule in the electronic ground state S_0, it can be absorbed and can lift the molecule into an electronically excited state (Figure 7-13). By spontaneous emission, the system can afterwards return to the ground state S_0. The correlation of the orbitals involved with the electron transition is depicted in Figure 7-14.

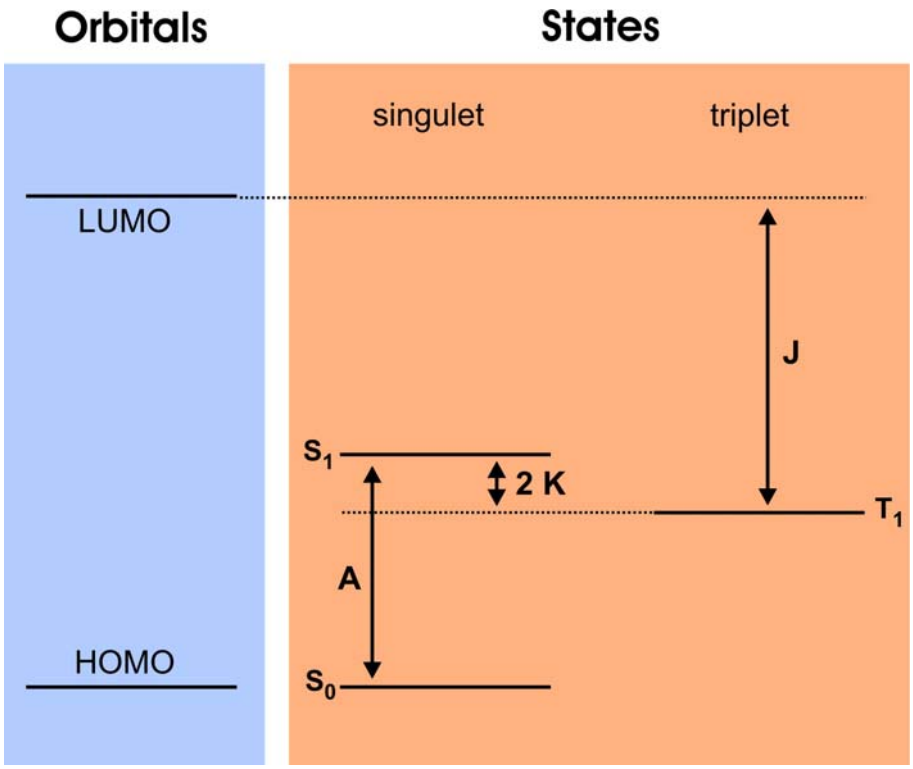

Figure 7-14: Energy scheme for the electron transitions between HOMO and LUMO.

The energy difference between the lowest unoccupied molecular orbital (LUMO) and the highest occupied molecular orbital (HOMO) is thereby higher than the energy A between the singulet ground state S_0 and the first excited singulet state S_1. The difference originates from different electron interactions (Coulomb J and exchange term 2K). Due to K > 0, the lowest triplet state T_1 lies always energetically lower than S_1. As a consequence of the configuration interactions, the HOMO-LUMO transition does not necessarily be the $S_0 \rightarrow S_1$ transition.

However, such transitions do not need to occur, moreover they exhibit certain probabilities for the corresponding transitions. Hereby, the oscillator strength $\mathbf{f_{01}}$ indicates the fraction of the electrons, which will take part in the respective transition. If **f** exhibits small values, the transition is declared as forbidden, while for values near 1, it is allowed. The quantum mechanical analogon is the transition dipole moment $\mathbf{M_{01}}$, which represents the change in dipole moment during the transition.

For molecules several rules apply. The "spin-interdiction" implies that the overall spin resp. the multiplicity **M = 2S + 1** needs to be retained. Therefore, transitions in between singulet states are allowed, while between triplet and singulet states the transitions are forbidden. Such a disappearance of transitions can also occur for

symmetry reasons ("symmetry-interdiction"). However, this interdiction can be circumvented, as the core motions reduce the symmetry and induce the occurrence of symmetry forbidden transitions. Another reason for the disappearance of the electronic transition dipole moment is the so-called "overlap-interdiction", which appears when the two orbitals, required for the transition, do not or show only a little spatial overlap.

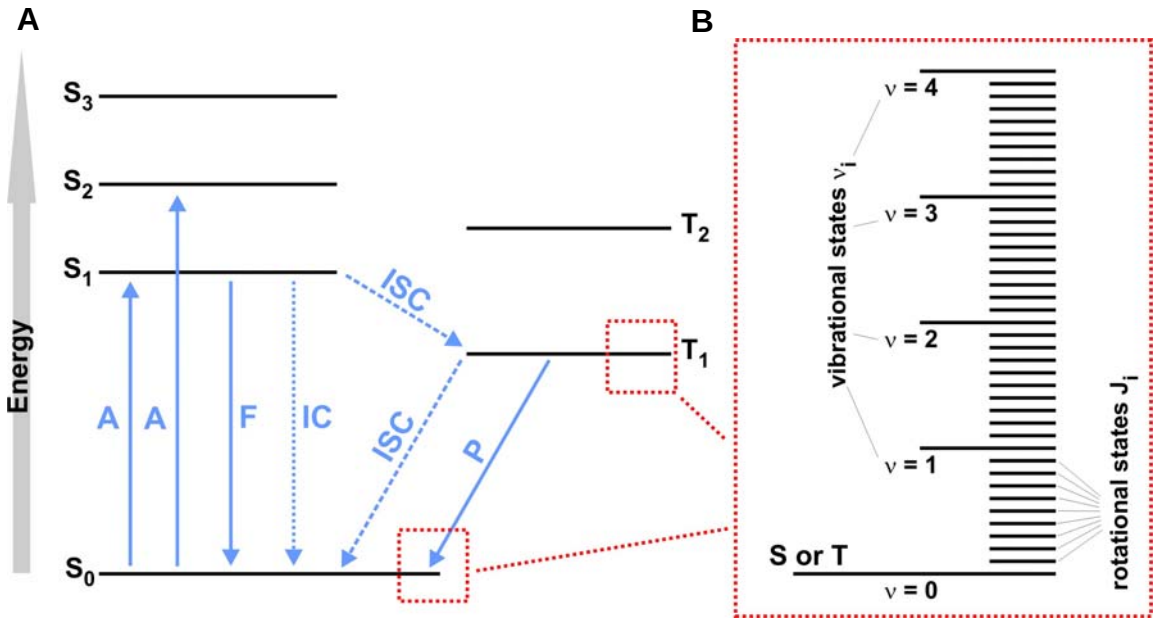

Figure 7-15: A) Jablonski diagram with the possible transitions (A: absorption, F: fluorescence, IC: internal conversion, ISC: intersystem crossing, P: phosphorescence); **B**) schematic representation of the superposition of the electronic vibration and rotational states.

In summary, by absorption processes one observes transitions from the ground state, which is usually a singulet state S_0, to other energetically higher singulet states S_1, S_2 and so on (Figure 7-15A). The return to S_0 commonly occurs from S_1 (seldom from other singulet states) by fluorescence or by a radiationless deactivation process (internal conversion). Radiationless spin reversion processes (intersystem crossing) lead to triplet states, which despite the "spin-interdiction", can return to the S_0 state by phosphorescence or another radiationless intersystem crossing.

In contrast to atoms, molecular electronic states show relatively broad energy bands, which is caused by a superposition of vibrational and rotational states. As shown in Figure 7-15B each term in the Jablonski diagram is energetically splitted. Therefore, an energetical state with an energy $\mathbf{E_{total}}$ corresponds to a certain electronic vibrational and rotational state of the molecule leading to:

$$E_{total} = E_{electronic} + E_{vibrational} + E_{rotational}$$

For an electron transition, this leads to:

$$\Delta E_{total} = \Delta E_{electronic} + \Delta E_{vibrational} + \Delta E_{rotational}$$

As presented in Figure 7-15B the electronic part is always far larger than the vibrational, which is again far more pronounced than the rotational part. In addition to the processes, shown in the simplified Jablonski diagram (Figure 7-15A), the relaxation **R** can appear, which is a radiationless decay within an electronic state. For spectra recorded in solution, the rotational contributions cannot be observed, moreover the bands consist of vibrational states. Depending on the compound, the absorptions are more or less resolved, whereby a higher resolution is expected for rigid molecules.

According to the Frank-Condon principle, the probability for a transition is maximized for a vertical transition of the energy-hypersurface, meaning that all parameters (bond lengths, bond angles, conformation, solvation cage, etc.) are retained. It has to be noted that the vibrational part of the transition from the lowest vibrational state ($\nu = 0$) of the ground state S_0 to the different vibrational states ($\nu' = 0, 1, \ldots$) of the excited states S_n ($n = 1, 2, \ldots$) do not show identical transition probabilities.

According to the definitions introduced by Clar (α, β, p) for the description of PAHs, J. R. Platt developped a corresponding nomenclature, originating from the group theory.

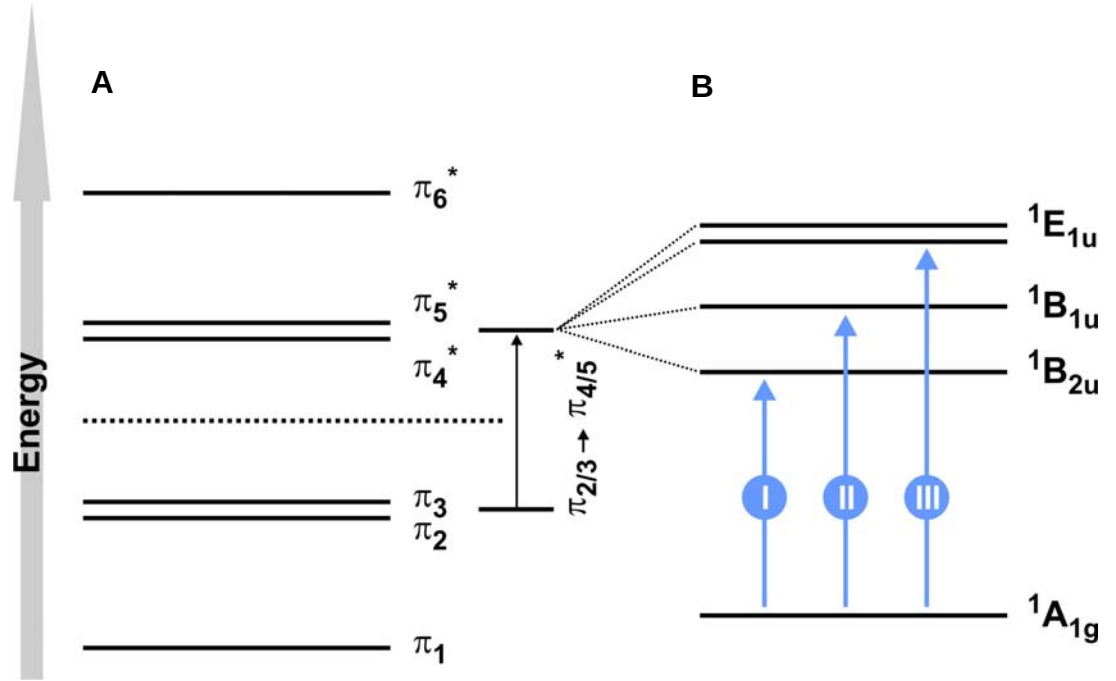

Figure 7-16: A) Energy scheme of the p-orbitals for benzene; **B**) electron excitations in benzene (for description of transition I to III see Table 7-1 below)

Transition		Platt	Clar
I	$^1A_{1g} \rightarrow {}^1B_{2u}$	$^1A \rightarrow {}^1L_b$	α
II	$^1A_{1g} \rightarrow {}^1B_{1u}$	$^1A \rightarrow {}^1L_a$	p
III	$^1A_{1g} \rightarrow {}^1E_{1u}$	$^1A \rightarrow {}^1B$	β

Table 7-1: Description of the electron excitation processes seen in Figure 7-16.

In the case of benzene, the π_2/π_3 (HOMO) and π_4^*/π_5^* (LUMO) orbitals form pairs of orbitals with identical energies (degeneration; Figure 7-16). The four possible electron transtions $\pi_{2/3} \rightarrow \pi_{4/5}^*$ lead from the $^1A_{1g}$ ground state to the excited singulet states $^1B_{2u}$, $^1B_{1u}$ and $^1E_{1u}$. The last state is degenerated as indicated by the symbol E. Due to the electron correlation, the three excites states differ in their energetical level, resulting in the observed electronic transitions (α, β, p).

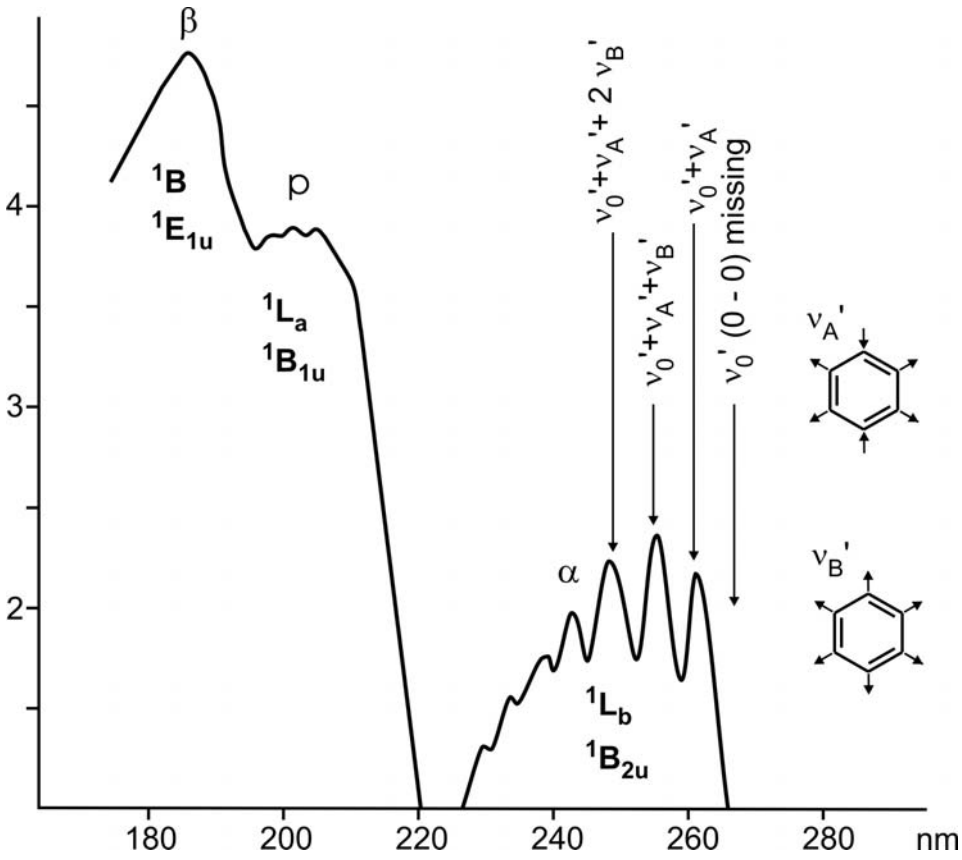

Figure 7-17: Absorption spectra of benzene.

In the UV/vis of benzene the strongly structured p- and α-bands correspond to symmetry-forbidden transitions (Figure 7-17). The p-band borrows intensity from the symmetry-allowed transition (β-band). Due to the "symmetry-interdiction" the vibrational 0 → 0 transition is missing in the α-band. The vibration ν_A' is disturbing the hexagonal symmetry and leads to the band located at the longest wavelengths. Further vibrational bands follow in a linear relation, corresponding to the symmetric pulsation vibration ν_b'.

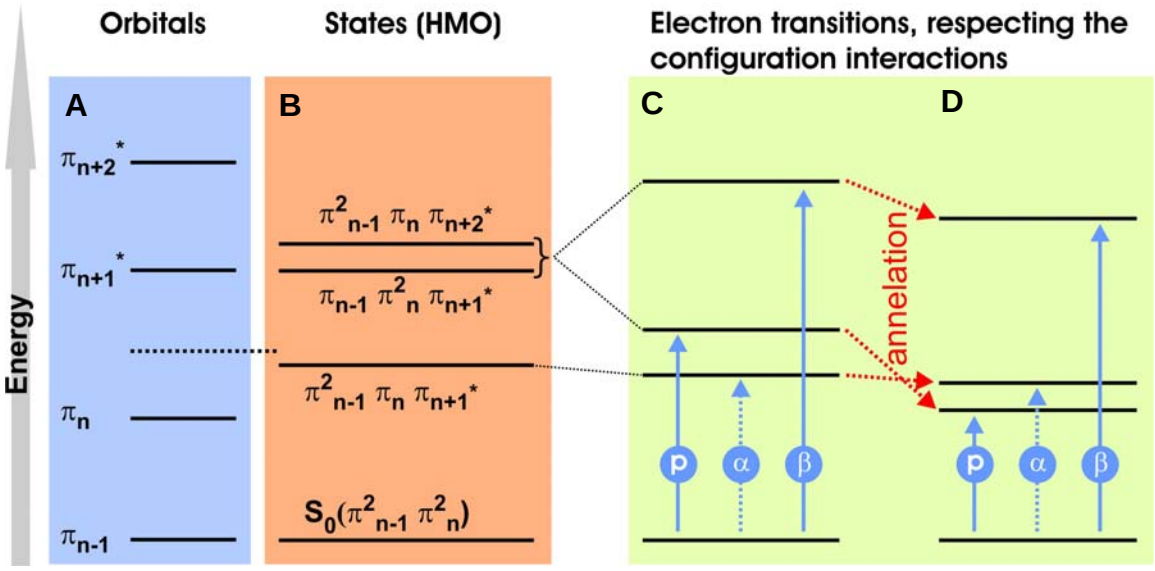

Figure 7-18: A) energy scheme of the π-orbitals for PAHs; B) state diagram according to HMO calculations; **B**) electron transitions by taking into account the configuration interactions for **C**) smaller PAHs and **D**) after annealation, when the α- band is overtaken by the p-band.

In contrast to benzene, the two highest occupied (π_{n-1} and π_n) and the two lowest unoccupied (π_{n+1}^* and π_{n+2}^*) molecular orbitals of PAHs are not anymore degenerated. Between them four electron transitions are possible (Figure 7-18C) With additional annelation, the α, β and p-bands are bathochromically shifted, whereby it is possible that the p- can cover or overtake the α-band (Figure 7-18D). It has to be pointed out that by all means the HOMO-LUMO transitions corresponds to the p-band.[3,4]

Influence of Distortion of the Aromatic Component upon the Electronic Spectra

The influence of the distortion of an aromatic entity onto its electronic properties has been studied extensively in the field of [n]paracyclophanes (Figure 7-19). The known [n]paracyclophanes[5,6] with values fo *n* from 16 down to 10 did not show any surprising features. As the value of *n* decreases below 9, the synthesis of the molecules becomes more difficult.

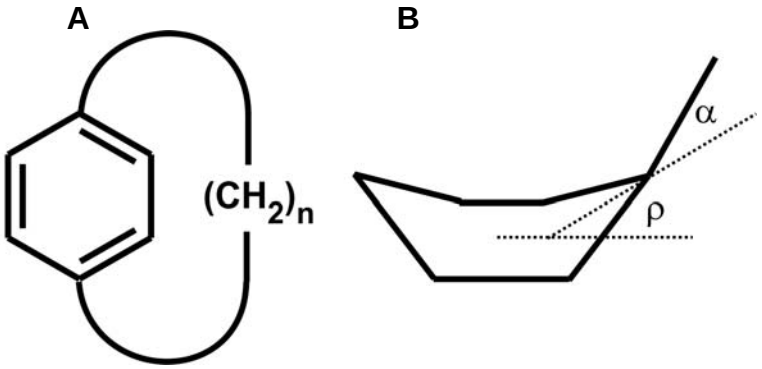

Figure 7-19: A) [n]paracyclophanes; **B**) angles used for description of the bending of the aromatic core.

The physical property, which was already long ago observed to be a function of the ring bending, is the UV spectrum. Increasingly out-of plane deformation of the benzene ring leads to a bathochromic shift of the three transitions appearing in the UV spectrum. This has been additionally investigated from a theoretical point of view. Another appearance of such a bathochromic shift, upon the distortion of the aromatic moiety has also been observed for perylene derivatives.[7-9] Therefore, it can be concluded that a distortion of an aromatic moiety will lead to bathochromic shift in the electronic spectra of the compounds.

Conjugation Effects Regarding the Electronic Spectra

The importance of an appropriate conformation for the electronic properties of aromatic compounds have been extensively studied for poly(p-phenylene)s (PPP) (**7-3**) in the recent years (Figure 7-20).[10] This type of materials has attracted a great interest, due to the fact that upon doping the compounds act as excellent organic conductors and

that polymers with PPP backbones can be used as active components in blue light emitting diodes.

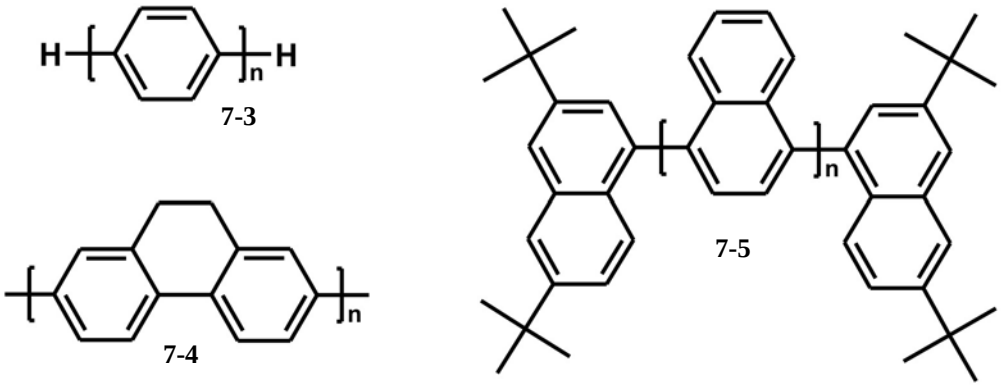

Figure 7-20: Structures of poly(paraphenylene) PPP (**7-3**), poly(phenantrene) PPT (**7-4**) and oligo-(1,4-naphtylene) (**7-5**), where n = 1-4

In the parent oligo- or poly(*p*-phenylene)s, the steric interactions between the *ortho*-hydrogens cause the planes of neighboring aryl rings to adopt dihedral angles up to 23°, which significantly reduces the π-overlap and thus prevents extended π-conjugation.[11,12] By replacing the hydrogens by larger groups, even greater dihedral angles and results in a more pronounced disturbance of the π-orbital overlap along the PPP backbone and a reduction of the effective conjugation length (ECL).[13] Such distortions from planarity of the linear backbone result in hypsochromic shifts in the UV/vis spectra.[12]

The planarization of oligo- and poly(*p*-phenylene)s to maximize the extent of conjugation by enhancing the π-orbital overlap has been of noteable interest for a number of years. One example for planarized derivatives, in which the electronic characteristics of the PPP π-electron system are better retained, are oligomers and polymers with 5,6-dihydrophenantrene-3,8-diyl repeat units (poly(phenantrene)s) PPT (**7-4**). This system, which establishes a bridging between adjacent phenyl rings, maintains flexibility and is not fully planarized. Nevertheless, the investigation of the UV/vis convergence behavior for the series of **7-4** revealed an ECL of n_{ECL} = 19 (whereby n is the number of phenyl rings in the linear backbone), which is nearly twice as high as the one of the parent PPP (**7-3**) ($n_{ECL} \approx 7$).

Another interesting example is the oligo-(1,4-naphtylene) series (**7-5**). Within this series, almost no change in the bathochromic shift can be observed. This result reflects the significant steric interaction between adjacent nahpthalene units that leads to a

ground state configuration in which neighboring naphthalene entities adopt a nearly orthogonal orientation.[14]

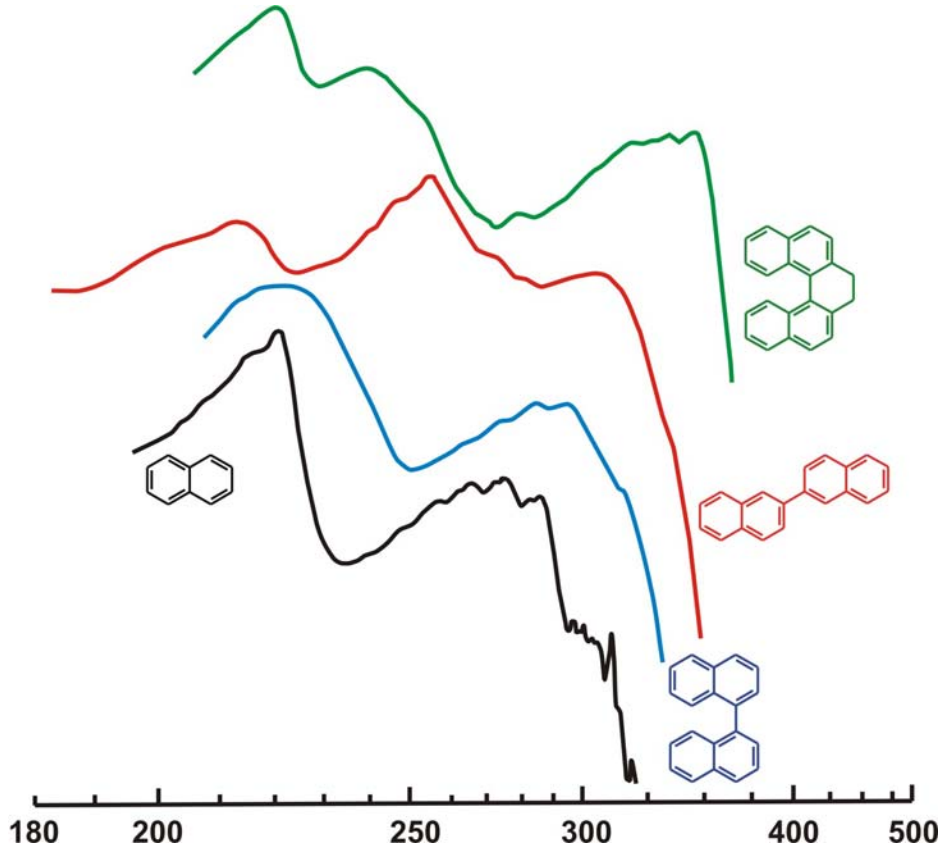

Figure 7-21: Electronic spectra of benzene, 1,1'-binaphtyl, 2,2'-binaphtyl and 3,4-dihydrodibenzo[c,g] phenanthrene

As shown in Figure 7-21, the influence of the conformation of aromatic compounds upon the shift of the UV/vis bands is not only restricted to PPPs. Also smaller examples reveal that the correct arrangement of the aromatic moieties is a prerequisite to achieve a bathochromic shift of the respective absorption bands. For example, almost no difference in the shift of the absorption bands can be observed for naphthalene and the 1,1'-binaphtyl, although the 1,1'-binaphtyl contains formally a far larger aromatic system than naphthalene. This result is in accordance to the observations obtained from the oligo-(1,4-naphtylene) series. By changing to the 2,2'-binaphtyl case, where the naphthalene moieties can adopt an improved conformation similar to PPP (**7-3**), also a bathochromic shift can be observed (approx. 30 nm). However, this shift is not very distinct, pointing towards the already discussed steric interactions between the *ortho*-

hydrogens. Similar to the PPT example (**7-4**), for the 3,4-dihydrodibenzo[c,g]phenanthrene, where the ethane-1,2-diyl bridge forces the two naphthalene units into a more favorable conformation for an extension of the π-electron conjugation, a more pronounced bathochromic shift can be detected (approx. 70-80 nm).

In conclusion it can be said, that for a pronounced π-electron conjugation between aromatic moieties, resulting in a bathochromic shift of the UV/vis absorption bands, a certain confined conformation between the moieties has to be adopted.

Determination of Fluorescence Quantum Yield

The fluorescence quantum yield (ϕ_F) is the ratio of absorbed photons relative to the ones emitted by fluorescence. In other words, the quantum yield describes the probability of the excited state to be deactivated by fluorescence rather by another non-radiative mechanism.

The most reliable method, first described by Williams et al.,[15] to determine this value (ϕ_F) is the comparison of the investigated compound with well characterized standard samples with known ϕ_F values. Basically, the solutions of the standard and test samples with identical absorbance at the same excitation wavelength can be assumed to absorb the same number of photons. Therefore a simple ratio of the integrated fluorescence intensities of the two solutions (recorded under identical conditions) will yield the ratio of the quantum yield values. As the value for the standard sample is known, it is trivial to calculate ϕ_F for the test sample.

The actual measurement is slightly more complicated as some facts have to be considered. While on one hand concentration effects (self-quenching) can play a role, on the other, the possible use of different solvents for the standard and the test sample will have some effect. In addition, the validity of the standard sample has to be ensured. These arguments can be taken into account by working at a carefully chosen concentration range and by acquiring the spectra at a number of different absorbances (concentrations) and ensuring linearity across the concentration range. In addition, by using different solvents for the two samples, the solvent refractive indices have to be integrated into the ratio calculations. The standard sample can be cross calibrated with another to verify its ϕ_F value.

Experimental Considerations

Standard samples: The standard samples should absorb at the excitation wavelength of choice for the test sample. If possible, they should also emit in a similar region to the test sample. A number of lists of fluorescent standard samples are available:[16,17]

Compound	Solvent	Literature Quantum Yield	Emission range / nm	Reference
Cresyl violet	Methanol	0.54	600-650	*J. Phys. Chem.* **1979**, *83*, 696
Rhodamine 101	Ethanol + 0.01% HCl	1.00	600-650	*J. Phys. Chem.* **1980**, *84*, 1871
Quinine sulfate	0.1M H_2SO_4	0.54	400-600	*J. Phys. Chem.* **1961**, *65*, 229
Fluorescein	0.1M NaOH	0.79	500-600	*J. Am. Chem. Soc.* **1945**, 1099
Norharmane	0.1M H_2SO_4	0.58	400-550	*J. Lumin.* **1992**, *51*, 269
Harmane	0.1M H_2SO_4	0.83	400-550	*J. Lumin.* **1992**, *51*, 269
Harmine	0.1M H_2SO_4	0.45	400-550	*J. Lumin.* **1992**, *51*, 269
2-methylharmane	0.1M H_2SO_4	0.45	400-550	*J. Lumin.* **1992**, *51*, 269
Chlorophyll A	Ether	0.32	600-750	*Trans. Faraday Soc.* **1957**, *53*, 646
Zinc phthalocyanine	1% pyridine in toluene	0.30	660-750	*J. Chem. Phys.* **1971**, *55*, 4131
Benzene	Cyclohexane	0.05	270-300	*J. Phys. Chem.* **1968**, *72*, 325
Tryptophan	Water, pH 7.2, 25C	0.14	300-380	*J. Phys. Chem.* **1970**, *74*, 4480
2-Aminopyridine	0.1M H_2SO_4	0.60	315-480	*J. Phys. Chem.* **1968**, *72*, 2680
Anthracene	Ethanol	0.27	360-480	*J. Phys. Chem.* **1961**, *65*, 229
9,10-diphenyl anthracene	Cyclohexane	0.90	400-500	*J. Phys. Chem.* **1983**, *87*, 83

Table 7-2: List of standard materials and their literature quantum yields.

Concentration range: To reduce reabsorption effects,[18] absorbances in the fluorescence cuvette should not exceed 0.1 *at and above* the excitation wavelength (Figure 7-22). Above this level, non-linear effects can be observed due to inner filter effects. The maximum allowable value of the recorded absorbance is in relation to the path length of the absorption cuvette (10mm → 0.1, 20mm → 0.2 and so on).

Procedure:

1) Recording of the absorption spectrum of the sample and the solvent background. Determine the absorbance at the excitation wavelength (max. 0.1, see above).

2) Recording of the fluorescence spectrum of the same solution. Determine the integrated fluorescence intensity (area of the fluorescence spectrum).
3) Repeat steps 1) and 2) for all the solutions differing in concentration of the sample (if possible five different concentrations and the blank solvent).
4) Plotting a graph of the integrated fluorescence intensity *vs.* the absorbance. A straight line should result, which intersects the 0/0 value.
5) Repeat steps 1) to 4) for the remaining samples.

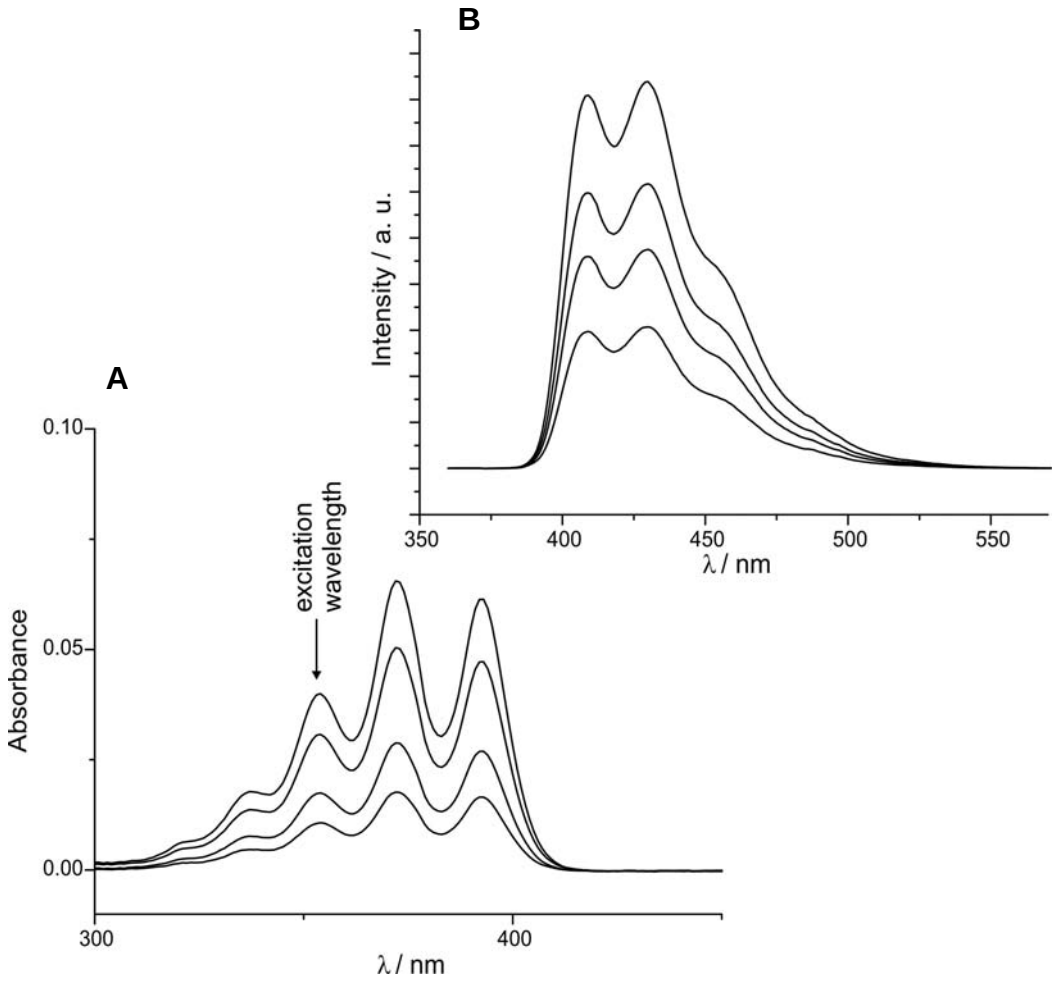

Figure 7-22: Example of an **A**) absorption and **B**) emission data set for four different concentrations of a sample.

Note: All fluorescence spectra need to be acquired with constant slit widths.

Evaluation: The obtained gradients of the graphs are proportional to the quantum yield of the respective sample. The absolute values are calculated using the standard samples, which have a fixed and known fluorescence quantum yield value, according to the following equation:

$$\Phi_X = \Phi_{ST} \cdot \left(\frac{Grad_X}{Grad_{ST}} \right) \cdot \left(\frac{\eta_X^2}{\eta_{ST}^2} \right) \qquad \text{Eq. 7-7}$$

The subscripts *X* and *ST* denote test and standard sample respectively. ϕ is the fluorescence quantum yield and *Grad* the gradient (Figure 7-23) from the plot of the integrated fluorescence intensity *vs.* the absorbance. η denotes the refractive indices of the solvents.

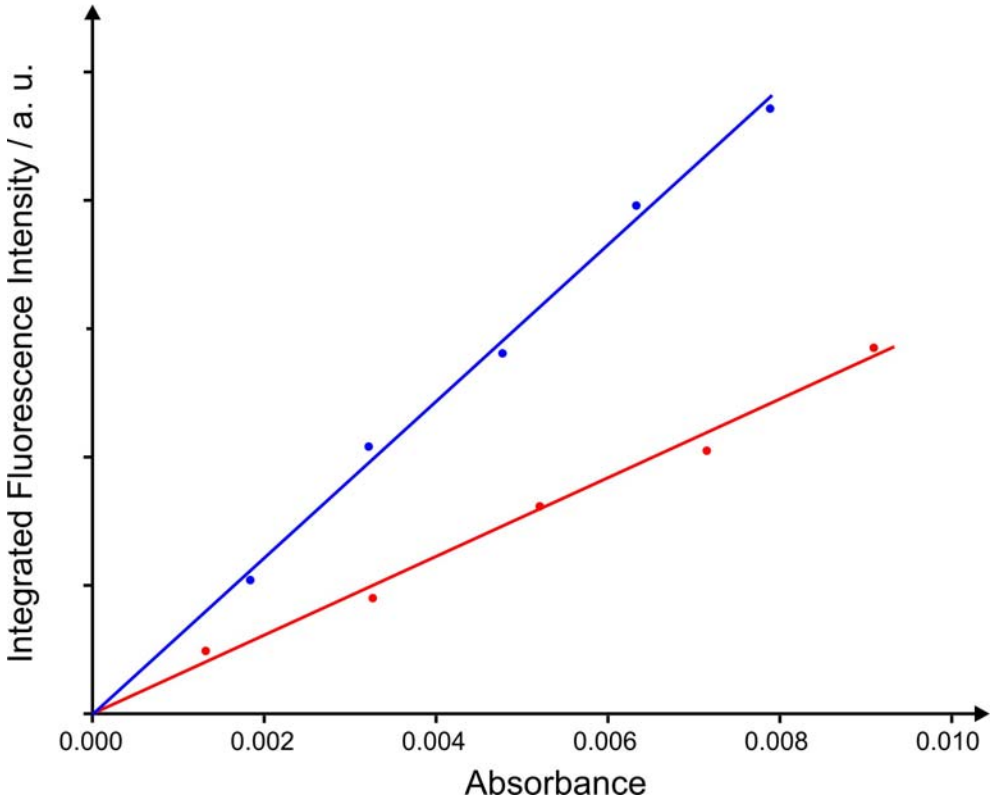

Figure 7-23: Linear plots for two samples. The gradient is proportional to the fluorescence quantum yield of the sample. The conversion into an absolute value is achieved by the equation

References

[1] E. Clar *Polycyclic Hydrocarbons* **1964**, Academic Press.

[2] E. Clar *The Aromatic Sextet* **1972**, John Wiley and Sons.

[3] E. Clar *Angewandte Chemie-International Edition* **1956**, *68*, 528.

[4] E. Clar, O. Kuhn *Annalen der Chemie-Justus Liebig* **1956**, *601*, 181.

[5] N. L. Allinger, J. T. Sprague, T. Liljefors *J. Am. Chem. Soc.* **1974**, *96*, 5100.

[6] L. W. Jenneskens, F. J. J. de Kanter, P. A. Kraakman, L. A. M. Turkenburg, W. E. Koolhaas, W. H.de Wolf, F. Bickelhaupt *J. Am. Chem. Soc.* **1985**, *107*, 3716-3717.

[7] G. Seybold, G. Wagenblast *Dyes Pigm.* **1989**, *11*, 303.

[8] L. T. Scott, P. C. Cheng, M. M. Hashemi, M. S. Bratcher, D. T. Meyer, H. B. Warren *J. Am. Chem. Soc.* **1997**, *119*, 10963.

[9] S. Hagen, M. S. Bratcher, M. S. Erickson, G. Zimmermann, L. T. Scott *Angew. Chem. Int. Ed. Engl.* **1997**, *36*, 406.

[10] R. E. Martin, F. Diederich *Angew. Chem. Int. Ed.* **1999**, *38*, 1350.

[11] J. M. Tour *Adv. Mater.* **1994**, *6*, 190.

[12] J. J. S. Lamba, J. M. Tour *J. Am. Chem. Soc.* **1994**, *116*, 11 723.

[13] H. Meier, U. Stalmach, H. Kolshorn *Acta Polym.* **1997**, *48*, 379.

[14] K. H. Koch, K. Müllen *Chem. Ber.* **1991**, *124*, 2091.

[15] A. T. R. Williams, S. A. Winfield, J. N. Miller *Analyst* **1983**, *108*, 1067.

[16] J. R. Lakowicz *Principles of Fluorescence Spectroscopy* **1999**, Kluwer Academic/Plenum Press, 2nd edition, New York.

[17] J. C. Scaiano *Handbook of Organic Photochemistry* **1989**, CRC Press.

[18] S. Dhami, A. J. de Mello, G. Rumbles, S. M. Bishop, D. Phillips, A. Beeby *Analyst* **1983**, *108*, 1067.

I HOMO-Levels in Relation to the Size of the Aromatic Entity

The relation between the size of PAHs and the absolute values of the energetical levels of their molecular orbitals have been investigated intensely for the rylene series. Theoretical studies predicted for this series a very narrow band gap, which is a prerequisite for a pronounced intrinsic conductivity that does not need to be induced by doping. In Figure 7-24, the calculated band structures of poly(*peri*-naphthalene) is presented, which has been achieved by Brédas et al.[1] with the so-called valence effective Hamiltonian (VEH) technique.[2,3]

As can be seen, the HOMO-level shows in the calculations a strong increase with increasing size of the aromatic moiety of the rylene drivatives. In addition, it is expected that the LUMO level will decrease, leading towards poly(*peri*-naphthalene) to a reduced band gap of merely 0.44 eV. The theoretically assumed lowering of the band gap with respect to the increasing size of the rylene backbone was also experimentally proven by

A. Bohnen et al. in a series of rylene derivatives.[4] Therefore, it can be assumed that by an increase of the aromatic moiety of PAHs, also the energetical levels of the HOMOs will increase, which will make the compounds more susceptible to oxidation.

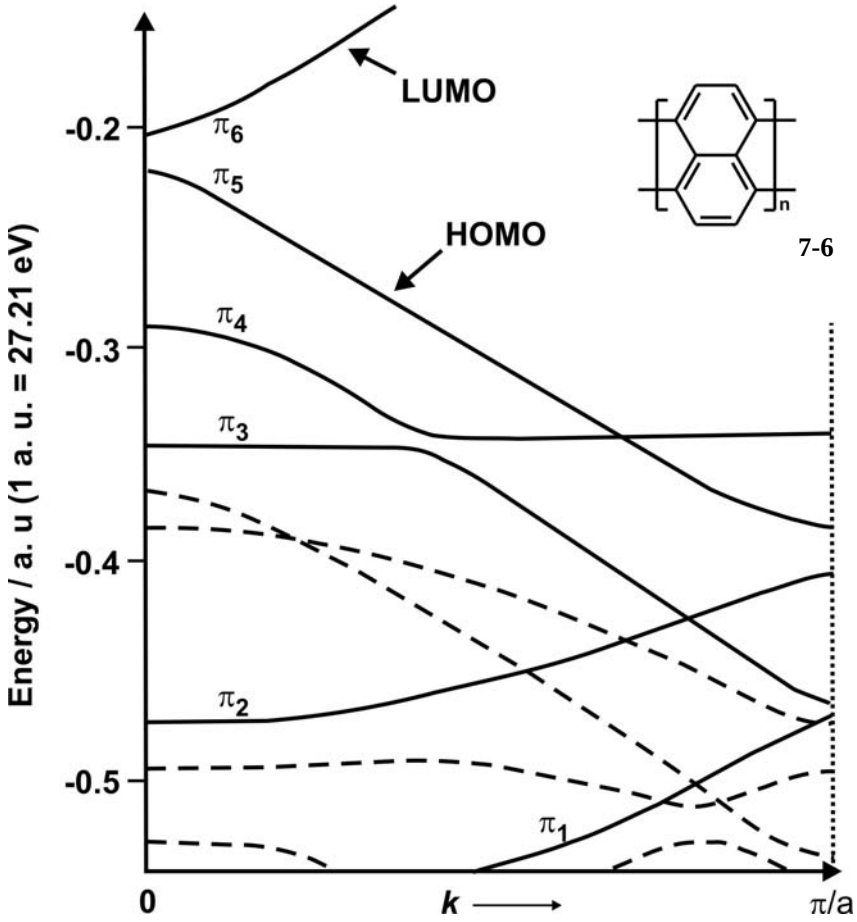

Figure 7-24: VEH band structure of poly(perinaphtalene); a is the length of the unit cell

References

[1] J. L. Bredas, R. H. Baughmann *J. Chem. Phys.* **1985**, *83*, 1316.

[2] G. Nicolas, P. Durand *J. Chem. Phys.* **1979**, *70*, 2020.

[3] G. Nicolas, P. Durand *J. Chem. Phys.* **1980**, *72*, 453.

[4] A. Bohnen, K. H. Koch W. Lüttke, K. Müllen *Angew. Chem.* **1990**, *102*, 548.

Publications

D. Wasserfallen, I. Fischbach, N. Chebotareva, M. Kastler, W. Pisula, F. Jäckel, M. D. Watson, I. Schnell, J. P. Rabe, H. W. Spiess, K. Müllen *Influence of Hydrogen-Bonds on the Supramolecular Order of Hexa-peri-hexabenzocoronene Derivatives* Advanced Functional Materials, **2005**, *15*, 1585-1594.

D. Wasserfallen, M. Kastler, W. Pisula, Y. Fogel, Z. Wang, K. Müllen *Suppressing Aggregation in a Large Polycyclic Aromatic Hydrocarbon* Journal of the American Chemical Society, **2006**, *128*, 1334-1339.

D. Wasserfallen, G. Mattersteig, V. Enkelmann, K. Müllen *Synthesis and Crystal Structures of Extremely Crowded Oligophenylenes as Model Precursors to "Cubic Graphite"* **2006** - submitted

W. Pisula, M. Kastler, D. Wasserfallen, T. Pakula, K. Müllen *Exceptionally Long-Range Self-Assembly of Hexa-peri-hexabenzocoronene with Dove-Tailed Alkyl Substituents* Journal of the American Chemical Society **2004**, *126*, 8074-8075.

M. Kastler, W. Pisula, D. Wasserfallen, T. Pakula, K. Müllen *Influence of Alkyl Substituents on the Solution- and Surface-Organization of Hexa-peri-hexabenzocoronenes* Journal of the American Chemical Society **2005**, *127*, 4286-4296.

J. M. Warman, J. Piris, W. Pisula, M. Kastler, D. Wasserfallen, K. Müllen *Charge Recombination via Intercolumnar Electron Tunnelling through the Lipid-like Mantle of Discotic Hexabenzocoronenes* Journal of the American Chemical Society **2005**, *127*, 14257-14262.

W. Pisula, M. Kastler, D. Wasserfallen, F. Nolde, C. Kohl, T. Pakula, K. Müllen *Pronounced Supramolecular Order in Discotic Donor–Acceptor Mixtures* Angewandte Chemie International Edition **2006**, *45*, 819-823.